

# **COMPUTER AIDED ANALYSIS, DESIGN AND OPTIMIZATION OF MULTISTORIED BUILDING SUBJECTED TO SEISMIC AND WIND LOADING**

S. M. Z. Islam\* & M. Menaz

*Department of Civil Engineering, Rajshahi University of Engineering and Technology, Rajshahi,  
Bangladesh*

*\*Corresponding Author: smzislam190@yahoo.com*

## **ABSTRACT**

An economical structural system which would mitigate undesirable cost due to seismic and wind loads. Seismic and wind loading should consider carefully in Building design in Bangladesh which is situated highly earthquake and tornado/typhoon pron area. The objective of this research is to analysis, design and optimization of multistoried building subjected to seismic and wind loading using ETABS and OPTIMA software respectively. Two case study of computer aided analysis, design and optimization of multi-storied building subjected to seismic and wind loading have been conducted in this research. The base shear, seismic load of different floor level and seismic shear of different floor level are calculated in this study. An extensive analysis and design works was conducted on column axial load, column-beam shear & moment for eight storied residential building considering combination of dead load, live load and earthquake load according to BNBC-2013. The deflection of various members, inter-storey drift, lateral displacement of the whole structure and stress of all members were checked comparison with limiting value of the design criteria. Moreover, a research is conducted on 67 storied tall building to determine the size and stiffness of the variable structural elements due to the lateral combined wind load resisting system. After the preliminary design, the various cross section of beams and column were reduced by considering their efficiency. Finalize the optimum member sizes in which the volume of concrete and quantity of steel is saved to precise amount and maximize the usable floor area by satisfying the design criteria. Finally, the optimum member sizes increase the floor area and saving cost up to 12.24% and 10-30% for seismic and wind loading respectively.

Keywords: Building; computer aided analysis; design and optimization; seismic and wind loading

## **INTRODUCTION**

Structural engineers are facing the challenge of striving for the most efficient and economical design solution while ensuring that the final design of a building must be serviceable for its intended function, habitable for its occupants and safe over its design life-time. Generally, the design of buildings must satisfy earthquakes or severe wind storm loading criteria. The building should have sufficient strength and stiffness to control deflection and prevent any structural damage or collapse. Deflection of various members, inter-storey drift and lateral drift performance is a principal concern in the seismic design of building structures. The economic design of elements of building structures for various levels of lateral drift performance under multiple levels of earthquake loads is generally a rather difficult and challenging task. Chan and Zou (2004) conducted a research on drift performance optimization for reinforced concrete buildings under earthquake loads using optimality criteria approach. An efficient computer-based optimization technique has been developed for lateral stiffness design of tall buildings by Chan (1997), Chan and Sui (1997). They developed an efficient computer-based optimization technique for lateral stiffness design of tall buildings. The optimization technique, based on a rigorously derived Optimality Criteria (OC) approach, is capable of optimizing large-scale tall steel and or reinforced concrete buildings subject to multiple static wind drift and dynamic wind-induced vibration design constraints.

The effectiveness of the state-of-the-art optimization technique has been demonstrated through its actual design application on a number of the tallest buildings in Hong Kong Chan (2001, 2004). Field

application projects optimized by OPTIMA software is shown in Fig. 1. Chan (2004). These actual applications represent a major advance in the use of structural optimization techniques for practical tall building designs, it should be noted that the research has been primarily focused on the elastic wind drift performance of tall buildings. ETABS software used for optimization of selected field applied projects as shown in Fig. 2. Much effort is still needed to extend the current optimization technique to inelastic seismic design of multi-story buildings. Recent trends to construct increasingly slender and taller buildings which are wind-sensitive. Very often, such slender and tall buildings different member size and stiffness may experience over design or under design. Optimization technique can overcome this problem. Therefore a research is needed for effective analysis, design and optimization technique of multistoried building. Selected Building This paper presents an effective analysis, design and optimization technique of multistoried building subjected to seismic and wind loading using ETABS and OPTIMA. Optimization technique always improves the quality of design, increase the floor area and saving cost.



Fig. 1: Selected building projects optimized by OPTIMA in Hong Kong, China



Fig. 2: Selected building projects optimized by ETABS in Rajshahi, Bangladesh

## METHODOLOGY

The emerging structural optimization technology provides a promising design tool to automate the structural synthesis process and to aid in searching for the best design to meet various design requirements. Transforming structural optimization theory into design practice of realistic civil

engineering structures has always been regarded a difficult task. An extensive research to analysis, design and optimization of multi storied building is conducted subjected to seismic and wind loading using ETABS and OPTIMA software respectively. A eight story residential building is considered for analysis, design and optimization subjected to seismic loading using ETABS. Although there exist powerful finite element software for precise prediction of dynamic seismic responses of structures, structural optimization of large-scale building structures for various levels of elastic and inelastic seismic performance under multiple levels of earthquake events is generally a challenging and difficult task.

Recent attempts have been made to develop an automatic optimal elastic and inelastic seismic drift design of concrete framework structures Chan and Zou (2004), Zou and Chan (2004, 2005a) and base-isolated building systems Chan (2005b). Research in the past normally expressed dynamic response performance constraints by calculating sensitivity derivatives of equations of motion with respect to design variables. Such a sensitivity formulation may be straightforward; but it requires enormous instantaneous sensitivity computations and may lead to divergent solution fluctuations. The recent studies have shown that a more stable seismic drift responses modeled by various response spectrum, time history and pushover analysis methods can be formulated accurately by the Principle of Virtual Work Chan and Zou (2004), Zou and Chan (2004, 2005a). Once the structural form of a building is established, the major effort is to size the structural members to satisfy all safety and wind-induced stability and serviceability design requirements. For a general tall building structure composed of  $t_s = 1, 2, \dots, N_s$  skeletal steel,  $i_c = 1, 2, \dots, N_c$  concrete frame elements and  $i_t = 1, 2, \dots, N_t$  concrete shear wall panels, the optimal element sizing design can be formulated as follows.

$$\text{Minimize } \text{Cost}(A_{i_s}, B_{i_c}, D_{i_c}, t_{i_s}) = \sum_{i_s=1}^{N_s} w_{i_s} A_{i_s} + \sum_{i_c=1}^{N_c} w_{i_c} B_{i_c} D_{i_c} + \sum_{i_t=1}^{N_t} w_{i_t} t_{i_t} \quad (1)$$

This formulation was considered subject to top drift constraints, inter storey drift constraints, wind induced acceleration constraints, element strength constraints, steel element, sizing constraints, concrete element width sizing, constraints, and concrete element depth sizing constraints, concrete wall thickness sizing constraints. Similarly, a sixty five story tall building is considered for optimization subjected to wind tunnel loading using OPTIMA software. Building model was generated, assign load, analysis, design and optimization have been completed according to the requirements of the selected building code. OPTIMA has been based on an integrated system approach as outlined in Fig. 3.

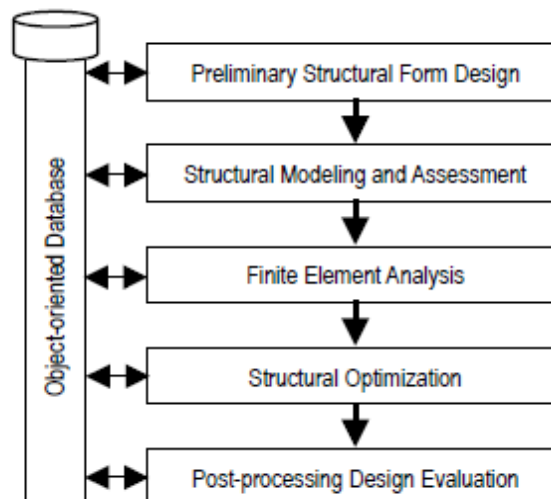


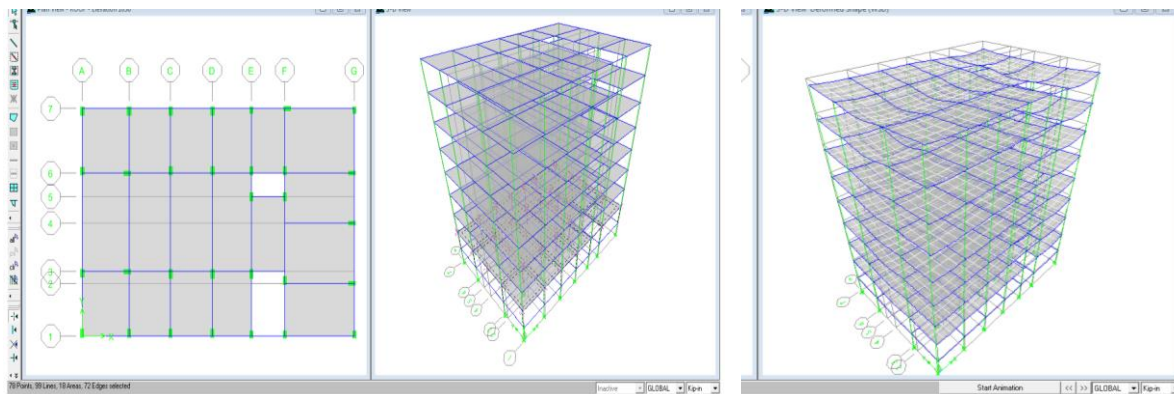
Fig. 3: Integrated design work flow

Optimal design formulation is included in this study. All of these modeling and analysis options are completely integrated with a wide range of steel and concrete design features. In this paper, the Optimality Criteria (OC) method, which has been widely used in the aerospace industry Venkayya (1989) and shown to be very effective in lateral drift design of tall buildings Chan (1992, 1997, 2001) and Chan et al (1995) will be extended to minimize the cost of tall symmetric steel buildings subject

to wind-induced acceleration performance constraints expressed in terms of the natural frequency of the building. In this approach, a set of necessary optimality conditions for the optimal design is first derived and a recursive algorithm is then applied to search for the optimal design indirectly by satisfying the set of optimality conditions.

## RESULTS AND DISCUSSIONS

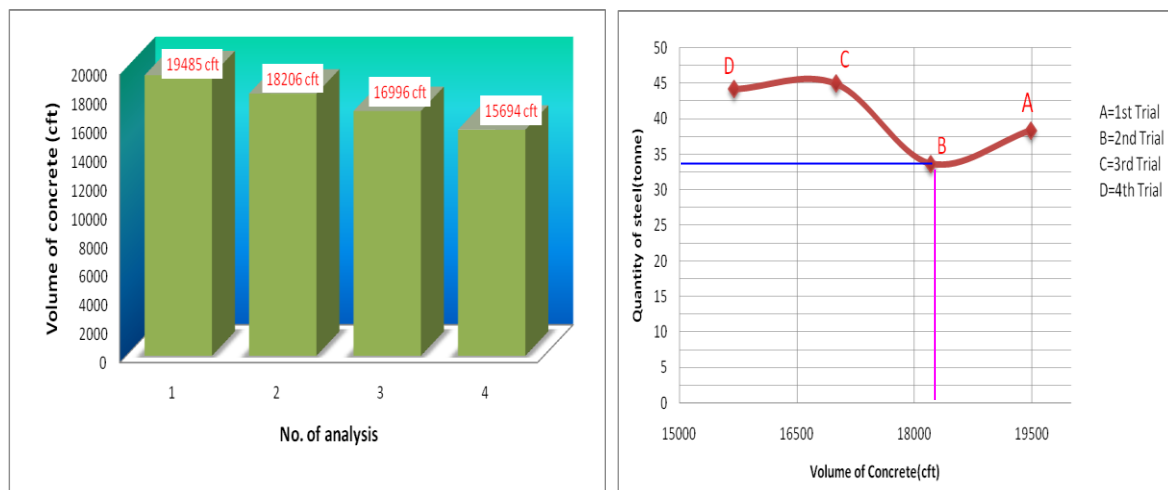
Building model and deflected shape of the building by ETAB'S subjected to earthquake load is shown in Fig. 4. Fig 5 presents the variation of quantity of concrete vs No. of trial analysis and quantity of steel vs volume of concrete. Optimum point was found at point B. Optimal structure design is becoming increasing significant due to limited material resources. Fig. 6-7 presents the optimal design modeling and results form numerical analysis. The members which is shown red colour in the work density diagram shown are considered as the relative efficient members (or the critical members) of the structure under the given set of design constraints as shown in Fig. 5 and 6. In this model, the efficient members under the given set of wind load are found. Economy in design can be achieved through an optimization procedure by aiming to find the most efficient structure that will satisfy the design criteria.



(a) Generation of the building model

(b) Deflected Shape of the structure

Fig.4: Generation of building and deflected shape of the building by ETAB'S

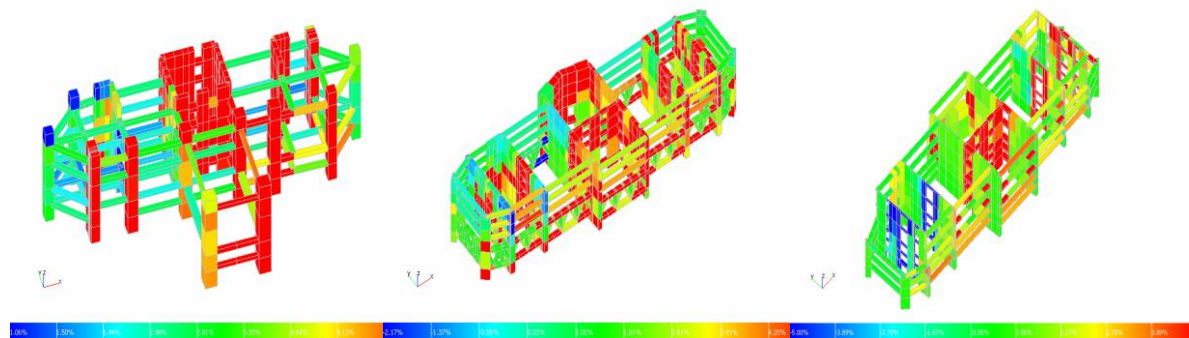


(a) Variation of concrete – No. of trial analysis.

(b) Variation of quantity of steel vs volume of concrete

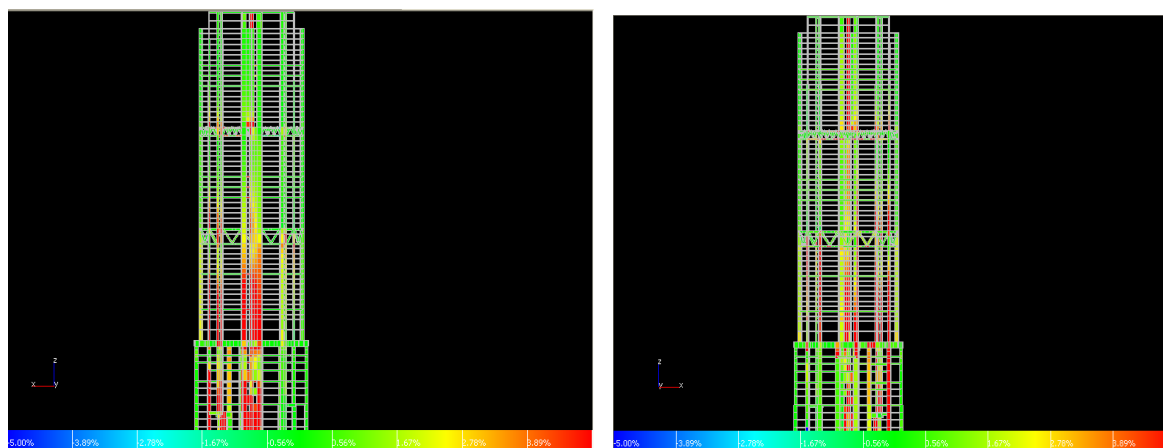
Fig. 5: Variation of quantity of concrete vs No. of trial analysis and quantity of steel vs volume of concrete

The cost comparison of initial model of 67 storied tall build subjected to wind loading and optimized model is shown Table 1. The optimum member sizes increase the floor area and saving cost up to 12.24% and 10-30% for seismic and wind loading respectively.



(a) Work density of 6-10 floor (b) Work density of 51-55 floor (c) Work density of 68-73 floor

Fig. 6: Work density of different floor using OPTIMA



(a) Front view

(b) back side view

Fig 7: Over all work density of Front view and back side view.

Table 1. Initial and optimized model comparison using OPTIMA

Item	Initial design Model	5 <sup>th</sup> Cycle optimized design model
Drift (Overall)	1 / 424.52	1 / 424.52
Total Column Member (No.)	380	380
Total Beam Member (No.)	2,897	2,905
Total Wall (No.)	7,357	7,358
Brace (No.)	94	102
Total Structure Element (No.)	10,728	10,744
Total length of element	11,414	11,520
Total planar area (m <sup>2</sup> )	1,704	1,810
Total volume of element (m <sup>3</sup> )	14,157	13,850
Total cost (\$)	4.59 x 10 <sup>7</sup>	(Approx.) 4.11 x 10 <sup>7</sup>
Cost Saving		= 0.48 x 10 <sup>7</sup>

## CONCLUSIONS

Structural optimization is an advanced computational technique, which replaces the traditional trial-and-error design procedure by a systematic goal-oriented design synthesis process. Remarkable progress has been made on developing an optimization procedure for element sizing optimization of practical tall buildings. The effectiveness of the state-of-the-art optimization software OPTIMA has been well attested through applications to the design of numerous tallest building projects in Hong Kong and Bangladesh. While some initial successes in practical structural optimization have been demonstrated in the lateral stiffness and serviceability design of tall buildings, research is still needed to advance the field of structural optimization to further develop innovative techniques for a wider spectrum of design problems associated with practical engineering of buildings. The efficient members under the given set of wind load are found. Economy in design can be achieved through an optimization procedure by aiming to find the most efficient structure that will satisfy the design criteria. The optimum member sizes increase the floor area and saving cost up to 12.24% and 10-30% for seismic and wind loading respectively. Efficient structural design also leads to a better foundation design, even in difficult soil conditions.

## ACKNOWLEDGEMENT

The authors gratefully acknowledge the Hong Kong University of Science and Technology, Hong Kong, China and Rajshahi University of Engineering and Technology, Rajshahi-6204, Bangladesh

## REFERENCES

- Chan, CM; Grierson, DE and Sherbourne, AN 1995. Automatic optimal design of tall steel building frameworks. *Journal of Structural Engineering ASCE*,121:838–47.
- Chan, CM. 1997. How to optimize tall steel building frameworks. *Guide to Structural Optimization. ASCE Manuals and Reports on Engineering Practice*, 90: 165–195.
- Chan, CM. 2001. Optimal lateral stiffness design of tall buildings of mixed steel and concrete construction. *The Structural Design of Tall Buildings*,10:155–177.
- Chan, CM. 1992. An optimality criteria algorithm for tall buildings design using commercial standard sections. *Journal of Structural Optimization*, 5: 26–9.
- Chan, CM. 2006. Optimal lateral stiffness design of tall buildings of mixed steel and concrete construction. *Journal of the Structural Design of Tall Buildings*, 10:155–77.
- Chan, C.-M. 2004. *Advances in structural optimization of tall building in Hong Kong*. Keynote lecture presented in the Third China-Japan-Korea Joint Symposium on Optimization of Structural and Mechanical Systems, Kanazawa, Japan.
- Chan, C-M and Zou, XK. 2004. Elastic and inelastic drift performance optimization for reinforced concrete building under earthquake loads. *Earthquake Engineering and Structural Dynamics*, 33 (8): 929-950.
- Chan, CM and Zou, XK. 2004. Elastic and inelastic drift performance optimization for reinforced concrete buildings under earthquake loads. *Earthquake Engineering and Structural Dynamics*, 33:929–950.
- Chan, CM and Sun, SL.1997. Optimal drift design of tall reinforced concrete building frameworks. *Advances in Structural Optimization*; Frangopol DM and Cheng FY (ed.), American Society of Civil Engineers: New York, 31–42.
- Venkayya, VB. 1989. Optimality Criteria: a basic multidisciplinary design optimization. *Computational Mechanics*, 5:1–21.
- Zou, X.-K. and Chan, C.-M. 2004. Integrated time history analysis and performance-based design optimization of base-isolated concrete buildings. *Proc. 13th World Conference on Earthquake Engineering*, Vancouver, Canada, Aug. 1-6,1314.
- Zou, X.-K. and Chan, C.-M., 2005a. An optimal resizing technique for seismic drift design of concrete buildings subjected to response spectrum and time history loadings. *Computers and Structures*, 83(19-20):1689–1704
- Zou, X.-K. and Chan, C.-M., 2005b. Optimal seismic performance-based design of reinforced concrete buildings using nonlinear pushover analysis. *Journal of Engineering Structures*, 27(8): 1289-1302.

## **TENSILE STRENGTH BEHAVIOUR OF BOLTED & SCREWED CONNECTIONS OF THIN STEEL SHEET AT ELEVATED TEMPERATURE**

S. M. Z. Islam\* & M. A. Islam

*Department of Civil Engineering, Rajshahi University of Engineering and Technology, Rajshahi, Bangladesh*

*\*Corresponding Author: smzislam190@yahoo.com*

### **ABSTRACT**

Thin profiled steel sheets are commonly connected to the underlying purlins or steel trusses/frame by drilling or tapping of screws and bolts. Fire resistance is quite important for thin steel structures due to the fact that the material properties of structural steel become sensitive when temperature exceeds approximately 400°C. The objective of this research is to investigate the structural behaviour of screw and bolted connection of thin profiled steel sheet after elevated temperature. A total of 108 connection coupon test including 48 connected specimens at high temperature tensile tests were conducted to investigate the material deterioration of the thin profiled sheet steels at elevated temperature. A series of test was conducted for bolts and screw connections in form of single and double shear conditions of thin profiled sheet steels from 25 °C to 1250°C temperatures. The investigation was also varied in bolt size, screw size, bolt arrangement, screw arrangements and 7 different temperatures. The failure modes and ultimate strength of shear of bolted and screwed connections of thin profiled sheet steels after elevated temperatures are presented. Based on the test results, it was found that the material properties of the profiled steel sheets were found to deteriorate and bolted is better than screwed connections after elevated temperatures. The comparison between the deterioration of the tested connection strengths and that of the material properties at elevated temperatures showed a similar tendency of reduction.

Keywords: Bolted and screw connection; elevated temperatures; failure modes; thin sheet steel; ultimate strength

### **INTRODUCTION**

Bolted and screwed are two conventional connection types which are widely used in light gauge and thin steel structures as shown in Fig. 1. Makelainen and Miller (1983) carried out tensile tests of cold-formed galvanized sheet steel Z33 at elevated temperatures using transient state and steady state methods. Behaviour of bolted and screwed connections have been investigated by different researches (LaBoube and Sokol, 2002; Lim and Young, 2007; Lu et al. 2009; Moze and Beg, 2011; Nithyadharan, and Kalyanaraman, 2011). The current design specification for cold-formed steel structures, such as the North American Specification (2007), Australian/New Zealand Standard (2005) and the Eurocode 3 (2006), provide design rules for bolted and screwed connections. These design rules are categorized by different failure modes. However, these design rules of the bolted and screwed connections for cold-formed steel structures in these specifications are slightly different. Various terms may be adopted by different specifications to define a similar failure mode. It should be noted that the design rules for screwed and bolted connection in the current design specifications of cold-formed steel structures are only applicable at ambient temperature condition. The North American Specification (2007), Australian/New Zealand Standard (2005) for cold-formed steel structures improved the bearing factors in the design rules of bearing failure based on hundreds of test specimens conducted by Rogers and Hancock (1998,1999, 2000) at ambient temperature.

The fire resistance of steel structures is an important issue that engineers need to consider. A series of equations was proposed to predict the material properties of cold-formed steel at elevated temperatures based on coupon test results Chen and Young (2007). The experimental investigation on single shear bolted connection specimens of thin sheet steels tested at elevated temperatures using steady state test method is reported by Shu and Young (2011). It was shown that the current design

equations of single shear bolted connections in the American (2007), Australian/New Zealand (2005) and European specifications (2006) provide conservative predictions at elevated temperatures by substituting the deteriorated material properties. However, experimental investigation on shear of screw and bolted connections of thin sheet steels at elevated temperatures using the transient state method is limited. There is no research on such connections after elevated temperature. Therefore, an investigation is needed to know the structural behaviour of screw and bolted connection of thin profiled steel sheet after elevated temperature. In this study, the structural behaviour of 48 single-double shear bolted and screw connections fabricated were investigated experimentally by varied in bolt size, screw size, bolt arrangement, screw arrangements and 7 different temperatures.

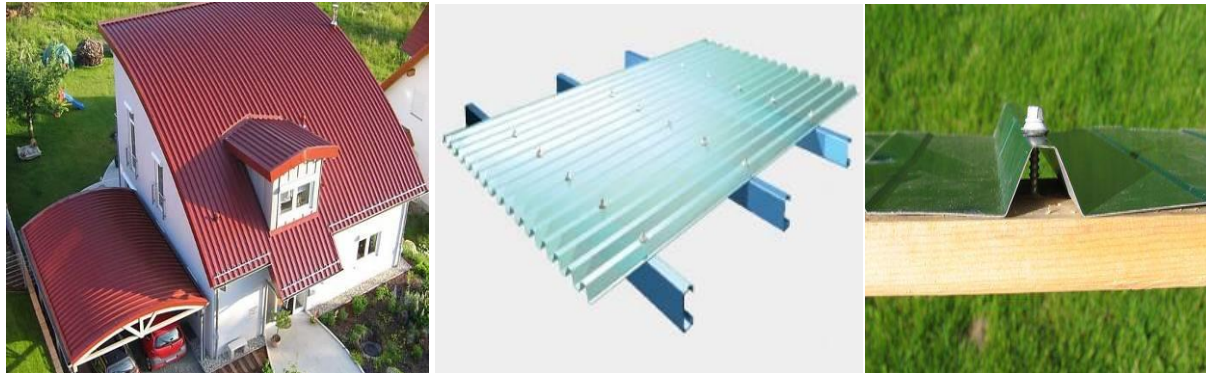
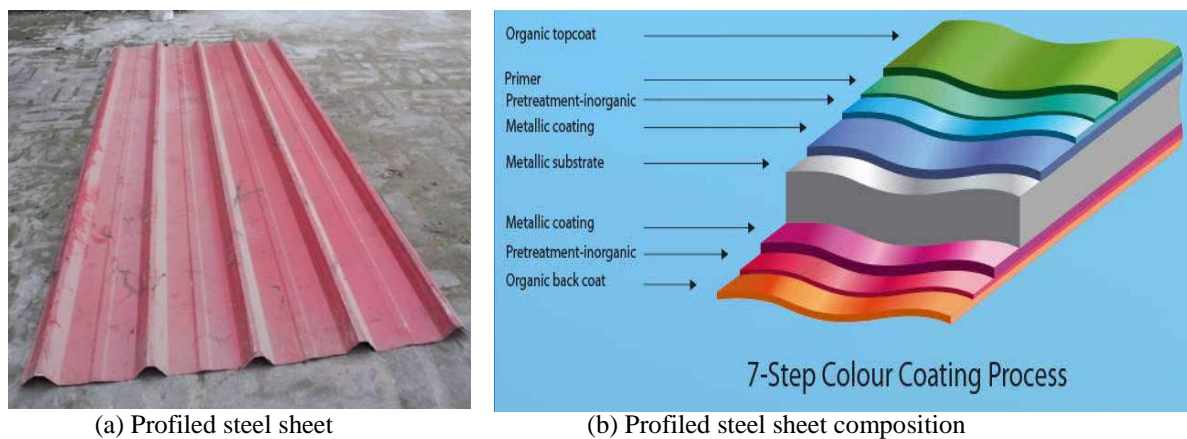


Fig. 1: Field application of profiled steel sheet using bolted and screwed connections

## METHODOLOGY

### *Material Properties*

Profiled steel sheet and composition layer of profiled steel sheet is shown in Fig. 2. The tensile coupons were prepared and tested according to the American Society for Testing and Materials Standard, ASTM and the Australian Standard AS 1391 for the tensile testing of metals using 12.5 mm wide coupons. Different heat insulating material which is used in this study is shown in Fig. 2.



(a) Profiled steel sheet

(b) Profiled steel sheet composition

Fig.2: Profile steel sheet and its composition

### *Test Specimen*

A total of 108 connection specimen including 48 connection specimens at elevated temperature were experimentally investigated in this study. In the first step, 60 specimens were tested by connecting with bolts and screws of 3 different diameter of 5.90 mm, 4.70 mm and 4.30 mm for single shear and double shear conditions to find out suitable connection specimen and optimum bolt and screw dia. Comparing the results for bolted connections the suitable connection type with the optimum bolt diameter was identified for both single shear and double shear conditions. In second step, 48 connection test were conducted using suitable connection type with the optimum bolt diameter which



was heated in different elevated temperatures of 25, 250, 500, 700, 850, 1000, 1250 °C. At first, the profiled steel sheets were cut with the snipping tools of certain dimensions 300 mm x 200 mm. The test was also conducted in two different arrangement of bolt and screw. There are mainly two types connection was adopted for this experiment such as bolt and screw are placed parallelly or vertically. B2-P (Two bolt parallel connection) test specimen and B2-V (Two bolt vertical connection) test specimen were adopted for the single shear and double shear bolted connections. The B2-P-test specimen and B2-V-test specimen were connected from end to end with bolts of diameter 5.90 mm, 4.70 mm, 4.30 mm both for single shear and double shear condition as shown in Fig. 3.

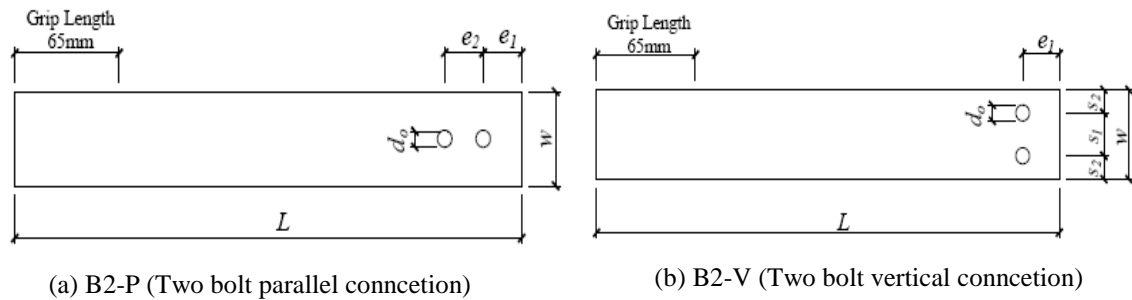


Fig. 3: Connection details for two bolt parallel and vertical connections

### Test Procedure

A series of bolted and screwed connection tests were conducted in this study. The bolted and screwed connection tests were conducted by a servo-controlled hydraulic Universal Testing Machine which is mainly used for the coupon tests. Drilling and connecting of tensile test specimen is shown in Fig 4. The connection specimens were set into the grip of the machine as shown in Fig. 5. A pair of grip apparatus was specially fabricated in order to provide pin assembly at both ends of the test specimen. Two special gaskets were inserted in the grips, so that the shear surface of the single and doubly lapped specimen was purely vertical in-line to the loading direction. Clips linked with iron wire were used to prevent the extent of out-of-plane curling at the end of the profile steel sheet. After that, tensile load was applied gradually and the tensile stresses obtained from the machine were recorded at the room temperature. Then, suitable connection type, arrangement with the optimum bolted & screwed diameter specimens were heated in different elevated temperatures of 25, 250, 500, 700, 850, 1000, 1250 °C as shown in Fig 6.

### RESULTS AND DISCUSSIONS

A total of 108 connections including 48 connections at elevated temperature specimens varied in bolt-screw size, arrangement were tested in 7 different temperatures namely, 25, 250, 500, 700, 850, 1000 and 1250°C. The failure modes of steel connections were observed carefully and most of the cases the bearing failure occurred as shown in Fig 7-8 and Table 1. Diameter of 4.7 and 4.3 mm for screw and bolt connections were found better performance for single shear and double shear respectively.



Fig. 4. Drilling and connecting of tensile test specimen



Fig. 5: Test setup of tensile test specimen



Fig. 6: Specimen at different temperature

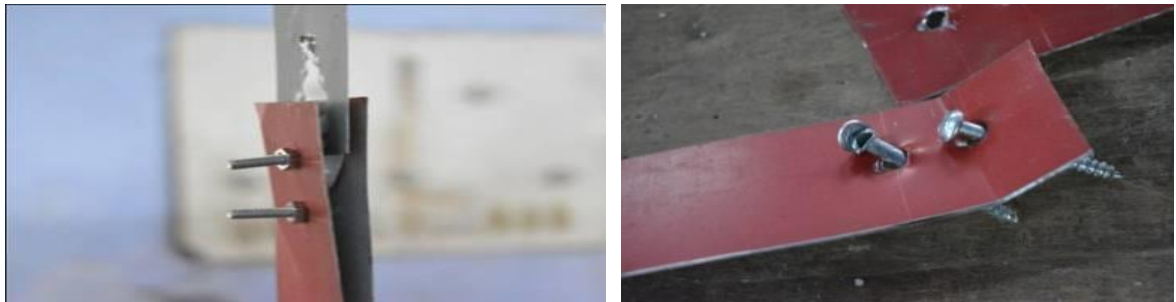


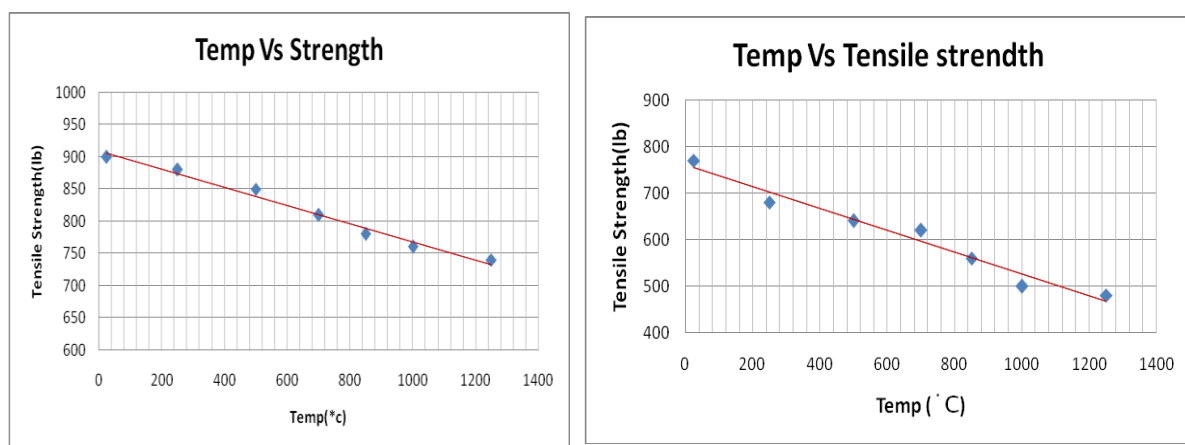
Fig.7: Tested failure mode of screw and bolt connection



Fig. 8: Bearing failure after elevated temperature

Table 1: Comparison of single and double shear tensile of screw connection after elevated temperatures

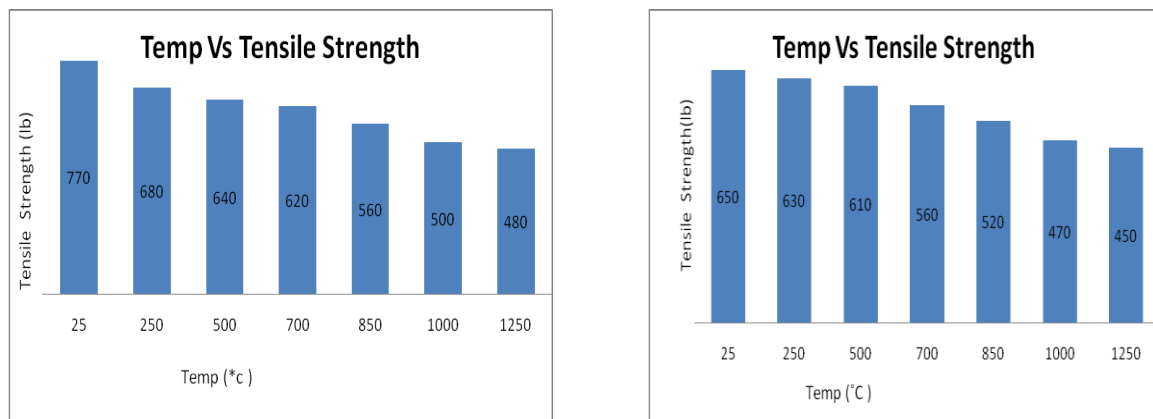
Specimen	Length L (mm)	Width W (mm)	Temp (°C)	Tensile Strength (lb)		Failure mode
				Single shear	Double shear	
S2-P- 12	300	50	25	640	560	Bearing Failure
S2-P- 13	300	50	250	600	545	Bearing Failure
S2-P- 14	300	50	500	560	525	Bearing Failure
S2-P- 15	300	50	700	510	485	Bearing Failure
S2-P- 16	300	50	850	480	450	Bearing Failure
S2-P- 17	300	50	1000	430	410	Bearing Failure
S2-P- 18	300	50	1250	410	390	Bearing Failure



(a) Bolted single shear

(b) Bolted double shear

Fig. 9: Comparison of tensile strength of single and double shear bolted connection after elevated temperatures



(a) Bolt connection

(b) Screw connection

Fig. 10: Comparison of tensile strength of bolted and screwed double shear connection after elevated temperatures

Based on the test results, two bolt or screw parallel connections are proved better performance than vertical arranged at elevated temperature. Single shear screwed and bolted connections are suitable than double shear screwed and bolted connection as shown in Table 1. and Fig. 9. It was found that the tensile strength of profiled steel sheet decreases linearly after the elevated temperatures as shown

in Fig.9. Moreover, it may be concluded that the bolted connections are more satisfactory than the screwed connections after the elevated temperatures as shown in Fig 10.

## CONCLUSION

A series of test program on the structural behaviour of single-double shear, bolted and screwed connections of thin sheet steels at elevated temperatures has been presented. A total of 108 including 48 connections at elevated temperature specimens varied in bolt-screw size, arrangement were tested in 7 different temperatures namely, 25, 250, 500, 700, 850, 1000 and 1250°C. According to the test results, bearing failure mode were found most of the specimen at elevated temperature. The optimum diameter of 4.7 and 4.3 mm for screw and bolt connections were found for single shear and double shear respectively. Based on test results, two bolt or screw parallel connections are proved better performance than vertical arrange at elevated temperature. Single shear screwed and bolted connections are found suitable than double shear screwed and bolted connection. It was found that the tensile strength of profiled steel sheet decreases linearly after the elevated temperatures. Furthermore, it may be concluded that the bolted connections are more satisfactory than the screwed connections at the elevated temperatures. The comparison of the test strengths of single-double shear bolted-screwed connections with the tensile strengths of the material properties of the corresponding sheet steels obtained from the coupon tests has a similar tendency of deterioration at elevated temperatures.

## ACKNOWLEDGEMENT

The authors gratefully acknowledge the Abul Khair (AKS) Steel Mills Dhaka, Bangladesh for supplying the test specimens.

## REFERENCES

- AISI S100. 2007. North American Specification for the Design of Cold-Formed Steel Structural Members, *American Iron and Steel Institute*, AISI S100-2007, AISI Standard.
- AS/NZS 4600, 2005. Cold-formed Steel Structures, Australian/New Zealand Standard, AS/NZS 4600:2005, Sydney, Australia, Standards Australia, 2005.
- Chen, J and Young, B. 2007. Experimental investigation of cold-formed steel material at elevated temperatures. *Thin-Walled Structures*, 45(1): 96-110.
- EC3, 2006. Eurocode 3 – Design of Steel Structures – Part 1-3: General Rules Supplementary Rules for Cold-formed Members and Sheeting. Brussels: European Committee for Standardization, EN 1993-1-3:2006.
- LaBoube, RA and Sokol, MA. 2002. Behavior of screw connections in residential construction. *Journal of Structural Engineering*, 128(1): 115-118.
- Lim, JBP and Young, B. 2007. Effects of elevated temperatures on bolted moment-connections between cold-formed steel members. *Engineering Structures*, 29(10): 2419-2427.
- Lu, W; Makelainen, P and Outinen, J. 2009. Behaviour of screwed shear sheeting connection in fire. *Application of Structural Fire Engineering*, 411-446.
- Moze, P and Beg, D. 2011. Investigation of high strength steel connections with several bolts in double shear. *Journal of Constructional Steel Research*, 67(3): 333-347.
- Nithyadharan, M and Kalyanaraman, V. 2011. Experimental study of screw connections in CFS-calcium silicate board wall panels. *Thin-Walled Structures*, 49(6): 724-731.
- Rogers, CA and Hancock, GJ. 1998. Bolted connection tests of thin G550 and G300 sheet steels. *Journal of Structural Engineering*, 124(7): 798-808.
- Rogers, CA and Hancock, GJ. 1999. Bolted connection design for sheet steels less than 1.0 mm thick. *Journal of Constructional Steel Research*, 51:123-146.
- Rogers, CA and Hancock, GJ. 2000. Failure modes of bolted-sheet-steel connections loaded in shear. *Journal of Structural Engineering*, 126(3): 288-296.
- Yan, S. and Young B. 2011. Tests of single shear bolted connections of thin sheet steels at elevated temperatures – Part I: Steady state tests. *Thin-Walled Structures*, 49(10):1320-1333.

## **NOBLE USE OF SHAPE MEMORY ALLOY IN SEISMIC RETROFIT OF MULTI-SPAN SIMPLY SUPPORTED ELEVATED HIGHWAY**

A. K. M. T. A. Khan\* & M. A. R. Bhuiyan

*Department of Civil Engineering, Chittagong University of Engineering and Technology, Chittagong, Bangladesh*

*\*Corresponding Author: thohidul.ce@gmail.com*

### **ABSTRACT**

Laminated rubber bearings (LRB) are one of the widely used isolation devices in elevated highway for mitigation of seismic induced damages. This isolation bearing has some consequences problems due to strong motions which may causes detrimental effects such as instability of the bearing, pounding, unseating problems of the deck and permanent deformation of the bearings. Shape memory alloy (SMA) bars are known for their super-elastic properties, which have been utilized in various applications in the fields of engineering and science. More recently, these materials have been evaluated for applications in the domain of earthquake engineering. SMAs are unique materials with a substantial potential for retrofitting of elevated highway when incorporated with LRB. The novelty of SMAs lies in their ability to undergo large deformations and return to their undeformed shape through stress removal or shape memory effect. SMAs also have some surprising thermo-mechanical properties, including super-elasticity and hysteretic damping. All these features make this materials a promising solution for blending with LRB to minimize possible seismic risk of bridges which further justified by nonlinear dynamic analysis. This study investigates the effectiveness of SMA based rubber bearing (SRB) in compare to lead rubber bearing to reduce the seismic vulnerability of an elevated highway when subjected to far-field (FF) ground excitations that are spectrally matched to a target design spectrum. The seismic response quantities in the analysis include the absolute maximum values of pier displacement, bearing displacement, deck displacement, deck acceleration, bearing force and residual displacement. The numerical result shows that, the SMA bars are effective in limiting the seismic responses, particularly the residual displacement when blended with LRB. The combined strengths obtained from LRB and SMA bars offers an optimum synergy for bridge retrofitting. Both the Ni-Ti and Cu-Be-Al SMA alloy based rubber bearing proves their superiority in compare to the lead rubber bearing and the evidences focused by the analytical scheme.

**Keywords:** Shape memory alloy bar; laminated rubber bearing; nonlinear dynamic analysis; super-elasticity behaviour; seismic performance; retrofitting; elevated highway

### **INTRODUCTION**

Laminated rubber bearings are one of widely used devices in seismic isolation of bridges and buildings. They are revealed the ability to carry vertical loads in compression and to accommodate shear deformations. The rubber layers, reinforced with steel shims, reduce the freedom to bulge by increasing the vertical stiffness of the bearing. Three types of laminated rubber bearings are widely used as seismic isolation devices: natural rubber bearing (RB), lead rubber bearing (LRB), and high damping rubber bearing (HDRB). RB occupies flexibility property and small damping and hence it has been used to accommodate the thermal movement, the effects of pre-stressing, creep, and shrinkage of superstructure of elevated highway or it has been used in seismic isolation by combining with other energy dissipation devices, such as lead, steel and viscous damper, etc. (Khan et al., 2015). Other two types of bearings possess high damping which are developed and widely used in various civil infrastructures including bridges in many countries, especially in Japan and USA (Khan, 2016). HDRB possess a variety of mechanical properties, which are influenced by their compounding effect, nonlinear elasto-plastic behaviour and temperature and strain-rate dependent viscosity property (Bhuiyan, 2009; Khan, 2016). Lead rubber bearings also acquire all the mechanical properties of

HDRB with reduced extent (Bhuiyan, 2009; Khan, 2016). LRB experiences some consequence-problems when subjected to strong earthquake excitations, especially the near field (NF) earthquake ground motions (Ozubulut and Hurlebaus, 2011a; 2011b). The unfortunate coincidence of the natural period of the seismically isolated bridge with that of the NF earthquakes amplifies the seismic responses of isolation system. In particular, LRB experiences large horizontal deformation under NF earthquakes which cause detrimental problems, such as instability of the bearings, pounding and unseating problems of the bridge deck (Choi, 2005; Khan, 2016). In recent years, a number of attempts are reported, by combining LRBs and shape memory alloy (SMA) in seismic isolation of highway bridges, to partially solve the above mentioned limitations (Khan et al., 2015). The super-elasticity accompanied by hysteresis property of the SMA allows it to fabricate with LRBs to reduce the residual deformation of the bridge system for sustainable seismic protection (Khan, 2016).

The objective of this work is to carry out seismic performance analysis of a bridge acted upon by far field (FF) earthquake ground accelerations in longitudinal direction. In this regard, nonlinear dynamic analysis of a bridge pier using a direct time integration approach is carried out. Two types of isolation bearings are employed in the analysis: lead rubber bearing (LRB) and smart material based laminated rubber bearing (SRB). The LRB (Fig.1a) is manufactured by alternating rubber layers with steel shims along with lead plugs to be inserted through bearing while the SRB (Fig.1b) comprises Ni-Ti and Cu-Be-Al based SMA wires with natural rubber bearing. In nonlinear dynamic analysis, the force-displacement behaviours of LRB and SRBs are evaluated using visco-elasto-plastic models. In addition, bilinear and linear elastic models are used for the bridge pier and deck, respectively. The variation of seismic responses of the bridge due to the use of LRB and SRBs are explored in the study. The bridge responses considered in this study include the peak values of pier displacement, bearing displacement, deck displacement, deck acceleration, bearing force and residual displacement. The comparison shows that the seismic responses of the bridge are affected by the use of two types of isolation bearings; more specifically, the residual displacements of the bridge pier are distinctly reduced in the case of SRBs in compare to LRB for all FF ground motions considered (Khan, 2016).

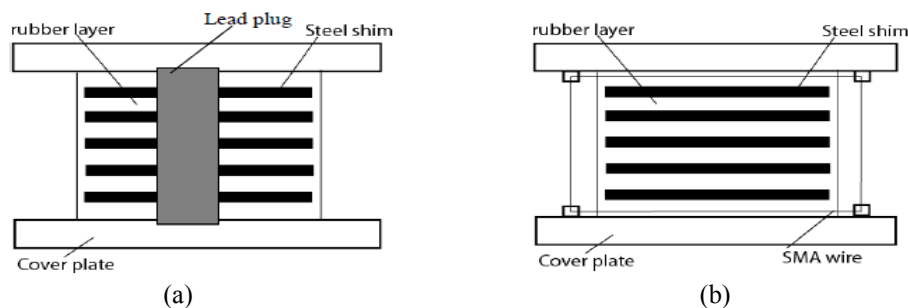


Fig.1: Schematic details of (a) Lead Rubber Bearing (LRB) and (b) Shape Memory Alloy (SMA) based Rubber Bearing (SRB) (After Khan, 2016)

## MODELING OF ELEVATED HIGHWAY

### *Physical Model of the Elevated Highway*

A typical three-span continuous elevated highway, isolated by LRB and SRBs, is used in the current study. The bridge consists of continuous reinforced concrete (RC) deck-steel girder isolated by LRB and SRBs installed below the steel girder supported on RC piers. The superstructure consists of 260 mm RC slab covered by 80 mm of asphalt layer. The height of the continuous steel girder is 1800 mm. The mass of a single span elevated highway deck is  $600 \times 10^3$  kg and that of a pier is  $240 \times 10^3$  kg. The mass calculation procedure will be available in literature (Khan, 2016). The substructure consists of RC piers and footings supported on shallow foundation. The representative physical model as well as analytical model of the elevated highway is tried to given hereunder (Fig.2). The dimensions and material properties of the deck and piers of elevated highway with footings are given in Table 1.

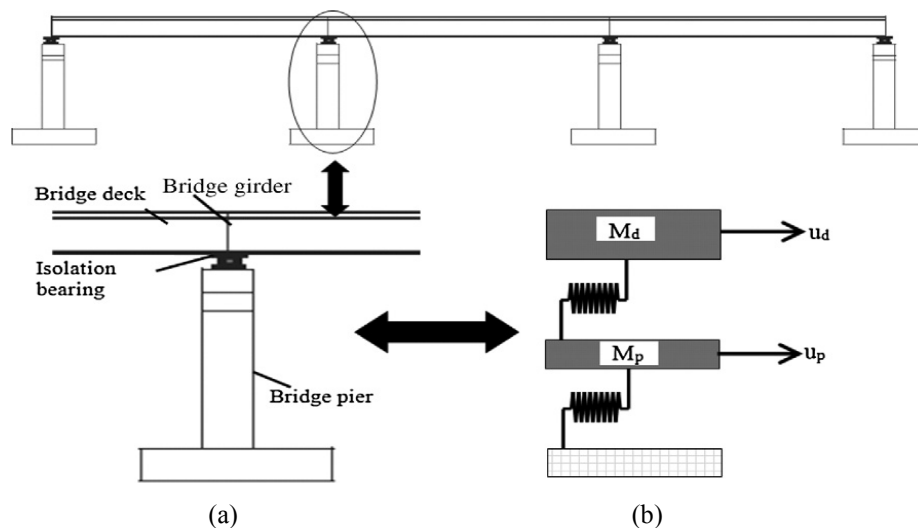


Fig.2: Modelling of the elevated highway (a) physical model and (b) analytical model (After Khan, 2016)

Table 1: Geometries and material properties of the elevated highway (After Khan et al., 2015)

Properties	Specifications
Cross-section area of the pier cap (mm <sup>2</sup> )	2000x12000
Cross-section area of the pier body (mm <sup>2</sup> )	2000x9000
Height of the pier (mm)	15000
Young's modulus of elasticity of concrete (N/mm <sup>2</sup> )	25000
Young's modulus of elasticity of steel (N/mm <sup>2</sup> )	200000

## ANALYTICAL MODEL OF THE ELEVATED HIGHWAY

### Modelling of the Elevated Highway

The elevated highway model is simplified into a two-degree of freedom (2-DOF) system: one at the deck level and the other at the pier top level of the elevated highway. This simplification holds true only when the superstructure of elevated highway is assumed to be rigid in its own plane which shows no significant structural effects on the seismic performance of the elevated highway when subjected to earthquake ground acceleration in longitudinal direction. The mass proportional damping of the pier of elevated highway is considered in the analysis. Equations that govern the dynamic responses of the 2-DOF system can be derived by considering the equilibrium of all forces acting on it using the d'Alembert's principle. In this case, the internal forces are the inertia forces and the restoring forces, while the external forces are the earthquake induced forces. Equations of motion are given as,

$$m_p \ddot{u}_p(t) + F_p(u_p, t) - F_{is}(t) = -m_p \ddot{u}_g(t); \quad (1a)$$

$$m_d \ddot{u}_d(t) + F_{is}(t) = -m_d \ddot{u}_g(t); \quad (1b)$$

where,  $m_p$ ,  $m_d$ ,  $u_p$  and  $u_d$  are the masses and displacements of pier and deck, respectively.  $\ddot{u}_p$  and  $\ddot{u}_d$  are the accelerations of pier and deck, respectively.  $\ddot{u}_g$  is the ground acceleration.  $F_p$  is the internal restoring force of the pier.  $F_{is}$  is the restoring force of the isolation bearings (LRB and SRB). The unconditionally stable Runge Kutta 4<sup>th</sup> order method is used in the direct time integration of the equations of motion (Eq. 1a and Eq. 1b) (Bhuiyan, 2009; Khan et al., 2015; Khan, 2016).

### **Modelling of the Pier of Elevated Highway**

The pier is restricted to participate in energy absorption in the elevated highway in addition to the isolation bearing. The secondary plastic behaviour was expected to be lumped at bottom of the pier where plastic hinge is occurred. The plastic hinge of the pier is modeled by nonlinear spring element. Four hysteresis models for the nonlinear spring are usually used in the nonlinear dynamic analysis of an elevated highway: elasto-plastic model, bilinear model, Clough degradation model, and tri-linear Takeda model. In the current study, the nonlinear spring element is modeled using the bilinear model. The ratio of the post yield stiffness with elastic stiffness is considered as 0.01 (Khan, 2016).

### **Modelling of the LRB and SRB**

The experimental investigations of LRB have revealed the four different fundamental properties, which together characterize the typical overall response: (i) a dominating elastic ground stress response, which is characterized by large elastic strains, (ii) a finite elasto-plastic response associated with relaxed equilibrium states, (iii) a finite strain-rate dependent viscosity induced overstress, which is portrayed by relaxation tests, and (iv) a damage response within the first cycles, which induces considerable stress softening in the subsequent cycles. Considering the first three properties, a strain-rate dependent constitutive model for the LRB was developed by Bhuiyan (2009) which is verified for sinusoidal excitations and subsequently implemented in seismic analysis using professional software (Resp-T, 2006). The geometries and material properties of LRB are presented by Table 2.

Table 2: Geometries and materials properties of the laminated rubber bearing (After Khan, 2016)

Sl. No.	Particulars	Value
01	Cross section of the bearing (mm <sup>2</sup> )	1000000
02	Thickness of the rubber layers (mm)	200
03	Number of rubber layers	6
04	Thickness of steel layer (mm)	3.0
05	Nominal shear modulus of rubber (MPa)	1.2

The constitutive model of SMAs is very complicated in a sense that it depends upon many factors, such as strain rates, strain magnitude and strain history. Three categories of constitutive models are used for characterizing the super-elasticity and damping properties of SMA bar, such as parametric, nonparametric and differential equation-based models (Khan et al., 2015). However, the differential equation-based constitutive model is widely used for SMAs since it is capable of using in continuum mechanics based finite element algorithms considering small and finite deformations and subsequently in finite element based professional software packages. In realization, the complexity of replicating the mechanical behaviour of SMAs by the use of phenomenological models, three versions of the models are used in seismic applications. The models include a simplified model, which is constructed based on experimentally obtained data; a thermo-mechanical model, which considers the stress-strain-temperature relationship in SMAs; and a thermo-mechanical model, which also takes into account the cyclic loading effects in SMAs. In recognizing the intricacy of the phenomenological models considering the thermo-mechanical behaviour of SMAs, a simplified model (Bhuiyan and Alam, 2013) is used to model the SRBs. Table 3 shows the geometries and material properties of the Copper-Beryllium-Aluminium (Cu-Be-Al) and Nitinol (Ni-Ti) SMA wires used in this study.

Table 3: Geometries and materials properties of SMA wires used in the analysis (After Khan, 2016)

Sl. No.	Particulars	SMA bar (Cu-Be-Al)	SMA bar (Ni-Ti)
01	Modulus of Elasticity (N/mm <sup>2</sup> )	32040	72000
02	Yield Strength (N/mm <sup>2</sup> )	235	270
03	Length of Wires (mm)	2500	2500
04	Cross Sectional Area (mm <sup>2</sup> )	600	600



## SEISMIC GROUND ACCELERATION

By Caltrans (2004), if the structure under consideration is within 10 miles (approx. 15 km) of a seismic fault can be classified as NF. Ground motions outside this range are classified as FF motions. Current study considers a suite of five FF ground motion records of medium to strong earthquakes with peak ground acceleration (PGA) values ranging from 0.243g to 0.728g (Fig.3(a) to 3(e)). Fig.3(f) shows the characteristics of the ground motions performing response spectrum analysis with 5 percent damping ratio. Here, the dominant periods of the ground motion records delimited by 0.2 to less than 1.0 sec which cover the wide range of natural period of bridge structures (Khan, 2016).

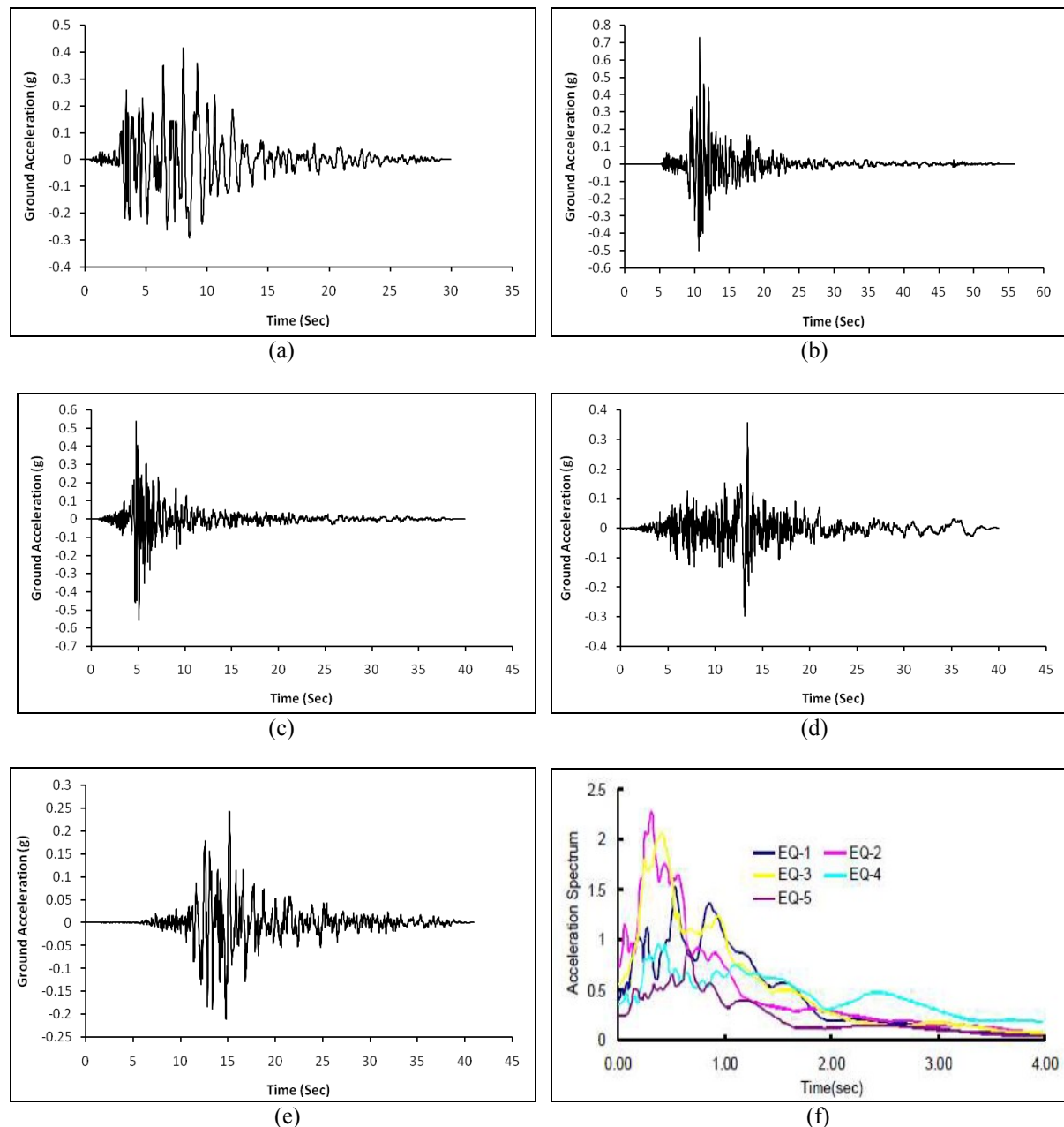


Fig.3 Acceleration time histories of far field seismic ground motion records; (a) EQ-1, (b) EQ-2, (c) EQ-3, (d) EQ-4, (e) EQ-5 and (f) Acceleration response spectra

## NUMERICAL RESULTS AND DISCUSSION

In comparative assessment, a few standard response parameters obtained for each earthquake ground motion are addressed in the subsequent subsections: pier displacement, bearing displacement, deck acceleration, deck displacement, residual displacement of the deck of elevated highway after earthquake and bearing force (Bhuiyan and Alam, 2013). Each response parameter of the system

equipped with LRB is compared with SRBs. For convenience, Ni-Ti SMA based laminated rubber bearing is expressed by “SRB 1” and Cu-Be-Al SMA based laminated rubber bearing is expressed by “SRB 2”. The numerical outcomes of a single representative earthquake (EQ-2) were placed in this article due to page limitation. Numerical outcomes for rest of the seismic records are available in literature (Khan, 2016). Fig.4 to Fig.10 presents typical responses of the elevated highway for EQ-2. The trends of the results obtained from absolute maximum responses by nonlinear dynamic analysis are exhibits through Fig.11 to Fig.13. The simulation results are summarized in Table 4 for both the LRB and SRBs when considering far field ground motion record EQ-1 to EQ-5 respectively.

### ***Pier Displacement***

The pier displacement decreases with increase in energy dissipation but increases with increase in the bearing forces. Therefore, the SRBs usually produce larger pier displacement than LRB. Fig.4 to Fig.6 exhibits time histories of the pier displacement due to EQ-2 when considering LRB, SRB 1 and SRB 2, respectively. Fig.11 confirmed that, the LRB and SRB 2 possess maximum (48.145mm) and minimum (38.180 mm) pier displacements whereas SRB 1 possess in the middle (41.301 mm) for seismic ground motion EQ-1. Again, Fig.11 argued that, the SRB 1 and LRB possess maximum (81.334 mm) and minimum (57.874 mm) pier displacements whereas SRB 2 possess in the middle (80.546 mm) for seismic ground motion EQ-2. Similarly, Fig.11 established that, the LRB and SRB 1 possess maximum (32.688 mm) and minimum (26.203 mm) pier displacements whereas SRB 2 possess in the middle (30.333 mm) for seismic ground motion EQ-3. Furthermore, Fig.11 says that, the SRB 1 and LRB possess maximum (47.943 mm) and minimum (36.150 mm) pier displacements whereas SRB 2 possess in the middle (44.721 mm) for seismic ground motion EQ-4. Moreover, Fig. 4.36 revealed that, the LRB and SRB 2 possess maximum (37.774 mm) and minimum (33.564 mm) pier displacements whereas SRB 1 possess in the middle (37.717 mm) for ground motion EQ-5.

### ***Bearing Displacement***

The bearing displacements are obtained from relative displacements between deck and pier. Bearing displacement increases with the decrease in energy dissipation of the bearings as revealed from Fig.10. It appears from the Figs.7 to Fig.9 that, the residual displacements of SRBs are bigger in magnitude than LRB, which correspond to the observations of the pier displacements. Fig.7 to Fig.9 exhibits time histories of the bearing displacement due to EQ-2 when considering LRB, SRB 1 and SRB 2, respectively. Fig.12 confirmed that, the SRB 1 and LRB possess maximum (202.703 mm) and minimum (185.765 mm) bearing displacements whereas SRB 2 possess in the middle (200.621 mm) for ground motion EQ-1. Again, Fig.12 argued that, the SRB 2 and LRB possess maximum (241.884 mm) and minimum (193.969 mm) bearing displacements whereas SRB 1 possess in the middle (195.929 mm) for ground motion EQ-2. Again, Fig.12 established that, the LRB and SRB 1 possess maximum (71.969 mm) and minimum (62.099 mm) bearing displacements whereas SRB 2 possess in the middle (65.508 mm) for ground excitation EQ-3. Furthermore, Fig.12 says that, the SRB 2 and LRB possess maximum (157.302 mm) and minimum (140.609 mm) bearing displacements whereas SRB 1 possess in the middle (155.262 mm) for ground motion EQ-4. Moreover, Fig. 4.37 revealed that, the LRB and SRB 2 possess maximum (130.473 mm) and minimum (117.673 mm) bearing displacements whereas SRB 1 possess in the middle (119.893 mm) for ground excitation EQ-5.

### ***Residual Displacement***

The residual displacement of the bearing is computed by taking the arithmetic average of the stable absolute values of the last 5 to 15 sec of the time history of bearing displacements as obtained from the dynamic analysis of the system for each earthquake (Khan, 2016). The residual displacements of SRBs are smaller than LRB for all earthquakes as presented in tenth column of Table 4. For seismic ground motion record EQ-1, Fig.13 confirmed that, the LRB and SRB 2 possess maximum (7.796 mm) and minimum (2.980 mm) residual displacements whereas SRB 1 possess in the middle (3.165 mm). Again, for seismic ground motion record EQ-2, Fig.13 argued that, the LRB and SRB 1 possess maximum (7.928 mm) and minimum (3.141 mm) residual displacements whereas SRB 2 possess in the middle (3.456 mm). Similarly, for seismic ground motion record EQ-3, Fig.13 established that, the LRB and SRB 2 possess maximum (8.114 mm) and minimum (3.031 mm) residual displacements

whereas SRB 1 possess in the middle (3.203 mm). Furthermore, for seismic ground motion record EQ-4, Fig.13 says that, the LRB and SRB 2 possess maximum (10.135 mm) and minimum (3.673 mm) residual displacements whereas SRB 1 possess in the middle (3.737 mm). Moreover, for ground motion record EQ-5, Fig.13 revealed that, the LRB and SRB 2 possess maximum (7.696 mm) and minimum (2.881 mm) residual displacements whereas SRB 1 possess in the middle (3.178 mm).

Table 4: Absolute maximum seismic responses of LRB, SRB 1 & SRB 2 due to Earthquake EQ-1 to EQ-5

EQ	Time (Sec)	PGA (g)	Bearing Type	Bearing Disp. (mm)	Deck Acc. (m/sq.s)	Pier Disp. (mm)	Deck Disp. (mm)	Bearing Force (kN)	Residual Disp. (mm)
EQ-1	30	0.416	LRB	185.765	4.337	48.145	172.321	1241.323	7.796
EQ-1	30	0.416	SRB 1	202.703	5.143	41.301	211.943	1616.841	3.165
EQ-1	30	0.416	SRB 2	200.621	4.557	38.180	202.573	1394.977	2.980
EQ-2	60	0.728	LRB	193.969	6.174	57.874	218.873	1219.012	7.928
EQ-2	60	0.728	SRB 1	195.929	5.726	81.334	201.989	1587.320	3.141
EQ-2	60	0.728	SRB 2	241.884	5.962	80.546	247.160	1608.637	3.456
EQ-3	40	0.555	LRB	71.969	5.521	32.688	65.431	793.803	8.114
EQ-3	40	0.555	SRB 1	62.099	5.491	26.203	63.276	815.710	3.203
EQ-3	40	0.555	SRB 2	65.508	5.490	30.333	63.054	764.116	3.031
EQ-4	40	0.358	LRB	140.609	3.590	36.150	138.975	1006.031	10.135
EQ-4	40	0.358	SRB 1	155.262	3.632	47.943	171.956	1351.781	3.737
EQ-4	40	0.358	SRB 2	157.302	3.691	44.721	166.166	1182.712	3.673
EQ-5	40	0.243	LRB	130.473	2.837	37.774	126.366	998.194	7.696
EQ-5	40	0.243	SRB 1	119.893	2.893	37.717	122.745	1139.470	3.178
EQ-5	40	0.243	SRB 2	117.673	2.868	33.564	117.655	995.744	2.881

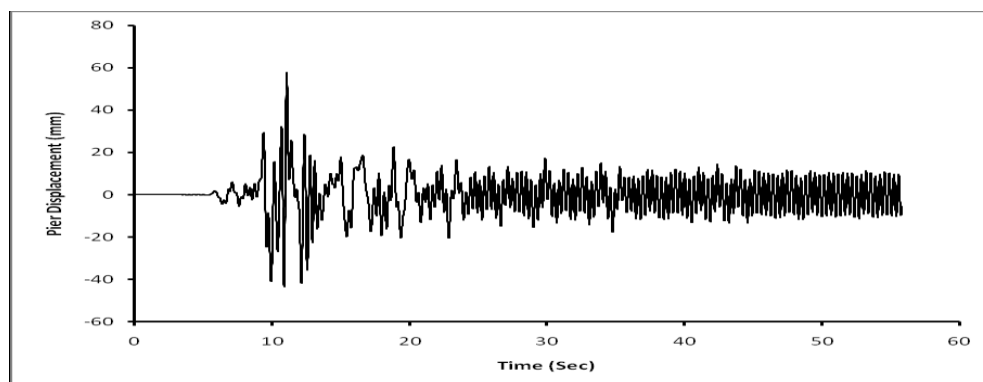


Fig.4: Pier displacement due to EQ-2 when considering LRB

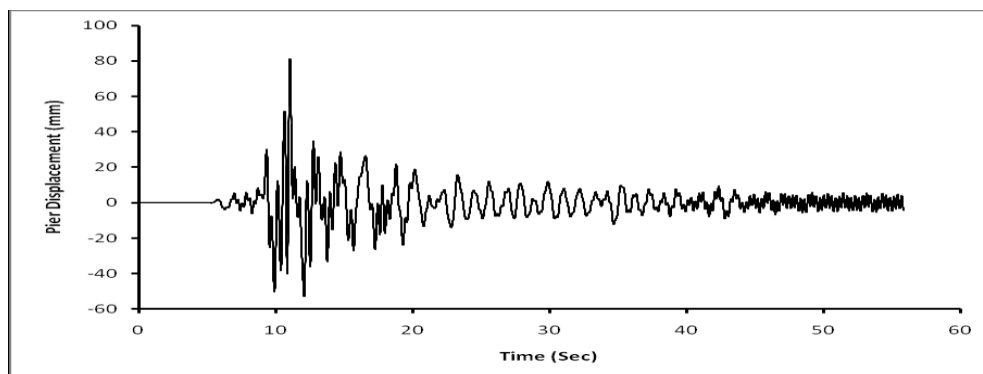


Fig.5: Pier displacement due to EQ-2 when considering SRB 1

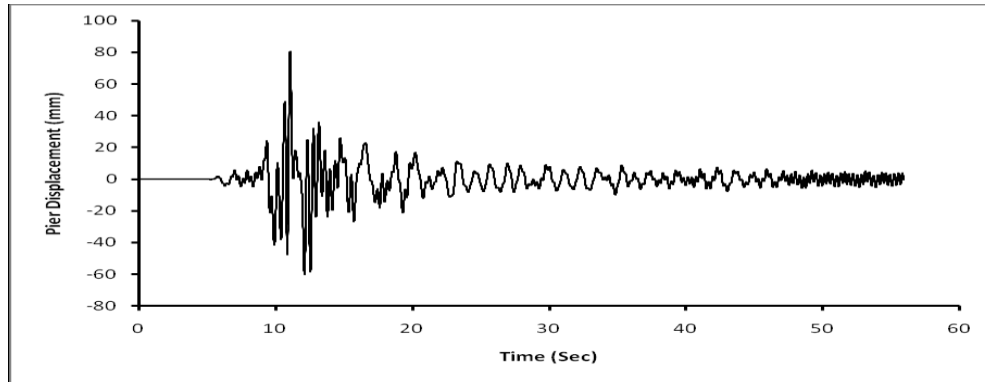


Fig.6: Pier displacement due to EQ-2 when considering SRB 2

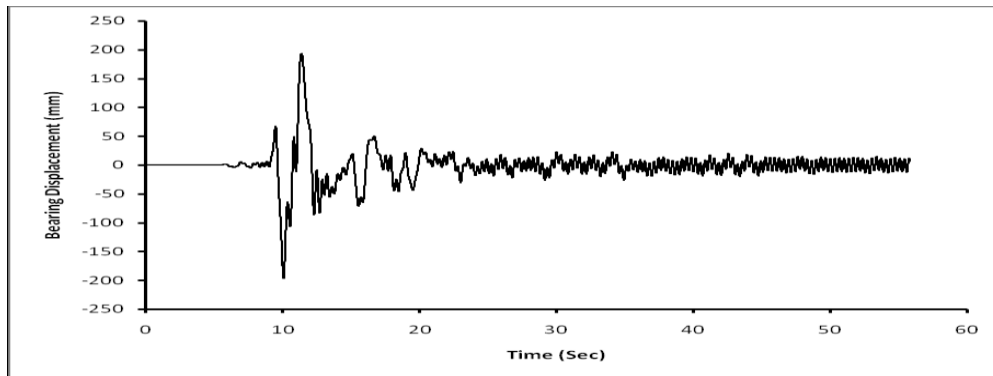


Fig.7: Bearing displacement due to EQ-2 when considering LRB

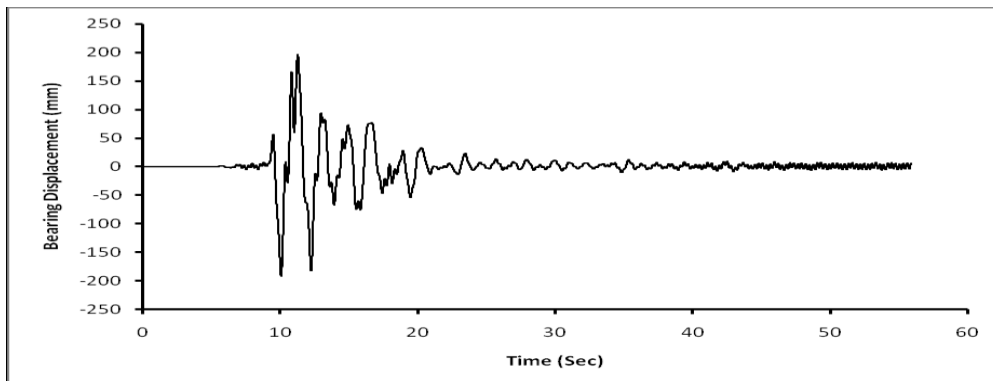


Fig.8: Bearing displacement due to EQ-2 when considering SRB 1

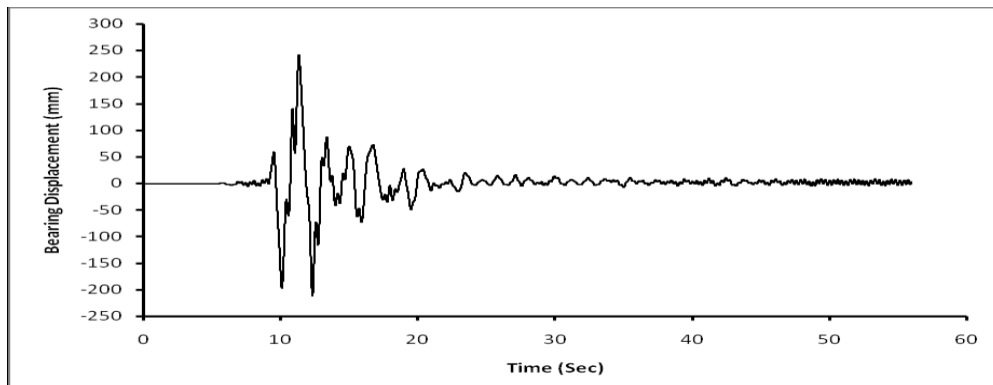


Fig.9: Bearing displacement due to EQ-2 when considering SRB 2

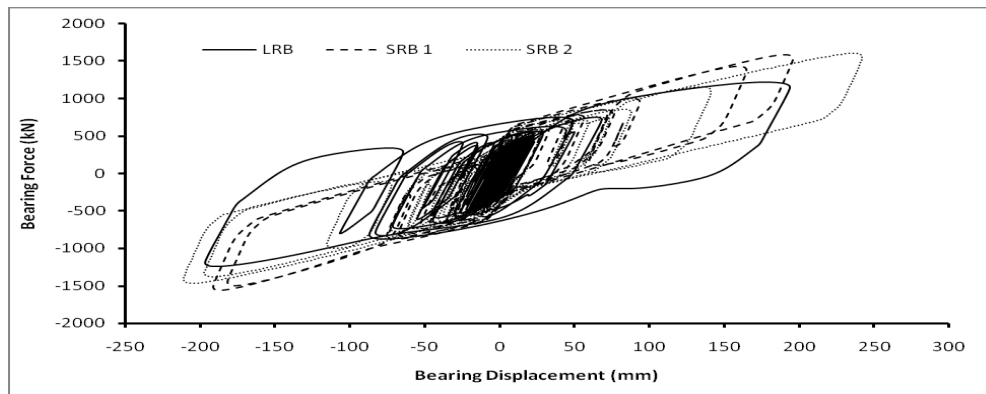


Fig. 10: Comparison of force-displacement relationship for LRB, SRB 1 and SRB 2 due to EQ-2

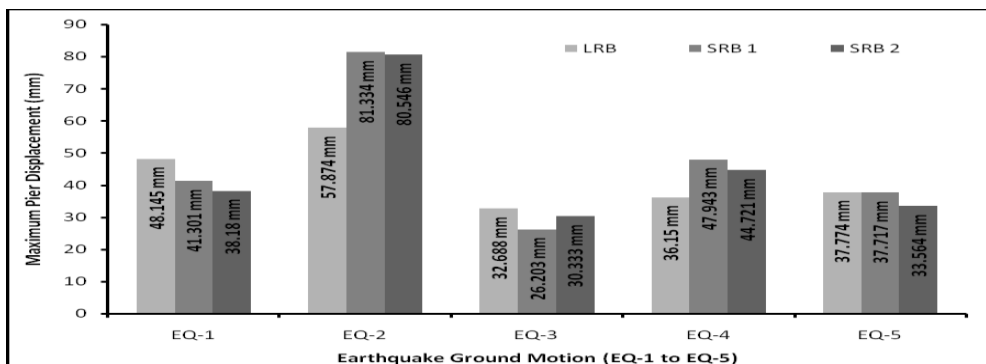


Fig. 11: Comparison of maximum pier displacement for LRB, SRB 1 and SRB 2 due to EQ-1 to EQ-5

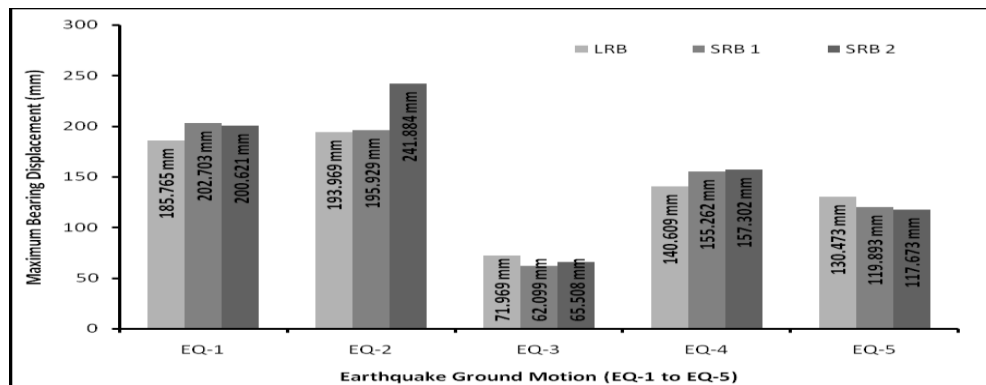


Fig. 12: Comparison of maximum bearing displacement for LRB, SRB 1 and SRB 2 due to EQ-1 to EQ-5

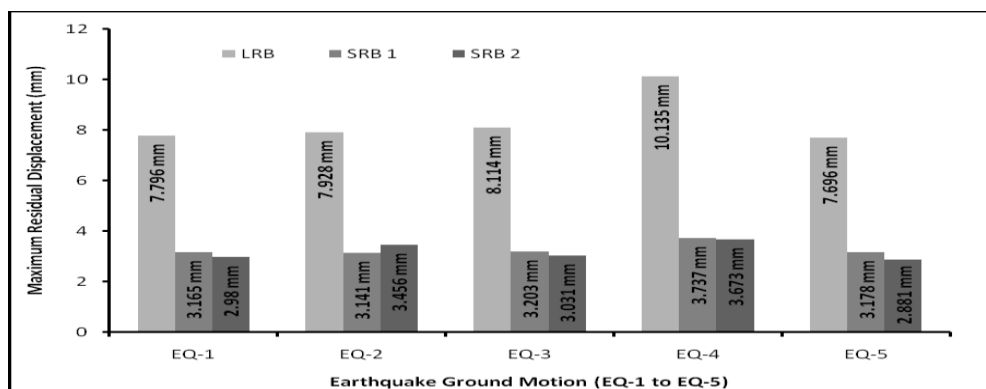


Fig. 13: Comparison of maximum residual displacement for LRB, SRB 1 and SRB 2 due to EQ-1 to EQ-5

## CONCLUDING REMARKS

This study presents the seismic performance assessment of an elevated highway isolated by lead rubber bearing (LRB) and SMA based natural rubber bearing (SRB). Two types of SRB have been employed in this analysis to initiate the seismic performance assessment of elevated highway by nonlinear dynamic analysis. These are Ni-Ti based laminated rubber bearing (SRB 1) and Cu-Be-Al based laminated rubber bearing (SRB 2). The nonlinearity of the bridge pier was considered by employing a bilinear force-displacement relationship developed by Bhuiyan (2009). A fixed restraint condition at bottom of the pier was considered. A complicated strain-rate dependent constitutive model for the LRB was used where as a visco-elasticity based analytical model was utilized for SRBs (Bhuiyan and Alam, 2013). The seismic performance considered in this studies are pier displacement, deck displacement, bearing displacement, deck acceleration, bearing force and residual displacement (Khan et al., 2015). The numerical results have revealed that, the SRBs satisfactorily restrain the residual displacement of the deck and the displacement of the pier of elevated highway for a suite of five FF ground motion records considered in this study. However, for deck and bearing displacements, the elevated highway with LRB has usually resulted in smaller responses in compared to SRBs. Almost a similar trend was observed in the case of deck accelerations. The early activation of hardening effect of SRBs in compared to LRB might have significant effect on the seismic responses of the system. The LRB designed in this study shows a larger dissipation of energy than that of SRBs. From the numerical analysis, it appears that not only the magnitude but the other characteristics of earthquake ground motions also have significant effect on the seismic responses of the elevated highway which should be carefully considered at design phase.

## REFERENCES

- Bhuiyan, AR. 2009. *Rheology modeling of laminated rubber bearings*, PhD dissertation, Graduate School of Science and Engineering, Saitama University, Japan.
- Bhuiyan, AR and Alam, MS. 2013. Seismic performance assessment of highway bridges equipped with superelastic shape memory alloy-based laminated rubber isolation bearing, *Engineering Structures*, 49:396–407.
- California Dept. of Transportation (CALTRANS), 2004. *Seismic Design Criteria*, Sacramento, USA.
- Choi, E; Nam, T and Cho, B. 2005. A new concept of isolation bearings for highway steel bridges using shape memory alloys, *Canadian Journal of Civil Engineers*, 32:957–967.
- Khan AKM TA; Bhuiyan, MAR and Alam, MS. 2015. Use of Ni-Ti shape memory alloy bars in seismic retrofit of multi-span elevated highway, *Proceedings of the National Conference of Earthquake and Environmental Disaster (NCEED - 2015)*, CUET, Chittagong, Bangladesh.
- Khan, AKM, TA. 2016. *Use of Shape Memory Alloy in Seismic Retrofit of Multi-Span Simply Supported Elevated Highway*, PGD Project Report, IEER, CUET, Chittagong, Bangladesh.
- Ozbulut, OE and Hurlbaas, S. 2011a. Optimal design of superelastic-friction base isolators for seismic protection of highway bridges against near-field earthquakes, *Earthquake Engineering & Structural Dynamics*, 40: 273–291.
- Ozbulut, OE and Hurlbaas, S. 2011b. Seismic assessment of bridge structures isolated by a shape memory alloy or rubber-based isolation system, *Smart Materials and Structures*, IOP Publishing Ltd, 20: 1-12.
- Resp-T, 2006. *User's Manual for Windows*, Version 5.

## **VIBRATION MITIGATION AND CONTROL OF 15 STORIED RC BUILDING VIA ACTIVE CONTROL**

M. S. Miah\*

*Department of Civil Engineering, University of Asia Pacific, Dhaka, Bangladesh  
\*Corresponding Author: mshamim@uap-bd.edu*

### **ABSTRACT**

The civil structures are getting slender in vertical direction over the last few decades in order to meet the need of the modern cities. Typically, those structures are often used as symbolic status of the national pride in addition to the conventional purposes. However, tall structures are prone to extreme vibration such as earthquakes. Hence it is essential to provide especial safety measure to those structures, for instance, appropriate vibration mitigation solution. The seismic hazard is a worldwide challenge, hence, in order to solve the aforementioned problem many attempts have been made over the last several decades. In this study, a reinforced building is considered to address the associated problems related to vibration mitigation. And mostly, the structures in Bangladesh are not properly designed for dynamic loads such as earthquake. Herein nonlinear dynamic analysis is performed of a 15 storied reinforced concrete building studied and performances are evaluated. It is assumed that three dampers will be placed into the building at different floors level. To do this end, an advanced modelling technique known as state space modelling is adopted. And the linear-quadratic regulator (LQR) is employed as control law. The concept of active control is adopted and numerical simulations are performed via MATLAB/SIMULINK®.

Keywords: Earthquakes; reinforced concrete buildings; nonlinear dynamic analysis; state space modeling; linear-quadratic regulator

### **INTRODUCTION**

Modern cities around the globe are having skyscrapers due to several reasons such as to build a city inside city to save more space, to make an icon of the country, etc. Those structures incredibly prone to dynamic loads such as earthquake. The aforementioned problem is driving the engineers and scientist to find better solution for its survival by keeping the structures in safe condition. Even though, the skyscrapers are capable of solving mass accommodation problem but they cost millions. Therefore, it is essential to make those structures structurally sound by providing better technological solution. Typically, all most all of the civil structures are prone to extreme vibrations, in particular, modern structures i.e., slender/tall buildings, bridges are critical in terms of vibration mitigation. There are several alternatives available and broadly can be categories as follows; (i) passive control, (ii) active control and (iii) hybrid control. The performances may vary significantly depending on the selection of the control technology mentioned before. For instance, passive control devices are safe and reliable but these technologies are not capable of tuning in real-time. In order to avoid the aforementioned drawbacks, the active control technology has been successfully used in many structures (Dyke 1996; Preumont, 2004) as an alternative. A detail study has been performed by (Preumont, 2004) where the advantages of adopting active control as a tool for extreme vibration mitigation is reported. However, the semi-active control devices such as magnetorheological (MR) damper a particular type of hybrid control e.g. semi-active control can be used an alternative of active and passive control systems (Bhowmik, 2011; Dyke, 1996; Miah et al., 2015). There are different types of semi-active control devices and the behavior modelling of a very specific type of MR damper is studied by (Bhowmik, 2011). The possibility of implementation of a rotational type MR damper in combination with real-time model updating is studied in (Miah et al., 2015 and 2016). In order to adopt active or semi-active control scheme a control algorithm is essential. Hence, herein a simple but optimal control algorithm so called the linear-quadratic regulator (LQR) is employed. The efficacy of the LQR scheme has been verified by several researchers (Anderson and Moore, 1989; Mobaieen, et

al. 2012; Miah et al., 2015; Weber and Maślanka, 2012).

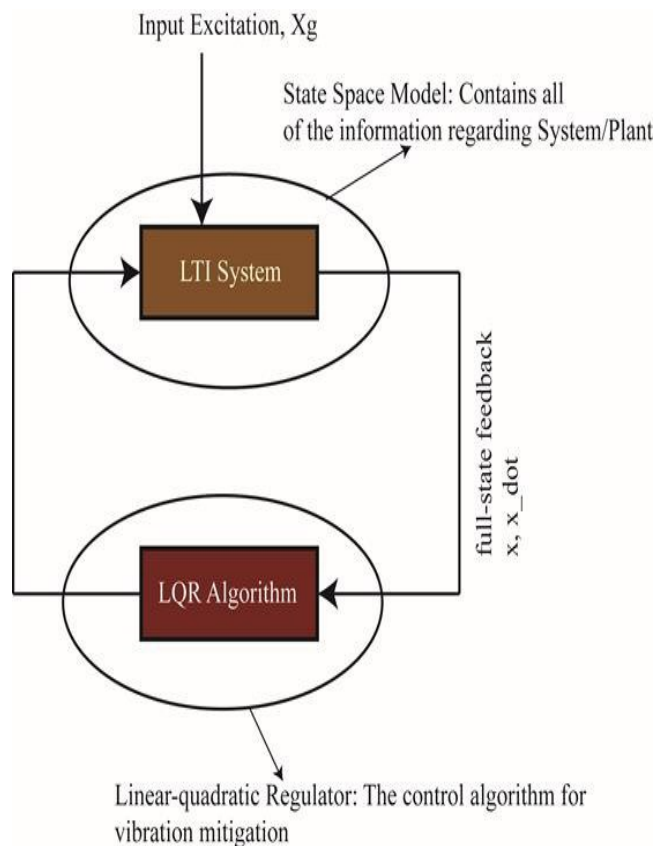


Fig. 1. Implemented control in closed-loop form.

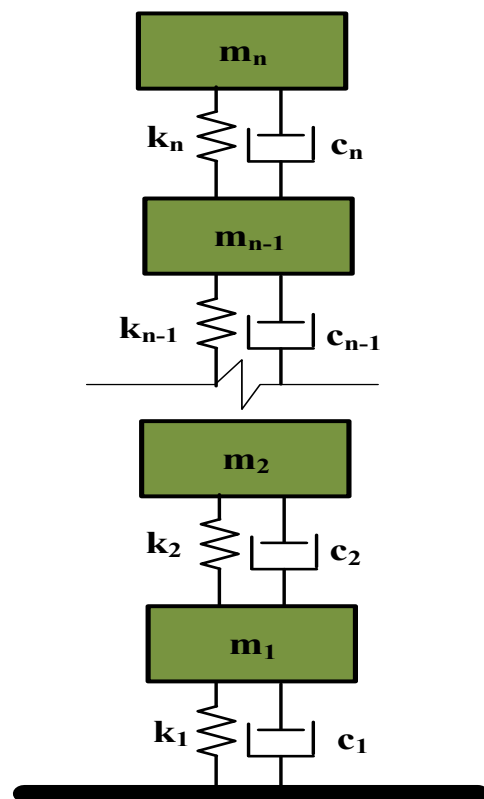


Fig. 2. The mass-spring-damper model of the 15-DOF system

Over the last few decades, due to the economic growth and the scarcity of the land has encouraged to build tall structures and it is taking serious attention all over in Bangladesh. However, the use of vibration mitigation technology is very limited in Bangladesh. Even, it is rarely that the designers are taking proper design measures for extreme dynamic loads due to several reasons; (i) project cost, (ii) lack of expertise especially in the area of vibration mitigation and control, (iii) lack of knowledge regarding nonlinear dynamic analysis and so on. Typically, the equivalent static analysis (ESA) or response spectrum analyses (RSA) are done for seismic/lateral loads analyses. The main focuses herein are to reduce the vibration of structures under seismic/dynamic loads. To do this end, the state space modelling (SSM) technique is used and linear-quadratic regulator (LQR) is employed as control law. A 15 storied reinforced concrete (RC) building frame is considered for the investigations and the response of the system is evaluated under dynamic loads.

## METHODOLOGY

### Problem Statement

It is mentioned in the previous section that, in this work, a sample 15 storied RC building is considered for the numerical implementations and the mass-spring-damper model is depicted in [Fig. 2]. The foregoing structure is simplified by 15 degree of freedoms (DOF) to avoid modeling complexity. Additionally, the system is presumed to be linear time-invariant (LTI) system. In order to avoid the modelling complicity, the SSM formulation is adopted presented by Eq. (1-2). And the numerical simulations are performed via the use of MATLAB/SUMILINK®. The control loop is presented by block diagram in [Fig. 1]. The structure is subjected to dynamic loads (harmonic type



excitation) as shown in [Fig. 1] by Xg. The structure is then coupled with the LQR control law where active control mechanism is employed. The aim of the control is to impose more supplementary damping to the system. The structure is assumed to be underdamped for all of the modes. There are two major equations for the SSM, the first equation is known as the system or process equation given by

$$\dot{x}(t) = Ax(t) + Bu(t) \quad (1)$$

$$A = \begin{bmatrix} 0_{n \times n} & I_{n \times n} \\ -(M^{-1}K)_{n \times n} & -(M^{-1}C)_{n \times n} \end{bmatrix}; M = \begin{bmatrix} m_1 & \dots & 0 \\ \vdots & \ddots & \vdots \\ 0 & \dots & m_n \end{bmatrix} \quad (1a)$$

where  $A$  represents the system matrix which contains mass, stiffness and damping information of the structure,  $B$  is the input matrix that contains both exogenous excitation and control force,  $\dot{x}$  is the time derivate of the state vector  $x$ , state vector  $x$  contains displacement and velocity vector of the system,  $u$  is the input vector,  $t$  is the time vector and  $n$  represents the number of floors. The process equation Eq.(1) requires an accompanied equation known as the measurement equation

$$y(t) = Cx(t) + Du(t) \quad (2)$$

where  $C$  indicates the output matrix, herein all of the displacement, velocity and accelerations are observed and  $D$  represents the feed-forward matrix. The structure is assumed to have each floor weight of 50000 Kg and the stiffness of  $70 \times 10^6$  N/m. The simulations are performed for 100 seconds with a sampling frequency of 500 Hz. The excitation force is applied at the first resonant frequency of the structure for the evaluation of the extreme loading case. In order to see the after load effect, the excitation was turned off after 66.67sec. And the simulations are performed for the following cases; (i) only one damper is placed at 1<sup>st</sup> floor level, (ii) two dampers are placed at 1<sup>st</sup> and 15<sup>th</sup> floor level, (iii) three dampers are placed at 1<sup>st</sup>, 5<sup>th</sup> and 15<sup>th</sup> floor level of the structure. In a nutshell, the system matrices are assumed to be in a simplified form e.g. diagonal matrix.

### **The Linear-Quadratic Regulator (LQR)**

The linear-quadratic regulator is considered to be one of the most widely accepted full-state feedback optimal control algorithm. The simplicity and robust performance of the LQR attracts researchers and control engineers to use it for vibration mitigation and control applications. However, a serious drawback of this scheme is that all of the floors displacement and velocity information are needed which is quite difficult to get. Hence in order to maximize the performance by minimizing the cost a limited sensor information is commonly used which is known as the linear-quadratic Gaussian (LQG). The LQG is a combination of the LQR and linear Kalman filter. Herein, it is assumed that the sensors are available in all of the floors and the following cost function  $J$  is minimized reclusively for every time-step

$$J = \sum_{n=0}^N (x_n^T Q x_n + u_n^T R u_n) \quad (3)$$

The first part of the above equation ( $x_n^T Q x_n$ ) represents the contribution of the system response (e.g. displacement and velocity) and the second part ( $u_n^T R u_n$ ) means the controller contribution. Typically, it is always expected that in order to get the most out of the controller more weight needs to be placed on the first part of the equation in comparison to the second part. The weighting factors are controlled by the parameters  $Q$  and  $R$ . Interested reader may obtain more detail about the LQR algorithm and its applications via the following articles (Anderson and Moore, 1989; Mobaieen, et al. 2012; Miah et al., 2015; Weber and Mašlanka, 2012).

### **RESULTS AND DISCUSSIONS**

The simulations are performed in a nearly real-time platform so-called SIMULINK<sup>®</sup>. In order to perform analyses, the 15-DOF system has bring into a formulation known as the SSM. Additionally, the weighting parameters  $Q$  and  $R$  of the LQR control algorithm is adjusted for the vibration

mitigation of the structure. It is mentioned earlier that the simulation of the 15 storied RC building is connected with dampers at different floor levels of the structure. In Addition to the SIMULINK<sup>®</sup>, MATLAB<sup>®</sup> 2012a package is also used for numerical implementations. The results of different floors level are compared. Firstly, the displacement and velocity response of 1<sup>st</sup> floor in [Fig.3-4]. And the response of the 15<sup>th</sup> floor level is compared for different damper combinations in [Fig.5-6]. For the visualization purpose there is a full-time history 0-100 sec and a zoomed view of 50-60 sec. In the above mentioned figures, the blue line indicates the uncontrolled case (what would happen without any damper), the black line represents the controlled case for the case damper is placed at the first floor level, the green line shows the what would happen when two dampers are used, one at first floor level and the second one is at fifteenth floor level. And the red line represents the three dampers case here three dampers are placed at 1<sup>st</sup>, 5<sup>th</sup> and 15<sup>th</sup> floor levels of the structure. It can be summarized from all of figures that two and three dampers cases are capable of mitigating the response significantly. Even, only one damper may also assist to reduce the vibration quite efficiently. Along with the aforementioned figures the 10<sup>th</sup> floor's responses e.g. displacement and velocity are compared in [Fig.7-8]. And finally, the controller's hysteretic loops for full-time history are evaluated and stable closed-loop response are observed in [Fig.9-10].

The studied approach is a compact mathematical formulation that makes the whole process faster. Even though, very good results are observed but further investigations are essential for practical implementations. Hence, further study will investigate the performances under different alternatives for the real-time implementations.

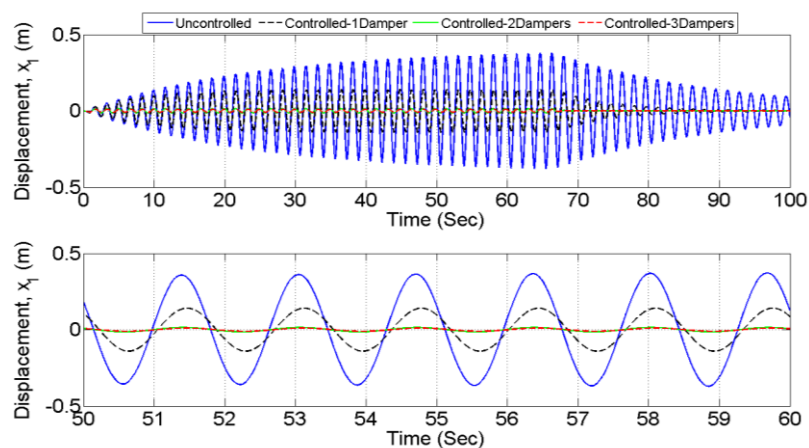


Fig. 3. The comparison of 1<sup>st</sup> floor displacement uncontrolled versus controlled cases; (a) full time history 0-100sec, (b) zoomed 50-60sec

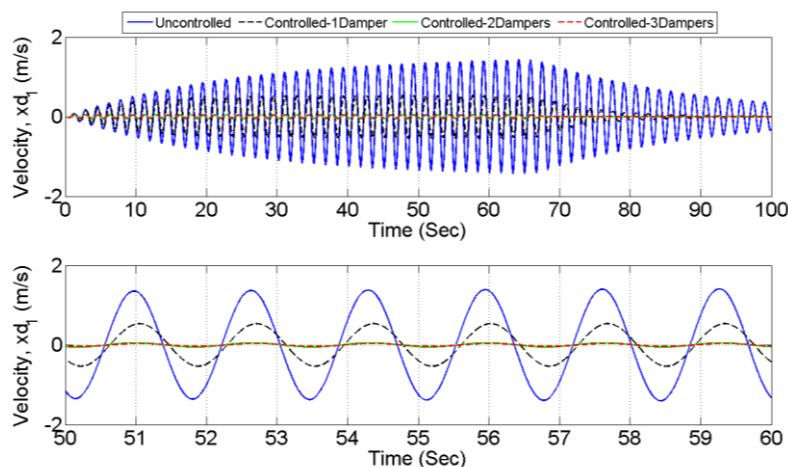


Fig. 4. The comparison of 1st floor velocity uncontrolled versus controlled cases; (a) full time history 0-100sec, (b) zoomed 50-60sec

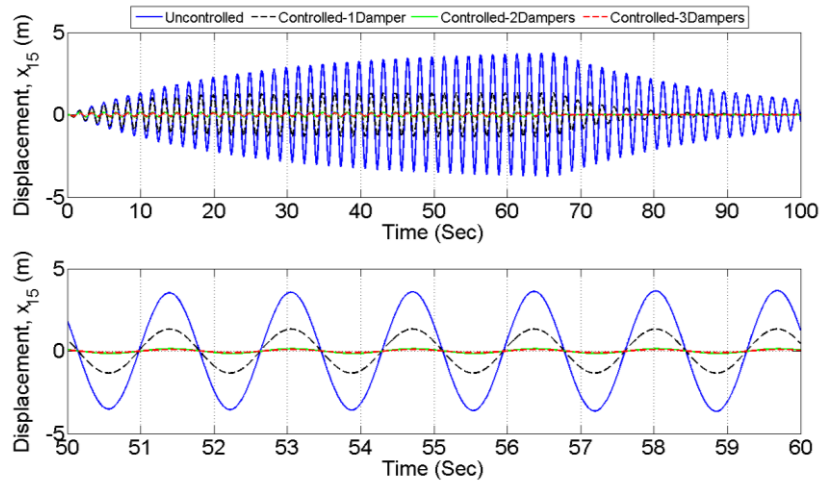


Fig. 5. The comparison of 15<sup>th</sup> floor displacement uncontrolled versus controlled cases; (a) full time history 0-100sec, (b) zoomed 50-60sec

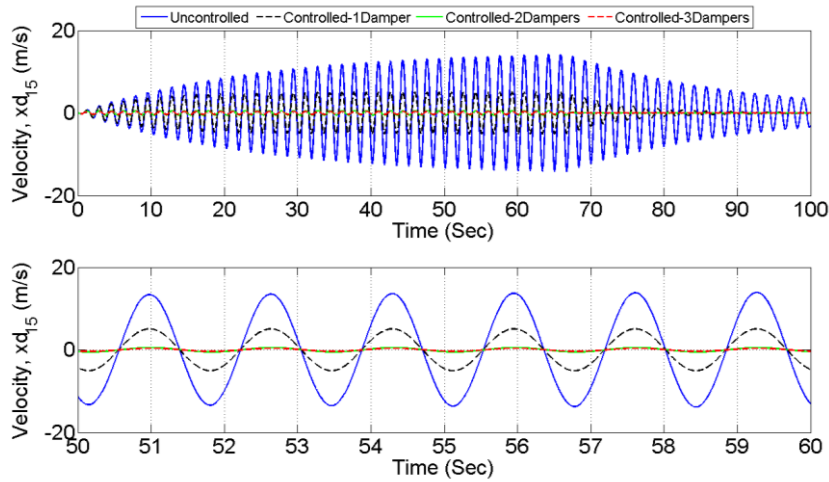


Fig. 6. The comparison of 15<sup>th</sup> floor velocity uncontrolled versus controlled cases; (a) full time history 0-100sec, (b) zoomed 50-60sec

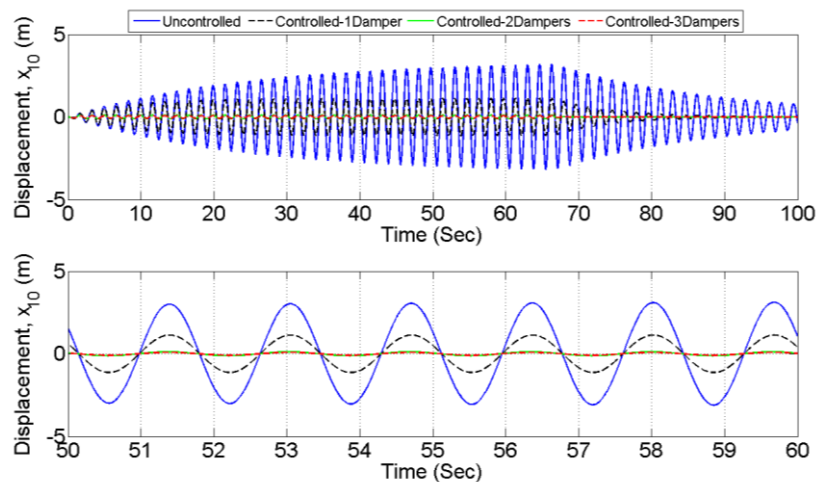


Fig. 7. The comparison of 10<sup>th</sup> floor displacement uncontrolled versus controlled cases; (a) full time history 0-100sec, (b) zoomed 50-60sec

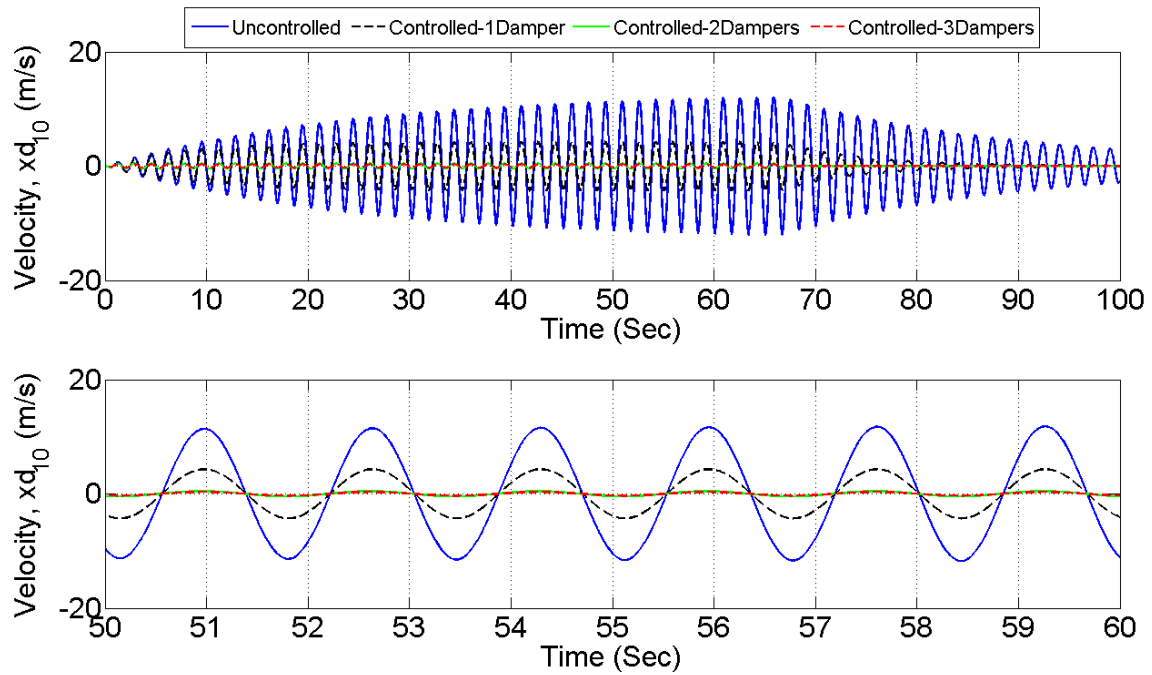


Fig. 8. The comparison of 10<sup>th</sup> floor velocity uncontrolled versus controlled cases; (a) full time history 0-100sec, (b) zoomed 50-60sec

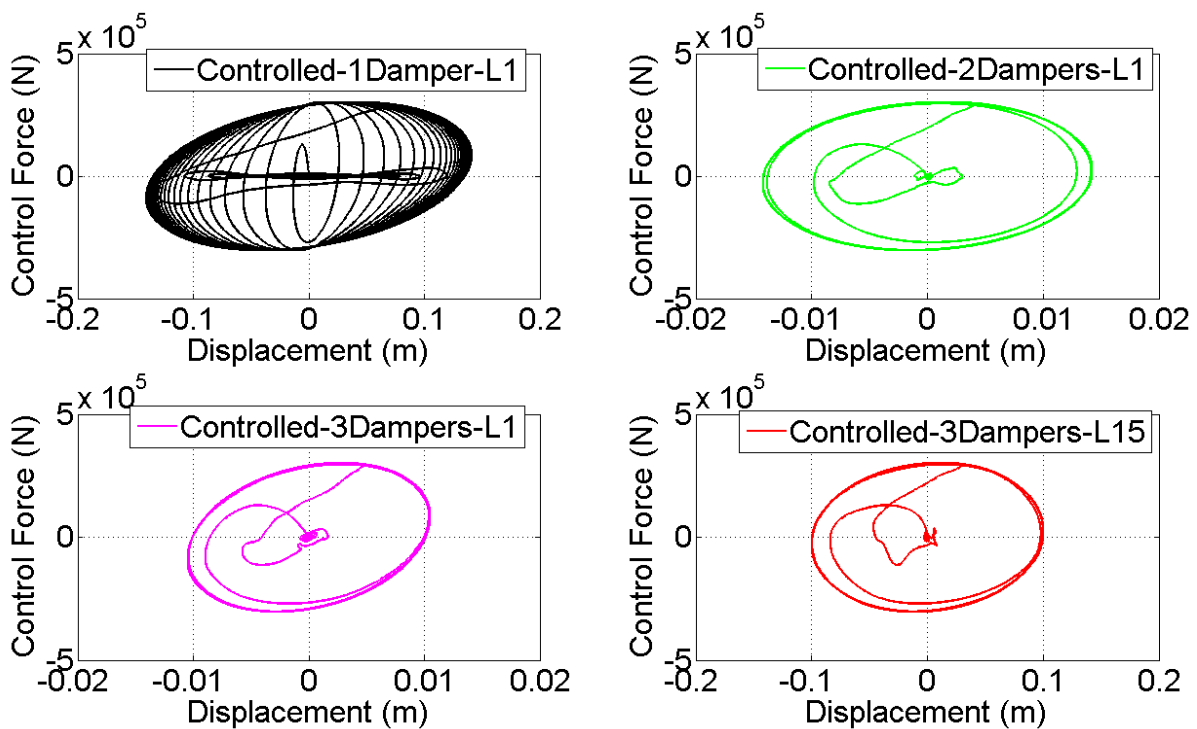


Fig. 9. The control force versus collocated displacement trajectory

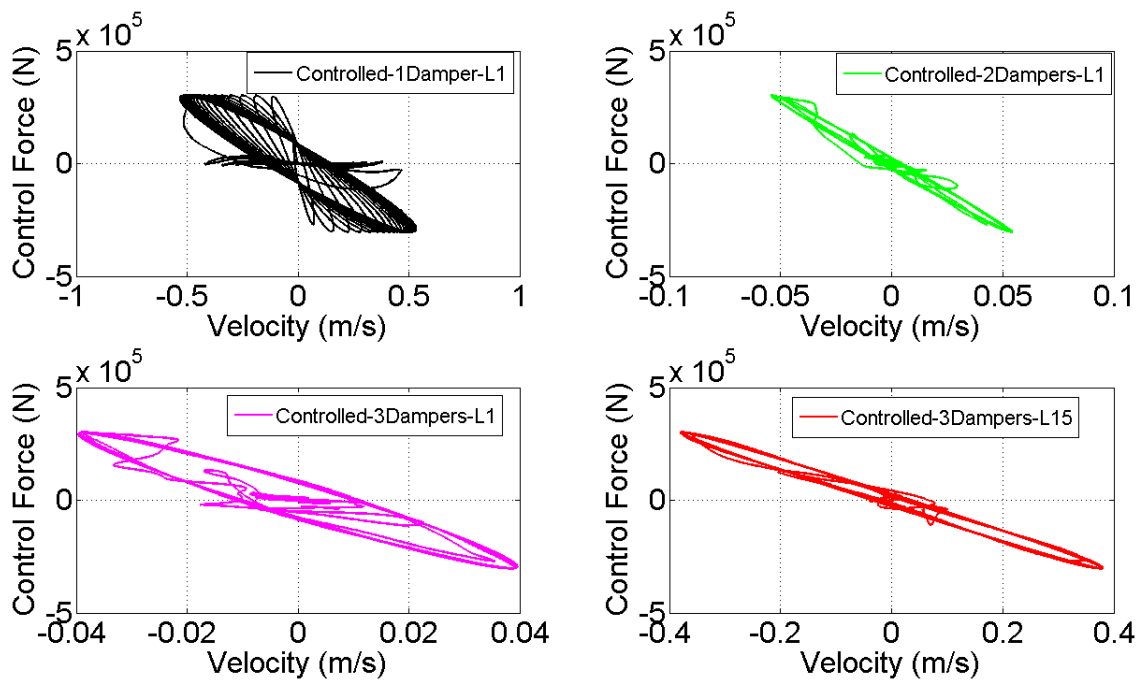


Fig. 10. The control force versus collocated velocity hysteresis

## CONCLUSIONS

This paper addresses the vibration mitigation and control problem which is quite crucial in the area of structural engineering in general. The aforementioned problem even more serious issue in Bangladesh due to the lack of proper analysis and design for dynamic loads as well as vibration mitigation and control. Hence keeping the above mentioned issues in mind herein a 15 storied RC building is studied and active control is employed for vibration mitigation. The goal is achieved by combining the system with the LQR scheme. And all of the floors information are assumed to be measured and feed into the controller in order to produce the active control force. The overall outcome of the work shows that a significant reduction of structural vibration is possible. The choice of the number of dampers and their locations may have a significant impact on overall performance of the structure in terms of vibration mitigation. Designer may choose the option according to his/her project needs. Herein a full-state feedback type control scheme has been deployed, however, in future a more realistic scenario i.e., limited sensors scenario will be investigated.

## ACKNOWLEDGEMENTS

The author appreciates the support of the department of Civil Engineering at University of Asia Pacific (UAP), Dhaka, Bangladesh.

## REFERENCES

- Anderson, B.D.O. and Moore, J. B. 1989. *Optimal Control Linear Quadratic Methods*, Englewood Cliffs, Prentice-Hall, NJ: USA.
- Bhowmik, S. 2011. *Modelling and Control of Magnetorheological Damper: Real-time implementation and experimental verification*, Technical University of Denmark, DCAMM Special Report No. S139, Lyngby, Denmark.
- Dyke, S. 1996. *Acceleration feedback control strategies for active and semi-active control systems: modeling, algorithm development, and experimental verification*. University of Notre Dame, Notre Dame, Indiana, USA.
- Miah, M. S., Chatzi, E. N. and Weber, F. 2015. Semi-active control for vibration mitigation of structural systems incorporating uncertainties, *Smart Materials and Structures*, 24(5):055016, doi: 10.1088/0964-1726/24/5/055016.
- Miah, M. S., Chatzi, E. N. and Weber, F. 2013. Semi-active control of structural systems with

uncertainties using an unscented Kalman filter, *Research and Applications in Structural Engineering, Mechanics and Computation*, Edited by Alphonse Zingoni, CRC Press, 61-66, doi:10.1201/b15963-13.

Mobaieen, S., Mohamady, B., Ghorbani, H., and Rabii, A. 2012. Optimal Control Design Using Evolutionary Algorithms with Application to an Aircraft Landing System, *Journal of Basic and Applied Scientific Research*, 2(2), 1876–1882.

Miah, M. S., Chatzi, E. N., Dertimanis, V. K., and Weber, F. 2016. Real-time experimental validation of a novel semi-active control scheme for vibration mitigation, *Structural Control and Health Monitoring*, (First published: 15 May 2016), <http://doi.org/10.1002/stc>.

Preumont, A. 2004. *Vibration control of active structures: an introduction (2nd ed.)*, Kluwer Academic Publishers, Dordrecht: Kluwer, The Netherlands.

Weber, F. and Maślanka, M. 2012. Frequency and damping adaptation of a TMD with controlled MR damper, *Smart Materials and Structures*, 21(5), 055011. <http://doi.org/10.1088/0964-1726/21/5/055011>.

## **ELECTROCHEMICAL CORROSION BEHAVIOR OF AL-SI HYPOEUTECTIC ALLOY IN SIMULATED SEAWATER ENVIRONMENT**

A. Hossain<sup>1\*</sup>, F. Gulshan<sup>2</sup> & A.S.W. Kurny<sup>2</sup>

<sup>1</sup>*Kailashtilla MSTE Plant, Sylhet Gas Fields Limited (A company Petrobangla, Energy and Mineral Resources Division), Sylhet, Bangladesh*

<sup>2</sup>*Department of Materials and Metallurgical Engineering, Bangladesh University of Engineering and Technology, Dhaka, Bangladesh*

\*Corresponding Author: [ah\\_buetmmesgfl@live.com](mailto:ah_buetmmesgfl@live.com)

### **ABSTRACT**

The aim of this study is to investigate the corrosion behavior of artificially peakaged Al-Si hypoeutectic alloy in simulated seawater environment. The electrochemical corrosion behavior of the thermal treated Al-Si alloy in simulated seawater was investigated using potentiodynamic polarization and electrochemical impedance spectroscopy (EIS) techniques. A representative set of samples was recovered and laboratory tests performed to evaluate the type and degree of corrosion attack. In potentiodynamic polarization test corrosion rate, current, potential and morphology were revealed. Corrosion resistance or charge transfer resistance ( $R_{ct}$ ) and simulated seawater resistance assessed by electrochemical impedance spectroscopy (EIS) test. Optical Light Microscopy (OLM) and Scanning Electron Microscopy (SEM) were employed to characterize the corroded surface and to observe the extent of pitting. Pronounced effect of pitting was observed in presence of Cl<sup>-</sup> for Al-Si alloy.

Keywords: Al-6Si alloy; electrochemical corrosion; scanning electron microscopy (SEM)

### **INTRODUCTION**

Al-Si alloys with silicon as a major alloying element constitute a class of material, which provides the most significant part of all shaped castings manufactured, especially in the aerospace and automotive industries. Al-Si Alloy make composite have become a substitute material in automobile industries especially in making of piston, cylinder blocks and other engineering components. They are also being considered as a potential in making of impellers, agitators etc. in marine structural applications because of their enhanced physical, mechanical and tribological properties (Singh et al., 2010; Shabestari and Moemeni, 2004). Al-Si alloys with silicon as a major alloying element constitute a class of material, which provides the most significant part of all shaped castings manufactured, especially in the aerospace and automotive industries. This is mainly due to the outstanding effect of silicon in the improvement of casting characteristics, combined with other physical properties such as mechanical properties and corrosion resistance. In general, an optimum range of silicon content can be assigned to casting processes (Rooy, 1988; Shabestari and Moemeni, 2004). Owing to their light weight, suitable strength and strong resistance to corrosion, aluminum alloys are used in a broad spectrum of engineering applications. The corrosion resistance of aluminum is attributed to an exceptionally stable oxide film that forms on its surface. This film is resistant to attack from water and oxygen in a wide range of temperatures and pH levels, making aluminum alloys useful in a variety of environments (Claycomb and Sherwood, 2004).

However, service life of any material mainly depends on its corrosion resistance in the surrounding environment. For example, if Al-Si alloy make AMC are used in marine environment, their susceptibility to pitting corrosion is likely to be increased in the presence of chlorides ions. The presence of aggressive ions like chloride creates extensive localized attack Chloride ions adsorb on the metal surface and destroy the existing passive oxide film that leads to a localized attack in the form of pitting corrosion. Since pitting corrosion is a main problem of AMC, different approaches have been made to control pitting corrosion by halide ions (Garrigues et al., 1995; Singh et al., 2010). In addition, it is well known that the corrosion behavior of aluminum alloys is significantly affected

by the presence of particles in the matrix. Particles that contain Al, Cu and Mg tend to be anodic relative to the alloy matrix, while those that contain Al, Cu, Fe and Mn tend to be cathodic relative to the matrix (Wei et al., 1998). Although the metallurgical and micromechanical aspects of the factors controlling microstructure, unsoundness, strength and ductility, and corrosion resistance of alloys are complex, it is well known that solidification processing variables are of high order of importance. The cooling rate during solidification defines the fineness of the dendritic network. The solute redistribution, the anodic or cathodic electrochemical behaviour of each component of the alloy and the scale of dendrite spacings and thermal treatment are the main microstructural characteristics affecting the corrosion resistance of the alloy (Osório et al., 2011).

The increasing demand from many industries for improved properties in materials has stimulated the development of new materials. In this context, various new materials such as the Al-Si alloys have been considered. Despite the excellent mechanical and physical properties of the Al-Si-Mg alloys, their corrosion resistance in aggressive environments is not yet well known. In recent years some work has been carried out to evaluate the corrosion resistance of these alloys in different media (Staley and Lege, 1993; Anand et al., 1997; Traldi et al., 2001; Traldi et al.2003).

The aim of this research paper is to evaluate the electrochemical corrosion properties Al-6Si heat treated alloy in simulated seawater environment.

## EXPERIMENTAL PROCEDURE

### *Materials preparation*

The Al-6Si alloy was utilized by melting Al-7Si-0.3Mg (A356) alloy and adding Al into the melt. After casting and solidification into a permanent steel mould of the alloy, suitable specimens were cut and used for the experiments. The samples were homogenised (500°C for 24hr) and solutionized (540°C for 2hr) and finally artificially aged (225°C for 1hr). After heat treatment the rectangular samples (30mm x 10mm x 5mm) were prepared for metallographical observation and finally subjected to electrochemical test. Deionized water and analytical reagent grade sodium chloride (NaCl) were used for preparation of 0.1M simulated seawater. All measurements were carried out at room temperature.

### *Electrochemical Measurements*

Potentiodynamic Polarization Measurements-A computer-controlled Gamry Framework TM Series G 300™ and Series G 750™ Potentiostat/ Galvanostat/ZRA were used for the electrochemical measurements. The Potentiodynamic polarization studies were configured in cells [Fig. 1], using three-electrode assembly with a saturated calomel reference electrode, a platinum counter electrode and the sample as working electrode in the form of coupons of exposed area of 0.50 cm<sup>2</sup> or 10mm x 5mm. Only one 10mm x 5mm surface area was exposed to the test solution and the other surfaces were covered with Teflon tape and allowed to establish a steady-state open circuit potential (OCP). The potential range selected was -1 to +1V and measurements were made at a scan rate of 0.50 mV/s. First 100s applied for achieving steady state OCP and for potential -1V to +1V immersion time was about 67 minutes. The corrosion current ( $I_{corr}$ , measured by Butler-Volmer equation), corrosion potential ( $E_{corr}$ ), pitting corrosion potential ( $E_{pit}$ ) and corrosion rate (mpy) were calculated from Tafel curve. The tests were carried out at room temperature in solutions containing 0.1M of NaCl at a fixed and neutral pH value. No stirring applied and the experiments carried out in a closed cell. The corroded samples were cleaned in distilled water and examined by optical light and scanning electron microscope.

Electrochemical Impedance Measurements-As in potentiodynamic polarization test, three electrode cell arrangements were also used in electrochemical impedance measurements. Rectangular samples (10mm x 5mm) were connected with copper wire and adopted as working electrodes for impedance measurements. EIS tests were performed in 0.1M NaCl solution at room temperature over a frequency range of 100 kHz to 0.2 Hz using a 5mV amplitude sinusoidal voltage. The 10mm x 5mm sample surface was immersed in 0.1M NaCl solution (corrosion medium). All the measurements were performed at the open circuit potential (OCP). The test cells were maintained at room temperature and the NaCl solution was refreshed regularly during the whole test period. The impedance spectra were



collected, fitting the experimental results to an equivalent circuit (EC) using the Echem Analyst TM data analysis software and evaluating the solution resistance ( $R_s$ ), polarization resistance or charge transfer resistance ( $R_{ct}$ ) and double layer capacitance ( $C_p$ ) of the thermal treated alloy.

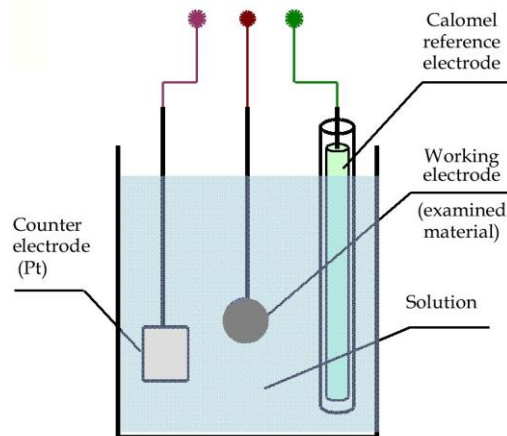


Fig. 1: Schematic representation of the three-electrode system cell

## RESULTS AND DISCUSSION

### Impedance Measurements

Table 1. shows the Electrochemical Impedance Spectroscopy (EIS) test results.

Table 1: Impedance test results

Alloy Code	$R_s(\Omega)$	$R_{ct}(k\Omega)$	$C_p(\mu F)$	OCP(V/SCE)
Al-6Si alloy	40.37	15.57	1.259	-0.8454

A large fluctuation in open circuit potential for the alloy was seen during the time of 100s exposure (Table1). After a period of exposure the OCP fluctuation decreased and reached steady state. The steady state OCP of the alloy is -0.8454V. The OCP values mainly depend on the chemical compositions and thermal history of the alloy.

Impedance measurements-The data obtained were modeled and the equivalent circuit that best fitted to the experimental data is shown in Fig.2.  $R_s$  represent the ohmic solution resistance of the electrolyte.  $R_{ct}$  and  $C_p$  are the charge transfer resistance and electrical double layer capacitance respectively, which correspond to the Faradaic process at the alloy/media interface. Fig. 3. a shows the Nyquist diagrams (suggested equivalent circuit model shown in Fig. 2) of the Al-6Si alloy in simulated seawater. In Nyquist diagrams, the imaginary component of the impedance ( $Z''$ ) against real part ( $Z'$ ) is obtained in the form of capacitive-resistive semicircle for each sample.

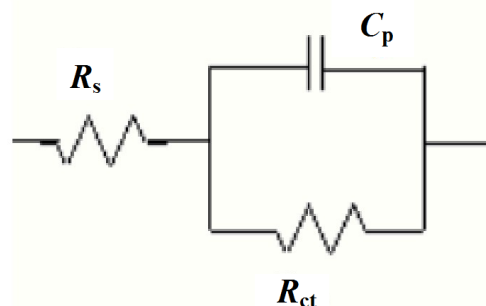


Fig. 2: Electrical equivalent circuit used for fitting of the impedance data of Al-6Si alloy in seawater

Fig.3.a shows the Nyquist diagrams (suggested equivalent circuit model shown in Fig.2) of the Al-6Si alloy in 0.1M NaCl in de-mineralized (DM) water. In Nyquist diagram, the imaginary component of the impedance ( $Z''$ ) against real part ( $Z'$ ) is obtained in the form of capacitive-resistive semicircle for the sample.

Fig.3.b shows the experimental EIS results in Bode magnitude diagram for Al-6Si alloy. Bode plot show the total impedance behavior against applied frequency. At high frequencies, only the very

mobile ions in solution are excited so that the solution resistance ( $R_s$ ) can be assessed. The solution resistance ( $R_s$ ) of the alloy is  $40.37\Omega$ , which is very negligible with respect to  $R_{ct}$  and the electrolyte behaves as a good ionic conductor. For the Al-6Si alloy, the charge transfer resistance ( $R_{ct}$ ) value in simulated seawater is  $15.57k\Omega$ , and this indicates the corrosion resistance of the alloy.

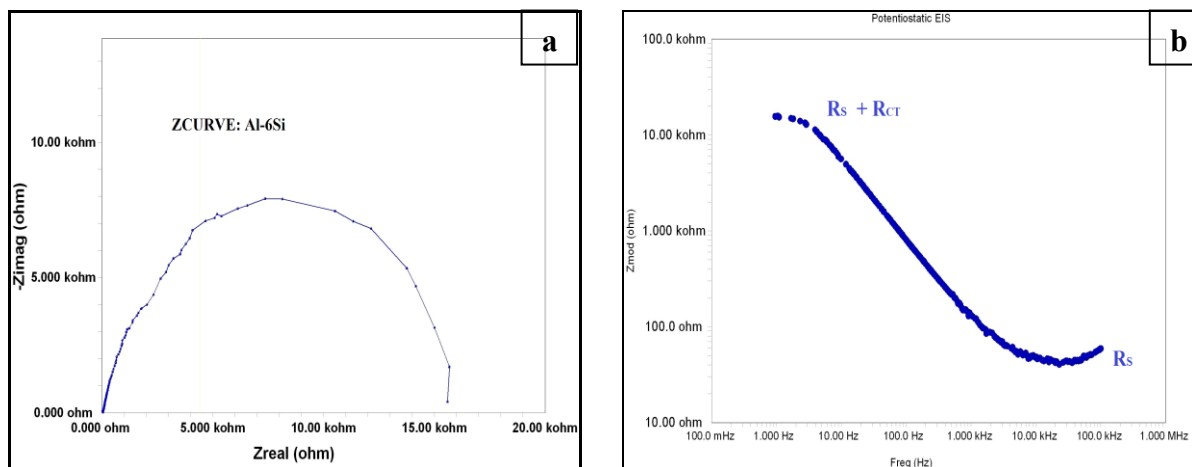


Fig. 3: (a) Nyquist plot and (b) Bode plot for Al-6S alloy in simulated seawater

### Potentiodynamic Polarization Measurements

Table 2 shows the potentiodynamic polarization test results obtained from the electrochemical tests.

Table 2: Potentiodynamic polarization test results

Alloy code	$I_{corr}(\mu A)$	$E_{corr}(mV)$	$E_{pit}(mV)$	Corrosion rate(mpy)
Al-6Si alloy	6.300	-764	-480	5.287

A Potentiodynamic polarization curve of Al-6Si alloy in simulated seawater is shown in Fig. 4. The different intermetallic compounds can lead to the formation of micro-galvanic cells because of the difference of corrosion potential between intermetallics and  $\alpha$ -aluminum matrix. The corrosion potential of Al-6Si alloy is  $-764mV$  and Pitting potential ( $E_{pit}$ ) is  $-480mV$ . The  $I_{corr}$  value, in simulated seawater is  $6.3\mu A$ , and the corresponding corrosion rate is  $5.287mpy$ .

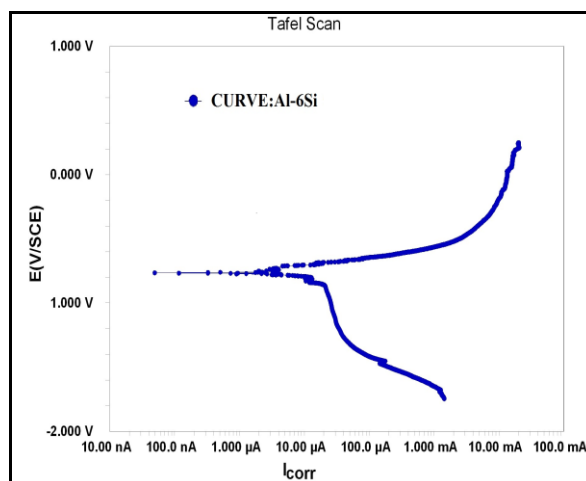


Fig. 4: Potentiodynamic polarization curves of peakaged Al-6Si alloy in simulated seawater

### Microstructural Investigation

The microstructure of the selected as-corroded samples was observed under OLM and SEM. There was evidence of corrosion products of intermetallic compounds in all the samples examined. Besides, several pits were visible in all the samples examined. It is probable that the pits are formed by the intermetallics dropping out from the surface due to the dissolution of the surrounding matrix. However, it is also possible that the pits are caused by selective dissolution of the intermetallic/or

particles of the second phase precipitates. The forms of corrosion in the studied Al-6Si alloy are not completely uniform and predominantly pitting corrosion as obtained by the OLM and SEM. Samples were characterized by OLM and SEM following potentiodynamic polarization tests. The peakaged Al-6Si alloy exhibited pits on their surface (Fig.5.a & Fig.5.b), which apparently had nucleated randomly. Conversely, the exposed surface of the alloy exhibited a corrosion product covering the surface after polarization. The optical micrographs (Fig 5.a) also showed that there was no corrosion in the fragmented and modified Al-Si eutectics.

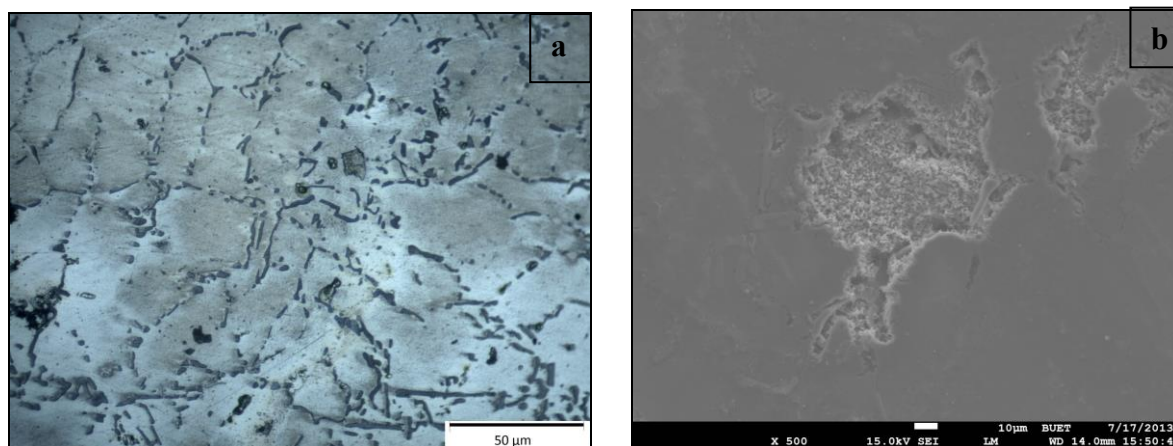


Fig. 5: (a) OLM and (b) SEM images show the damage surface morphology of as-corroded Al-6Si alloy in simulated seawater

## CONCLUSION

The electrochemical impedance technique has been found to be appropriate to investigate the corrosion behavior of Al-Si hypoeutectic alloy in simulated seawater environment. The impedance results indicate the presence of a surface oxide and the polarisation results indicate this oxide to be at least partially permeable.

- ❖ From the EIS test, the solution resistance ( $R_s$ ) of the alloy is  $40.37\Omega$  and this environment is a good ionic conductor. The  $R_{ct}$  value in simulated seawater is  $15.57k\Omega$ , corrosion resistance of the alloy.
- ❖ From the linear polarization and Tafel extrapolation plot, the  $I_{corr}$  value, in simulated seawater is  $6.3\mu A$ , and the corresponding corrosion rate is  $5.287mpy$ . In the anodic region, the Al-Si hypoeutectic alloy shows the lower corrosion resistant.
- ❖ Electrochemical results showed that simulated sea water is more accelerated the pitting corrosion. The forms of corrosion in the studied alloy are pitting corrosion as obtained from the OLM and SEM microstructures study with pits observations.

## ACKNOWLEDGEMENTS

The authors are thankful to the Pilot Plant and Process Development Centre (PP & PDC) at BCSIR laboratories, Dhaka for carried out the electrochemical corrosion tests.

## REFERENCES

- Anand, S; Srivatsan, TS; Wu, Y and Lavernia, EJ. 1997. Processing, microstructure and fracture behavior of a spray atomized and deposited aluminium-silicon alloy. *Journal of Materials Science*, 32: 2835-2848.
- Claycomb, GD; Sherwood, PMA. 2002. Investigation of surface oxides on aluminum alloys by valence band photoemission. *J Vac Sci Technol A*, 20(4): 1230-1236.
- Fontana, MG and Greene, ND. 1987. Corrosion Engineering. *McGraw-Hill book Company*, New York.
- Garrigues, L; Pebere, N and Dabosi, F. 1995. An investigation of the corrosion inhibition of pure aluminum in neutral and acidic chloride solutions. *Electrochim Acta*, 41(7): 1209-1215.

- Osório, WR; Siqueira, CA; Santos, CA and Garcia, A. 2011. The Correlation between Electrochemical Corrosion Resistance and Mechanical Strength of As-Cast Al-Cu and Al-Si Alloys. *Int. J. Electrochem. Sci.*, 6: 6275 – 6289.
- Rooy, EL. 1988. Aluminum and Aluminum Alloys in Castings: Metals Handbook. *ASM International*, Metals Park, Ohio, USA, 15: 743-770.
- Scamans, GM; Hunter, JA and Holroyd, JHN. 1989. Corrosion of aluminium-a new approach. *Proc. of 8th Inter. Light metals Congress*, Leoban Wien, 699-705.
- Shabestari, SG and Moemeni, H. 2004. Effect of copper and solidification conditions on the microstructure and mechanical properties of Al-Si-Mg alloys. *J. Mater. Proc. Technol.* 153/4: 193-198.
- Singh, IB; Singh, M; Das, S and Yengeswaran, AH. 2010. Corrosion behaviour of sol-gel Al<sub>2</sub>O<sub>3</sub> coated Al-Si alloy in 3.5% NaCl solution. *Indian Journal of Chemical technology*, 17: 419-424.
- Staley, JT; Lege, DJ. 1993. Advances in aluminium alloy products for structural applications in transportation. *J Physique IV, Colloque C7, supplément au Journal de Physique III*, 3: 179-190.
- Traldi, SM; Rossi, JL and Costa, I. 2001. Corrosion of spray formed Al-Si-Cu alloys in ethanol automobile fuel. *Key Engineering Materials*, 189-191: 352-357.
- Traldi, SM; Rossi, JL and Costa, I. 2003. An electrochemical investigation of the corrosion behavior of Al-Si-Cu hypereutectic alloys in alcoholic environments. *Revista de Metalurgia Suplemento S*, 81(34):86-90.
- Wei, RP; Chin-Min, L and Gao, M. 1998. A Transmission electron microscopy study of constituent-particle-induced corrosion in 7075-T6 and 2024-T3 aluminum alloys. *Metallurgical Mater Trans A*, 29A:1153-1160

## **NON-METALLIC INCLUSIONS CONTENT IN MEDIUM CARBON STRUCTURAL STEELS AND DEFORMATION BEHAVIOR DURING HOT ROLLING**

A. Hossain<sup>1\*</sup>, F. Gulshan<sup>2</sup> & A. S. W. Kurny<sup>2</sup>

<sup>1</sup>*Kailashtilla MSTE Plant, Sylhet Gas Fields Limited (A company Petrobangla, Energy and Mineral Resources Division), Sylhet, Bangladesh*

<sup>2</sup>*Department of Materials and Metallurgical Engineering, Bangladesh University of Engineering and Technology, Dhaka, Bangladesh*

*\*Corresponding Author: ah\_buetmmesgfl@live.com*

### **ABSTRACT**

Non-metallic inclusions found in steel can affect its performance characteristics. Their impact depends not only on their quality, but also, among others, on their size and distribution in the steel volume. The amount of non-metallic inclusions found in medium carbon steel under industrial conditions. Molten steels are cast into what are usually known as pencil ingots/billets and do not have any refining facilities. In absence of proper refining and quality control, these ingots/billets usually contain slags, non-metallic inclusions, inhomogeneities and deformed bars produced from these pencil ingots/billets contain significant amount of slags and inclusions. Finished products of these pencil ingots are in general of inferior quality and give substandard reinforcing bars. Proper refining (ladle refining) of induction melted assorted scrap can give fairly clean and refined liquid steels. Reinforcing bars produced from such refined melts are generally free from inclusions and slags. The amount of non-metallic inclusions was determined by optical and extraction methods. Inclusions are characterized by measuring ranges. Metallographic studies of the deformed bars show the deformation behavior of the inclusions.

Keywords: Non-metallic inclusions; structural steel; deformation behavior

### **INTRODUCTION**

Advances in steelmaking during the last six decades have resulted in steel grades with very low level of impurities. In recent years, new “clean and ultra-clean” steels have been developed and commercialized by steel producers around the world, thereby responding to the current and future market demands of steel having significantly improved mechanical properties (Niclas et al., 2015). In Bangladesh most of the steel bars used for reinforcement of concrete are produced by melting iron and steel scrap in induction furnaces. Because of the nature of induction heating, the melt in the furnace is continuously stirred and complete separation of inclusions cannot take place (Millman, 1999). An induction furnace is a melting unit. Very little, if any, refining takes place in an induction furnace. Thus the quality of steel produced in an induction furnace is directly related to the quality of scrap and other raw material. In Bangladesh only limited number of steelmaking units use ladle refining furnaces for enhancing the quality of steel produced (Millman, 1999; Amit and Ojha, 1997). In many instances molten steel is poured into moulds to produce pencil ingots. The moulds are themselves massive castings with a square, rectangular, round or polygonal cross-section. The growth and development of steel plants has coincided with the introduction and acceptance of continuous casting. In some plants ladle metallurgy has also been introduced. Few of them have gone for inert (argon or nitrogen) gas purging in order to reduce inclusion content, gas content and make composition and temperature in the ladle homogeneous. Ladle metallurgy incorporates inert gas stirring for homogenization of temperature and composition of the steel in the ladle as well as for floatation of inclusions. For continuous casting, inert gas stirring of steel in the ladle has become a standard practice to improve the quality of steel.

The quantity and quality of non-metallic inclusions is determined mostly by the steel melting technology. Out-of furnace treatment regimes are also introduced to minimize the quantity of non-metallic inclusions. The quantity of non-metallic inclusions in steel is relatively low, nevertheless, they have a significant impact on the structure, technological and strength parameters of the resulting alloy (Lis, 1999; Wypartowicz and Podorska, 2006; Lis, 2002; Fernandes et al., 2003). The distribution of inclusions is an equally important factor. Single inclusions and clusters of inclusions exert different effects. Large, individual inclusions can produce discontinuities that grow rapidly under variable load. During processing, the shape and distribution of micro particles change, and impurities undergo anisotropic deformation. Non-metallic inclusions play a special role in the process of steel hardening. Due to differences in the physical properties of steel and inclusion-forming phases, structural stresses are formed along inclusion boundaries (Kocańda, 1985; Wang et al., 2012; Bao et al., 2012; Yang et al., 2006; Murakami et al., 1989). Most non-metallic inclusions present in steel have detrimental effects on properties, which will lead to poor formability of the product as well as problems associated with fatigue life. In addition to improved formability, cleaner steel also benefits the coating and corrosion resistant properties. Cleanliness requirements for steel products are often measured in total oxygen, and maximum particle size (Zhang and Thomas, 2003).

A literature analysis shows that, for these steels, the phenomena occurring during their use with respect to their microstructure and non-metallic inclusions have been analyzed most deeply. Fatigue tests are a particularly sensitive method for testing a material's durability. A comparison of fatigue properties and the size of impurities suggests that Sub-microscopic inclusions in high-plasticity steel inhibit dislocation motion. Inclusions absorb energy which contributes to the formation of discontinuities and slows down decohesion. Their results set strict criteria as to the allowable steel impurity. In hard steels, reduced mechanical properties at changing loads are unambiguously attributed to non-metallic inclusions (Lipiński and Wach, 2010; Barrie et al., 2008; Park and Park, 2014; Gulyakov et al., 2012; Srivastava et al., 2014; Lipiński and Wach, 2010; Spriestersbach et al., 2014; Evans et al., 2014; Lipinski and Wach, 2009; Roiko et al., 2012; Shih and Araki, 1973; Genel, 2005).

The aim of this study was to determine the extent of variation of inclusion content with the liquid metal processing routes and analyze dimensional structure of non-metallic inclusions in the reinforced bars.

## EXPERIMENTAL PROCEDURE

This study was based on analysis of samples collected from the process stream of a steel plant in Bangladesh (Fig.1). Care was always exercised to collect a representative sample. The plant concerned produces different grades of deformed bars from ingots produced in metal moulds (pencil ingots) and also from billets produced by a continuous casting machine. The plant has a ladle refining furnace and samples of continuously cast billets, both ladles refined and not refined, were collected.

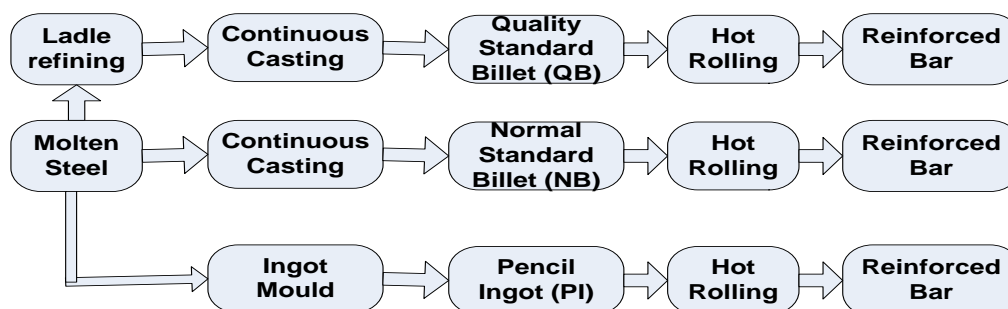


Fig 1: Flow diagram of different route of processing reinforcing bar

A number of pencil ingots of different heats, normal standard billets and quality standard billets were chemically analyzed. The chemical compositions of the samples were examined and the heats chosen for further work was based on carbon equivalent factor. The sampling procedure of any heterogeneous material is of great importance. Two methods of sampling are advocated random

sampling and representative sampling. Representative sampling is best achieved by taking samples equally spaced throughout the bulk. This method of sampling is perfectly satisfactory. Inclusion content may be determined either by a macroscopic or a microscopic method. The advantages of microscopic method are that, the character or type of inclusions may be determined and extremely small inclusions are revealed. Specimens or metallographic assessment of inclusions were prepared by using standard techniques of polishing. Extreme care was used to ensure that the inclusions are retained. It was not always possible to retain all the inclusions. However, this did not affect the result because the cavities in the samples were counted as inclusions. Many investigators have preferred to estimate the inclusion content in steels without recourse to arbitrary standards, primarily because the personal factor in these methods is reduced to as rational a basis as possible. Several methods have been suggested for assessing the inclusion content in steel. Inclusion content was estimated by the method of direct counting and measurement of inclusions on metallographic samples (Kjerrmann and Jernkont, 1929). Both longitudinal and transverse sections were examined. The locations of inclusion analysis were selected randomly. For understanding the deformation behavior, the SEM with EDX analysis was performed on the finished rolled reinforced bars. The chemical compositions (as determined by optical emission spectroscopy) of ingot, normal standard billet and quality standard billet are listed in Table 1.

Table 1: Chemical compositions of the ingots/billets

Heat No	Chemical Composition						Carbon Equivalent = %C + % Mn/6
	%C	%Mn	%Si	%P	%S	%N	
PI	0.33	1.12	0.24	0.04	0.04	0.03	0.52
NB	0.32	1.15	0.25	0.04	0.04	0.03	0.51
QB	0.31	1.14	0.31	0.03	0.04	0.04	0.50

Note: PI=Pencil Ingot, NB=Normal Standard Billet and QB=Quality Standard Billet

## RESULTS AND DISCUSSION

### *Inclusion Distributions*

Steel ingots or billets produced commercially are heterogeneous in nature. The exact distribution of the non-metallic inclusions in an ingot or billet is not known, but experience suggests that it could vary from top to the bottom or first to the end and also centre to the outside of an ingot or billet. Differences between ingots or billets in the same cast have also been observed. The magnitude of these differences is largely dependent on steel making and casting conditions.

The results of inclusion contents are given in Table 2. During the assessment, different particle sizes were measured and monitored. The inclusion sizes and distributions were found to be affected by the melting, handling and/or processing technique. The casting quality requirements were met regardless of the particle size ranges detected in the molten metal just before the pouring operation. The pencil ingot contains higher content inclusions than casting billets and gives inferior mechanical properties. Proper liquid metal treatment (ladle refining) with synthetic slag ensured lower number inclusions in the quality billets and reinforcing bars produced from these billets give better mechanical properties.

Table 2: Inclusion distributions in ingot/billet

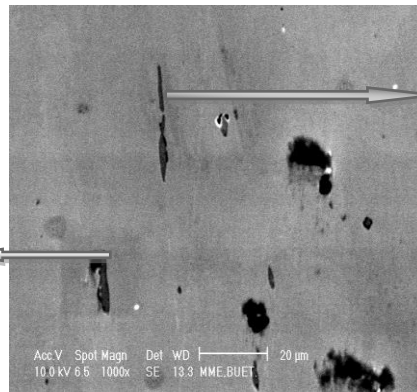
Heat No	Inclusions size distribution, $\mu\text{m}$					Total Number of Inclusions / $\text{cm}^2$
	3-10	10-20	20-30	30-40	>40	
PI	22150	784	890	252	16	24092
NB	11895	458	334	24	3	12714
QB	10125	451	22	7	00	10605

### *Metallurgical Observations*

Samples polished in the rolling direction were taken from each reinforcing bars. These are examined under the optical microscope and scanning electron microscope. All the reinforcing bars had a ferrite/pearlite matrix typical of C/Mn steels with a carbon content of about 0.3%. All the steels contained inclusions of the oxide, carbide, sulphide or complex types.

**EDX Analysis:**

Element	% of wt	Comments
Fe	23.84	Mainly Sulphides (FeS, MnS) and some oxides
Mn	35.46	
Si	0.39	
Al	0.32	
O	1.94	
S	26.17	
C	11.88	



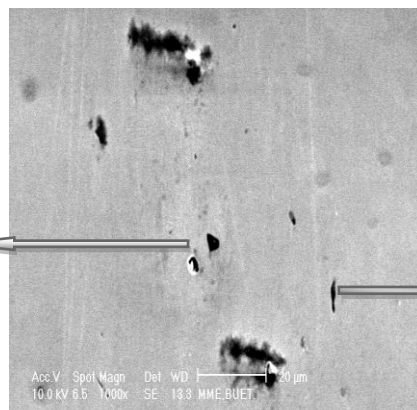
**EDX Analysis:**

Element	% of wt	Comments
Fe	65.89	Mainly carbides(Fe <sub>3</sub> C, Mn <sub>3</sub> C)and some oxides
Mn	23.74	
Si	0.52	
Al	0.45	
O	1.98	
S	0.38	
C	7.11	

Fig 2: SE image sulphide and carbide type's inclusions; chemical composition (mass %) of the inclusions, inclusions detected by EDX microanalysis in the deformed bars and shapes after rolling

**EDX Analysis:**

Element	% of wt	Comments
Fe	53.3	carbides (Fe <sub>3</sub> C, Mn <sub>3</sub> C), silicate and oxides( FeO, MnO, SiO <sub>2</sub> , Al <sub>2</sub> O <sub>3</sub> )
Mn	24.26	
Si	1.10	
Al	0.91	
O	7.51	
S	0.00	
C	12.92	



**EDX Analysis:**

Element	% of wt	Comments
Fe	52.18	Mainly carbides
Mn	19.04	
Si	7.12	
Al	3.69	
O	0.00	
S	0.00	
C	17.94	

Fig 3: SE image oxides and carbides type inclusions, inclusions distinguished by EDX and depending on their shapes after rolling

The shape change of inclusions after multi-pass hot rolling and EDX results are showed in Fig. 2 and Fig.3. During rolling the plastic inclusions change shape and therefore their size, whilst the harder types of inclusions are not affected by reduction. Inclusions in the form of thin films located on grain boundaries are especially dangerous for steel quality. These are usually low-melting oxysulphide inclusions precipitated in liquid state during steel solidification. They weaken the intergranular bonds, especially at elevated temperatures (red shortness). After rolling or forging the sulphide type inclusions are elongated and rolled out to some extent with the working/rolling direction (Fig.2). Elongated MnS found in the deformed bars. Inclusion particles with sharp edges may be quite dangerous; these are usually high melting inclusions (Malkiewicz and Rudnik, 1963; Baker, et al., 1976; Belchenko and Gubenko, 1983). Rounded off inclusion particles are considered less harmful. They are formed by substances which have low melting point and are poorly wettable by the metal. Small carbide type inclusions are retaining their shape (Fig.3) and particle size, refractory and brittle one breaks up. A low concentration of inclusions in steel is not, by itself, the guarantee of high quality because the inclusions may be concentrated in particular places of an ingot or billet.

Fig.4.a shows the Optical micrograph of elongated inclusion. The size of the elongated sample indicates the degree of reduction of the material from ingot or billet to deformed bars. With increasing reduction, the plastic inclusions change shape and therefore their size, whilst the harder types of inclusions are not affected by reduction. Inclusion particles with sharp edges (Fig. 4.b) may be also quite dangerous; these are usually high-melting inclusions, i.e. with the melting point above the temperature of molten metal. They often serve as stress concentrators in the metal and as sites for the beginning of fracture. If such an inclusion passes onto the surface of an article (a ball bearing, rail, etc.) it will crumble out soon and cause premature failure of the article. Rounded off inclusion



particles (Fig.4.c) are considered less harmful. They are formed by substances which have a low melting point and are poorly wettable by the metal.

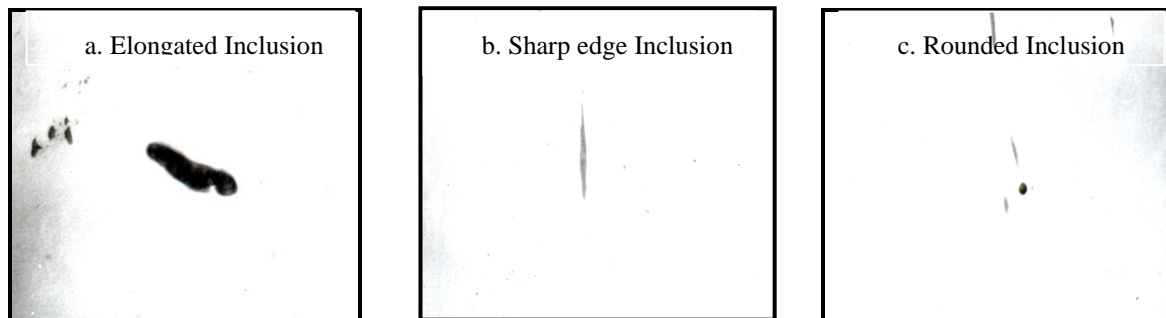


Fig. 4: Optical micrographs showing (a) elongated, (b) sharp edge and (c) rounded off inclusion after hot rolling

## CONCLUSIONS

The nature, size, shape and distribution of inclusions have been studied. It was found that most of the inclusions were Mn, Al and Si based complex silicate or oxide or carbide precipitates. Structural steel from pencil ingot contain larger size ( $>40\ \mu\text{m}$ ) and higher number ( $24092/\text{cm}^2$ ) inclusions. Deformed bars produced from normal casting billets (without treatment) content lower size and number inclusions. Inclusions level in the reinforced bars produced from quality standard billet (ladle refining) are lower number and size ( $<40\ \mu\text{m}$ ) than pencil ingots or normal standard billets. During deformation (hot rolling) sulphide type inclusions are elongated and rolled out and elongated MnS found in the deformed bars. Small carbide type inclusions are retaining their shape and particle size, refractory and brittle one breaks up.

## ACKNOWLEDGMENTS

The authors wish to record on his sincere thanks to BASHUNDHARA STEEL COMPLEX LIMITED (An enterprise of BASHUNDHARA GROUP) for permitting him to undertake this study and to the honorable Ex. Executive Director of BSCL Engr. M.A. H. Serajee for his encouragement and support.

## REFERENCES

- Amit, C and Ojha, C. 1997. Production of quality steel at TATA Steel. *Asia Steel*, 98-102.
- Bao, Y; Wang, M and Jiang, W. 2012. A method for observing the three-dimensional morphologies of inclusions in steel. *International Journal of Minerals, Metallurgy and Materials*, 19(2): 111-115.
- Baker, TJ; Gove, KB and Charles, JA. 1976. Inclusion deformation and toughness anisotropy in hot-rolled steels. *Metals Technology*, 3: 1183-1193.
- Barrie, RL; Gabbb, TP; Telesman, J; Kantzos, PT; Prescenzi, A; Biles, T and Bonacuse, PJ. 2008. Effectiveness of shot penning in suppressing fatigue cracking at non-metallic inclusions in Udimet 720. *Materials Science and Engineering A*, 474: 71-81.
- Belchenko, GI and Gubenko, SI. 1983. Deformation of nonmetallic inclusions during steel rolling. *Russian Metallurgy*, 4: 66-69.
- Evans, MH. 2014. Confirming subsurface initiation at non-metallic inclusions as one mechanism for white etching crack (WEC) formation. *Tribology International*, 75: 87-97.
- Fernandes, M; Pires, J; Cheung, N; and Garcia, A. 2003. Investigation of the chemical composition of nonmetallic inclusions utilizing ternary phase diagrams. *Materials Characterization*, 49: 437-443.
- Gulyakov, VS; Vusikhis, AS; and Kudinov, DZ. 2012. Nonmetallic Oxide Inclusions and Oxygen in the Vacuum Jet Refining of Steel. *Steel in Translation*, 42(11): 781-783.
- Genel, K. 2005. Estimation method for the fatigue limit of case hardened steels. *Surface & Coatings Technology*, 194: 91-95.
- Kjerrmann, H and Jernkont, Ann. 1929,113, pp.181-199.
- Kocańda, S. 1985. *Fatigue cracking of metals*. Warsaw: WNT.
- Lipiński, T and Wach, A. 2010. The Share of Non-Metallic Inclusions in High-Grade Steel for Machine Parts. *Archives of Foundry Engineering*, 10(4): 45-48.

- Lipinski, T and Wach, A. 2009. Non-metallic inclusions structure dimension in high quality steel with medium carbon contents. *Archives of Foundry Engineering*, 3(9): 75-78.
- Lipiński, T and Wach, A. 2010. The influence of out furnace processing on the exploitational propriety the middle carbon high quality constructional steel. *Archives of Foundry Engineering*, 1(10): 93-96.
- Lis, T. 1999. Out furnace lay reducing dirt interpolations non - metallic processing. *Metallurgist - Metallurgic Messages*, 2: 54-61.
- Lis, T. 2002. Application of stereological procedures for quantitative assessment of dispersive oxide phase. *Steel Research*, 73(5).
- Malkiewicz, T and Rudnik, S. 1963. Deformation of non-metallic inclusions during rolling of steel. *J. Iron Steel Inst.*, 201: 33-38.
- Millman, MS. 1999. Quality Steel from the EAF. 57th Electric Furnace Conference Proceedings, Pittsburgh (USA), 14-17 November. *The Iron and Steel Society*.15-28.
- Murakami, Y; Kodama, S & Konuma, S. 1989. Quantitative evaluation of effects of non-metallic inclusions on fatigue strength of high strength steels. I: BASIC fatigue mechanism and fatigue facture stress and the size and location of non-metallic inclusions. *International Journal of Fatigue*.11 (5): 291-298.
- Niclas, A; Andrey, K and Pär GJ. 2015. The Effect of Different Non-Metallic Inclusions on the Machinability of Steels, *Materials 2015*, 8: 751-783, doi: 10.3390/ma8020751.
- Park, JS and Park, JH. 2014. Effect of Slag Composition on the Concentration of Al<sub>2</sub>O<sub>3</sub> in the Inclusions in Si-Mn killed Steel. *Metallurgical and Materials Transactions B*. 45B: 953-960.
- Shih, T.Y. & Araki, T. 1973. The effect of nonmetallic inclusion and microstructures on the fatigue crack initiation and propagation in high strength carbon steel. *Transaction Journal Steel Institute Japanese*, 1: 11-19.
- Spriestersbach, D; Grad, P and Kerscher, E. 2014. Influence of different non-metallic inclusion types on the crack initiation in high-strength steels in the VHCF regime. *International Journal of Fatigue*, 64: 114-120.
- Srivastava, A; Ponson, L; Osovski, S; Bouchaud, E; Tvergaard, V and Needleman, A. 2014. Effect of inclusion density on ductile fracture toughness and roughness. *Journal of the Mechanics and Physics of Solids*, 63: 62-79.
- Roiko, A; Hänninen, H and Vuorikari, H. 2012. Anisotropic distribution of non-metallic inclusions in a forged steel roll and its influence on fatigue limit. *International Journal of Fatigue*, 41: 158-167.
- Wang, XH, Jiang, M, Chen, B. and Li, HB. 2012. Study on formation of non-metallic inclusions with lower melting temperatures in extra low oxygen special steels. *Science China Technological Sciences*, 55(7): 1863-1872.
- Wypartowicz, J and Podorska, D. 2006. Control of chemical composition of oxide-sulphide inclusions during deoxidation of steel with manganese, silicon and titanium. *Metallurgist- Metallurgic Messages*, 73(3): 91-96.
- Yang, ZG; Zhang, JM; Li, SX; Li, GY; Wang, QY; Hui, WJ and Weng, YQ. 2006. On the critical inclusion size of high strength steels under ultra-high cycle fatigue. *Materials Science and Engineering*, A 427: 167-174.
- Zhang, L and Thomas, BG. 2003. State of the Art in Evaluation and Control of Steel Cleanliness – Review. *ISIJ International*, 43(3): 271–291.

## **EFFECT OF 0.5WT% CR ADDITION ON THE MECHANICAL PROPERTIES AND MICROSTRUCTURE OF HEAT TREATED PLAIN CARBON LOW ALLOY STEEL**

A. Hossain<sup>1\*</sup>, F. Gulshan<sup>2</sup>, M. M. Ali<sup>2</sup> & A. S. W. Kurny<sup>2</sup>

<sup>1</sup>*Kailashstilla MSTE Plant, Sylhet Gas Fields Limited (A company Petrobangla, Energy and Mineral Resources Division), Sylhet, Bangladesh*

<sup>2</sup>*Department of Materials and Metallurgical Engineering, Bangladesh University of Engineering and Technology, Dhaka, Bangladesh*

*\*Corresponding Author: ah\_buetmmesgfl@live.com*

### **ABSTRACT**

Alloy addition increases the tensile strength with increasing lesser amount of ductility for the development of high strength low alloy steels (HSLA). Improvement of mechanical properties and microstructures, heat treatment was carried out which provide high strength, high yield point combined with adequate ductility and toughness. An attempt has been taken to study the effect of 0.5wt% Cr on structure and properties of ~ 0.10% carbon (low carbon) steel. Samples of the steels were annealed and normalized by R.F. Generator machine from their respective heat treatment temperatures. The standard tensile specimens made from the annealed and normalized steel bars were tested to obtain data on tensile properties such as yield strength, ultimate tensile strength, percentage of elongation and percentage of reduction in area. 0.5wt% Cr content steel (Steel-2) shows the better yield strength and tensile strength but poor ductility than plain carbon steel (Steel-1) in the heat treated conditions. The corresponding heat treatments change the microstructures of the examined alloys.

Keywords: Plain carbon steel; heat treatment; tensile properties; microstructure

### **INTRODUCTION**

During the last decades, there has been a great demand for steels with higher mechanical strength, sufficient ductility and toughness. Moreover, the lightness of the steel is attractive, as in the automobile and aircraft applications. These requirements can be achieved by an increase in carbon content in a limited way, but even in the heat-treated condition the maximum strength of alloy steel can reach 700 MPa above this value; the ductility dramatically decreases (Avner, 1974). Heat treated alloy steels provide high strength, high yield point, combined with appreciable ductility even in large sections. The use of plain carbon steels frequently necessitates water quenching accompanied by the danger of distortion and cracking, and even so only thin sections can be hardened throughout. For resisting corrosion and oxidation at elevated temperatures, alloy steels are essential. High-strength low-alloy (HSLA) steels, or micro-alloyed steels, are designed to provide better mechanical properties and/or greater resistance to atmospheric corrosion than conventional carbon steels in the normal sense because they are designed to meet specific mechanical properties rather than a chemical composition. The HSLA steels have low carbon contents (0.05-0.25% C) in order to produce adequate formability and weldability, and they have manganese contents up to 2.0%. Small quantities of chromium, nickel, molybdenum, copper, nitrogen, vanadium, niobium, titanium and zirconium are used in various combinations (Aver, 1974; Hossain and Kabir, 2006).

According to the Alloy Steels Research Committee (ASRC): "Carbon steels are regarded as steels containing not more than 0.5% manganese and 0.5% silicon, all other steels being regarded as alloy steels (American Society for Metals, 1964). The basic alloying elements added to steel are manganese, lead, nickel, chromium, molybdenum, vanadium, niobium, silicon and cobalt. The effect heat treatment of low-alloy steel was extensively studied by many researchers during the last decades (Frihat, 2015). Low-alloy steels constitute a category of ferrous materials that exhibit mechanical properties superior to plain carbon steels as the result of additions of alloying elements such as nickel,

chromium, molybdenum and niobium. For many low-alloy steels, the primary function of the alloying elements is to increase hardenability in order to optimize mechanical properties and toughness after heat treatment. In some cases, however, alloy additions are used to reduce environmental degradation under certain specified service conditions (Aver, 1974; Hossain and Kabir, 2006).

Mechanical properties of steels are strongly connected to their microstructure obtained after heat treatments that are generally performed in order to achieve a good hardness and/or tensile strength with sufficient ductility (Mebarki et al., 2004). Currently, there is a strong interest in the effect of cooling rate on the mechanical properties and microstructure of industrial processed steels. It has been shown that oil quenching produce an essentially ferrite-martensite dual phase structure with about 4 volume pct of fine particle and thin film retained austenite. In contrast, the slower air cooling results in a larger amount (about 10 volume pct) of retained austenite in addition to the ferrite and martensite phases. On the other hand, with the applied cooling rate increasing, the transformed structure evolves from granular bainite, lower bainite, self-tempered martensite, to finally martensite without self tempering (Qiao et al., 2009). Among them, self-tempered martensite, obtained in the transformed specimens cooled with rates of 25 - 80°C/min, exhibits the highest hardness values due to the precipitation of fine carbides.

It has been shown that yield strength increases with increasing cooling rate, while ultimate tensile strength and strain-to-failure is unaffected. Although many papers have been published on the effect of cooling rate on the tensile behaviors of steel (Chao and Gonzales-Carrasco, 1998; Perdrix et al., 2000; Serre and Vogt, 2008) there has been little research on the effects of cooling rate on the microstructure and micro-hardness (Nagpal and Baker, 1990; Lu et al., 2009).

The influence of Mn, Cr and Mo on hardenability is well known. These elements promote the formation of hard phases such as bainite and martensite. Chromium, manganese (both having high affinity for oxygen) and molybdenum all enhance hardenability. Cr, Mo and Mn influence on the formation of bainite and/or martensite during continuous cooling of medium-carbon steels and respective mechanical properties (Sarasola, et al., 2005; Sulowski and Cias, 2011). It was investigated the effects of Cr and Ni on low carbon steel with undissolved carbide particles on the refining the austenite grain size (Razzak, 2011). Low carbon steel with Cr content showed a lower Widmanstatten ferrite content, whereas the proportion of acicular ferrite was increased. Acicular ferrite improves the toughness and acts as an obstacle to cleavage fracture. Higher impact absorption energy was measured in a specimen with finer acicular ferrite structures. Cr is a ferrite-stabilizing element and increases the corrosion resistance of plain carbon low alloy steel (Lee and Lee, 2015).

The present study is aimed at understanding the effect of 0.5wt% Cr addition on the mechanical properties and microstructures of heat treated plain carbon low alloy steels.

## **EXPERIMENTAL PROCEDURE**

Two different steels containing about 0.10 % carbon were used in this study. The compositions of the steels are presented in Table 1. Steel-1 is the base steel with which the structure and properties of the Steel-2 compared. The steels were made in an air induction furnace. All the melts were poured into a cylindrical metal mould and sound ingots were produced. These ingots were rolled down to 16mm diameter bars.

The heat treatments of the specimens were carried out in the Induction R. F. Generator (Radio Frequency). The steels were held at their respective heat treatment temperatures for pre selected periods. Then they were allowed to cool at two different cooling rates, namely 67, ~4°C/min. These cooling rates indicate the natural cooling or normalizing (67°C/min) and annealing (4°C/min). The heat treated bars were then machined into standard tensile specimens with a nominal diameter and minimum parallel length of 3.99 mm and 25 mm respectively.

The tensile specimens were then tested with a Universal Tensile Testing Machine (INSTRON) to obtain data on yield strength (YS), ultimate tensile strength (UTS), percentage of elongation (%EL), and percentage of reduction in area (% RA).

For metallographic observation, the heat treated specimens were taken for micro examination. The samples were then ground, polished up to gamma-aluminum powder and then etched in 2% nital. The microstructure of these specimens was then studied with the help of an optical microscope and

photograph of these structures of each specimen were taken. Chemical compositions of the examined steels have shown in Table.1.

Table 1: Chemical compositions of the examined steels

Steel Name	Composition weight percentage						
	C	Si	Mn	S	P	Cr	Fe
Steel-1	0.10	0.28	1.18	0.021	0.028	-	Bal.
Steel-2	0.11	0.20	1.28	0.022	0.022	0.5	Bal.

## RESULTS AND DISCUSSION

### Tensile Properties

The results of the tensile test of the heat treated (both annealed and normalized) tensile specimens of the Steel-1 and Steel-2 are shown in Fig.1. It is evident from Fig.1.a that yield strength of the Steel-2 is higher than the Steel-1. Between the alloy steels; Steel-2 with Cr produces the higher yield strength than Steel-1 all over the applied heat treatment. This indicates that chromium increase the yield strength. A similar trend was found with the ultimate tensile strength of these steels. Chromium (Cr) in the form of CrC precipitates increases the strength by means of precipitation strengthening. CrC also pins the grain boundaries and inhibits the grain growth. This results in grain refinement and hence higher strength.

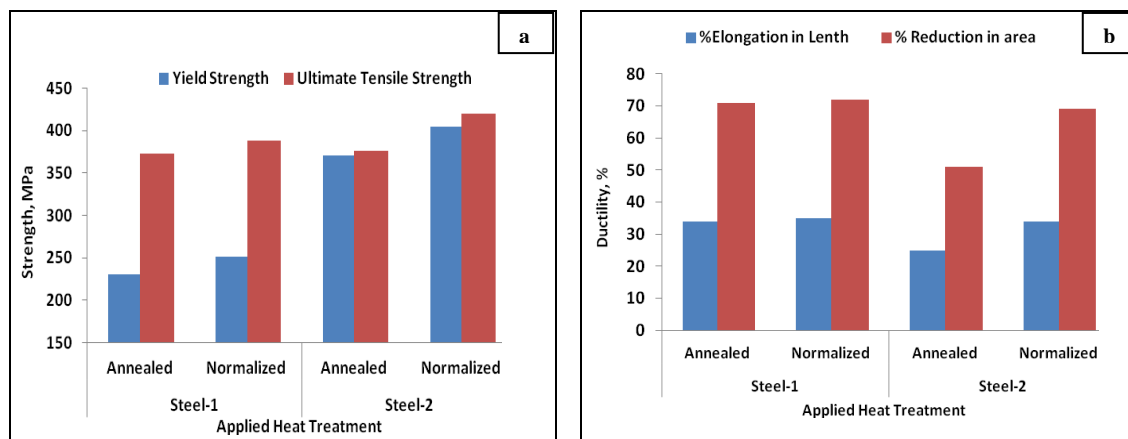


Fig 1: (a) Tensile strength and (b) Ductility at annealed and normalized condition

Fig.1.b shows that ductility i.e. percentage of elongation and reduction in area in Steel-1 and Steel-2 in both annealed and normalized condition. Steel-2 showed lower percentage of elongation than Steel-1 in both heat treatment conditions. This may be due to the presence of precipitates (CrC in Steel-2). This indicates that CrC is harmful for increasing the ductility. The percentage of reduction in area also decreases due to present CrC. This happens because ductile behaviour is normally inversely proportional to yield strength.

### Microstructural Investigation

The microstructure of annealed and normalized Steel-1 and Steel-2 are shown in Fig.2.a and Fig.2.b respectively. It has been observed that Steel-1 showed regular ferrite pearlite structure in the annealed condition (Fig.2.a) and fine ferrite pearlite & few Widmanstatten structure & bainite in the normalized condition (Fig.3.a). The finer structure in the normalized condition is due to the faster cooling rate. In the annealed condition Steel-2 revealed regular ferrite pearlite structure (Fig.3.b) finer than Steel-1 revealed ferrite pearlite. In the normalized condition Steel-1 showed some Widmanstatten structure along with regular ferrite pearlite. The amount of Widmanstatten structure is only small in Steel-1. The Steel-2 showed only regular ferrite pearlite in the normalized condition (Fig.3.b). Optical microscopy also revealed finer ferrite pearlite in Steel-2 than plain carbon Steel-1.

Steel-2 showed more or less same grain size of ferrite pearlite compared to Steel-1. Steel-1 is a plain carbon steel. It does not contain any alloying element. So, there are no second phase particles to

inhibit grain growth. In the annealed condition Steel-1 also revealed very fine ferrite pearlite in some areas. This may be due to the segregation effect. The finest grain size in Steel-2 containing Cr and Cr is due to the precipitation of finer CrC during cooling. For this reason Steel-2 showed finest grain size than Steel-1.

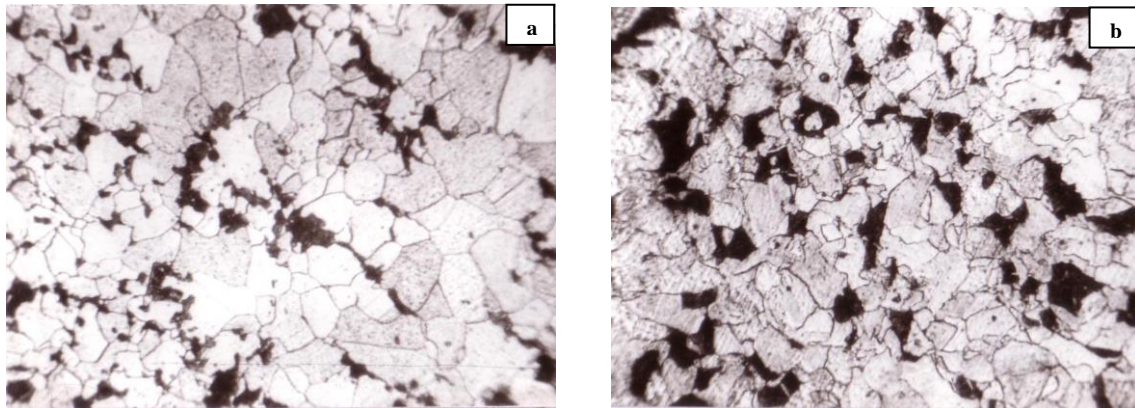


Fig 2: Optical microstructures of (a) Steel-1 and (b) Steel-2 at annealed condition, X600

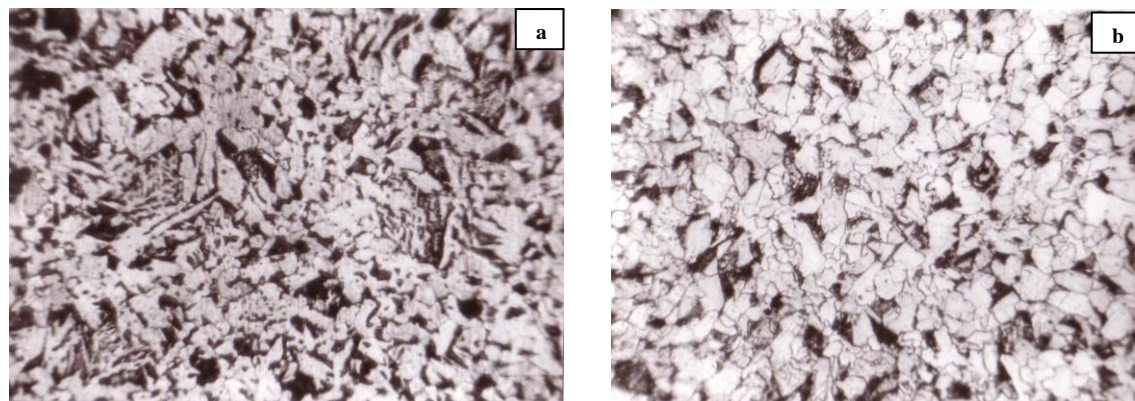


Fig 3: Optical microstructures of (a) Steel-1 and (b) Steel-2 at Normalized condition, X600

## CONCLUSION

Heat treatment affects the microstructure and tensile properties of the experimental low alloy steels remarkably. At annealed condition, Cr in Steel-2 revealed regular ferrite pearlite structure, finer than plain carbon Steel-1. Steel-2, it has been observed that fine ferrite pearlite & few Widmanstatten structure & bainite in the normalized condition (faster cooling rate). The yield and ultimate tensile strength of Cr content Steel-2 is higher than steel-1 but the ductility is lower all over the heat treated condition.

## REFERENCES

- American Society for Metals, 1964. Metal Handbook. Vol. 2. 8th Edition, *American Society for Metals*, Materials Park, Ohio.
- Avner, SH. 1974. Introduction to Physical Metallurgy. 2nd Edition, McGraw-Hill Book Company, New York.
- Chao, J and Gonzales-Carrasco, JL. 1998. Influence of cooling rate on room temperature tensile behaviour of thermally oxidised MA 956. *Mater. Sci. Technol.* 14: 440.
- Frihat, MH. 2015. Effect of Heat Treatment Parameters on the Mechanical and Microstructure Properties of Low-Alloy Steel. *Journal of Surface Engineered Materials and Advanced Technology*, 5: 214-227, <http://dx.doi.org/10.4236/jsemat.2015.54023>
- Hossain, A and Kabir, MA. 2006. *Heat Treatment of Low Alloy Steels*. B.Sc. Engg. Thesis, Department of Materials and Metallurgical Engineering, Bangladesh University of Engineering and Technology, Dhaka.

- Lee, H and Lee, H. 2015. Effect of Cr Content on Microstructure and Mechanical Properties of Low Carbon Steel Welds. *Int. J. Electrochem. Sci.*, 10: 8028 – 8040.
- Lu, Z; Faulkner, RG; Riddle, N; Martino, FD and Yang, K. 2009. Effect of heat treatment on microstructure and hardness of Eurofer 97, Eurofer ODS and T92 steels. *J. Nuc. Mater.* 415: 386-388.
- Mebarki, N; Delagnes, D; Lamelse, P; Delmas, F and Levallant, C. 2004. Relationship between microstructure and mechanical properties of a 5% Cr tempered martensitic tool steel. *Mat. Sci. Eng. A.*, 387-389: 171-175.
- Nagpal, P and Baker, I. 1990. Thermal vacancies and the yield anomaly of Fe Al. *Metallurgical Transactions*, 21A: 2281.
- Perdrix, F; Trichet, MF; Lbonnontien, J; Cornet, M and Bigot, J. 2000. Influence of nitrogen on the microstructure and mechanical properties of Ti–48Al alloy. *J. Phys.* 10: 223.
- Qiao, ZX; Liu, YC; Yu, LM and Gao, ZM. 2009. Effect of cooling rate on microstructural formation and hardness of 30CrNi3Mo steel. *App. Phy. A.* 95: 917.
- Razzak, MA. 2011. Heat Treatment and Effects of Cr and Ni in Low Alloy Steel. *Bulletin of Materials Science*, 34: 1439-1445. <http://dx.doi.org/10.1007/s12034-011-0340-9>.
- Sarasola, M; Sainz, S and Castro, F. 2005. In: Proc. of Euro PM2005, Prague, Czech Republic. PM Low Alloy Steels 4. EPMA, 1: 349.
- Serre, I and Vogt, JB. 2008. Mechanical properties of a 316L/T91 weld joint tested in lead–bismuth liquid. *J. Nuclear Mater.*, 376: 330.
- Sulowski, M and Cias, A. 2011. The effect of sintering temperature on the structure and mechanical properties of sintered Fe-Mn-Cr-Mo-C structural steels. *Powder Metallurgy Progress*, 11(1-2): 123-131.

# **FIELD SURVEY OF THE HISTORICAL AND ARCHAEOLOGICAL BUILDINGS IN CHITTAGONG CITY, IDENTIFICATION OF FAULTS AND RECOMMENDATION OF PROBABLE RETROFITTING MEASURES**

F. Parvin<sup>1\*</sup>, M. A. Yusuf<sup>2</sup> & O. A. Chowdhury<sup>3</sup>

<sup>1</sup>*Health Engineering Department, Chittagong, Chittagong, Bangladesh*

<sup>2</sup>*Civil Engineering Department, Port City International University, Chittagong, Bangladesh*

<sup>3</sup>*Civil Engineering Department, Southern University Bangladesh, Chittagong, Bangladesh*

*\*Corresponding Author: lipi.parvin@gmail.com*

## **ABSTRACT**

The history of Chittagong is very royal for many branches of history. The oldest archaeological and historical buildings are one of them. Near about 53 number of historic building are situated in Chittagong. Most of them are about to ruin due to age and lack of maintenance. At the same time the buildings have experienced different types of natural disaster like earthquake, flood, landslide, cyclone etc. Our most valuable traditional oldest archaeological and historical buildings are now at vulnerable condition due to frequent occurrences of natural disaster specially for earthquake and landslide. It is high time to take necessary steps to keep these buildings safe. Here we conduct a preliminary and detail survey on Chandanpura Mosque, CRB (Chittagong Railway Building), Zia Memorial Museum, Chittagong Railway Station (old), Chittagong Railway School, Chittagong Polytechnic Institute, Chittagong Club and Chittagong Court Building. Various dimensions of structure and other features collected by physical measurement from existing building's and prepare their floor plan, front elevation, sectional elevation. By visual observation we identified their visible faults. Then categorized them in plaster cracks, brick wall cracks, corrosion in steel, horizontal cracks in the beam, vertical cracks in the column. Then recommend probable retrofitting measures in civil engineering practice according to identified problem.

Keywords: Historical Building; traditional value; vulnerability; cracks; retrofitting

## **INTRODUCTION**

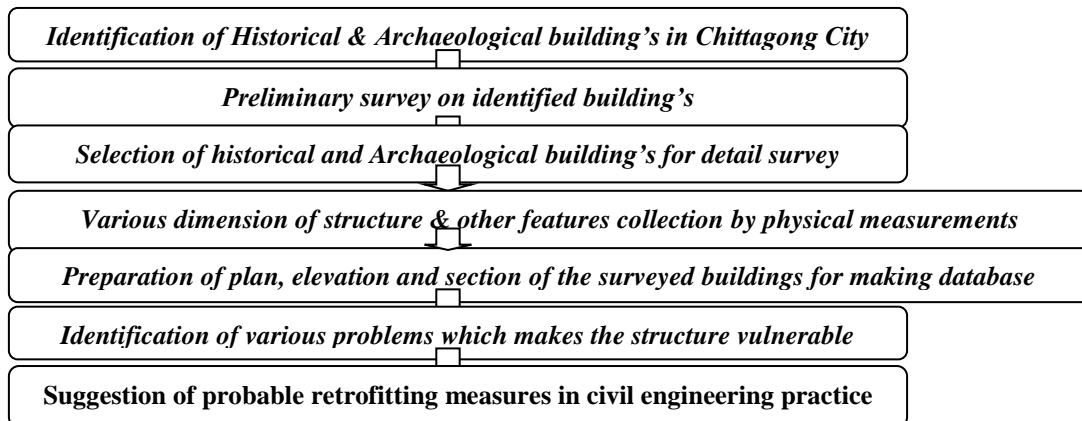
Notable numbers of buildings are carrying our tradition, culture & history. Many Buildings are informally constructed in a traditional manner without formal design by qualified Engineers or Architects. Now a days this is become our responsibility to save this structures to conserve their traditional, historical and archaeological value.

Chittagong is also very important for its many historical & archaeological buildings. Such buildings involve stone, brick, concrete block, rammed earth and wooden post, combination of some or all above materials. For last six decade these buildings are completely out of proper maintenance on time. As a result they are almost nearby to damage before design life time. It is high time to take necessary action to save these structures. Most of them have not been designed for seismic loads. Recent earthquakes have shown that many such buildings are seismically vulnerable and should be considered for retrofitting. Retrofitting is the process of saving the structure from damage and strengthens the structure. Different conventional retrofitting techniques are available to increase the strength or ductility of these historical and archaeological building.



## METHODOLOGY

Methodology of the work are given below as a work flow diagram



### **Identification of Historical & Archaeological building's**

For identifying a project as a historical & Archaeological a building must satisfied three common criteria e.g. Age, Integrity of a Building and Significance.

**Age:** A building must be "old enough" at least 50 years old to be considered historic. In another way a structure must be old enough to have been studied by historians, architectural historians or archaeologists. This latter perspective allows some types of properties that are less than 50 years old to be considered as "historic".

**Integrity:** For physical integrity a building, structure, landscape feature, historic site, or historic district must be relatively unchanged. For an archaeological site, integrity means that the site must be relatively undisturbed, with its patterns and layers of artifacts and other archaeological evidence relatively intact.

**Significance:** Finally and most importantly a property must be significant to be considered historic. Significance is defined in three ways: (1) through direct association with individuals, events, activities, or developments that shaped our history or that reflect important aspects of our history; (2) by embodying the distinctive physical and spatial characteristics of an architectural style or type of building, structure, landscape, or planned environment, or a method of construction, or by embodying high artistic values or fine craftsmanship; or (3) by having the potential to yield information important to our understanding of the past through archaeological, architectural, or other physical investigation and analysis.

### **Preliminary survey on identified building's**

We have conducted a preliminary survey of identified buildings by a questionnaire survey form shown in **Table 1**

### **Data collection**

We collect data by field measurement and for required data we create a data base.

### **Preparation of Plan, Elevation & section**

From surveyed data and field measurement we have prepared floor plan, front elevation and sectional elevation of surveyed buildings.

### **Fault identification**

From visual investigation and field visit we have identified different types of fault on the existing structures e.g. plaster crack, beam column crack, ceiling crack, reinforcement corrosion, slab & stair problems, masonry wall crack.

### **Retrofitting measures**

After identification of all types of faults we recommend required retrofitting measures.

## RESULTS AND DISCUSSIONS

The 2<sup>nd</sup> largest city and sea port of Bangladesh, Chittagong has its past glory. During the 18th and 19th centuries Chittagong was under the British rule. For this reason different important historical and archaeological buildings were constructed in here in different times. The Preliminary Survey results are shown in Table 2

Table 1: Questionnaire survey form for preliminary survey

Sl. No.	Description of building	Information	Notes
01	Name		
02	Address		
03	Name and type of owner		Private/government
04	Name of Architect		
05	Name of Engineer		
06	Use of building		Residential/ office/ commercial/ industrial
07	Type of structure		Load bearing/frame
08	Open ground storey	Yes / No	
09	Heavy machinery or any other type of large mass	Yes / No	
10	Expansion / Separation joints		
11	Photograph / sketch		Attach with sheet
12	Structural drawings available	Yes / No	
13	Architectural drawings available	Yes / No	
14	Geotechnical report available	Yes / No	
15	No. of Storey		

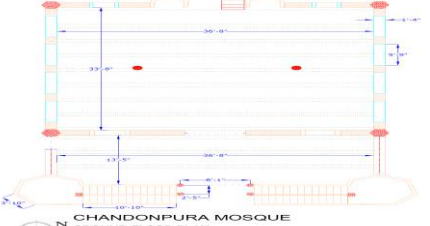
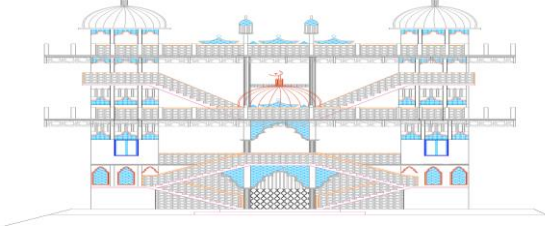
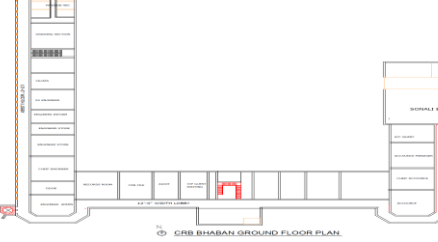
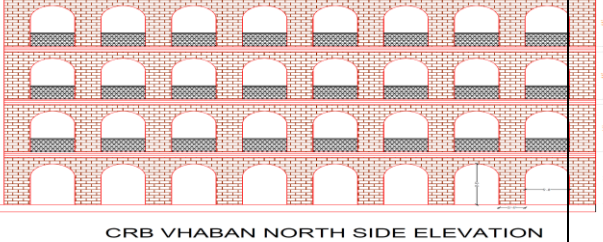
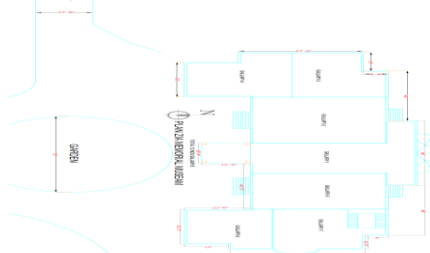
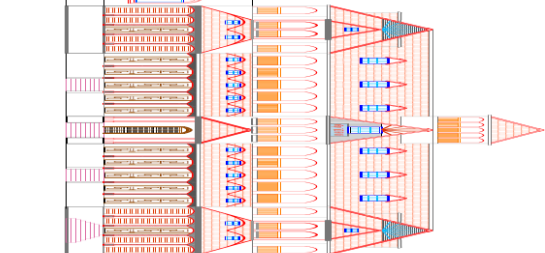
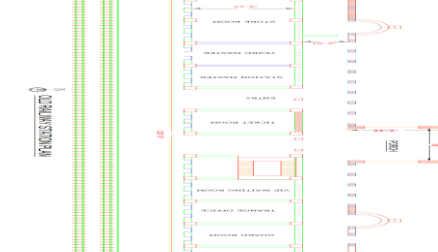
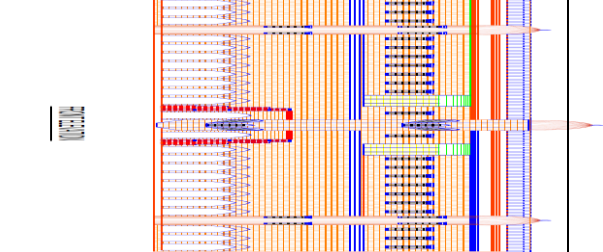
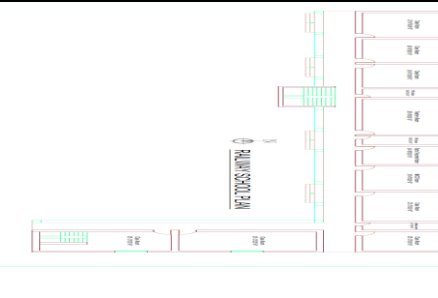
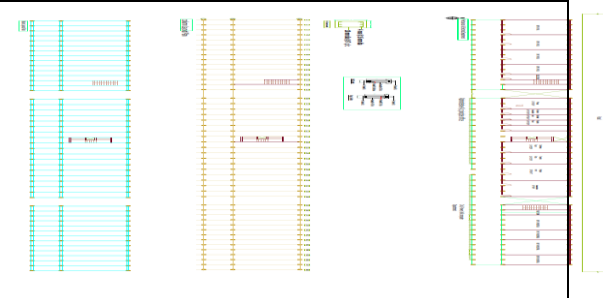


Table 2: Preliminary survey results

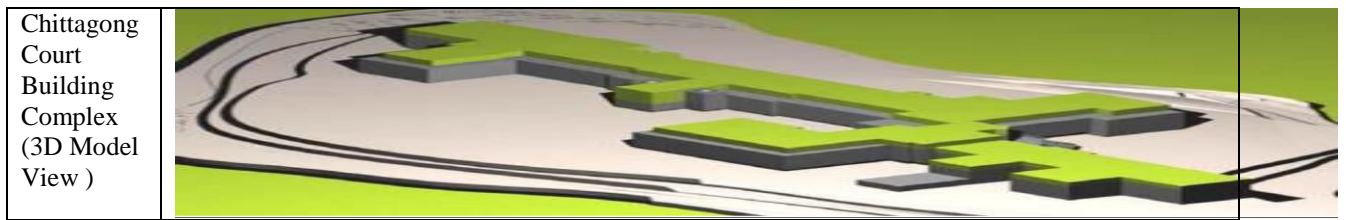
Sl. no.	Name of the building & Location	Established Year	No. of storied	Previously Retrofitted	Type of Structure
1.	Chandanpura Mosque<Andarkilla>	1920	02	No	Bricks masonry & RCC Structure
2.	CRB (Chittagong Railway Building)<S.S.Khaled Road>	British Victorian Period.	03	No	Bricks masonry
3.	Zia Memorial Museum<S.S.Khaled Road>	1913	02	No	Bricks masonry
4.	Chittagong Railway Station(old) <Kotowali>	1972.	02	Yes	Bricks masonry
5.	Chittagong Railway School <Pahartoli station road>	1936	02	No	Bricks masonry
6.	Chittagong Polytechnic Institute <East Nasirabad>	1962	03	No	R.C.C. frame structure
7.	Chittagong Club Ltd. <S.S.Khaled Road>	1875	03	Yes	R.C.C. frame structure
8.	Chittagong Court Building<Kotowali>	1953	03	No	Bricks masonry

### *Preparation of Plan, Elevation & section*

Different floor plan and elevation drawn from collected data of the surveyed buildings shown in Table 3

Table 3: Drawing of surveyed building







<p>Chandanpura Mosque                  ( Floor Plan &amp; Front Elevation )</p>	 <p>CHANDANPURA MOSQUE                  GROUND FLOOR PLAN</p>	 <p>FRONT ELEVATION</p>
<p>CRB                  (Chittagong Railway Building)                  (Ground floor plan and North side elevation)</p>	 <p>CRB SHABAN GROUND FLOOR PLAN</p>	 <p>CRB SHABAN NORTH SIDE ELEVATION</p>
<p>Zia Memorial Museum                  (Ground floor plan and Front elevation)</p>	 <p>ZIA MEMORIAL MUSEUM                  GROUND FLOOR PLAN</p>	 <p>FRONT ELEVATION</p>
<p>Chittagong Railway Station                  (Old)                  (Ground floor plan and Front elevation)</p>	 <p>CHITTAGONG RAILWAY STATION (OLD)                  GROUND FLOOR PLAN</p>	 <p>FRONT ELEVATION</p>
<p>Chittagong Railway School Building and Chittagong Polytechnic Institute                  (Ground floor plan)</p>	 <p>CHITTAGONG RAILWAY SCHOOL BUILDING AND CHITTAGONG POLYTECHNIC INSTITUTE                  GROUND FLOOR PLAN</p>	 <p>FRONT ELEVATION</p>
<p>Chittagong Club                  (Ground floor, 1<sup>st</sup> floor, Mezzanine floor plan)</p>	 <p>CHITTAGONG CLUB                  GROUND FLOOR PLAN</p>	 <p>CHITTAGONG CLUB                  MEZZANINE FLOOR PLAN</p>

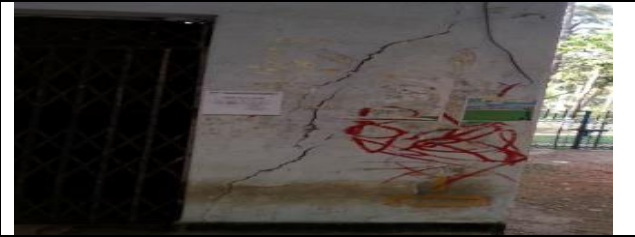
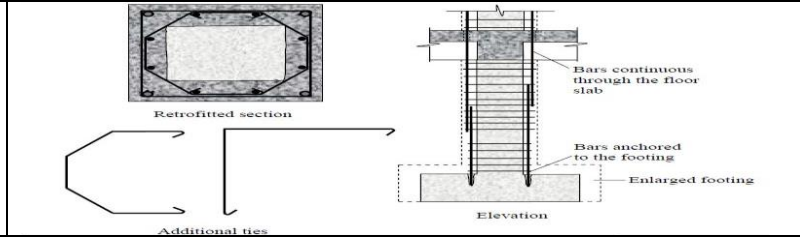

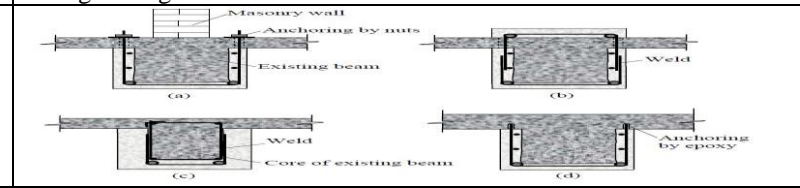

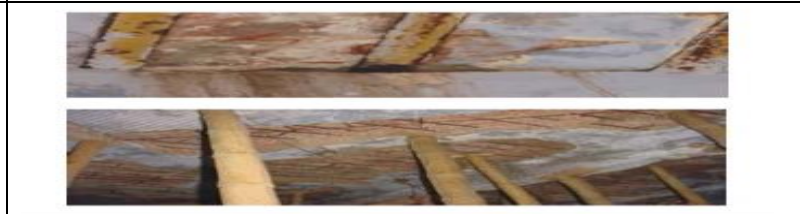
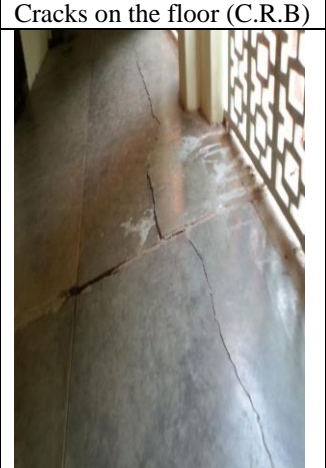


**Identified problems and their probable retrofitting measures**

During detailed survey of structure identified problems and their probable retrofitting measures in civil engineering practice are shown in **Table 4**

**Table 4:** Identified problems and their probable retrofitting measures

<b>Crack in Ancillary part &amp; plaster of the structure</b>		
Cracks in railing and corrosion of steel (Chandanpura mosque).	Cracks in railing (Chandanpura mosque)	Cracks in the wall plaster (C.P.I).
		
<b>Repair technique:</b> Plaster should remove properly in cracks area. Then apply de-salt chemical in the wall and re plaster . Ancillary part like railing crack fault should recast.		
<b>Crack in the wall</b>		
Cack in the wall (C.R.B)	Corrosion in the wall (C.R.B)	Cracks in the wall (old fire service building)
		
<p><b>Repair technique:</b> Cracks that are small in width (<math>\leq 0.75</math> mm) can be effectively repaired by pressure injection of epoxy (IS 13935: 1993).The surfaces are thoroughly cleaned of loose materials. Injection ports are placed along the length of the cracks on both sides, at intervals approximately equal to the thickness of the member. Low viscosity epoxy resin is injected into the ports sequentially, beginning at the port at the lowest level and moving upwards one by one. The resin is pushed through the packer till it is seen flowing from the other end or from a port higher than where it is injected. The port is closed at this juncture and the packer is moved to the next higher port.</p> <p>Larger cracks will require larger packer spacing depending on thickness of the member. Vacuum injection has a typical fill level of 95 percent and can fill cracks as small as 0.025 mm. A similar technique can be applied to strengthen weak walls.</p> <p><b>Re-pointing:</b> For re-pointing, first the wall should be made wet and all loose debris cleared. The joints that are to be re-pointed should be raked to a depth of 2 times the joint height. Next fresh mortar should be placed by trowels. The mortar should be non-shrinking type. The re-pointed portion should be cured properly.</p> <p><b>Grout Filling:</b> Selected cells in a hollow block masonry wall can be filled with grout. Filling the voids with grout will increase the compressive strength and make the wall more impermeable to water penetration. The inside of the cavity should be pre-wetted, then drained prior to grouting.</p> <p><b>Crack Stitching:</b> It is possible to introduce internal ties in a masonry wall by drilling a hole, placing a bar and finally grouting the hole. A similar ‘pinning technique’ can be used for stitching cracks in the walls and strengthening the arches.</p>		
<b>Cracks in the column</b>		
Cracks in column (C.P.I)	<b>Repair technique:</b> Column jacketing method can be applied for re-strengthening the column	

	
<p><b>Cracks in the Beam</b></p>	
<p>Crack &amp; corrosion of steel in beam (C.P.I)</p>	<p><b>Repair technique:</b> Beam jacketing method can be applied for re-strengthening the beam</p>
	
<p><b>Ceiling fault</b></p>	
<p>Corrosion of steel on roof (C.P.I)</p>	<p>Corrosion of steel on roof (Court building)</p>
	
<p><b>Repair technique:</b> Ceiling should re plaster after removing the old damaged plaster immediately to prevent steel corrosion and in R.B slab (reinforced brick) steel section can be repaired by applying anti corrosion chemical.</p>	
<p><b>Cracks on the floor</b></p>	
	<p><b>Repair Technique :</b> Large Cracks and Crushed Material For cracks with width larger than 6 mm or in regions where brickwork or concrete is crushed, the following procedure is suitable.</p> <ol style="list-style-type: none"> <li>1. Removed loose material in the crack.</li> <li>2. If necessary, the crack is dressed to have a V groove.</li> <li>3. At wide cracks, fillers like flat stone chips can be used.</li> <li>4. To prevent widening of the cracks, they can be stitched</li> </ol> <p>The stitching consists of drilling small holes of diameter 6 to 10 mm on both sides of the crack, cleaning the holes, filling up these with epoxy mortar and anchoring the legs of stitching dogs (U-shaped steel bars of diameter 3 to 6 mm with short legs). The stitching dogs can have variable length and orientation. The spacing of the reinforcement should be reduced at the ends of the crack. Stitching will not close the crack, but it prevents further propagation and widening of the crack. The stitching will stiffen the area near the vicinity of the crack.</p>

## CONCLUSION AND RECOMMENDATION

### CONCLUSION

In a sense of social & professional responsibility of an Engineer we take some step as starting of the preservation of Historical and Archaeological buildings. From above study we saw that identified problems are not a major problems at all. These can be easily retrofitted by suggested retrofitting measures in civil engineering practice in a economic way. Problem is lack of awareness, lack of regular repair & maintenance. In this way we throw our most valuable Historical and Archaeological buildings in a threat.

### RECOMMENDATION:

- This paper can be used for conservation of these historic Structures.
- Prepared database can be used for taking priority of treatment at vulnerable stage.

- Can prepare a master plan for restoring the Historical Buildings in future.
- Data base can be used for the numerical modelling to get the specific retrofitting technique of this building.

#### **REFERENCES**

- Handbook on Repair and Rehabilitation of RCC Buildings (2002), Central Public Works Department.  
Hand Book on Seismic Retrofit of Building, Central Public Works Department.  
IS13945, Repair and Seismic Strengthening of Buildings –Guidelines, Bureau of Indian Standards, New Delhi, 1993.  
Shri. Pravin B. Waghmare “MATERIALS AND JACKETING TECHNIQUE FOR RETROFITTING OF STRUCTURES” International Journal of Advanced Engineering Research and Studies E-ISSN2249 – 8974.  
UNDP/UNIDO Project RER/79/015,”Repair and strengthening of Reinforced Concrete, Stone and brick Masonry Buildings”, Building Construction Under Seismic Conditions in the Balkan Regions, 1983, United Nations Industrial Development Programme, Australia, Vol.5.

## STATIC & TIME HISTORY ANALYSIS OF RCC STRUCTURE: A COMPARATIVE STUDY

S. A. Haque<sup>1</sup>, T. Haque<sup>2\*</sup>, S. Sanjida<sup>1</sup> & Y. Masud<sup>1</sup>

<sup>1</sup>Department of Civil Engineering, Ahsanullah University of Science & Technology, Dhaka, Bangladesh

<sup>2</sup>Department of Water Resources Engineering, Bangladesh University of Engineering and Technology, Dhaka, Bangladesh

\*Corresponding Author: tamanna.haque.himi@gmail.com

### ABSTRACT

This paper reports on the response of RCC structures over time due to Static and Dynamic loading. Here structures with different span lengths are modeled. Three different cases based on span lengths are considered (Case-01: Length/Breadth (L/B) ratio 0.60, Case-02: L/B ratio 0.80 and Case-03: L/B ratio 0.95). These structures are designed within reasonable drift limits and analyzed for probability of occurrence of the most unfavorable effect resulting from the combination of different loads. The effect of same loading on different span lengths are compared with each other. The effects of four Earthquakes of different magnitudes: Imperial Valley 1940 (Magnitude-6.95), Imperial Valley 06 (6.53), Imperial Valley 07 (5.01) and Imperial Valley 08 (5.62) – on the same structure are determined by Time History Analysis and results are compared with each other. This paper highlights on the variations observed in Column Bending Moment, Column Shear Force and Joint Displacements due to Static and Time history analysis. From the analysis, it is found that Maximum Moment for dynamic analysis is 245% of the Maximum Static Moment, Maximum Shear for dynamic analysis is 167% of the Maximum Static Shear and Maximum Joint Displacement for dynamic analysis is 255% of the Maximum Static Joint Displacement.

Keywords: Static Analysis; time history analysis; column bending moment; column shear force; joint displacement

### INTRODUCTION

Earthquake forces are random in nature and unpredictable, the engineering tools need to be sharpened for analyzing structures under the action of these forces. Earthquake loads are required to be carefully modeled so as to assess the real behavior of structure with a clear understanding that damage is expected but it should be regulated. Various simplified nonlinear analysis procedures and approximate methods to estimate maximum inelastic displacement demand of structures are proposed in the literature. Within this framework, two analysis tools are currently offered with different levels of complexity and of required computational effort, nonlinear static analysis (Pushover) and nonlinear dynamic analysis (Time-history).

A full time history analysis will give the response of a structure over time during the application of dynamic loading. Time history analyses are required to define the real seismic response of structures, especially for irregular, highly ductile, critical or higher modes induced structures.

The main objectives of this paper are-

- Determination of the displacement and ductility demands of a building structure, which may exhibit inelastic behavior during an earthquake.
- Determination of the nonlinear behavior of building structures by utilizing time-history analyses of various deformation levels.

### METHODOLOGY

#### Model Development

The building model considered for this study is a ten-storied building.

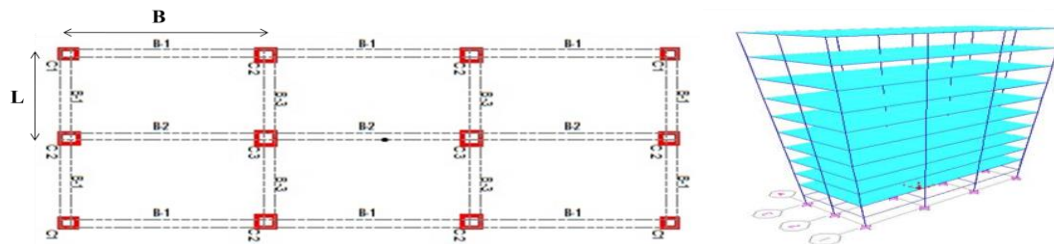


Fig. 1: Plan Layout (Left), 3D view of the structure (Right)

Table 1: Different Span length

Case	Length	Breadth
01. (L/B= 0.60)	12'	20'
02. (L/B= 0.80)	12'	15'
03. (L/B= 0.95)	12'	13'

All structural models consist same beam-column layout; just the spacing between columns varies. All building models of Ordinary Moment Resisting Frame have been developed with Concrete beam, column and 6'' concrete slab. Material properties for all members is 4000 psi and yield stress is 60 ksi. Here fixed support condition has been selected. The effects on the structures are analyzed using SAP2000 V-14 software.

Loads that act on structures can be divided into three general categories. They are:

- Dead load: The dead loads are Floor finish (25 psf), Partition Walls (20 psf), which will act along with the self-weight of the beam, column & slab.
- Live load: Live Load 60 psf has been used according to the BNBC.
- Lateral load: Two types of lateral loads are considered – Wind Load and Earthquake Load.

These loads are applied using ten different combinations according to BNBC. These combinations are:

- |   |  |
|---|--|
| i) 1.4 DL + 1.7 LL                            | vi) 1.05DL + 1.275 LL + 1.405 EQ <sub>X</sub>  |
| ii) 1.05DL + 1.275 LL + 1.275 W <sub>X</sub>  | vii) 1.05DL + 1.275 LL - 1.405 EQ <sub>X</sub> |
| iii) 1.05DL + 1.275 LL - 1.275 W <sub>X</sub> | viii) 1.05DL + 1.275 LL + 1.405EQ <sub>Y</sub> |
| iv) 1.05DL + 1.275 LL + 1.275 W <sub>Y</sub>  | ix) 1.05DL + 1.275 LL - 1.405EQ <sub>Y</sub>   |
| v) 1.05DL + 1.275 LL - 1.275 W <sub>Y</sub>   | x) ENVELOPE                                    |

In this study, we have also used four different earthquake data. They are:

- Imperial Valley 1940 of Magnitude 6.95
- Imperial Valley 06 of Magnitude 6.53
- Imperial Valley 08 of Magnitude 5.62
- Imperial Valley 07 of Magnitude 5.01

## RESULT AND DISCUSSION

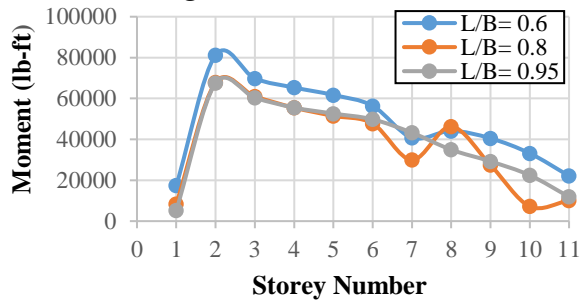
Variations are observed on the effects of same parameters such as Column Bending Moment, Column Shear Force and Joint Displacements.

### Static Analysis

Different structures are analyzed with the same arrangements of beams and columns, but with three different L/B ratios of 0.6, 0.80 and 0.95. In case of static loading the structures are analyzed for probability of occurrence of most unfavorable effects resulting from different load combinations provided by BNBC. Effects of the same type of loading on different spans are described below:



### Column Bending Moment



### Column Shear Force

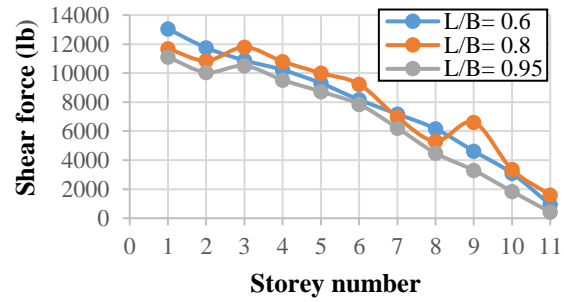


Fig. 2: Moment distribution and Shear force distribution of Column C1 along different story levels

For Column C1 the maximum moment 81155.85 lb-ft is obtained at Ground Floor of the structure with L/B ratio 0.6 and minimum moment 5234.15 lb-ft is obtained at Base Level with L/B ratio 0.95. For Column C1 the maximum shear 13047.7 lb is obtained at Base level of the structure with L/B ratio 0.6 and minimum shear 422.57 lb is obtained at Roof Level with L/B ratio 0.95

### Joint Displacement due to Static Loading (Wind-X and Wind-Y)

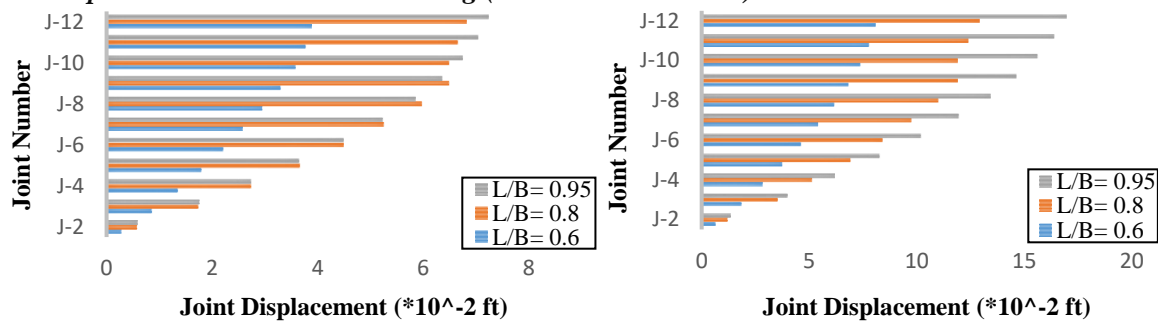


Fig. 3: Joint Displacement due to Static Loading Wind-X (Left) and Wind-Y (Right)

For Wind-X and Wind-Y the maximum joint displacement  $7.24 \times 10^{-2}$  ft is observed at joint-12 and  $16.97 \times 10^{-2}$  ft is observed at joint-12 of the structure with L/B ratio 0.95. Again, minimum joint displacement  $0.28 \times 10^{-2}$  ft is observed at joint-02 and 0.64 ft. at joint-02 with L/B ratio 0.6.

### Joint Displacement due to Static Loading (EQ-X and EQ- Y)

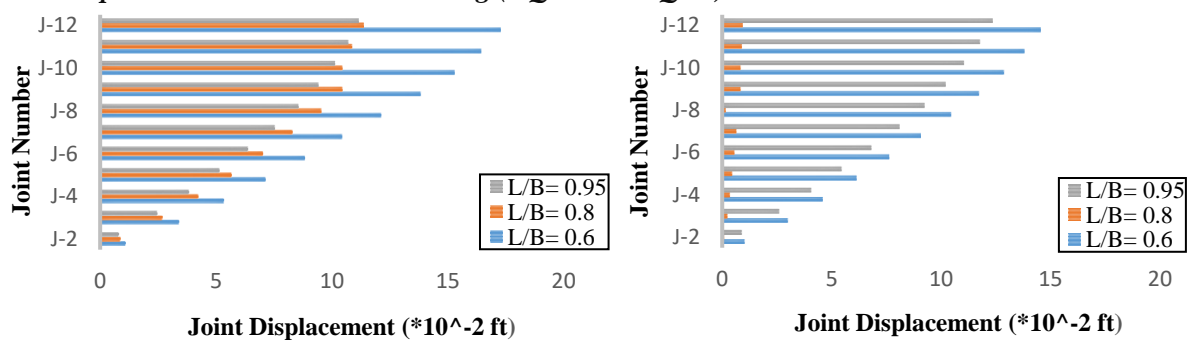


Fig. 4: Joint Displacement due to Static Loading Earthquake-X (Left) and Earthquake-Y (Right)

For Earthquake-X and Earthquake-Y the maximum joint displacement  $17.28 \times 10^{-2}$  ft is observed at joint-12 and  $14.56 \times 10^{-2}$  ft is observed at joint-12 of the structure with L/B ratio 0.60. Again, minimum joint displacement is  $0.82 \times 10^{-2}$  ft is observed at joint-02 with L/B ratio 0.95 and  $0.08 \times 10^{-2}$  ft. is observed at joint-02 with L/B ratio 0.80.

### Time History Analysis

Time history analysis is a step by step analysis of the dynamic response of a structure to a specified loading that may vary with time. The dynamic time history analysis is used to determine the dynamic

response of a structure through the direct numerical integration of the dynamic equilibrium equations. Here the dynamic time history analysis is done to analyze parameters like Column Bending Moment, Column Shear force and Joint displacement. Two types of comparisons are shown here:

### Comparison of Effects of Different Span Length

In this study different structures are analyzed with the same arrangements of beams and columns, but with three different Length/Breadth (L/B) ratios of 0.6, 0.80 and 0.95. Time History Analysis is done only for Earthquake data 'Imperial Valley 1940' of magnitude 6.93 for different L/B ratios of 0.6, 0.80 and 0.95 .

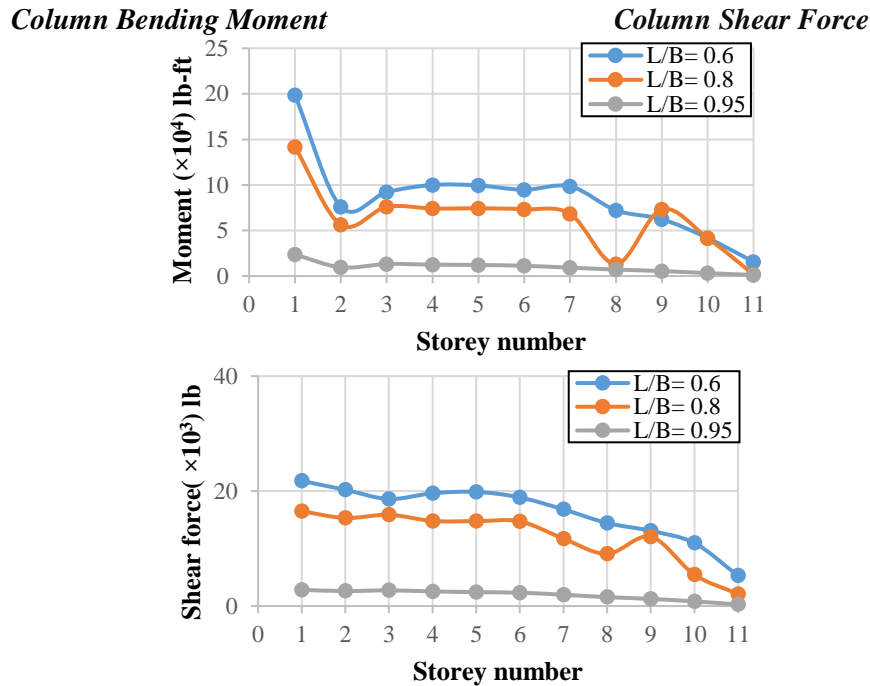


Fig. 5: Moment distribution and Shear force distribution of Column C1 along different story levels

For Column C1 the maximum moment  $19.86 \times 10^4$  lb-ft is obtained at Base level of the structure with L/B ratio 0.6 and minimum moment  $0.12 \times 10^4$  lb-ft is obtained at Roof Level with L/B ratio 0.95. For Column C1 the maximum Shear  $21.78 \times 10^3$  lb is obtained at Base level of the structure with L/B ratio 0.6 and minimum Shear  $0.28 \times 10^3$  lb is obtained at Roof Level with L/B ratio 0.95

### Joint Displacement due to Dynamic loading

Joint displacement due to Dynamic Loading (Earthquake data of Imperial Valley 1940 of magnitude 6.93) along the X - direction at different elevations (from Joint-02 to Joint-12) is shown below:

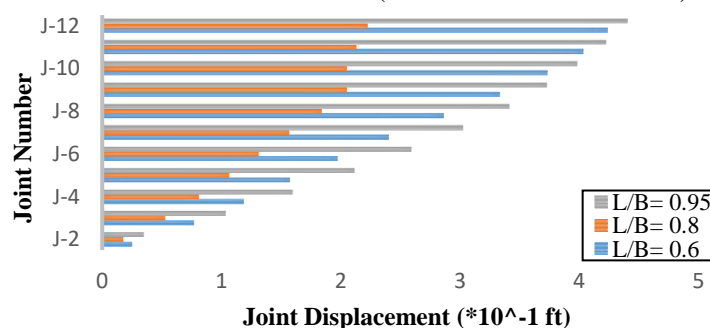


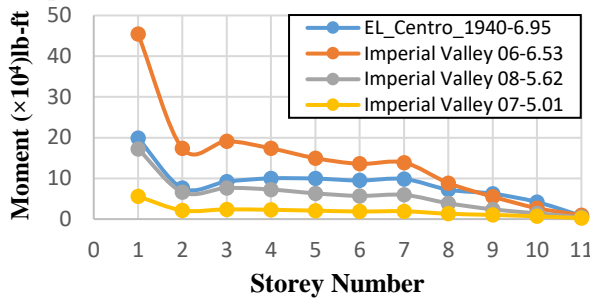
Fig. 6: Joint Displacement due to Dynamic Loading

Maximum joint displacement  $4.405 \times 10^{-1}$  ft is observed at Joint-12 of the structure with L/B ratio 0.95. Again, minimum joint displacement is observed at joint-02 with L/B ratio 0.80, the value of which is  $0.1752 \times 10^{-1}$  ft.

### Comparison of the Effects of Four Different Earthquakes

The effects of four earthquakes are compared for the same structure of L/B ratio 0.6. Comparisons are done for Column Bending Moment and Column Shear Force by Time History analysis using SAP.

#### Comparison for Column Bending Moment



#### Comparison for Column Shear Force

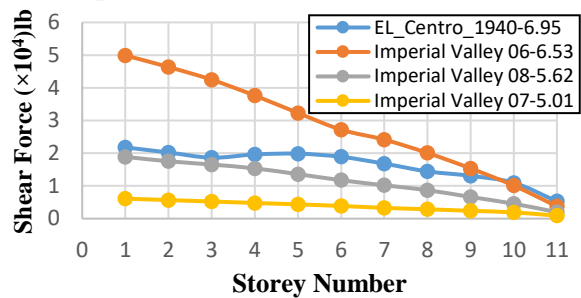


Fig. 7: Moment distribution and Shear Force distribution of Column C1 along different story levels

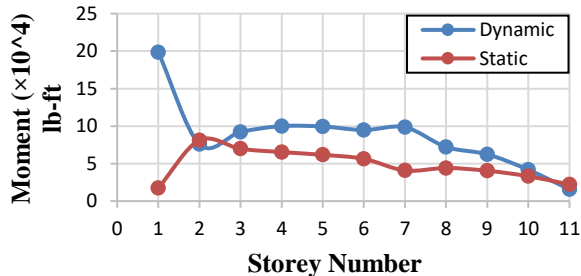
For Column C1 maximum moment  $45.43 \times 10^4$  lb-ft at Base Level of the structure for earthquake Imperial Valley 06 (magnitude 6.53) and minimum moment  $0.24 \times 10^4$  lb-ft and  $0.91 \times 10^4$  lb-ft is obtained at Roof Level for earthquake Imperial Valley 07 (magnitude 5.01)

For Column C1 maximum shear  $4.989 \times 10^4$  lbs. is obtained at Base Level of the structure for earthquake Imperial Valley 06 (magnitude 6.53) and minimum shear  $0.09 \times 10^4$  lbs. is obtained at Roof level for earthquake Imperial Valley 07 (magnitude 5.01).

#### Comparison between Static and Dynamic (Time History Analysis)

Two types of analysis have done here. Static for different load cases and dynamic time history analysis for Earthquake Data 'Imperial Valley 1940' (magnitude 6.95). Variations are observed on the effects of same parameters such as Column Bending moment, Column Shear force and joint displacements.

#### Variation in Column Bending Moment



#### Variation in Column Shear Force

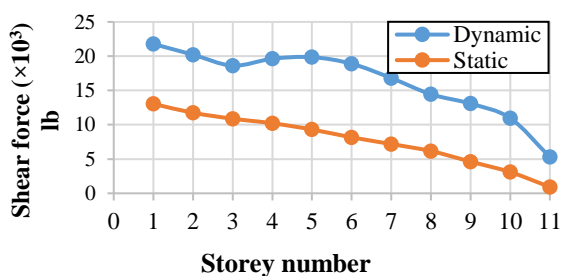


Fig. 8: Variation in Column Bending Moment for (C1), Variation in Column Shear Force for (C1)

Here it is observed that for dynamic analysis the value of moment ( $19.46 \times 10^4$  lb-ft/ft) at base level is maximum, for static analysis at the same level we get the minimum moment value ( $1.74 \times 10^4$  lb-ft). From the Column shear force graph we can see that the values of Column Shear Force for C1 are higher in dynamic analysis whereas that is lower for static analysis.

#### Variation in Joint Displacement

For Joint Displacement variation in the result obtained from static (Wind-X, Wind-Y, EQ-X and EQ-Y) and dynamic analysis is shown below:

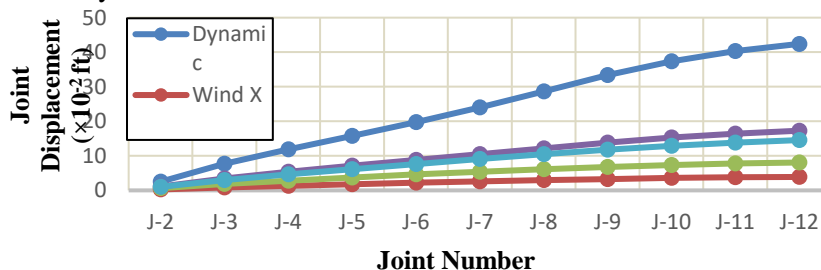


Fig. 9: Variation in Joint Displacement for static and dynamic analysis

The above curves show the variation of joint displacement due to static and dynamic loadings. Due to dynamic loading joint displacement is much higher than that of any static loadings (Wind-X, Wind-Y, EQ-X, and EQ-Y).

## CONCLUSION

In this study structures with different span lengths are modeled to attain adequate stiffness against lateral loading and designed within reasonable drift limits and according to other safety parameters. The outcomes of this study are discussed below:

### ***Variation due to different Span Length***

- 1) For same plan layout, values of Bending Moments (BM) of Columns decrease with increasing span length.
- 2) The variation of Column Shear Force (SF) is similar to the variation of Bending Moments of Columns. Shear Force in Columns also decreases with increasing span length.
- 3) Joint Displacement increases with the increasing elevation of the joint from ground level.

### ***Variation due to four different Magnitudes***

- 1) Column Bending Moment and Column Shear Force each increases with the increasing magnitude of earthquake data.
- 2) Column Bending Moment and Shear Force decreases and joint displacement increases with the increasing elevation above ground level.
- 3) We also observe an exception. For Imperial Valley 06 each parameter shows considerably higher values, though its magnitude is smaller (i.e. 6.53) than that of Imperial Valley 1940 (6.95).

### ***Variation due to Static and Dynamic Analysis***

- 1) ***Column Bending Moment*** - Maximum moment for dynamic analysis is  $19.86 \times 10^4$  lb-ft at Base Level of Column C1 for L/B=0.60 which is 245% or 2.45 times of the Maximum Static Moment (81155.85 lb-ft at the Ground Level of Column C1 for L/B=0.60)
- 2) ***Column Shear Force*** - Maximum shear for dynamic analysis is  $21.78 \times 10^3$  lb at Base Level of Column C1 for L/B=0.60 which is 167% or 1.67 times of the Maximum Static Shear (13047.7 lb at Base Level of Column C1 for L/B=0.60).
- 3) ***Joint Displacement*** - Maximum Joint Displacement for Dynamic Analysis is  $4.41 \times 10^{-1}$  ft at Joint-12 for L/B=0.95 which is 255% or 2.55 times of the Maximum Static Joint Displacement ( $17.28 \times 10^{-2}$  ft at Joint-12 for L/B=0.60 due to EQ-X).

## REFERENCES

- Atkinson, GM. 2009. Earthquake time histories compatible with the 2005 National Building Code of Canada uniform hazard spectrum. *Canadian Journal of Civil Engineering*, 36: 991-1000.
- Izmir, Dokuz Eylul University, Turkey "A Comparative Study on Nonlinear Static and Dynamic Analysis of RC Frame Structures."
- Lew, M; Naeim, F. 2008. Challenges in specifying ground motions for design of tall buildings in high seismic regions of the United States. *Proceedings of the 14th World Conference on Earthquake Engineering*, Beijing, China.
- Malaga-Qhuquitaype, C; Bommer, J; Pinho, R and Stafford, P. et al. 2008. Selection and scaling of ground-motion records for nonlinear response-history analysis based on equivalent SDOF systems. *Proceedings of the 14th World Conference on Earthquake Engineering*, on CD-ROM, Beijing, China.
- Naeim, F and Lew Marshall. 1995. On the use of design spectrum compatible time histories. *Earthquake Spectra*, 11(1): 111-127.

## **SEISMIC VULNERABILITY ASSESSMENT OF EXISTING RCC BUILDINGS IN CHITTAGONG CITY: A CASE STUDY OF 8 NO. SHULAKBAHAR WARD**

A. Barua\*, S. Chakraborty, R. A. Adnan, M. A. Islam & M. A. Hasan

*Department of Civil Engineering, Southern University Bangladesh, Chittagong, Bangladesh*

*\*Corresponding Author: anirbanbarua4@gmail.com*

### **ABSTRACT**

Chittagong is the largest port city and commercial capital of Bangladesh which has many development activities as like of planned residential areas, but over the last 30 years the unchecked development in Chittagong has been resulted in little resilience to earthquake. So now-a-days it is very important to identify buildings that are high vulnerable. This paper represents the seismic vulnerability of RCC buildings of 8 no. Shulakbahar ward, Chittagong by using Turkish method based on a number of structural parameters like soft story, pounding effects, apparent quality etc. at level-I survey and two parameters like redundancy and strength index are also calculated at level-II survey that determined on the basis of engineering knowledge and observation. In this method, the discriminate scores obtained from two discriminate functions are combined in an optimal way to classify existing buildings as “safe”; “unsafe”; “moderate” from level-I survey and those moderate group buildings are further analyzed in Level-II survey and obtained the high risk and low risk group, moderate risk group.

Keywords: Turkish method; soft story index; pounding effect; stiffness index; strength index

### **INTRODUCTION**

Earthquake is caused due to tectonic movements in the earth's crust. Earthquake is also occurred away from plate boundaries at weaknesses in the earth's crust known as faults. In case of Bangladesh which is possibly one of the country's most vulnerable to potential earthquake threat and damage because the location of Bangladesh close to the boundary of two active plates: the Indian plate in the west and the Eurasian plate in the east and north. For this reason the country (e.g. Chittagong) is always under a potential threat to earthquake at any magnitude at any time, which might cause catastrophic death tolls in less than a minute. In the basic seismic zoning map of Bangladesh, Chittagong region has been laid under Zone II, has seismic coefficient of 0.15, which means this area (Chittagong) under the high risk of earthquake. According to Global Hazard Assessment Program (GSHAP), the most hazardous division in Bangladesh is the Port City Chittagong. About 80-90 percent of buildings and physical infrastructures in Chittagong are vulnerable to future massive earthquake measuring 6-7 magnitudes on the RS, as most of these were not designed to withstand against seismic load. Hilly terrain of this city corporation area may create huge land slide during a heavy earthquake. Now evaluation of the seismic resistance and the assessment of possible damage are quite imperative in order to take preventive measures and reduce the potential damage to civil engineering structures and loss of human lives during possible future earthquakes.

The objective of this study is to compile a database of R.C.C. buildings to make a vulnerability analysis of those structures of the selected area in 8 No. Shulakbahar ward, to classify the buildings into seismically safe or unsafe as well as to identify the buildings that are highly vulnerable.

### **OBSERVED AREA**

The study area is Shulokbahar R/C/A at ward no.8 of Chittagong City Corporation situated on the bank of Karnaphuli River.



Fig. 1: Study Area Shulakbahar Ward

## METHODOLOGY

There are several methods to determine seismic risk assessment such as FEMA 154 (1988), FEMA 310 (1998), EURO CODE 8, NewZeland Guideline, Modified Turkish Method, NRC guideline, IITK-GSDM method, Japan method. All the methodologies have common objective to determine the risk of building due to earthquake. Among these Turkish Method of simple survey procedure is adopted for this case study for the study area of 8 No Shulakbahar ward.

## TURKISH METHOD

In recent times, after the 1999 earthquake in the cities of Kocaeli and Duzce, Government of Turkey and Japan International Cooperation Agency (JICA) came forward for implementing a regional seismic assessment and rehabilitation program. Researchers from various universities were involved in this program supported by the Government of Turkey and JICA. In this method a simple two-level Seismic Assessment Procedure for a building stock was proposed (Sucuoglu and Yazgan 2003). In this most vulnerable buildings that may undergo severe damage in a future earthquake are identified. The first level (Level - I) is known as “Walk Down Evaluation”. This simple level does not require any analysis. In this level the street survey procedure based on simple structural and geotechnical parameters that can be observed easily from the sidewalk. In second level (Level - II), the observers enter the basement and ground stories of the buildings for collecting the simplest structural data.

### *Level – I: (The Walk Down Evaluation procedure)*

In this level of observation some structural parameters that have been observed during the field surveys and selected for representing building vulnerability are given below.

### *Survey Parameters*

- (a) Number of Stories [Up to seven stories]: This is the total number of floors above the ground level.
- (b) Existence of a soft Storey [Yes or No]: A soft storey usually exists in a building when one particular storey, usually employed as a commercial space, has less stiffness and strength compared to the other stories.
- (c) Existence of heavy Overhangs [Yes or No]: Heavy balconies and overhanging floors in multistory RC buildings shift the mass center upwards; accordingly give rise to increased seismic lateral forces and overturning moments during earthquakes.
- (d) Apparent Building Quality [Good, Moderate or Poor]: A close relationship has been observed between apparent quality and experienced damage during recent earthquakes in Turkey.
- (e) Existence of short Columns [Yes or No]: Frames with partial infill’s lead to the formation of short columns which sustain heavy damage since they are not designed for the high shear forces due to shortened heights that will result from a strong earthquake.
- (f) Pounding Effect [Yes or No]: When there is no sufficient clearance between adjacent buildings, they pound each other during an earthquake as a result of different vibration periods. Uneven floor levels aggravate the effect of pounding.
- (g) Topographic Effects [Yes or No]: Buildings on slopes steeper than 30 degrees have stepped foundations, which cannot distribute ground distortions evenly to structural members above.

(h) Local Soil Conditions [Stiff or Soft]: The intensity of ground motion at a particular site predominantly depends on the distance the causative fault and local soil conditions. As there exists a strong correlation between PGV and the shear wave velocities of local soils (Wald 1999), in this study the PGV is selected as to represent the ground motion intensity. The PGV map in the JICA (2002) report has contour increments of 20 cm/s<sup>2</sup>. The intensity zones in Istanbul are expressed accordingly, in terms of the associated PGV ranges.

Zone I : 60<PGV<80 cm/s<sup>2</sup>

Zone II : 40<PGV<60 cm/s<sup>2</sup>

Zone III: 20<PGV<40 cm/s<sup>2</sup>

Based on their number of stories and the seismic hazard level at the site buildings are assigned different base scores as shown in Table given below.

Table 1: Base scores and vulnerability scores for concrete buildings, (Sucuoglu et al., 2003)

No. of Stories	Base Scores(BS)			Vulnerability Scores(VS)					
	Zone I	Zone II	Zone III	Soft Story	Heavy Overhang	Apparent Quality	Short Column	Pounding	Topographic Effects
1 or 2	100	130	150	0	-5	-5	-5	0	0
3	90	120	140	-15	-10	-10	-5	-2	0
4	75	100	120	-20	-10	-10	-5	-3	-2
5	65	85	100	-25	-15	-15	-5	-3	-2
6 or 7	60	80	90	-30	-15	-15	-5	-3	-2

### Building Seismic Performance

The vulnerability parameters of a building are obtained from walk down surveys and its location is determined, the seismic performance score PS can be calculated by the following equation:

$PS = (BS) - \sum (VSM) \times (VS)$ ; Where, *BS* is the Base Score (Defined in Table 1),  $\sum (VSM)$  is the Summation of Vulnerability Score Multiple (Defined in Table 2), *VS* is the Vulnerability Scores (Defined in Table 1)

Table 2: Vulnerability Parameters, (*VSM*)

Soft storey	Does not exist = 0, Exist = 1
Heavy overhangs	Does not exist = 0, Exist = 1
Apparent quality	Good = 0, Moderate = 1, Poor =2
Short columns	Does not exist = 0, Exist = 1
Pounding effect	Does not exist = 0, Exist = 1
Topographic effects	Does not exist = 0, Exist = 1

### Level - II (Preliminary Assessment)

Yucemen et al. 2004, Ozcebe et al. (2003) and Yakut et al. (2003) employed the discriminant analysis technique to develop a preliminary evaluation methodology for assessing seismic vulnerability of existing low- to medium-rise RC buildings in Turkey. The procedure is applicable to RC frames and frame-wall structures, having the stories up to seven. The main objective of the procedure is to find the buildings that are highly vulnerable to damage.

Definition of the discriminating parameters and the procedure to be followed are introduced below:

Table 3: Variation of LSCVR and IOCVR values with number of stories

n	LSCVR	IOCVR
3 or less	0.383	-0.425
4	0.430	-0.609
5	0.495	-0.001
6	1.265	0.889
7	1.791	1.551

Table 4: Variation of CMC values with soil type and distance to fault

Soil Type	Shear Wave Velocity (m/s)	Distance to Fault (km)				
		0-4	5-8	9-15	16-25	>26
B	>760	0.778	0.824	0.928	1.128	1.538
C	360-760	0.864	1.000	1.240	1.642	2.414
D	180-360	0.970	1.180	1.530	2.099	3.177
E	<180	1.082	1.360	1.810	2.534	3.900

By comparing the CV values with associated DI value calculate performance grouping of the building for life safety performance classification (LSPC) and immediate occupancy performance classification (IOPC) as follows:

If  $DI_{LS} > CV_{LS}$  take  $PG_{LS}=1$

If  $DI_{LS} < CV_{LS}$  take  $PG_{LS}=0$

If  $DI_{IO} > CV_{IO}$  take  $PG_{IO}=1$

If  $DI_{IO} < CV_{IO}$  take  $PG_{IO}=0$

## RESULTS & DISCUSSIONS

After analyzing data, among 500 buildings 191 buildings are unsafe, 215 buildings are safe and 94 buildings are moderate category that is shown in Fig. 2.

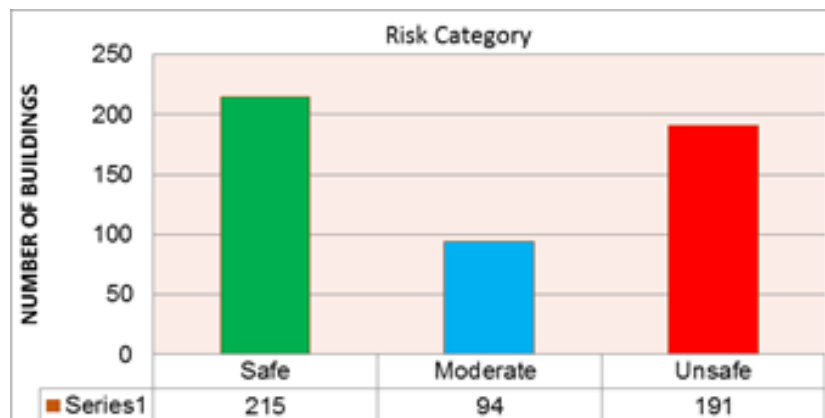


Fig. 2: Number of vulnerable buildings

The study can be summarized as follows:

- The vulnerability factor which is the most severe in study area recognized with soft story in 41.2% and heavy overhanging in 24% building found at level I survey. In case of level II survey 50% buildings have soft storey problem and 26% found heavy overhanging problem.
- The moderate apparent quality of the buildings is ensured by 55% and 12% in level I and II survey respectively. About 14.4% buildings have poor apparent quality found at level II survey.
- From the Level I survey results, the pounding and topographic effects of the buildings covered maximum percentage 6% and 8% respectively. In case of Level II survey these effects were found for 12% and 8% building respectively.
- The redundancy and strength index at level II survey were found in case of 28% and 8% buildings respectively.

## CONCLUSION

- 1) This study mainly targets to attract the interest on the present situation of Chittagong earthquake by seismic vulnerability assessment based on Turkish method.
- 2) The results of the first level and the second level investigations indicated that, in general consistent results, which further indicated that walk down survey provides a realistic priority ordering for the second level investigations.
- 3) Some buildings, which were assigned moderate at the end of first level, may be ranked in the high seismic risk group buildings by the second level survey.



## REFERENCES

- Ahmed, MA; Saha, AR and Dhar, AS. 2008. *Earthquake Vulnerability Assessment of Cox's Bazar District*. Dhaka: Ministry of Food and Disaster Management
- Ahmed, MM. 2013. *Seismic Vulnerability Assessment of Building and Application of HYDE-System for Retrofitting*. M.Sc. thesis, Chittagong University of Engineering & Technology; Chittagong, Bangladesh
- BNBC 1993. Bangladesh National Building code, Housing and Building Research Institute, Mirpur, Dhaka, Bangladesh
- BNBC 2006. Bangladesh National Building code, Housing and Building Research Institute, Mirpur, Dhaka, Bangladesh
- CDMP. 2009. *Seismic Hazard & Vulnerability Assessment of Dhaka, Chittagong & Sylhet City Corporations*. Comprehensive Disaster Management Programme, Bangladesh.
- GSHAP. 1992. World Seismic Map. Global Seismic Hazard Assessment Programme. [seismo.ethz.ch/GSHAP](http://seismo.ethz.ch/GSHAP)
- Gulkan, P and Sozen, MA. 1999. Procedure for Determining Seismic Vulnerability of Building Structures. *ACI Structural Journal*, 96(3): 336-342.
- Sucuoglu, H and Yazgan, U. 2003. Simple Survey Procedures for Seismic Risk Assessment in: Urban Building Stocks. *Seismic Assessment and Rehabilitation of Existing Buildings*, NATO Science Series IV/29, pp. 97-118.

## **AN EXACT SOLUTION OF POST-BUCKLED NONLINEAR BEAM ON AN ELASTIC FOUNDATION**

M. M. Rana\* & A. S. M. Z. Hasan

*Department of Civil Engineering, Rajshahi University of Engineering and Technology, Rajshahi, Bangladesh*

*\*Corresponding Author: masud.ce08@gmail.com*

### **ABSTRACT**

This paper is concerned with buckling problem of flexible beams on an elastic foundation for free vibration. An exact solution for the post-buckled geometric nonlinear beam with clamped-clamped and clamped-hinged end conditions are presented in this paper. The cubic nonlinearity of the governing equation of motion is induced due to the mid-plane stretching, which is considered in the analysis. The critical buckling load, associated mode shape, the effect of foundation stiffness, and vibration behavior are obtained. The optimum locations of an internal hinge and the optimum buckling force are also investigated for various foundation stiffness of the nonlinear beam on an elastic foundation.

Key words: Buckling; exact solution; hinge; free vibration; nonlinear beam

### **INTRODUCTION**

Buckling is a static instability of structures due to in-plane loading and solving the nonlinear buckling problem for a given axial load results in the post buckling configurations [Nayfeh and Emam 2008]. A plenty of research has been carried out on the subject of buckled beam [Fang and Wickert 1994, Nayfeh et al. 1995, Addessi et al. 2005, Zhang et al. 2005, Li and Batra 2007, Emam and Nayfeh 2009, Xia et al. 2010], plates [Chen 1994, Librescu and Lin 1997] and rods [Whiting 1997, Wang 1997, Li et al. 2002] for many years. Among them, Nayfeh et al [1995] and Chen [1994] were formulated the static buckled configurations to obtain buckled shapes and their associated natural frequencies with the fixed and simply supported post-buckled beams. The governing equations of the nonlinear buckled beams were induced a geometric nonlinearity in the most of the researches. The geometric nonlinearity is due to the mid-plane stretching, which is taken into account in the present study. Fang and Wickert [1994] studied the static deformation of micro-machined beams under prescribed in-plane compressive stress by analytical and experimental means based on geometrically nonlinear imperfect beam. Addessi et al. [2005] investigated free un-damped in-plane vibrations of shear undeformable beams around their highly buckled configuration neglecting rotary inertia effects. Zhang et al. [2005] investigated the secondary bifurcations and tertiary states of a beam resting on nonlinear foundation. They used a three mode Galerkin discretization to produce a set of nonlinear algebraic equilibrium equations and then the algebraic equations were solved by numerically using the root solving and pseudo-arch-length method.

In the recent years, Li and Batra [2007] studied the buckling and the post buckling deformation of uniformly heated pinned-pinned and fixed-fixed Euler-Bernoulli beams supported on linear elastic foundations. They used the shooting method to compute the buckling modes and transitions among them by solving analytically the linear problem. Recently, Xia et al. [2010] investigated the static bending, post buckling and free vibration of nonlinear micro-beams. This study established a nonlinear non-classical Euler-Bernoulli beam model for micro-scale beam by using the modified couple stress theory.

Buckling of column/beam is basic in elastic stability. In some cases beam may have to provide interior joints or internal hinge. The internal hinge may be necessary in designs to facilitate the opening of doors and hatches or other swivel motions. Previously, the buckling force and optimum hinge location on fundamental frequency had been investigated on beams [Wang and Wang 2001, Lee et al. 2003, Cheng et al. 2003] and plates [Xiang et al. 2001, 2003, Gupta and Reddy 2002]. Also, exact vibration solutions of structural members were summarized by Wang et al. [2005]. In the

recent years, buckling of column [Wang 2008] and an infinite beam [Wang 2010] with the internal hinge attached to an elastic foundation have been investigated. Most the works available in the literature for determination of internal hinge location of a beam are the linear vibration problem except Cheng et al. [2003] is a nonlinear random response. Nonlinear vibration of buckling problems of beam with an internal hinge is rare in the literature. The aim of the present study is to determine the optimum location of internal hinge and critical buckling forces at various foundation stiffness of nonlinear beam for clamped-clamped (C – C) and clamped-hinged (C – H).

In this study, an exact solution of the governing differential equation is presented. The geometric nonlinearity is governed due to the mid-plane stretching of the beam; as a result the governing equation is formulated with a cubic nonlinearity. Two types of end conditions of the geometric nonlinear beam such as C – C and C – H on an elastic foundation are taken into account for the analysis of the buckling problem. Exact vibration solutions for internal hinge locations and optimum buckling force corresponding to various foundations stiffness are also investigated for C – C and C – H nonlinear post-buckled beam on an elastic foundation.

### THEORY

The governing equation of motion of nonlinear vibration of the Euler-Bernoulli beam on elastic foundation including the effect of mid-plane stretching [Barari et al. 2011] is as follows

$$EI\hat{W}'''' + m\hat{W}\dot{\hat{W}} + \xi\hat{W}\dot{\hat{W}} + \hat{F}\hat{W}'' + \hat{K}_f\hat{W} - \left(\frac{EA}{2L} \int_0^L (W')^2 dx\right) \hat{W}'' = \hat{P}\cos(\hat{\Omega}\hat{t}) \quad (1)$$

Where, the prime indicates the derivative with respect to  $\hat{x}$ , over dot indicates the derivative with respect to  $\hat{t}$  and  $\hat{W}$  denotes the transverse displacement by the mid-plane stretching of the beam on elastic foundation. The  $m$  is the mass per unit unreformed length, cross section area  $A$ , moment of inertia  $I$ , length of the beam  $L$ , Young's modulus of the beam  $E$ , damping coefficient of the beam  $\xi$ , foundation coefficient of modulus  $K_f$ , axial force acting on the beam  $\hat{F}$ , excitation amplitude  $\hat{P}$ , excitation frequency  $\hat{\Omega}$ . For the convenience, the following non-dimensional variables are used

$$x = \frac{\hat{x}}{L}, W = \frac{\hat{W}}{r}, t = \hat{t} \sqrt{\frac{EI}{mL^4}}, F = \frac{\hat{F}L^2}{EI}, \xi = \frac{\xi L^2}{\sqrt{mEI}}, r = \sqrt{\frac{I}{A}}, K_f = \frac{K_f L^4}{EI}, \text{ and } P = \frac{\hat{P}L^4}{rEI} \quad (2)$$

Where,  $r$  is the radius of gyration of the cross section of the beam, therefore, equation (1) can be written as

$$W'''' + \dot{W} + \xi\dot{W} + FW'' + K_f W - \frac{1}{2}W'' \int_0^L (W')^2 dx = P\sin(\Omega t) \quad (3)$$

The associated boundary conditions for C – C and C - H beam is as follows:

$$W = 0 \text{ and } W' = 0 \text{ at } x = 0, L \quad (4)$$

$$W = 0 \text{ and } W' = 0 \text{ at } x = 0 \quad (5a)$$

$$W = 0 \text{ and } W'' = 0 \text{ at } x = L \quad (5b)$$

### BUCKLING FORMULATION

Consider the time dependent, damping factor and force terms are zero, the buckling problem can be obtained from Eq. (3) is as follow

$$W''''(x) + FW''(x) + K_f W(x) - \frac{1}{2}W''(x) \int_0^L (W'(x))^2 dx = 0 \quad (6)$$

#### Exact Solution

The integral is constant [Nayfeh and Emam 2008] in Eq. (6) for given  $W(x)$ . So, consider  $Q$  denotes this constant

$$Q = \frac{1}{2} \int_0^L (W')^2 dx \quad (7)$$

Substituting Eq.(7) into Eq. (6), the results can be expressed as

$$W'''' + \lambda W'' + K_f W = 0 \quad (8)$$

where  $\lambda = F - Q$  represents the critical buckling load and Eq. (8) is a fourth order ordinary differential equation whose general solution can be expressed into three types [Wang 2008].

Case 1, if  $\lambda^2 > 4K_f$ , the solution can be written

$$W(x) = C_1 \sin(\alpha x) + C_2 \cos(\alpha x) + C_3 \sin(\beta x) + C_4 \cos(\beta x) \quad (9a)$$

$$\text{Where } \alpha = \sqrt{\frac{\lambda - \sqrt{\lambda^2 - 4K_f}}{2}} \quad \text{and} \quad \beta = \sqrt{\frac{\lambda + \sqrt{\lambda^2 - 4K_f}}{2}} \quad (9b)$$

Case 2, if  $\lambda^2 = 4K_f$ , the solution can be written

$$W(x) = C_1 \sin(\alpha x) + C_2 \cos(\alpha x) + x C_3 \sin(\alpha x) + x C_4 \cos(\alpha x) \quad (9c)$$

$$\text{Where } \alpha = \sqrt{\frac{\lambda}{2}} \quad (9d)$$

Case 3, if  $\lambda^2 < 4K_f$ , the solution can be written

$$W(x) = C_1 e^{-\alpha x} \sin(\beta x) + C_2 e^{-\alpha x} \cos(\beta x) + C_3 e^{\alpha x} \sin(\beta x) + C_4 e^{\alpha x} \cos(\beta x) \quad (9e)$$

$$\text{Where } \alpha = (K_f)^{\frac{1}{4}} \cos\left(\frac{\theta}{2}\right), \beta = (K_f)^{\frac{1}{4}} \sin\left(\frac{\theta}{2}\right), \text{ and } \theta = \pi - \tan^{-1}\left(\frac{\sqrt{\lambda^2 - 4K_f}}{\lambda}\right) \quad (9f)$$

In this study, we consider only the case 1,  $\lambda^2 > 4K_f$ , therefore the general solution of the different types of end conditions of the nonlinear beam are as follows:

### C – C beam

Applying the boundary condition of Eq. (4) for clamped-clamped beam, we have

$$C_2 + C_4 = 0 \quad (10)$$

$$\alpha C_1 + \beta C_3 = 0 \quad (11)$$

$$C_1 \sin(\alpha) + C_2 \cos(\alpha) + C_3 \sin(\beta) + C_4 \cos(\beta) = 0 \quad (12)$$

$$\alpha C_1 \cos(\alpha) - \alpha C_2 \sin(\alpha) + \beta C_3 \cos(\beta) - \beta C_4 \sin(\beta) = 0 \quad (13)$$

The determinant of the coefficient matrix of equations (10) – (13) represents the characteristic equation. Therefore, the following characteristic equation can be obtained

$$2\alpha\beta - 2\alpha\beta \cos(\alpha) \cos(\beta) - (\alpha^2 + \beta^2) \sin(\alpha) \sin(\beta) = 0 \quad (14)$$

The Eigen-values are determined by solving the Eq.(14). Now the mode shapes are given by

$$W(x) = d \left[ -\left(\frac{\beta}{\alpha}\right) \sin(\alpha x) - \frac{\alpha \sin(\beta) - \beta \sin(\alpha)}{\alpha(\cos(\alpha) - \cos(\beta))} \cos(\alpha x) + \sin(\beta x) + \frac{\alpha \sin(\beta) - \beta \sin(\alpha)}{\alpha(\cos(\alpha) - \cos(\beta))} \cos(\beta x) \right] \quad (15)$$

Where,  $d$  is a constant to be determined. The expression of mode shapes  $W(x)$  governs both the symmetric and anti-symmetric mode shapes. The buckle configuration  $W(x)$  satisfies the boundary condition as well as the following condition due the mid stretching of the beam.

$$\lambda = F - Q = F - \frac{1}{2} \int_0^L (W')^2 dx \quad (16)$$

Substituting Eq. (15) into Eq. (16), a relationship with the variables  $F$ ,  $K_f$ ,  $d$  and  $\lambda$  are obtained. Therefore, for a given axial load  $F$ , the constant  $d$  corresponding to any  $\lambda$  can be determined, and subsequently, the mode shapes of beam can be obtained by using the Eq. (15)

Simplify the Eq. (14) the symmetric mode is as follows

$$(\alpha + \beta) \sin\left(\frac{\alpha}{2} - \frac{\beta}{2}\right) + (\alpha - \beta) \sin\left(\frac{\alpha}{2} + \frac{\beta}{2}\right) = 0 \quad (17a)$$

$$\tan\left(\frac{\alpha}{2}\right) = \left(\frac{\beta}{\alpha}\right) \tan\left(\frac{\beta}{2}\right) \quad (17b)$$

Simplify the Eq. (14) the anti-symmetric mode is as follows

$$(-\alpha - \beta) \sin\left(\frac{\alpha}{2} - \frac{\beta}{2}\right) + (\alpha - \beta) \sin\left(\frac{\alpha}{2} + \frac{\beta}{2}\right) = 0 \quad (18a)$$

$$\tan\left(\frac{\alpha}{2}\right) = \left(\frac{\alpha}{\beta}\right) \tan\left(\frac{\beta}{2}\right) \quad (18b)$$

### C – H beam

Similarly, satisfying the boundary conditions Eq. (5) the characteristic equation for the clamped-hinged beam can be written as

$$(\alpha^2 - \beta^2)(\alpha \cos(\alpha) \sin(\beta) - \beta \cos(\beta) \sin(\alpha)) = 0 \quad (19)$$

The Eigen-values are determined by solving the Eq. (19). Again the mode shapes yield Eq. (15) and the critical buckling load can be determined after determining the constant  $d$  by using the Eq. (19). The characteristic equations and Eigen-values for various end conditions of beam on elastic foundation are summarized in Table 1.

Table1 The Eigen values for various end conditions of beam on elastic foundation

End conditions of beam	Eigen values when $\beta=0.3$ by using Eqs. (14) and (19) for C – C and C – H beams, respectively
C – C	6.298, 8.971, 12.575, 15.451, 18.858
C – H	4.483, 7.752, 10.889, 14.084, 17.212

## RESULTS AND DISCUSSION

The nonlinear post-buckled vibrations of beam on an elastic foundation are analyzed with C – C and C – H. The results are presented in the following Sections with non-dimensional parameters such as length of the beam, axial force, static deflection and foundation stiffness. Figure 1 shows flexible beam on elastic foundation subjected to the axial load, (a) without internal hinge and (b) with internal hinge.

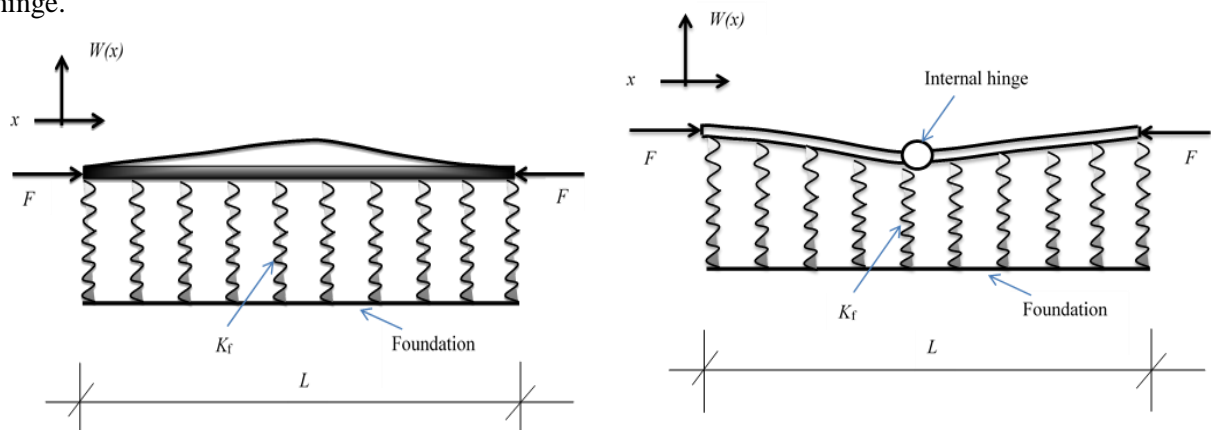


Fig. 1: A flexible beam on elastic foundation subjected to the axial load, (a) without internal hinge and (b) with internal hinge

Fig. 2: illustrates the non-dimensional static deflection with respect to various foundations for C – C and C – H beam. The first two modes bifurcation diagrams for non-dimensional static deflection as a function of non-dimensional foundation stiffness are presented in Figure 2a-b. The non-dimensional static deflections are plotted of the point at  $x = 0.3L$ . As the foundation stiffness decreases from the first critical stiffness at  $K_f = 38.00$  and  $28.76$ , the straight position loses stability and therefore, the buckling is formulated for C – C and C – H beam respectively in Figure 2a-b. The stability analysis is not included in this study.

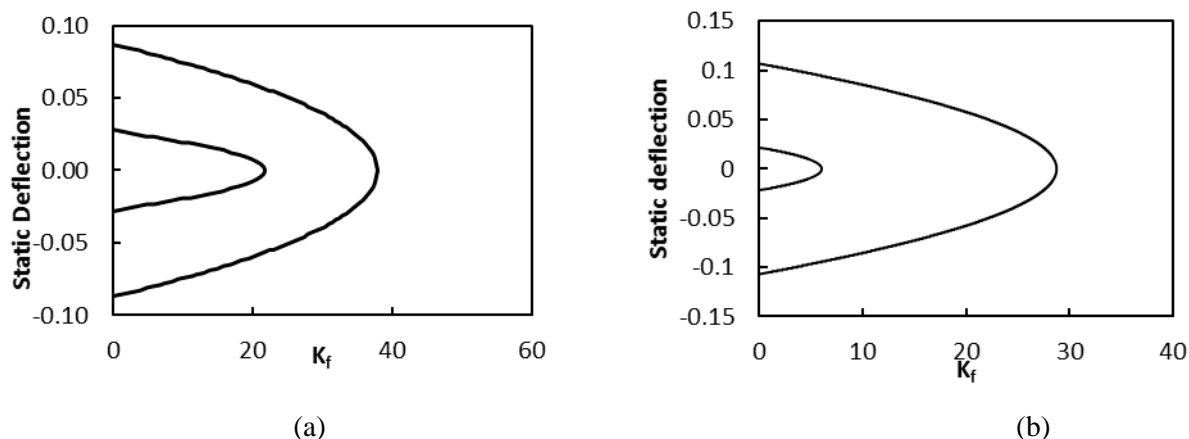


Fig 2 Non-dimensional static deflection corresponding to foundation stiffness of 1<sup>st</sup> and 2<sup>nd</sup> mode (a) C – C beam and (b) C – H beam.

Fig. 3 shows the non-dimensional critical buckling load obtained from exact solution for C – C and C – H beam. The first two modes bifurcation diagrams for non-dimensional deflection as a function of non-dimensional axial force are presented in Figure 3a-b. The non-dimensional static deflections are plotted at  $x = 0.3L$  with the foundation stiffness when  $K_f = 1$ . As the axial load increase from the 1<sup>st</sup> mode critical buckling load at  $F/\pi^2 = 4.105$  and  $2.038$ , the straight position loses stability and thus, the buckling is formulated for C – C and C – H beam in Figure 3a-b. The stability analysis is not included in this study. It can be seen that the critical axial force are increasing with increasing the foundation stiffness in Table 2a-b for C – C and C – H beam respectively.

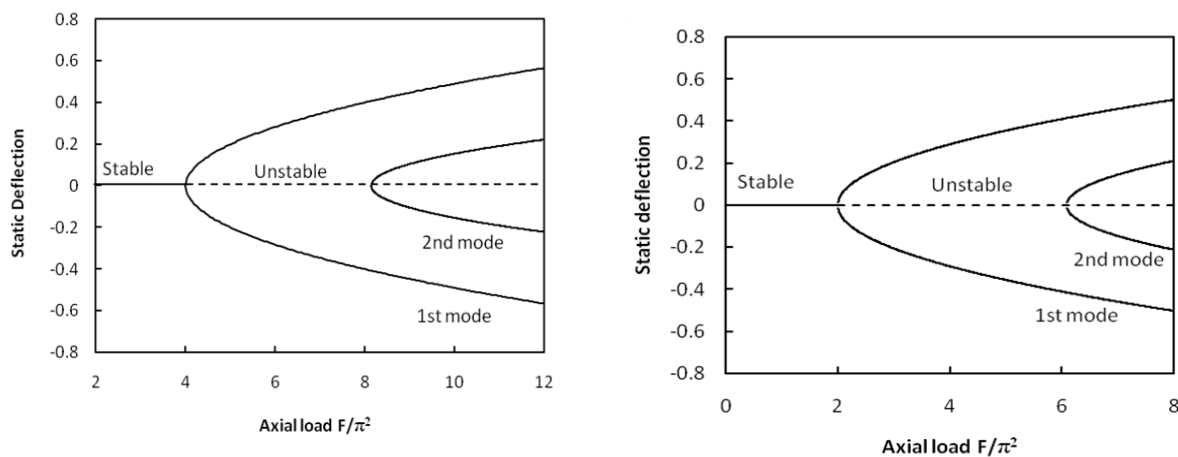


Fig. 3 Non-dimensional static deflection corresponding to axial load of 1<sup>st</sup> and 2<sup>nd</sup> mode (a) C – C beam and (b) C – H beam.

Table 2 a The critical buckling force at various  $K_f$  for C – C beam.

$K_f$	Axial load $\frac{F}{\pi^2}$ at $x = 0.3L$		
	1 <sup>st</sup> mode	2 <sup>nd</sup> mode	3 <sup>rd</sup> mode
1	4.015	8.148	16.014
5	4.035	8.158	16.019
10	4.061	8.170	16.026
15	4.086	8.183	16.032
20	4.112	8.195	16.039

Table 2 bThe critical buckling force at various  $K_f$  for C – H beam.

$K_f$	Axial load $\frac{F}{\pi^2}$ at $x = 0.3L$		
	1 <sup>st</sup> mode	2 <sup>nd</sup> mode	3 <sup>rd</sup> mode
1	2.038	6.083	12.006
5	2.078	6.097	12.013
10	2.127	6.113	12.022
15	2.174	6.130	12.030
20	2.221	6.147	12.039

On the other hand, the phase diagram of C – H beam has a non-closed trajectory and the shape of the curve is more likely kidney shape. The nature of the phase diagram of the C – H beam demonstrates that the nonlinearity dominates in the system of C – H beam on elastic foundation at 1<sup>st</sup> mode vibration. Moreover, the trajectory of the C- H beam originates at the centre of the displacement and velocity; and the trajectory is vertically i.e. velocity axis symmetric. In addition, there is a common or fixed centre of the phase trajectories in the all cases of foundation stiffness for C – H beam.

## CONCLUSIONS

An exact solution is presented to solve the nonlinear vibrations of post-buckled beam on an elastic foundation with C – C and C – H end conditions. The effect of foundation stiffness, critical buckling force and interesting vibration behaviors are investigated. The exact vibration solutions for axially loaded nonlinear beams on an elastic foundation with an internal hinge are obtained. The optimum non-dimensional buckling forces are investigated corresponding to the different foundation stiffness for C – C and C – H beam. The result shows that the foundation stiffness is greatly influenced to the buckling force of the beam with an internal hinge. The result obtained from the bifurcation diagrams and the internal hinge locations are useful for practical application with such kind of axially loaded nonlinear beam on an elastic foundation.

## REFERENCES

- Addressi, A; Lacarbonara, W and Paolone, A. 2005. Free in-plane vibrations of highly buckled beams carrying a lumped mass. *Acta Mechanica*, 180: 133-156.
- Barari, A; Kaliji, HD; Ghadimi, M and Domairry, G. 2011. Non-linear vibration of Euler-Bernoulli beams. *Latin American Journal of Solids and Structures*, 8: 139-148.
- Cheng, GF; Lee, YY and Mei, C. 2003. Nonlinear random response of internally hinged beams. *Finite Elements in Analysis and Design*, 39(5-6): 487-504.
- Emam, SA and Nayfeh, AH. 2009. Post buckling and free vibrations of composite beams. *Composite Structures*, 88: 636-642.
- Fang W and Wickert, JA. 1994. Post buckling of micromachined beams. *J. Miromech. Microeng*, 4: 116-122.
- Gupta, PR and Reddy, JN. 2002. Buckling and vibration of orthotropic plates with an internal line hinge. *International Journal of Structural Stability and Dynamics*, 2(4): 457-486.
- Lee, YY; Wang, CM and Kitipornchai, S. 2003. Vibration of Timoshenko beams with internal hinge. *Journal of Engineering Mechanics*, 129(3): 293-301.
- Li, S; Zhou, YH and Zheng, X. 2002. Thermal postbuckling of a heated elastic rod with pinned-fixed ends. *Journal of Thermal Stresses*, 25: 43-56.
- Li, SR and Batra, RC. 2007. Thermal buckling and post buckling of Euler-Bernoulli beams supported on nonlinear elastic foundations. *AIAA Journal*, 45 (3): 712-720.
- Librescu, L and Lin, W. 1997 Postbuckling and vibration of shear deformable flat and curved panels on a non-linear elastic foundation. *International Journal of Non-linear Mechanics*, 32(2): 211-225.
- Nayfeh, AH and Emam, SA. 2008. Exact solution and stability of post buckling configurations of beams. *Nonlinear Dynvol*, 54: 395-408.

- Nayfeh, AH; Kreider, W and Anderson, TJ. 1995. Investigation of natural frequency and mode shapes of buckled beam. *AIAA Journal*, 33 (6): 1121-1126.
- Xia, W; Wang, L and Yin, L. 2010. Nonlinear non-classical microscale beams: Static bending, postbuckling and free vibration. *International Journal of Engineering Science*, 48: 2044-2053.
- Chen HP. 1994. Free vibration of prebuckled and postbuckled plates with delamination. *Composites Science and Technology*, 51: 451-462.
- Wang, CY. 1997. Post-buckling of a clamped-simply supported elastic. *International Journal of Non-linear Mechanics*, 32(6): 1115-1122.
- Wang, CY and Wang, CM. 2001. Vibration of a beam with an internal hinge. *International Journal of Structural Stability and Dynamics*, 1(1): 163-167.
- Wang, CM; Wang, CY and Reddy, JN. 2005. Exact solutions for buckling of structural members. CRC Series in Computational Mechanics and Applied Analysis.
- Wang, CY. 2008. Optimum location of an internal hinge of a uniform column on an elastic foundation. *Journal of Applied Mechanics*, 75: 034501(1-4).
- Wang, CY. 2010. Buckling of a weakened infinite beam on an elastic foundation. *Journal of Engineering Mechanics*, 136(4): 534-537.
- Whiting, AIM. 1997. A Galerkin procedure for localized buckling of a strut on a nonlinear elastic foundation. *International Journal of Solids and Structures*, 34(6): 727-739.
- Xiang, Y; Wang, CM and Wang, CY. 2001. Buckling of rectangular plates with internal hinge. *International Journal of Structural Stability and Dynamics*, 1(2); 169-179.
- Xiang, Y; Wang, CM; Wang, CY and Su, GH. 2003. Ritz buckling analysis of rectangular plates with internal hinge. *Journal of Engineering Mechanics*, 129(6): 683-688.
- Zhang, Y; Murphy, KD. 2005. Secondary buckling and tertiary states of a beam on a non-linear elastic foundation. *International Journal of Non-linear Mechanics*, 40: 795-805.



## REPLACEMENT OF TRADITIONAL COARSE AGGREGATE

M. J. Islam<sup>1\*</sup>, S. A. Shafian<sup>2</sup> & N. Sarwar<sup>2</sup>

<sup>1</sup>Department of Civil Engineering, Military Institute of Science and Technology, Mirpur, Dhaka, Bangladesh

<sup>2</sup>Department of Civil and Environmental Engineering, Islamic University of Technology, Gazipur, Bangladesh

\*Corresponding Author: mjislam@iut-dhaka.edu

### ABSTRACT

Plastic waste disposal has become one of the most important issues in today's world because of its non-biodegradable nature. Using plastic in construction practice has become popular in recent years. In this study plastic is used in concrete as replacement of coarse aggregate, both crushed stone and brick chips, and compared their various fresh and hard properties to find out its applicability in structural concrete. Both crushed stone and brick chips are partially replaced with polypropylene (10% and 20% by volume) and the results are compared with concrete without any polypropylene. After conducting extensive tests, it can be concluded that polypropylene can be used as a partial replacement (10% by volume) of coarse aggregate for construction practice.

Keywords: Polypropylene, Compressive Strength, Workability, Tensile Strength.

### INTRODUCTION

In 2013, around 299 million tons of plastics were produced which was about 4% more than the production in 2012. In America alone around 31750 thousand tons of plastic waste was introduced in the municipal solid waste in 2012. During the year 2010 – 2011, some 750 thousand tons of recycled plastic waste was produced in Bangladesh (Islam, M.J et.al, 2015). Non-biodegradable behavior is the main problem with plastic materials which leads to congestion and pollution of the environment. Polypropylene (PP) is a cheap and plentiful thermoplastic used in a wide variety of applications including food packaging, textiles, laboratory equipment, automotive components, and polymer banknotes. Because of its wide application it is also turned out in significant amount as solid waste material. In 2012, 34.20% of PP was found in the total plastic products as durable goods in the municipal solid waste in the USA. So surely it has made people's lives much easier but it also has a difficult disposal system, negative environmental impact and other consequences. Some research works were previously conducted where plastic wastes were used as a replacement for aggregate in concrete. Based on the literature review, it is evident that PP performs better as a replacement of aggregate in concrete compare to other form of plastics. In the present study fresh and dry properties of concrete with PP used as partial replacement of coarse aggregate has been investigated. Tests have been carried out to compare the compressive and tensile strengths, slump test and unit weight of 10% and 20% PP replaced concrete with the conventional concrete (0% replacement).

### METHODOLOGY

Using plastic in construction practice is a modern idea. In order to achieve the desired outcome, a lot of experiments have been performed. The ideas were to find out the workability, compressive as well as tensile strength of the sample concrete cylinder and also to inspect the uniqueness of the material.

### Materials:

For the research work, three different types of coarse aggregates have been used, Stone chips, Brick chips and recycled Polypropylene (PP). The grading of the coarse aggregate were done according to ASTM C33. For fine aggregates, Local sand has been collected and used. Burnt clay brick were purchased from the local market and then crushed into desired sizes. Crushed stones were purchased from local market according to desired shapes. Shredded polypropylene (PP) was used as coarse aggregate in this research

work.. PP aggregate were prepared through a process . At first, scrap plastic had been collected and washed, and then it had been melted and cooled into certain shape. Those cooled plastic bars can be shredded into specific sizes.

Unit weight, fineness modulus ,specific gravity and absorption capacity of coarse and fine aggregates used are summarized in the table provided following. Materials properties have been found out doing specific tests in the laboratory according to the ASTM standards.

**Table-1:** Properties of aggregate

Description	Crushed Stone	Brick Chips	Sand	Polypropylene (PP)
Maximum size	19 mm	19 mm	-	19mm
Bulk specific gravity	2.61	6.54	2.25	0.85
Apparent specific gravity	2.58	2.43	2.43	-
Water absorption	1.05%	14.3%	3.40%	0.80%
Fineness modulus	7.29	6.54	2.60	7.29

**Mix design:**

Mix design for the concrete specimens is proposed for both types of aggregates(Stone Chips and Brick Chips).For both cases,two different water cement ratios were chosen along with three different types of replacements. The water cement ratios were .45 and .55.

Both Stone chips and Bricks chips are replaced by PP(Polypropylene) and thus mix design for 1 m<sup>3</sup>concrete has been proposed. Three different replacement ratios by volume were chosen and thus three different cases were proposed for both type of aggregates. The proposed cases were

a) with no PP,b)With 10% PP by volume and c) With 20% by volume .

Following tables shows the mix design for the concrete specimens. WC45P0 = water-cement ratio 0.45 and 0% PP replacement, WC55P0 = water-cement ratio 0.55 and 0% PP replacement, WC45P10= water-cement ratio 0.45 and 10% PP replacement, WC55P10= water-cement ratio 0.55 and 10% PP replacement, WC45P20= water-cement ratio 0.45 and 20% PP replacement, WC55P20= water-cement ratio 0.55 and 20% PP replacement. BWC45P0 = water-cement ratio 0.45 and 0% PP replacement, BWC55P0 = water-cement ratio 0.55 and 0% PP replacement, BWC45P10= water-cement ratio 0.45 and 10% PP replacement, BWC55P10= water-cement ratio 0.55 and 10% PP replacement, BWC45P20= water-cement ratio 0.45 and 20% PP replacement, BWC55P20= water-cement ratio 0.55 and 20% PP replacement..

**Table 2:** Mix Design for 1 m<sup>3</sup> concrete(Stone chips replaced with PP)

Designation	Cement (kg)	Water (kg)	Sand (kg)	Crushed Stone (kg)	PP (kg)
<b>Water/Cement ratio = 0.45</b>					
WC45P0	340	153	539	1251	-
WC45P10	340	153	539	1126	40.5
WC45P20	340	153	539	1001	81.0
WC45P30	340	153	539	876	121.5
<b>Water/Cement ratio = 0.55</b>					
WC55P0	340	187	514	1192	-
WC55P10	340	187	514	1073	38.6
WC55P20	340	187	514	954	77.2
WC55P30	340	187	514	834	115.8

**Table 3:** Mix Design for 1 m<sup>3</sup> concrete(Brick Chips replaced with PP)

Designation	Cement (kg)	Water (kg)	Sand (kg)	Brick Chips (kg)	PP (kg)
<b>Water/Cement ratio = 0.45</b>					
BWC45P0	340	153	539	1251	-
BWC45P10	340	153	539	1126	40.5
BWC45P20	340	153	539	1001	81.0
BWC45P30	340	153	539	876	121.5
<b>Water/Cement ratio = 0.55</b>					
BWC55P0	340	187	514	1192	-
BWC55P10	340	187	514	1073	38.6
BWC55P20	340	187	514	954	77.2
BWC55P30	340	187	514	834	115.8

## RESULTS

For determining the applicability of polypropylene in concrete following test were performed and their results are shown in the graphs for better perceptive.

### *Effects on Slump values:*

Slump test is done to find out the workability of the concrete .The workability depends on various factors like size and shape of the aggregates, water-cement ratios etc. As previously stated, two conventional aggregates,Stone chips and brick chips were partially replaced by Polypropylene, workability seems to increase for both cases with the increment of replacements. Following graphs shows the comparison among various replacements made with Polypropylene.

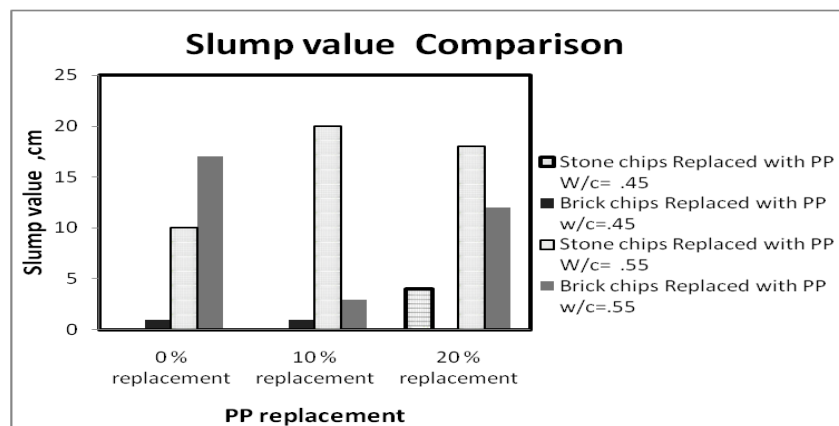


Fig 1:Slump values of Conventional Concrete with PP replaced Concrete with Stone chips and Brick Chips

### *Effects on Compressive strengths:*

Compressive strength of the sample cylinders were measured for both type of replacements.Compressive strength tests were done after 7 days and 28 days of casting.

For Stone chips replaced with PP,increments in strengths were 14% and 69% for 10% replacements and for both water cement ratio respectively than conventional concrete. Similarly for brick chips,anincrements in strengths were observed 9% and 4% for 10 % replacements and for both water cement ratio respectively than conventional concrete .This increase in strength may be caused due the rough and edgy surface texture of the PP aggregates. However, with further increase in PP content in concrete (20% replacements) decrease in strength trend was observed for Stone chips and Brick chips replaced concrete.Following figures shows the comparison of compressive strength of 7 days and 28 days of all types of replacements for both Stone chips and Brick chips.

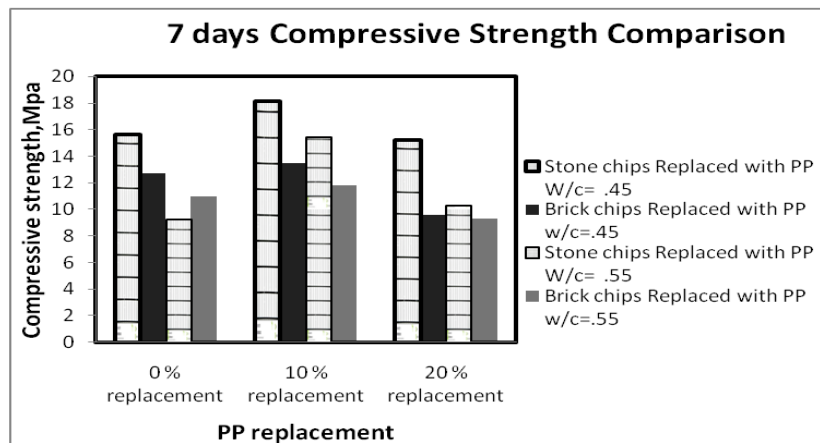


Fig 2:Compressive Strength (28 days) of PP replaced Concrete with Stone chips and Brick Chips

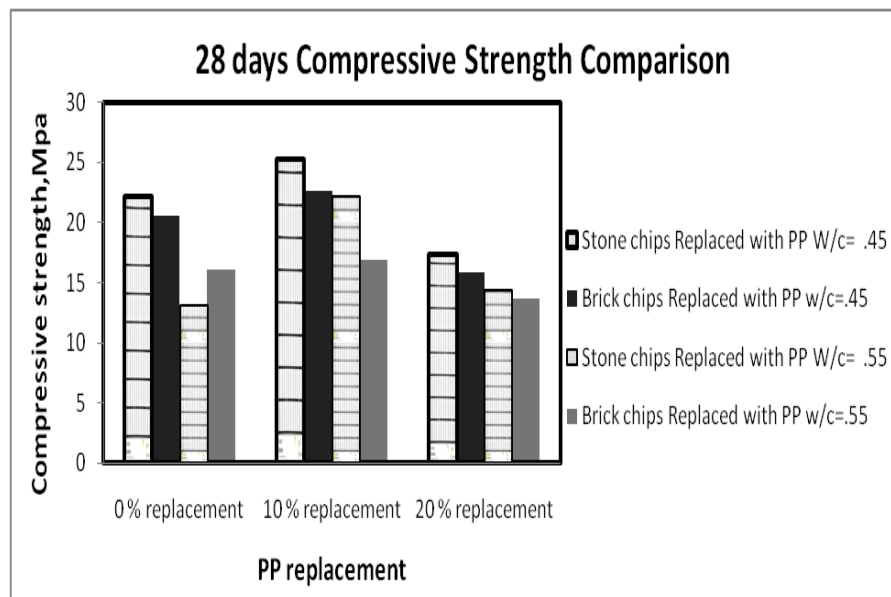
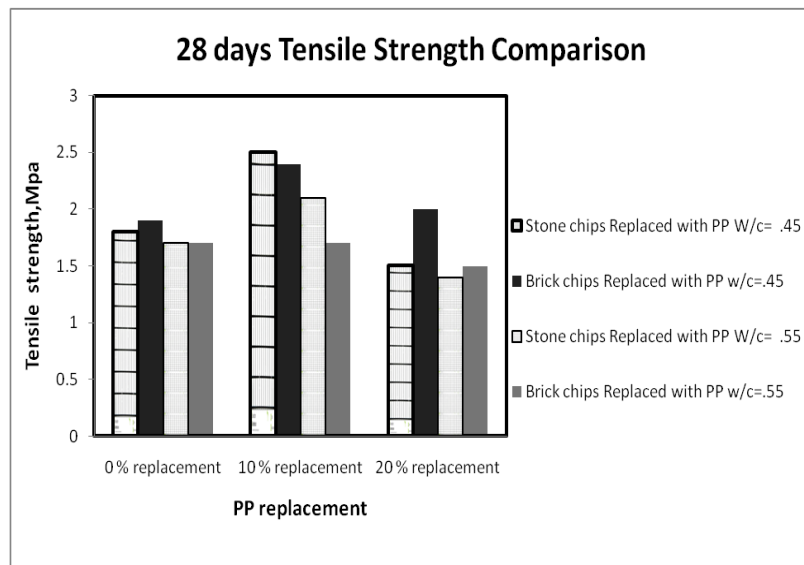


Fig 3:Compressive Strength (7 days) of PP replaced Concrete with Stone chips and Brick Chips

**Effects on Tensile Strength:**

For both of aggregates (Stone chips and Brick chips) replaced with Polypropylene, showed increment in tensile strength with certain increase of Polypropylene. In 10% replacements of Stone chips with PP ,for both water cement ratios, tensile strength increased certain amount than regular concrete .For further replacement(20% by volume) ,strength seemed to be decreased for both water cement ratios.Similarly for Brick chips replaced concrete ,also shows the similar trend.

Following graphs shows the values of tensile strength of both types of aggregates with two different water cement ratios.



**Fig 4:**Tensile Strength (28 days) of PP replaced Concrete with Stone chips and Brick Chips

#### DISCUSSIONS:

After investigating the above data appropriately, following conclusion can be provided ;

1. Compare to the concrete with no PP, 10 % PP replaced concrete in case of stone chips showed a significant increase in both compressive and tensile strengths However, with 20% replacement showed opposite trend.
2. For the brick chips replacements, 10% PP replaced concrete showed better results than other concrete in the case of compressive as well as tensile strengths.
3. For both cases, density of the concrete reduced significantly for PP replaced concrete.
4. But overall, polypropylene replacement with crushed stone chips showed better results than brick chips replaced concrete. This type of concrete may be used for structural purpose having low density as well as high strength.

#### REFERENCES

- Siddique, R, Khatib, J, Kaur, I. : Use of recycled plastic in concrete: A review, Waste management, Vol. 28(10), 1835-1852, 2008
- Hasnat, A, Sayem, A. S. M., Tousif, F. and Islam, M. J.: Recycling of waste plastic in concrete as coarse aggregate, in 1st IUT International Seminar on Sustainability and Durability of Concrete, December 2014, Gazipur, Bangladesh.
- Islam, M.J, Islam, A.K.M.R and Meherier, M.S: An Investigation on Fresh and Hardened Properties of Concrete while Using Polyethylene Terephthalate (PET) as Aggregate, in proceeding World Academy of Science, Engineering and Technology International Journal of Civil, Structural, Construction and Architectural Engineering Vol. 9(5), 2015
- Islam, M.J, Sarwar, N. and Shafian, S. A :An Investigation of Concrete Properties with Polypropylene (PP) as Partial Replacement of Coarse Aggregate

Mathew, P, Varghese, S, Pau, T and Varghese, E: Recycled Plastics as Coarse Aggregate for Structural Concrete, International Journal of Innovative Research in Science, Engineering and Technology Vol. 2(3), 2013

Municipal Solid Waste Generation, Recycling, and Disposal in the United States Tables and Figures for 2012, U.S. Environmental Protection Agency Office of Resource Conservation and Recovery February 2014, [http://www.epa.gov/solidwaste/nonhaz/municipal/pubs/2012\\_msw\\_dat\\_tbls.pdf](http://www.epa.gov/solidwaste/nonhaz/municipal/pubs/2012_msw_dat_tbls.pdf)

Worldwatch Institute, Global Plastic Production Rises, Recycling Lags,  
<http://www.worldwatch.org/global-plastic-production-rises-recycling-lags-0>

## COMPRESSIVE STRENGTH BEHAVIOR OF CONCRETE USING RICE HUSK ASH AS SUPPLEMENTARY TO CEMENT

M. A. Hasan<sup>1\*</sup>, M. A. Islam<sup>1</sup>, Z. Ahmed<sup>1</sup> & I. Ahmad<sup>2</sup>

<sup>1</sup>Department of Civil Engineering, Southern University Bangladesh, Chittagong, Bangladesh

<sup>2</sup>Department of Civil Engineering, Chittagong University of Engineering and  
Technology, Chittagong, Bangladesh

\*Corresponding Author: hasancuet90@gmail.com

### ABSTRACT

Throughout the world cement, mortar and concrete cubes are the most widely used construction material the expanded use of the technologist for its use in aggressive. Concrete is a composite material composed of aggregate bonded together with a fluid environments cement which hardens over time. Concrete refers to Portland cement concrete or to concretes made with other hydraulic cement, such as cement found. However, road surfaces are also a type of concrete, "Asphaltic concrete", where the cement material is bitumen. The main aim of the study is to select the most effective proportion of rice husk ash that can be used in replacing cement in concrete. In this study a total 45 no. of 4inch concrete cubes were casted with fresh water using water cement ratio 0.485 with different replacement level of cement (100:0, 95:5, 90:10, 85:15, and 80:20). Concrete cubes were tested for compressive strength at 3 days, 7days &28 days. The compressive strength of the various concrete specimens is observed to increase with the age of curing and decrease as the percentage of RHA content increase among the different concrete mix, the optimum partial replacement of RHA continent is found to be 10%.

Keywords: Rice Husk Ash (RHA); cement; water cement ratio; cubes; compressive strength

### INTRODUCTION

Concrete is a composite material composed of coarse granular material (the aggregate or filler) embedded in a hard matrix of material (the cement or binder) that fills the space between the aggregate particles and glues them together. Concrete is the most widely used construction material in the world. It is used in many different structures such as dam, pavement, building frame or bridge. Also, it is the most widely used material in the world, far exceeding other materials. Rice husk ash is an industrial waste possess some of the cementing properties that can be economically utilized as the replacement of cement in producing concrete. RHA is collected from rice mills but it may be obtained using basket burner whereas rice husk burned at 250 degree centigrade temperature. RHA is a carbon neutral green product. Lots of ways are being thought for disposing them by making commercial use of this RHA. RHA is a good super-pozzolan. This super-pozzolan can be used in a big way to make special concrete mixes (Concrete –Chapter 5). There is a growing demand for fine amorphous silica in the production of special cement and concrete mixes, high performance concrete, high strength, low permeability concrete, for using in bridges, marine environments, nuclear power plants etc. This market is currently filled by silica fume or micro silica, being imported from Norway, China and also from Burma. Due to limited supply of silica fumes in Bangladesh and the demand being high the price of silica fume has risen to as much as US\$ 500 ton in Bangladesh. From RHA we can manufacture organic micro-silica / amorphous silica, with silica content of above 89%, in very small particle size of less than 35 microns – Silica-pozzolan for application in High Performance Concrete (Obilade, I.O.). The goal of the study is to reduce the construction cost as well as to utilize the environmental polluted material and also to introduce a new binding material as a partial replacement of cement which is environmentally benefitted.

### METHODOLOGY

Out of many tests applied to the concrete, compressive strength test is the most important which gives an idea about all the characteristics of concrete. By this single test one judge that whether concreting

has been done properly or not. In this study 4in. Cubes of concrete were used in this study. Casting and curing of concrete cubes have been completed by using fresh water. Various parameters have been used in this laboratory investigations such as concrete mix ratio: Cement-Sand-aggregate ratio is 1:1.5:3; Percentage of rice husk as a partial replacement of cement: 0%, 5%, 10%, 15%, 20%; Percentage of rice husk ash as a partial replacement of cement: 0%, 5%, 10%, 15%, 20%; Exposure period: 3 days, 7 days, 28 days. For mixing, water-cement ratio 0.485 has been used in this experimental work. At first some specimens were carried out from curing water in this study. Then each one was put in the open air for 24 hours for drying. After drying, the cubes were scaled by an inch scaled and then placed in the compressive strength testing machine. In the testing position, the cube was at right angles to the as-cast position so that the weaker and stronger parts (Parallel to one another) were extended from plate to plate. The load on the cube should be applied at a constant rate of stress equal to 0.2 to 0.4 Mpa/second (30 to 60psi/second). Finally, the data would be recorded which was got from compressive strength testing machine.

## RESULTS AND DISCUSSIONS

Compressive strength values of test specimen's in compressive strength testing machine (for different mix ratio, curing period) have been shown in Table 1:

Table 1: Compressive Strength value of test Specimen

Rice Husk	Curing Period	3 days			7 days			28 days		
Plane	Compressive Strength(psi)	1690	1619	1619	1831	1690	1479	2816	3520	3661
	Average	1642.66			1666.66			3332.33		
5% Rice Husk Ash	Compressive Strength(psi)	1084	1549	1436	1513	1197	1408	2535	2323	3732
	Average	1356.33			1372.33			2863.33		
10% Rice Husk Ash	Compressive Strength(psi)	1619	1197	1338	1338	1831	2183	3943	4506	3732
	Average	1384.66			1784			4060.33		
15% Rice Husk Ash	Compressive Strength(psi)	1349	1319	1338	1253	1331	1842	2464	3661	3520
	Average	1335			1475			3215		
20% Rice Husk Ash	Compressive Strength(psi)	1197	1056	774	1338	1127	1056	2064	3561	3520
	Average	1009			1173.67			3048		

Variation of compressive strength vs curing period and compressive strength vs different cement, rice husk ash ratio are given below:

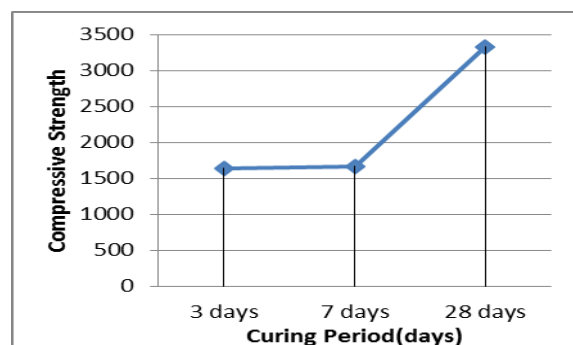


Fig. 1: Compressive Strength VS Curing Period relation for concrete specimen {C:RHA=100:0, Sand: Cement=1:1.5}

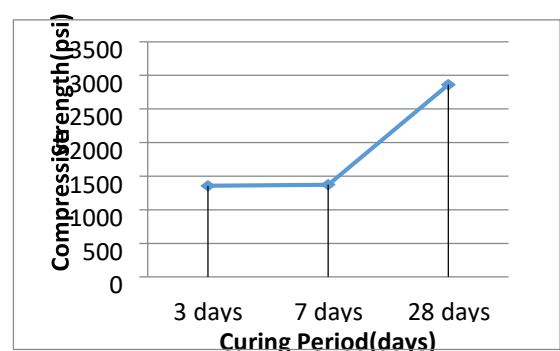


Fig. 2: Compressive Strength VS Curing Period relation for concrete specimen {C:RHA=95:5, Sand: Cement=1:1.5}



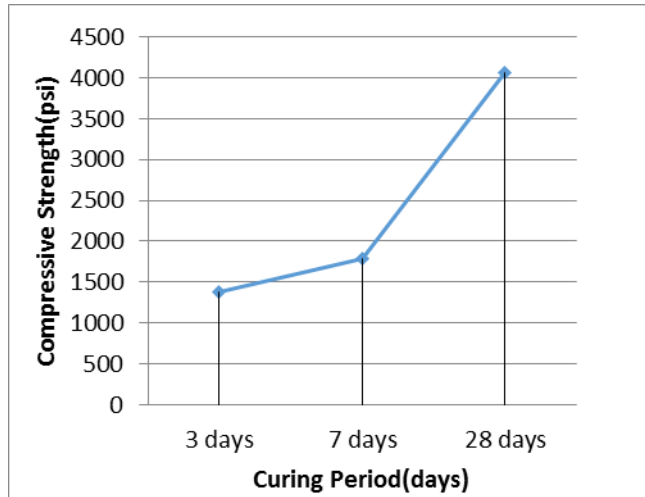


Fig. 3: Compressive Strength VS Curing Period for concrete specimen {C:RHA=90:10, Sand: Cement=1:1.5}

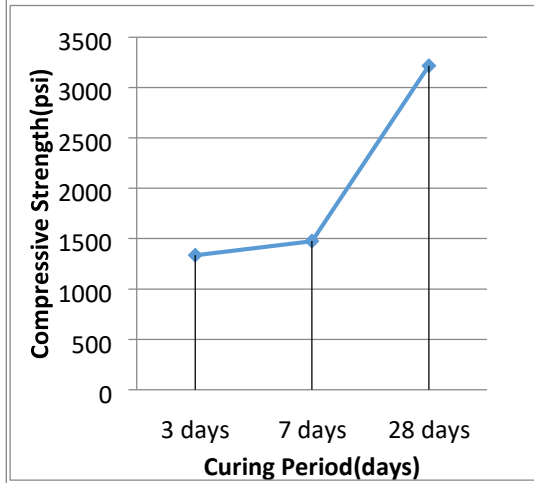


Fig. 4: Compressive Strength VS Curing Period for concrete specimen {C:RHA=85:15, Sand: Cement=1:1.5}

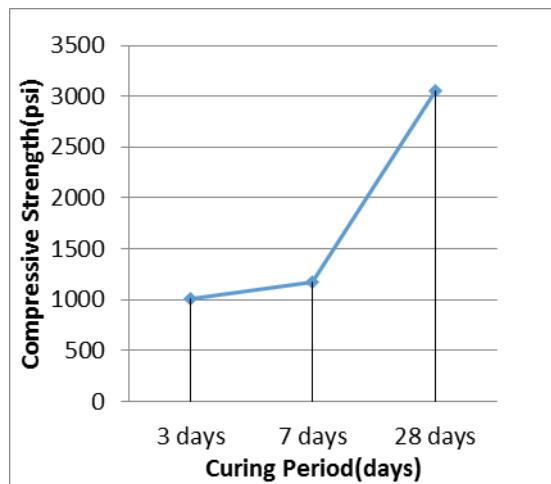


Fig. 5: Compressive Strength VS Curing Period for concrete specimen {C:RHA=80:20, Sand: Cement=1:1.5}

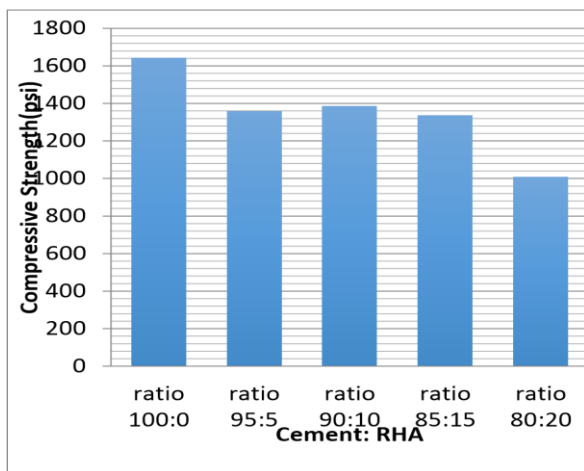


Fig. 6: 3 days compressive strength of concrete with various C:RHA ratio (Cement:Sand=1:1.5)

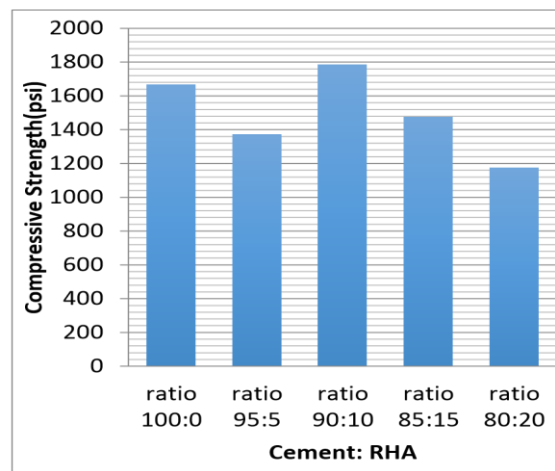


Fig. 7: 7 days compressive strength of concrete with various C:RHA ratio (Cement:Sand=1:1.5)

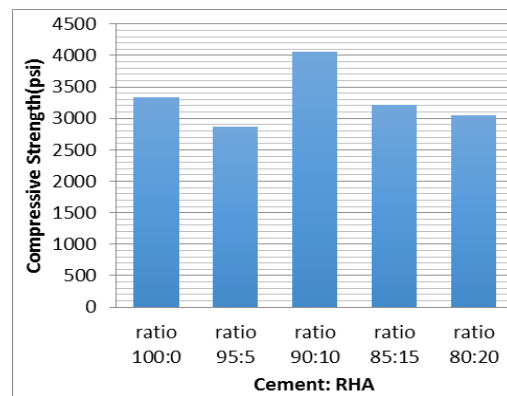


Fig. 8: 28 days compressive strength of concrete with various C:RHA ratio (Cement:Sand=1:1.5)

## CONCLUSION

Based on studies following results are made: For all mixes the compressive strength of the specimen increases with the age of curing and decreases as the RHA content increases. The replacement of cement content of the mix by 10% RHA is very close and greater in some case to 100% cement mix with regards to its compressive strength. The optimum replacement level of cement with RHA is found as 10%.

## REFERENCES

- Agarwal, SK. 2006. Pozzolanic activity of various siliceous materials. *Cem. Concr. Res.*, 36(9):1735-9.
- Chindaprasirt, P and Rukzon, S. 2008. Strength, Porosity and Corrosion resistance of Ternary Blend Portland Cement, Rice Husk Ash and Fly Ash Mortar. *Construction and Building Materials*, 22:1601-1606.
- Aziz, M.A. ;ED:1995 “*Engineering Materials*”.
- Mehta, PK. 1989. Rice husk ash as mineral admixture in concrete. *In: proceedings of the 2<sup>nd</sup> international seminar on durability of concrete: aspect of admixtures and industrial byproducts*, 131-136.
- Moyad, N; Khalaf, AL and Yousif, HA.1978. Use of rice husk ash in concrete. *International Journal of Cement Composites and Lightweight Concrete*, 6(4): 241-8.
- Rodriguez, GS. 2006. Strength development of Concrete with Rice Husk Ash. *Cement and Concrete Composites*, 28: 158-160.

## **SEISMIC VULNERABILITY ASSESSMENT OF EXISTING BUILDINGS IN CHITTAGONG CITY: A CASE STUDY ON RAMPUR WARD**

M. R. Mukhlis<sup>1\*</sup>, S. A. Tangina<sup>2</sup>, M. I. Mostazid<sup>3</sup> & M. R. Hoque<sup>2</sup>

<sup>1</sup>*Institute of Earthquake Engineering Research, Chittagong University of Engineering and Technology, Chittagong, Bangladesh*

<sup>2</sup>*Department of Civil Engineering, Southern University Bangladesh, Chittagong, Bangladesh*

<sup>3</sup>*Department of Civil Engineering, Hajee Mohammad Danesh Science and Technology University, Dinajpur, Bangladesh*

*\*Corresponding Author: raihan.ce@live.com*

### **ABSTRACT**

A strong earthquake affecting a major urban area like Chittagong city may result in destructions of massive proportions and may have disastrous consequences for the entire nation. Chittagong, located in the south eastern part of Bangladesh, is a strategically and commercial capital of the country. The study area situated at no.25 Rampur ward of Chittagong City Corporation with more than 30,000 populations. The study methodology comprised of the most popular method of modern Turkish, where about eight individual parameters were surveyed like soft story, pounding effects, apparent quality etc. at level I survey. Based on the selected parameters, performance score has been assigned to individual buildings by which the buildings have been classified as damage category of safe, moderate and unsafe at level I survey. A total of 400 buildings have been surveyed in the study area of interest. Among those 400 buildings 179 buildings are safe, 39 buildings are unsafe and 182 buildings are of moderate category after level I survey. The important outcome of the study is the complete building inventory of the study area identifying the damage category.

Keywords: Seismic vulnerability assessment; Turkish method; Rampur ward; Chittagong city

### **INTRODUCTION**

By its geographical position, Bangladesh is being treated as one very vulnerable country with its high risk of earthquake hazard. The Indian plate is moving ~60 mm/yr in a northeast direction and subducting at the rate of 45 mm/yr under the Eurasian and 35 mm/yr under the Burmese plates in the north and east, respectively (Bilham, 2004).

When the rocks along a weak region in the earth's crust reach their strength, a sudden movement takes place and opposite sides of the fault suddenly slips and release the large elastic strain energy stored in the interface rocks. The sudden slip at the fault causes the earthquake. A violent shaking of the earth when large elastic strain energy released spreads out through seismic waves that travels through the body along the surface of the earth. Most earthquakes in the world occur along the boundaries of the tectonic plates. Earthquakes can also occur far from the edges of plates, along faults. They are more common near the edges of the plates (UPSeis, 2016).

Bangladesh stands on the northeastern corner of the Indian plate while Chittagong is situated over Chittagong-Tripura Fold Belt (CTFB). Most of the active faults within CTFB is thought to be secondary faults and deformations related to the rupture of the Tripura segment shown in [Fig. 1]. However, a part of these faults may generate large earthquakes separately from the plate boundary fault like the 1918 Srimongal earthquake. However, it is difficult to separate active structures from the secondary structures (Morino et. al., 2013). Some active faults within Chittagong have been shown in [Fig. 2] among which Sitakund fault, Patia fault, Sitapahar fault, Kalabunia fault have potentials to produce some significant earthquakes. Sitakund fault zone is located at Northwest side of Chittagong city and the nearest fault from main city.





Fig. 5: Building ID 01



Fig. 6: Building ID 56

### SEISMIC VULNERABILITY ASSESSMENT

Current approaches in seismic vulnerability evaluation methods can be classified in three main groups depending on their level of complexity. The first, most simple level is known as “Walk down Evaluation.” Evaluation in this first level does not require any analysis and its goal is to determine the priority levels of buildings that require immediate intervention. The procedures in FEMA 154 (1988), FEMA 310 (1998) Tier 1 and the procedure developed by Sucuoglu and Yazgan (2003) are examples of walk down survey procedures. The second level or Preliminary assessment methodologies (PAM) are applied when more in-depth evaluation of building stocks is required. In this stage, simplified analysis of the building under investigation is performed based on a variety of methods. These analyses require data on the dimensions of the structural and non-structural elements in the most critical story. The procedures by FEMA 310 (1998) Tier 2 and Ozcebe et al. (2003), later complemented by Yakut et al. (2003) can be listed as the examples of preliminary survey procedures. It is possible to survey large building stocks by employing the preliminary evaluation methodologies within a reasonable time span. The procedures in third level employ linear or nonlinear analyses of the building under consideration and require the as-built dimensions and the reinforcement details of all structural elements. In the present study only first level has been covered for seismic vulnerability assessment of buildings in study area.

#### **Walk down Evaluation (Level – I)**

For level-I assessment the procedure developed by Sucuoglu and Yazgan (2003) has been used. The first survey level is conducted from the sidewalk by trained observers through walk-down visits. A street survey procedure must be based on simple structural and geotechnical parameters that can be observed easily from the sidewalk. The time required for an observer for collecting the data of one building from the sidewalk is expected not to exceed 10 minutes. The parameters that are selected for representing building vulnerability in this study are the following:

1. The number of stories above ground (1 to 7)
2. Presence of a soft story (Yes or No)
3. Presence of heavy overhangs, such as balconies with concrete parapets (Yes or No)
4. Apparent building quality (Good, Moderate or Poor)
5. Presence of short columns (Yes or No)
6. Pounding between adjacent buildings (Yes or No)
7. Local soil conditions (Stiff or Soft)
8. Topographic effects (Yes or No)

Each parameter reflects a negative feature of the building system under earthquake excitations on a variable scale (Sucuoglu and Yazgan, 2003)

The intensity of ground motion at a particular site predominantly depends on the distance of the causative fault and local soil conditions. As there exists a strong correlation between PGV and the shear wave velocities of local soils (Wald, 1999), in this study the PGV is selected as to represent the ground motion intensity. As for Chittagong no PGV map is available, the intensity zones are expressed accordingly, in terms of the associated PGV ranges as developed for Istanbul.

Zone I:  $60 < PGV < 80 \text{ cm/s}^2$

Zone II:  $40 < PGV < 60 \text{ cm/s}^2$

Zone III:  $20 < PGV < 40 \text{ cm/s}^2$

Based on their number of stories and the seismic hazard level at the site buildings are assigned different base scores as shown in Table 1.

Table 1: Base Scores and Vulnerability Scores for Concrete Buildings (Ahmed et al. 2012)

Number of Stories	Base Scores(BS)			Vulnerability Scores(VS)					
	Zone I ( $60 < PGV < 80$ )	Zone II ( $40 < PGV < 60$ )	Zone III ( $20 < PGV < 40$ )	Soft Story	Heavy Overhang	Apparent Quality	Short Column	Pounding Effects	Topography Effects
1 or 2	100	130	150	0	-5	-5	-5	0	0
3	90	120	140	-15	-10	-10	-5	-2	0
4	75	100	120	-20	-10	-10	-5	-3	-2
5	65	85	100	-25	-15	-15	-5	-3	-2
6 or 7	60	80	90	-30	-15	-15	-5	-3	-2

### Building Seismic Performance

Once the vulnerability parameters of a building are obtained from walk down surveys and its location is determined, the seismic performance score PS can be calculated by using Eq. (1). The base scores (BS), the vulnerability scores (VS) and the vulnerability score multiplies (VSM) to be used in Eq. (1) are defined in Tables 1 and 2, respectively

$$PS = (BS) - \sum (VSM) \times (VS) \quad (1)$$

Table 2: Vulnerability Parameters (VSM) (Ahmed et al. 2012)

Soft story	Does not exist=0	Exists=1
Heavy overhangs	Does not exist=0	Exists=1
Apparent quality	Good = 0;	Moderate = 1; Poor =2
Short columns	Does not exist=0	Exists=1
Pounding effect	Does not exist=0	Exists=1
Topographic effects	Does not exist=0	Exists=1

Buildings are classified into three risk groups in this study based on the calculated Seismic performance score (PS) as shown in following Table 3.

Table 3: Risk Groups Based on Seismic Performance Score (PS)

Risk Groups	Performance Score Range
Unsafe	$PS \leq 30$
Moderate	$31 < PS \leq 60$
Safe	$61 < PS \leq 100$

## RESULTS AND DISCUSSIONS

Total number of structure in this area is almost residential, where most of the percentages are moment resisting RC frame. A total of 400 RC buildings were surveyed in case of Level I survey. Among 400 buildings 34 two storied, 77 three storied, 139 four storied, 102 five storied and 48 six storied buildings exist in the study area as shown in [Fig. 7]. After assessing the overall survey parameters, among 400

buildings 277 buildings have heavy overhangs problem, 11 buildings have short column problem, 110 buildings have soft story problem, 186 buildings have pounding possibilities and in terms of apparent quality 53 buildings are poor, 91 building are good and 256 building are average as shown in [Fig. 8]. At end of Walk down evaluation survey, according to their seismic performance score building are classified into three categories of safe, unsafe and moderate as shown in [Fig. 9]. Finally, [Fig. 10] shows that among 400 buildings 179 buildings are safe, 39 buildings are unsafe and 182 buildings are of moderate category after level I survey.

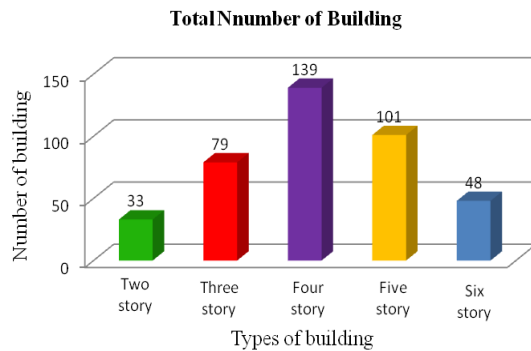


Fig. 7: Total Number of different storied Buildings

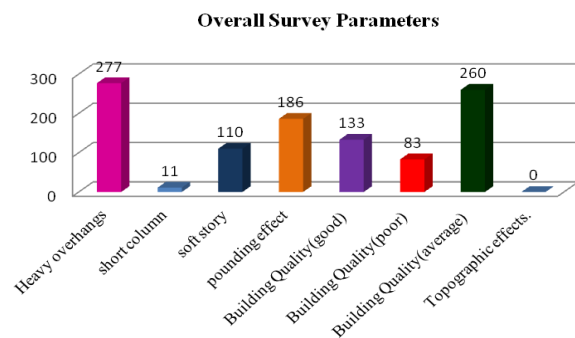


Fig. 8: Vulnerability Parameters after Walk down Evaluation

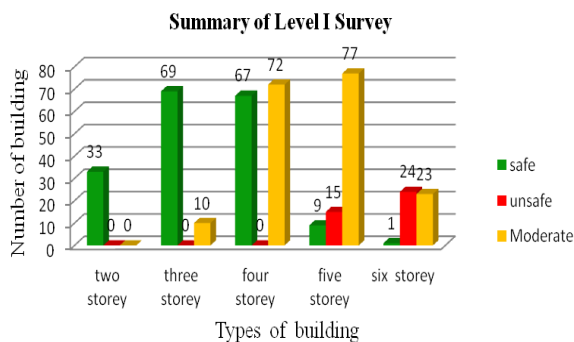


Fig. 9: Summary of Level I Survey

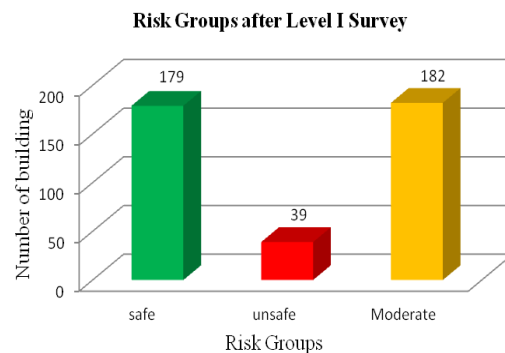


Fig. 10: Risk Groups after Level I Survey

## CONCLUSIONS

- ❖ From this assessment, soft story in 27.5%, pounding effect in 46.5%, short columns in 2.75%, and heavy overhanging in 24% building among 400 buildings in study area have found at level I survey.
- ❖ From the level-I survey results we found Apparent Building Quality (Average) in 64% building, Apparent Building Quality (Good) in 23% building, and Apparent Building Quality (Poor) in 13% building.
- ❖ Among 400 buildings 179 (45%) buildings are found to be safe, 39 (10%) buildings are found to be unsafe and 182 (45%) buildings are found to be moderate in terms of their performance score (PS) value after level I survey.
- ❖ Those 39 unsafe buildings and 182 moderate buildings should be taken under further assessment to identify their vulnerable structural component and retrofit thereafter as early as possible on priority basis.

## REFERENCES

Ahmed, M; Khaleduzzaman, KM; Siddique, NA and Islam, S. 2012. Earthquake Vulnerability Assessment of Schools and Colleges of Sylhet, a North-eastern City of Bangladesh. *SUST Journal of Science and Technology*, 19(5):27-34.

- Al-Hussaini, TM; Hossain, TR and Al-Noman, MN. 2012. Proposed Changes to the Geotechnical Earthquake Engineering Provisions of the Bangladesh National Building Code. *Geotechnical Engineering Journal of the SEAGS & AGSSEA*, 43(2): 1-7.
- Alam, MJ. 2011. Earthquake Risk in Bangladesh, *University of Kassel*, [online], Available at: <http://www.unikassel.de/fb14/stahlbau/eartheng/downloads/Earthquake%20risk%20in%20Bangladesh%20Prof.%20Jahangir%20Alam.pdf> [Accessed 20July, 2016].
- Bilham, R. 2004. Earthquakes in India and the Himalaya: tectonics, geodesy and history. *Annals of Geophysics*, 47 (2/3): 839-858.
- FEMA 154, 1988. A Hand Book on Rapid Visual Screening of Buildings for Potential Seismic Hazards, *Federal Emergency Management Agency*, Washington DC, USA
- FEMA 310, 1988. Hand book of Seismic Evaluation of Buildings-A prestandard, *Federal Emergency Management Agency*, Washington DC, USA
- FEMA 356, 2000. Prestandard and Commentary for the Seismic Rehabilitation of Buildings, *Federal Emergency Management Agency*, Washington DC, USA
- Morino, M and Kamal, ASMM. 2003. *Report of active fault mapping in Bangladesh: Paleo-seismological study of the Dauki fault and the Indian-Burman plate boundary fault*. Comprehensive Disaster Management Programme (CDMP II), Ministry of Disaster Management and Relief, Govt. of Bangladesh, 3-9.
- Ozcebe, G; Yucemen, MS; Aydogan, V and Yakut, A. 2003. Preliminary Seismic Vulnerability Assessment of Existing Reinforced Concrete Buildings in Turkey- Part I: Statistical Model Based on Structural Characteristics. *Seismic Assessment and Rehabilitation of Existing Buildings*, NATO Science Series IV/29, 29-42.
- Sucuoglu, H and Yazgan, U. 2003. Simple Survey Procedures for Seismic Risk Assessment in Urban Building Stocks. *Seismic Assessment and Rehabilitation of Existing Buildings*, NATO Science Series IV/29, 97-118.
- Wald, DJ; Quirarano, V; Heaton, TH; Kanamori, H; Scrivner, CW and Worden, CB. 1999. Trinet Shake Maps: Rapid Generation of Peak Ground Motion and Intensity Maps for Earthquakes in Southern California. *Earthquake Spectra*, 15(3): 537-555.
- Yakut, A; Aydogan, V; Ozcebe, G and Yucemen, MS. 2003. Preliminary Seismic Vulnerability Assessment of Existing Reinforced Concrete Buildings in Turkey -Part II: Inclusion of Site Characteristics. *Seismic Assessment and Rehabilitation of Existing Buildings*, NATO Science Series IV/29, 43-58.
- UPSeis, 2016, Where Do Earthquakes Happen, *Michigan Technological University*, [online], Available at: <http://www.geo.mtu.edu/UPSeis/where.html> [Accessed 21July, 2016].



## **A COMPARATIVE STUDY ON PHYSICAL PROPERTIES OF CEMENT: ASTM AND BDS EN STANDARDS**

M. A. A. Siddique\*, M. S. Islam & U. K. Halder

*Department of Civil Engineering, Bangladesh University of Engineering and Technology, Dhaka,  
Bangladesh*

*\*Corresponding Author: [alamin@ce.buet.ac.bd](mailto:alamin@ce.buet.ac.bd)*

### **ABSTRACT**

Reinforced concrete (RC) is widely used in civil infrastructure due to cheap labor and availability of construction materials. Cement is used as a binding material for different ingredients of members of these structures. At present, Bangladesh's cement industry has become the 40th largest market in the world. In Bangladesh, different types of cement are produced and are followed BDS EN 197-1:2003 standard for the standardization. In addition, a standard such as ASTM is widely used as specifications for construction of civil infrastructures. There are some differences of the requirements and specifications as well as testing procedure and evaluation of quality of cement considering BDS EN and ASTM. Since cement is a global product for construction industry, a comparison among the requirements and specifications of cement using different standards might become necessary. A review study has been conducted to figure out the different specifications and requirements for the properties of cement following ASTM and BDS EN. In addition, an experimental program is carried out to determine the different physical properties such as normal consistency, initial and final setting time, and compressive strength of cement. Two types of cement such as Ordinary Portland Cement (OPC) and Portland Composite Cement (PCC) are considered in the experimental program. OPC grade 52.5N and PCC grade 42.5N are used. Specimen preparation and testing have been conducted for each cement sample on the same day. From the experimental results, it has been shown that compressive strength of cement for OPC 52.5N grade following ASTM standard is found to be 71% higher at 28 days than that from the minimum requirement. However, this strength is shown to be 22% higher at 28 days following BDS EN standard.

Keywords: Cement; standards; ASTM; BDS EN; grades; setting time; compressive strength

### **INTRODUCTION**

The development of cement industry in Bangladesh dates back to the early-fifties but its growth in real sense started only about a decade. Till 1990, about 95 percent of the country's demand for cement had been met through import. The country has been experiencing an upsurge in cement consumption for last 6/7 years. The transition of traditional low rise buildings to high rise ones has pushed up the use of cement. Increase in demand for cement has soared up due to mainly the property sector boom and infrastructure development in the country. With the implementation of large-scale infrastructure projects, exhilarated pace of urbanization, construction of apartment buildings and multi-storey shopping complexes in urban areas, and changes in the taste and economic condition to a large number of rural people, aspiring for modern houses, the demand for cement has been gaining momentum by the day. Now, cement industry in Bangladesh has become the 40th largest market in the world. Bangladesh is producing different types of cements following BDS EN (Bangladesh Standard- European Norm) 197-1:2003 standard. In addition, ASTM (American Society for Testing and Materials) standard is still widely used around the world for the specifications and requirements in different development projects. From the earlier studies, it has been shown that the requirements and specifications for each standard vary from one to another. However, for a global construction material, a comparison among the specifications, requirements and test results following different standards might become necessary. Therefore, the main objective of this paper is to identify the requirements and specifications for cements considering BDS EN and ASTM. In addition, an experimental program is conducted to determine the different physical properties such as normal

consistency, initial and final setting time, and compressive strength of cement following both the standards. The obtained test results are compared with the requirements following both the standards.

### COMPARISON OF REQUIREMENTS FOLLOWING BDS EN AND ASTM STANDARDS

Two types of cement categories such as Ordinary Portland Cement (OPC) and Portland Composite Cement (PCC) are widely used around the world as binding materials for concrete. PCC is also known as blended cements in many standards. OPC Type-I is the most common type of cement in use which has more than 95% clinkers. It conforms with the Bangladesh Standard BDS EN 197-1:2003 CEM-I 52.5, European Standard EN 197 type CEM-I, and American Standard ASTM C150 PC Type I. OPC is the most common type of cements which is used in general concrete construction when there is no exposure to sulphates in the soil or groundwater. PCC is a variation of OPC which includes a mixture of a pozzolanic material having a portland cement clinker ranges from 65% to 79% and is widely used in Bangladesh. Pozzolan or similar materials such as volcanic ash, clay, slag, silica, fume, fly ash, or shale are used in different types of blended cements. It conforms to BDS EN 197-1:2003 CEM-II/B-M (S-V-L) 42.5 and ASTM C595 Types of IP/IS/IL/IT. Physical requirements such as compressive strength, initial and final setting time in ASTM standard are provided in C150 and C595 for OPC and PCC cements, respectively. BDS EN197-1:2003 specify the physical requirements for both the cement types. OPC and PCC grades are identified considering 28 days compressive strength of cement. 42.5 MPa strength is normally used for CEM II type and 52.5 MPa is used for CEM I type. In both cases, specification for initial setting time is provided. However, both the initial and final setting time of cement are considered in ASTM standard. Compressive strength of cement at 2 and 28 days are required following BDS EN while 3, 7, and 28 days strength requirements are followed in ASTM. Letters "N" and "R" are used in BDS standard to specify the normal strength and high early strength requirements for a cement grade. Table 1 provides the compressive strength and setting time requirements following BDS EN and ASTM both for OPC and PCC cements. From the table, it is observed that specifications for initial setting time are different for different grades of cements as per BDS EN. However, no requirement for final setting time is provided. On the other hand, both the initial and final setting time are provided in ASTM standard as requirements. Initial setting time is the same both for OPC and PCC as per ASTM.

Table 1: Comparative requirements for physical properties of OPC and PCC cements

STANDARDS	BDS EN				ASTM	
	BDS EN 197-1:2003				C 150	C 595
	42.5N	42.5R	52.5N	52.5R	OPC	PCC
Compressive Strength (MPa)						
-2 days	≥ 10	≥ 20	≥ 20	≥ 30		
-3 days	---	---	---	---	12	13
-7 days	---	---	---	---	19	20
-28 days	42.5 to 62.5	42.5 to 62.5	≥ 52.5	≥ 52.5	28	25
Setting Time (minutes)						
-Initial Setting Time (min.)	≥ 60	≥ 60	≥ 45	≥ 45	45	45
-Final Setting Time (min.)	---	---	---	---	375	420

### EXPERIMENTAL PROGRAM

An experimental program is carried out to assess the different physical properties following ASTM and BDS-EN standards. Two types of cement such OPC and PCC are considered. OPC with grade 52.5N and PCC with 42.5N are used in the present study. Normal consistency, setting time and compressive strengths are determined for each case following ASTM and BDS EN standards. Although 2 days and 28 days compressive strengths are required for cement following BDS EN standard, compressive strengths at 3, 7, and 28 days are evaluated to assess the development of strength with age as well as for a comparative study.

## PREPARATION OF SPECIMENS AND EXPERIMENTAL RESULTS

### (a) Normal consistency and setting time of cement

The amount of water that brings the cement paste to a standard condition of wetness is called normal consistency. Both the ASTM and BDS EN standards use manual Vicat apparatus to determine the normal consistency of cement as a percentage of dry cement. The suitable temperature for this test is  $(23 \pm 2)^\circ\text{C}$  and relative humidity is more than 50% according to ASTM C187. The temperature shall be maintained  $(20 \pm 2)^\circ\text{C}$  and a relative humidity of not less than 50% following BDS EN 197-1. The same diameter and the weight of the plunger are used for measurements. According to ASTM, the cement paste shall be in normal consistency when the plunger rod settles to a point  $10 \pm 1\text{mm}$  below the original surface in 30 sec after being released. However, the paste is considered in a normal consistency when the distance produce between the plunger and base plate of the mould of  $6 \pm 2\text{ mm}$  in 30 sec after being released. Table 2 shows the normal consistency values of OPC considering both the ASTM and BDS standards while table 3 shows those values for PCC.

For the determination of initial and final setting time of cement, the same Vicat apparatus is used with a needle diameter of approximately 1 mm. The same temperature and relative humidity as mentioned for the normal consistency test is used. The cement mould using the same amount of water as used for consistency is kept in moist cabinet or moist room for 30 min after moulding without being disturbed as per ASTM C191. The elapsed time between the initial contact of cement and water and the penetration of 25 mm into the paste is the Vicat time of setting or Vicat initial time of setting. The final setting time is obtained when the needle does not sink visibly into the paste. On the other hand, the filled mould and base plate is placed in the container filling with water so that surface of the paste is submerged to a depth at least 5 mm as per BDS EN 196-3. After sometime the paste is lifted from water and kept under the needle. The needle is released freely. Penetration into the paste is calculated after 30 minutes of releasing. The time elapsed between zero time (starting time of mixing of cement and water in a mixer) and the time at which the distance between the needle and the base plate ( $6 \pm 3$ ) mm measured to the nearest minute is the initial setting time of the cement. The mould is then inverted to determine the final setting time. Final set are made on the face of the specimen originally in contact with the base-plate. The elapsed time is measured from zero to that at which the needle first penetrates only 0.5 mm into the specimen as the final setting time. Tables 2 and 3 provide test results both for the initial and final setting time of OPC and PCC, respectively. From the tables, it is shown that both the cements satisfied the ASTM and BDS standard requirements. Initial setting time is higher for PCC than that of OPC and is matched better with BDS EN requirements.

Table 2: Normal consistency and setting time for OPC 52.5N cement

Test standard	Consistency (%)	Initial setting time (min)	Final setting time (min)
ASTM	26	167	273
BDS-EN	30	165	240

Table 3: Normal consistency and setting time for PCC 42.5N cement

Test standard	Consistency (%)	Initial setting time (min)	Final setting time (min)
ASTM	26	182	240
BDS-EN	32	195	255

### (b) Compressive strength of cement

Cement as a binding material in concrete or mortar is usually subjected to compressive stresses. Mortar is a mixture of cement and sand in a specified ratio on which the strength of the mortar depends. The mechanical strength of hardened cement is most important for structural use. According to ASTM C109, compressive strength of the hydraulic cement mortars is determined by using 2 inch or 50 mm cube specimens as shown in Fig. 1(a). Room temperature should be maintained  $(23 \pm 3)^\circ\text{C}$  and a relative humidity should be above 50%. A 2.75 parts of sand is mixed with 1 part cement where as water–cement ratio should be 0.485. The sand used for making test specimens shall be natural

silica sand conforming to the requirements for graded standard sand in specification C778. Hand tamping is used in a layer of mortar about 1 inch or 25 mm (approximately one half of the depth of the mold) in all of the cube compartments. In each cube compartment, 32 times in about 10s in 4 rounds, each round to be at right angles to the other and consisting of eight adjoining strokes over the surface of the specimen is used. When the tamping of the first layer in all of the cube compartments is completed, the compartments are filled with the remaining mortar and then tamping is done as specified for the first layer as shown in Fig. 1(b). The prepared test specimens are shown in Fig. 1(c). Immediately upon completion of molding, the test specimens are kept in moist room or moist closet for 24 hours. Then the specimen is kept in the water mixing with lime water for determining compressive strengths at 3, 7, and 28 days.



(a) Mould for compressive strength test (b) Hand tamping for compaction (c) ASTM mould with mortar  
Fig.1: ASTM mould, hand compaction and specimens for compressive strength test of cement

Compressive strength is determined on prismatic test specimens 40 mm x 40 mm x 160 mm in size as shown in Fig. 2(a) following BDS EN standard. These specimens are cast from a batch of plastic mortar containing cement- sand ratio of 1:3 with a water-cement ratio of 0.50. According to EN 196-1 CEN standard sand is used in preparation of mortar. CEN reference sand is a natural, siliceous sand consisting preferably of rounded particles and has a silica content of at least 98%. The moisture content is less than 0.2% expressed as a percentage by mass of the dried sample. The mortar is prepared by mechanical mixing and is compacted in a mould using a standard jolting apparatus as shown in Fig. 2(b). The specimens in the mould are stored in a moist atmosphere for 24h and then the demoulded specimens are stored under water until strength testing. The prepared specimens for compressive strength test are shown in Fig. 2(c). For a comparative study, these specimens are prepared and tested on the same day as done for ASTM specimens.



(a) Mould for compressive strength test (b) Jolting apparatus for compaction (c) BDS EN mortar filled moulds  
Fig.2: BDS EN standard mould, jolting apparatus for compaction and prepared mortar specimens

From the experimental results, it is shown that all the tested specimens satisfied the minimum strength requirements both for ASTM and BDS EN standards. Figs. 3(a) and 3(b) present the compressive strength results of cement mortars for OPC and PCC, respectively. As mentioned earlier, cement grades OPC 52.5N and PCC 42.5N are used in the experimental program.

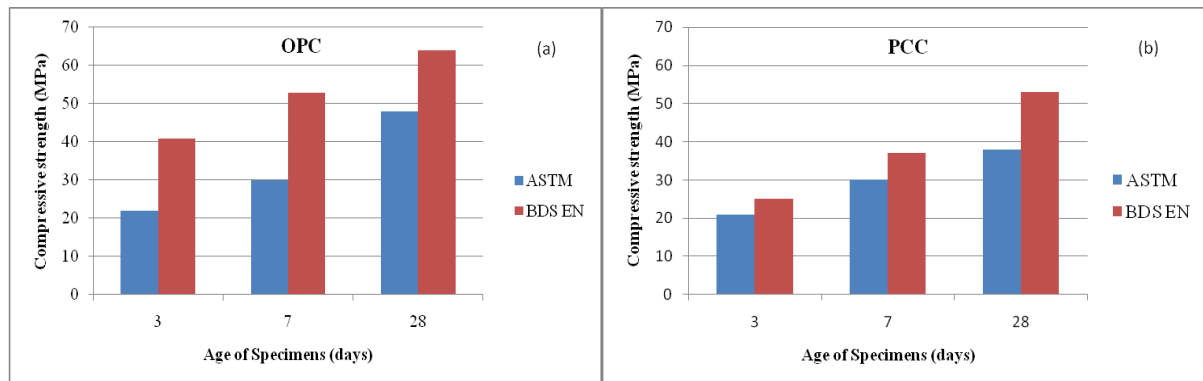


Fig. 3: Test results for compressive strength of cements (a) OPC and (b) PCC

A comparative study between the requirements and obtained compressive strength is also conducted both for ASTM and BDS EN standards. Figs. 4(a) and 4(b) show the required minimum and obtained strengths for ASTM and BDS EN standards, respectively. The comparison is done both for OPC and PCC strength requirements as shown in the figure. It is observed that obtained test results are well above both for OPC and PCC as per ASTM requirements. The rate of gaining cement compressive strength with age is shown well pattern for both the grades of cement. At 28 days, an increase in compressive strength of 71% for OPC and that of 52% for PCC is reported. On the other hand, an increase of compressive strength at the age of 28 days is obtained only 22% for OPC and 24% for PCC as per BDS EN standard.

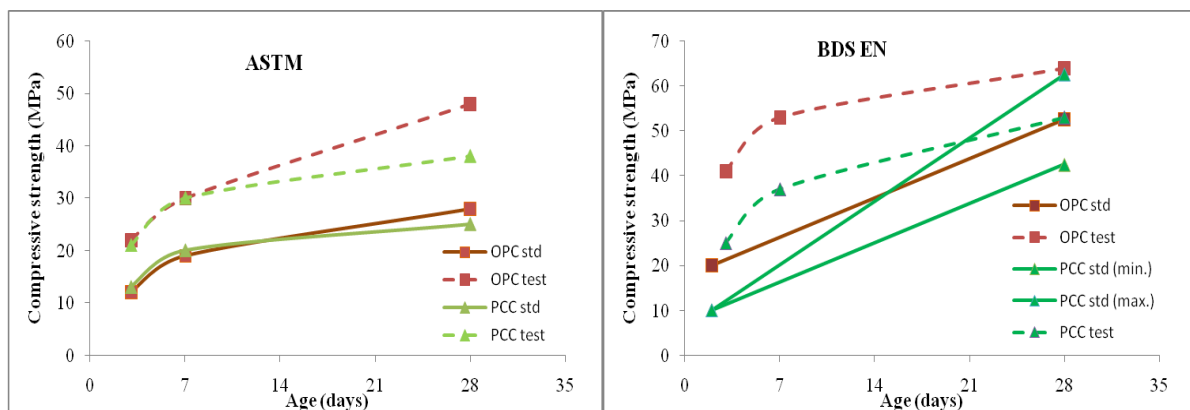


Fig. 4: Comparison of compressive strength requirements and obtained results (a) ASTM and (b) BDS EN

From the study of standard requirements and experimental results, it is observed that the minimum compressive strength requirements for cement are lower values in ASTM than those of BDS EN. Also, initial setting time is the same both for OPC and PCC as per ASTM. Compressive strength enhancement at 28 days is shown higher for OPC than those of PCC following ASTM. However, this enhancement in the strength for tested cement sample is almost the same both for OPC and PCC following BDS EN.

## CONCLUSIONS

A review study is conducted on different specifications and requirements for the different properties of cements following ASTM and BDS EN standards. An experimental program is also conducted to determine the different physical properties such as normal consistency, initial and final setting time, and compressive strength of cement. Both OPC and PCC types of cement are considered in the study. OPC grade 52.5N and PCC grade 42.5N are used in the experimental program. Specimen preparation and testing have been done on the same day for each grade of cement samples.

Following conclusions can be drawn from the present study:

- Requirements for initial setting time is provided in BDS EN while both the initial and final setting time are considered in ASTM.

- Specification for initial setting time of tested cement sample is matched better with BDS EN standard.
- Minimum compressive strength values for OPC and PCC are very close following ASTM while those values are well separated as per BDS EN.
- For OPC 52.5N, an enhancement of compressive strength at 28 days is obtained 71% higher than that of the required value as per ASTM while that value is only 22% higher following BDS EN.
- Strength enhancement ratio is higher for OPC than that of PCC as per ASTM while that enhancement is almost the same both for OPC and PCC following BDS EN.

### **ACKNOWLEDGMENTS**

Experimental studies of this paper were carried out under the undergraduate program in Bangladesh University of Engineering and Technology (BUET), Dhaka, Bangladesh. Authors are thankful to all lab technician/assistants of Civil Engineering Department, BUET for their assistance during the experimental study.

### **REFERENCES**

- ASTM C109: Standard Test Method for Compressive Strength of Hydraulic Cement Mortars (Using 2-in. or [50-mm] Cube Specimens, West Conshohocken, PA, USA.
- ASTM C150: Standard Specification for Portland Cement, West Conshohocken, PA, USA.
- ASTM C187: Standard Test Method for Normal Consistency of Hydraulic Cement, West Conshohocken, PA, USA.
- ASTM C191: Standard Test Methods for Time of Setting of Hydraulic Cement by Vicat Needle, West Conshohocken, PA, USA.
- ASTM C595: Standard Specification for Blended Hydraulic Cements, West Conshohocken, PA, USA.
- ASTM C778: Standard Specification for Standard Sand, West Conshohocken, PA, USA.
- BDS EN 196-1:2005(E): Method of Testing Cement- Part 1: Determination of strength, BSTI, Bangladesh.
- BDS EN 196-3:2005(E): Method of Testing Cement- Part 3: Determination of setting time and soundness, BSTI, Bangladesh.
- BDS EN 197-1:2003: Cement- Part 1: Composition, specifications and conformity criteria for common cements, BSTI, Bangladesh.

## **AN EXPERIMENTAL STUDY: STRENGTH PREDICTION MODEL AND STATISTICAL ANALYSIS OF CONCRETE MIX DESIGN**

R. Rumman\*, B. Bose, M. A. B. Emon, T. Manzur & M. M. Rahman

*Department of Civil Engineering, Bangladesh University of Engineering and Technology, Dhaka, Bangladesh*

*\*Corresponding Author: rubaiya.rumman@gmail.com*

### **ABSTRACT**

The predominant criterion for assessing concrete quality is its 28-day compressive strength. Concrete mix design by ACI method is popularly used in Bangladesh for producing concrete of required strength, but for determining its compressive strength one has to wait 28-day after casting. Predicting 28-day compressive strength of concrete has been a significant research challenge for many years. In this work, early age strength of concrete was considered as the tool for concrete strength prediction so that early age, for example 7-day, strength can be regarded as another criterion for concrete quality assessment. Although prediction of 28-day strength from early strength data is already proposed by ACI, it is still not used by construction Engineers in the country. Considering its potential as a powerful tool in mix design, extensive laboratory research has been carried out focusing on this specific area using locally available materials. Three hundred concrete cylinders were cast varying their water cement ratio, cement content, aggregate cement ratio and concrete strength at 7 and 28 days was observed. Along with predicting 28-day compressive strength from early strength data this paper also analyses the standard deviation of the data set to check its acceptability.

Keywords: Concrete; mix design; ACI method; compressive strength; early strength; standard deviation

### **INTRODUCTION**

Majority of structures found in Bangladesh are made of concrete. The guideline generally followed in this country for producing concrete is the one provided by ACI mix design (ACI Committee 211. 1-91). The criterion used is primarily 28-day strength of concrete. However, often it becomes necessary to predict 28-day strength from early age strength of concrete. There is no Code prescribed formula for such prediction. As a result, a number of research endeavours have been carried out in this field (Hasan & Kabir, 2012; Abd Elaty, 2013; Telisak et al., 1991) and different strength prediction models have been proposed. Telisak et al. (1991) studied the applicability of some non-destructive test methods for assessing concrete strength in field and Abd Elaty (2013) proposed a new model for predicting concrete strength using data taken from previous research papers (Colak, 2006; Givi et. al, 2011; Wild et. al, 1995 and Han & Kim, 2004). Hasan and Kabir (2012) took data from a previous experimental study conducted in Patiala (Garg, 2003) and proposed a mathematical model, then validated it using an experimental data set of 23, prepared using materials found in Bangladesh. However, mathematical model developed using test data of samples prepared by local materials and larger sample size may provide more accurate prediction of strength. With this end in view, a research endeavour is conducted using locally available materials in Bangladesh and then proposing a model to predict 28-day strength based on early age test data.

The objectives of this research were to:

- Conduct a detailed experimental study with large sample size (consisting of 300 cylinders) to observe the 7-day and 28-day compressive strength of concrete having different water cement ratios and cement content.
- Obtain simplified equations to predict 28-day strength from 7-day strength of concrete based on different water-cement ratios.
- Validate the equations with results obtained from previous researches.

- Obtain normal distribution curves of 28-day strength at different characteristic strength and find out the statistical variance for each band of experimental data.

## METHODOLOGY

The mix design of concrete has been carried out as per ACI Mix Design Method (ACI Committee 211.1-91). The concrete samples were prepared using locally available materials. Stone Chips were used as coarse aggregate and local sand with fineness modulus 3.09 was used as fine aggregate. Gradation curves for coarse aggregate and fine aggregate are shown in Fig. 1 and Fig. 2, respectively.

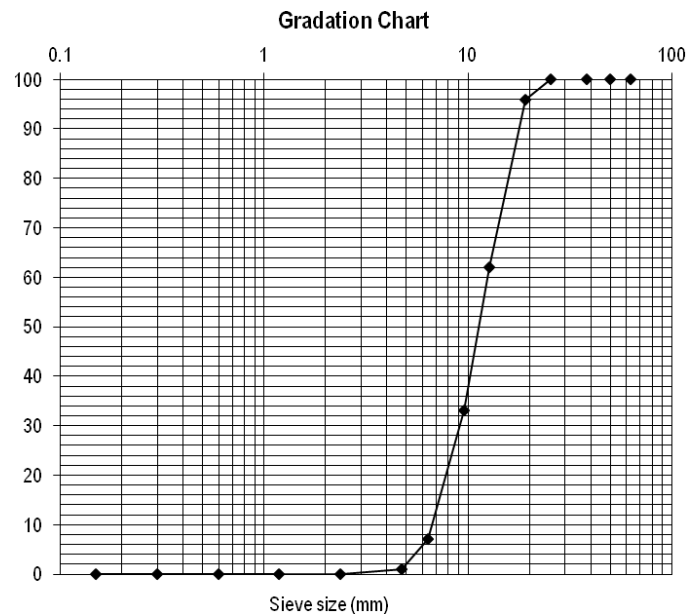


Fig. 1: Gradation curve for coarse aggregate

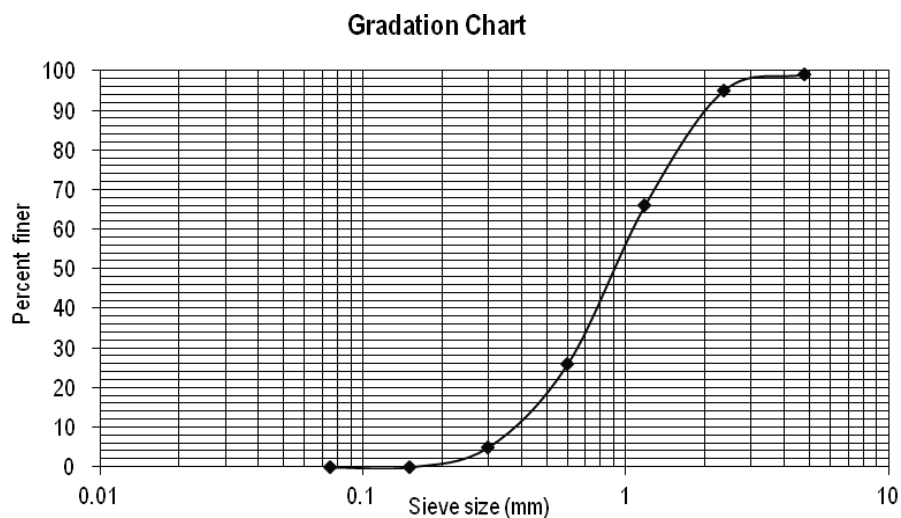


Fig. 2: Gradation curve for fine aggregate

The compressive strength of the cylinders has been tested conforming to the ASTM specifications (ASTM C39 / C39M - 16a). Following self-explanatory figures (Fig. 3) show the total procedure of mix design and compressive strength test of concrete in concise form.



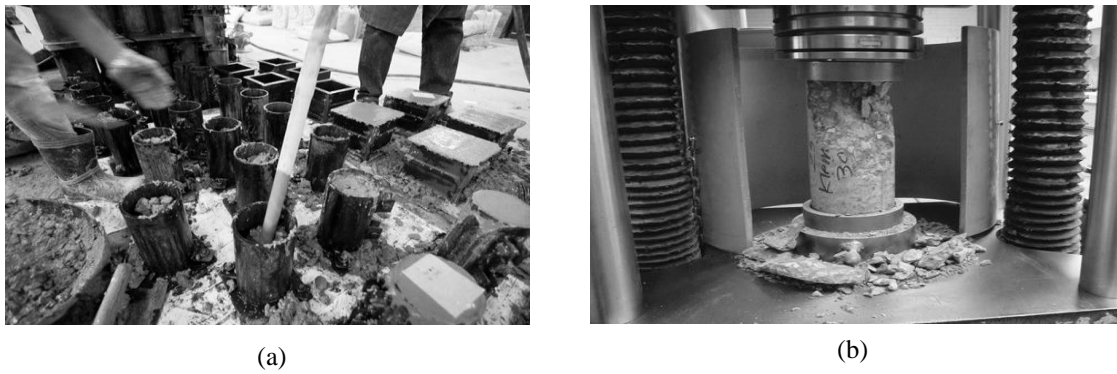
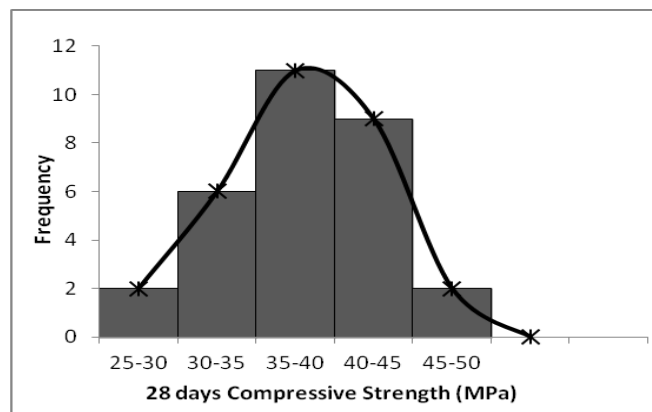


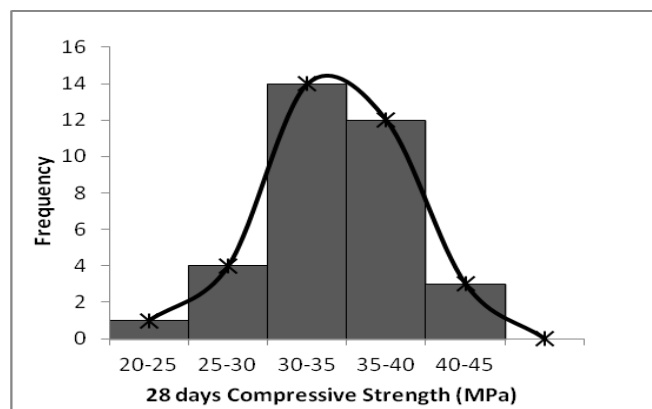
Fig. 3: (a) Compaction of the freshly cast cylinders and cubes (b) Determination of compressive strength of

### STATISTICAL ANALYSIS

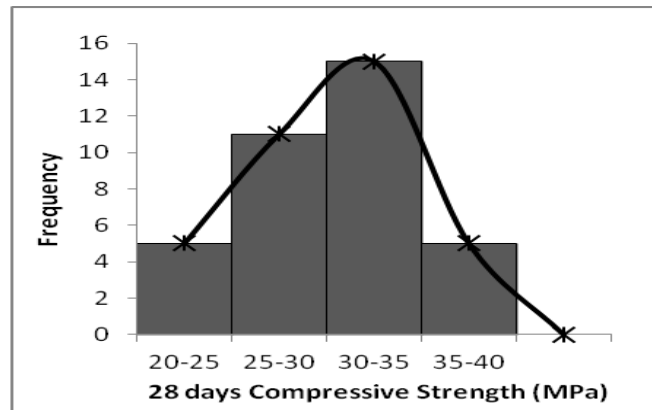
The experimental data obtained for 28-day compressive strength based on the characteristic strength were tallied and normal distribution curves were drawn. The results, as shown in the graphs below (Fig. 4), show fairly bell shaped normal distribution curves as were expected. Standard deviations of the experimental data from characteristic strength were determined for each of the three target strength data; each consisting 30 (or more) data sets as specified by ACI Committee 118 (1991).



(a)



(b)



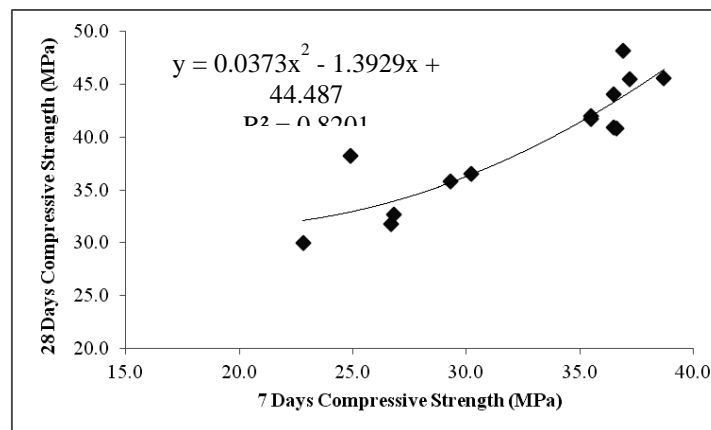
(c)

Fig. 4: Normal Distribution of 28-day compressive strength obtained in the laboratory based on the characteristic strength of (a) 43.75 MPa, (b) 37.5 MPa and (c) 34.35 MPa

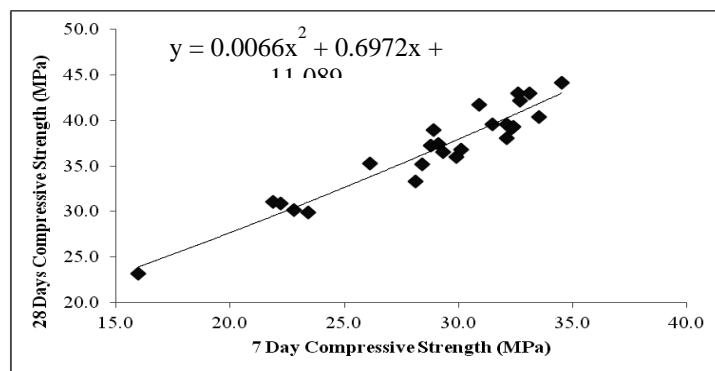
Standard deviations of the three range of compressive strength data set were calculated to be 5.43 MPa, 4.52 MPa and 4.88 MPa respectively whereas the mean strength of the data ranges were calculated to be 38 MPa, 34 MPa and 29 MPa respectively. The standard deviation values are relatively low, so the acceptability of the utilized experimental strength results is verified.

## RESULTS AND DISCUSSIONS

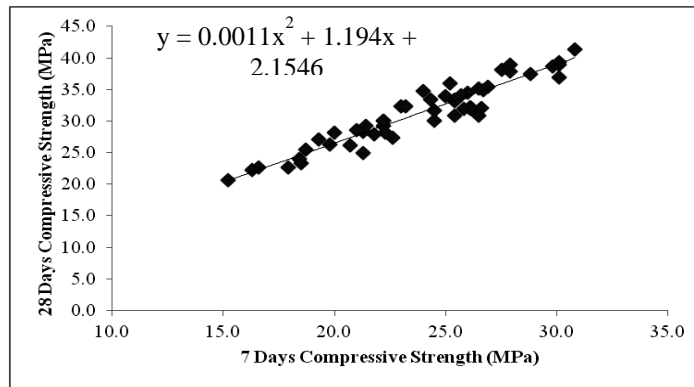
A mix design data set of 100 was taken varying their water cement ratio (w/c) and cement content. Fine aggregate to total aggregate ratio (fa/ta) and aggregate gradation were kept constant (0.40). Their water cement ratio was varied from 0.35 to 0.5. All the data were then divided into three ranges of w/c ratio: 0.35 to 0.40, 0.41 to 0.44 and 0.45 to 0.50. 28-day strength versus 7-day strength values were plotted for these three ranges of w/c.



(a)



(b)



(c)

Fig. 5: Plot of 28-day versus 7-day compressive strength at water cement ratio of (a) 0.35 to 0.40 (b) 0.41 to 0.44 and (c) 0.45 to 0.50

The above three figures (Fig. 5) show the plots of 28-day compressive strength versus 7-day compressive strength for the three-different water cement ratio range. They show the regular trend of increasing 28-day strength resulting from increased 7-day strength.

#### DERIVATION AND VALIDATION OF MODEL

The next step was to determine three sets of equations which would assist in predicting 28-day strength from 7-day strength. The following three equations were developed [Eq. (1), Eq. (2) and Eq. (3)] for w/c ratio ranges of 0.35 to 0.40, 0.41 to 0.44 and 0.45 to 0.50, respectively.

$$y = 0.0373x^2 - 1.3929x + 44.487 \quad (1)$$

$$y = 0.0066x^2 + 0.6972x + 11.089 \quad (2)$$

$$y = 0.0011x^2 + 1.194x + 2.1546 \quad (3)$$

Where, y is the 28-day compressive strength and x is the 7-day compressive strength of a specific sample. As can be seen from the  $R^2$  values, the experimental data reasonably satisfies the proposed equations.

Table 1: Validation of previous research results with the derived equations

w/c Range	w/c	7-day strength	28-day predicted strength	28-day Actual strength
		MPa	MPa	MPa
upto 0.4	0.4	23.33	32.29262	32.34
	0.35	39.29	47.34012	47.29
	0.375	34.76	41.1378	41.5
0.41-0.44	0.42	18.04	25.8144	24.64
	0.42	26.15	33.83401	34.2
	0.44	20	27.673	25.97
0.45-0.50	0.47	21.26	28.03623	27.67
	0.48	23.38	30.67161	30.9
	0.5	20.36	26.92042	27.51

The derived equations were validated using data taken from previous researches (Kamal & Rumman, 2014; Garg, 2003; Hasan & Kabir, 2012). Table 1 shows the validation of the three equations for three water cement ratios ranges. From Table 1, it can be observed that for each range of water cement ratio, the 28-day predicted strength and actual strength are almost similar. Numerically, a maximum deviation of 4.8% is observed.

## CONCLUSIONS

ACI mix design, although generally used all over the globe, may need modifications at different regions of the world due to differences in ambient conditions and materials. Equations and statistical data obtained from this study from rigorous experimental research can assist the practicing engineers of the country and south-east Asian regions as an important tool in early evaluation of a concrete mix. In addition, early prediction of strength may assist in taking important decisions regarding quality control of concrete work. Such decision may save both time and cost of a construction project.

## REFERENCES

- ACI Committee 318. (1999). *Building code requirements for structural concrete; (ACI 318-99); and commentary (ACI 318R-99)*. Farmington Hills, Mich: American Concrete Institute.
- ACI 211 (1991, Reapproved in 2002). Standard Practice for Selecting Proportions for Normal Heavyweight, and Mass Concrete, ACI 211.1-91. *Manual of Concrete Practice*, 1–38.
- Abd elaty, M. A. A. (2013). Compressive strength prediction of Portland cement concrete with age using a new model. *HBRC Journal*, 10(2), 145–155. <http://doi.org/10.1016/j.hbrcj.2013.09.005>
- ASTM C39 / C39M - 16a Standard Test Method for Compressive Strength of Cylindrical Concrete Specimens, ASTM International, West Conshohocken, PA, 2016, [www.astm.org](http://www.astm.org)
- Colak, A. A new model for the estimation of compressive strength of Portland cement concrete, *Cement and Concrete Research* 36 (7) (2006) 1409–1413.
- Hasan, M., & Kabir, A. (2012). Early Age Tests to Predict 28 Days Compressive Strength of Concrete Compressive strength of concrete Mix-design data. *Awam International Conference on Civil Engineering*, (AUGUST 2012), 376–383. <http://doi.org/10.13140/2.1.3296.2249>
- Han, S.-H., Kim, J.-K., Effect of temperature and age on the relationship between dynamic and static elastic modulus of concrete, *Cement and concrete research* 34 (7) (2004) 1219–1227.
- Hewlett, P.C., Lea's Chemistry of Cement and Concrete, *Elsevier Butterworth-Heinemann*, New York, 2005 (Chapter 6).
- Givi, A., Rashid, S., Aziz, F., Salleh, M., The effects of lime solution on the properties of SiO<sub>2</sub> nanoparticles binary blended concrete, *Composites B* 42 (3) (2011) 562–569.
- Kamal, M. R., & Rumman, R. (2014). *Durability Characteristics of CEM II Cement Concretes* (B.Sc. Thesis). Bangladesh University of Engineering and Technology.
- Rishi Garg. (2003). *Concrete Mix Design Using Artificial Neural Network*. Thapar Institute of Engineering and Technology.
- Telisak, T., Carrasquillo, R. L., & Fowler, D. W. (1991). *Early Age Strength of Concrete: A Comparison of Several Nondestructive Test Methods* (Vol. 1198–1F).
- Wild, S. S., Sabir, B. B., Khatib, J. M., Factors influencing strength development of concrete containing silica fume, *Cement and Concrete Research* 25 (7) (1995) 1567–1580.

## EFFECT OF SUGAR ON SETTING TIME OF PORTLAND CEMENT

A. F. Mazumder\*

*Department of Civil Engineering, Presidency University, Dhaka, Bangladesh*

*\*Corresponding Author: mazumder\_buet@yahoo.com*

### ABSTRACT

Setting time is affected while concreting in hot weather condition. To prevent concrete to set early due to adverse effects of hot weather, admixtures are usually incorporated in it. On the other hand emergencies may arise, due to traffic congestion and for massive concreting, to increase the setting time. The objective of this paper is to investigate the effect of sugar as a retarding/accelerating admixture on Type - I and Type - V Portland Cement paste. The setting time tests were performed for different concentration (0 to 0.25%) of sugar. Sugar was added with water, and then mixed with cement. The test result revealed that for lower concentration (0.01~0.08%), sugar acts as retarding agent and for higher concentration (over 0.17~0.19%), sugar acts as accelerating agent. Optimum concentration was found to be 0.073% and 0.05% for Type - I and Type - V cement respectively.

Keywords: Initial Setting Time; final setting time; cement; sugar; admixture

### INTRODUCTION

Traffic congestion has triggered on time arrival of concrete truck on construction site. In addition, high temperature also lowers the setting time of concrete. When water is added to cement, paste is formed which gradually stiffens and then hardens. The stiffening of cement paste is called setting. Normal setting of cement is associated with the hydration of Tri-calcium silicate ( $C_3S$ ) and formation of the calcium silicate hydrate (C-S-H gel). Due to the conditions of hot weather, there is rapid evaporation of water from the surface of the fresh cement paste/concrete. As a result, the cement paste or concrete sets rapidly than its normal setting and reduces the length of time for concreting operations. So, less time is available for placing, compaction and finishing. That would lead to porous concrete and loss of strength. So, there is rise of demand of efficient retarder for cement paste/ concrete.

Retarding admixtures are mainly based on materials having lignosulfonic acids and their salts, hydroxy-carboxylic acids and their salts, sugar and their derivatives and inorganic salts such as borates, phosphates, zinc and lead salts. Retarding effects of a retarder depends upon a number of factors including dosage of the admixture, time of addition to the mix and curing conditions. Some admixtures act as retarders when used in small amounts but behave as accelerators when used in large amounts. For example, sugar behaves as a set retarder but the small amount of sugar will virtually prevent the setting of cement (Ashworth, 1963; Jumadurdiyev et al., 2005; Abalaka, 2011; Abalaka, 2011).

Owing to the retardation of ordinary Portland cement, sugar falls into three categories: non-retarding, good retarders and most effective retarders. The non-retarding sugars,  $\alpha$ -methyl glucoside and  $\alpha$ ,  $\alpha$ -trehalose are effectively non-retarding; the retarding sugars glucose, maltose, lactose and cellobiose, are grouped together as good retarders; and sucrose and raffinose are the most effective retarders (Thomas and Birchall, 1983). Because of retarding action of retarder, the one day strength of concrete is reduced. However, ultimate strength is reported to be improved by using set controlling admixtures. Rate of drying shrinkage and creep would increased by using retarders, but the ultimate values cannot increase.

The main objective of this study is to investigate the possibilities of using sugar as retarding agent for Type I and Type V cement. The specific objective of this study is to determine the optimum dosages of sugar for both types of cement and its effect on setting time.

### METHODOLOGY

The length of time for a mixed preparation of materials to reach a state of hardness, measured from the start of the mixing. The end point for dental materials is usually determined by a penetration test. The

setting and hardening of cement is a continuous process, but two points are distinguished for test purposes. The initial setting time is the interval between the mixing of the cement with water and the time when the mix has lost plasticity, stiffening to a certain degree. It marks roughly the end of the period when the wet mix can be molded into shape. The final setting time is the point at which the set cement has acquired a sufficient firmness to resist a certain defined pressure. It is different for different types of cement, depends upon the type of project in which it is being used. Initial setting time of ordinary Portland cement should be maximum 45 minutes according to the British Standard. Final setting time of cement should not be more than 10 hours.

To investigate the effect of sugar as a retarding agent, normal consistency test was undertaken according to ASTM C187. After completing normal consistency test, with the known consistency (water/cement ratio) six samples were tested to measure initial and final setting time according to ASTM C191. At first, one sample was tested without adding sugar to the mixture (control specimen). Then initial and final setting time was recorded, to know the actual situation of the cement. Then rest 5 samples were tested with different concentration of sugar, added to the mixture by mixing with water as a percentage of cement. The concentrations of sugar were taken as 0.05%, 0.10%, 0.15%, 0.20% and 0.25%. Then for all the samples initial and final setting time were recorded and compared with the control specimen. To find out optimum dosage of sugar Newton's Forward Interpolation method was adopted.

## RESULTS AND DISCUSSIONS

Six specimens were tested to find out initial and final setting time. Among the specimens, one was control specimen without sugar content and other five specimens were having increasing amount of sugar. The amount of sugar was added as the percentage of cement content in the mixture. The concentration was 0.05%, 0.10%, 0.15%, 0.20% and 0.25%. Then following the same procedure initial and final setting were recorded for different concentration of sugar. Table 1 shows the experimental results.

Table 1: Sugar Concentration, Initial and Final Setting Time

Sugar added as the percentage of cement	Weight of sugar added (gm)	Setting Time			
		Type I Cement		Type V Cement	
		Initial (minutes)	Final (minutes)	Initial (minutes)	Final (minutes)
0	0	135	215	187.8	600
0.05	0.325	378	780	690.8	900
0.1	0.65	373	675	313.4	720
0.15	0.975	219	510	190	510
0.2	1.3	50	420	111.9	356
0.25	1.625	23	360	35.7	240

The outcome of this research is discussed below:

- The normal consistency was found to be 0.26 and 0.28 for Type I and Type V cement respectively.
- For lower concentration (up to 0.08%), sugar acts as retarder and for higher concentration (more than 0.17~0.19% approximately), sugar acts as accelerator comparing with the control specimen (without sugar).

The optimum sugar content for which highest amount of retardation was 0.073% (using Newton's Forward Interpolation Method) and 0.05% approximately for Type I and Type V cement respectively.

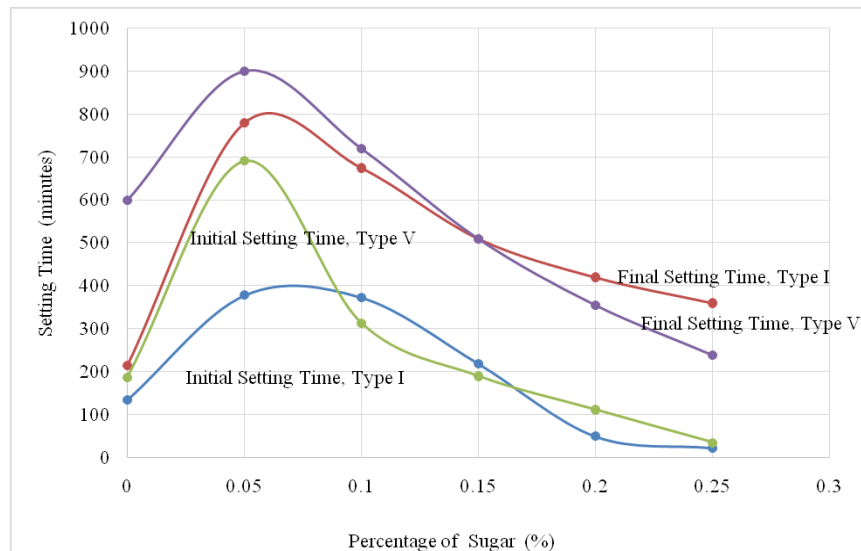


Fig. 1: Setting Time Vs Concentration of Sugar Diagram

Discussion can be made about result:

- The setting time of cement is highly affected by sugar and amount of sugar to be added to get additional time (in case of retardation) or reduce the time (in case of acceleration) before set, can be found out from Fig. 1.
- The retarding effects of sugar, when added to a mix, continue until it is removed from the solution by reaction with  $C_3A$  from the cement or by some other way, it is removed and incorporated into the hydrated material (Khan and Ullah, 2004).
- For higher concentration of sugar, setting time had decreased. The exact cause of this abnormal behavior of the retarding admixture to accelerate the initial set is not known. However, it was reported by some researchers that in addition to the reaction between lime and pozzolana, some other reaction between  $C_3A$  or its hydration products and pozzolana can occur (Plowan and Cabera, 1984). There may be some reaction between the pozzolana and the admixture to form some compounds giving rigidity to the paste earlier than that obtained by the hydration products of the cement. According to the opinion of the Author of this paper, higher concentration of sugar increases the reactivity of  $C_3A$ .

## CONCLUSIONS

This research was undertaken to investigate the retarding action of sugar on setting time of cement paste. All other variable was kept constant, except the concentration of sugar. From the result of initial and final setting time it can be reported that

- Up to optimum sugar content (0.06-0.08%), sugar can be used as a retarding admixture for hot weather countries.
- Above 0.20% sugar content can be used as a accelerator for cold weather countries.
- Optimum concentration can be chosen for highest amount of setting time.
- From the graph below, extra time required for transporting, placing, compacting and finishing can be calculated and for that corresponding sugar concentration should be added to have desired initial setting time. This curve was drawn for 0 to 0.08% of sugar content by interpolating the data from 0 to 0.05% concentration. Otherwise, for required additional initial setting time, sugar concentration can be calculated from the equations and added to actual initial setting time.

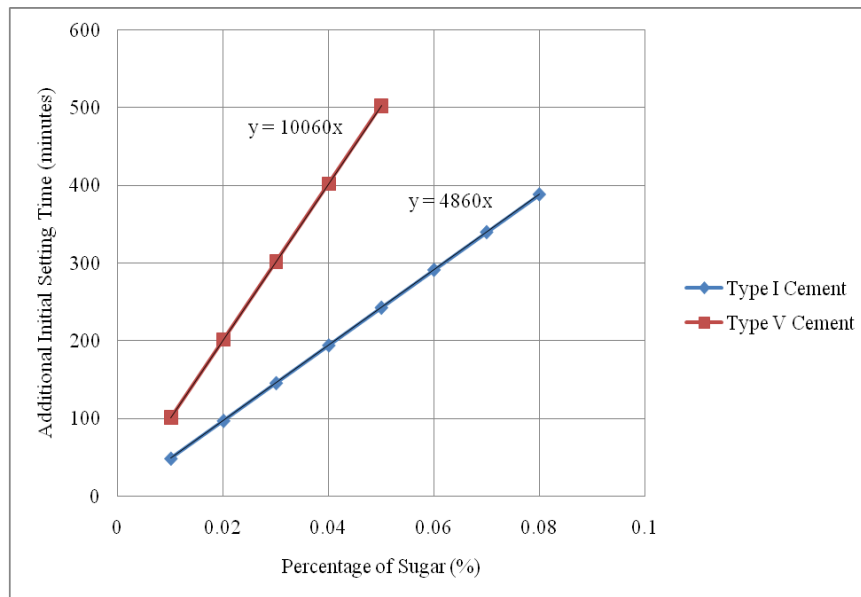


Fig. 2: Initial Setting Time Vs Sugar Concentration

### ACKNOWLEDGMENTS

Tests of this study were undertaken in concrete laboratory of King Fahd University of Petroleum and Minerals (KFUPM).

### REFERENCES

- Abalaka, AE. 2001. Effects of Sugar on Physical Properties of Ordinary Portland Cement Paste and Concrete. *AU J.T.*, 14(3): 225-228.
- Abalaka, AE. 2011. Comparative Effects of Cassava Starch and Simple Sugar in Cement Mortar and Concrete. *ATBU Journal of Environmental Technology*, 4(1).
- Ashworth, R. 1963. Some Investigation into the use of sugar as an admixture to concrete. *Proc. Inst. Civ. Eng.*, 31: 129-145.
- Jumadurdiyev, A; Ozkul, MH.; Saglam, AR. and Parlak, N. 2005. The Utilization of Beet Molasses as a Retarding and Water-reducing Admixture for Concrete. *Cement and Concrete Research*, 35: 874-882.
- Khan, B. and Ullah, M. 2004. Effect of a Retarding Admixture on the Setting Time of Cement Pastes in Hot Weather. *Eng. Sci. Vol.* 15(1): 63-79.
- Plowan, C and Cabera, JG. 1984. Mechanism and Kinetics of Hydration of C3A and C4AF. *Cement and Concrete Research*. 14(2): 238-248.
- Thomas, NL and Birchall, JD. 1983. The Retarding Action of Sugar on Cement Hydration. *Cement and Concrete Research*. 13: 830-842.



## **PROPERTIES OF STEEL FOR THE REINFORCEMENT OF CONCRETE IN BANGLADESH**

M. A. A. Siddique\*

*Department of Civil Engineering, Bangladesh University of Engineering and Technology, Dhaka,  
Bangladesh*

*\*Corresponding Author: [alamin@ce.buet.ac.bd](mailto:alamin@ce.buet.ac.bd)*

### **ABSTRACT**

This paper presents the statistical analysis of test results for different properties of steel for the reinforcement of concrete in Bangladesh. A number of tests have been conducted on reinforcing bars having different steel grades such as 276 MPa (40 ksi), 414 MPa (60 ksi) and 500 MPa (72 ksi). These bars have been used or will be intended to use for a wide range of structural applications such as buildings, bridges, flyover, culverts, road drainage networks etc. These include constructions by government and semi-government organizations, private as well as developer companies. From the experimental results, it is observed that tested diameters of rebars are usually lesser than that of the specified nominal diameter. This trend is found more dominant for 500 MPa bars than that of 276 MPa and 414 MPa bars. Average yield strength of rebars satisfies the minimum standard requirements set forth by ASTM and BDS ISO. The ratio between tensile strength to the yield strength and percent elongation are observed higher both for 276 MPa and 414 MPa bars than those of 500 MPa bars. Higher coefficient of variation is shown for bars with yield strength of 414 MPa.

Keywords: Reinforcing bar; grade; yield strength; tensile strength; percent elongation

### **INTRODUCTION**

Three types of steel reinforcement bars (rebars) such as hot-rolled (HR), cold twisted deformed (CTD), and thermo-mechanically treated (TMT) have been used in concrete structures. HR rebars are produced through hot rolling followed by a slow cooling to an ambient temperature. The high yield strength of the bar is obtained by raising carbon as well as manganese contents, and to a great extent, by cold twisting. CTD bars are produced by cold working process, which is basically a mechanical process that involves stretching and twisting of mild steel, beyond the yield plateau, and subsequently releasing the load. There has been an increasing demand for high strength deformed bars. TMT bars were introduced in Bangladesh in the last decade. Thermo mechanical treatment is an advanced heat treatment process in which hot bars coming out of last rolling mill stand are rapidly quenched through a series of water jets. Rapid quenching provides intensive cooling of surface resulting in the bars having hardened surface with hot core. The rebars are then allowed to cool in ambient conditions. During the course of such slow cooling, the heat released from core tempers the hardened surface of martensite while core is turned into ferrite-pearlite aggregate composition (Islam, 2010). The design of reinforced concrete (RC) structures in Bangladesh was dominated by the use of steel reinforcement with a yield strength,  $f_y$ , equal to 276 MPa (40 ksi) and 414 MPa (60 ksi). Currently, 500 MPa (72 ksi) rebars are widely used in concrete industry. ACI 318 (ACI 2011) and AASHTO (2012) edition of the AASHTO LRFD Bridge Design Specifications permit the use of rebars beyond 552 MPa. Earlier versions of these codes, the yield strength of rebars was limited to 552 MPa as the behaviour of structural members using rebars with yield strength above 552 MPa was not well documented. Use of high strength bars for design could provide various benefits to the concrete construction industry by reducing member cross-sections and reinforcing quantities, which would lead to savings in materials, shipping, and placement costs. However, the use of high strength reinforcements such as 500 MPa bars is not fully utilized in design practice in Bangladesh. This may be due to the fact that the behaviour of structural RC members having reinforcing steel with yield strength of 500 MPa is not well documented. However, upcoming BNBC-2015 might permit the use of reinforcing bar up to 600 MPa considering different ductility classes following BDS ISO standards. This ductility class depends on

tensile strength-to-yield strength (TS/YS) ratio and specified characteristic value of elongation at maximum force,  $A_{gt}$ . According to H. Bachmann (2000), RC structures may be classified as moderate ductile when  $TS/YS \geq 1.15$  and  $A_{gt} \geq 6\%$  are met and high ductility having  $TS/YS \geq 1.25$ . In addition, no maximum limit is specified for upper yield strength of the rebars. Although, 500 MPa bars are now currently in use for the construction industry in Bangladesh, there is a concern in structural behaviour of concrete members having high strength rebars. If a higher strength reinforcing steel is used in concrete but not fully accounted for in design phase, there may be an inherent overstrength in the members that has not been properly taken into account in the design phase. Overstrength in one member may result in unanticipated higher loads being transmitted to adjacent members or joints affecting assumed structural behaviour. This concern is most critical for members in seismic areas or when progressive collapse state is considered.

In structural design, uncertainties in loadings, design and constructions are considered by load factors and strength reduction factors. The purpose of these factors is to limit the probability of structural failure to an acceptable low level. For the case of material property variations, the variability of the physical and mechanical properties of reinforcing steel affects the performance of RC structures. In Bangladesh, these properties have minimum requirements, as detailed by ASTM A615 and BDS ISO 6935-2. These standards do not set maximum limits for yield strengths except ASTM A706. Designers normally use the minimum values in design without considering the true strength of rebars. This may be of concern because member behaviour can differ from the assumed response if material properties are significantly higher than those used in the design. If the reinforcement is too strong in RC flexural member, it will be over-reinforced and this can result in brittle failure with the concrete crushing before the steel yields. Therefore, the objective of this paper is to evaluate the variability of mechanical properties of reinforcing steel produced in Bangladesh and to analyze the degree to which manufacturers satisfy the minimum requirements established by ASTM and BDS standards. The study is conducted statistically by analyzing the tested rebar data. Trends in the data are evaluated based on different grades and bar sizes. Cross-sectional properties such as diameter as well as weight per meter length are considered. For the mechanical properties, yield strength (YS), tensile strength (TS), strength ratio (TS/YS), and percent elongation (%) are considered. General data descriptors are used, including mean, standard deviation, coefficient of variation, minimum and maximum values for each grade and bar size. These results would provide the quality assessment of reinforcing bars for concrete used in construction sectors in Bangladesh.

## **METHODOLOGY**

A statistical analysis has been carried out on the tested data to evaluate the variability in the properties of steel reinforcements. Cross-sectional property such as nominal weight as well as actual diameter and mechanical properties such as yield and tensile strengths, strength ratio (TS/YS) and percent elongation are assessed in terms of the requirements as set forth by ASTM and BDS. Three grades of rebars such as 276 MPa, 414 MPa and 500 MPa are considered in the study. Available diameters range from 10 mm to 20 mm for 276 MPa bars whereas 8 mm to 25 mm are considered for 414 MPa and 500 MPa rebars. In addition, 28 mm, 32 mm and 40 mm are considered for 500 MPa bars and 32 mm for 414 MPa bars. All the reinforcing bars were tested in universal testing machine to obtain the mechanical properties of rebars following ASTM A370.

## **RESULTS AND DISCUSSIONS**

In this paper, a statistical analysis is conducted to evaluate the physical and mechanical properties of rebars and to compare these properties with requirements set forth by ASTM and BDS standards. Table 1 presents the number of specimens tested in the laboratory for different grades and bar sizes. These rebars are tested in the year of 2015-16 and are used or intended to use for a wide range of structural applications. From the analysis, it is observed that average diameter of 20 mm rebar having grades of 500 MPa and 414 MPa are obtained 19.9 mm with a lower standard deviation and coefficient of variation (CoV) for 500 MPa than those of 414 MPa bar. However, average diameter is obtained 20.1 mm for 276 MPa bar with a higher standard deviation and a higher CoV. These statistical values can be determined for other bar diameters as well as for different grades of rebars. Fig. 1 shows the variation of 20 mm bar dia for three grades as well as average dia vs. nominal values.

Table 1: Number of rebar specimens used for analysis

Grade ksi (MPa)	Bar size (mm)									
	8	10	12	16	20	22	25	28	32	40
40(276)	---	162	193	175	147	---	---	---	---	---
60(414)	12	216	164	187	179	12	118		17	---
72(500)	45	324	278	364	375	21	168	15	18	12

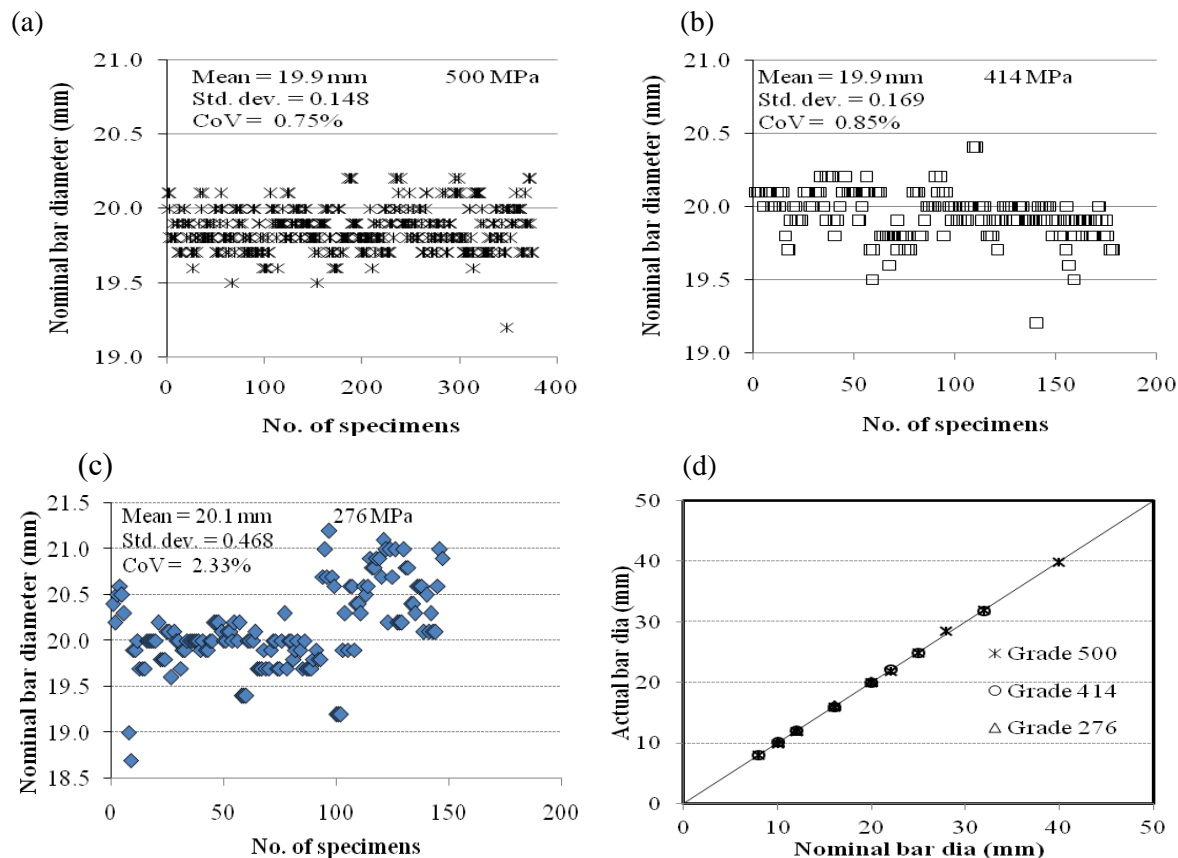


Fig.1: Variation of 20 mm bar diameters for different grades of rebars (a) 500MPa (b) 414 MPa (c) 276 MPa and (d) average bar dia for three grades

Fig. 2 shows the variation of yield strength, tensile strength, TS/YS ratio and percent elongation for 500 MPa rebars with maximum and minimum values for each parameters. From Fig. 2(a), it is observed that a wide range of yield strength is obtained with a minimum 325 MPa for 12 mm bar and a maximum 750 MPa for 8 mm bar. A number of specimen fall below the minimum yield strength values. Similar trend is observed for tensile strength, TS/YS ratio and percent elongation as shown in Figs. 2(b), 2(c) and 2(d), respectively. Figures 3 and 4 present the variations of the same parameters as mentioned in Fig. 2 for the rebar grades 414 MPa and 276 MPa, respectively. From these figures it is observed that average yield strength is well above the standard minimum criteria. However, a higher strength variation is observed for 12 mm of 500 MPa and 16 mm of 414 MPa bars. Percent elongation as well as strength ratio values are higher for 414 MPa and 276 MPa bars than those of 500 MPa bars. Fig. 5 shows CoV of different parameters for three grades of rebars. From this figure, it is shown that a higher CoV is observed for yield strength and strength ratio of 414 MPa bars than those of 500 MPa bars. However, CoV for percent elongation is comparable for the tested three grades of rebars as shown in Fig. 5(d)

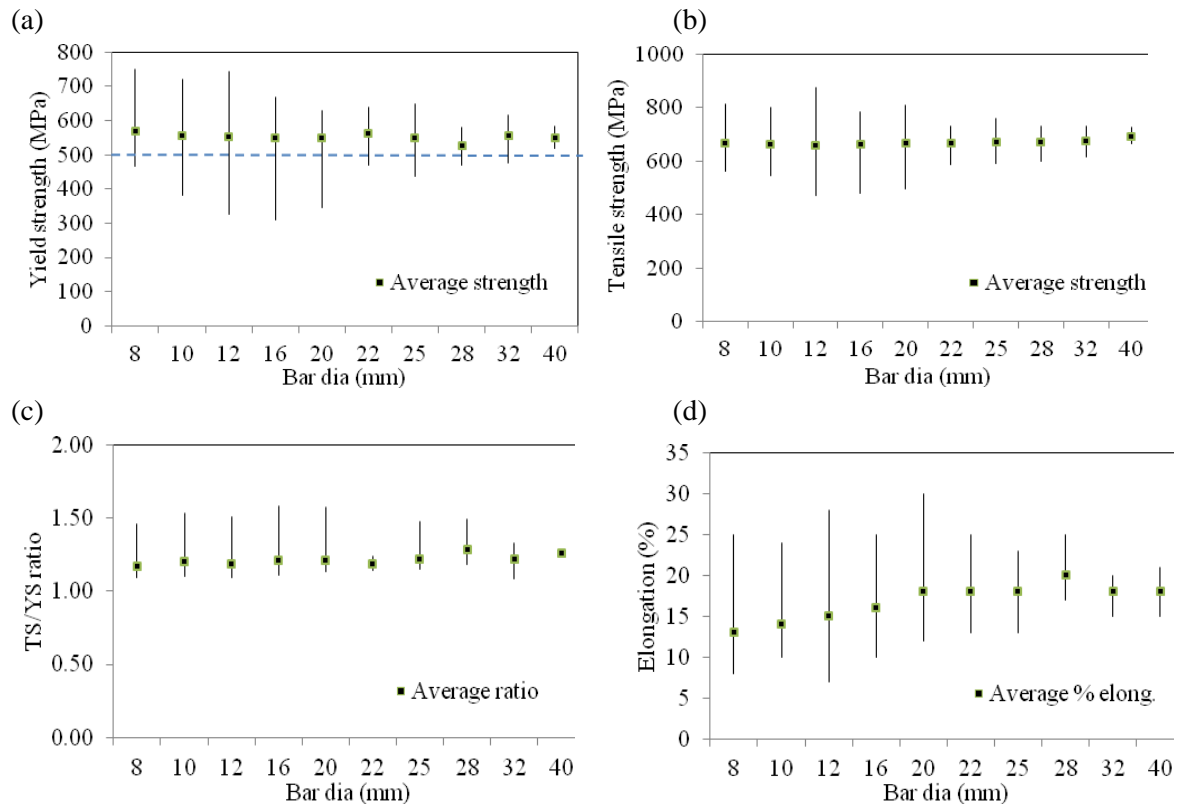


Fig.2: Variation of different properties of 500 MPa rebars (a) Yield strength (b) Tensile strength (c) Strength ratio (TS/YS) (d) Percent elongation

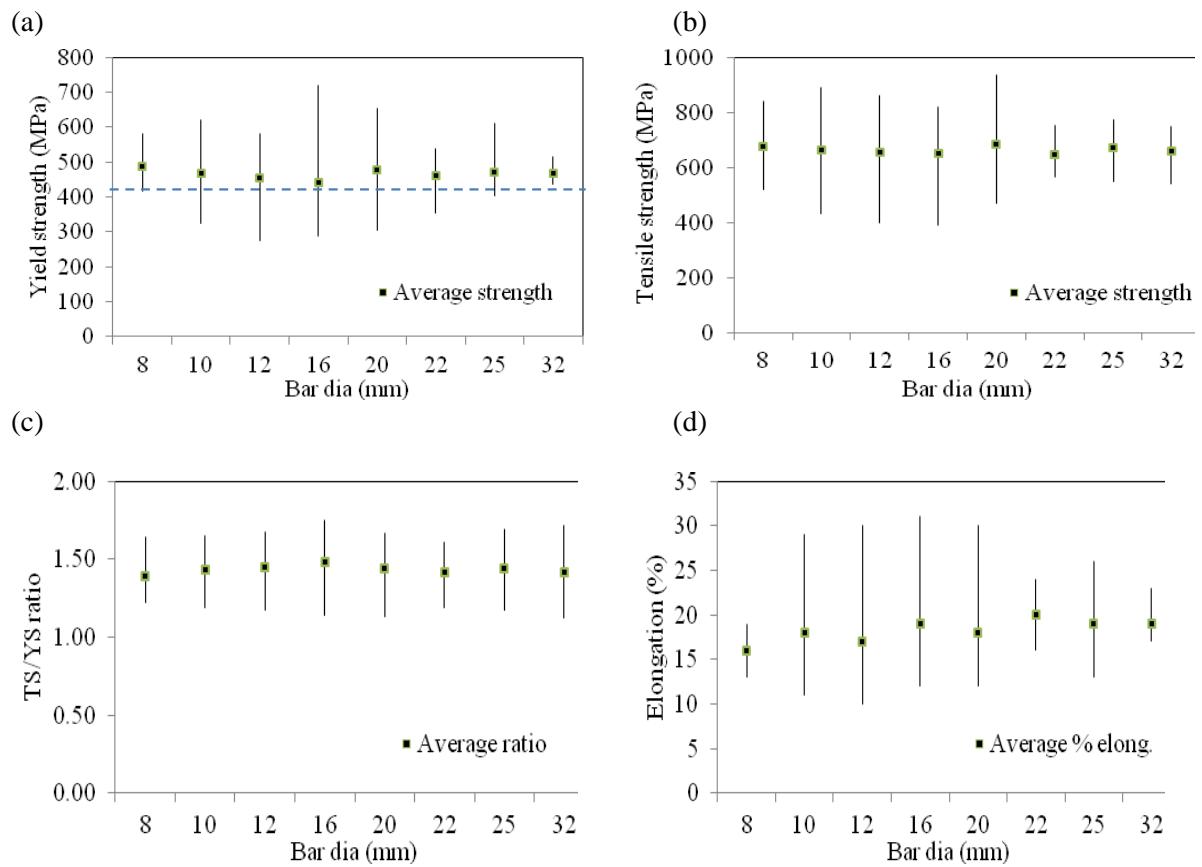


Fig.3: Variation of different properties of 414 MPa rebars (a) Yield strength (b) Tensile strength (c) Strength ratio (TS/YS) (d) Percent elongation

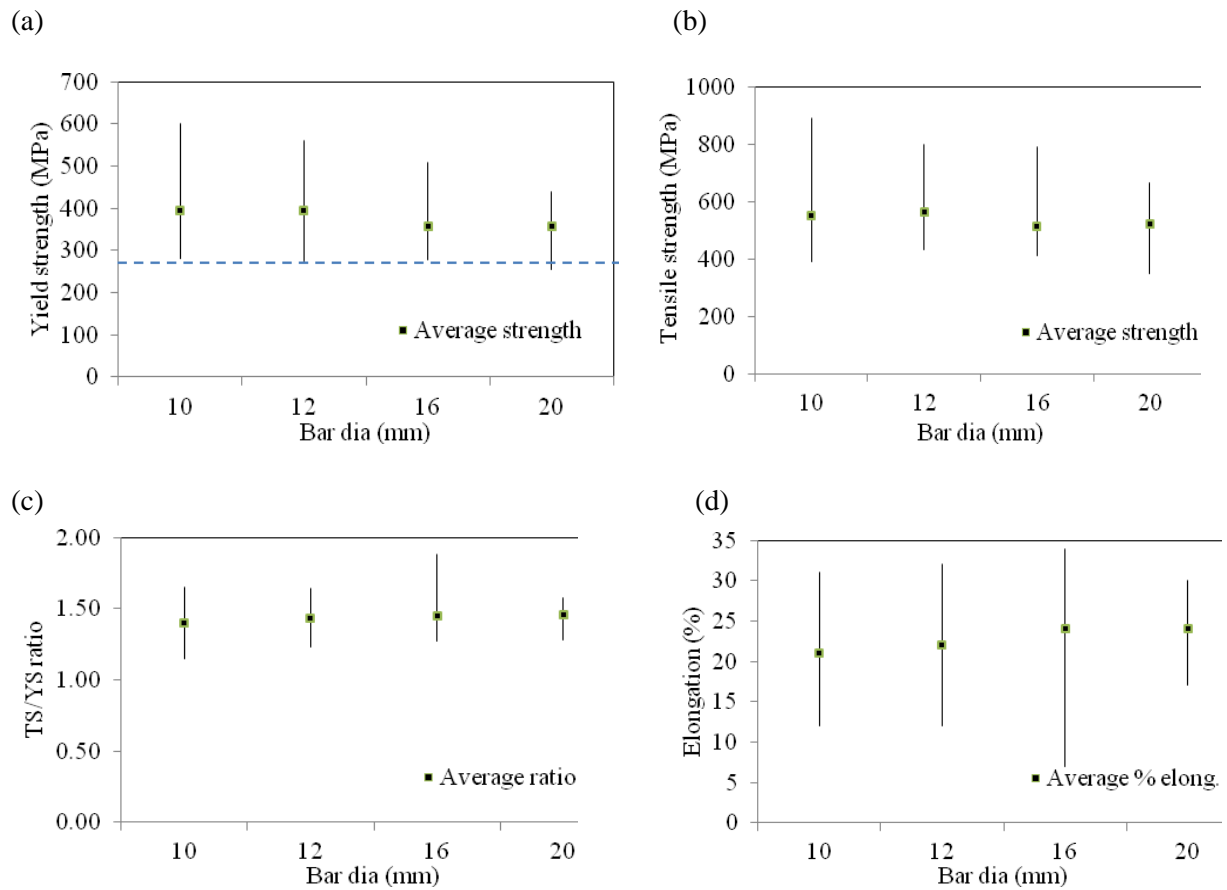


Fig. 4: Variation of different properties of 276 MPa rebars (a) Yield strength (b) Tensile strength (c) Strength ratio (TS/YS) (d) Percent elongation

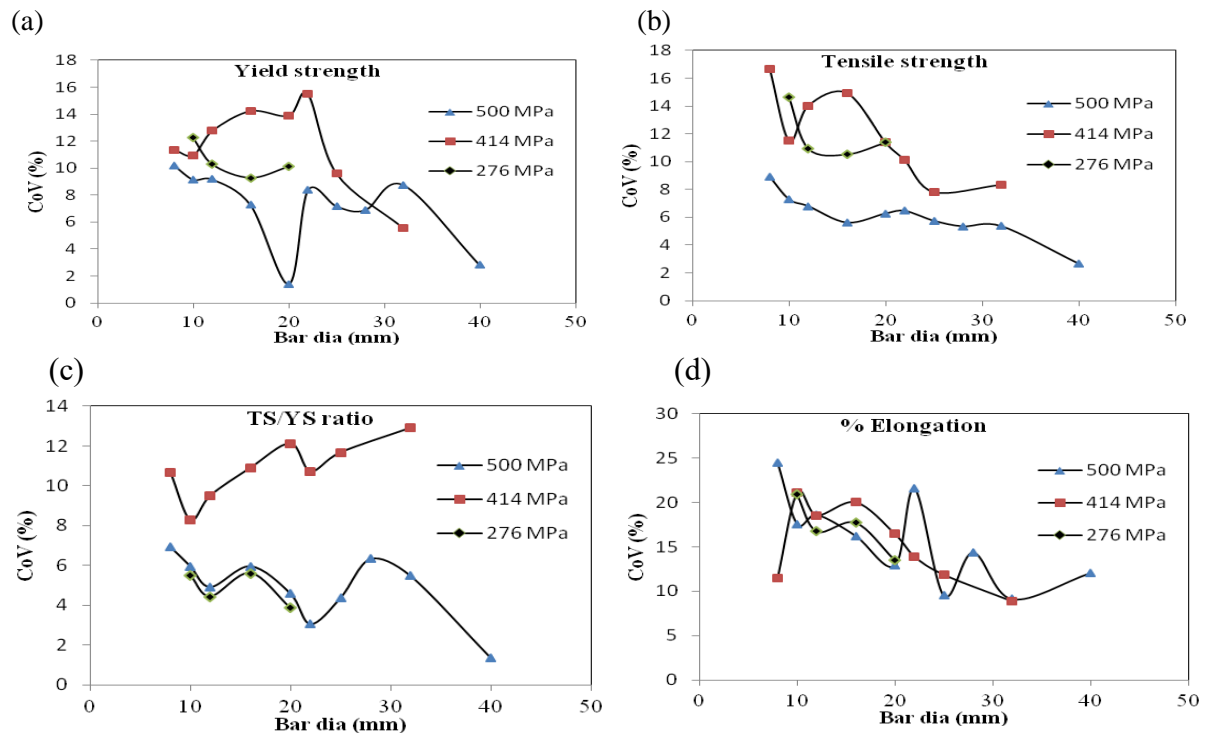


Fig. 5: Variation of CoV for three grades of rebars (a) Yield strength (b) Tensile strength (c) TS/YS ratio (d) Percent elongation

## **CONCLUSIONS**

A statistical analysis is conducted in this paper to evaluate the physical and mechanical properties of reinforcing bars and to assess the quality of the rebars used in concrete construction in Bangladesh. Three grades such as 500 MPa, 414 MPa and 276 MPa are considered. A wide range of rebar diameters from 8 mm to 40 mm are considered for wide areas of construction applications by government and private sectors. Following conclusions can be drawn from the present study:

- Average yield strength values for all the tested specimens satisfy the minimum yield strength requirements set forth by ASTM and BDS standards.
- Tensile strength-to-yield strength ratio and percent elongation are observed higher values for 414 MPa and 276 MPa bars than those of 500 MPa bars.
- Higher CoV are obtained for yield strength values of 414 MPa bars than those of 500 MPa and 276 MPa bars. However, almost the same CoV is shown for percent elongation for three grades of rebars.

## **ACKNOWLEDGMENTS**

The author would like to express his gratitude to BRTC, BUET for providing the experimental data. The author is also thankful to all lab technician/assistants of SM lab, Department of Civil Engineering, BUET for their assistance in conducting the tests.

## **REFERENCES**

- AASHTO .2012., AASHTO LRFD Bridge Design specifications, 6th Ed. Washington, DC.
- American Concrete Institute (ACI). 2011. Building Code requirements for reinforced concrete and commentary, ACI 318-11/ACI 318R-11, Farmington Hills, MI, USA.
- ASTM. 2014. Standard test methods and definitions for mechanical testing of steel products, A 370-14, West Conshohocken, PA, USA.
- ASTM. 2014. Standard specification for deformed and plain carbon steel bars for concrete reinforcement, A615/A615M-14, West Conshohocken, PA, USA.
- ASTM. 2014. Standard specification for deformed and plain low-alloy steel bars for concrete reinforcement, A706/A706M-14, West Conshohocken, PA, USA.
- Bachmann, H. 2000. Problems relevant to poor ductility properties of european reinforcing steel. *12th World conference on Earthquake Engineering*, Auckland, New Zealand.
- Bangladesh Standards and Testing Institution (BSTI). 2015. Steel for the reinforcement of concrete- Part 2: Ribbed bars, BDS ISO6935-2, Tejgaon, Dhaka, Bangladesh.
- Housing and Building Research Institute (HBRI). 2006. Bangladesh National Building Code (BNBC), Mirpur, Dhaka, Bangladesh
- Islam, MA. 2010. Thermomechanically treated advanced steels for structural applications. *Proceedings of MARTECC 2010, The International Conference on Marine Technology*, BUET, Dhaka, Bangladesh, pp. 149-153.

## **EFFECT OF BASE ISOLATION AND DIFFERENT BRACING SYSTEM TO IMPROVE BUILDING PERFORMAMCE UNDER EARTHQUAKE EXCITATIONS**

F.T. Zahura<sup>\*</sup>, S. A. Javed & R. Naznin

*Department of Civil Engineering, Ahsanullah University of Science and Technology, Dhaka,  
Bangladesh*

*\*Corresponding Author: fatema.ce@aust.edu*

### **ABSTRACT**

The performance of different types of frame with base isolator and Rectangular shape frames with different types of bracing under earthquake is investigated to know the building response. A 20 story SAC frame was selected for this study and the base isolated frame is introduced to compare with the rectangular shape frames. Modal time period and frequency are compared between base isolated frame and rectangular frame with bracing. Displacement and drift is compared with the rectangular frame bracing and base isolated frame. The results show that base isolator reduce the inertia forces introduced in the structure due to earthquake by shifting the fundamental time period of the structure. The displacement of a base isolator frame is 42% higher than the E Bracing frame for the case of EI Centro and hereby increases the flexibility of the structure.

Keywords: Base isolation; bracing system; rectangular frame; SAC frame

### **INTRODUCTION**

Earthquake is one of the most uncertain loads in nature. It cannot be predicted when and with how much energy it will be generated. Like other loads, it cannot be calculated precisely or forecasted with reasonable accuracy. Due to the unpredictable nature of the load it has always been a challenging task for structural researchers and professionals to prepare any guideline. Therefore, the behaviour of different types of frame under earthquake should be determined. The technique of base isolation has been developed in an attempt to mitigate the effects on buildings and their contents during earthquake attacks and has been proven to be one of the more effective methods for a wide range of seismic design problems on buildings in the past two decades. Seismic isolation consists essentially of the installation of mechanisms which decouple the structures and their contents from potentially damaging earthquake-induced ground motions. This is achieved by mounting the structure on an isolation system with considerable horizontal flexibility so that during an earthquake, when the ground vibrates strongly under the structure, only moderate motions are induced within the structure itself. During earthquakes, the conventional structure without seismic isolation is subjected to substantial Story drift, which may lead to damage or even collapse of building (Hoq, S.M. 2010). Whereas the isolated structure vibrates almost like a rigid body with large deformations or displacements endured by the isolation bearings. The lateral forces of the isolated building are not only reduced in magnitude but also fairly redistributed over the floors, which further mitigates the overturning moment of the structure (Peng-Hsiang et al. 1998). The aim of this paper is to model and investigate a SAC frame with base isolation system to minimize contents related damage by controlling acceleration response and keep allowable resonance range. Maison, B. F et al. (1999) studied the effect of semi-rigid connections within the SAC program. But, in those studies all the connections were considered as partially restrained (FEMA-355c). Thus base isolated frames and bracing frames are selected which were subjected to four earthquake records from four different frequency earthquake. These are for El Centro, Northridge, Array and Kobe earthquakes. The control frame was selected to be the rectangular frame based on the SAC frame geometry. The aspect ratio and geometrical dimensions were same to obtain their earthquake response which included lateral displacement, inter-story drift. For the first part of the investigation, time period and frequency compared between base isolated frame and rectangular frame with bracing. In the second part of the study displacement and drift is compared with the rectangular frame with different types of

bracing and base isolated frame to identify the effect of base isolation. Finally a 20 story of SAC frame (FEMA-355e) as a case study has been taken into consideration through simulated analysis for both, with and without base isolation systems. Fig. 1 represents the 20 story of SAC frame. Fig. 2 to fig. 4 shows the sac frame with Cross bracing, E bracing and inverted V bracing. Numerical analyses are applied in order to observe dynamic behaviour of such structures under seismic loads.

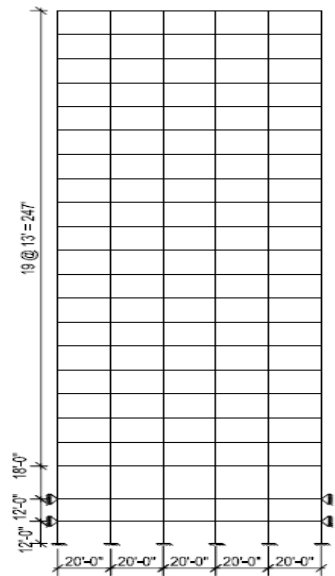


Fig. 1: Twenty Story SAC Frame

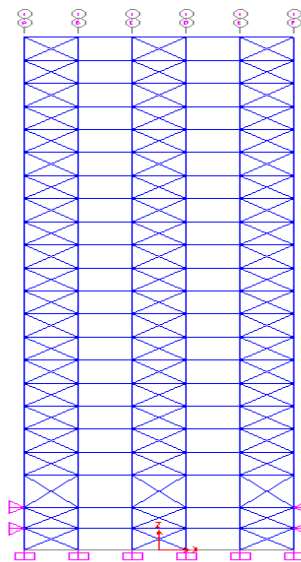


Fig. 2: SAC frame with cross bracing

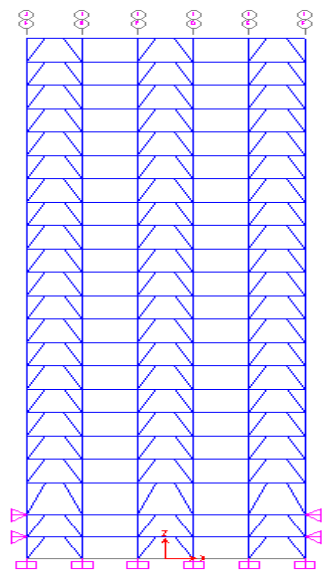


Fig. 3: SAC frame with E bracing

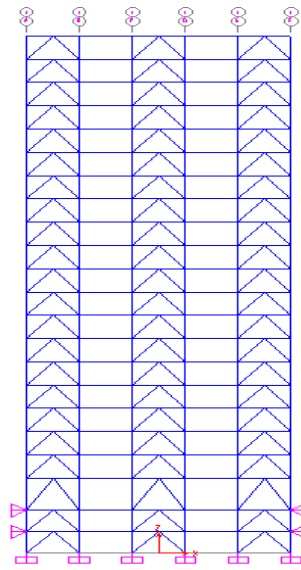


Fig. 4: SAC frame with inverted V bracing

## METHODOLOGY

A 20 story 5-bay frame is used to observe the effect of earthquake on medium high-rise building. All the member sizes are W14 X 283. All the frames are analyzed under four different earthquake excitation data. These earthquakes reflect a wide variation in frequency content. Later a base isolator has been proposed to see the effect of behavior of the frame. The base isolator has been constructed by placing the rubber isolator between the building and the foundation of the rectangular frame. This isolated frame has the same height and width ratios as the rectangular shape. All member sizes, joint loads and uniformly distributed loading were kept the same for both the shapes. For each earthquake results of rectangular, braced frames are compared with base isolator frame. Comparison is accomplished with the help of Time history analysis and modal history analysis by using SAP2000 software. All the connections are considered to be rigid. Total dead load and 25 percentage of live load are considered for



calculating member mass. Results include top displacements and inter story drifts. All the results are plotted to compare the performance of individual shape under earthquake excitations. The time steps and the step size for different earthquakes are listed in the Table 1. Corresponding time period and frequencies for first ten modes are also determined.

Table 1: Time steps and step size

Earthquake	Number of output time steps	Output time step size
EICentro	2674	0.02
Array	3939	0.01
Northridge	2990	0.005
Kobe	3000	0.02

## RESULTS AND DISCUSSIONS

Comparison between the time period and frequency of the moment resisting frame with the other bracing frames are obtained from the SAP2000 software. Time periods and frequencies are tabulated in Table 2 and Table 3.

Table 2: Time periods of different types of bracing

Mode	Time Period (sec)				
	Moment Resisting Frame	Base Isolator Frame	Cross Bracing Frame	E Bracing Frame	Inverted V Bracing Frame
1	2.612	2.824	1.774	1.843	1.753
2	0.860	0.929	0.499	0.576	0.501
3	0.481	0.592	0.318	0.314	0.318
4	0.338	0.517	0.227	0.293	0.233
5	0.301	0.364	0.217	0.221	0.215
6	0.268	0.297	0.177	0.191	0.171
7	0.241	0.272	0.134	0.168	0.143
8	0.203	0.219	0.112	0.145	0.111
9	0.183	0.198	0.096	0.115	0.102
10	0.169	0.182	0.093	0.110	0.094

Table 2 shows the maximum time period 2.824 sec is obtained for base isolated frame and minimum 1.753 sec for inverted V bracing frame. Using of base isolator increases time period and decreases frequency. Table 2 shows that moment resisting frame has 2.612 sec time period and after introducing base isolator time period increases and frequency decreases. Among all types of frames inverted V frame shows minimum time period.

Table 3: Frequency of different types of bracing

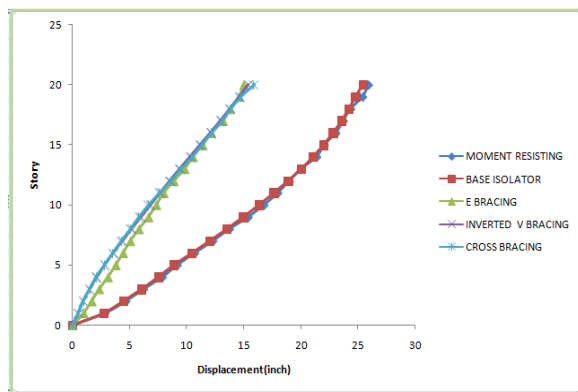
Mode	Frequency (cyc/sec)				
	Moment Resisting Frame	Base Isolator Frame	Cross Bracing Frame	E Bracing Frame	Inverted V Bracing Frame
1	0.382	0.354	0.563	0.542	0.570
2	1.162	1.075	2.001	1.735	1.992
3	2.076	1.688	3.143	3.181	3.136
4	2.959	1.931	4.406	3.408	4.285
5	3.321	2.747	4.593	4.510	4.629
6	3.864	3.368	5.633	5.230	5.829
7	4.150	3.669	7.435	5.923	6.966
8	4.914	4.554	8.920	6.883	8.930
9	5.466	5.037	10.340	8.647	9.764
10	5.912	5.493	10.679	9.042	10.562

Table 3 shows that minimum frequency 0.354 cyc/sec is obtained for base isolated frame and maximum 0.57 cyc/sec for inverted V bracing frame. Using of base isolator frequency decreases. Table 3 shows that moment resisting frame has 0.382 cyc/sec frequency and after introducing using base isolator frequency reduces.

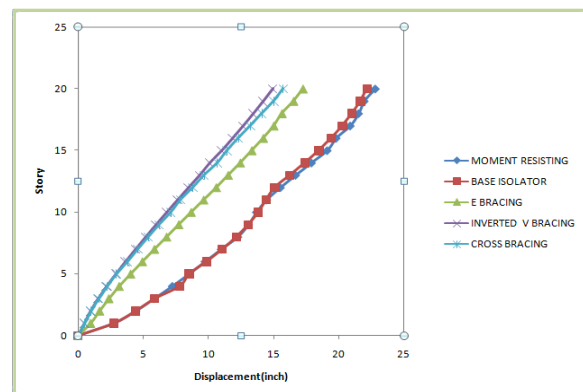
Graphical presentation of displacement profile for all frames with different earthquakes considering El Centro, Northridge, Kobe, Array earthquakes are shown in Fig. 5 and Fig. 6. Table 4 shows displacement for 10% earthquake. Displacement for Elcentro and Array earthquakes increases to 25.45 inches and 22.18 inches which was 25.91 inches and 22.86 inches for simple moment resisting frame. By increasing displacement base isolator decreases time period.

Table 4: Displacement for 10% earthquake

Displacement (inch)					
Earthquake	Moment resisting frame	Base isolator frame	Cross Bracing Frame	E Bracing Frame	Inverted V bracing frame
El Centro	25.91	25.45	15.9	15.00	15.36
Array	22.86	22.18	15.72	17.24	14.93



a) El Centro



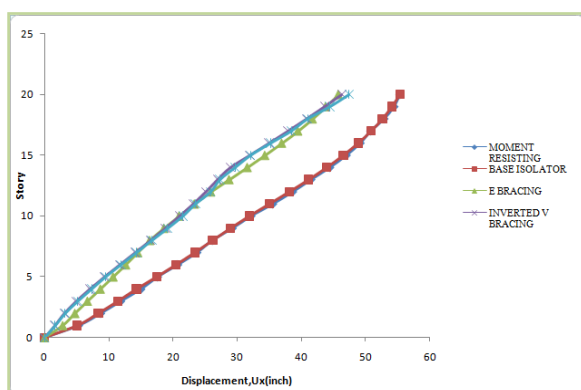
b) Array

Fig. 5: Displacement profile for 10 % earthquake El Centro and Array

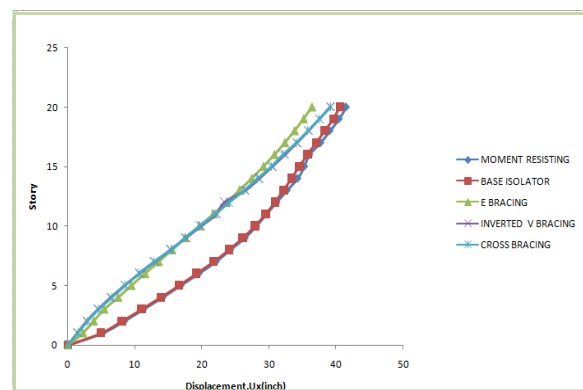
Table 5 shows maximum displacement for 2% earthquake. Displacement for Northridge earthquakes increases to 55.36 inches which was 55.34 inches for simple moment resisting frame. But displacement for Kobe earthquakes decreases to 40.56 inches which was 41.47 inches for simple moment resisting frame.

Table 5: Displacement for 2% earthquake

Displacement(inch)					
Earthquake	Moment resisting frame	Base isolator frame	E bracing frame	Inverted V bracing frame	Cross bracing frame
Northridge	55.34	55.36	45.8	46.26	47.41
Kobe	41.47	40.56	36.39	39.08	39.22



a) Northridge



b) Kobe

Fig. 6: Displacement profile for 2 % earthquake Northridge and Kobe

Fig. 7 and Fig. 8 shows the inter story drift profile for rigid rectangular frame with different types of framing and base isolator for four types of earthquake.



## **ACKNOWLEDGMENTS**

The support provided by Ahsanullah University of Science & Technology in the form of a computer laboratory support for this study is very much appreciated.

## **REFERENCES**

- FEMA-355C. 2000. *State of the Art Report on Systems Performance of Steel Moment Frames Subject to Earthquake Ground Shaking*. SAC Joint Venture for the Federal Emergency Management Agency, Washington, DC.
- FEMA-355E. 2000. *State of the Art Report on Past Performance of Steel Moment-Frame Buildings in Earthquakes*. SAC Joint Venture for the Federal Emergency Management Agency, Washington, DC.
- Hoq, SM. 2010. *Effect of frame shape and geometry on the global behavior of rigid and hybrid frame under earthquake excitations*. M.Sc. Thesis, The University of Texas, Arlington, USA
- Maison, BF and Kasai, K. *Seismic Performance of 3 and 9 Story Partially Restrained Moment Frame Buildings*. SAC/BD-99/16, (1999).
- Peng-Hsiang, Charng. 1998. *Base isolation for multistory building structures*. Ph.D Thesis, University of Canterbury, New Zealand

## **NUMERICAL SIMULATION OF BEAM WITH WEB OPENING**

A. F. Mazumder & A. A. Sarfin\*

*Department of Civil Engineering, Presidency University, Dhaka, Bangladesh*

*\*Corresponding Author: A. A. Sarfin*

### **ABSTRACT**

Transverse opening in RC beams allows the utility line to pass through the structure and encourages the designer to reduce the height of the structure leading to an economical design. Because of sudden changes in the dimension of cross section of the beam; the corners of opening would be subjected to stress concentration and it is possible to induce transverse cracks in the beam. Also it can reduce the stiffness, which leads to excessive deflection, both elastic and plastic, under service load. The main objective of this paper is to study the deflection and stress of beam, numerically using COMSOL, with and without of square web opening and to provide additional reinforcement to overcome excessive deflection and stress. To overcome the excessive deflection in the beam, two additional reinforcement bars across the width were provided. COMSOL result showed that deflection was reduced because of providing additional reinforcement. Similarly, both elastic and plastic stresses increase with the increment of the size of web opening which can be reduced with additional reinforcements, though bars with higher diameters do not have any significant effect on plastic and elastic stresses.

Keywords: RC beam; web opening; additional reinforcement; COMSOL

### **INTRODUCTION**

A beam is a structural element that is capable of withstanding load primarily due to bending. The bending force induced into the material of the beam as a result of the external loads, own weight, and external reactions. In the construction of modern building, many pipes and ducts are necessary to accommodate essential services like water supply, sewage, air-conditioning, electricity, telephone, computer network etc. Usually, these pipes and ducts are placed underneath the soffit of the beam and for aesthetic reasons, are covered by a suspended ceiling, thus creating a “dead space”. In each floor, the height of this dead space that adds to the overall height of the building depends on the number and depth to be accommodated. The depth of ducts or pipes may range from a couple of centimetres to, as long as, half a meter. An alternative arrangement can be undertaken by allowing these ducts to pass through the transverse opening of the floor beams. This arrangement of building services leads to significant reduction in the headroom and results in a more compact design. For small building, saving may not be significant compared to the overall cost. But for multi-storey buildings, any saving in story height multiplied by the number of stories can represent a substantial saving in total height of structures, length of air conditioning and electrical ducts, plumbing risers, walls and partition surfaces, and overall load on the foundation. Some researcher studied this phenomenon and tried to give practical and economical solution (Amiri et al, 2011; Chen et al, 2008; Mansur, 2006; Vasehiamiri and Alibygle, 2004).

The main objective of this study is to understand the behaviour of a beam with web opening. The specific objective of this study is to observe the deflection and stress of beam with & without of web opening and to provide additional reinforcement to overcome excessive deflection and stress.

### **METHODOLOGY**

In this study, a simply supported solid beam (control specimen) had been analyzed by commercially available software COMSOL 4.3b. Then the same beam with different web openings (Table 1) had been analyzed and deflection and stress had been recorded and compared with the deflection and stress of the control beam.

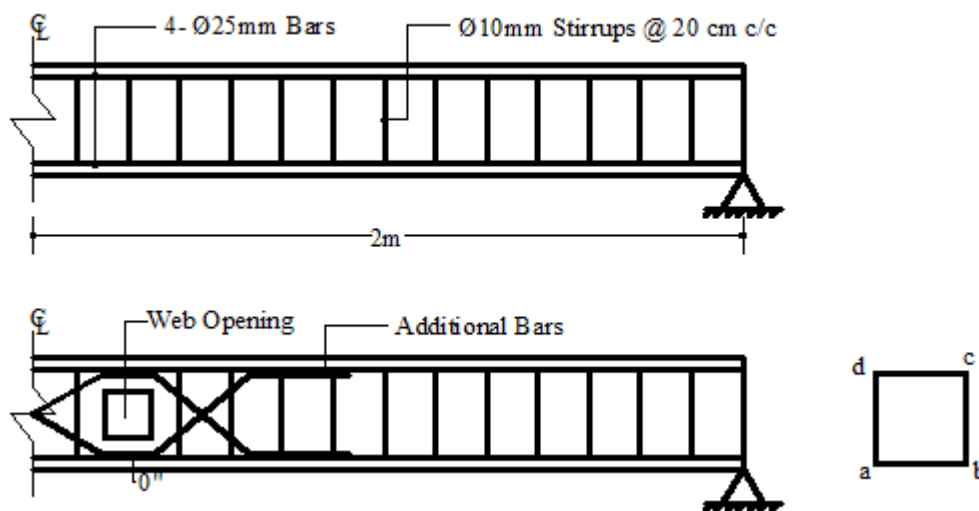


Fig. 1: Details of Beam, Web Opening and Additional Reinforcement

### Beam Specification

To observe the effect of the opening in the web of a beam, 12 simply supported beams were modelled and analyzed in COMSOL. Specification of the beam is shown in Table 1 with reinforcement detailing (Fig. 1). 25 mm bar was used as longitudinal main bar with clear cover of 3.25 cm and 10 mm bar was used as stirrups with a spacing of 20 cm c/c distance. Plastic strain increased near the hollow with the increase of web opening. Strain localization was observed in the top of the web opening and in higher opening areas. So, two additional reinforcements were provided to cope up with strain localization and huge strain.

Table 1: Solid Beam Specification

Specifications	Beam
Length	4 m
Width	30 cm
Depth	50 cm
Main Reinforcement	25 mm (4, in each corner with 3.25 cm clear cover)
Additional Reinforcement (25 × 25 cm)	10, 12, 14, 16 mm (2, spacing 10 cm c/c)
Stirrups	10 mm (spacing 20 cm c/c)
Load Applied	200,000 N/m <sup>2</sup> (Pressure)
Support Condition	Simply Supported

### Material Properties

In this study, 12 beams were analyzed. Two materials were used- concrete and structural steel. The uniaxial compressive and tensile strength of concrete were assumed to be 30 MPa and 3 MPa, respectively. The density, modulus of elasticity, and Poisson's ratio of concrete were assumed to be 2400 kg/m<sup>3</sup>, 26 GPa, and 0.25, respectively. Density, modulus of elasticity, and Poisson's ratio of steel were assumed to be 7850 kg/m<sup>3</sup>, 200GPa, and 0.3, respectively.

### RESULTS AND DISCUSSIONS

Both elastic and plastic deflections at mid span increase with the increment of the size of the web opening (Fig. 2). It has been observed that additional reinforcements have reduced both elastic and

plastic deflections. The mid-span deflection of beam with 25 mm square web opening reduces gradually from 2.3796 mm to 2.31854mm (elastic) and 3.38365 mm to 3.2083 mm (plastic) as the diameter of additional reinforcement increases up to 16 mm.

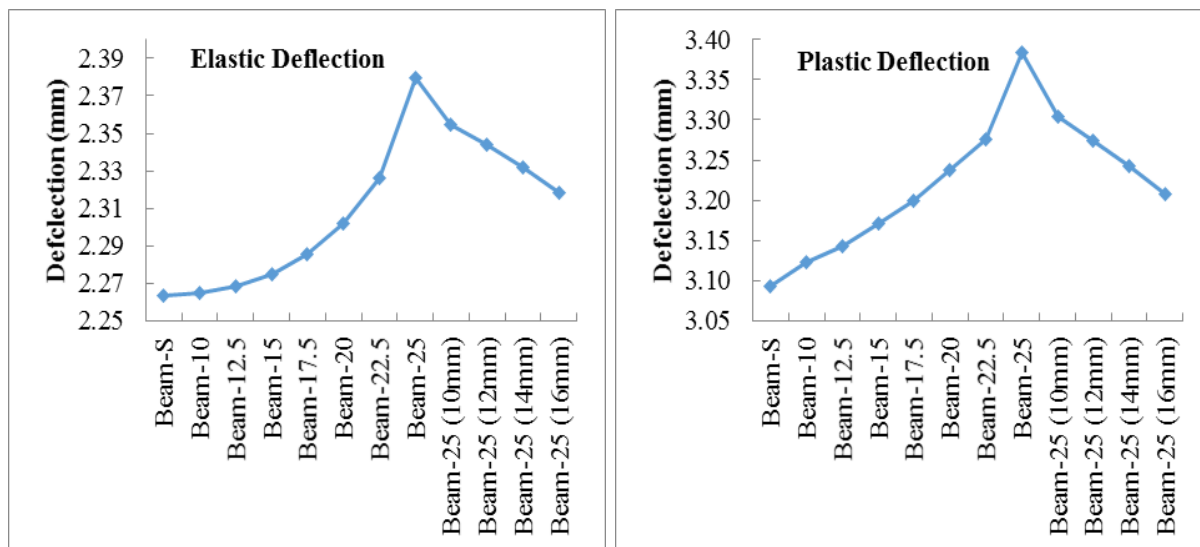


Fig. 2: Elastic and Plastic Deflection of Beams at Mid-Span

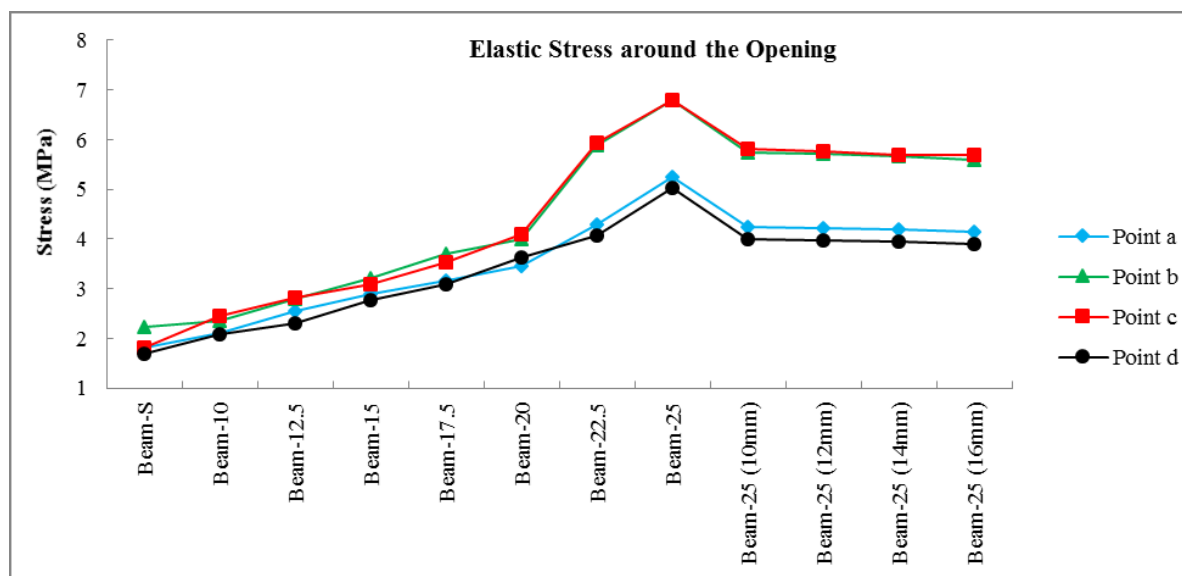


Fig. 3: Elastic Stresses of Beam around Web Opening

It has been observed from Fig. 3 that elastic stresses gradually increases as the dimension of the square web openings increase from 10 mm to 25 mm. Stresses at points 'a' and point 'd' as well as stresses at points 'c' and point 'b' are almost similar (Fig. 1). It should be noted that points (a, d) and points (b, c) are located at the same horizontal distance from centerline. After the inclusion of 10 mm additional reinforcements to the model, elastic stress decreases sharply. As the diameter of additional bars increases, elastic stresses decrease, though the change is not as prominent as that of the model with 10 mm additional bars.

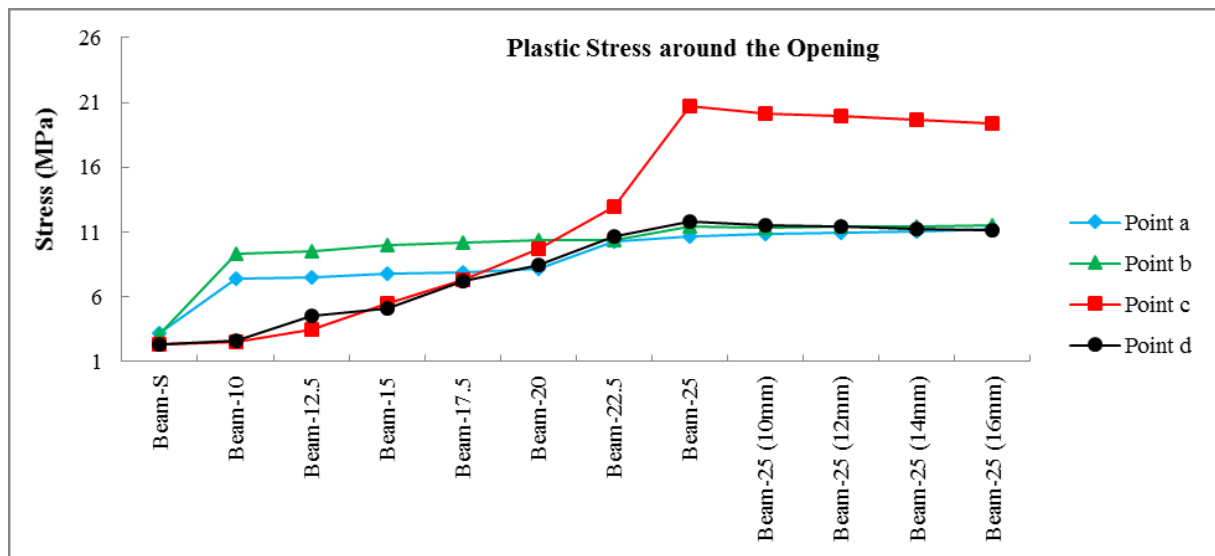


Fig. 4: Plastic Stresses of Beam around Web Opening

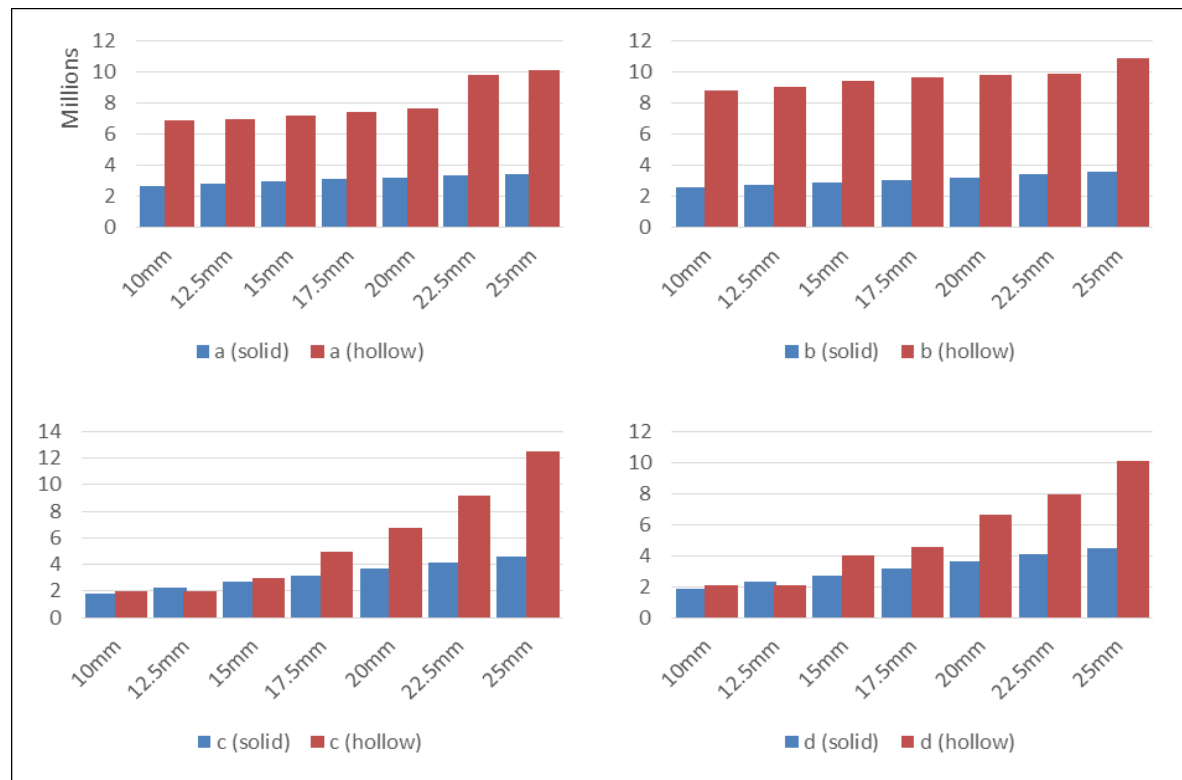


Fig. 5: Plastic Stress at Points a, b, c and d for both Solid and Hollow Beams (MPa)

For plastic stress, as shown in Fig. 4, stresses increase as the dimension of the opening increases. Plastic stresses at points 'a' and 'b', both of which are below neutral axis, increases sharply as the opening has been introduced. After that, stresses increase gradually for points 'a', 'b' and 'd'. Point 'c' undergoes excessive plastic stress compared to other three points. Additional bars have decreased plastic stress, similar to elastic stresses, though increasing diameter has very negligible effect.

It should be noted that as the dimension of web opening increases, distance of four points (a, b, c and d) from neutral axis is also increased. So, for better understanding, graphs in Figure 5 compare the plastic stresses in solid beam and plastic stresses in hollow beams at the same four points mentioned above. All four graphs in Figure 5 show that each of the four points undergoes significant plastic stresses due to web openings, which gradually increases as the size of openings has been increased.



## CONCLUSIONS

In this study, 12 simply supported beams, with different size of web opening, were analysed by commercially available software COMSOL 4.3b. For all beams, the elastic and plastic deflection and stresses were recorded and compared. It can be concluded that

1. Beams with web opening undergo excessive elastic and plastic deflection under service load. The deflection gradually increases with the increment of cross sectional area of beam web opening.
2. Maximum deflection was found to be 3.38365 mm at 25 cm square opening.
3. Maximum elastic and plastic stresses were found to be 6.3 MPa and 20.3 MPa respectively, at the corner of 25 mm square web opening.
4. After providing two additional reinforcement with 10, 12, 14, 16 mm diameter bars, the deflections were found to be decreased significantly.
5. Stresses were found to be decreased significantly for two 10 mm additional reinforcement. But for 12, 14 and 16 mm bars, stresses were found to be similar and deflection were reduced significantly. So, addition of bars with higher diameter increases the local stiffness of the beam.
6. Stresses induced in four corners were found to be much higher than that of the solid beam. It happens due to stress concentration.

So, as the area of web opening was increased, deflection at mid-span and stresses (elastic and plastic) at four corners of the opening were also increased. To overcome excessive deflection, additional reinforcements should be provided with proper arrangement.

## REFERENCES

- Amiri, S; Masoudnia, R; Pabarja, AA. 2011. The study of the effects of web openings on the concrete beams. Australian Journal of Basic and Applied Sciences, 5(7): 547-556, 2011 ISSN 1991-8178.
- Chen, CC; Li, CY; Kuo, MC. 2008. Experimental study of steel reinforced concrete beams with web openings. The 14th World Conference on Earthquake Engineering, October 12-17, 2008, Beijing, China.
- Mansur, MA. 2006. *Design of Reinforced concrete beams with web openings*. 6th Asia-Pacific Structural Engineering and Construction Conference (APSEC 2006), 5 – 6 September, 2006. Kuala Lumpur, Malaysia.
- Vasehiamiri, J; Alibygle, MH. 2004. Effect of small circular opening on the shear and flexural behavior and ultimate strength of reinforced concrete beams using normal and high strength concrete. 13th World Conference on Earthquake Engineering, Vancouver, B.C., Canada, August 1-6, 2004, Paper No. 3239.

## **CORRELATION BETWEEN TEMPERATURE CHANGE AND EARTHQUAKE IN BANGLADESH**

A. Hossain\*, F. Kabir & K. Roy

*Department of Civil Engineering, Rajshahi University of Engineering & Technology, Rajshahi,  
Bangladesh*

*\*Corresponding Author: ahmedhossain090001@gmail.com*

### **ABSTRACT**

With more than 160 million people, Bangladesh is ranked as 8th most populous place on earth. Bangladesh has a tropical monsoon climate characterized by heavy seasonal rainfall, high temperatures and high humidity. Natural disasters such as floods, tornadoes and earthquakes affect the country yearly. Geographical location of Bangladesh makes it ideally suited to earthquake. Scientists have come to recognize that it sits at the juncture of several active tectonic plate boundaries. Study area are selected as Sylhet, Barisal, Cox's bazar, Dhaka, Rangpur and Rangamati district based observatories. The seismic data is of duration between 1988 and 2008. This paper introduced the feasibility of the approach and methods to find a possible correlation between temperature change and earthquake.

Keywords: Temperature; earthquake; tectonic plate; seismic data

### **INTRODUCTION**

In the past, a great number of thermal deviation associated with strong earthquakes were recorded in China. This aroused seismologists to consider the possibility of predicting earthquakes by monitoring the changes in temperature. Analysis of seismicity with temperature shows that strong earthquakes are associated with thermal deviation and measuring temperature can be used to monitor and predict earthquakes. In general, the deviation starts to appear in more than one month before a strong earthquake with covering area of thousands Km<sup>2</sup>. Temperature abnormally increases 1<sup>0</sup> C or more in one month, and 2<sup>0</sup> C or more, even 10<sup>0</sup> C in a half month. The epicenter locates within the anomaly area (Huangguangsi; Luo Zhaofu). The Chinese succeeded in warning the local population about a large Earthquake in Haicheng (a city in northern China) in 1975. The magnitude of the Earthquake on the Richter scale was 7.3. As a consequence of the warning, people were moved from several areas within the city to the outskirts. The City's inhabitants numbered 500,000. It was estimated that 90% of the buildings in the city collapsed in the earthquake, resulting in 2,000 people losing their lives. It has been estimated that the warning saved the lives of thousands of people, perhaps as Many as 100,000 (Celin Wangetal., 2006). The notion that earthquake prediction was possible was gaining impetus. The Chinese prediction was based on a number of observations. To name a significant few, they observed small earthquakes, changes in the levels and chemical content of ground water, changes in surface elevation, as well as changes in the magnetic field and electrical signals. Koshiyama (1976), who was actually involved in a survey, at the time of the measurement, particularly the deviated ground disturbance just before (probably one or two hours) the Tonankai earthquake of 7 December, 1944. According to his description, a strong wind was blowing, so the author further examined the weather conditions and observed the velocity of the wind and the atmospheric temperature at the Hamamatsu weather station. This figure does not show any anomalous weather condition during the period before and after the Tonankai earthquake. In particular, the velocity of the wind was not very high immediately prior to the earthquake. So it is not reasonable to attribute the systematic anomalous change in levelling data to a change in weather conditions. In Northern areas of Pakistan, from 1961 to 2005, collected data in this period shows increase in earthquake frequency. The main factors for increase in earthquake frequency can be the temperature. Increase of temperature is

causing glaciers to melt thus releasing pressure on Earth below which in turn possibly rebounds, causing earthquakes (Usman, M., Qureshi, S.N. and Amir, 2010). Some recent research has found a correlation between a sudden relative spikes in atmospheric temperature 2-5 days before an earthquake. It is speculated that this rise is caused by the movement of ions within the earth's crust, related to an oncoming earthquake. Scientists analyzing the March 11, 2011 earthquake in Japan reported a sudden spike in the temperature in the atmosphere above the quake site detected just before the event. Bangladesh is extremely vulnerable to seismic activity. Accurate historical information on earthquakes is very important in evaluating the seismicity of Bangladesh. Information on earthquakes in and around Bangladesh is available for the last 250 years. The earthquake record suggests that since 1900, more than 100 moderate to large earthquakes occurred in Bangladesh, out of which more than 65 events occurred after 1960. This brings to light an increased frequency of earthquakes in the last 30 years. This increase in earthquake activity is an indication of fresh tectonic activity or propagation of fractures from the adjacent seismic zones. So, it is important to know about the trend of earthquake that has occurred in the past so that we can prepare ourselves for the future. At a glance, several factors that were incorporated with earthquakes are temperature variation, wind velocity, changes in the levels and chemical content of ground water, changes in surface elevation as well as changes in the magnetic field and electrical signals. The aim of this paper is to find out possible relationship between temperature variation and earthquake to know about the possible trend of earthquakes ahead.

## METHODOLOGY

The temperature data and seismic data contains twenty year period from 1988 to 2008. To find temperature change, maximum temperature of the specific day on which earthquake occurred and maximum temperature of five days before it is found out. The temperature data is provided by Bangladesh Meteorological Department and seismic data are collected from Earthquake-report.com website. Following recent earthquakes in Bangladesh were taken into study (Data courtesy: NOAA Natural Hazards database).

Table 1: List of Earthquakes in Bangladesh (1988-2008)

Date		Earthquake location in Bangladesh			Earthquake Parameters	
Year	Month	Day	Location	Zone	Focal Depth (Km)	Magnitude
1988	February	6	Sylhet	I	33	5.8
1989	June	12	Barisal	III	6	5.1
1999	July	22	Cox's Bazar	II	10	4.2
2001	December	19	Dhaka	II	10	4.5
2002	June	20	Rangpur	II	40	4.5
2003	July	26	Rangamati	II	10	5.7
2007	November	7	Rangamati	II	29	5.1
2008	January	12	Rangamati	II	34	5.0

Table 2 contains date and temperature data for selected areas collected from Bangladesh Meteorological Department

## RESULT AND DISCUSSION

Figure 1 to 8 summarizes graphical representation for the data obtained from table 1 and table 2. The earthquake ensued in February 6, 1988 at 14:50 hit Sylhet with a magnitude of 5.8. [Fig. 1] shows temperature data of previous five days before that earthquake. Temperature variation is in ascending order until the day earthquake occurred. [Fig. 2] Shows ascending and descending variation of temperature just before the day earthquake hit Barisal with a magnitude of 5.2.

Table 2: TEMPERATURE DATA AND DATE OF EARTHQUAKE ENSUED

Place	Date and Maximum temperature ( ° C)						Temperature Difference
<b>Sylhet</b>	1/2/88	2/2/88	3/2/88	4/2/88	5/2/88	6/2/88	1.7
	27.8	28	28.3	30	30	28.3	
<b>Barisal</b>	7/6/89	8/6/89	9/6/89	10/6/89	11/6/89	12/6/89	2.1
	32.6	34	34.5	33	33	32.4	
<b>Cox's Bazar</b>	17/7/99	18/7/99	19/7/99	20/7/99	21/7/99	22/7/99	2
	32	31.5	29	28.1	31	30	
<b>Dhaka</b>	14/12/01	15/12/01	16/12/01	17/12/01	18/12/01	19/12/01	1.2
	24.5	26.7	25.7	26.9	26	25.7	
<b>Rangpur</b>	15/6/02	16/6/02	17/6/02	18/6/02	19/6/02	20/6/02	1.5
	28.5	29.5	30.5	29	27.9	29	
<b>Rangamati(2003)</b>	21/07/03	22/07/03	23/07/03	24/07/03	25/07/03	26/07/03	0.2
	31.8	31.8	34.5	33.4	33.6	34.7	
<b>Rangamati(2007)</b>	2/11/07	3/11/07	4/11/07	5/11/07	6/11/07	7/11/07	1
	31.5	27.2	30.4	29.5	29.4	30.5	
<b>Rangamati(2008)</b>	7/1/12	8/1/12	9/1/12	10/1/12	11/1/12	12/1/12	0.2
	26.4	26.6	27.2	27	27.8	27.6	

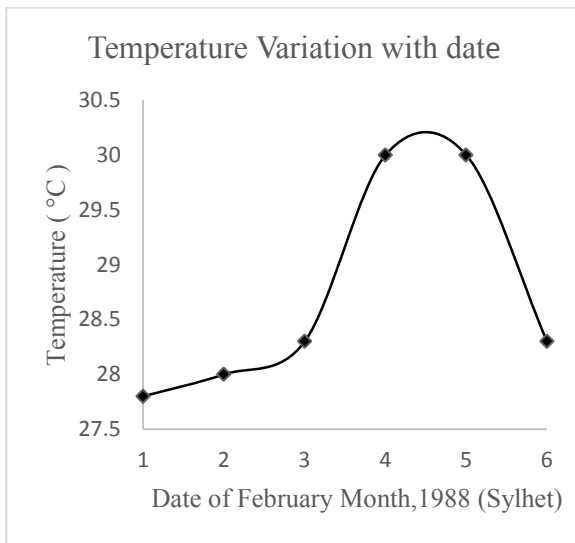


Fig. 1: Temp. Data for 1/2/1988 to 6/2/1988

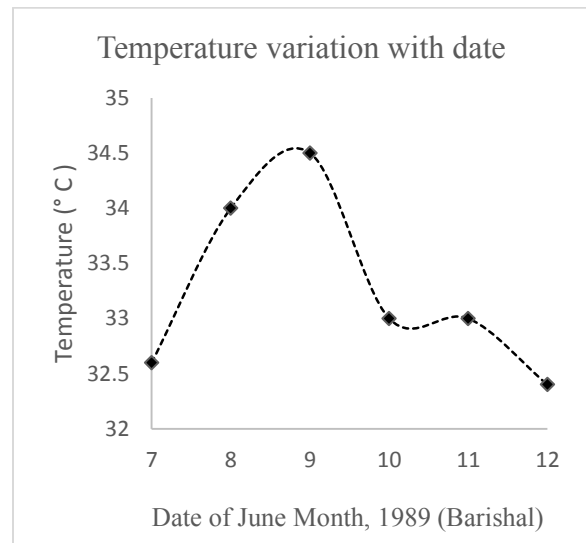


Fig. 2: Temp. Data for 7/6/1989 to 12/6/1989

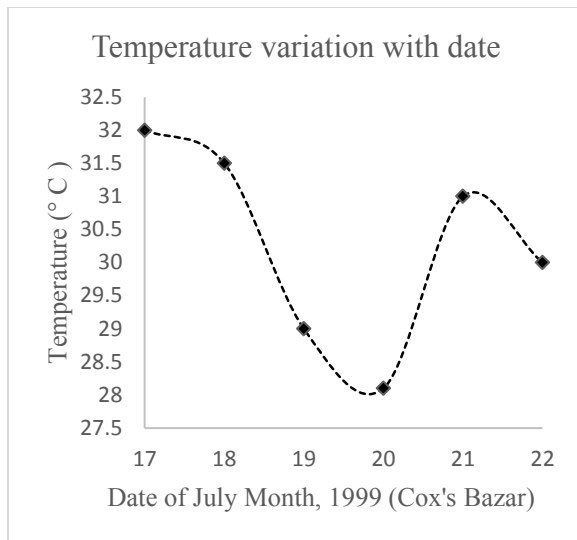


Fig. 3: Temp. Data for 17/7/1999 to 22/7/1999

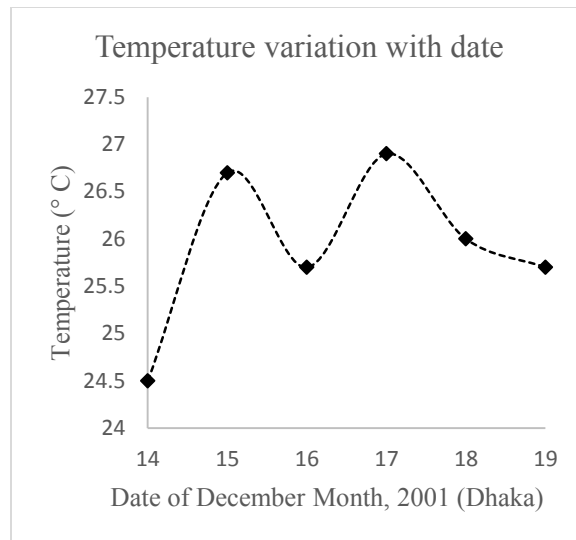


Fig. 4: Temp. Data for 14/12/2001 to 19/12/2001

On 22 July, 1999 at Maheshkhali Island in Cox's Bazar, earthquake occurred with a magnitude of 4.2. It was severely felt around Maheshkhali Island and the adjoining sea. Focusing into the temperature variation in [Fig. 3], temperature continued to fall down up to 20th July, but raised to 31° just before the day earthquake occurred. The earthquake of December 19, 2001 with magnitude of 4.5 and focal depth of 10 km was located very close to Dhaka city. [Fig. 4] shows temperature variation close to sine curve type for this earthquake.

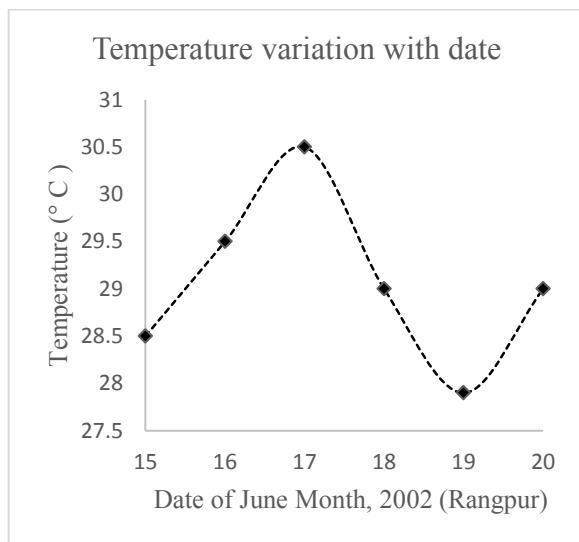


Fig. 5: Temp. Data for 15/6/2002 to 20/6/2002

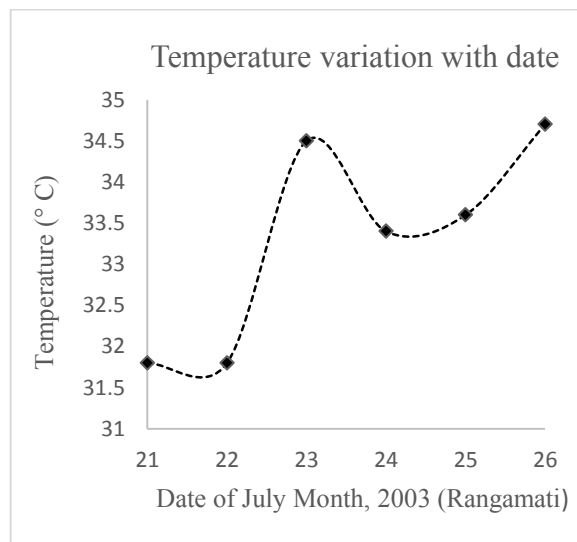


Fig. 6: Temp. Data for 21/7/2003 to 26/7/2003

Fig. 5 shows sine curve variation of temperature for the earthquake occurred in 20/6/2002 in Rangpur.

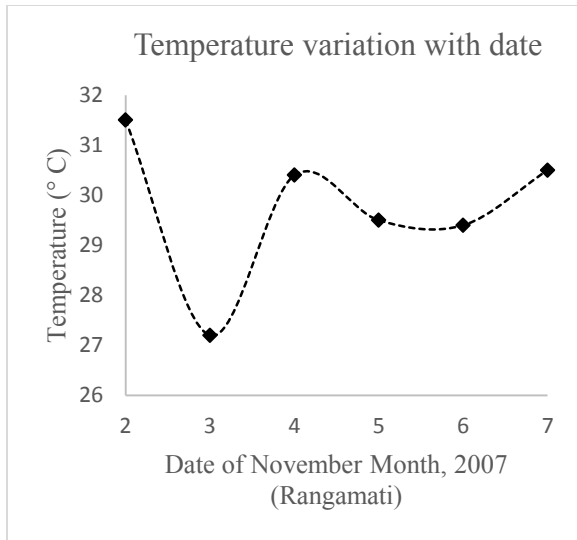


Fig. 7: Temp. Data for 2/11/2007 to 7/11/2007

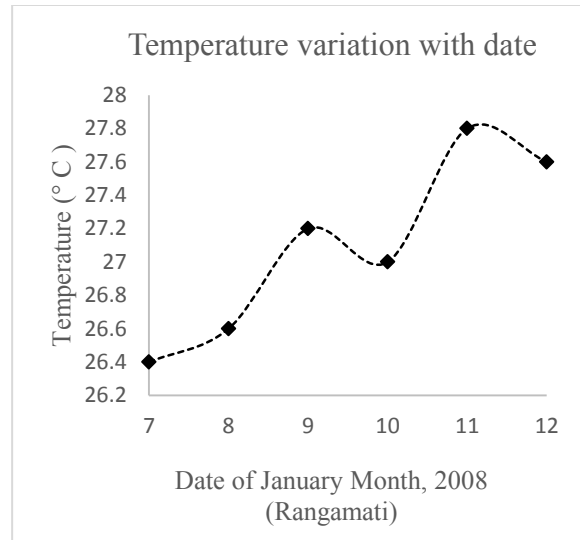


Fig. 8: Temp. Data for 7/1/2008 to 12/1/2008

Fig. 6, 7, 8 shows temperature variation with date for earthquakes occurred in 2003, 2007, 2008 respectively for Rangamati district. Of them, Fig. 6 and Fig. 7 temperature variations are quite similar trend.

Considering temperature difference obtained from table 2, following graph is plotted.

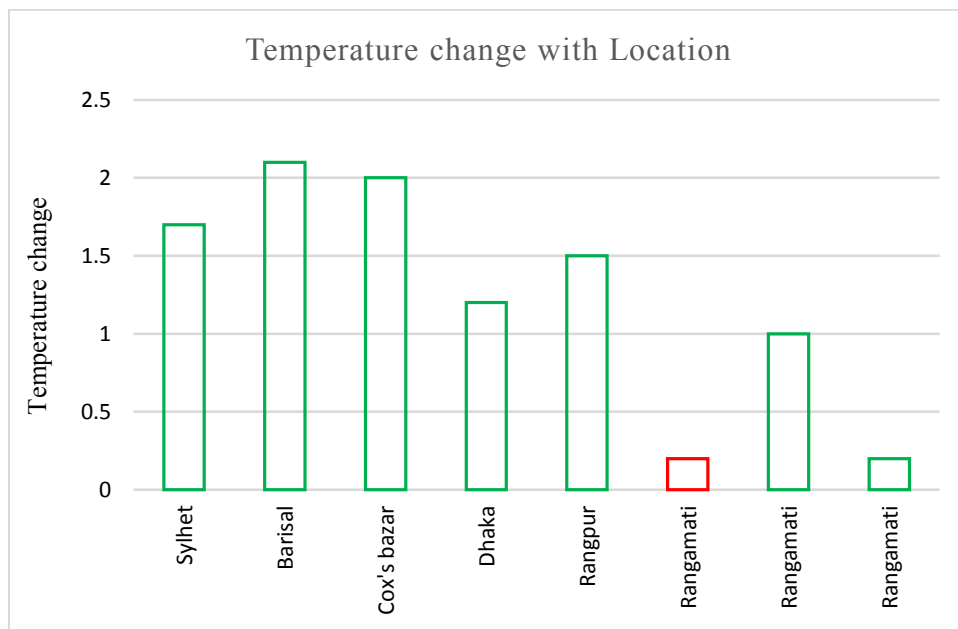


Fig. 9. Temperature change data with different earthquake location in Bangladesh

Fig. 9 shows temperature change for different earthquake location in Bangladesh. Green line indicates decrease in temperature and red line indicates increase in temperature. Temperature decrease for Sylhet, Barisal, Cox's Bazaar, Dhaka, Rangpur, Rangamati (2007) and Rangamati (2008) district is  $1.7^{\circ}$ ,  $2.1^{\circ}$ ,  $2^{\circ}$ ,  $1.2^{\circ}$  and  $1.5^{\circ}$ ,  $1^{\circ}$ ,  $0.2^{\circ}$  C respectively. Only increase in temperature change is  $0.2^{\circ}$  C for Rangamati District earthquake in 2003.

## CONCLUSIONS:

Bangladesh is extremely vulnerable to seismic activity. Accurate historical information on earthquakes is very important in evaluating the seismicity of Bangladesh. Information on earthquakes in and around Bangladesh is available for the last 250 years. The earthquake record suggests that since 1900, more than 100 moderate to large earthquakes occurred in Bangladesh, out of which more than 65 events occurred after 1960. This brings to light an increased frequency of earthquakes in the last 30 years. This increase in earthquake activity is an indication of fresh tectonic activity or propagation of fractures from the adjacent seismic zones. From analysis, considering earthquakes occurred in 2003, 2007 and 2008 with temperature change (positive and negative) following graph is obtained for Rangamati district which is located in zone 3 of earthquake zoning map.

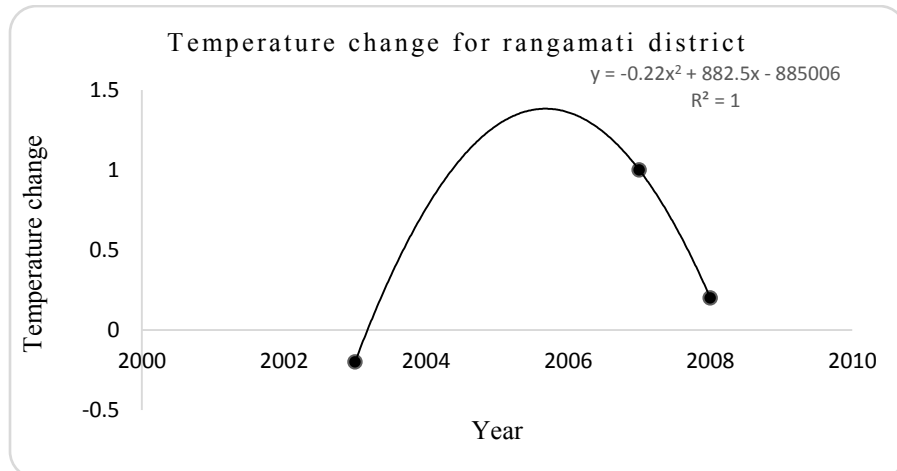


Fig. 10. Temperature change data (positive and negative) for Rangamati District

From Fig. 10, if obtained trend line (polynomial of second order  $y = -0.22x^2 + 882.5x - 885006$  of  $R^2=1$ ) is further analysed, it can lead to predict earthquakes ahead. Other temperature data can lead to be decisive in finding correlations between temperature change and earthquake for other zones.

## ACKNOWLEDGEMENT

Special acknowledgement to Atlas, Seismic Risk Assessment in Bangladesh Ministry of Disaster Management and Relief, Government of the People's Republic of Bangladesh which was first published in May 2015.

## REFERENCE

- Effects of Temperature Increase on Earthquake Frequency and Depth in Northern Pakistan 2010  
International Conference on Biology, Environment and Chemistry IPCBEE vol.1 (2011) © (2011)  
IACSIT Press, Singapore  
<http://earthquake-report.com/2014/05/11/important-historic-earthquakes-in-bangladesh/>  
[http://webcache.googleusercontent.com/search?q=cache:http://blogs.discovermagazine.com/80beats/2011/05/23/finally-a-way-to-predict-earthquakes-atmospheric-temp-spiked-before-japan-quake/#.VzgXI\\_197IU](http://webcache.googleusercontent.com/search?q=cache:http://blogs.discovermagazine.com/80beats/2011/05/23/finally-a-way-to-predict-earthquakes-atmospheric-temp-spiked-before-japan-quake/#.VzgXI_197IU)  
Atlas, Seismic Risk Assessment in Bangladesh Ministry of Disaster Management and Relief, Government of the People's Republic of Bangladesh

# CORRELATION BETWEEN AGGREGATE CRUSHING VALUE OF COARSE AGGREGATE AND COMPRESSIVE STRENGTH OF CONCRETE

M. Nishat<sup>1\*</sup>, Z. M. Dalia<sup>1</sup> & R. Ahsan<sup>2</sup>

<sup>1</sup>Department of Civil Engineering, Presidency University, Dhaka, Bangladesh

<sup>2</sup>Department of Civil Engineering, Bangladesh University of Engineering and Technology, Dhaka,  
Bangladesh

\*Corresponding Author: mahitunnishatmitu@gmail.com

## ABSTRACT

Aggregate Crushing Value (ACV) is an index of loss of coarse aggregate (CA) under sustained loading. However, ACV is not considered in concrete mix design according to ACI 211.1(ACI 211.1, 2009). In this paper effect of ACV of CA on compressive strength of concrete has been explored. Coarse Aggregate was collected from five different sources. Concrete mix design was conducted for target strengths of 3000, 4000 and 5000 psi according to ACI. Total 135 Concrete cylinders were tested for compressive strength at 7, 14 and 28 days. ACV test for each type of Coarse aggregate was performed. Achieved strength Vs. ACV was plotted for each sample. It is observed that, compressive strength is inversely related to the ACV. Higher strength concrete is more dependent on ACV. To achieve target strength at 28 days, ACV should be less than 30, 29, and 28 for 3000 psi, 4000 psi and 5000 psi respectively.

Keywords: Aggregate crushing value; compressive strength; target strength; mix design

## INTRODUCTION

Concrete is a versatile engineering material consisting of cementing substance, aggregates, water and often controlled amount of entrained air. It is initially a plastic, workable mixture which develops strength from hydration due to reaction between cement and water. Concrete is said to be as man-made rock. Reason behind its popularity is its high strength, fire resistance, durability and workability.

Compressive strength of concrete is the most important property of concrete. This property depends on various factors (constituting material properties and their proportion, method of preparation, curing, test condition). Aggregate Crushing Value (ACV) is one of the important properties of coarse aggregate.

ACV gives a relative measure of resistance to crushing under gradually applied compressive load. Thus ACV is inversely related to strength of coarse aggregate.

In concrete pavement design ACV of coarse aggregate is given much importance. In concrete mix design ACV of coarse aggregate is not considered. ACV may have effect on the strength gaining of concrete.

The objective of the study is to observe the variation of compressive strength of concrete with different coarse aggregates, the variation of aggregate crushing value of different coarse aggregates, strength gain of concrete with time for different coarse aggregates and to establish a relation between aggregate crushing value of coarse aggregate and compressive strength of concrete.

In the study, Portland Composite Cement (PCC) has not been used. Only Ordinary Portland Cement (OPC) has been used. Same type of fine aggregate has been used for all tests. Admixture has not been used for concrete mix.

## METHODOLOGY

Concrete cylinder test was performed in the laboratory using cylindrical molds (4"× 8") according to ASTM standard C 470(ASTM C470, 2009). Total 135 concrete cylinders were tested. Five different CA samples were collected from different sources named Fazilpur, Meghalaya, Volagonj, Priggable and Aluvutu. Two sizes of aggregates were used. One is 1/2" and the other is 3/4". Total fifteen sets of mix design was conducted using the five samples of aggregate for three different target strength 3000 psi,



4000 psi, 5000psi. The process of concrete mix design and determination of Aggregate Crushing Value according to ACI 211.1(ACI 211.1, 2009) and BS 812-110 standards (BS 812-110, 2009)was used in our project work respectively. For ACI mix design procedure required material information are Sieve analyses of both fine and coarse aggregates (ASTM C136, 2006), unit weight (ASTM C29, 2009), specific gravities, and absorption capacities of fine aggregates (ASTM C128, 2009) and coarse aggregates (ASTM C127, 2007).

**Properties of coarse aggregate**

The aggregate properties that were determined during the study are given in the following Table.

Table 1: Properties of Coarse Aggregates of Five Sources

Properties of Aggregate	Name of Aggregate				
	Meghalaya	Fazilpur	Volagonj	Priggable	Aluvutu
Bulk Specific Gravity(OD Basis)	2.6	2.5	2.6	2.52	2.52
Bulk specific Gravity(SSD Basis)	2.67	2.6	2.64	2.6	2.6
Apparent Specific Gravity	2.79	2.76	2.71	2.73	2.74
Absorption Capacity (%)	2.6	3.7	1.6	3.2	3.2
Unit weight (kg/ m <sup>3</sup> )	1480	1560	1560	1690	1700
Moisture content (%)	1.197	3.17	0.42	1.24	2.98
Aggregate Crushing Value(ACV)	23	24	23	30	26

**RESULTS AND DISCUSSIONS**

In this study, compressive strength and ACV of various samples has been determined. The results are shown in Figures 1 to 3.

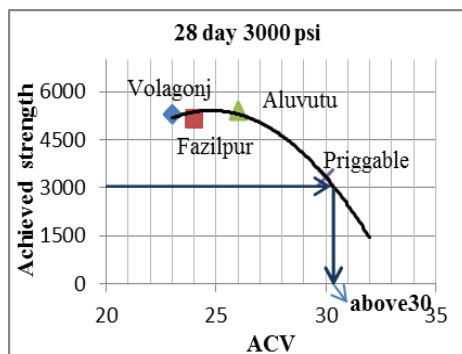


Fig. 1

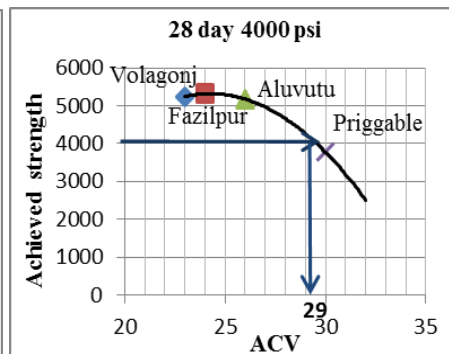


Fig. 2

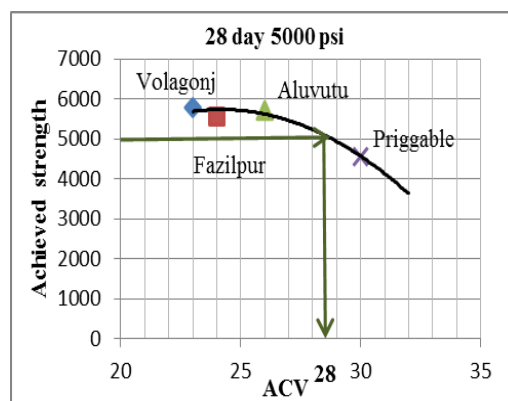


Fig. 3

Fig. 1 shows that, Compressive strength has an inverse relationship with the ACV. It also shows that all stones have reached 3000 psi in 28 days. Aluvutu, Fazilpur and Volagonj have reached greater than the target strength 3000 psi. To achieve 3000 psi, ACV should be less than 30.

Fig. 2 shows that, all the stones except Priggable have reached strength beyond 4000 psi in 28 days. For 4000 psi, deviation from the points of the curve is lesser than that of 3000 psi strength curve. To achieve 4000 psi, ACV should be less than 29.

Fig. 3 shows that, all the stones except Priggable have reached strength beyond 5000 psi in 28 days. For 5000 psi, deviation from the points of the curve is lesser than that of 4000 psi strength curve. To achieve 5000 psi, ACV should be less than 28.

### Differences in Pattern in Strength Gain of Concrete with Time

Strength gain of concrete cylinders at 7, 14 and 28 days have been shown in the same graph for 3000 psi, 4000 psi and 5000 psi.

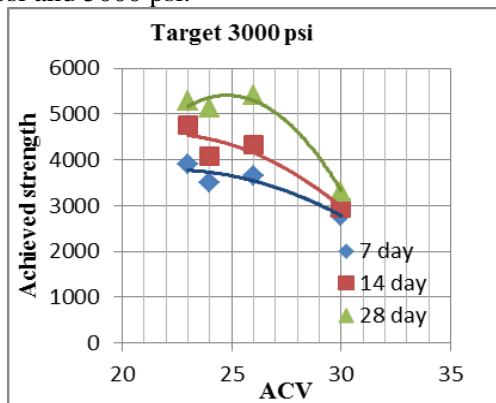


Fig. 4

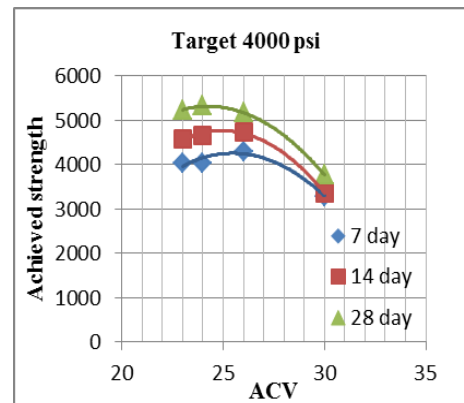


Fig. 5

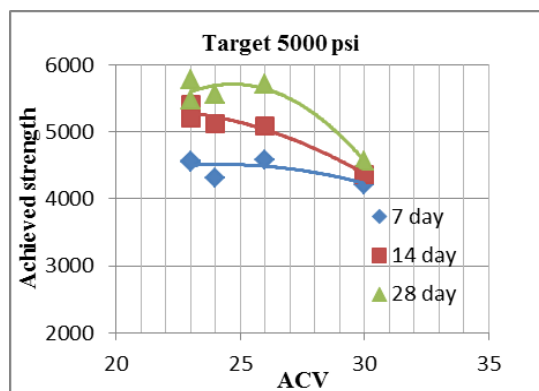


Fig. 6

Fig. 4 shows that, with the increase of time, the nature of graph tends to be more erratic. Fig. 5 shows that, the curves at 7, 14 and 28 day follow almost similar pattern. Fig. 6 shows that, the curves at 7, 14 day follow almost similar pattern. But the 28 day curve is slightly of different pattern.

From Fig. 5 to 6, it is observed that-

- Graphs for 3000 psi and 4000 psi strengths are more erratic in nature than 5000 psi strength.
- Though Volagonj and Meghalaya have same ACV, but they have different compressive strengths.

### CONCLUSIONS

This study gives a general scenario of strength development characteristics of concrete for different coarse aggregates having different ACV. It can be expected that these findings will be useful for construction of concrete structure.

Observing the obtained experimental results for concrete with different coarse aggregate having different ACV, the following conclusion can be drawn:

- Higher strength (4000 psi & 5000 psi) concrete is more dependent on ACV than lower strength (3000 psi).
- To achieve 3000 psi, 4000 psi and 5000 psi strength at 28days, concrete should have coarse aggregate having ACV less than 30, 29 and 28 respectively.
- For higher strength concrete, differences between strengths for various coarse aggregate are decreased. So Compressive Strength Vs ACV curve is smoother for higher strength concrete.
- For 7days, all the samples have achieved 65% of target strength.
- For 14days, all the samples have achieved 90% of target strength for 3000 psi target strength. But in case of 4000 psi and 5000 psi target strength, only Priggable could not achieve 90% of target strength.

### **ACKNOWLEDGMENTS**

Thanks to Almighty Allah for His graciousness, unlimited kindness and with the blessings of whom the good deeds are fulfilled.

We would like to extend our heartfelt appreciation to all who have contributed to the study especially:

- Our thesis supervisor, Dr. Raquib Ahsan, professor, Department of Civil Engineering, BUET
- Concrete lab assistants of Department of Civil Engineering, BUET
- Our parents and family
- NDE, the aggregate supplier
- The Civil Department of BUET

### **REFERENCES**

- American Concrete Institute (ACI). 2009. *Standard Practice for Selecting Proportions for Normal Heavy Weight and Mass Concrete*, ACI 211.1
- American Society for Testing and Materials (ASTM). 2009. *Standard Specification for Molds for Forming Concrete Test Cylinders Vertically*, ASTM C470.
- American Society for Testing and Materials (ASTM). 2006. *Standard Test Method for Sieve Analysis of Fine and Coarse Aggregate*, ASTM C136.
- American Society for Testing and Materials (ASTM). 2003. *Standard Test Method for Bulk Density ("Unit Weight") and Voids in Aggregate*, ASTM C29.
- American Society for Testing and Materials (ASTM). 2007. *Standard Test Method for Density, Relative Density and Absorption of Fine Aggregate*, ASTM C128.
- American Society for Testing and Materials (ASTM). 2007. *Standard Test Method for Density, Relative Density and Absorption of Coarse Aggregate*, ASTM C127.
- British Standards (BS). 2009. *Testing Aggregates-Methods for Determination of Aggregate Crushing Value (ACV)*, BS 812-110.

## **PERFORMANCE EVALUATION OF REINFORCED CONCRETE GARMENTS BUILDINGS LOCATED IN MODERATE SEISMIC ZONE OF BANGLADESH**

A. K. M. G. Murtuz\*, K. B. Jalal, K. Islam & S. M. Muniruzzaman

*Department of Civil Engineering, Military Institute of Science and Technology, Dhaka, Bangladesh*

*\*Corresponding Author: golam.murtuz@ce.mist.ac.bd*

### **ABSTRACT**

In this study, the seismic performance of three existing reinforced concrete garment buildings located in moderate seismic zone (0.20g) of Bangladesh has been investigated according to proposed Bangladesh National Building Code (BNBC-2014). Three dimensional analytical models of these buildings have been developed to assess different performance indices. Performance parameters such as average column compressive stress, realization rate of longitudinal reinforcement for columns, shear force capacity ratio and the moment capacity ratio were computed using the analytical model developed in finite element platform. The performance of these structural properties are evaluated in two step process - in the first step considering only the effect of gravity loads and later considering the seismic loading as per Bangladesh National Building Code along with the contribution of the vertical loads. Result shows that, columns in the ground floor level are highly susceptible to collapse due to inadequate longitudinal reinforcement and lack of shear reinforcement to provide adequate lateral confinement. Most of these columns also possess a threat of premature failure due to inadequate shear capacity under earthquake hazard.

Keywords: Garment buildings; seismic performance; capacity ratio; finite element analysis

### **INTRODUCTION**

Bangladesh garment industry has went through a rapid expansion to approximately 5600 garments factory with approximately 4 million workers working under this sector (BGMEA website). In financial year 2015, Ready Made Garments (RMG) industry exported garment products of 24.49 billion USD that accounts for about 80% of the country's foreign earnings (Wadud & Huda, 2016). Despite the huge contribution of garment industry in country's economic development, the infrastructure system of this sector is now being castigated due to the recent incident of 'Rana Plaza' collapse which caused a total death of over 1138 workers. Furthermore few past earthquakes in nearby region of Bangladesh such as 2011 Sikkim earthquake (M=6.9) and the devastating 2015 Nepal earthquake (M=7.8) that jolted Bangladesh with long duration shaking have garnered attention among the stakeholder and researchers to evaluate the performance of structural properties of these garment buildings (Al-Hussaini et. al., 2015). Moreover, the recent Myanmar earthquake (2016) revealed the inadequacies of current reinforced concrete building stocks in Bangladesh which resulted in 11 tilted buildings sustaining different damage level in Chittagong city. One of these buildings has been assessed and suggested for demolition due to the sustained damage posed by the earthquake ground motion.

The damages in RC structures due to past earthquakes around the world are of similar nature and are attributed to virtually very few parameters like inadequate design and detailing, inferior material quality, construction malpractices, change in occupancy category over time, presence of different distress due to environmental conditions etc. (Ergun et. al., 2015; Sezen et. al., 2003; Kaplan et. al., 2004; Dogangun, 2004). The existing garment building stock comprises most of these inadequacies in advance with accommodating a large number of garment workers. Hence, they possess a great risk of casualties as well as monetary losses due to infrastructural damage and a passive impact due to hindrance in manufacturing garment products. The performance of structural properties of these buildings under earthquake hazard is thus a primary measures for their seismic vulnerability assessment and hence to ensure the margin against collapse.

The seismic performance evaluation of large number of reinforced concrete garment buildings in Bangladesh necessitates a simplified method over the detailed structural evaluation. The detailed assessment seems practically impossible and rather extravagant for structures with minimum level of vulnerabilities. Hence, the parameters and structural variables affecting the performance of the garment buildings should be determined through a preliminary assessment. At the same time the preliminary assessment procedure needs to represent the true behavior of the buildings under earthquake loading. Previous researches have been conducted to investigate the contribution of different structural performance indices such as concrete quality, number of floors, lateral confinement in the seismic performance of reinforced concrete buildings (Ergun et. al., 2015; Inel et. al., 2010). The current study aims at to investigate the effect of abovementioned parameters on seismic performance of the garment buildings. For this purpose, three reinforced concrete garment buildings in moderate seismic zone with different floor height is considered to represent the current garment building stock in Bangladesh.

### **DESCRIPTION OF SELECTED GARMENT BUILDINGS**

In order to attain the aforementioned objectives that is effect of structural properties on seismic performance of reinforced concrete garment buildings, a total of three RCC garment buildings from moderate seismic zone (0.20g) of Bangladesh have been selected for the current study. The three buildings have further been classified into three specific categories namely well designed, moderately designed and poorly designed depending on the design consideration while constructing the building. Well-designed building represent the current design code and considers the seismic design provision mentioned as per the Bangladesh National Building Code (BNBC), whereas the poorly designed building lacks proper design guideline and has been constructed based on local practices without following any particular design specification. In contrary, the moderately designed garment building follows basic design guideline but doesn't consider any specific seismic design code for construction. They are classified and named as Well designed low-rise building; moderately designed mid-rise building and poorly designed mid-rise building. All the three buildings are selected in a way so that they represent the low to mid-rise building stocks of current reinforced concrete garment buildings in the moderate seismic zone of Bangladesh. The floor system of all the buildings comprises of solid slabs of 125mm for poorly designed building and 200mm for both moderately designed and well-designed buildings. Properties of the selected buildings are presented in Table 1.

Table 1: Selected garment factory building parameters

Building Parameters	Well Designed	Moderately Designed	Poorly Designed
Number of storey	3	7	5
Bottom storey height (m)	6.75	4.7	5
Typical storey height (m)	5.75	3.5	4
Plan area (m <sup>2</sup> )	1180	3147	336
Plan irregularities	Regular	Irregular	Regular
Vertical irregularities	Regular	Irregular	Irregular
Bays in X-Z plane	8	6	6
Bays in Y-Z plane	2	9	2
Infill wall (Peripheral)	Brick Masonry Wall	No Infill Wall	Brick masonry Wall
Structural System	Beam-Column Moment Resisting Frame	Beam-Column Moment Resisting Frame	Beam-Column Moment Resisting Frame
Concrete strength (MPa)	28	21	21
Rebar yield strength (MPa)	413	413	413

The loading conditions considered for the analysis are divided into two steps. In the first step of analysis only the dead loads (buildings self-weight, partition wall load and floor finishes) and live loads for special occupancy structures are considered as per Bangladesh National Building Code (BNBC'14). Both the live loads and floor finish loads are applied as uniformly distributed shell loads and the partition wall loads are applied as both shell loads and uniformly distributed on peripheral beams of the buildings. The magnitude of live loads considered are of 3.8 kN/m<sup>2</sup> for well-designed and poorly designed buildings and 4.8 kN/m<sup>2</sup> for moderately designed building. A uniformly distributed load of 1.2 kN/m<sup>2</sup> has been applied for floor finish loadings. Furthermore the second stage of loading consists of earthquake and wind loads in addition to the basic gravity loadings. The seismic design category "C" has been considered for all the three buildings. Cross sectional properties and reinforcement detailing of the structural concrete columns considered for the analysis are represented in the study of Murtuz et. al., 2015.

## METHODOLOGY

Three different reinforced concrete garment buildings of varying height have been considered to represent the low and midrise building stock of Bangladesh. All the necessary design data regarding structural properties of the buildings are obtained from the as build drawing provided by the designer of these buildings. In this study, the performance of the buildings are assessed in two loading steps i.e. considering only the gravity loadings and later considering the earthquake loading as per proposed Bangladesh National Building Code (BNBC'2014) along with the gravity loads applied in step 1. The average column compressive stresses ( $\sigma_{ca}$ ) were computed as the ratio of the total weight of the building and total column cross sectional area in the ground floor level and the average stresses at ground floor base ( $\sigma_{ga}$ ) were calculated by dividing the sum of gravity loads by the total floor area in the ground level.

$$\sigma_{ca} = (\sum DL + \sum LL) / A_{g, col} \quad (1)$$

$$\sigma_{ga} = (\sum DL + \sum LL) / A_{g, gf} \quad (2)$$

Here, DL = dead load considered in the building, LL = Total live load considered,  $A_{g, col}$  = Column x-sectional area in ground floor level and  $A_{g, gf}$  = Total floor area in the ground level.

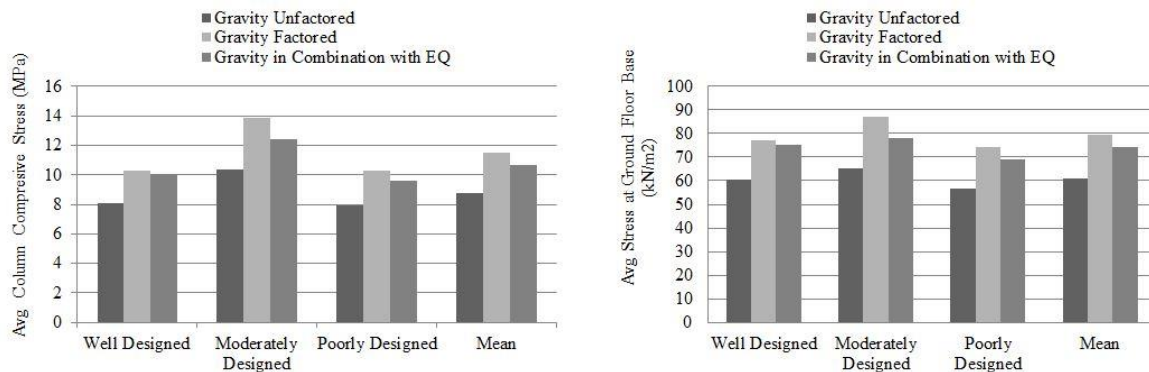


Fig. 1: Variation of (a) Average Column Compressive Stress ( $\sigma_{ca}$ ) and (b) Average Stress at Ground Floor Base ( $\sigma_{ga}$ )

The realization rates of longitudinal reinforcement have been obtained from the analysis result of the buildings. Two sets of realization rate and reinforcement optimization factor for all the columns in the ground floor levels are obtained in the two steps of analysis and their variation due to the employment of earthquake load is compared for each column in the ground floor level. The realization rate and optimization factor of longitudinal reinforcement is calculated following the stated Eq. (3) and Eq. (4).

$$\text{Reinforcement Realization Rate (RRR)} = (\sum A_{s, req} / \sum A_{s, pr}) / n \quad (3)$$

$$\text{Reinforcement Optimization Factor (ROF)} = (\sum A_{s, pr} - \sum A_{s, req}) / \sum A_{s, pr} \quad (4)$$

Here,  $A_{s, req}$  = Total reinforcement area required,  $A_{s, pr}$  = Total reinforcement area provided and  $n$  = Total number of columns/beams considered.

Finally, the shear force capacity ratio ( $V_{cr}$ ), normalized shear capacity ratio ( $V_{ncr}$ ) and the moment capacity ratio ( $M_{cr}$ ) in the two orthogonal directions of the buildings are calculated following Eq. (5), (6) and (7) bellow –

$$V_{cr} = (\sum V_{cap} / V)_{X \text{ and } Y} \quad (5)$$

$$V_{ncr} = (\sum V_{cap} / \sum W)_{X \text{ and } Y} \quad (6)$$

$$M_{cr} = (\sum M_{cap} / M_o)_{X \text{ and } Y} \quad (7)$$

Here,  $V_{cap}$  and  $V$  represent the shear capacity of individual column in the ground floor level and the base shear demand considering the seismic loading in two orthogonal directions. The moment capacity ratio is determined in the similar fashion as the ratio of moment capacity of the columns ( $M_{cap}$ ) with the overturning moment ( $M_o$ ) at the base of the building. Details description of the above parameters can be found in Ergun et. al., (2015).

## RESULTS AND DISCUSSIONS

The result obtained from the study is used to evaluate the properties of structural components in the ground floor level to check their performance under existing loading condition and expected behaviour under earthquake loading. The Mean of average column compressive stress as shown in Fig. 1(a) is found to be 11.48 N/mm<sup>2</sup> under factored gravity loads which is well below the specified concrete column compressive strength of 21 N/mm<sup>2</sup>. Hence, it can be concluded that the column cross sectional area are adequate against the existing gravity loading condition and thus justifies the fact that they are still functioning under service loading without undergoing any major damage. The variation of average ground floor stress level is represented in Fig. 1(b). The maximum average stress at ground floor base is observed for moderately designed building and the other two buildings follows similar average stress rate at the ground floor base level.

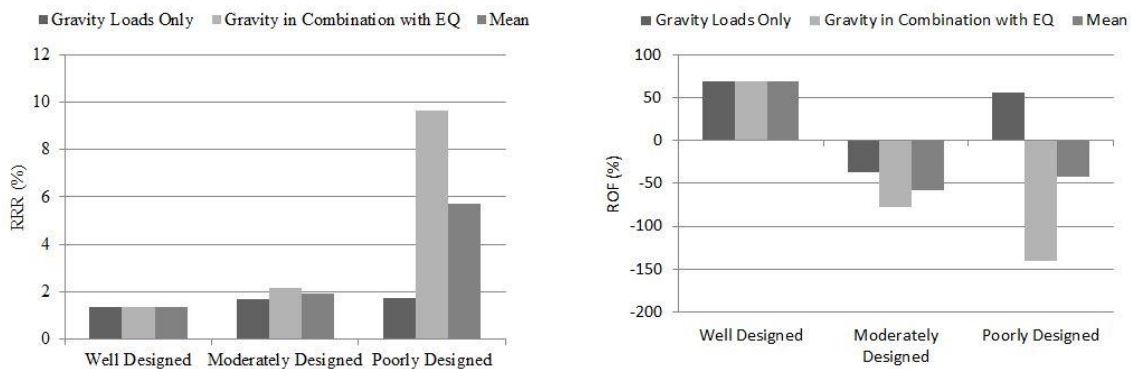


Fig. 2: Variation of (a) Reinforcement Realization Rate (RRR) and (b) Reinforcement Optimization Factor (ROF) for the three garment factory buildings

However, the average reinforcement realization rate as shown in Fig. 2(a) under gravity loads in combination with earthquake loading is found to be 9.62 for poorly designed building whereas the value is only 1.34 for well-designed building. Result clearly depicts that the column in the ground floor level of poorly designed building are extremely under-reinforced and thus expected to undergo severe damage due to design level earthquake. The more deliberate view of the reinforcement deficiency or surplus is presented in Fig. 2(b) as the Reinforcement Optimization Factor (ROF) for all the three buildings. Result shows that the design reinforcement requirement for well-designed building is far less than the provided reinforcement area and hence they are represented in the positive side of the bar charts. In contrary, moderately designed and poorly designed buildings follows a negative trend that shows the deficiency in total reinforcement area provided for these buildings.

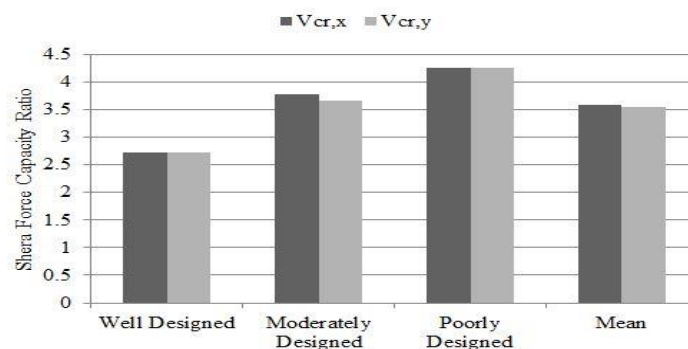


Fig. 3: Shear Force Capacity Ratio of selected garment buildings under earthquake loading

The maximum normalized shear force capacity ratio (the ratio of total shear force capacity of the ground floor columns to that of the total building weight) for the ground floor column as presented in Fig. 4 is computed as 0.26 for poorly designed building which exceeds the limiting value of 0.25 and thus showing inadequate shear capacity of reinforced concrete columns under lateral loading posed by earthquake excitation. All other buildings have lower normalized shear capacity ratio than the poorly designed building and hence predicting safe against shear failure. Variation in Shear Force Capacity Ratio for all the three buildings are illustrated in Fig. 3, where the base shear is calculated according to the Bangladesh National Building Code (BNBC) and the shear capacity of the column sections are computed considering the effect of concrete and transverse reinforcement as specified by the design data of the examined buildings. Result shows a linear increase from well-designed building towards poorly designed buildings having the maximum shear force capacity ratio for the poorly designed building.

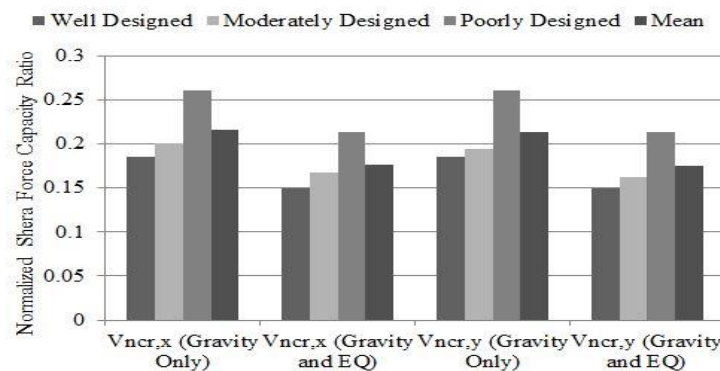


Fig. 4: Normalized Shear Capacity Ratio of examined garment buildings

The Moment Capacity Ratio and the Normalized Moment Capacity Ratio are illustrated in Fig. 5 and Fig. 6 respectively. The ratio of moment capacity as computed by dividing the ultimate moment capacity of the ground floor columns to that of the overturning moment at the base of each building considered. The normalized moment capacity in both the orthogonal direction (global X and Y axes) has further been computed with respect to the total building weights. Maximum moment capacity is obtained with the well-designed building whereas the minimum capacity is observed for the poorly designed garment building.

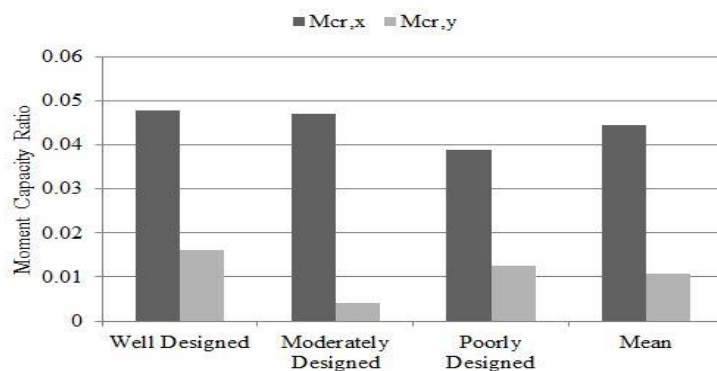


Fig. 5: Moment Capacity Ratio of the selected buildings in two orthogonal direction

## CONCLUSION

The study conducted investigates different performance parameters for three different buildings classified as well-designed, moderately designed and poorly designed according to their design philosophy and consideration of loadings from earthquake excitation. Comparing the results obtained from the investigation, the following conclusion can be drawn –

- Average column compressive stress for all the three designed buildings were far below the specified concrete compressive strength and hence prove that the design of these buildings inevitably considers the effect of gravity loads. It can also be inferred that the buildings under investigation are still functioning without any damage is due to their capacity to sustain the



gravity loads but their performance under earthquake events are questionable resulting from the increased shear and moment demand posed by the seismic excitation.

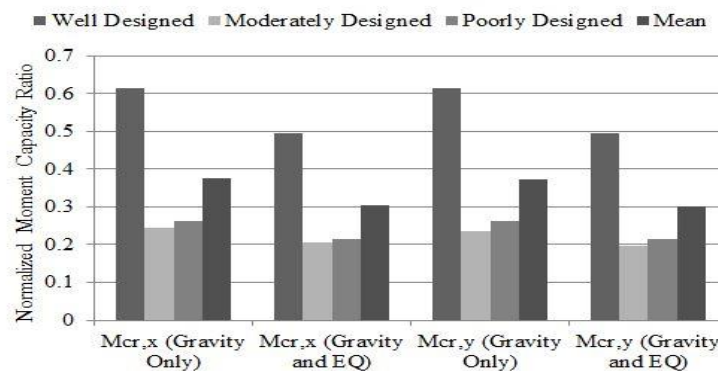


Fig. 6: Normalized Moment Capacity Ratio for the examined buildings under different loading conditions

- Result shows that two of the buildings (presented as moderately designed and poorly designed) lacks the required longitudinal reinforcement area required to sustain the designed level earthquake and hence making them under-reinforced building during any earthquake events. So it can be concluded that catastrophic damage due to brittle structural failure could takes place during any moderate level earthquake event.
- From the result of shear force capacity ratio and normalized shear force capacity ratio it can be concluded that the columns in the ground floor level satisfy the requirements to sustain against shear failure except the poorly designed building where the ratio exceeds slightly beyond the critical value.
- Overturning moments generated due to the seismic action shows insufficiency of the buildings capacity to resist demand and hence making them vulnerable against earthquake loadings.

## REFERENCES

- Al-Hussaini, TM; Chowdhury, IN; Noman, MNA. 2015. Seismic Hazard Assessment for Bangladesh - Old and New Perspectives. *First International Conference on Advances in Civil Infrastructure and Construction Materials*, MIST, Dhaka, Bangladesh, 14–15 December 2015.
- Bangladesh Garment Manufacturers and Exporters Association (BGMEA) Website. (<http://www.bgmea.com.bd/>)
- Dogangun, A; 2004. Performance of reinforced concrete buildings during the May 1, 2003 Bingol earthquake in Turkey. *Engineering Structures*. 26: 841–856.
- Ergün, A., Kıraç, N., & Başaran, V. (2015). The evaluation of structural properties of reinforced concrete building designed according to pre-modern code considering seismic performance. *Engineering Failure Analysis*, 58, 184-191.
- İnel, M; Özmen, HB; Şenel, ŞM; Meral, E; and Palancı, M. 2010. Evaluation Of Factors Affecting Seismic Performance Of Low And Mid-Rise Reinforced Concrete Buildings. *9<sup>th</sup> International Congress On Advances In Civil Engineering*. Trabzon: Turkey.
- Kaplan, H; Yilmaz, S; Binici, H; Yazar, E; and Cetinkaya, N. 2004. May 1, 2003 Turkey — Bingol earthquake: damage in reinforced concrete structures. *Engineering Failure Analysis*. 11: 279–291.
- Murtuz, A.K.M.G., Islam, K., Alam, M.S., Jalal, K.B., Priti, R.J. (2015). Performance Assessment of Existing RC Garment Manufacturing Factory Buildings: Case Study in the Context of Bangladesh. *Proceedings of First International Conference on Advances in Civil Infrastructure and Construction Materials*, 14-15th December 2015, Dhaka, Bangladesh.
- Sezen, H; Whittaker, AS; Elwood, KJ; and Mosalam, KM. 2003. Performance of reinforced concrete buildings during the August 17, 1999 Kocaeli, Turkey earthquake, and seismic design and construction practice in Turkey. *Engineering Structures*. 25: 103–114.
- Wadud, Z., & Huda, F. Y. (2016). Fire Safety in the Readymade Garment Sector in Bangladesh: Structural Inadequacy Versus Management Deficiency. *Fire Technology*, 1-22.

## **PARAMETRIC STUDY ON GFRP REINFORCED SHORT CONCRETE COLUMNS**

T. Mahmood, M. A. Morshed\* & M. Begum

*Department of Civil Engineering, Bangladesh University of Engineering and Technology, Dhaka,  
Bangladesh*

*\*Corresponding Author:anan.morshed@gmail.com*

### **ABSTRACT**

This paper summarizes the results of eight parametric columns reinforced with GFRP rebars. Nonlinear 3D finite element models have been developed using ABAQUS finite element code to investigate the compressive behaviour of GFRP reinforced square concrete columns. The load versus deflection response of the parametric columns was formulated using the static riks solution strategy. The parametric study was conducted to investigate the influence of -- the concrete compressive strength, reinforcement ratio and spacing of ties on ultimate axial load capacity and deflection of GFRP reinforced short columns. The results are presented in detail in the paper.

Keywords: Fibre Reinforced Concrete, Finite Element (FE) Modelling, Glass Fibre Reinforced Polymer (GFRP), Non Linear Analysis, Parametric study.

### **INTRODUCTION**

Most of the building columns and bridge piers are often in need of high corrosion resistance and high yield strength. The use of concrete structures reinforced with fibre reinforced polymer (FRP) composite materials has been growing to overcome the common problems caused by corrosion of steel reinforcement (ACI Committee 440 2007). The use of internal reinforced FRP bars can be a cost-effective alternative for upgrading the performance of concrete columns. Extensive experimental research have been conducted by research groups on the behavior of GFRP rebars used as internal reinforcement for beams, slabs and pavements (ACI Committee 440, CSA S806- 02, Benmokrane et al., 1998). These efforts have contributed greatly in improving our knowledge on analyzing and designing concrete structures reinforced with FRP bars in flexure and shear. On the other hand, the behavior of GFRP RC compression members is less defined. Previous experiments carried out by Kobayashi et al., 1995, De Luca et al. 2009, Tobbi et al. 2012, etc. studied the behavior of FRP reinforced columns. Tobbi et al., 2012 conducted an experimental research studying the behaviour of square concrete columns reinforced with GFRP bars under concentric loading. To extend the range of applications of GFRP reinforced columns in practice and to enhance the limited data on square columns reinforced by GFRP rebars, a parametric analysis is required using a validated analytical model.

### **METHODOLOGY**

A nonlinear finite element model for GFRP reinforced column was developed using ABAQUS finite element code. Detail description of the model has been included in Morshed et al. 2016. A damage plasticity model was used in the analysis to simulate the behaviour of reinforced concrete. The perfect bonding between FRP rebars and concrete was simulated using embedded element algorithm. A static Riks formulation was implemented to trace the stable load-displacement history of FRP reinforced concrete up to failure. The load was applied through displacement control technique. This model have been verified against the results from Tobbi et al. 2012. The numerical analysis results of the model are found to be in good agreement with the experimental results. The FE model as shown in Figure 1 is used here to conduct the parametric study. A comparative graphical results have also been plotted and shown in Figure 1.

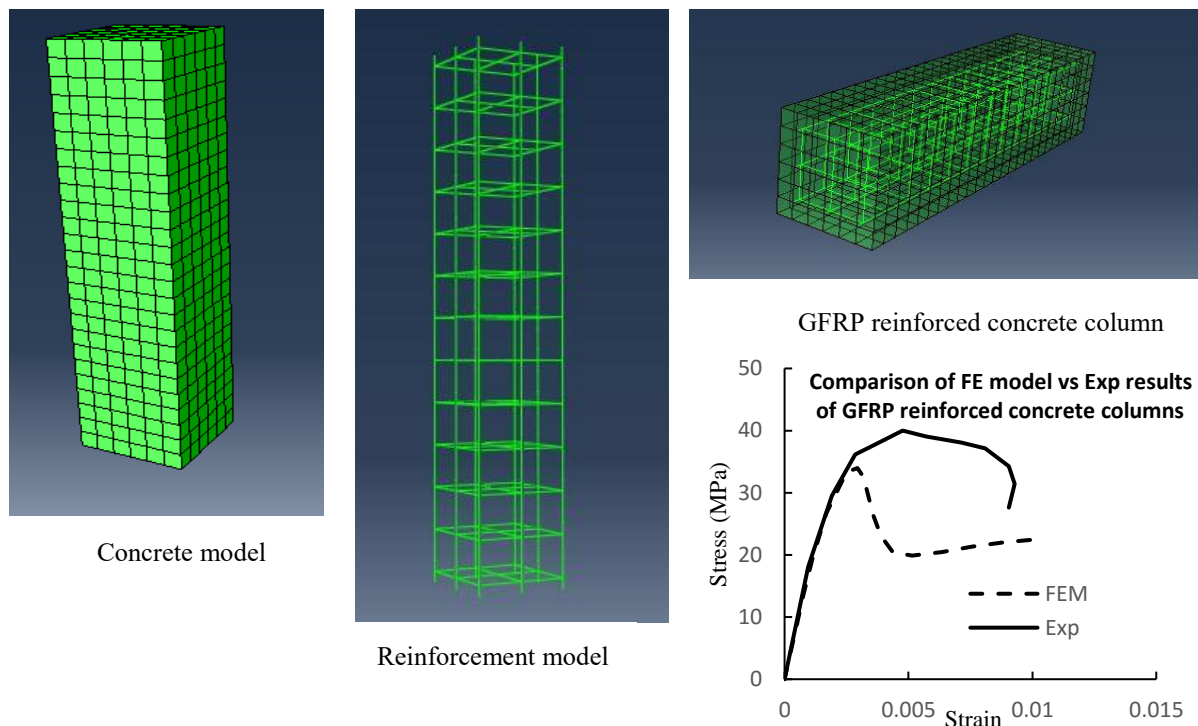


Fig. 1: FE Model of validated GFRP reinforced concrete columns (Morshed et al., 2016)

### DESIGN OF PARAMETRIC STUDY

The finite element model generated in the published research will be used to conduct a detailed parametric study on the behaviour of GFRP reinforced square concrete columns.

#### Variable Parameters

For designing the parametric study, the concrete compressive strength, reinforcement ratio and spacing of ties are identified as the most important geometric variables. The geometric and material properties of the columns designed for parametric study are included in Table 1. The specimens are named as PCX-Y-Z where X, Y and Z represent concrete compressive strength in MPa, reinforcement ratio (%) and tie spacing in mm respectively.

Table 1 Geometric and material properties of parametric columns

Column Specimen	Concrete compressive strength $f_{cu}$ MPa	Reinforcement	Reinforcement Ratio %	Tie spacing mm
PC33-1.85-120	33	8- $\phi$ 19 mm bars	1.9	120
PC33-3.21-120	33	8- $\phi$ 25 mm bars	3.2	120
PC33-1.85-330	33	8- $\phi$ 19 mm bars	1.9	330
PC33-3.21-330	33	8- $\phi$ 25 mm bars	3.2	330
PC25-1.85-120	25	8- $\phi$ 19 mm bars	1.9	120
PC25-3.21-120	25	8- $\phi$ 25 mm bars	3.2	120
PC25-1.85-330	25	8- $\phi$ 19 mm bars	1.9	330
PC25-3.21-330	25	8- $\phi$ 25 mm bars	3.2	330

### Fixed Parameters

For all column specimens following parameters have been kept constant:

- Column dimensions: 350 X 350 X 1400 mm(Tobbi et al., 2012, Morshed et al., 2016)
- Loading pattern: Displacement Controlled until failure at a rate of 0.002mm/s
- Boundary conditions: One end fixed.

### RESULTS AND DISCUSSIONS ON PARAMETRIC STUDY

The output parameters that have been extracted from the analysis are: Load and deflection. The axial load and deflection data are directly obtained from the Abaqus simulation. The summary of the results is shown in Table 2. The load versus deflection curves are then generated from the numerical analysis is investigated in this study.

Table 2 Results of parametric study

Column Specimen	Ultimate	Deflection at ultimate load
	Load, $P_u$	$\Delta_u$
	(KN)	mm
PC33-1.85-120	4161	2.6
PC33-3.21-120	4318	2.6
PC33-1.85-330	4109	2.4
PC33-3.21-330	4258	2.6
PC25-1.85-120	3225	2.4
PC25-3.21-120	3350	2.2
PC25-1.85-330	3179	2.2
PC25-3.21-330	3306	2.4

### Effect of Concrete Compressive Strength, $f_{cu}$

To evaluate the influence of varying concrete compressive strength on axial load capacity, two compressive strength of concrete 33 MPa and 25 MPa were considered as presented in Figure 2.

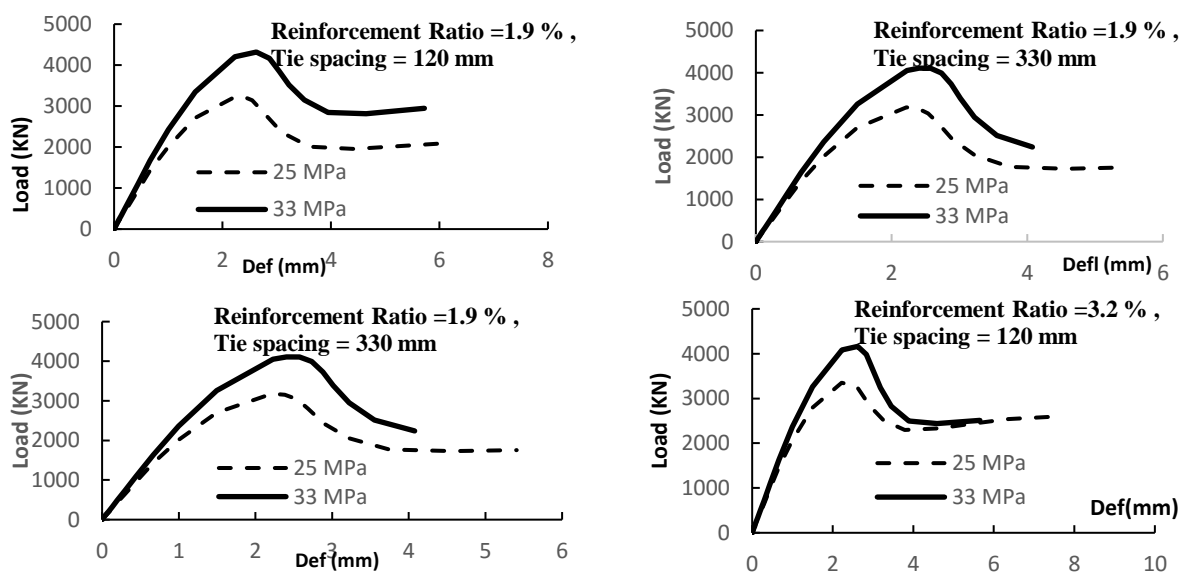


Fig. 2: Effect of concrete compressive strength

All of the specimens confirmed significant increase of an average of 23% in ultimate capacity when characteristic concrete compressive strength was increased by 25 %. The curves show a higher initial stiffness for that of compressive strength 33 MPa. However, no noteworthy change was observed in deflection at peak strength.

**Effect of Reinforcement Ratio,  $\rho$  %**

To evaluate the influence of varying reinforcement ratio on axial load capacity, two reinforcement ratio of 1.9% and 3.2% were considered as presented in Figure 3.

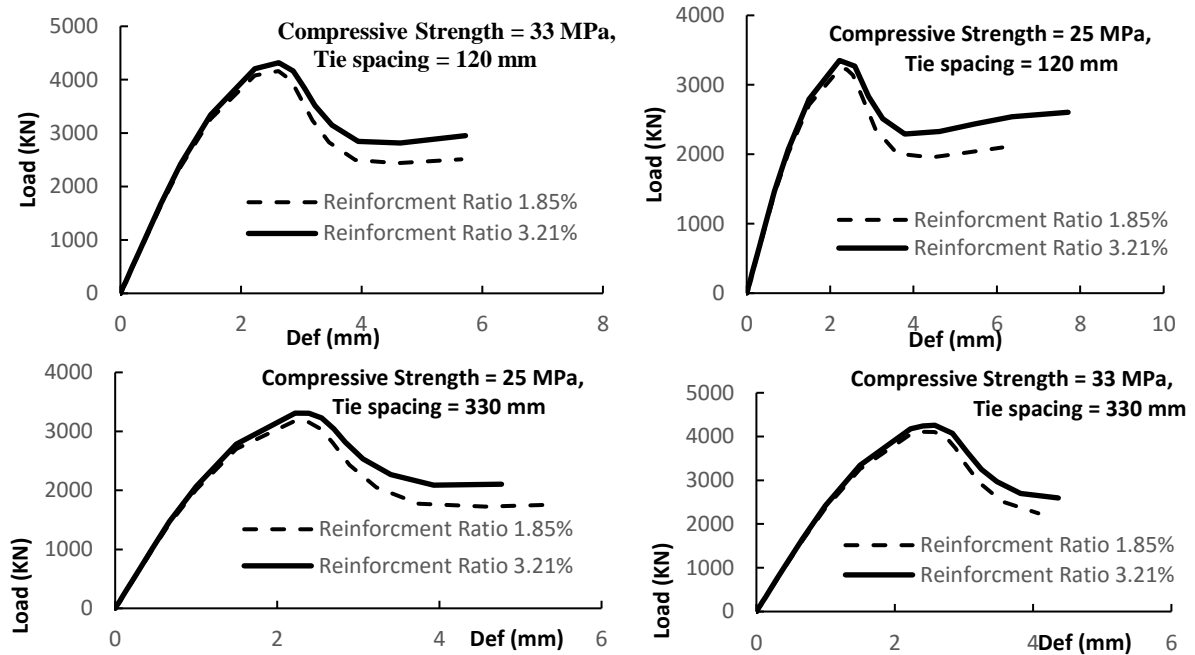


Fig. 3: Effect of reinforcement ratio

All of the specimens confirmed increase in ultimate capacity when reinforcement ratio was increased by 73%. However for the columns with concrete strength 25 MPa and tie spacing 330 mm, the increase in ultimate capacity due to increase in reinforcement ratio was more compared to others. The curves show almost same initial stiffness for the two reinforcement ratios. As predicted, the ductility of the columns increases due to increase in reinforcement ratio.

### Effect of Tie spacing, $s$ (mm)

To evaluate the influence of varying tie spacing on axial load capacity, two spacing of 120 mm and 330 mm were considered as presented in Figure 4.

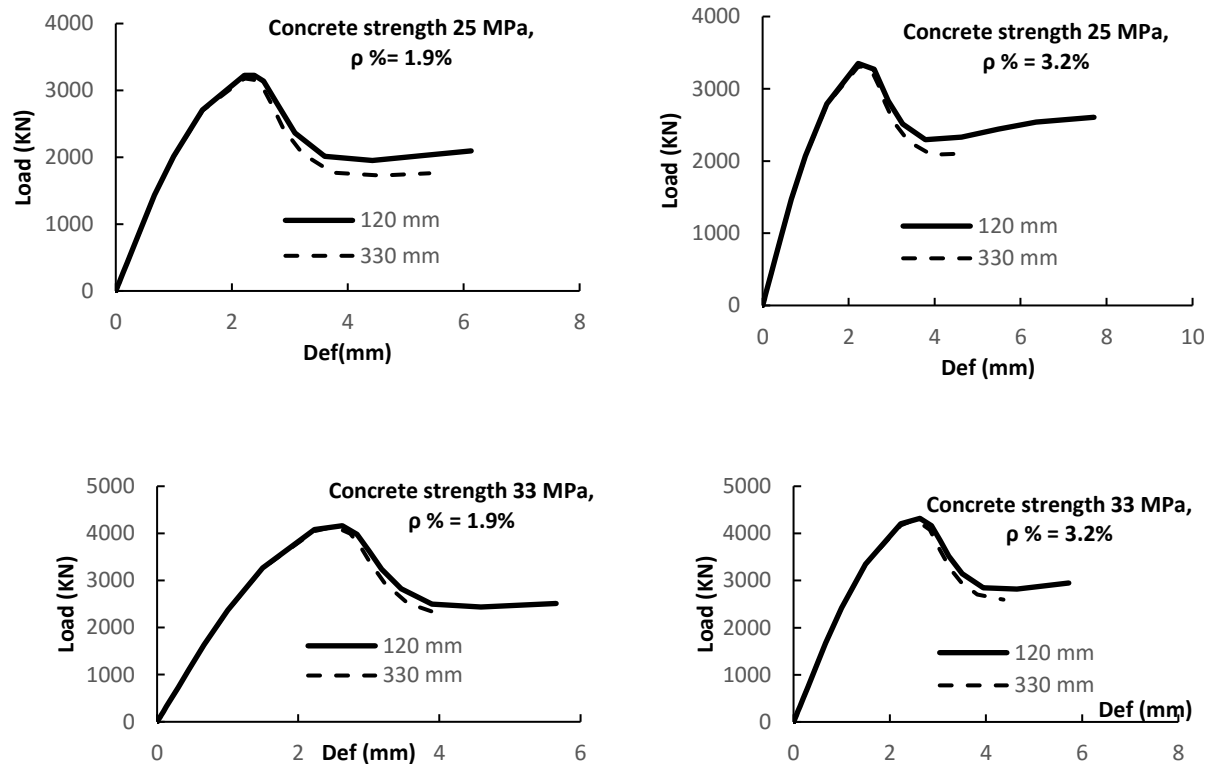


Figure 4 Effect of tie spacing.

All of the specimen confirmed increase of around 1.4% in ultimate capacity when tie spacing was decreased by almost 3 times in identical configuration. Thus, smaller the spacing, the increased confinement efficiency. In addition, the tie spacing controlled the buckling of the longitudinal bars. As predicted, the ductility and toughness (larger deformation region) of the columns improved due to increased transverse reinforcement ratio.

### ULTIMATE CAPACITY AND CODE PROVISIONS

The nominal capacity of an axially loaded RC column  $P_n$  is given by the following equation

$$P_n = 0.85 f'_c (A_g - A_s) + f_y A_s \quad (1)$$

The 0.85 reduction factor suggested by the ACI Building Code (ACI Committee 318 2008) in capacity is mainly attributed to the differences in size and shape of RC columns and the concrete cylinder. CSA S806-02 permits the use of FRP bars as longitudinal reinforcement in columns subjected to axial load only, without taking into account the FRP bars' contribution in calculating the ultimate capacity of the columns, as shown in the following equation

$$P_n = 0.85 f'_c (A_g - A_s) \quad (2)$$

Figure 5 compares the axial strength computed,  $P_n$ , according to the equation as suggested by Kobayashi and Fujisaki, 1995 (Eq. (3)) considering the contribution of GFRP bars in compression to be equal to 35% of GFRP tensile strength.

$$P_n = 0.85 f'_c (A_g - A_s) + 0.35 f_y A_s \quad (3)$$

Clearly, Eq. (1) overestimates column maximum capacity by 25% as evident from the  $P_n / P_u$  factor from figure 5. Conversely, ignoring the contribution of FRP longitudinal bars would underestimate maximum capacity. Setting GFRP compressive strength at 35% of the GFRP tensile strength made it possible to accurately predict the maximum axial load, as shown in Fig.5

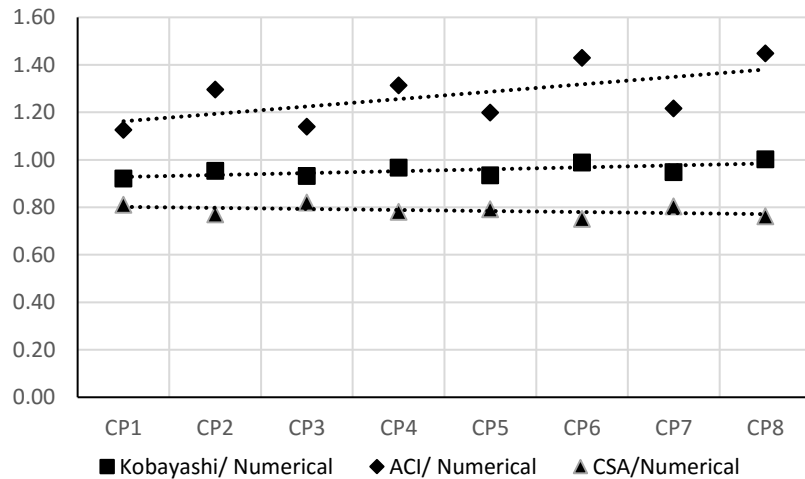


Fig. 5: Comparison of theoretical model to numerical model.

Table 2: Comparison between numerical and theoretical values by Kobayashi (1995) model, Eq. (3)

Column Specimen	Numerical Load, $P_u$	Theoretical Load, $P_n$ , by Eq3	% Error ( % $\Delta$ )	$\frac{P_n}{P_u}$
	KN	KN	%	
PC33-1.85-120	4161	3832	8.6	0.92
PC33-3.21-120	4318	4120	4.8	0.95
PC33-1.85-330	4109	3832	7.2	0.93
PC33-3.21-330	4258	4120	3.3	0.97
PC25-1.85-120	3225	3014	7.0	0.93
PC25-3.21-120	3350	3314	1.1	0.99
PC25-1.85-330	3179	3014	5.5	0.95
PC25-3.21-330	3306	3314	0.2	1.00

## SUMMARY AND CONCLUSIONS

A parametric study was undertaken to study the behaviour of GFRP reinforced concrete columns. It was found that the gain in ultimate axial load capacity ranges from 22-23% with 24% increase in concrete compressive strength. The reinforcement ratio was increased by 73% and the gain in ultimate load capacity varied from 3.5-5.8 %. The reinforcement ratios modelled were 1.9% and 3.2%. The gain in ultimate axial load capacity was found to be around 1.4% with reduction in tie spacing by 3 times. Finally, setting the GFRP compressive strength at 35% of the GFRP maximum tensile strength in code provisions produced a reasonable estimate of ultimate capacity compared to the experimental results.

## REFERENCES

- ACI Committee 440. Guide for the design and construction of structural concrete reinforced with FRP bars, 440.1R-06. American Concrete Institute, Farmington Hills, MI (2006).  
A. De Luca, F. Matta, and A. Nanni. Structural response of full-scale reinforced concrete columns with internal FRP reinforcement under compressive load. *9th International*

*Symposium on Fiber Reinforced Polymer Reinforcement for Concrete Structures (FRPRCS-9)*, ed. D. Oehlers, M. Griffith, and R. Seracino, July 13–15, 2009, Sydney, Australia, CD-ROM, 4 (2010).

Benmokrane, B. and Rahman, H. (1998). “Durability Of Fiber-Reinforced Polymer (FRP) composite for construction”, *Proceedings of the First International Conference on Durability of Composites for Construction*, Sherbrooke, Quebec, Canada, Aug. 5-7, 692 .

Canadian Standards Association, 2002, “Design and Construction of Building Components with Fiber-Reinforced Polymers (CAN/CSA S806- 02),” Canadian Standards Association, Mississauga, ON, Canada, 177 pp.

K. Kobayashi and T. Fujisaki. Compressive behavior of FRP reinforcement in non-prestressed concrete members. *Proceedings, 2nd International RILEM Symposium on Non-Metallic (FRP) Reinforcement for Concrete Structures (FRPRCS-2)*, Ghent, Belgium, 267–274 (1995).

Morshed, M.A.; Mahmood, T.; and Begum, M. (2016). Finite Element modelling and analysis of short concrete columns reinforced with GFRP bars. *International Journal of Advance Civil Engineering and Technology* [online]. 1(1): 1-14.

Available at: <http://mantechpublications.com/admin/index.php/IJoACET/issue/view/37>

Tobbi, H.; Farghaly, A. S.; and Benmokrane, B., 2012. Concrete Columns Reinforced Longitudinally and Transversally with GFRP Bars. *ACI Structural Journal*, 109(4) July-Aug., 551-558.



# **STUDY OF CONCRETE PROPERTIES INCORPORATING WASTE GLASS**

S. Y. Morshed\* & K. M. S. Islam

*Department of Civil Engineering, Khulna University of Engineering & Technology, Khulna,  
Bangladesh*

*\*Corresponding Author: yadmorshed@gmail.com*

## **ABSTRACT**

A few of the world's waste glass is recycled into new glass. This study is an attempt to recycle the waste glass by replacing natural sand with crushed waste glass in concrete. The objectives of this investigation are to study the strength of concrete made with 100% replacement of natural sand by glass sand (glasscrete) and also to compare the result with concrete made with natural sand. The results show that glasscrete gain less strength than normal concrete and require less w/c ratio. On the other hand, glasscrete have greater elastic modulus than normal concrete.

Keywords: waste glass; glasscrete; concrete; strength and elastic modulus

## **INTRODUCTION**

Concrete is the most widely used artificial substance on earth owing to its remarkable versatility as a construction material (Crow, 2008). The annual concrete production exceeding 2 billion metric tons per year across the world. One shortcoming of concrete as a construction material is the harmful effects on the environment posed by the production of its components (Roskos et al., 2014).

The generation of waste is vastly increased due to rapid growth of population and industry. So, worldwide recycling of waste materials has become a serious issue. The closed loop recycling technique is considered as the most appropriate practice to recycle waste materials. However, sometimes, because of high cost enforced from sorting and cleaning processes of waste material, the closed loop cannot be applied in recycling process. For example, the closed loop recycling process is not viable to recycle contaminated mixed-color waste recycled glass in glass industry because it required high cost for sorting and cleaning and inconsistency in the properties of the contaminated mixed-color waste recycled glass (Taha and Nounu, 2010).

Numerous research works were performed to examine the opportunity of reusing waste recycled glass in concrete and construction industry as alternative solution to reduce the generated bulk of mixed-color waste recycled glass, and establish solid ground for clear understanding and further investigation (Dhir et al., 2004; Jin et al., 2000; Shayan and Xu, 2003). Most of the past research on the use of glass aggregates in concrete engrossed on the mitigation of the deleterious alkali-silica reaction (ASR). ASR develops when aggregates with highly amorphous silicates (e.g., glass) are in contact with the alkaline pore solution of concrete. This contact causes dissolution of the silicates and formation of ASR gel, which swells and might crack the concrete (Wright et al., 2014).

This investigation was performed to study the strength of concrete made with 100% replacement of natural sand by glass sand (glasscrete) and also to compare the result with concrete made with natural sand. This study will present the results of a research effort focused on developing a green concrete for structural application made with Portland Composite Cement (PCC) as a binder material and crushed waste glass as fine aggregate.

## **METHODOLOGY**

One of the most important tasks of this study was collection of waste glass and preparation of glass aggregate. The main ingredient of study waste glass was collected from locally available glass stores, domestic wastes and wastes of construction work [Fig. 1]. The glass was crushed to sand size using a standard Los Angeles (LA) abrasion machine to obtain a fineness modulus similar to the natural sand used in this study [Fig.2]. Although the FM is a rough estimation of consistency across mixtures, its

simplicity evaluation provides a basis for quality control of workability (Mindess et al., 2003). The coarse glass aggregate was collected by separating from the crushed aggregate using a No. 4 ASTM standard sieve. Crushed glass passed through on NO. 4 sieve was used as fine aggregate.



Fig. 1: Collected Waste Glass



Fig. 2: Fine Glass Aggregate

The natural sand used in this thesis was locally available river sand, locally known as Sylhet sand, adhering to ASTM C33 (ASTM, 2011), with a saturated surface dry (SSD) specific gravity of 2.4, water absorption 4.1% and fineness modulus (FM) of 2.9. The dry rodded unit weight of the natural sand was determined 1600 kg/m<sup>3</sup>. The glass sand adhered to the ASTM C33 (ASTM, 2011) gradation and had a specific gravity of 2.6 and water absorption 0.00%. The FM was maintained at 2.9 ± 0.1. The glass sand also had dry rodded unit weight of 1795 kg/m<sup>3</sup>. The natural coarse aggregate used in this research was crushed stone chips adhered to the ASTM C33 (ASTM, 2011) gradation as a #57 coarse aggregate with a dry rodded unit weight of 1495 kg/m<sup>3</sup>, SSD specific gravity of 2.73, and water absorption 0.70%.

Table 1: Proportion of concrete mixtures (kg/m<sup>3</sup>)

Mix Design	Cement	Coarse Aggregate	Fine Aggregate		Water	Design Strength (psi)
			Natural Sand	Glass Sand		
N1	465.12	930	803.06	-	200	5000
G1	465.12	900	-	793.19	200	5000
N2	363.64	930	777.36	-	200	4000
G2	363.64	900	-	870.71	200	4000
N3	333.33	930	800.45	-	200	3500
G3	333.33	900	-	895.72	200	3500
N4	307.69	930	819.99	-	200	3000
G4	307.69	900	-	916.89	200	3000
N5	285.71	930	836.73	-	200	2500
G5	285.71	900	-	935.03	200	2500

Proportioning of concrete was performed according to the ACI 211.1 standard volumetric proportioning method. Concrete was mixed according to ASTM C192 (ASTM, 2007) using a standard concrete mixture. 100mm×200mm concrete cylinders were cast and compacted according to ASTM C31 (ASTM, 2000) in two layers with 25-rod blows per layer. Concrete cylinders were cast for various desired strength [Table 1] and compressive strength was tested at 1, 3, 7 and 28 days after casting. Elastic modulus was determined at 28 days after casting. In Table 1 the mixture identifier starts with N refers natural sand and G refers glass sand.

## RESULTS AND DISCUSSION

The compressive strength development over time between the glasscrete and the conventional natural sand mixtures that were designed for a 28-day compressive strength of 5,000 psi (G1 and N1) and 4000 psi (G2 and N2) are shown in Fig. 3 and Fig. 4 respectively. It is observed that glasscrete always gain less compressive strength than concrete made with natural sand.

Both N1 and G1 exceed their design strength 5000 psi at 28 day but conventional concrete gains more strength than glasscrete. The strength difference between them is 6.42% of their designed strength. The same observes for N2 and G2 mixtures whose desired strength was 4000 psi at 28 days and strength difference is 11.4%.

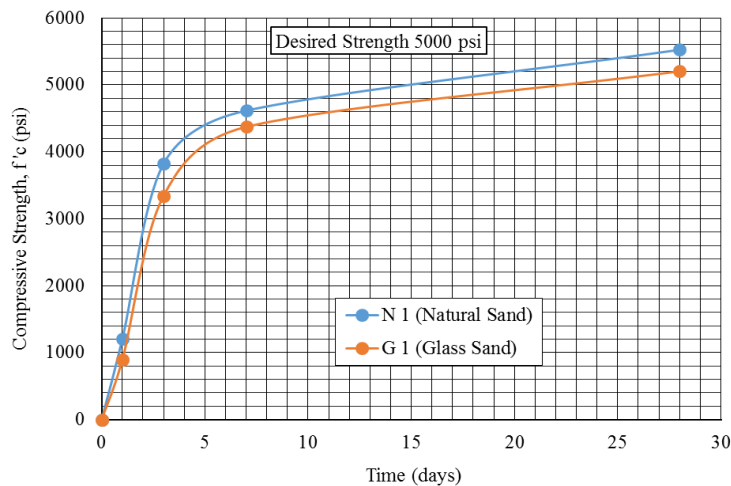


Fig. 3: Compressive Strength Gain Curve for N1 and G1 Mixtures

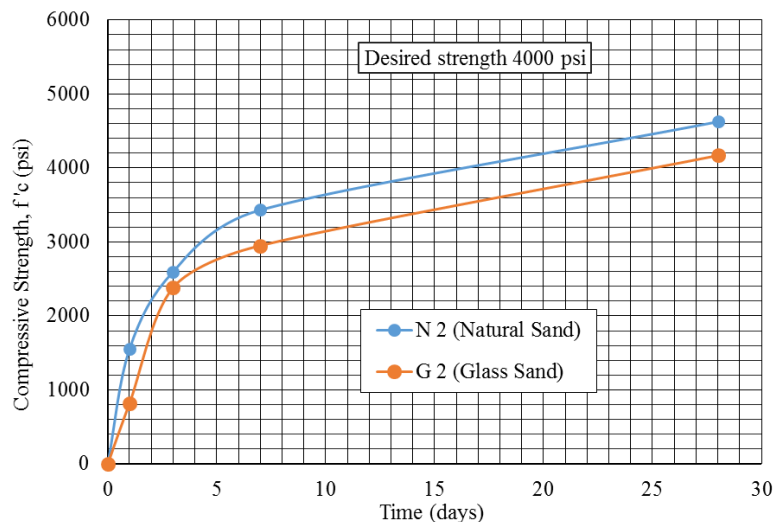


Fig. 4: Compressive Strength Gain Curve for N2 and G2 Mixtures

As concrete matures, the weaker bonding of glass aggregate to hydrated cement paste may become the weak link, which controls the compressive failure of glasscrete mixtures. Natural sand may allow for a better bond with cement paste given its greater surface roughness and moisture absorption capacity. Correlations were determined between the w/cm and the compressive strength at seven [Fig. 5] and 28 [Fig. 6] days, for glasscrete and natural sand concrete mixtures. Exponential regression curves were fitted with the experimental results and the correlation coefficients are offered. These figures may serve as design tools for proportioning concrete mixtures containing recycled glass fine aggregates to achieve a target compressive strength. For example, Fig.6 shows that to design a glasscrete mixture with 28-day strength of 4,000 psi, w/cm= 0.51 is required, whereas this strength is achieved in a conventional mixture with w/cm =0.55.

Elastic modulus of both glasscrete and conventional concrete was determined at 28 days after casting. A comparison of elastic modulus is presented in Fig. 7. It is observed that for 100% sand replacement (glasscrete) always attain higher elastic modulus than conventional concrete for all mixtures. So glasscrete is stiffer than conventional concrete.

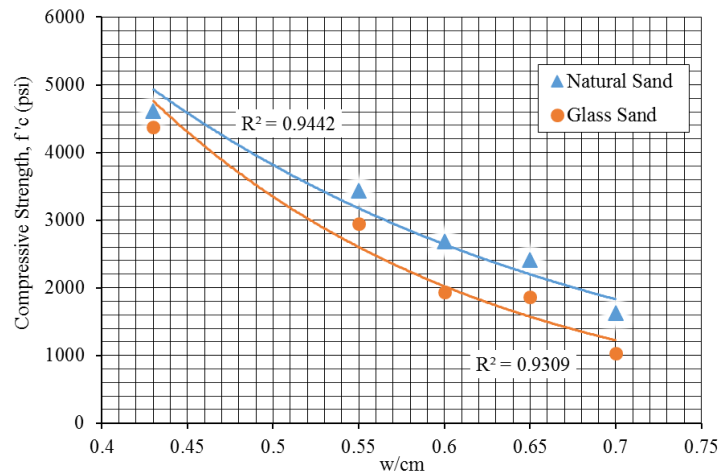


Fig. 5: Relation between w/cm and compressive strength at 7 days

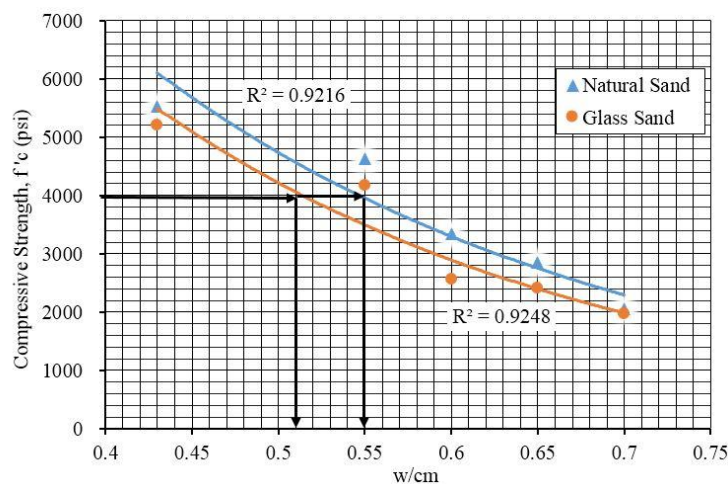


Fig. 6: Relation between w/cm and compressive strength at 28 days

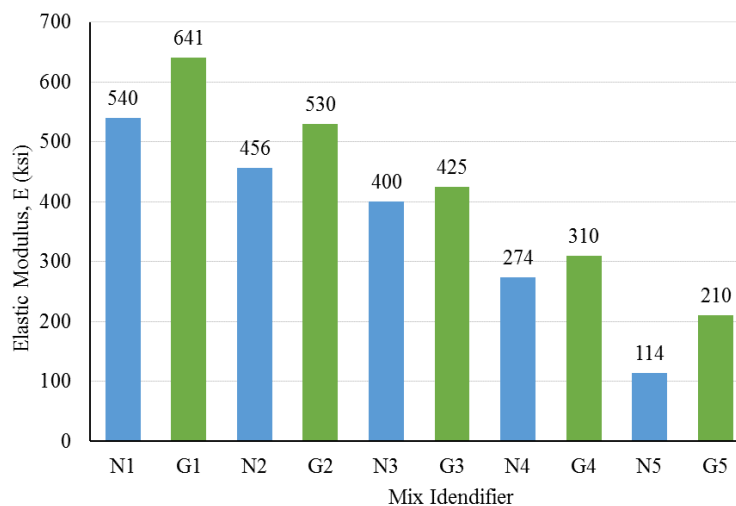


Fig. 7: Elastic modulus Comparison of natural sand concrete and glasscrete

## CONCLUSION

This paper studied the performance of conventional concretes and concretes containing 100% glass sand as replacement of natural concrete (glasscrete). This study found that glasscrete always attain less compressive strength than conventional concrete for a similar w/cm ratio. Similarly for a definite desired strength glasscrete required less w/cm ratio than conventional concrete. This may happen for a lower fracture toughness of glass particles and weaker bond between glass aggregates and cement paste.

The empirical correlations that were developed in this study might be useful in practicing glasscrete mixtures. On the other hand, for a similar w/cm ratio glasscrete always attain larger elastic modulus compared to conventional concrete. Hence, glasscrete exhibits more stiffness than conventional concrete.

## REFERENCES

- ASTM. 2000. *Standard Practice for Making and Curing Concrete Test Specimens in the Field*. C31, West Conshohocken, PA.
- ASTM. 2007. *Standard practice for making and curing concrete test specimens in the laboratory*. C192-07, West Conshohocken, PA.
- ASTM. 2011. *Standard specification for concrete aggregates*. C33-11, West Conshohocken, PA
- Crow, JM. 2008. The concrete conundrum. *Chem. World*, 5(3): 62–66.
- Dhir, RK; Dyer, RK and Tand, MC. 2009. Alkali-silica reaction in concrete containing glass. *Mater. Struct.*, 42(10): 1451–1462.
- Jin, W; Meyer, C and Baxter, S. 2000. Glasscrete—concrete with glass aggregate. *ACI Mater. J.*, 97(2): 208–213.
- Mindess, S; Young, J and Darwin, D. 2003. *Concrete*, 2nd Ed., Pearson Education, Upper Saddle River, NJ
- Roskos, C; White, T and Berry, M. 2014. Structural performance of self-cementitious fly ash concrete with glass aggregates. *Journal of Structural Engineering*, ASCE, B4014010-1-10.
- Shayan, A and Xu, A. 2004. Value-added utilization of waste glass in concrete. *Cem. Concr. Res.*, 34(1): 81–89.
- Taha, B and Nounu, G. 2009. Utilizing waste recycled glass as sand/ cement replacement in concrete. *J. Mater. Civ. Eng.*, 10.1061/ (ASCE) 0899-1561(2009)21:12(709), 709–721.
- Wright, J; Cartwright, C; Fura, D and Rajabipour, F. 2014. Fresh and Hardened Properties of Concrete Incorporating Recycled Glass as 100% Sand Replacement. *J. Mater. Civ. Eng.*, 10.1061/ (ASCE) MT.1943-5533.0000979, 04014073.

# **PRESENT STATUS OF APPLICATION OF STRENGTHENING AND REPAIRING TECHNIQUES FOR COLUMN JACKETING AND ITS OUTLOOK IN BANGLADESH**

J. Wasim\* & AKMH Julkernine

*Department of Civil Engineering, Bangladesh University of Engineering and Technology, Dhaka,  
Bangladesh*

*\*Corresponding Author: wasim@jaherwasim.com*

## **ABSTRACT**

With better understanding of seismic demand on structures and with our recent experiences with large earthquakes near urban centers, the need of seismic retrofitting is well acknowledged especially in the ready-made garments sector in Bangladesh. This paper summarizes and reviews the use of the industrial structures strengthened and repaired with column jacketing in Bangladesh with respect to realistic case studies. According to different codes and engineering practices retrofit measures may vary considerably. The paper will be introducing and evaluating retrofit measures using column jacketing based on FEM modeling and in perspective to existing seismic conditions. Seismic analysis has been conducted based on nonlinear time history analysis using SAP2000 a product of Computer and Structure Inc. in basic frame and retrofitted frame. The study results are discussed in detail both in diagrams and with a simple formula. Based on the suggested procedure, seismic retrofitting has been carried out by using the ACI-562 guideline.

Keywords: Retrofit; ACI-562; SAP2000; column jacketing; Bangladesh

## **INTRODUCTION**

The massive 7.9 magnitude earthquake in Nepal (2015) and its climbing death toll have raised the heavyweight cautionary signal for Bangladesh and the surrounding's about colossal earthquake. So now a day detailed engineering assessment and retrofitting measures are a vital issue in this Asian zone. Retrofitting is the modification of existing structures to make them more resistant to earthquake by optimizing the strength, ductility and earthquake loads (O. R. Chowdhury et al, 2015). Earthquake load is generated from the site seismicity, mass of the structures, important of buildings, degree of seismic resistant etc. Due to variety of structural condition of building, it is hard to develop typical rules for retrofitting. Each building has different approaches depending upon the structural deficiencies. Hence engineers are needed to prepare and design the retrofitting approaches. In the design of retrofitting approach, the engineers must comply with the building codes. The results generated by adopting retrofitting techniques must fulfil the minimum requirements on the building codes such as deformation, detailing strength etc. In view of this, the paper will be assessing a case study of an existing six storied industrial building. This building is used mainly for light factory operations including operational offices, dining, and sewing, cutting, finishing and finished goods storage. A plan view of this building has shown in Fig. 1.

## **METHODOLOGY**

This paper presents seismic retrofits technique suitable for improving the local and global response performance of existing reinforced concrete industrial buildings that was designed for mainly gravity load and situated in low to moderate seismic zone of Bangladesh. Retrofit schemes are developed to focus on redistributing damage throughout the structure providing a control of story deformations. This is achieved by retrofitting using column jacketing method, thereby a low-cost solution with minimal structural disturbance. A six-storied industrial building has been used as a case study for this research. Several visits were made to check and collect data to assess building stability through scanning, rebar

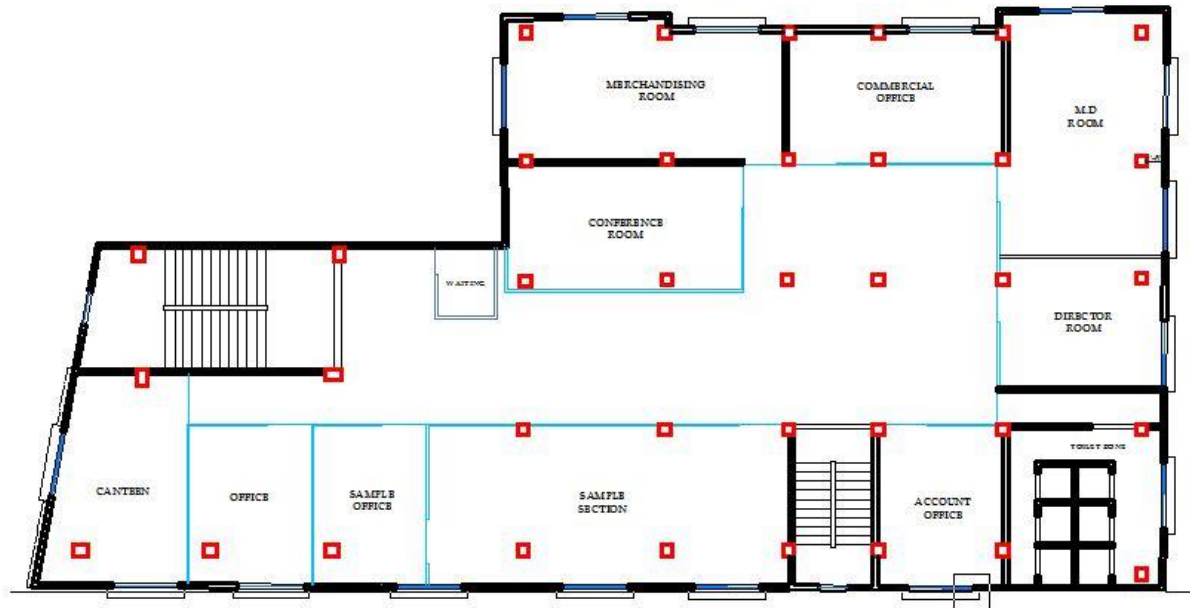


Fig. 1: Plan View of a 6 Storied Industrial Building

testing and core cutting on rcc column, beam and slab of different levels of the building. To assess and analyse data, followed the code of BNBC, the guide line of Accord, Alliance and National Tripartite Plan of Action (NTPA) on structural integrity, using ACI-562 code to evaluate concrete strength from core test results. Finite element software ETABS (a product of Computer and Structure Inc.) was used to analyse different types of load calculation and developed a 3D model of existing building structure and based on the evaluation a retrofit model was also developed.

### ***Geotechnical Investigation***

From soil report it has found the structure is built on soft soil (SD Type, SPT < 15) in zone 2 (moderate seismic intensity zone) of Bangladesh Seismic map.

### ***Strength Assessment of Concrete***

To assess the strength of the concrete, core test has conducted on January 2016. According to the core test result of the concrete strength varies between 1580 psi and 3700 psi. Considering all these, concrete strength value of 1683 psi was found as per ACI-562 and this value was considered in the analysis.

### ***Test of Collected Steel Sample***

Rebar samples collected from the building showed 63 ksi yield strength according to laboratory test results. To be in accordance with real-time scenario 60 ksi yield strength was considered for the assessment.

### ***Scanning of Structural Member***

To verify the reinforcement in the existing columns, beams and slabs, Ferro scanning was performed. Reinforcements were scanned at twenty locations at different floor levels. Three locations are at level 1 (two beams and one column), five locations are at level 2 (four columns and one slab), seven locations are at level 3 (four columns, one slab and two beams) and another five locations are at level 6 (four columns one slab).

## **STRUCTURAL ANALYSIS**

### ***Structural Model***

Finite element analysis has been performed for this building based on as-built structural and architectural layout. The building has beam supported slab system (level-1, 2, 3) and edge supported

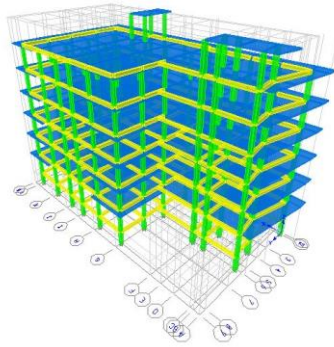


Fig. 2: 3D Finite Element Model of the 6 Storied Building

slab system (level-4, 5, 6). Beams and columns were modeled with appropriate frame elements. The slab was modeled with shell elements. Fig. 2 shows the 3D model of the building.

### Boundary Condition

For this 6-storied industrial building with pile foundation, it is reasonable to assume that the bases of columns are fully restrained in all directions both translational and rotational. Thus, all the nodes at the bottom of each column were rendered fully restrained against all sort of displacement in the node.

### RESULTS

After finite element analysis, a several number of columns of the structure were found to be inadequate. Design Load to Structural Element Capacity of Column (D/C Ratio) for columns in Level-1 are shown in Table-1. Inadequate columns are to be considered as those with D/C ratio greater than 1 and marked in red in the table. Concrete column jacketing has been applied by encasing existing columns in concrete jacket with longitudinal and transverse reinforcement as shown in fig-3. The columns have an increased size and added reinforcement so that their flexural capacity becomes greater than that of the joining beams. For the columns at the ground floor level, the added column reinforcement was anchored into the pile cap as foundation has defined as fixed. Transverse reinforcement has added to the potential plastic hinge regions in base columns to provide adequate rotational ductility and enhance shear capacity. The concrete used for this retrofit technique is a high-performance material that has the

Table 1: D/C Ratio of Level-1 Columns

Grid Line	A	B	C	D	E	F	G	H	I	J	K	L
1							2.18	1.91	2.37	2.34	2.33	
1C												O/S
2	1.61			1.75		1.66						
3							2.66	1.98	2.06	2.01	2.42	2.24
4			1.71			1.67						
5							2.95	2.01	1.99	1.97	2.02	2.11
6		1.36				1.64						
7							1.88	1.95	1.96	1.97	1.95	1.95
8							2.55	2.02	1.90	1.92	2.01	1.89
	N	O	P	Q	R	S	T	U	V	W	X	Y
1A							2.51	2.58				
1B	1.65			2.23		1.87						



characteristic properties of low shrinkage, high strength ( $f'_c = 6$  ksi), and superior bond adhesion by epoxy coating to existing concrete members.

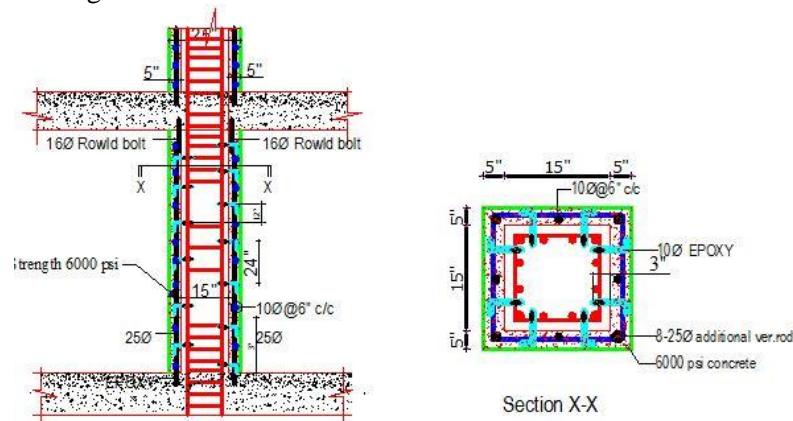


Fig. 3 : Concrete Column Jacketing Technique

Another finite element model has been developed to investigate the structure Load/Capacity ratio after retrofitting. After retrofitting the design load to structural element capacity are as follows in Table 2.

Table 2: D/C Ratio for Level-1 Columns after Retrofitting

Grid Line	A	B	C	D	E	F	G	H	I	J	K	L
1							0.44	0.38	0.39	0.36	0.33	
1C												0.32
2	0.42			0.21		0.41						
3							0.42	0.35	0.34	0.33	0.34	0.33
4			0.48			0.47						
5							0.44	0.35	0.24	0.24	0.27	0.31
6		0.43				0.43						
7							0.39	0.27	0.23	0.23	0.24	0.24
8							0.37	0.25	0.19	0.19	0.24	0.25
	N	O	P	Q	R	S	T	U	V	W	X	Y
1A							0.89	0.91				
1B	0.81			0.96		0.82						

Column jacketing method was incorporated in the structural retrofit model using SD section design process in the ETABS finite element software. The column sections were increased by 5 inches on each side by reinforced concrete jacketing method (Teran & Ruiz, 1992).

### Time History Analysis

The retrofit solutions outlined in the previous section provide local retrofit measure for frame structures. However, the global effectiveness of this retrofit measure in a structure is not completely obvious. Application of this certain types of retrofit measure may not be beneficial to overall structural performance. Global verification of integrating the local retrofit measures throughout the structure is most effectively evaluated by using inelastic dynamic analysis programs. In this study, nonlinear time history analysis was performed using SAP2000 (a product of CSI Inc.) implemented by Modak-Sotelino Generalized algorithm (Sukomol & Elisa, 2002) in pre-retrofit frame and retrofitted frame. It has seen that, in retrofitted frame story drift was decreased in a significant manner with respect to the original sub assemblage. Story drift data has shown in fig 4.

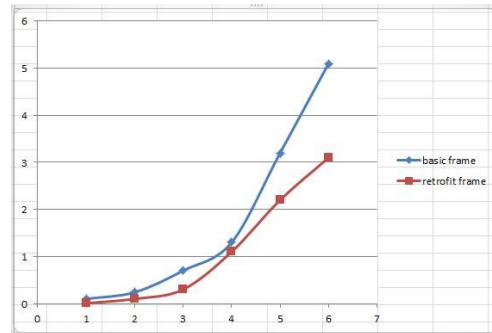


Fig. 4: Story Drift in Pre-Retrofit Frame and Retrofit Frame

## ACKNOWLEDGEMENTS

The author would like to thank Mr Saiful Mahmud for his advice and help in data collection for this study.

## CONCLUSIONS

Based on the present study, the following conclusions can be drawn:

- Concrete jacketing of columns and encasing the joint region in a reinforced fillet is an effective but the most labour-intensive strengthening method due to difficulties in placing additional joint transverse reinforcement.
- Retrofitting by column jacketing decrease storey drift in a large extent.
- It is important to obtain accurate as-built information and analytical data to perform a seismic evaluation of the existing structure and to select the appropriate retrofitting strategy
- Further research should be conducted to improve the selection of appropriate retrofit techniques using criteria based on performance, economy and constructability

## REFERENCES

- Chowdhury, OR; Wasim, J and Julker Nine, AKMH. 2015. Detail Engineering Analysis of Assessment of Retrofit Measures of Existing Structures Using Column Jacketing Method. *Proceedings of First International Conference on Advances in Civil Infrastructure and Construction Materials. (CICM 2015) Dhaka, Bangladesh, 14 – 15 December, 2015.*
- Computer and Structures Inc., ETABS Nonlinear Version 9.7, California, USA.
- Computer and Structures Inc., SAP2000, California, USA.
- Modak, S and D Sotelino, E. 2002. The generalized method for structural dynamics applications Article · Jul 2002 · *Advances in Engineering Software.*
- Teran, A and Ruiz, J. 1992. Reinforced concrete jacketing of existing structures. *Earthquake Engineering, 10<sup>th</sup> World Conference (ISBN 9054100605), Balkema, Rotterdam.*

## **EFFECT OF LOCALLY AVAILABLE FLY ASH AS PARTIAL REPLACEMENT OF CEMENT ON CONCRETE STRENGTH**

M. R. Kamal<sup>1\*</sup> & R. Rumman<sup>2</sup>

<sup>1</sup>*Department of Civil Engineering, Sonargaon University, Dhaka, Bangladesh*

<sup>2</sup>*Department of Civil Engineering, Bangladesh University of Engineering and Technology, Dhaka, Bangladesh*

*\*Corresponding Author: rubayat.kamal@gmail.com*

### **ABSTRACT**

Cement industry is the most energy intensive of all manufacturing industries of recent time. So various solutions are currently under investigation with the aim of reducing the environmental impacts of cement production; and one of them is replacing cement with fly ash. Fly ash is a naturally-occurring by-product from the coal combustion process which is used as a partial replacement of cement. Because fly ash use displaces cement use, it also reduces the need for cement production – a major energy user and source of greenhouse gas emissions. Fly ash being less expensive, increased percentage of fly ash replacement results in cost reduction of concrete. Due to its pozzolanic effects, fly ash also enhances the compressive strength and durability of concrete. In Bangladesh, Portland Composite Cement (PCC), which contains certain percentages of fly ash and other supplementary cementing materials, is becoming popular nowadays, but its exact composition is not mentioned by the production companies. This paper investigates the effect of locally available fly ash as partial replacement of cement and tries to determine an optimum percentage of fly ash for maximum strength; making the concrete economical in the process. It was found that 10% fly ash replacement provided maximum compressive strength.

Keywords: Fly ash; compressive strength; Portland Composite Cement; Ordinary Portland Cement

### **INTRODUCTION**

Fly ash, consisting of spherical and glassy particles, is a residue produced from combustion of coal. Presently in Bangladesh, it is estimated that 1.3 million cubic feet of fly ash is produced per annum from thermal power plants, and is estimated to reach an alarming crescendo of 9.5 million cubic feet by 2018 (Tamim et al., 2013). Dumping of this huge amount of fly ash is a big concern. Experts estimate that cement production contributes to about 7% of carbon dioxide emissions from human sources. If all the fly ash generated each year were used in producing concrete, the reduction of carbon dioxide released because of decreased cement production would be equivalent to eliminating 25% of the world's vehicles. ("Fly Ash & The Environment | Headwaters Resources," n.d.) Fly ash replacement also helps in reducing the cost of concrete as fly ash is cheaper than cement. Several investigations have already been carried out by researchers all over the world to study the effect of fly ash replacement on compressive strength of concrete (Berryman et al., 2005; Pitroda et al., 2012; Thomas, 2007; Kumar, et al., 2014). (ASTM C618 - 03 Standard Specification for Coal Fly Ash and Raw or Calcined Natural Pozzolan for Use in Concrete) However, very few researches are found regarding locally produced fly ash of Bangladesh. Farooque et al. (2010) investigated the pozzolanic activity of fly ash collected from Meghna Cement Factory. Sultana et al. (2014) studied the influence of rice husk ash (collected from a rice mill of Joypurhat) and fly ash (locally produced in thermal power plant of Boropukuria) on properties of clay samples collected from Naogaon. Islam et al., (2015) also used fly ash from Boropukuria power plant as a replacement of clay and made fly ash bricks. Muhit e al. (2013) studied fly Rainbow Holdings Limited, Dhaka as partial replacement of cement and found 10% replacement as optimum in terms of strength. In this study, fly ash collected from Boropukuria thermal plant was used as a partial replacement of cement and its effect on concrete compressive strength was observed.

## EXPERIMENTAL PROGRAM

The experimental program was planned to study the effect of locally produced fly ash as partial replacement of cement on the compressive strength characteristics of hardened concrete at different curing ages. The details of the program including different materials used test conducted are summarized below.

### Materials

- Cement: ASTM (C-150 Type-I Portland Cement was used as binding material.
- Fly ash: Fly ash collected from Boropukuria thermal power plant was used as a supplementary cementing material. The fly ash was of class F according to ASTM (C618 – 03) as already analysed and classified by previous researchers (Khan et al.,2013; Tamim et al., 2013).
- Aggregate: 20 mm downgrade and 10 mm downgrade stone chips in the ratio of 60:40 were used as coarse aggregate and Sylhet sand was used as fine aggregate for preparing the test specimens.

### Mix Design

Two different grade concrete mixes, M25 and M40, were produced having water cement ratio of 0.50 and 0.40 respectively using 10%, 20 %, 30% and 50% fly ash replacement. Percent replacement of fly ash was done by weight of cement. Table 1 shows the mix designs used for preparing the concrete specimens.

Table-1: Mix designs used for preparing sample

Mix No	Characteristic Strength	Coarse Aggregate	Fine Aggregate	Cement	Water	W/C Ratio
	(MPa)	(kg)	(kg)	(kg)	(kg)	--
1	25	1250	618	380	190	0.5
2	40	1225	605	450	180	0.4

### Compressive Strength Test of Cylindrical Concrete Specimens

Compressive strength test on concrete specimens was done according to the specifications of ASTM test method for Compressive Strength of Cylindrical Concrete Specimens (ASTM C39 / C39M - 16a). Compressive strength test was carried out on 4" X 8" cylindrical concrete specimens at 3, 7 and 28 days. Procedure for mixing and casting of fresh concrete cylinders and determination of compressive strength are shown in the self-explanatory figures below (Fig. 1).



Fig. 1(a): Weighing of fly ash



Fig. 1(b): Mixing and casting of cylinders

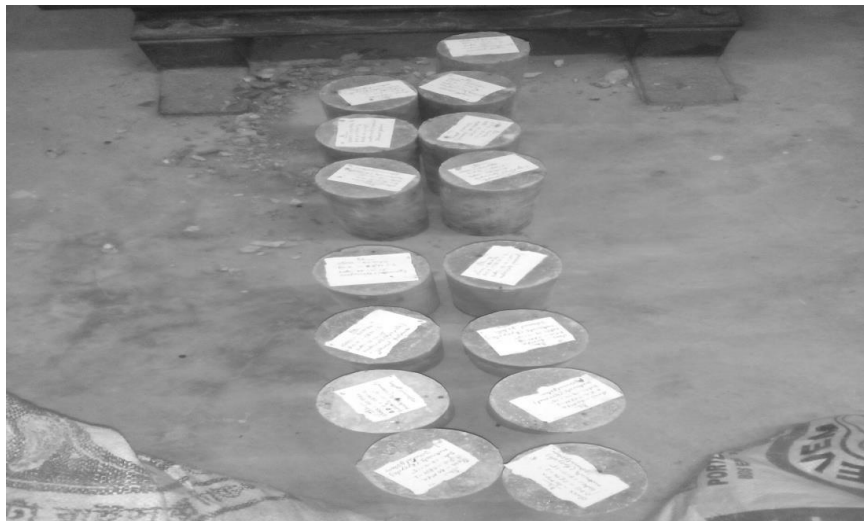


Fig. 1(c): Cylinders prepared for compressive strength test



Fig 1(d): Crushing of cylinder

Fig. 1: Compressive strength test of cylindrical concrete specimens

## RESULTS AND DISCUSSIONS

Fig. 2 and Fig. 3 show the comparison of compressive strength for different percentages of fly ash replacement of M25 and M40 grades respectively.

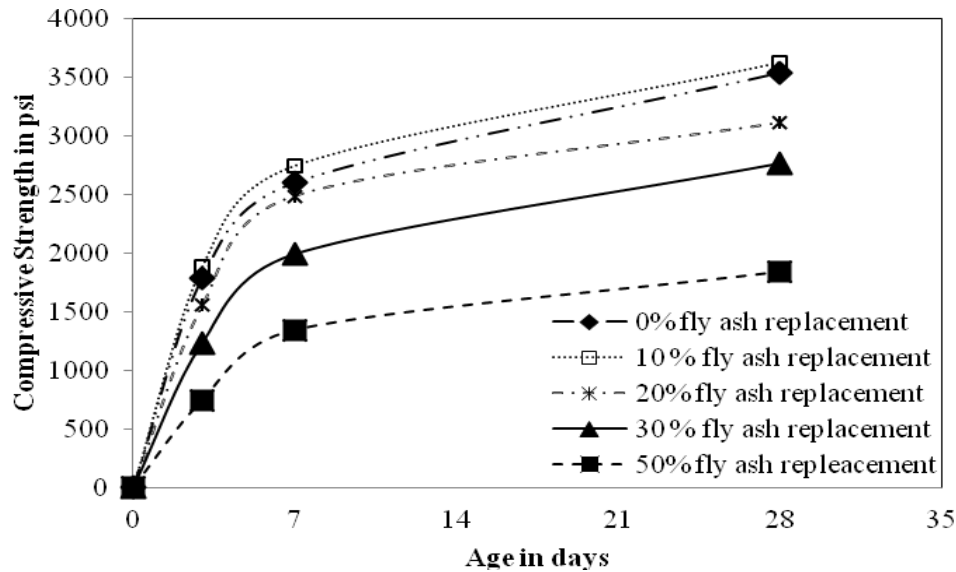


Fig. 2: Variation of compressive strength with age for different percentages of fly ash replacement of M25 grade concrete

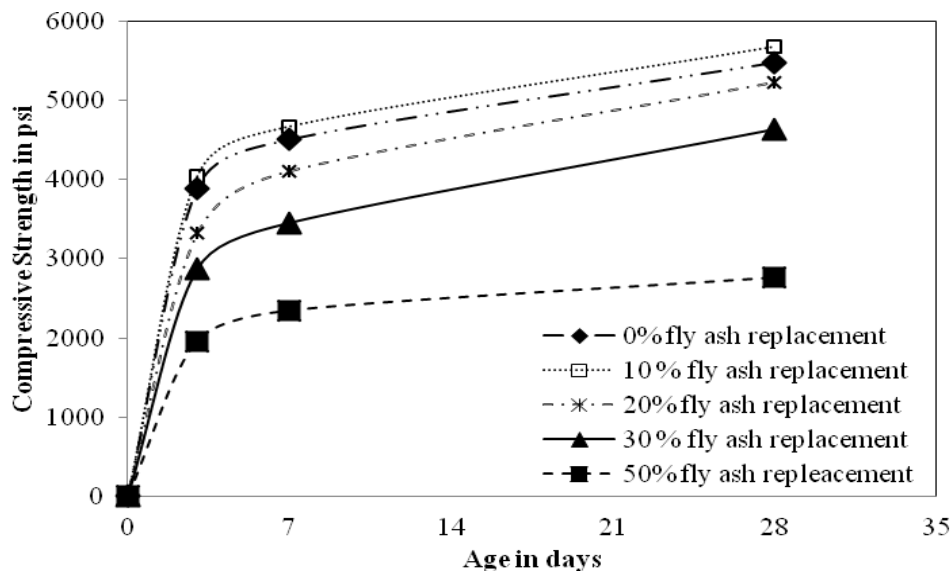


Fig. 3: Variation of compressive strength with age for different percentages of fly ash replacement of M40 grade concrete

From the graphs, it can be seen that for both M25 and M40 grade concretes, 10% fly ash replacement provided the highest compressive strength at all ages. The 2<sup>nd</sup> highest strength was achieved using OPC cement with no fly ash replacement. Compressive strength of M25 and M40 grade concretes with 10% fly ash replacement were 2.4% and 3.5% higher than that of OPC cement concretes respectively. After 10%, with increasing percentages of fly ash, compressive strength decreased and 50% fly ash replacement provided the lowest strength at all curing ages.

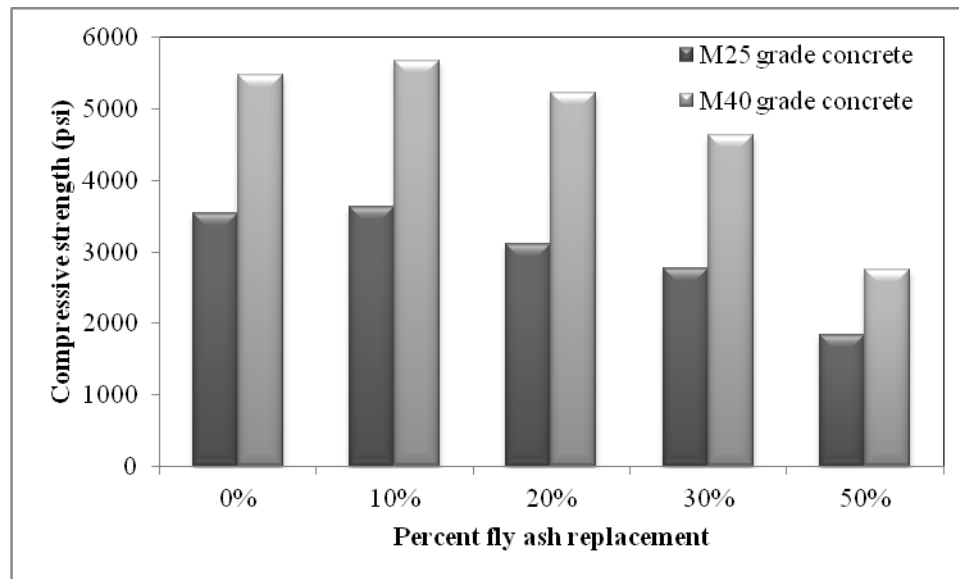


Fig. 4: Variations of 28 day compressive strength of M25 and M40 grade concretes for different percent replacement of fly ash

Fig. 4 presents a bar chart showing variations of 28 day compressive strength of both the concrete grades for different percent replacements of fly ash. Since 28 day strength is taken as concrete compressive strength so this strength was used for drawing the bar chart. This bar chart represents the comparison of the percent replacement of fly ash better.

## CONCLUSIONS

Bangladesh has a vast resource of fly ash produced in Boropukuria thermal power plant and it has potential to be extended in the future. The proper use of local fly ash can solve the major problems of its disposal and reduce the consumption of energy and resources. This experimental exercise has helped to study the effect of replacing cement with fly ash at different percentages on concrete compressive strength, which is generally used in Bangladesh as a property for concrete quality control. The conclusion that can be drawn from this research is that, 10% fly ash replacement provided the maximum compressive strength of concrete for both grades. This strength is even higher than that of concrete made with Type I Ordinary Portland Cement. Since fly ash is less expensive than cement and its production generates less Carbon dioxide and also since it provides greater strength, 10% fly ash replacement could be considered as optimum.

## ACKNOWLEDGMENTS

The authors wish to gratefully acknowledge the support of the concrete laboratory of Sonargaon University (SU) for technical support and students of section M-8 for their cooperation.

## REFERENCES

- ASTM C39 / C39M - 16a Standard Test Method for Compressive Strength of Cylindrical Concrete Specimens. ASTM International, West Conshohocken, PA, 2016, [www.astm.org](http://www.astm.org).
- ASTM C150 / C150M-16e1, Standard Specification for Portland Cement, ASTM International, West Conshohocken, PA, 2016, [www.astm.org](http://www.astm.org)
- ASTM C618-03, Standard Specification for Coal Fly Ash and Raw or Calcined Natural Pozzolan for Use in Concrete, ASTM International, West Conshohocken, PA, 2003, [www.astm.org](http://www.astm.org)
- Berryman, C., Zhu, J., Jensen, W., & Tadros, M. (2005). High-percentage replacement of cement with fly ash for reinforced concrete pipe. *Cement and Concrete Research*, 35(6), 1088–1091. <http://doi.org/10.1016/j.cemconres.2004.06.040>
- Farooque, K., Yeasmin, Z., Alam, S., Alam, A., & Zaman, M. 2010. Pozzolanic Activity of Fly Ash. *Bangladesh Journal of Scientific and Industrial Research*, 45(4), 303–308.
- Fly Ash & The Environment | Headwaters Resources. (n.d.).
- Khan, M. A. A., Saha, M. S., Sultana, S., Ahmed, A. N., & Das, R. C. 2013. Coal Fly Ash of

- Barapukuria Thermal Power Plant, Bangladesh: Physico Chemical Properties Assessment and Utilization. *International Journal of Scientific & Engineering Research*, 4(11), 1456–1460.
- Kumar, S. A., Kumar, S. A., & Arora, T. R. 2014. Effect of Fly Ash as A Cement Replacement on The Strength of Concrete. *International Journal of Engineering and Advanced Technology (IJEAT)*, 4(2), 185–187.
- Michael Thomas, U. of N. B. 2007. Optimizing the Use of Fly Ash in Concrete. *Concrete Thinking for a Sustainable World, Portland Cement Association*.
- Muhit, I. B., Ahmed, S. S., Amin, M. M., & Raihan, M. T. 2013. Effects of Silica Fume and Fly Ash as Partial Replacement of Cement on Water Permeability and Strength of High Performance Concrete. In *Int. Conf. on Advances in Civil Engineering, AETACE* (pp. 1–8).
- Pitroda, J., Zala, L. B., & Umrigar, F. S. 2012. Experimental Investigations on Partial Replacement of Cement with Fly Ash in Design Mix Concrete. *International Journal of Advanced Engineering Technology E*, 3(4), 126–129.
- Robiul Islam, Monjurul Hasan, Rezaul Karim, M. F. M. Z. 2015. Properties of Fly Ash Brick Prepared in Local Environment of Bangladesh. *International Journal of Civil, Environmental, Structural, Construction and Architectural Engineering*, 9(12), 1496–1500.
- Sultana, M. S., Hossain, M. I., Rahman, A., & Khan, M. H. 2014. Influence of Rice Husk Ash and Fly Ash on Properties of Red Clay. *Journal of Scientific Research*, 6(63), 421–430. <http://doi.org/10.3329/jsr.v6i3.15343>
- Tamim, M. M., Dhar, A., & Hossain, M. S. 2013. Fly ash in Bangladesh- An Overview. *International Journal of Scientific & Engineering Research*, 4(5), 809–812.



## **OPTIMUM FIBRE CONTENT FOR TENSILE STRENGTH OF FIBRE REINFORCED MICRO-CONCRETE**

B. H. Javed\* & A. A. Sarfin

*Department of Civil Engineering, Bangladesh University of Engineering and Technology, Dhaka, Bangladesh*

*\*Corresponding Author: javed.buet@gmail.com*

### **ABSTRACT**

Fibre reinforced concrete is one of the most promising construction techniques and repairing materials of modern times. Polyester fibre is, by far, the front runner in the field of reinforcing fibres from long ago. On the other hand, micro-concrete technology is a new trend where the size of coarse aggregate is reduced significantly without compromising the strength of concrete. Here along with strength, workability is ensured using chemical admixture (Super plasticizer). In micro-concrete, polyester fibre is mainly used for increasing its tensile strength. So in this research, it was aimed to determine the optimum fibre content at which micro-concrete will hold sufficient tensile strength without deteriorating other major properties. So in this research fibre content was varied from 0.1 to 0.5% by volume and it was found for the addition of polyester fibre compressive strength increases up to 43 percent and splitting tensile strengths increase up to 30 percent with respect to control.

Keywords: Micro-concrete; polyester fibre; optimum content

### **INTRODUCTION**

Micro-concrete technology is a new trend where the size of coarse aggregate is reduced significantly without compromising the strength of concrete. Now a days it is mainly used for retrofitting purposes for its various inherent characteristics (pattanaik, 2009; Lakshmanan et al., 2006). As the size of coarse aggregate is kept smaller than usual size, it can be pumped easily to the desired height. Not only that, it requires less compaction than conventional concrete and it is also easy to handle. The main advantage of using this concrete is its capability of using in congested area where the spacing of reinforcement is kept small for different purposes (Habert & Roussel, 2009). On the other hand for retrofitting purpose, tensile strength of concrete is also considered as an important property of concrete for different application. For example, for retrofitting measures of beam-column joints where sufficient shear reinforcement has not been provided, the tensile strength of concrete may help to make it ductile. Increasing tensile strength of concrete using fibres is a popular technique from long ago. In this research the tensile strength of micro-concrete will be tested using different content of Polyester fibre. Then the optimum dose of fibre will be determined at which concrete would hold sufficient tensile strength without deteriorating other properties like compressive strength and slump.

### **METHODOLOGY**

At first micro-concrete mixture with proportion Cement: CA: FA=1:1:1.5) was prepared for casting at least thirty 4 inch x 8 inch concrete cylinder. In this research 5mm downgraded crushed stone was used as coarse aggregate. Superplasticizer (Master Gelenium) was added 6ml/kg of cement to get desired workability. Then the mixture was equally divided into six groups and then Polyester fibre was added at different proportion on volume basis of total concrete (0.1%, 0.2%, 0.3%, 0.4%, 0.5%) to different groups (Hossain, 2015). One group was kept without fibre and it was used as control mix for the comparison with other groups.



Fig. 1: Recron-3S polymer modified fibre.

Table 1: Properties of Recron-3S fibres.

Properties	Recron 3S
Type	Polyester
Cross section	Modified triangular
Form	Monofilament (Micro)
Specefic gravity	1.36
Tensile strength (MPa)	578
Modulous of elasticity (MPa)	17240
Length (mm)	12 $\pm$ 1, 18 $\pm$ 1
Equivalent diameter (mm)	0.0375
Aspect ratio	320 and 480

Before casting in the mould, concrete will be tested from each group for their slump according to ASTM C143 and the change of slump with different content of Polyester fibre will be measured. After 24 hours the moulds will be removed and the cylinders will be kept in water tub for 28 days curing. After 28 days curing from each group three cylinders will be tested for their compressive strength according to ASTM C39/C39M, three cylinders will be tested for tensile strength ASTM C496/496M. Thus “The percentage of optimum fibre content” will be determined for steel and Synthetic fibre at which micro-concrete would hold sufficient tensile strength without deteriorating other properties.

Table 2: Properties of Coarse aggregate and Fine Aggregate

Basic Property	Coarse aggregate	Shylet sand
Unit Weight	1584.9 kg/m <sup>3</sup>	1554.30 kg/m <sup>3</sup>
Specific Gravity	2.804	2.709
Absorption capacity	2.95%	2.67%
Fineness modulous	4.95	2.92

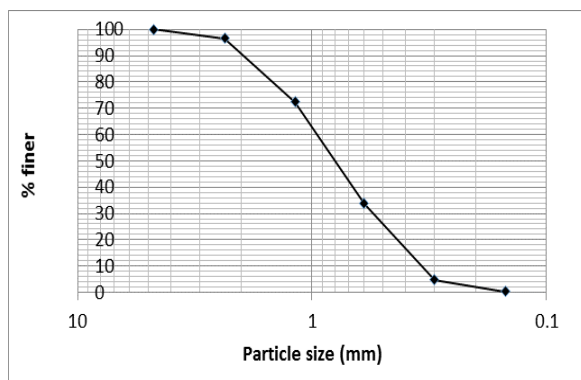


Fig. 2: Gradation curve of fine aggregate (Sylhet sand)

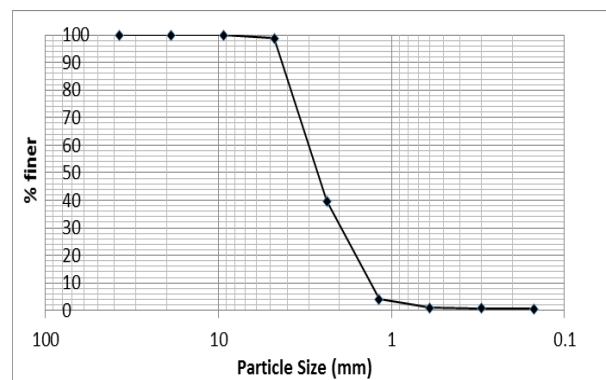


Fig. 3: Gradation curve of coarse aggregate (crushed stone)

## RESULTS AND DISCUSSIONS

The graphical representation of the results of concrete cylinder found from concrete testing laboratory is given below. In the figure PFRMC means Polyester Fibre Reinforced Micro concrete.

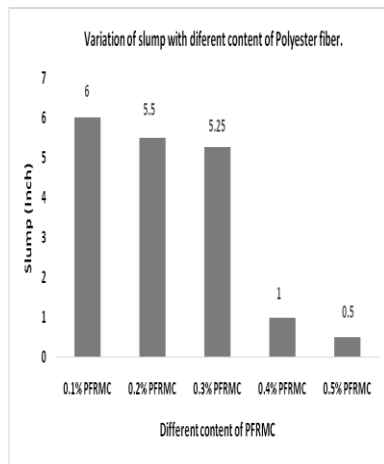


Fig. 4: Slump Vs. fibre content

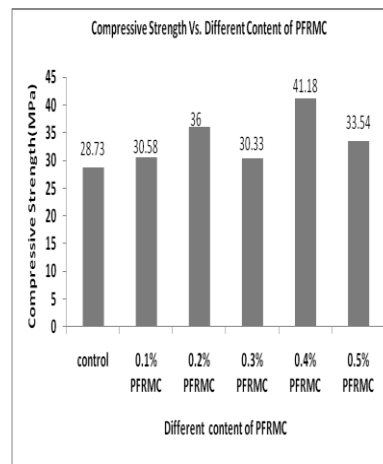


Fig. 5: Compressive strength Vs. Fibre content

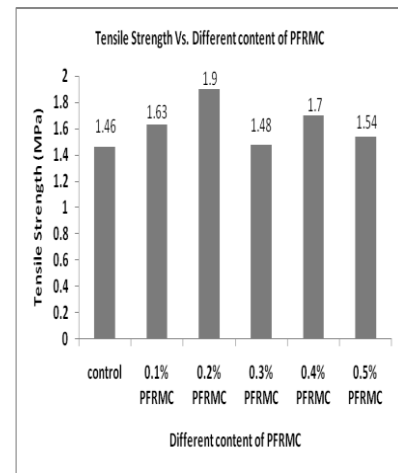


Fig. 6: Tensile strength Vs. fibre content

It was found with the increases of Polyester fibre content the value of slump decreases and after 0.3% Polyester fibre content the amount of concrete slump reduces significantly. Though this property can be improved by using admixture (Superplasticizer) but it can be said fibre content has influence on slump of concrete. On the other hand fibre content and attributes do not have direct influence on compressive strength properties of fibre reinforced concrete but the extent of this effect depend largely on preferential orientation of the fibres which is impracticable to control in such case. In this case for Polyester fibre it was found for different content of fibre the increase of compressive strength don't follow a regular pattern. The maximum increase of compressive strength was 43 percent with respect to control and was found at 0.4 percent Polyester fibre content. On the other hand it was found for different content of polyester fibre the maximum increase of tensile strength is 30.14 percent for 0.2 percent polyester fibre content and at this content the increase of compressive strength was 25.3 percent.

## CONCLUSIONS

- From the graphical presentation, it is easily noticed that 0.2% polyester fibre content is the optimum content at which micro concrete will hold sufficient tensile strength along with compressive strength and slump.
- Though at 0.4% fibre content concrete shows more compressive strength but considering slump and tensile strength it was not defined as optimum fibre content.

## ACKNOWLEDGMENTS

All staffs and members of Concrete laboratory and Strength of materials laboratory of Bangladesh University of Engineering and Technology.

## REFERENCES

- ASTM C39/ C39M. 2003. Standard Test Method for compressive Strength of Cylindrical Concrete Specimens. *ASTM International, West Conshohocken, PA, USA.*
- ASTM C469/ C469M. 2002. Standard Test Method for Static Modulus of Elasticity and Poisson's Ratio of Concrete in Compression. . *ASTM International, West Conshohocken, PA, USA .*
- Pattanaik, SC. 2009. Structural Strengthening of Damaged RCC Structures with Polymer Modified Concrete. *In Proceedings of Workshop on Rehabilitation and Retrofitting of Structures, IIT Mumbai.*
- Lakshmanan, N; Muthumani, K and Krishnamoorthy, TS. 2006. Retrofitting of Reinforced Concrete Structures Using Wrapping Techniq
- Habert, G and Roussel, N. 2009. Study of two concrete mix-design strategies to reach carbon mitigation objectives. *Cement and Concrete Composites, 31(6): 397-402.*
- Hossain, T. 2015. *Experimental Investigation on Performance of Interior Beam Column Joints Retrofitted with Ferrocement and Polyester Fibre Reinforced Concrete.* Department of Civil Engineering Bangladesh University of Engineering and Technology.

## **SEISMIC PERFORMANCE IMPROVEMENT OF FLAT PLATE STRUCTURES BY PROVIDING SHEAR WALL**

M. A. R. Bhuiyan\*, I. Ahmed & S. M. M. Hasan

*Department of Civil Engineering, Bangladesh University of Engineering and Technology, Dhaka,  
Bangladesh,*

*\*Corresponding Author: ashiqbuetcivil@gamil.com*

### **ABSTRACT**

The slab system that is supported by columns without any column line beams is known as flat plate. Board strips of the slabs centred on the column lines in each direction serve the same function as the beams. Flat slab systems are also susceptible to significant reduction in stiffness resulting from cracking that occurs from construction loads, service loads, gravity loads and lateral loads. The brittle punching failure due to transfer of shear forces and unbalanced moments between slabs and columns in flat plate structures causes serious problems. Flat plate construction is mainly used as the vertical load carrying system in structures where shear wall is responsible for lateral capacity of structures. During earthquake shaking, when the crack forms, the sections are transformed from elastic to plastic state. So, Performance Based Analysis or Pushover Analysis was done here to find actual behaviour of the structure in earthquake. As a result of using of shear wall the capacity spectrum curve meets with demand spectrum curve at less deformation representing the performance evaluation of shear wall. Shear wall increases the lateral (earthquake) capacity of flat plate structures tremendously.

Keywords: Pushover analysis; capacity spectrum curve; demand spectrum curve

### **INTRODUCTION**

Now a days, flat plate structure is widely used due to the many advantages it possesses over conventional moment-resisting frames. It provides low building heights, unobstructed space, architectural flexibility, easier framework and shorter construction time. However it suffers low transverse stiffness due to lack of deep beams. This may lead to potential damage even when subjected to earthquake with moderate intensity. Bangladesh is situated adjacent to the plate margins of India and Eurasia where devastating earthquakes occurred in the past. Widespread damage of structures and loss of thousands of life in the country will happen due to earthquakes. The primary focus of the present study is structural damage estimation of flat plate building with shear wall and without shear wall designed as per BNBC (2006). The objective of this study is to find out the efficiency of shear wall as a solution for flat plate structures against earthquake loading and the effective way to model shear wall in ETABS 9.6.

### **METHODOLOGY**

Some medium rise i.e. five storied, ten storied and fifteen storied flat plate structures are modeled and analyzed with the help of finite element software ETABS 9.6. The building is 3X3 bays residential building, located in Dhaka. Length of each bay is 20 feet. There are sixteen columns in the flat plate structure. Typical storey height is 10 feet. The height from ground level to the bottom of foundation is 6 feet. Earthquake load are calculated automatically by the program. Wind load is calculated according to BNBC. Standard load combinations are taken according to BNBC (2006). At first flat plate buildings are were analyzed without shear wall , then were analyzed with shear wall as wall element and at last shear wall was modeled as column whose length and width were equal to shear wall . The flat plate buildings were also analyzed as beam column frame where beam depth was taken as equal to slab depth and beam width was taken as the slab width for which uniform rotation across its width gives the same column displacement as the original slab. Capacity spectrum method (ATC 40) is employed for finding performance situation of the flat plate structures. Pushover analysis is used to evaluate the nonlinear behavior of the structure. To define hinge in shear wall false storey has been created of three feet height.

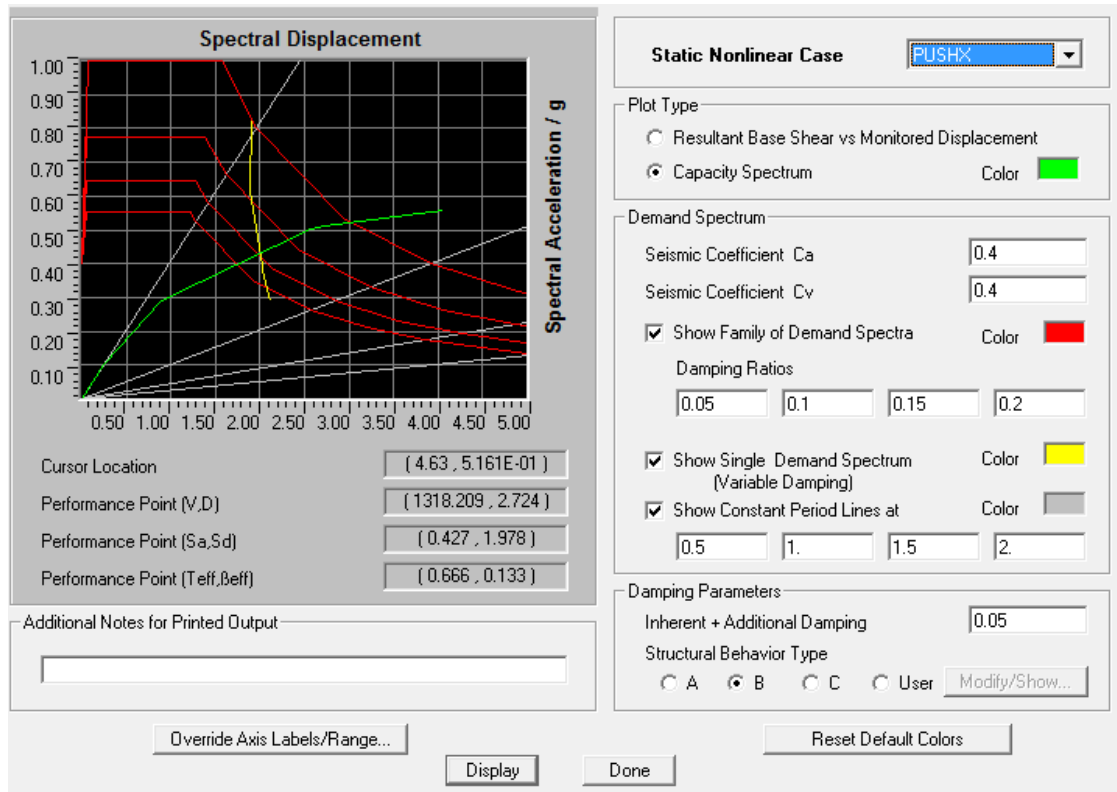


Fig. 1: Spectral acceleration vs. spectral displacement for five storied flat plate structure with shear wall as wall element

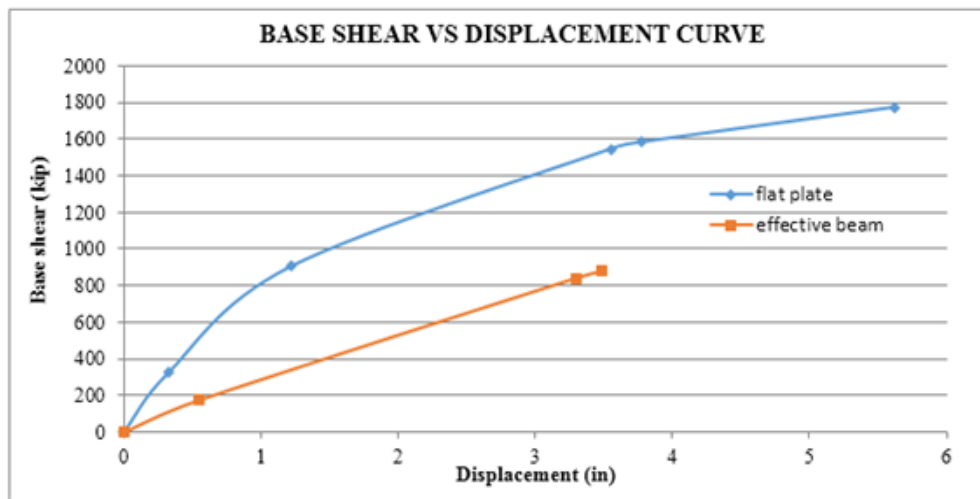


Fig. 2: Comparison of capacities between flat plate and beam column frame for five storied structure with shear wall modelled as wall element

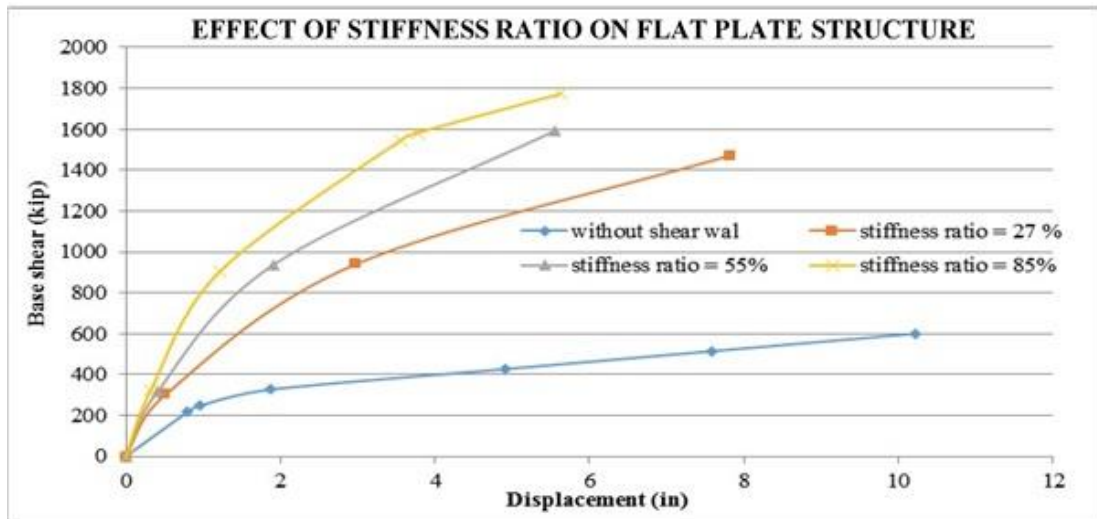


Fig. 3: Increasing trend of capacity for five storied flat plate structure with respect to stiffness ratio by shear wall modeled as wall element

Table 1: Design details of structural members

Member	Size (Inch)	
	Designed as purely flat plate	Designed as beam-column frame
Slab	5	Absent
Beam	24 X 18 (perimeter beam)	38 X 5 (exterior beam ) and 67 X 5 (interior beam)
Column	25 x25	25 x25
Grade beams	18 x 18	18 x 18

$$b_{eff} = K_{eff} * l \quad (1)$$

$$q_z = C_c C_1 C_z V_b^2 \quad (2)$$

$$p_z = G_z C_P q_z \quad (3)$$

Equation [1] is the formula for the calculation of effective beam width. Effective beam width ( $b_{eff}$ ) is a fraction of span length ( $l$ ) where span length and beam width must be in the same direction.  $K_{eff}$  is the effective beam width coefficient. Equation [2] and Equation [3] have been used for wind load calculation. In these equation  $q_z$ ,  $C_c$ ,  $C_1$ ,  $C_z$ ,  $V_b$ ,  $p_z$ ,  $G_z$  and  $C_P$  are sustained wind pressure at height  $z$  in  $KN/m^2$ , structure importance coefficient, velocity to pressure conversion coefficient, combined height and exposure coefficient, basic wind speed in  $km/hr$ , design wind pressure at height  $z$  in  $KN/m^2$ , gust coefficient and pressure coefficient for structures respectively.

## RESULTS AND DISCUSSIONS

Fig. 1 shows that the up to displacement of 1.2 inch the structures behaves elastically. At performance point spectral displacement is 1.978 inch and spectral acceleration is 0.427g. At performance point effective damping is 13.3 % and the effective time period of the structure is 0.666 sec. So, performance point falls in inelastic range. From Fig. 2 it is obvious that flat plate structures should not be modelled as equivalent beam-column frame (effective beam concept) rather it should be modelled as flat plate structures because in case of beam-column frame it shows less capacity as well as less ductility compared to flat plate structures. When shear wall is modelled as column it gives less capacity than that of wall element. So, shear wall should be modelled as wall element. As a result of using of shear wall the capacity spectrum meets with demand spectrum curve with less deformation representing the performance evaluation of shear wall. Though shear wall increases the lateral load (earthquake load) capacity, it decreases the ductility of the flat plate structures. With the increasing height of flat plate buildings capacity of the structure against earthquake load reduces while ductility increases. For all other cases either the structure is structure ten storied or fifteen storied the curve shape remains same; the difference is that the value varies. Also the results in X-direction is only shown in the figure. As the

structure is symmetric it will give same results in Y-direction. So, the interpretation on those cases have not been shown here.

### **CONCLUSIONS**

It is economical to use shear wall to the amount corresponding to 25% - 30% stiffness ratio (ratio of the stiffness of shear wall to the stiffness of all column including shear wall).

### **ACKNOWLEDGMENTS**

Dr. Ishtiaque Ahmed, Professor, Department of Civil Engineering, Bangladesh University of Engineering and Technology (BUET), Dhaka, Bangladesh.

### **Book**

BNBC. 2006. Bangladesh National Building Code, Housing and Building Research Institute, Mirpur, Dhaka, Bangladesh.

Sadi, S. 2009. *Estimation of Elastic Deflection of Flat Plate*. M. Sc. Engg. Thesis. Department of Civil Engineering, Bangladesh University of Engineering & Technology, Dhaka, Bangladesh.

## **ANALYSIS OF SLAB THICKNESS REQUIREMENT OF RCC SLAB IN ORDER TO PREVENT UNDESIRABLE FLOOR VIBRATION**

M. M. Orvin\*, K.M. Amanat & A. A. Kawsar

*Department of Civil Engineering, Bangladesh University of Engineering and Technology, Dhaka, Bangladesh*

*\*Corresponding Author: mmceorvin@gmail.com*

### **ABSTRACT**

Now-a-days, modern structures are becoming slender, irregular shaped and long spanned which are susceptible to floor vibration phenomena. The purpose of this study is to determine the minimum slab thickness of a RCC slab to prevent undesirable vibration that will not cause discomfort to occupants and compare the obtained result with (Rakib, 2013) who investigated on this previously. Though American Concrete Institute (ACI) provided code for minimum slab thickness requirement from static deflection criteria, it might not be sufficient for dynamic serviceability like vibration. An investigation based on 3D finite element modeling of a reinforced RCC floor subjected to gravity load including partition wall load is carried out to study the natural floor vibration. The ANSYS model verification is done and is validated by ETABS modeling. The variation of the floor vibration is studied for several parameters such as different slab thickness, span length and floor panel aspect ratio.

Keywords: Floor vibration; RCC floor; slab thickness; ANSYS modeling of RCC Floors

### **INTRODUCTION**

Modern construction techniques make use of lightweight materials to create long-span floors. These floors sometimes result in annoying levels of vibration under ordinary loading situations. In extreme cases this vibration can render the floor unusable by the human occupants of the building if it creates excessive discomfort to them. If the structures have the frequency below 10 Hz, then it creates resonance with human body. This resonance may cause discomfort to the people (Murray et al. 1993). The aim of the current study is to enlarge knowledge regarding the vibration response of a RCC building floor with change of different parameters. The variation of floor vibration is analyzed with change of slab thickness, floor panel aspect ratio and span length. A 3D finite element model of floor having three spans and bay will be developed. Verification of the built model is done by ETABS. Modal analysis is to be executed to determine mode shape and frequency. Analysis of the variation of natural floor frequency with variation of slab thickness, span and floor panel aspect ratio as well as analysis of the slab thickness with variation of span length and floor panel aspect ratio will be rendered. Finally the analyzed data is compared with M. Rakib (2013).

### **METHODOLOGY**

American Institute of Steel Constructions (AISC) Steel Design Guide, Series 11: Floor Vibrations Due to Human Activity (Murray et al. 1997) states that the floor system is satisfactory if the peak acceleration, due to walking excitation as a fraction of the acceleration of gravity,  $g$ , does not exceed the acceleration limit. DG11 states that from experience and records, if the natural frequency of a floor is greater than 9-10 Hz, significant resonance with walking harmonics does not occur. Bachman and Ammann (1987) recommend that concrete slab-steel framed floor systems have a minimum first natural frequency of 9 Hz. Wyatt (1989), however, has recently proposed design criteria for walking vibration for fundamental natural frequencies not less than 7 Hz. Ohlsson (1988) has recommends that floors not to be designed with fundamental frequencies below 8 Hz. Vibration design of floors guideline incorporated in RFCS report suggested that frequency is related to modal mass. This guideline sums up that for a certain modal mass of floor, safe zone is reached beyond a frequency in the range of 3-10 Hz.



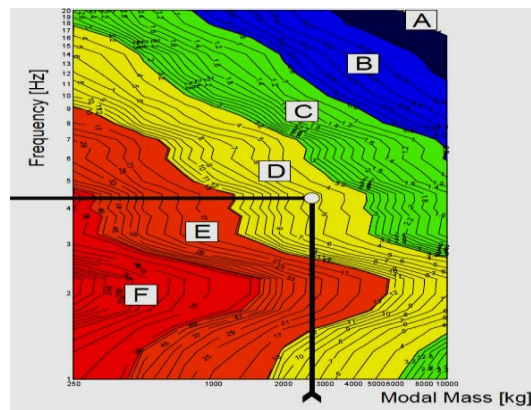


Fig. 1: Typical Frequency v/s Modal mass curve

Floors that have a natural frequency at or near 4-8 Hz may exhibit an excessive response because the input force component of the harmonic may coincide with the resonant frequency of the floor. The following Fig. 2 explains that human walking frequency mostly varies from 1.6 Hz to 8.8 Hz (Setareh, 2010). So building floor modes with natural frequencies in excess of 10 Hz is not usually excited by people walking. If the natural frequency of floor is more than 10 Hz, resonance will not occur for human excitation and discomfort to occupant is prevented.

The natural frequency of a floor can be calculated by the following formula that describes that with increase in stiffness the natural frequency of the system increases and

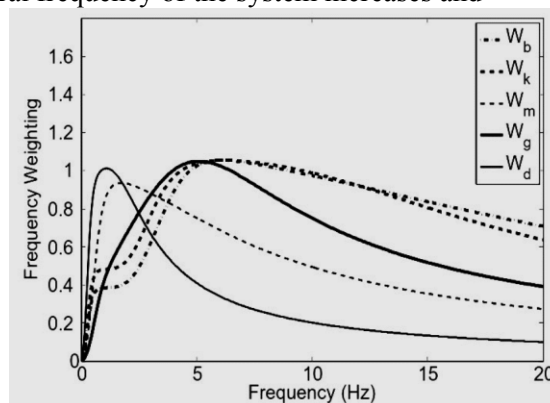


Fig. 2: Variation of the frequency weighting versus frequency (Setareh, 2010)

frequency decreases with the increase in mass of the structure. The formula follows:

$$\text{Natural Frequency, } f = \frac{1}{2\pi} \sqrt{\frac{\text{Stiffness}}{\text{Mass}}} \dots (1)$$

Finite element methods can be used to accurately predict the dynamic properties of reinforced concrete structure. ANSYS 11.0 is used in this study for its relative ease of use, detailed documentation, flexibility and vastness of its capabilities. ANSYS 11.0 is one of the most powerful and versatile packages available for finite element structural analysis. The verification of the model built in ANSYS 11.0 is done by building the model in ETABS 9.7. The x-z plane is acting as the horizontal plane in global co-ordinate system. To find the dynamic behavior of multistoried RC framed building, basic un-factored load case is considered as DL (self-weight, partition wall, floor finish). In calculation of column size determination, factored dead and live load is used.

Only self-weight of beams, columns and slabs and nonstructural load (Partition wall, floor finish) are considered as dead load case of the structure. All vertical loads except self-weight of beams, columns and slab are applied as mass on the structure. Total vertical load applied on the structure is  $25 \times 4.786 \times 10^{-5}$  N/mm<sup>2</sup> (25 psf) and  $50 \times 4.786 \times 10^{-5}$  N/mm<sup>2</sup> (50 psf) for floor finish and partition wall load respectively. Total live load applied on the structure is  $100 \times 4.786 \times 10^{-5}$  N/mm<sup>2</sup> (100 psf). This live load will only be used in determining the beam, column size. In modal analysis live load is not used.

In this study author made reinforced floor model with ANSYS 11. The model was analyzed with modal analysis to get the dynamic behavior such as frequency of that floor for different span length and floor panel aspect ratio (beta). The floor should be modeled as a three dimensional space frame with joints and nodes selected to realistically model the stiffness and inertia effects of the structure. Each joints or nodes should have six degrees of freedom, three translational and three rotational.

For this study, a building frame of one floor with three span and three bay (bay is the longer floor panel) has been analyzed for 3m, 4m, 5m, 6m, 7m, 8m, 9m,10m span length. Floor panel aspect ratios are considered as 1, 1.2, 1.4, 1.6, 1.8. The slab thickness is takes as 50 mm increment starting from 50 mm. The column size is calculated from the load imposed on the floor assuming that the floor is a typical floor of a 5 storied building. Beam size is taken as the function of slab thickness and span length. The plan, elevation and three dimensional view of model are shown in following Fig. 3:

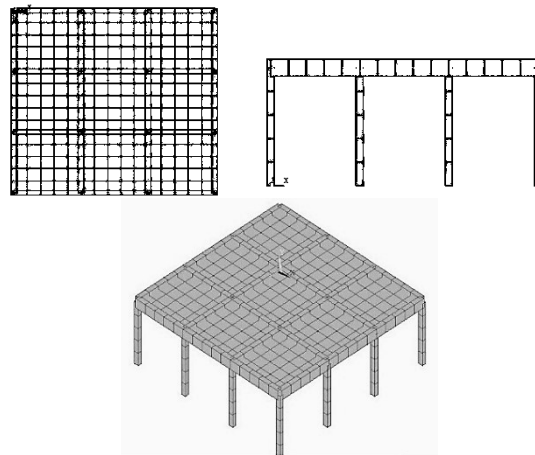


Fig. 3: Plan, 3D and Elevation of the Model

Modal analysis is used to calculate dynamic behavior of the floor (frequency). Every mode shape have a particular frequency. We have to be careful in determining the proper mode shape corresponding to the natural frequency of the floor. Initial shapes generally corresponds to sway shapes. The minimum natural frequency from mode shape must be defined carefully. Typical mode shapes are provided following in Fig. 4.

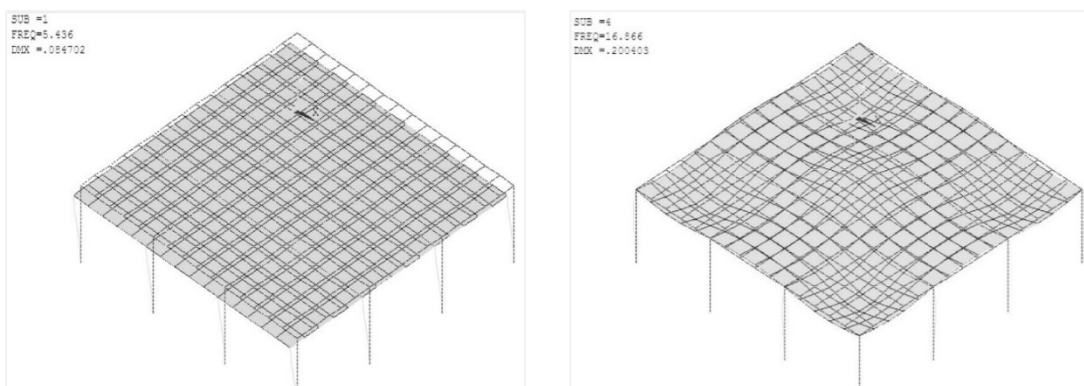


Fig 4: 1st Mode Shape, frequency 5.43 Hz and 4th Mode Shape frequency 16.87 Hz respectively

Validation of the ANSYS model is necessary in order to check whether the result found from ANSYS is accurate or not. A model is generated in software ETABS 9.7 and a particular mode shape frequency is checked whether it matches with that particular mode shape frequency of ANSYS model. From ANSYS, the natural frequency of the model floor (4<sup>th</sup> mode shape frequency) is 22.295 Hz. Three dimensional and elevation views are shown in Fig 3. From ETABS, the natural frequency of the model floor (4<sup>th</sup> mode shape frequency) is  $(1/0.0405)$  Hz = 23.25 Hz.

## RESULTS AND DISCUSSIONS

Analysis of determining minimum slab thickness for 10 Hz limit (Murray, 1997) for a building floor is modeled and parametric study with results will be discussed now. Parameters are taken based on practical values so that the actual building behavior under vibration will be same as the 3-D modeling frame. Only natural vibration of floor including 10 Hz criteria is studied. Comparison of ACI limit with 10 Hz criteria requirement including both present study and Rakib, (2013) is also discussed here. Typical curves are following:

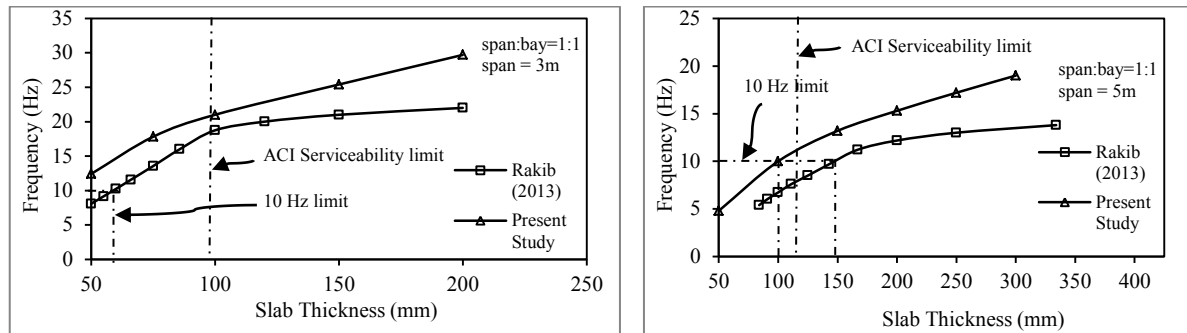


Fig. 5: Frequency v/s Slab thicknesses for floor panel aspect ratio 1.0 for 3m and 5m span

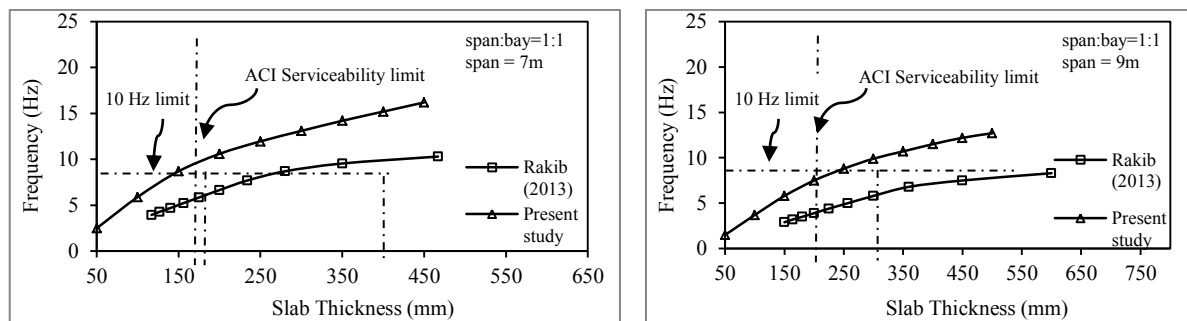


Fig. 6: Frequency v/s Slab thicknesses for floor panel aspect ratio 1.0 for 7m and 9m span

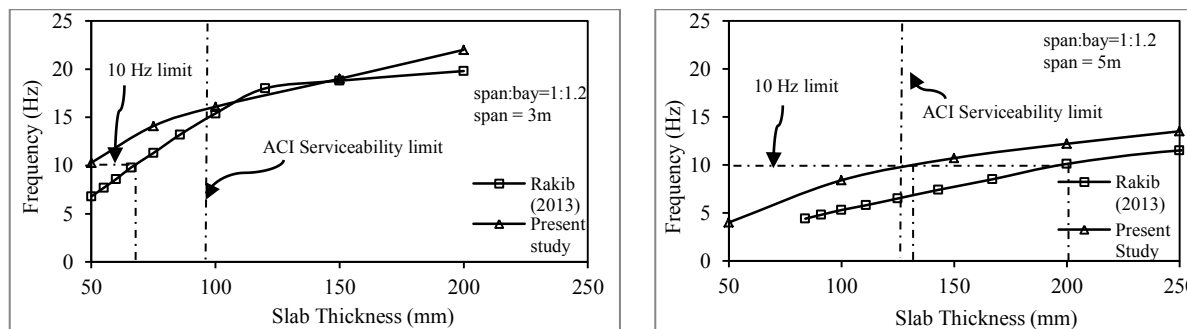


Fig. 7: Frequency v/s Slab thicknesses for floor panel aspect ratio 1.2 for 3m and 5m span

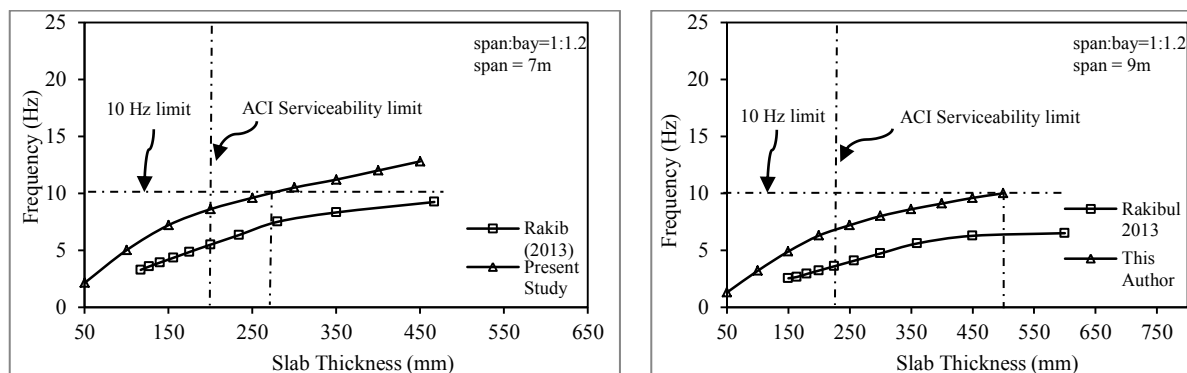


Fig. 8: Frequency v/s Slab thicknesses for floor panel aspect ratio 1.2 for 7m and 9m span

The natural frequency of floor is increasing with increase of slab thickness due to the fact that with increasing slab thickness, the beam and column size is also increased, due to self-weight of the slab. Hence increase the moment of inertia of structural elements and consequently increases the natural frequency of the floor. With increase of span length, the stiffness of the floor decreases, as a result the floor frequency is reduced. With increase of floor panel aspect ratio, the natural frequency of floor is decreasing. Increase of mass means decrease of natural frequency of the structure. But increased slab thickness increases the beam and column size that increases the moment of inertia and stiffness that increases the floor frequency.

For a particular curve, due to these two contradictory conditions, the initial part of the curves mentioned above in the figures are steeper when mass is small and when the mass is higher the curve becomes less steep. The frequency still increases due to increased stiffness. The typical shape of the curve obtained in this study is almost same as provided by Rakib (2013) but in comparison with Rakib (2013), it is seen that natural frequency is in the higher range found in this study than by Rakib (2013). In some curves provided by Rakib (2013), the frequency is very low resulting unrealistic slab thickness requirement.

Slab thickness fulfilling 10 Hz limit is plotted against various span length for various aspect ratio for both Present study and Rakib (2013) and compared with ACI Serviceability limit. Typical figures are shown in Fig. 9. Slab thickness fulfilling 10 Hz limit can also be plotted against various aspect ratio for various span for both 10 Hz limit and ACI limit. The slab thickness required for satisfying the 10 Hz limit, is increasing with the increase of span for a particular floor panel aspect ratio. Also, the larger the aspect ratio, the higher the slab thickness required for satisfying 10 Hz criteria. In comparison with Rakib (2013), it is seen that the 10 Hz limit curves provided by Rakib (2013) is higher than the curve provided by this author. It means that minimum slab thickness requirement is larger for Rakib's (2013) analysis and if the span length is large, the minimum slab thickness is sometimes found unrealistic.

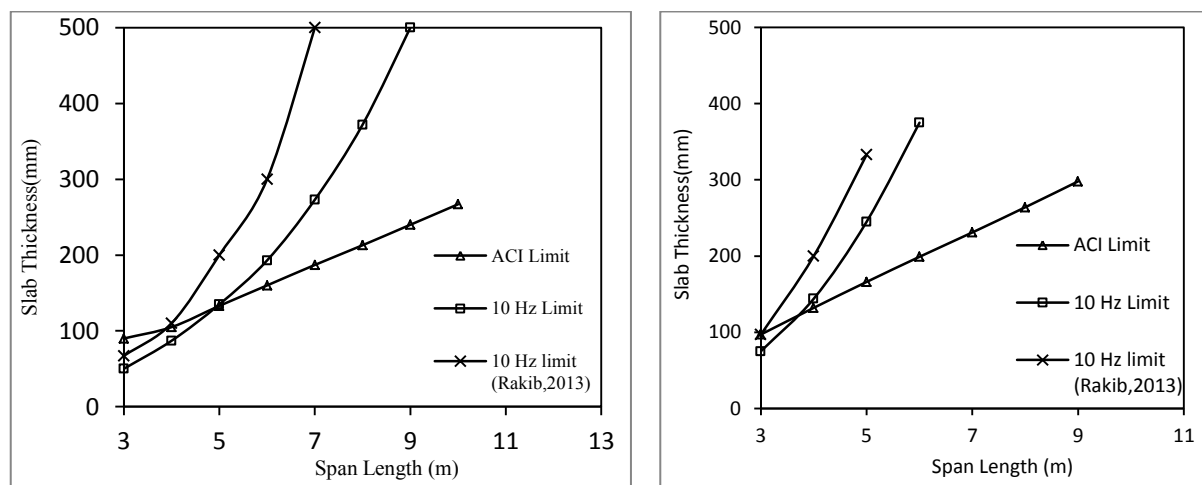


Fig. 9: Minimum Slab Thickness v/s Span length for aspect ratio of 1.2 and 1.6 respectively

## CONCLUSION

In the present study an investigation has been done to determine the required minimum slab thickness from dynamic serviceability. Minimum slab thickness determination and comparison with slab thickness requirement investigated by Rakib (2013) is done. Floor frequency is dependent to mass of floor as well as the stiffness of the floor system. Increasing mass decreases the frequency and increasing stiffness increases the floor frequency. Floor frequency decreases with increase of span length and floor panel aspect ratio. ACI serviceability limit may not be sufficient for preventing floor vibration while span and aspect ratio is larger.

The minimum slab thickness requirement provided by Rakib (2013) is in the higher side in comparison with this present study. It may be due to the fact that this study only considers single floor for the vibration analysis. Only a single floor vibration is analyzed here and understanding the proper mode shape and corresponding frequency is easier. On the other hand Rakib (2013) considered 3 floors, building vibration characteristics may be merged with the floor vibration phenomena. Also the column axial stiffness may be included in the analysis of Rakib (2013).

The current study has some limitations. The results are not sufficient to apply for all type of situations as so many other factors have not been considered. Advancement of current study can be done combining some other variables. The model was considered to be linearly elastic. To be more realistic with the results a finite element analysis with nonlinearly material properties can be performed. The asymmetric floor frames can be studied under the variables considered for symmetric frames. Different number of span and bay other than three can be studied. Study can be carried out for without partition wall load. Effect of result due to floor height change can be another part of study. Vibration effect due to other sources (machinery, traffic) can be studied. Only gravity load on floor is considered in the study.

### **ACKNOWLEDGMENTS**

The author wishes to express his deepest gratitude to Dr. Khan Mahmud Amanat, Professor, Department of Civil Engineering, BUET, Dhaka, for his continuous supervision all through the study. His systematic guidance, invaluable suggestions and affectionate encouragement at every stage of this study have helped the author greatly. A very special debt of deep gratitude is offered to the author's parents and his younger sister for their continuous encouragement and cooperation during this study.

### **REFERENCES**

- Allen, D.E. and Murray, T.M. 1993. Design Criteria For Vibration Due To Walking. *AISC Engineering J.*, 40(4), 117-129.
- Bachmann H. and Ammann W. 1987. Vibrations in Structures Induced by Man and Machine. *Structural Engineering Document 3e*, Chapter 1, 2, 3.
- European Commission – Technical Steel Research: Generalization of criteria for floor vibrations for industrial, office, residential and public building and gymnastic halls, *RFCS Report EUR 21972 EN, ISBN 92-79-01705-5, 2006, <http://europa.eu.int>*
- Murray T.M., Allen D.E. and Ungar E.E. 1997. *Design Guide No. 11*. "Floor Vibrations Due to Human Activity", American Institute of Steel Construction (AISC), Chicago, IL, Chapter 2, 4.
- Murray, T.M.; Allen, D.E. and Uger, E.E. 2003. Floor Vibration Due To Human Activities. *Steel Design Guide Series, AISC, Chicago*.
- Nilson A.H., Darwin D., Dolan C.W., "Design of Concrete Structures", 13th edition, Chapter 13, Page 437.
- Ohlsson S.V. (1988), "Springiness and Human-Induced Floor Vibrations- A Design Guide", D12:1988, Swedish Council for Building research, Sweden.
- Rakib, M. 2013. Minimum slab thickness of RC slab to prevent undesirable floor vibration. *BSc Thesis*, Bangladesh University of Engineering And Technology (BUET), Dhaka, Bangladesh.
- Setareh M. (2010), Vibration Serviceability Of A Building Floor Structure I: Dynamic Testing And Computer Modeling. *Journal Of Performance Of Construction Facilities*, ASCE.
- Wyatt T.A. 1989. Design Guide on the vibration of floors. *ISBM: 1 870004 34 5, The Steel Construction Institute*, Berkshire, England.

## **PROSPECT OF CONSTRUCTING REINFORCED BRICK MASONRY (RBM) STRUCTURES IN BANGLADESH**

M. S. Islam<sup>1\*</sup>, M. A. A. Siddique<sup>2</sup> & M. Begum<sup>2</sup>

<sup>1</sup>*Department of Civil Engineering, World University of Bangladesh, Dhaka, Bangladesh*

<sup>2</sup>*Department of Civil Engineering, Bangladesh University of Engineering and Technology, Dhaka, Bangladesh*

*\*Corresponding Author: shariful2@civil.wub.edu.bd*

### **ABSTRACT**

This paper presents a theoretical discussion on the subject of reinforced brick masonry (RBM) structures. It is intended as an overview of the types of available RBM and how they work. It discusses commonly applied terminology and models of mechanical behaviour that form a basis for understanding material performance without presenting mathematical details. Structure made with reinforced cement concrete (RCC) are not cheap and construction period of time is long. Moreover, they need extra shuttering cost. In addition, unreinforced brick masonry (URM) is weak in flexural and shearing resistance and hence they are very much vulnerable during an earthquake. They suffer severe damage under earthquake effects. On the other hand, RBM consist of both reinforcements and masonry. The two materials (masonry and reinforcement) complement each other, resulting in an excellent structural material. By reinforcing the masonry with steel reinforcements, the resistance to seismic loads and energy dissipation capacity can be improved significantly. The reinforcement provides additional tensile strength which can overcome the limitations in the use of URM. RBM shows the prospect of constructing low-to-mid rise masonry structures of residential buildings, hospitals and schools in the rural area of Bangladesh at a low cost and low construction period of time with adequate margin of safety.

Keywords: Bricks; reinforcement; earthquake; tensile; compressive strength; shearing resistance

### **INTRODUCTION**

Brick masonry is one of the oldest forms of building construction, and reinforcement has been used to strengthen masonry since 1813. Reinforced brick masonry (RBM) is a construction system where steel reinforcement in the form of reinforcing bars or mesh is embedded in the mortar or placed in the holes and filled with concrete or grout. This masonry has greatly increased resistance to forces that produce tensile and shear stresses. The reinforcement provides additional tensile strength which can overcome the limitations in the use of unreinforced masonry (URM). This results an excellent structural material by complementing two materials such as masonry and reinforcement. By reinforcing the masonry with steel reinforcement, the resistance to seismic loads and energy dissipation capacity can be improved significantly (PWD, India 1996). Reinforced brick masonry contributes huge amount of shearing resistance and gives lateral stability against earthquake. A number of experimental works were carried out on RBM beams to study the flexural and web reinforcement ratio on the ductility, ultimate flexural, shear strength and mode of failures. According to several research works, design of RBM can be performed using the ultimate strength design method similar to that used for reinforced concrete beams (Khalaf et al., 1983 and Taly N, 2001). Mohamad et al. (2005) carried out experimental tests on masonry prisms subjected to compression. The failure mechanism of masonry depends on the difference of elastic modulus between brick unit and mortar. Oliveira et al. (2000) carried out the tests on prisms under cyclic loading and the stress-strain behaviour of the brick prisms showed a bilinear pre-peak behavior. Gumaste et al. (2007) studied the properties of brick masonry using table moulded bricks and wire-cut bricks from India with various types of mortars. It is also found that strength of URM is notably lower in comparison to that of RBM. Reinforced cement concrete can overcome this situation but they are not cheap and requires longer construction period. RC construction needs shuttering cost. On the other hand, URM is weak in flexural and shearing resistance and very much vulnerable during

earthquake (Qazi et al., 2011). It is known that masonry structures have relatively low resistance to horizontal seismic forces and suffer severely during seismic forces (Priestley and Bridgeman, 1974). In earlier decades, masonry buildings mainly 4/5 storied were constructed as residential buildings, hospitals and schools. However, experience of past earthquakes has shown that a number of masonry structures are vulnerable to seismic actions and severe damage was observed (Dutta et al., 2013). Therefore, the main objective of this paper is to study the mechanical properties (compressive, tensile, flexure, shear, seismic performance, etc.) of RBM and discuss the feasibility of constructing RBM over URM in rural areas of Bangladesh.

## METHODOLOGY

Based on the literature available, a comprehensive investigation has been carried out to assess the effects of compressive and tensile strengths, modulus of elasticity, shear, flexure and seismic performance of RBM. Finally, all such results will be compared to URM. Finally, some discussions to the feasibility of constructing RBM in rural areas of Bangladesh will be provided.

### *Mechanical strength tested by various researchers*

Khan et al. (2012) conducted a research on compressive strength, diagonal tensile strength as well as modulus of elasticity, stress strain behavior of the unreinforced masonry prism having a size of length = 16 inch, height = 16", thickness = 9" for compressive strength according to ASTM C1314-11a. Diagonal tensile strength was calculated from diagonal compression tests on masonry prisms (27" x 27"x 9"), as shown in Fig 1. The cement to sand ratio was 1:6. Campione et al. (2016) tested both concentric and eccentric loading conditions as shown in Fig 2. In order to accomplish these tests, universal testing machine (UTM) was used. The loading area had a width equal to  $b = 0.5B$ , with  $B$  the side of the square transverse cross section. The eccentricity was equal to  $B/6$ .



(a)



(b)



(b)

Fig.1: Strength test of brick prisms, a) Compressive strength  
 b) Diagonal tension; Khan et al. (2012).

Fig 2: Compressive strength test a) Concentric  
 b) Eccentric; Campione et al. (2016)

Eccentric tests were carried out by loading the specimens on a reduced area with respect to the entire cross section, producing a disturbed region (D-region). Linear variable displacement transducers (LVDTs) were used to record the displacement of the prism. Table 1 shows the material properties of bricks and mortars that have been used by the researchers. Khan et al. (2012) obtained weak bond-between the bricks and mortar and, consequently, low diagonal tensile strength (7.3 psi) and compressive strength (438 psi). Freeda et al. (2013) found the compressive strength of unreinforced fly ash brick masonry was 34% more than the unreinforced clay brick masonry. The reinforced fly ash brick masonry was 20.7% more than the reinforced clay brick masonry. The introduction of wire mesh-in the clay brick masonry resulted in an increase of load carrying capacity by 25%. However, the main limitation of this study was the effects of moisture on the strength of brick masonry and the strength of eccentrically loaded brick work. Table 2 presents the summary of the results conducted by Campione et al. (2016), Freeda et al (2013), Khan et al. (2012), and Sakhthivel et al. (2016). The peak loads and compressive strengths of URM and RBM under concentric and eccentric loads are provided. It is found

from the results that rupture strain limit of URM is around 30 % lower than that of alternate steel grids (SG) of RBM and around 40% lower for every course of RBM as shown in Fig. 3.

Table 1: Mechanical properties of mortar and bricks

Sl no.	Description of the test	Value	Adopted from
1	Compressive strength of mortar, MPa	6.09	Khan et al. (2012)
2	Water absorption of bricks, %	23.0	Khan et al. (2012)
3	Elastic modulus of masonry, MPa	1230	Khan et al. (2012)
4	Specific weight of masonry material, Pcf	94	Khan et al. (2012)
5	Compressive strength of mortar, MPa	7.89	Campione et al. (2016)
6	Tensile strength of mortar, MPa	1.14	Campione et al. (2016)
7	Flexure strength of mortar, MPa	2.07	Campione et al. (2016)
8	Compressive strength of brick, MPa	7.83	Nayak and Dutta (2016)

Table 2: Results of compressive strength adopted from various researchers

Series	e = 0 (Concentric)		e = b/6 (Eccentric)	Adopted from
	Peak Load (KN)	Strength (MPa)	Peak Load (KN)	
UM	759	12.60	213	Campione et al. (2016)
SG every course	1125	17.39	281	
SG alternate course	942	15.08	253	
URM	-	1.70	-	Freeda et al (2013)
RBM	-	2.20	-	
URM	-	3.00	-	Khan et al. (2012)
RBM	-	4.20	-	
URM	8.56	-	-	Sakthivel et al. (2016)
RBM	22.48	-	-	

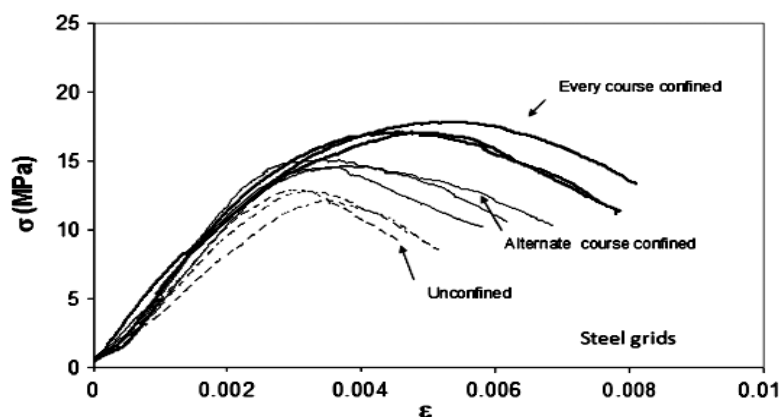


Fig 3: Stress-strain diagram of URM and RBM; Campione et al. (2016)

According to Sakthivel et al. (2016), RBM can be adapted where high compressive and diagonal tensile strength is required instead of RCC as shown in Fig. 4. During the diagonal compressive strength tests of URM and RBM, the result is found 8.56 kN and 22.487 kN, respectively in which capacity of RBM is 2.63 times higher than URM. Freeda et al. (2013) also conducted research on stress-strain behavior of URM and RBM with 10% and 20% replacement of fine aggregates with fly ash as shown in Fig 5. It is seen that rupture strain limit of unreinforced clay brick (CBP) is around 25% lower compared to reinforced clay brick (CBPR). Similar trend is observed for unreinforced clay brick with 10% and 20% replacement of fine aggregates with fly ash CBP10 and CBP20, respectively.





Fig 4: Uses of steel bar in masonry;  
 Sakthivel et al. (2016).

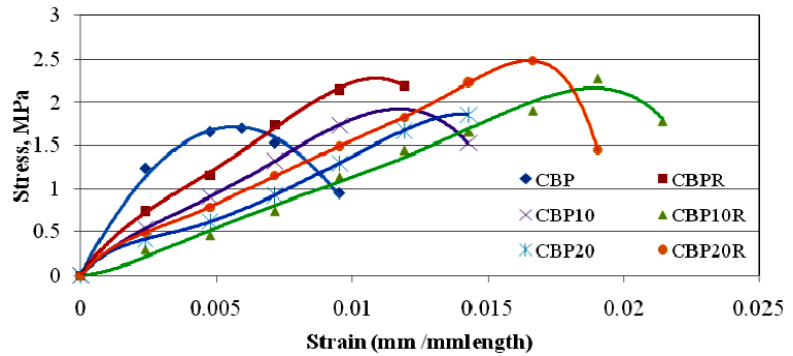


Fig 5: Stress-strain behavior of URM and RBM;  
 Freeda et al. (2013).

### Seismic behavior of masonry structures

Horizontal shear failure, corner/junction failure and failure of out-of-plane walls initiated by junction failure are the most common type of failures in unreinforced masonry structures when subjected to seismic excitation. Corner/junction is identified as the weakest portion of such structures. It is needed to improve the integrity of the structures to behave as a single unit and to ensure proper interlocking between orthogonal walls to reduce the casualties during earthquake. Keeping in view of the above mentioned facts, Nayak and Dutta (2016) used 12 mm thick poly propylene (PP) bands, steel wire mesh and reinforcing bars to strengthen URM walls for achieving better seismic performance as shown in Fig 6. Use of PP band and wire mesh help to improve the integrity of the structures. Horizontal reinforcing bars ensure proper interlocking between orthogonal walls. The shake table with a 1m x 1m single axis horizontal electro dynamic shaker capable of shaking 1000 kg mass with peak ground acceleration of 1g is used in the experimental study. All experiments were carried out under the same ground excitation. Since, the real acceleration time history available corresponding to various real earthquakes may be biased by their spectral shape and frequency content, a ground excitation in the form of swept sine motion had been used in all the cases. Thus, PGA is used as a parameter for damage indicator in the study.

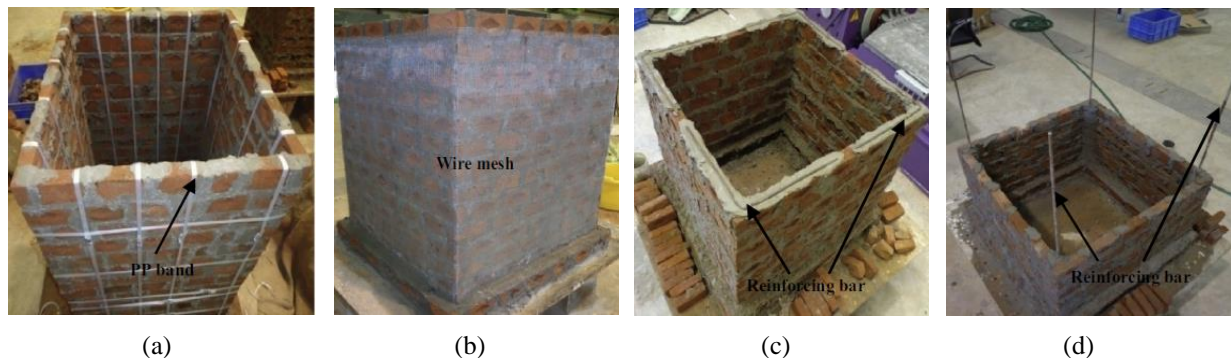


Fig 6: Construction of reinforced four sided walls: (a) PP band provided in form of grid; (b) steel wire mesh all around; (c) horizontal re bar at the junction and (d) vertical re bar at the corner; Nayak and Dutta (2016).

The study conducted by Nayak and Dutta (2016) was extended to assess seismic behavior of unreinforced masonry (URM) wall as well as different types of reinforced masonry walls (RMW). For free standing walls, it was seen that URMW was destroyed at a very low (0.5 g) PGA as shown in Fig. 7(a). On the other hand, reinforced masonry PP band wall (RMPPBW) was destroyed at a very high (2.0 g) PGA compared to the URMW. Similar trend was found in case of reinforced masonry walls wrapped with wire mesh horizontal wall (RMWMHWI, II) and reinforced masonry walls wrapped with wire mesh full height wall (RMWMFWI,II). Unreinforced L shaped masonry walls (URMLW) was also failed (0.84 g) to relatively lower PGA compared to reinforced masonry PP band L shaped masonry walls (RMPPBLW), reinforced masonry L shaped walls wrapped with wire mesh (RMWMLW) and reinforced masonry walls horizontal L shaped reinforcing bar (RMRBLW) as shown in Fig. 7(b).

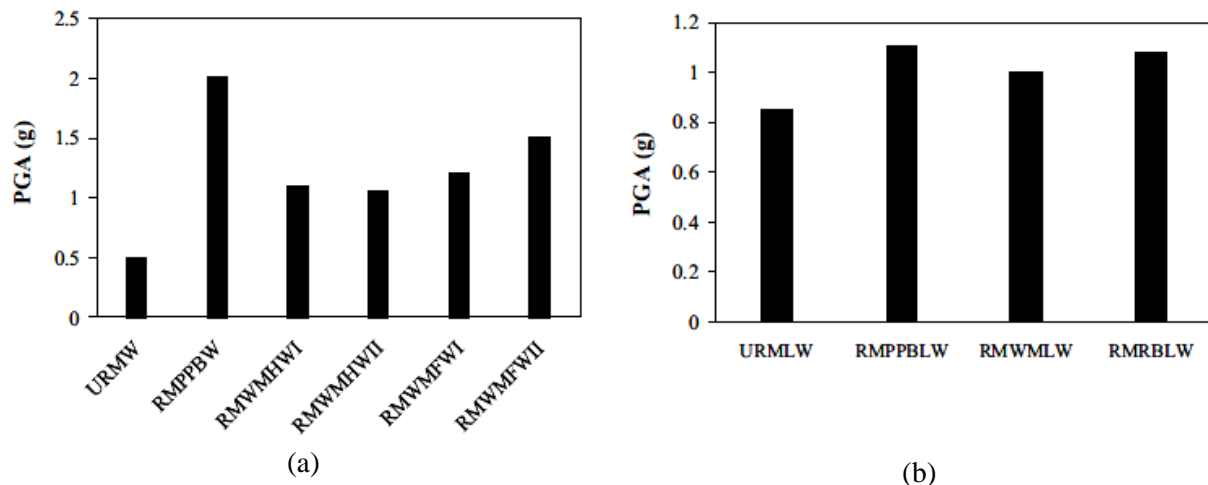


Fig 7: Comparison of strength in terms of PGA for: (a) free standing walls; (b) L-shaped walls adopted from Nayak and Dutta (2016).

According to Sakthivel et al. (2016), RBM can be adapted for high seismic zone buildings as shown earlier in Fig 4. It is shown that shear stress was obtained 361.32 kN/m<sup>2</sup> and 137.54 kN/m<sup>2</sup> for RBM and URM, respectively which is 263% higher than ordinary brick masonry (URM). Thus, it can be concluded that the use of steel embedded brick is one of the best solutions against brittle fracture in brick wall systems in shear. Also, it withstands higher seismic forces compared to ordinary brick structures. Hence, it can prevent a large of masonry structures from collapses and damages during seismic activities.

### Fractured surface

It is seen that URM failed both horizontal and vertical directions for compressive strength test. In case of seismic test, the condition was incendiary. On the other hand, reinforced masonry did not collapse fully. It is also said that a brittle failure is seen for URM. But for RBM only horizontal shear crack is seen and the failure mode is relatively ductile. Fig 8 shows different types of fractured patterns studied by Campione et al. (2016) and Nayak and Dutta (2016).

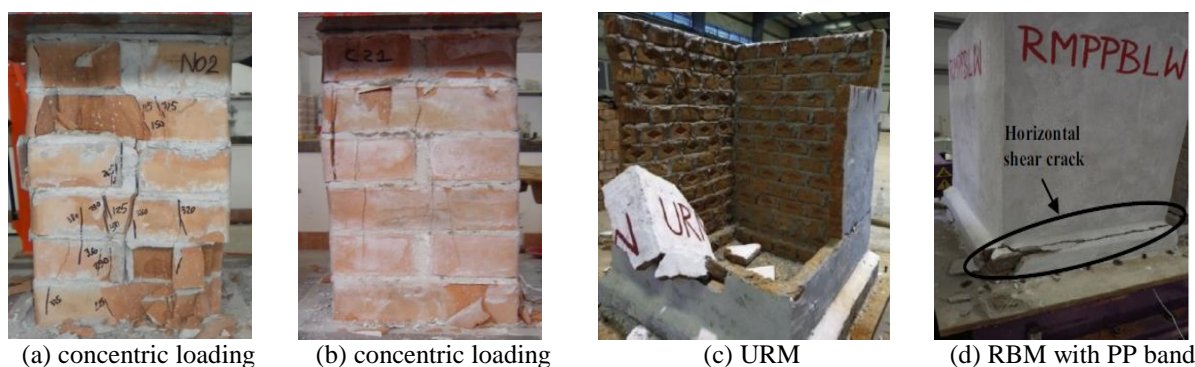


Fig 8: Fractured surface concentric (a) URM (b) RM with CFRP; adopted from Campione et al. (2016) (c) URM (d) RM with PP band; adopted from Nayak and Dutta (2016).

### CONCLUSIONS

In this paper, a theoretical discussion on the subject of reinforced brick masonry (RBM) structure is presented. It is intended as an overview of the mechanical properties of unreinforced brick masonry (URM) as well as RBM of various techniques adopted from literature. The effects of the confinement produced by steel wire, vertical and L shaped reinforcements are also reviewed. The main conclusions that can be drawn from the present study are given below:

- 1) The compressive strength of RBM is significantly higher than that of URM. Strength of RBM can be obtained 263% higher than that of URM.
- 2) Tensile strength and modulus of elasticity of RBM are in higher capacities compared to those of URM.
- 3) Rupture strain limit of RBM is significantly higher compared to that of URM.
- 4) It is seen high modulus of toughness for seismic resistant structures of RBM can be achieved compared to a very low modulus of toughness of URM.
- 5) It is also seen that for a seismic test, URM failed at a low level of PGA which is a vulnerable condition during earthquakes.
- 6) Brittle failure pattern is shown for URM in a seismic excitation whereas a relatively ductile fracture is shown for RBM.

Finally, by reinforcing the masonry with steel reinforcement, FRP, wire mesh, the resistance to seismic loads and energy dissipation capacity can be improved significantly compared to URM. The reinforcing materials are also cheap, easily available and can be easily installed. Therefore, RBM shows the prospect of constructing mid-rise residential buildings, hospitals and schools in the rural area of Bangladesh at a lower cost and low construction period of time with adequate safety.

## REFERENCES

- Campione G., Cavaleri L. and Papia M. 2016. Advanced strategies and materials for reinforcing normal and disturbed regions in brick masonry columns. *J. Compos. Constr.*, 20(4): 04016013.
- Dutta S.C., Mukhopadhyay P., and Goswami K. 2013. Augmenting strength of collapsed unreinforced masonry junctions: the principal damage feature due to moderate Indian earthquakes. *Nat Haz Rev ASCE.*, 14(4): 281–285.
- Freeda C.C., Tensing D. and Mercy S.R. 2013. Experimental study on axial compressive strength and elastic modulus of the clay and fly ash brick masonry. *Journal of Civil Engineering and Construction Technology*, 4(4): 134-141.
- Gumaste K.S., Nanjunda Rao K.S., Venkatarama Reddy B.V. and Jagadish K.S., 2007. Strength and elasticity of brick masonry prisms and wallettes under compression. *Materials and Structures*, 240-241.
- Khalaf F.M., Glanville J.I., and El Shahawi M. 1983. A Study of flexure in reinforced masonry beams. *Concrete International*, 5(6): 46–53.
- Khan S., Khan A.N., Elnashai A.S., Ashraf M., Javed M., Naseer A, and Alam B. 2012. Experimental seismic performance evaluation of unreinforced brick masonry buildings. *Earthquake Spectra*, Earthquake Engineering Research Institute, 3(28): 1269–1290.
- Mohamad G., Lourenço P.B. and Roman H.R. 2005. Mechanical behavior assessment of concrete block masonry prisms under compression. *International Conference on Concrete for Structures (INCOS 05)*, 261-266.
- Nayak S. and Dutta S.C. 2016. Failure of masonry structures in earthquake: A few simple cost effective techniques as possible solutions. *Engineering Structures*, 106: 53–67.
- Oliveira DV; Lourenço PB, and Roca P, 2000. Experimental characterization of the behavior of brick masonry subjected to cyclic loading. *12<sup>th</sup> International Brick/Block Masonry Conference*, Madrid, Spain, pp. 2119-2125.
- Priestley M. J. N. and Bridgeman, D. O. 1974. Seismic resistance of brick masonry walls. *Bull. New Zealand Nat. Soc. Earthquake Eng.*, 7(4), 167–187.
- Qazi A.U., Sharif M.B., Ilyas M. and Ramzan A. 2011. Critical review of reinforced masonry in seismic prone area for different codes, *Pakistan Journal of Science*, 63(2): 79-83.
- Sakthivel K.S., Murugan S., Kumar K.R. and Kumar G.R. 2016. Experimental study of reinforced brick masonry structures, *International Journal of Innovative Research in Science, Engineering and Technology*, 5(4) pp. 4852-4858.
- Technical notes on brick construction, 1996. Technical Paper No. 17, Public Works Department, Government of India.
- Taly N. 2001. *Design of reinforced masonry structures*. Mc Graw-Hill: New York, USA.

## **MONITORING BRIDGE DEFLECTION BY TOTAL STATION**

M. Kamruzzaman<sup>1\*</sup> & M. R. Haque<sup>2</sup>

<sup>1</sup>*Department of Civil Engineering, Rajshahi University of Engineering and Technology, Rajshahi, Bangladesh*

<sup>2</sup>*Department of Civil Engineering, Patuakhali Science and Technology University, Bangladesh*

*\*Corresponding Author: kzaman93@gmail.com*

### **ABSTRACT**

Bridges are an important part of road and transportation systems and deflection is an important index to evaluate the structural health of bridges. In this study, a method of measuring vertical bridge deflection by Refractorless Total Station (RTS) is introduced. A calibrated target board is fixed on the mid-span of the bridge girder and cross hair of the target board was observed remotely by RTS to assess the vertical deflection while passing railway locomotives and coaches. The study was conducted on major Railway Bridges in Bangladesh. It includes Hardinge Bridge, Bhairab Bazar Bridge, Akhaura Bridge, Ghorashal Bridge, Ghatina Bridge and Arani Bridge. The least count of the RTS was 1/8" (3.17mm) and monitored deflection ranges from 1/8" to 7/8" (3.17mm to 22.22mm) for all bridges. The results from the study reveal that the methods to monitor vertical deflection of bridges are quite simple, practical and reliable. It needs less manpower, time and has the potential to access bridge deflection with good accuracy.

Keywords: Total station; vertical deflection; target board

### **INTRODUCTION**

Measurement of deflections of bridges because of dynamic and semi-static loads is essential for their design, function, and structural health (Brownjohn et al. 2010; Bardakis and Fardis 2011), but until recently it was a rather unsolved problem. Moreover, deflection is an important index for safety evaluation of bridges. A high rate of deflection indicates the materials is significantly displaced which may bend, warp or shift in response to the imposed load. Lower rate of deflection indicates higher structural stiffness. Bridges whose deflections overpass the specified limit of design may increase damage accumulation and even collapse at any time, which pose a serious threat to people's lives and bring about a great loss of property. Now a day, monitoring bridge deflections is a challenge to the structural engineers.

There are some studies that report about major difficulty in testing bridges is the measurement of vertical deflections. Dial gauge, accelerometer, tiltmeter etc are traditional tools and methods to measure structural displacement and rotation. These tools must be installed, maintained, and frequently recalibrated to produce reliable results. The collected data from these tools need to be interpreted to obtain direct deflection results which in many cases is very complicated procedure and out of the control of the general structural engineers. The use of instruments such as mechanical dial gauges, linear potentiometers and linear variable differential transducers is usually not feasible. Access under a bridge structure is usually limited, which requires erecting temporary supports to mount the measurement instruments to the ground. Hence, a flexible surveying technique is needed to overcome these obstacles, and make the process of measurements easier and more accurate. These difficulties can be eliminated by using Refractorless Total Station (RTS), which offers the capability to measure the spatial coordinates of discrete points on a bridge without touching the structure.

Systematic measurements of deflections of bridges became possible with the invention of the Global Positioning System (GPS) (Roberts et al. 2004; Meng et al. 2007), on the condition that an unobstructed view of the horizon and of the satellites exists, which is not the case with various railway bridges in which the passing trains deform or even disrupt the satellite signal (Wieser and Brunner 2002). Stiros et. al. (2007) studied about the results of RTS monitoring of the Gorgopotamos Railway bridge in central Greece, a bridge over 100 years old with several openings of ~30m. This bridge was partly destroyed

and rebuilt twice, and its dynamic behaviour is practically unknown. Their study focused on the apparent vertical displacements of a reflector set at the mid-span of an opening, where maximum displacement was expected, during the passage of trains. The objective of the present study is to measure the vertical deflection of railway bridges of Bangladesh with the use of RTS which can measure deflection accurate to 1/8" or 3.17mm. This monitoring system is much easier to set up and use, reducing labour and time. The system has almost no site restrictions. This paper discussed the implementation of RTS and contrasts its use to traditional load testing monitoring equipment. In this survey work, RTS is used with target board instead of prism.

## METHODOLOGY

Vertical deflection of railway bridges was measured in three different methods. The study accepted deflection results of bridges only when three methods produce same result.

### Method 1: Observation of Target Board Only

For measuring mid-span deflection the study used calibrated target board as appeared in Fig 1, 2 and 3.

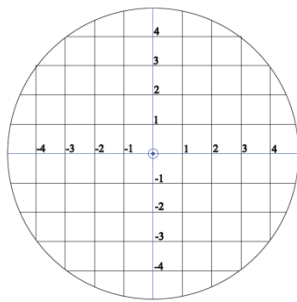


Fig 1: Calibrated Target Board  
 (Scale: 1 grid = 0.3in)

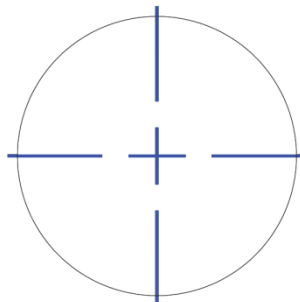


Fig 2: Cross hair of  
 Total Station

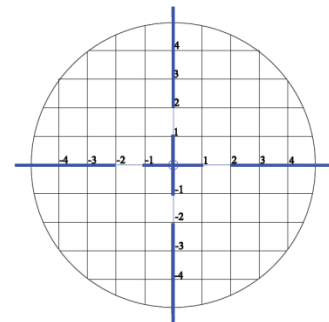


Fig 3: Cross hair of Total Station  
 coincides with origin (0, 0) of Target  
 Board at no Load

Calibrated target board (Fig. 1) was placed at mid-span (Fig. 4) of bridge and the cross hair (Fig. 2) of RTS was kept at origin (0, 0) of target board as like in Fig. 3 with no vehicular load (only dead load).

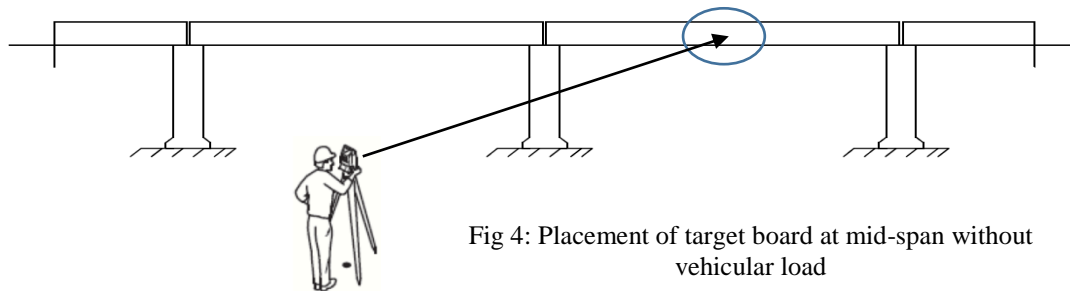


Fig 4: Placement of target board at mid-span without  
 vehicular load

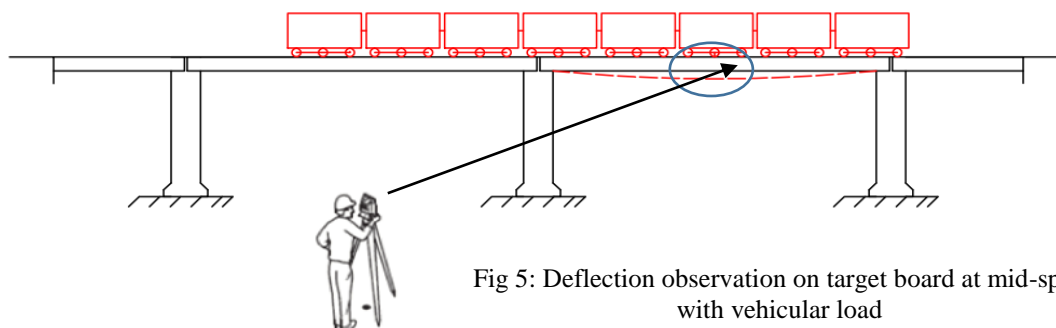


Fig 5: Deflection observation on target board at mid-span  
 with vehicular load

Due to passing of passenger coaches, locomotives and oil tankers, bridges undergo vertical deflections and the target board kept at mid-span moves downward. It was remotely observed by the RTS and the real differences between the cross hair of RTS and target board (as in Fig 5, 6) is observed by operator.

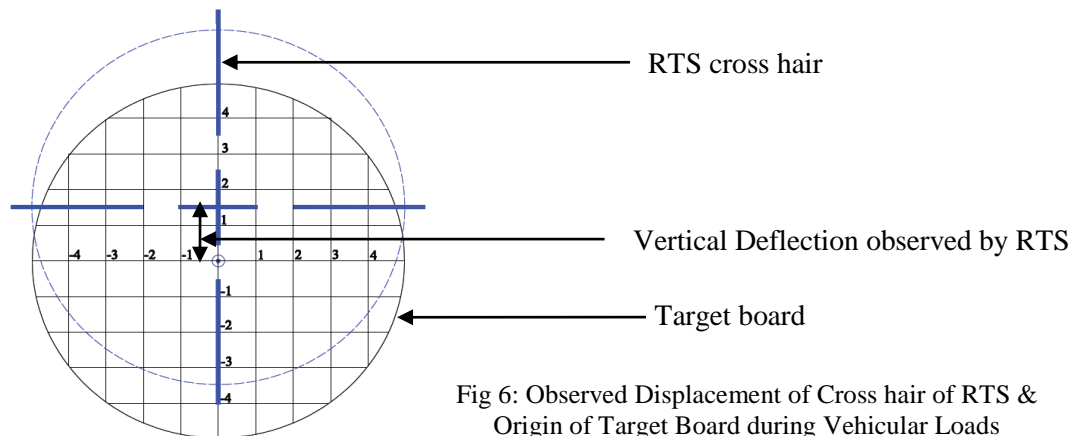


Fig 6: Observed Displacement of Cross hair of RTS & Origin of Target Board during Vehicular Loads

### Method 2: Observation of LASER on the Target Board

The calibrated target board was kept on the mid-span of the bridge and LASER was released from RTS to pass through the origin of the target board during no vehicular load. Afterwards, at loaded condition, while train passes, LASER released and the intersecting points observed on the target board as appeared in Fig. 7. The position of LASER from the origin of target board is the deflection as shown in Fig. 7.

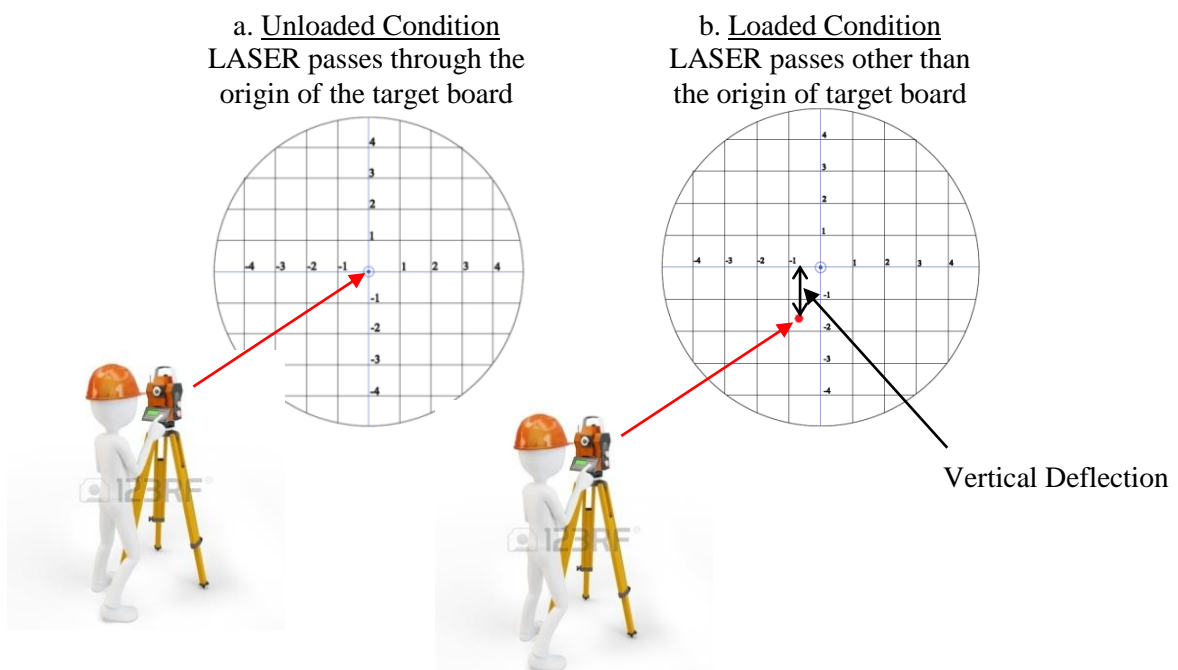


Fig 7: Observation of LASER Rays on the Target Board at Loaded & Unloaded Condition

### Method 3: Missing Line Measurement (MLM) by Total Station

MLM means missing line measurement which is used in RTS to measure horizontal distance (HD), vertical distance (VD) and slope distance (SD). At the beginning of this measurement, the origin of target board and the centre of cross hair of RTS were kept at same line of sight at unloaded condition. Then, at loaded condition, while the origin of target board moves downward, the centre of cross hair of RTS again sighted to the origin (0, 0) of target board. This readjustment of line of sight of RTS gives the value of HD, VD and SD. The VD usually gives the vertical deflection of the studied bridge.

## RESULTS AND DISCUSSIONS

In this study, six railway bridges were studied and the deflection results are presented in Table. 1.

Table 1: RTS Observed Deflection of Major Railway Bridges of Bangladesh

No.	Bridge Name	Span (ft)	Condition	Vertical Deflection (in)
1.	Hardinge Bridge	345' (105.18m)	For Locomotive	5/8" (15.88mm)
			For Passenger Coach	3/8" (9.53mm)
			For Oil Tanker	7/8" (22.22mm)
2.	Bairab bridge	335' (102.13m)	For Passenger Coach	3/4" (19.05mm)
3.	Ghatina bridge	206' (62.80m)	For Passenger Coach	3/8" (9.53mm)
4.	Arani bridge	54' (16.46m)	For Passenger Coach	1/8" (3.17mm)
5.	Akhaura bridge	105' (32.01m)	For Passenger Coach	5/8" (15.88mm)
6.	Ghorashal bridge	104' (31.70m)	For Passenger Coach	1/2" (12.7mm)

The results of field survey lead to the following conclusions:

1. AASHTO Standard Specifications for Bridges (2002) states that, for simple or continuous spans, deflection due to service live loads shall not exceed 1/800 of the span for Railway Bridge. Vertical deflection of bridges varies with respect to span length. According to AASHTO specification, deflections of all studied bridges are within allowable limit.
2. In case of Hardinge bridge, deflection is comparatively less with respect to span length.
3. In case of Akhaura bridge, deflection is comparatively high with respect to span length.
4. Using target board with RTS gives good accuracy for the measurement of vertical deflection.

## CONCLUSIONS

Use of RTS to monitor vertical deflection of major railway bridges is the concern of this paper. RTS has the potential to produce accurate results compared to the traditional deformation monitoring systems. Deflection estimation of major railway bridges in Bangladesh by three different measurement methods produce same vertical deflection results ranging from 3.17mm to 22.22mm. Thus, RTS measurements showed promising results and can be regarded as a powerful tool for monitoring bridge deflection.

## REFERENCES

- Bardakis, V and Fardis, M. 2011. A displacement-based seismic design procedure for concrete bridges having deck integral with the piers. *Bull. Earthquake Eng.*, 9(2): 537–560.
- Brownjohn, JMW; Magalhaes, F; Caetano, E and Cunha, A. 2010. Ambient vibration re-testing and operational modal analysis of the Humber Bridge. *Eng. Struct.*, 32(8): 2003–2018.
- Meng, X; Dodson, A and Roberts, G. 2007. Detecting bridge dynamics with GPS and triaxial accelerometers. *Eng. Struct.*, 29(11): 3178–3184.
- Psimoulis, P and Stiros, S. 2007. Measurement of deflections and of oscillation frequencies of engineering structures using robotic theodolites (RTS). *Eng. Struct.*, 29(12): 3312–3324.
- Roberts, GW; Meng, X and Dodson, A. 2004. Integrating a Global Positioning System and accelerometers to monitor deflection of bridges. *J. Surv. Eng.*, 130(2): 65–72.
- Wieser, A and Brunner, FK. 2002. Analysis of bridge deformations using continuous GPS measurements. *Proc., 2nd Conf. of Engineering Surveying, INGEO 2002*, Slovak University of Technology, Bratislava, Slovakia, 45–52.

## **LOAD BEARING CAPACITY OF UNREINFORCED MASONRY WALL AND STRENGTHENED BY UHPC**

A. F. Mazumder\*

*Department of Civil Engineering, Presidency University, Dhaka, Bangladesh  
\*Corresponding Author: mazumder\_buet@yahoo.com*

### **ABSTRACT**

The majority of existing masonry buildings using unreinforced masonry walls (URM) has been constructed for low service loads. These buildings consequently do not have enough capacity to dissipate the energy resulting from high service loads, the excitation action during event like earthquake. As a result, there is an urgent need to strengthen these walls in order to improve their ability to withstand to higher service loads. Several strategies for strengthening of masonry structures have been proposed and applied to increase the axial strength of masonry. The new generation of advanced concrete technology, ultra-high performance concrete (UHPC), has created enormous possibilities for innovative construction utilization. This work addresses the behavior of strengthening concrete block masonry walls subjected to axial compression loading and retrofitted by UHPC plastering on both sides of the wall, with mortar having microsilica as strength modifier and steel fibers as reinforcing additive.

Keywords: URM; UHPC; strengthening

### **INTRODUCTION**

Masonry wall is one of the most popular and common type of structural component in the world which has a long history and is beautiful in appearance, low cost and ease of construction. Masonry wall is the component of structures made from individual units laid in and bonded together by using mortar. The key advantages of masonry wall are the thermal mass of a building and protection of the building from fire has been increased, there is no requirement of painting and resulting reduced life-cycle costs and useful life cycle is 30 to 100 times higher than structural steel. Most common uses of masonry wall are for partition walls, structural wall, and retaining wall and even in heritage structures. It is well-known that those structural elements are constructed mainly of unreinforced masonry wall (URM). These URM walls are subjected axial load, earthquake load etc. URM walls can be used as load-bearing wall, if proper strengthening material is used. Some researchers had used CFRP, GFRP sheet and bars, textile reinforced mortar (Basaran et al, 2013; Vasconcelos et al, 2012; Mahmood et al, 2008; ElGawady et al, 2006; Zhao et al, 2003 for strengthening. URM wall can be more useful for load-bearing type of wall with proper strengthening techniques and cementitious material could be one of the possible solutions. Ultra-High Performance Concrete (UHPC), also referred as Ultra-High Performance Fiber Reinforced Concrete (UHPRFC), is a new generation of cement-based materials that was developed in France in the 1990s. UHPC is relatively a new generation of concrete optimized at the micro and nano-scale to provide superior durability and mechanical properties compared with conventional and high performance concretes. Improvements in UHPC are achieved through limiting the water-cementitious materials ratio ( $w/cm < 0.2$ ), optimizing particle packing, eliminating coarse aggregate, using specialized materials and implementing high temperature and high pressure curing regimes. In addition, randomly dispersed and short fibers are typically added to enhance the material's tensile and flexural strength, ductility and toughness. Some researcher studied the physical and mechanical properties of UHPC (Hakeem, 2012; Wang and Lee, 2007). The improved mechanical properties of UHPC give the indication to be used as strengthening material.

The main objectives of this study are a) to investigate the mechanical properties of block, mortar, and UHPC b) to investigate the axial capacity of Unreinforced Concrete Masonry Prism (NCMP) and c) to investigate the axial capacity of Unreinforced Concrete Masonry Prism Retrofit (NCMPR), which is UHPC plastered NCMP.



## METHODOLOGY

The load bearing capacity of unreinforced concrete masonry prisms were evaluated on the basis of axial load tests. In this test incrementally increased vertical load was applied to the prism. Experimental program included two tests conducted on two prisms. The first one was unreinforced masonry prism (NCMP), second one was unreinforced masonry wall but plastered by 12.5 mm thickness of UHPC on both sides of the wall (NCMPR).

### *Construction of Test Specimen*

In this study, two unreinforced concrete masonry prism were used under axial loading test. One of the prisms was made of concrete masonry blocks (400×200×100 mm) and Portland cement mortar. Another NCMP prism was plastered with UHPC by 12.5 mm thickness (NCMPR). The aspect ratio for all walls was kept to be 1. Height to thickness of the wall ratio was 60.

The key ingredients of UHPC include micro silica and steel fiber. There were two types of steel fibers used in the same mix. One of these steel fibers was straight and other one was hooked end. Hooked end steel fibers were used for better gripping and anchorage. The developed UHPC mix was utilized for strengthening. The UHPC was mixed in a horizontal pan mixer. After casting specimens were cured for 28 days under water curing process. After curing period was completed, the specimens were tested.

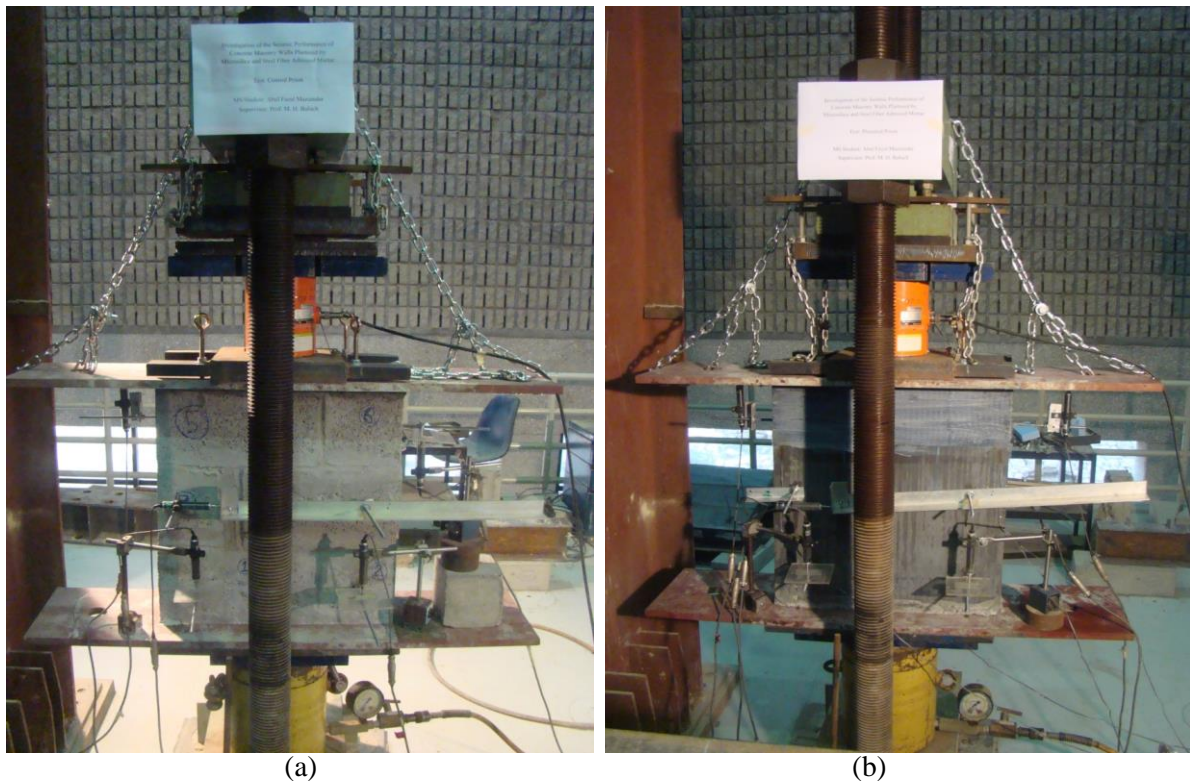


Fig. 1: Experimental Setup, (a) NCMP and (b) NCMPR

### *Experimental Setup, Instrumentation and Procedure*

According to ASTM C 1314 and European Standard EN1052-1(1999), masonry prisms (NCMP and NCMPR) were tested under uniaxial compressive load. To conduct the test, the prisms were placed in the proper position within a steel frame fabricated for purpose of testing under compressive load. Placing of the prism was critical issue, which the prism has to be perfectly aligned vertically and horizontally so that the application of vertical load using the hydraulic jack actuator will not result eccentricity when applying load. Laser leveler was used so that perfect alignment could be achieved. The axial compression forces were exerted on the prism through a steel plate attached to the top and bottom of the wall. High strength mortar (BASF EMACO S88C) was placed in top surface of the prism to ensure uniform distribution of the axial force on the prism without any stress localization. The wall deformations, vertical as well as horizontal, were captured and recorded using four vertical CDP-25 LVDTs and one horizontal CDP-25 LVDTs attached to the prisms at different positions [Figure 1].

### Material Properties

Mechanical properties of various wall components, like concrete masonry block unit, mortar, UHPC were found out by experimental tests. According to EN 772-1 European Standard 2000, compressive strength of concrete masonry blocks was obtained and average value was 9.46 MPa. Modulus of elasticity and Poisson ratio of concrete masonry blocks was 4 GPa and 0.15, respectively.

Blocks were attached in the walls by mortar. The water/cement and cement/sand ratio was kept to be 0.6 and 1/3 respectively. Compressive and flexural strength of mortar was 30 MPa and 2 MPa respectively. Specimens were tested after same age curing of walls. The modulus of elasticity was recorded to be 20.5GPa and Poisson ratio to be 0.18. In case of UHPC, average compressive strength found to be 128 MPa (150×150×150 mm specimens) in compression test and 11.5 MPa was found in direct tension test (Dog-Bone Test). The modulus of elasticity was obtained 45 GPa and Poisson ratio was 0.26.

### RESULTS AND DISCUSSIONS

The experimental work was carried out in two specimens. The maximum compressive strength was recorded to be 5.28 and 11.13 MPa for NCMP and NCMPR prisms, respectively. So, the axial strength was increased by 111% approximately for NCMPR, comparing with NCMP. The maximum displacement captured in case of NCMPR was 1.44mm, which was lower than the NCMP. So, the plaster made the NCMPR prism stiffer than NCMP. Axial load Vs vertical displacement diagram is shown in Figure 2.

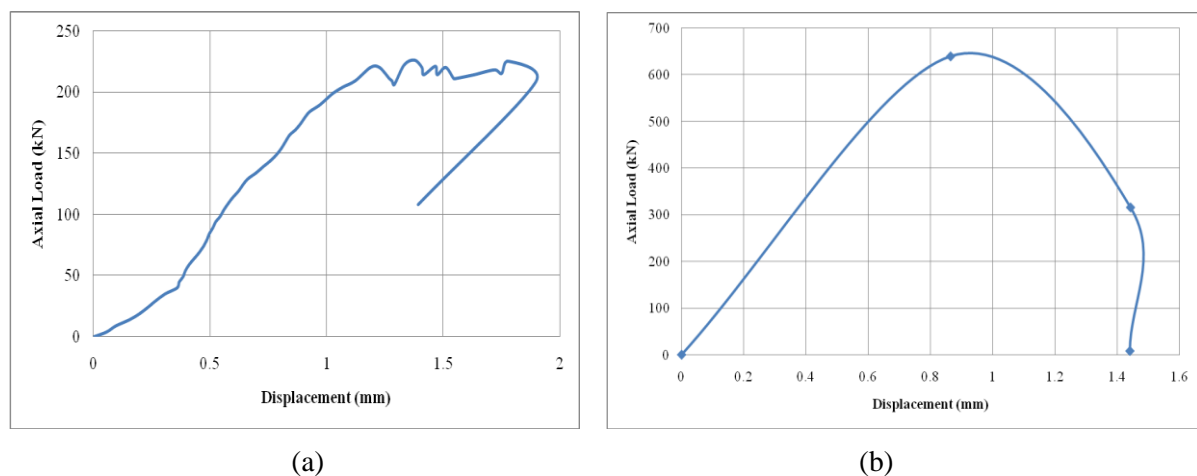


Fig. 2: Axial Load Vs Displacement Diagram, (a) NCMP and (b) NCMPR

### CONCLUSIONS

An innovative system for strengthening concrete masonry walls using UHPC plaster has been investigated. As a retrofit measure, UHPC plaster is congruous and compatible with the existing NCMP in contrast to other retrofitting techniques including use of CFRP and other non-cementitious materials. Following conclusions can be drawn from this study:

- UHPC plaster of plaster thickness to wall thickness ratio of 0.25 was able to increase the strength of the URM wall by an order of 111%.
- Use of UHPC plaster resulted in increase of overall stiffness of the URM wall.

### ACKNOWLEDGMENTS

This work was supported by Research Group (RG), King Fahd University of Petroleum and Minerals (KFUPM), under Funded Project RG1403-1/2, "Investigation of the Seismic Performance of Concrete Masonry Walls Plastered by Nanosilica and Steel Fiber Admixed Mortar".

### REFERENCES

Basaran, H; Demir, A and Bagci, M. 2013. The Behavior of Masonry Walls with Reinforced Plaster Mortar. *Advances in Material Science and Engineering*

- ElGawady, MA; Lestuzzi, P and Badoux, M. 2006. A Seismic Retrofitting of unreinforced Masonry Walls Using FRP. *Composites: Part B*, 37 : 148-162.
- Hakeem, IYA. 2012. *Characterization of an Ultra-High Performance Concrete*. King Fahd University of Petroleum and Minerals (KFUPM), Dhahran, Saudi Arabia.
- Mahmood, H; Russell, AP and Ingham, JM. 2008. Monotonic Testing of Unreinforced and FRP-Retrofitted Masonry Walls Prone to Shear Failure in an Earthquake. *The 14<sup>th</sup> World Conference on Earthquake Engineering*, October 12-17, 2008, Beijing, China.
- Vasconcelos, G; Abreu, S; Figueiro, R and Cunha, F. 2012. Retrofitting Masonry Infill Walls with Textile Reinforced Mortar. *15 WCEE, LISBOA 2012*.
- Wang, YC and Lee, MG. 2007. Ultra-High Strength Steel Fiber Reinforced Concrete for Strengthening of RC Frames. *Journal of Marine Science and Technology*, 15 (3): 210-218.
- Zhao, T; Xie, J and Li, H. 2003. Strengthening of Cracked Concrete Block Masonry Walls Using Continuous Carbon Fiber Sheet. *9th North American masonry conference*, South Carolina, Clemson, 156-67.

## **STRENGTH DEVELOPMENT OF PORTLAND COMPOSITE CEMENT AND ITS COMPARISON WITH PORTLAND CEMENT**

M. D. Karim\*

*Royal Cement Limited, Bara Kumira, Sitakund, Chittagong, Bangladesh  
\*Corresponding Author: dawoodkarim@gmail.com*

### **ABSTRACT**

Granulated Blast Furnace Slag (GBS) is a major by-product of steel manufacturing. Many research has been conducted on slag while used in cement. Here we will discuss the real life data of strength development for a period of three years of Portland Composite Cement using slag and limestone, and compare the same with development of strength with Portland Cement (OPC). This Paper presents the results of a test on the effect of Portland Composite Cement mixed with Slag and limestone as per CEM II ratios of BDS-EN 197-1:2003 (Equivalent of En 197) and compared the same with CEM I (OPC) of the same standard for the similar duration. This is of great value in the construction of mass concrete using CEM II as it would save a big amount of money, and on the other hand will provide similar strength like OPC. As slag and fly ash etc. were used for land filling (it will rise the sea level) only, steps were taken to manage these materials by mixing with cement all over the world for more than 75 years. Though the requirement of Cement having Slag has a tendency of lower early strength, but it becomes similar in later stages. The paper would try to establish that at 365 days both CEM I and CEM II show similar compressive strength results, but later on CEM II will show more strength than CEM I. The further development of strength even after 365 days would also be monitored.

Keywords: Granulated Blast Furnace Slag (GBS); Portland Composite Cement; Portland Cement or OPC; compressive strength

### **INTRODUCTION**

Granulated Blast Furnace Slag (GBS) originates in an iron blast furnace. Carefully controlled amounts of iron ore, along with limestone or dolomite, are fed into a blast furnace and heated to 1,480°C. When molten, the iron is kept for steel production and the slag is sent to a granulator. Here, the slag is rapidly quenched with large quantities of water and converts to a light coloured glassy sand-like material. The process minimizes crystallization and forms “granulated slag,” which is composed principally of calcium aluminosilicate glass. (Formation of this glass provides slag cement with its cementitious properties.) At this point, the slag is the consistency of fine sand. It is then dewatered and dried. Finally, the slag is interground with Portland cement clinker and limestone to make Portland Composite Cement. EN 197 or BDS EN 197 has allowed producing 27 types of cement which is mentioned in Table of the standard. In the table the CEM II B-M (S-L) allows to mix 21~35% slags and limestone with Portland cement clinker and Gypsum.

Composite cement of various types is the major cement produced in Bangladesh. Only around 20% of total produced cement in the country is OPC. Composite cement has been produced here since 2003 after being introduction of the standard BDS-EN 197: 2003. And all major formulation and expertise were provided from abroad. Very few RND works were done among any cement producers to learn any comparison between the newly introduced composite cement and OPC. To overcome this problem, Royal Cement conducted a comparison test between OPC and Composite cement having 15% Slag with no Limestone first in 2003, and later placed that data in various in-house seminars. That test was conducted with a span of one year, and since no Limestone was used the results may be claimed inconclusive. For that reason, in 2011 another similar test was conducted with a span of 3 years period. This has helped to achieve genuine experience of strength development of PCC, and share the same to others.

## METHODOLOGY

For the test ASTM test methods were followed; like for determination of setting time, ASTM C191, for Fineness ASTM C204 and finally for compressive strength ASTM C109 were followed. For compressive strength test ASTM Graded Sand conforming C778, 2 inch Cast iron cube moulds were used, Lime saturated water was used for curing which conforms to ASTM C511. The range of curing room temperature was 22.5°C~23.6°C. Humidity of curing room was more than 70%.

Both samples *i.e.* CEM I and CEM II B-M (S-L) should have similar physical properties like fineness and setting time, which are very important for such test. Same curing room, as well as same compressive strength testing machines (Pre Calibrated) were used which will eliminate errors due to machine, curing room condition etc.

20 sets (3 moulds in each set) of 2 inch moulds were prepared for each type of cement and they were broken using a calibrated compressive strength testing machine of 300 KN capacity. Samples were cured according to ASTM C109 and tested on 1 Day, 2 Days, 3 Days, 4 Days, 5 Days, 6 Days, 7 Days, 14 Days, 21 Days, 28 Days, 35 Days, 42 Days, 49 Days, 56 Days, 180 Days, 365 Days, 1.5 Years, 2 Years, 2.5 Years and finally for 3 Years.

All moulds were prepared and cured following ASTM C109 standard and they were prepared and cured simultaneously to eliminate all possible variables in an industrial test lab. For this reason, it is believed that the results are more conclusive and genuinely comparable to each other; and while put on the plot the graph was also amazingly accurate.

### Observations

Some slow development of strength were observed in CEM I (OPC) for the ages of 5~7 days, which was unexplainable. It was anticipated that this is due to the allowed possible standard deviation of the ASTM Test method.

Table 1: Mixing ratio of raw materials in the experimental cements

	Clinker	Slag	Limestone	Gypsum
CEM I	97.5%	--	--	2.5%
CEM II B-M (S-L)	65%	25.5%	7%	2.5%

Table 2: Chemical Composition of Raw Materials

	CaO	SiO <sub>2</sub>	Al <sub>2</sub> O <sub>3</sub>	Fe <sub>2</sub> O <sub>3</sub>	MgO	SO <sub>3</sub>	IR	LOI	Free lime
Clinker	66.10	19.28	7.82	3.26	1.03	1.68	2.40	0.31	0.89
Slag	40.26	31.60	17.20	0.82	4.81	1.16	3.2	0.78	--
Limestone	51.81	--	--	--	--	--	--	--	--
Gypsum	--	--	--	--	--	35.37	--	--	--

N.B.: Slag was totally dried out of moisture

Table 3: Physical Properties of cements

	Fineness	Residue on R90	Initial Setting Time	Final Setting Time
CEM I	367 m <sup>2</sup> /kg	0.2%	140 mins	180 mins
CEM II B-M (S-L)	365 m <sup>2</sup> /kg	2.8%	145 mins	190 mins

### Equations

The machine reading during breaking were in KN. Value in PSI were found using the following conversion formula;

$$KN = \frac{1000 \times 2.204lb}{9.81 \times 4sq.in^2}$$

## RESULTS AND DISCUSSIONS

For comparison the data is placed in two separate tables; Early Strength and Later Strength. The values of strength are in lb/in<sup>2</sup> or psi for easy understanding. The data were not rounded up for getting a more accurate curve in the table.

Table 4: Compressive Strength Results of the samples (Early Strength)

	1 Day	2 Days	3 Days	4 Days	5 Days	6 Days	7 Days	14 Days	21 Days	28 Days
CEM I (psi)	1180	2340	2677	3120	3315	3483	3876	4606	5112	5560
CEM II B-M (S-L) (psi)	768	1540	2078	2378	2640	2950	3080	3470	3820	4200

Table 5: Compressive Strength Results of the samples (Later Strength)

	35 Days	42 Days	49 Days	56 Days	180 Days	365 Days	1.5 Years	2 Years	2.5 Years	3 Years
CEM I (psi)	5861	5992	6011	6161	6254	6250	6300	6460	6460	6560
CEM II B-M (S-L) (psi)	4600	5000	5310	5740	6070	6340	6600	6840	7060	7110

After placing these values in a plot a figure is found which indicates that though Portland Composite Cement develops at a much slower late at early stage, but it shows higher strength on later stages.

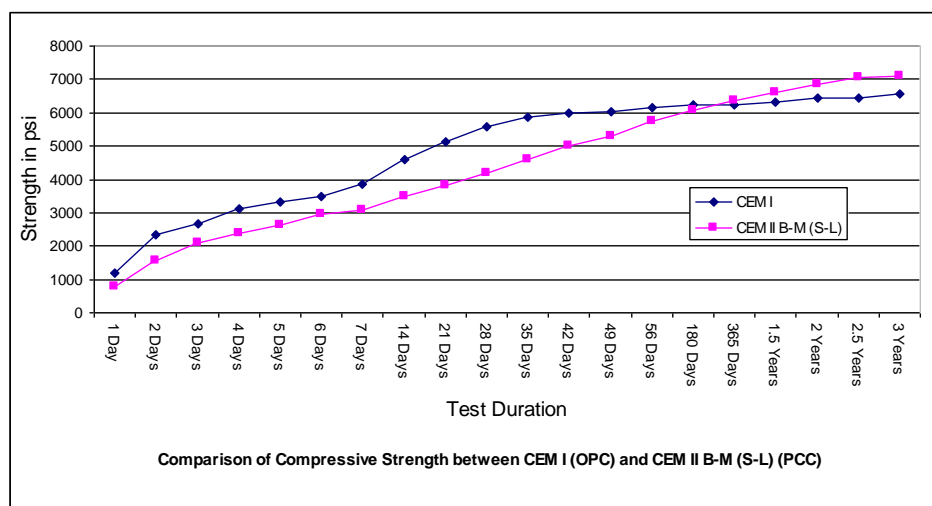


Fig 1: Comparison of Compressive Strength between CEM I (OPC) and CEM II B-M (S-L) (PCC)

It the Figure 1 one more observation can be found, whereas the strength of the OPC has a tendency to stabilise after 180 days or six month with only 4.8% development in rest of the time; the CEM II was clearly gaining strength day by day and the rising tendency of plot shows some upwards trend even at 3 years duration (17% increase in strength in the same time).

The benefits of limestone filler (LF) and granulated blast-furnace slag as partial replacement of portland cement are well established. However, both supplementary materials have certain shortfalls. LF addition to portland cement causes an increase of hydration at early ages inducing a high early strength, but it can reduce the later strength due to the dilution effect. On the other hand, BFS contributes to hydration after seven days improving the strength at medium and later ages.

Slag Cement has higher resistance to sulphate and salinity content sand and environment. When Portland cement hydrates, it forms calcium-silicate hydrate gel (C-S-H) (about 50~60%) and calcium hydroxide (Ca(OH)<sub>2</sub>) or C-H (about 20~25%). C-S-H is the "glue" that provides strength and holds the concrete together. Permeability is related to the proportion of C-S-H to Ca(OH)<sub>2</sub> in the cement paste. The higher the proportion of C-S-H to Ca(OH)<sub>2</sub>, the lower the permeability of the concrete as C-H is a by-product of the hydration process that does not significantly contribute to strength development in normal portland cement mixtures. When slag cement is used as part of the

cementitious material in a concrete mixture, it reacts with  $\text{Ca(OH)}_2$  to form additional C-S-H, which in turn lowers the permeability of the concrete.

When slag cement is incorporated in a concrete mixture, less heat is generated and thermal stress is reduced: Due to increased strength with slag cement, the total cementitious content can be reduced. Portland cement content is reduced by the percentage of slag cement used. Hydration characteristics of slag cement are such that the early rate of heat generation and peak temperature of the concrete are reduced.

The composite cement price is lower, thus bigger saving during volume usage.

The Quality of the material used are also another important criteria, the similar curve may not be achieved without getting similar type of GBS Slag.

In both of the studies it is found that at the age of 365 days both CEM I and CEM II are showing similar results, of which surprisingly CEM II has a bit higher strength. The result also indicates that the both CEM I and CEM II cement uses in the experiment has the tendency to gain strength even after 1 and 2 years. The tendency of the curve is still upwards even after 3 years.

## CONCLUSIONS

This plot indicates that cement containing slag may produce higher strength than OPC after systematic curing which is the main requirement for the development of concrete strength. As the civilisation develops, people are using up most of their environmental resources by manufacturing product like cement. A big volume of virgin raw materials is consumed each year to produce clinker for cement. This causes a vast release of Carbon-di-Oxide into the environment. The production of clinker cannot be stopped, but the volume can be reduced by using by-products like Granulated Blast Furnace Slag. About 300 KG of Slag is produced during production of one Metric Ton of Steel. And this huge amount of slag can help to reduce the stress on the environment by helping cement to gain similar results like OPC. PCC has many more benefit to the environment; such as less heat production, protection against chemical attack etc.

In contrast to the stony grey of concrete made with Portland cement, the near-white colour of GBS cement permits architects to achieve a lighter colour for exposed fair-faced concrete finishes, at no extra cost. To achieve a lighter colour finish, GBS cement also produces a smoother, more defect free surface. Dirt does not adhere to GBS concrete as easily as concrete made with Portland cement, reducing maintenance costs. GBS cement prevents the occurrence of efflorescence, the staining of concrete surfaces by calcium carbonate deposits.

In both of the studies it is found that at the age of 365 days both CEM I and CEM II are showing similar results, of which surprisingly CEM II has a bit higher strength. The result also indicates that the both CEM I and CEM II cement uses in the experiment has the tendency to gain strength even after 1 and 2 years. The tendency of the curve is still upwards even after 3 years.

## ACKNOWLEDGMENTS

Mr. Raihan Khan, Manager, Royal Cement Limited

Mr. Javed Iqbal, Dy Manager, Royal Cement Limited

## REFERENCES

Neville, AM and Brooks, JJ. 1999. *Concrete Technology*. London: Addison, Wesley Longman Limited. 29p.

Supplimentary Cementing Materials for Use in Blended Cement (RD112T), by Rachal J. Detwiler, Javed I. Bhatta and Shankar Bhattacharja, Portlan Cement Organisation (PCA). 14p, 26p.

## **PERFORMANCE EVALUATION OF BAMBOO AS REINFORCEMENT IN CONCRETE**

M. R. Awall\*, M. H. Ali, M. A. Rahman, M. A. Hossain & S. U. Khan

*Department of Civil Engineering, Rajshahi University of Engineering & Technology, Rajshahi,  
Bangladesh*

*\*Corresponding Author: robi95@gmail.com*

### **ABSTRACT**

Bamboo is a low cost construction material and is available in Bangladesh. So, it is more effective and economic in rural construction. Usually steel is used as reinforcement in concrete, but it is costly than any other materials. If bamboo is used as the replacement of steel, then the rural people can build bamboo reinforced concrete building. In this study, performance of bamboo as reinforcement in concrete has been investigated. Strength property of bamboo is observed by tensile test of bamboo sticks and suitability of bamboo as reinforcement in concrete has been evaluated by testing of slab and beam. Three types of sample having without node, middle node and node at a distance  $L/4$  of single and double seasoned are used for tensile test. Also, three types of beam are used for flexural test, namely plain concrete beam, single reinforced beam and doubly reinforced beam having same dimensions 750 mm length, 200 mm width and 250 mm depth. Again, two identical two way slabs of 750 mm width, 1200 mm length and 150 mm depth are used for slab test. In singly reinforced concrete beam the load carrying capacity is found about 2.2 times and for doubly reinforced beam about 3.0 times more than plain concrete beam. The ultimate load carried by slab is 78 kN and corresponding deflection is 2.17 mm. The doubly seasoned stick can increase the tensile and flexural stresses than single seasoned.

Keywords: Bamboo; reinforcement; seasoned stick; concrete beam; slab; flexural stress.

### **INTRODUCTION**

As Bangladesh is a developing country, the cost of housing is a major consideration. Although most of the houses in rural areas are made of wood, bamboo, brick which are easily available. Concrete is widely used construction material for its various advantages such as low cost, availability, fire resistance etc. But it cannot be used alone everywhere because of its low tensile strength. Therefore, generally steel is used in reinforce concrete. Though steel has a high tensile strength to complement the low tensile strength of concrete, use of steel should be limited since it is very costly and so much energy consuming in manufacturing process. Thus a suitable substitute of this with a low cost, environmental friendly and also a less energy consuming one, is a global concern; especially for developing country. Addressing all these problems, bamboo is one of the suitable replacements of reinforcing bar in concrete for low cost constructions. Bamboo is natural, cheap, widely available and most importantly strong in both tension and compression. The mechanical properties vary with height and age of the bamboo culm. Research findings indicate that the strength of bamboo increases with age. The optimum strength value occurs between 2.5 and 4 years and the strength decreases at a later age (Amada and Untao, 2001). The function of the nodes is to prevent buckling and they play a role of axial crack arresters. The tensile strength of bamboo can reach up to 370 MPa, which makes bamboo an attractive substitute to steel in tensile loading applications (Rahman et al., 2011).

Janseen (2000) conducted her study on Bamboo reinforced building and discusses the joints and building with pure Bamboo. Listed in her book are several things that are more of a hassle than steel reinforcement. Of those, the bonding between the Bamboo and concrete is considered the biggest problem due to absorption of water and smooth wall of the Bamboo culm. Vengala et al. (2004) constructed a prototype Bamboo reinforced concrete house and used an earthquake simulator to find that the house stood during a 7.8 (on the Richter scale) earthquake. They found no cracking in the concrete, the Bamboo to be extremely resilient to earthquakes, and the cost to be split in half compared to mud and brick construction. Lo et al. (2004) and Amada et al. (1997) investigated the mechanical and



physical properties of Bamboo. They conducted a thorough investigation into the structure and purposes of the nodes, which they found to strengthen the Bamboo culm. They also commented on the advantage of Bamboo has over other natural building materials with its fast growth rate. Amada and Untao (2001) studied the fracture properties of Bamboo. In contradiction to other studies, this study states that the tensile strength of Bamboo fibers almost corresponds to that of steel. The main discovery is that the fracture properties of Bamboo depend upon the origin of fracture. Ghavami (1995, 2004) discussed the mechanical properties of Bamboo, specifically pertaining to Bamboo in concrete. This study showed that the ultimate load of a concrete beam reinforced with Bamboo increased about 400% as compared to un-reinforced concrete. It was found that, compared to steel, there was lower bonding between the Bamboo and concrete, and the Bamboo had a Modulus of elasticity 1/15 of steel. This study concluded that Bamboo can substitute steel satisfactorily, and that there is a need to establish the characteristic strength of Bamboo for design purposes. In the current study, tensile property of bamboo is observed and performance of bamboo as reinforcement in concrete with replace of steel has been thoroughly investigated.

## METHODOLOGY

### *Bamboo*

Bamboo is a composite material, consisting of long and parallel cellulose fibres embedded in a ligneous matrix. The density of the fibres in the cross-section of a bamboo shell varies along its thickness. In this study, bamboo was given consideration for using as reinforcement for the construction of low-cost houses in Bangladesh. As a high demand of occupy houses in Bangladesh is highly increasing. Therefore, urgent and effective action is required to secure the demand in sustainable basis. Most bamboos are hollow. In the hollow inner area, some horizontal partitions called diaphragms. On the outside, these partitions are denote by a ring around the culm. A diaphragm and the ring on the outside together form a “node”. Branches grow from these nodes. The part between two nodes is called an inter-node. The internodes of most bamboos are hollow. They have a cavity. The wall of the culm is called simply the culm wall as shown in Fig. 1.

### *Preparation of bamboo sticks*

Bamboo preparation is essential for increasing its durability, long life and to prevent it from insects. After cutting the bamboo plant, it should be allowed to dry and season involves immersing the culms in stagnant or running water for four to six weeks to leach out the sugars. After that the wet bamboos are air-dried under shade. Air drying is necessary before using the bamboo as reinforcement for preventing

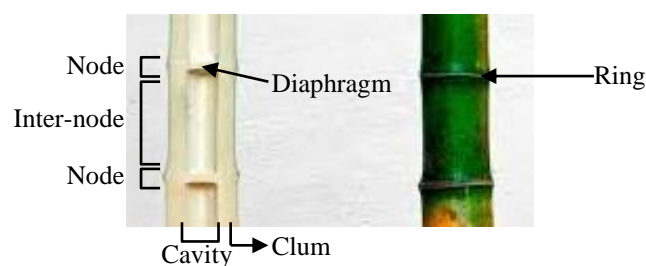


Fig. 1: Various parts of Bamboo culm

contraction and shrinkage because it may contain 50-60% moisture content depending on the season, area of growth and species. Usually, one or two week is used for full air drying (Janseen, 2000). During cutting great care should be taken not to split the specimen, because splitting will result in continuous tearing of fiber. Bamboo sticks are cut according to the size of the specimen and allowed to dry and again season for 30 days. When seasoned bamboo either split or whole is used as reinforcement, it should receive a waterproof coating to reduce swelling when in contact with concrete. Without some type of coating, bamboo will swell before the concrete has developed sufficient strength to prevent cracking and the member may be damaged. A dip coat of asphalt emulsion is used in this study shown in Fig. 2.

### **Tensile test of bamboo sticks**

Bamboo sticks are generally more popular than whole culms in construction works. In order to conduct the tensile strength test, bamboo stick samples are cut of 750 mm length and around 25 mm width shown in Fig. 3. The first set of tensile tests was conducted on bamboo samples having without node, second set of tensile test was conducted on bamboo sticks having single node at middle and third set of tensile test was conducted having node at L/4 distance. These all three sets are taken as single seasoned; also another set is taken doubly seasoned. Specimen was placed in Universal Testing Machine (UTM) and tensile load was being applied until failure. During these tensile tests, all tensile specimens were failed at node point. The maximum tensile strength is obtained for the sample having node at L/4 distance and tensile stress is increasing 6.4% in double seasoned stick than single seasoning shown in Table 1.



Fig. 2: Preparation of bamboo sticks (a) Seasoning (b) Air drying (c) Asphalt emulsion coating

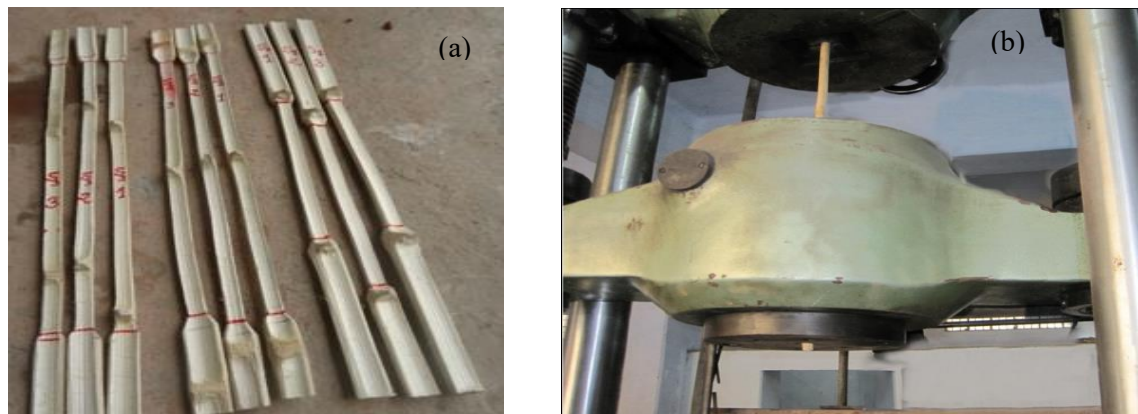


Fig. 3: Tensile strength test of bamboo sticks (a) bamboo sticks (b) testing under UTM machine

Table 1: Tensile stress of bamboo specimens

Seasoned type	Specimen type	Sample no.	Average Area (mm <sup>2</sup> )	Ultimate load (kN)	Stress (MPa)	Average Stress (MPa)
Single seasoned	Without node (S <sub>1</sub> )	1	177	22	124.30	118.5
		2	174.33	22	126.20	
		3	200	21	105.00	
	Middle node (S <sub>2</sub> )	1	185	19	102.70	116.72
		2	197	23	116.75	
		3	153	20	130.71	
Doubly seasoned	Node at L/4 (S <sub>3</sub> )	1	148.33	20	134.83	132.84
		2	162	21	129.60	
		3	141.67	19	134.11	
	Node at L/4 (S <sub>3</sub> )	1	154.5	22	142.39	141.31
		2	147	21	142.86	
		3	137	19	138.67	

**Preparation and testing of beam and slab**

In this research, three types of beam were used namely plain concrete beam, singly reinforced beam and doubly reinforced beam having same dimensions. In plain concrete beam, no bamboo stick was used. Three bamboo sticks were placed at the bottom with 25 mm clear cover in singly reinforced beams. Similarly, three bamboo sticks were placed at the top and bottom with 25 mm clear cover in the case of doubly reinforced beams shown in Fig. 4. When placing the bamboo, the top and bottom of the stems were altered in every row and the nodes were staggered. This ensured a fairly uniform cross-section of the bamboo reinforcement throughout the length of the member, and the wedging effect was obtained at nodes increased the bond between concrete and bamboo. After 28 days curing, beam was carefully placed under the testing machine (UTM) and supports were placed at the measured location of 100 mm inside from each end. Dial gauges were also provided at mid-span to calculate the deflection. After placing the beam, one point loading at the mid-span of the beam was applied gradually by controlled pumping unit. The deflection of the beam at mid-span was measured at regular interval of loading shown in Fig. 5.

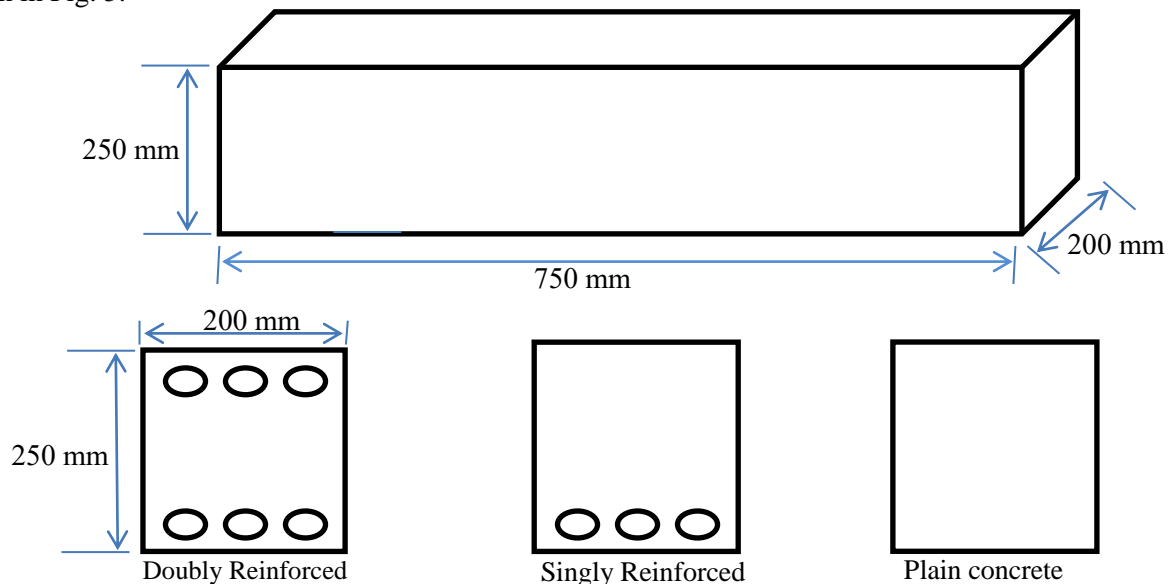


Fig. 4: Dimensions and cross-section of sample concrete beam



Fig. 5: Flexural test of beam



Fig. 6: Flexural test of slab

Also two identical two way slabs were used in dimension 1200 mm length, 750 mm width and 150 mm depth. Clear cover 25 mm is provided and bamboo reinforcements having uniformly spaced from center to center are ensured. After 28 days curing, slabs are tested under the universal testing machine (UTM). Dial gauges were also provided at mid-span to calculate the deflection. After placing the slab, line loading along length at the mid-span of the beam using I-beam was applied gradually by controlled pumping unit shown in Fig. 6.

## RESULTS AND DISCUSSIONS

Load-deflection curves of bamboo reinforced concrete beams are shown in Fig. 7. The ultimate load carrying capacity of plain concrete beam, singly reinforced with single seasoned (SB-SS), singly reinforced with double seasoned (SB-DS), doubly reinforced with single seasoned (DB-SS) and doubly reinforced with double seasoned (DB-DS) beam were found to be 32 kN, 66 kN, 67.5 kN, 88 kN and 89 kN respectively. Also the corresponding deflections were 0.69 mm, 2.94 mm, 3.11 mm, 3.90 mm and 3.92 mm respectively. From the test results, it can be observed that the maximum deflection of singly and doubly reinforcement beams are 4.5 and 6 times larger than the plain concrete beam respectively. Also in singly reinforced concrete beam (SB) the load carrying capacity is found about 2.2 times and in doubly reinforced beam (DB) about 3.0 times more than the plain concrete beam (PB). The doubly seasoned (DS) stick can increase 3% flexural stresses and 6% tensile stress than single seasoned (SS) stick. The ultimate load carried by slab is 78 kN with corresponding deflection 2.17 mm shown in Fig. 8. Flexure failure was occurred in each slab. From the test conditions, bamboo can potentially be used as substitute for steel reinforcement with treatment to control water absorption and to increase the bond. Steel reinforced concrete structures built in the past 30 years can reveal serious deterioration caused mainly by the corrosion of the steel reinforcement. Ghavami (2005) tested the bamboo reinforced beam, after that it has been exposed in open air climate. It can be observed that the

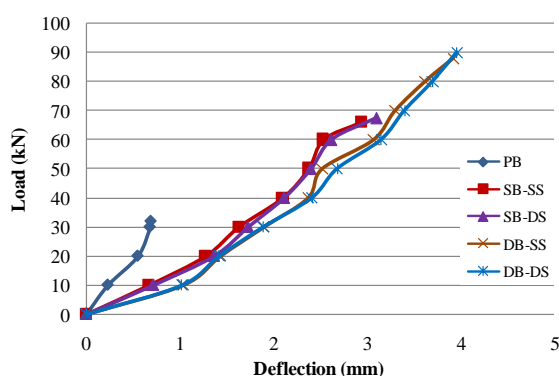


Fig. 7: Load-deflection curve of bamboo reinforced concrete beam

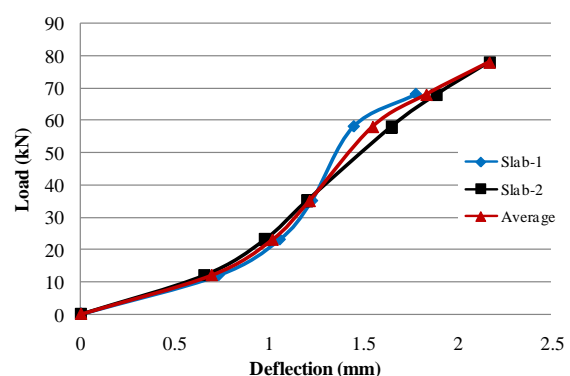


Fig. 8: Load-deflection curve of bamboo reinforced concrete slab

bamboo sticks of the beam reinforcement, treated against insects as well as for bonding with concrete, is steel satisfactory condition after 15 years. Therefore, the durability analysis shall be done before

employing it in important construction. Tensile strength of the bamboo shall be tested before designing structural members as it varies on soil condition, topography, water table, water absorption etc.

## CONCLUSIONS

For developing country like Bangladesh, the cost of housing is a major concern to the poor or, low-income people. Steel is mainly used as reinforcement which is very costly. Scientists and engineers are seeking for new materials as substitute of steel, the idea of using bamboo as reinforcement has gain popularity due to cheap, natural and also readily available. From test results, the load carrying capacity of singly bamboo reinforced concrete beam is increased about 2.2 times and that for doubly bamboo reinforced beam about 3.0 times than plain concrete beam having same dimensions. The ultimate load carried by slab is 78 kN with corresponding deflection 2.17 mm. The doubly seasoned bamboo sticks are more effective than single seasoned bamboo sticks. Tensile strength of bamboo is good enough. Bamboo is weak at node section and major failure occurs at node point. In the green material concept, the replacement of steel reinforcement can be possible by using bamboo for low cost construction. Moreover, there is a need to establish more characteristic strength of bamboo for design purpose based on experimental and rigorous statistical analysis.

## REFERENCES

- Amada, S and Untao, S. 2001. Fracture properties of bamboo. *Composites Part B: Engineering*, 32(5): 451-459.
- Amada, S, Ichikawa, Y, Munekata, T, Nagase, Y and Shimizu, H. 1997. Fiber texture and mechanical graded structure of bamboo. *Composites Part B: Engineering*, 28(1-2): 13-20.
- Ghavami, K. 1995. Ultimate load behavior of Bamboo-reinforced light weight concrete beams. *Cement & Concrete Composites*, 17(4): 281-288.
- Ghavami, K. 2005. Bamboo as reinforcement in structural concrete elements. *Cement & Concrete Composites*, 27(6): 637-649.
- Janseen, JJA. 2000. *Designing and building with Bamboo*, Technical Report no. 20, International Network for Bamboo and Rattan.
- Lo, TY, Cui, HZ and Leung, HC. 2004. The effect of fiber density on strength capacity of bamboo. *Materials Letter*, 58(21): 2595-2598.
- Rahman, MM, Rashid, MH, Hossain, MA, Hasan, MT and Hasan, MK. 2011. Performance Evaluation of Bamboo Reinforced Concrete Beam. *International Journal of Engineering & Technology*. 11(4): 113- 118.
- Vengala, J, Mohanthy, BN and Raghunath, S. 2004. Seismic performance of Bamboo housing- an overview. *World conference on earthquake engineering*, Vancouver, Canada, August 1-6.

## **CYLINDRICAL WEDGE-TYPE COMPRESSION FREE BRACING SYSTEM FOR MOMENT RESISTING FRAME STRUCTURES**

A. Das\* & M. A. Islam

*Department of Civil Engineering, Southern University Bangladesh, Chittagong, Bangladesh  
\*Corresponding Author: amritadascuet@gmail.com*

### **ABSTRACT**

In order to make the structure safe during seismic vibration, the structure can be strengthening by using different kinds of bracing system. If ordinary brace is used for this purpose, it will be buckled under lateral compressive load. This study will investigate the performance of the cylindrical wedge-type non-compressive bracing system. The whole experimental investigation has been done into two phases: in the first phase only uniaxial test has performed. In the second phase, the test has been performed by applying cyclic load through the hydraulic actuator on a half portal frame. The cylindrical wedge grip worked properly under compression by releasing the sacrificial steel, which prevent buckling of steel core. The hysteretic loops from tension load are not stable in size and slope even the same load. It is anticipated that non-linearity from the device itself or from the gripping device of the universal testing machine may cause this unstable hysteresis. The developed device needs some improvement to use in the inclined configuration. Pre-loaded spring as well as the improvement in steel casing for perfect alignment of both wedge and steel core might resolve problem from inclined configuration.

Keywords: Cylindrical; wedge-type; non-compressive; bracing system; buckling

### **INTRODUCTION**

In the present world, building of high rise structures is a common trend not only in the developed country but also in the developing country. Tall buildings had changed the scenario of the landscape of the major cities in the world. The main problem of Tall structures is normally susceptibility to earthquake and wind. It is noticeable that the life safety purpose has been served in conventional structural configuration at the cost of property loss or repair. As the demand of the tall building is increasing day by day, some advanced technology should be implemented in the design methodology.

After Kobe earthquake a survey has been done on the damage of structural members and connections with respect to structural type. Damaged structures are classified as having resisting braced or unbraced frames. Di et al. (2009) mentioned that from the survey it had been confirmed that majority of damaged buildings had unbraced moment frames (MRF) as earthquake resistant system.

Tremblay (Tremblay, 2002) observed that under a severe earthquake, a nonlinear response generally initiated when the compressive force in one of the braces reached to its ultimate value and buckling of that brace occurred. In other words, the main problem that is faced by conventional bracing is the buckling during compression. However, the members that act only in tension and moves freely in compression also decrease the effectiveness of the system. It is because until it reaches the start of the compressive point there is not that much buckling compressive strength. For this reason, Golafshani et al. (2006) suggested the development of such type of bracing mechanism that could endure tensile force every time with a resisting stiffness against earthquake excitation.

In this study, therefore the main focus will be not only on the mitigation of the problem associated with conventional bracing system but also on the behavior of tension only bracing member.

## METHODOLOGY

The method of doing test of this research work has been influenced by the technique of prestressing at which a small chuck plays main part to achieve goal. The strand chuck is also known as wedges, grippers and lock off.

### PREPARATION OF THE TEST ASSEMBLAGES FOR THE TEST

#### Cylindrical wedge-type non-compressive device

The Cylindrical wedge-type non-compressive device has three parts (i) Conical shaped Grip (ii) Outer cylinder (iii) Cover of the cylinder.

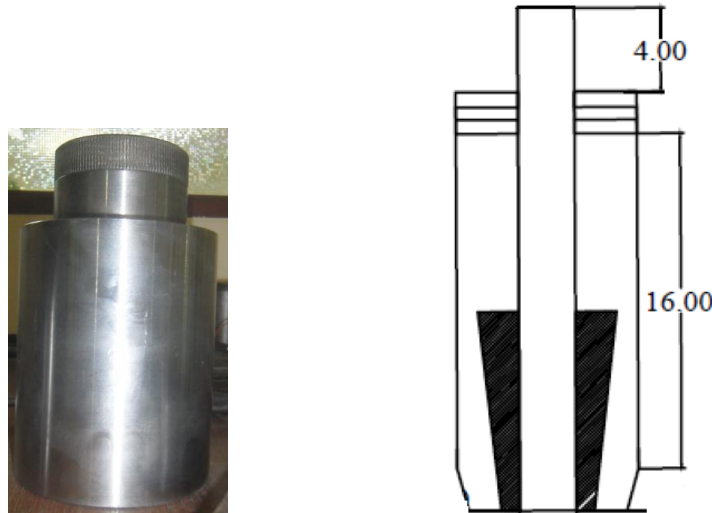


Fig. 1: (a) Outer cylinder (b) Cross sectional view of Cylinder with wedge grip (All dimensions are in cm)

#### Sacrificial Bar

For the UTM test, a 12mm diameter rod reduced to 9mm diameter in the yielding part has been used. Total six numbers of specimens are with this dimension. For the top part 27mm diameter bar with 12mm groove of 6cm length has been used as an adapter. From the top edge of 12mm bar 6cm length is threaded to screw inside the adapter rod.

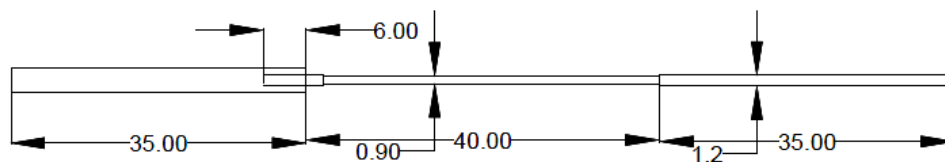


Fig. 2: Schematic diagram of specimen for uniaxial test (All Dimensions are in cm)

#### Loading protocol for testing

Since no specified loading protocol has been depicted in the past research for non-compressive bracing system, loading provision for BRB in Fema-450 has been chosen to do the final test.

#### Instrumentation

For the instrumentation purpose, load cell of capacity 50 ton, LVDT and strain gages were installed to measure force, the linear displacement and strain respectively. Strain gages are put at 5cm, 20cm and 35 cm from the bottom portion of yielding part. According to this placement, the strain gauges will be introduced in this report as top, middle and bottom strain gauge respectively. Finally all the instruments were connected to the data logger to record the respective data.

### Testing

After completing all the arrangement shown in figure 3, displacement control test has done following the loading protocol. Total six specimens have been tested by universal testing machine. This whole process has been controlled from the observing data of data logger. Among six, three specimens have been tested till rupture.



Fig. 3: Test set up for uniaxial testing at Structural Engineering laboratory at AIT

### Brace for actuator test

For the actuator test, 27 mm diameter rod reduced to 16mm diameter in yielding part has been used as bracing. Two piece of specimen are connected with a coupler. Only one specimen has been subjected to the test with hydraulic actuator.

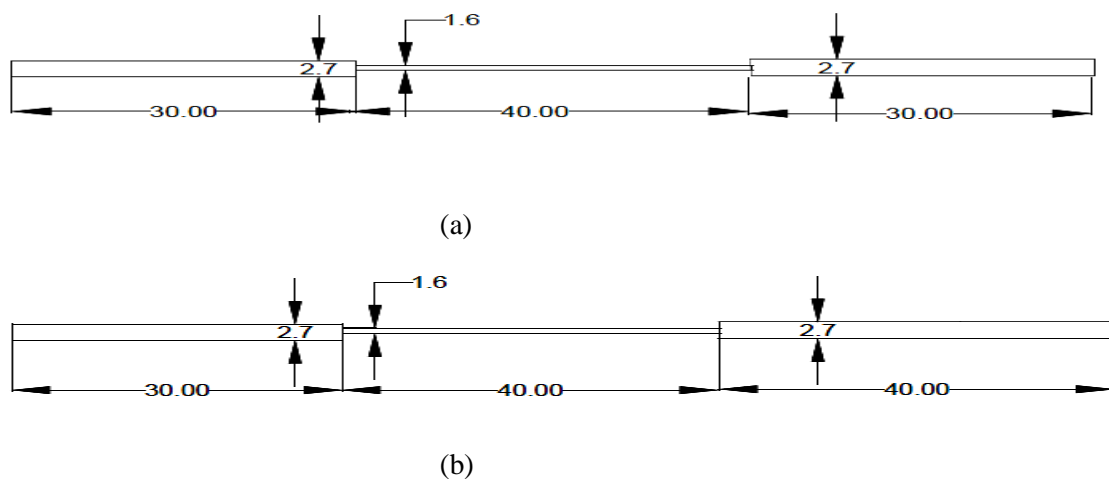


Fig. 4: Specimen for test with actuator (a) upper part (b) lower part (All Dimensions are in cm)

### Coupler

To avoid the yielding in the coupler, the area of the coupler kept higher than the expected yielding zone of 16mm diameter portion. The thickness of the coupler is 12mm and outer diameter is 51mm. Total length of coupler is 10cm.

### Steel plate

For the test with actuator, two steel plates are used. Between these two plates, one is used as gusset plate and another one is used as connector with the hinge support. Both plates are 10mm thick.



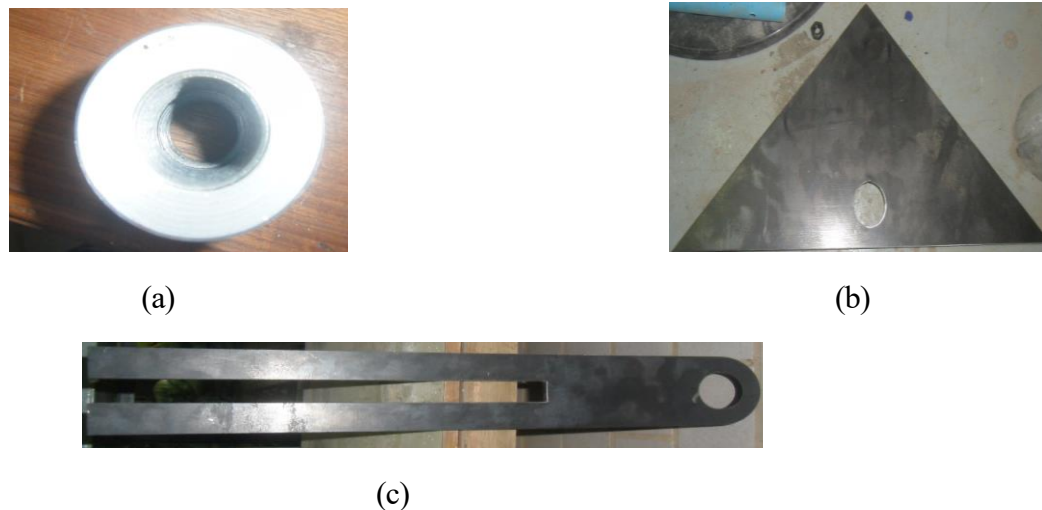


Fig. 5: (a) 12mm thick coupler (b) Gusset plate (c) Steel plate for using at the lower portion of bracing

#### ***Set up of Test Assemblages for second phase of final test***

The specimen has been subjected to quasi-static cyclic loading. Lateral load was applied at two (2) meter height from the center of the hinge pin by a hydraulic actuator with capacity of 30ton. All components in the frame are consisted with W250x76.0 kg/m. The frame is supported by a hinge. The brace has been connected to the gusset plate with help of two steel plates (figure 3). Both the steel plates were bolted in such a way that the outer cylinder of the energy dissipating device can be fit well in between. A clearance length of cm 15% of the yielding length of brace has been kept between the gusset plate and brace to restrain the brace from hitting the gusset plate. The another end of the brace has been welded with a steel plate of thickness 10mm and thus the plate has been connected to another hinge support.

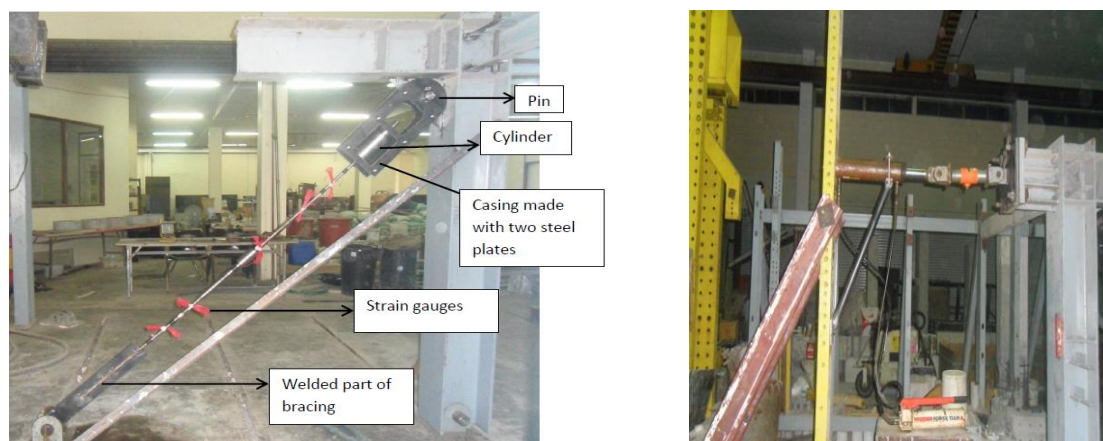


Fig. 6: Set up of brace with frame at Structural Engineering laboratory at AIT

#### ***Instrumentations***

Instruments were installed in order to measure the force, the displacement and the strain occurred during testing. LVDT has been placed at the tip of steel beam. Strain gages are placed at five positions. From the edge of top yielding part strain gages are provided at 5cm, 20 cm, and 36 cm distances. From the bottom edge of yielding part at 5cm and at 20 cm distance strain gages are provided.

### Test

After completion of the erection of the test assemblages the alignment has been checked. Then, the displacement transducers and the strain gages were connected to the data logger. Respective Coefficients of each LVDT, strain gage and load cell were adjusted to the data logger. All channels of the strain gages were checked to ensure that data were recorded to the data logger. Before starting the test, a zero reading was taken for all devices, except data from the actuator load cell. The lateral load implemented by the actuator to all assemblages according to the predetermined story drift. Steps of the movement in each story drift were divided into four steps. A movement to a peak backward position is termed as step one. At this time test assemblage was pushed by the actuator. In the same manner, step three was a movement to a peak forward position. In this case the, assemblage was pulled by the actuator. At Step two and four the assemblage returned to the initial position.

## RESULTS AND DISCUSSIONS

### Discussion on results got from the test with Universal Testing Machine (UTM)

#### Hysteretic Behavior

The behavior of the steel specimen under both tensile loading and cyclic axial loading perceived from the test can be explained from the force-displacement response diagram (figure 7a). The steel core did not exhibit general hysteretic behavior. For example, the hysteretic loops from tension load observed in the experiment are not stable in size and slope even the load are same. It is anticipated that non-linearity from the device itself or from the gripping device of the universal testing machine may cause this unstable hysteresis. Moreover, the specimen did not subject to any degradation of stiffness because of lateral deformation due to compression with the increment of displacement amplitude. In this research work, the slope of the hysteresis curve just after compression depended on the locking efficiency of both developed and existing UTM's lower grip.

#### Stress-Strain relationship

The entire specimens showed linear behavior with in the elastic range and after yielding there were some non-linearity in behavior of steel which was obvious. From the stress-strain diagrams (figure 7b) it is reflected the fact that during compression the grip unlocked properly as there was no negative strain values except the Poisson's strain values at the very beginning. The stress-strain diagram of the specimens underwent cyclic axial loading, did not show any compressive strain. It exposed the fact that the specimen did not suffer through any local buckling or fracture because of non-compressive device.

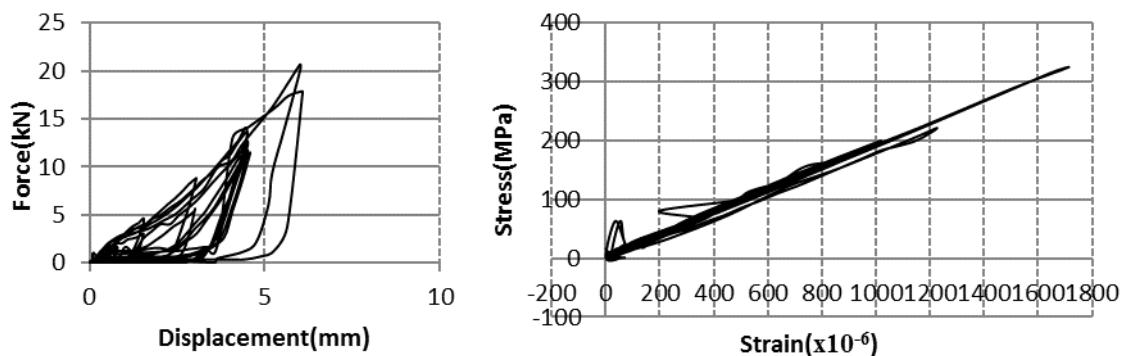


Fig. 7: (a) Force-displacement response of specimen (b) Stress-strain diagram of specimen

### Discussion on results got from the test with hydraulic actuator:

Final test has been performed by hydraulic actuator of capacity 30ton. After completing first step (6 cycles) of FEMA loading protocol it has been noticed that the recorded data of loading was very smaller than expectation as the developed grip did not hold the brace in tension.

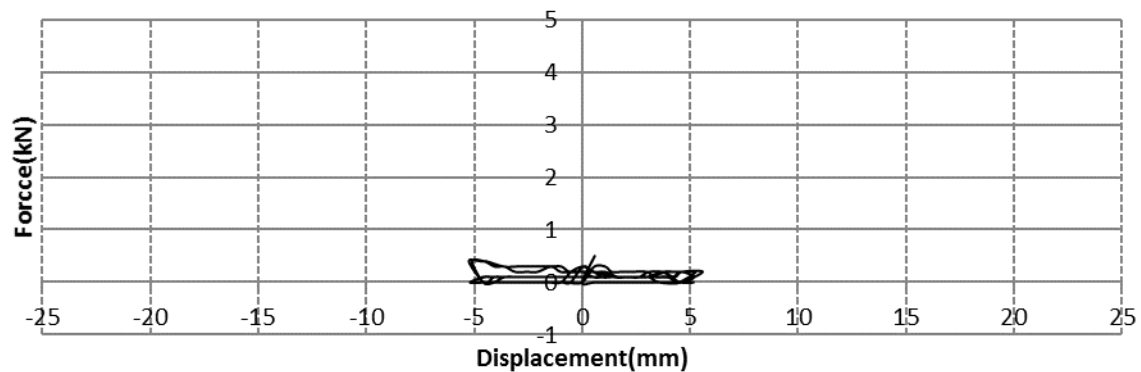


Fig. 8: Force - displacement response for 6 cycles of 5.3mm displacement

## CONCLUSIONS

The integrated intent of this research work is to develop a non-compressive device to disengage compression from bracing system. To verify the performance of the developed wedge-type grip, the entire experimental process has been divided into different phases. On the basis of the experimental results, the following conclusions can be drawn:

1. The cylindrical-wedge type compression free hysteretic energy dissipative device was experimented through various loading protocol and exhibit steel hysteretic behavior over steel plasticity under tension load. The device worked properly under compression by releasing the core plate (sacrificial steel), which prevent buckling of steel core.
2. The hysteretic loops from tension load observed in the experiment are not stable in size and slope even the load are same. It is anticipated that non-linearity from the device itself or from the gripping device of the universal testing machine may cause this unstable hysteresis.
3. The device, developed in this research, cannot be used in the inclined configuration since the orientation of wedges is affected by gravity. Pre-loaded spring to keep the wedge in place might help resolve the problem. Furthermore, the steel casing which keeps the core steel in proper alignment might resolve problem from inclined configuration.

## REFERENCES

- Di , S. L., & Elnashai, , A. S. (2009). Bracing systems for seismic retrofitting of steel frames. *Journal of Constructional Steel Research*, 65(2), 452-465.
- FEMA 356:Prestandard and commentary for the seismic rehabilitation of buildings,2000. Federal Emergency Management Agency.
- Golafshani, A. A., Rahani, E. K., & Tabeshpour, M. (2006, june 6). *A new high performance semi-active bracing system*. *Engineering structures*, 28(14), 1972-1982. Retrieved september 2014, from www.sciencedirect.com
- Hussain , S., Benschoten, P. V., Satari , M. A., & Lin, S. (2006). Buckling restrained braced frame (BRBF) structures: analysis, design and approvals issues. In Proceedings of the 75th SEAOC Annual Convention, Long Beach, (pp. 13-16).
- Kumar, K. S. (2012). A Design Methodology For Supplemental Damping For Seismic Performance Enhancement Of Frame Structures. . *Asian Journal Of Civil Engineering (Building And Housing)*, 13(5), 659-678.
- Lin, Y. Y. (2003). Direct displacement-based design for building with passive energy dissipation systems. *Engineering structures*, 25(1) , 25-37.
- Tremblay, R. (2002). Inelastic seismic response of steel bracing members. *Journal of Constructional Steel Research*, 58(5), 665-701.

## **EFFECT OF DELAY IN CASTING ON COMPRESSIVE STRENGTH OF CONCRETE**

M. J. A. Chy.\* , M. I. Kayes & SK. S. Ali

*Department of Civil Engineering, Bangladesh University of Engineering and Technology, Dhaka,  
Bangladesh*

*\*Corresponding Author: jakiulbuet08@yahoo.com*

### **ABSTRACT**

The casting of concrete may be delayed from the time of mixing due to many reasons, which can affect the compressive strength of concrete. This investigation showed that loose the casting delay causes considerable variation of the compressive strength of concrete. A large number of 4” inch by 8” inch cylinders have been cast for this study. The cylinders were cast at different times after mixing with water. The cylinders were tested at different dates to see the effect of curing time and age on compressive strength of concrete. OPC has been considered in this study for the testing compressive strength of concrete. The results of this study indicate that casting delay of concrete does not decrease the compressive strength rather it helps to enhance the strength. This investigation has been made for W/C ratio of 0.5 and 0.6 respectively. Results are quite encouraging which may invite interest to the researchers for further study by involving more parameters.

Keywords: Concrete; workability; compressive strength; water-cement ratio; mechanical properties; time independence; the strength of materials.

### **INTRODUCTION**

Concrete industries and especially ready mixed concrete industries are faced with a common problem is known as casting delay, which usually results in a considerable loss of workability, so that concrete may be unworkable. Delay in the production and delivery of ready-mixed concrete is inevitable, which is influenced by the location of construction sites in relation to the central batching plant and traffic conditions on the route. On the other hand, improper methods of handling, lack of site organization, work scheduling, and breakdown of equipment are some other causes of unexpected long delays. So in this research, it is tried to investigate the relation between casting delay compressive strength of concrete.

Most of us have a silly notion that the delay of the casting of concrete causes reduction of strength significantly. For this they try to place the concrete as soon as possible otherwise concrete may be unworkable. If delay casting is unavoidable, which causes a considerable loss of workability it is a common practice in our country to add some water into the concrete mix. The addition of extra water is known as Re-tempering with water. That is why it is required to know the effect of Delay casting of concrete and re-tempering with water on strength. Gonnerman and Woodworth investigated re-temp that it was a harmful practice as the strength is lowered due to increase in w/c ratio of the re-tempered mix.

By studying the behaviour of concrete made with locally available Ordinary Portland cement (OPC) casting both before and after initial setting time with two different water-cement ratios(0.6 or 0.5), anyone can create a general scenario of the strength gain characteristics of concrete. And which will be helpful for the construction planning of building construction spatially for ready mixed concrete industries? This will give idea how much strength will be reduced if water is added after initial setting time because sometimes people of our countries are used to add extra to increase workability of concrete

## **METHODOLOGY**

The properties of different ingredients of concrete (coarse aggregate, fine aggregate, and cement) would be tested. Then the amount of different ingredients of concrete for the target compressive strength of 3000 psi and 4000 psi would be calculated by ACI mixed design method of concrete of ordinary Portland cement (OPC). Concrete cylinders would be cast using OPC for two different target design strengths. The cylinder would be cast after a certain interval. Additional water would be mixed with 3 initial setting times. The sample would be cured continuously until they are tested. The compressive strength of concrete samples would be tested at 7 days, 14 days and 28 days of age of concrete. The graph would be plotted showing the compressive strength of concrete with age which would represent the compressive strength variation of concrete made with OPC at different delay casting of time. Also, the compressive strength variations of tempering with water would be studied.

Different physical properties of both fine and coarse aggregate would be tested according to ASTM codes. Fineness modulus, Unit weight and specific gravity of coarse aggregate would be performed according to ASTM C136, ASTM C29, and ASTM C127 respectively. Fineness modulus, bulk specific gravity and absorption capacity of fine aggregate would be performed according to ASTM C136 and ASTM C128 respectively. Normal consistency, initial and final setting time the direct compressive strength of cement mortar would be tested according to C 187, C191 and C109 respectively. Concrete testing is done by several steps such as preparation of mold, use of the batch mixture, controlled time of mixing, Placing and compacting the mixture, Vibration of concrete, Casting of concrete, Curing of concrete, Compressive strength test of concrete and finally calculate the compressive strength of concrete.

## **RESULTS AND DISCUSSIONS**

This study gives a general scenario of the strength development characteristics of concrete made with locally available Portland composite cement (PCC). These finding will be useful for design and construction planning of concrete structure especially for ready mix concrete industries for calculating the transportation time on the basis of delay casting time. My findings of this investigation are described in graph below:

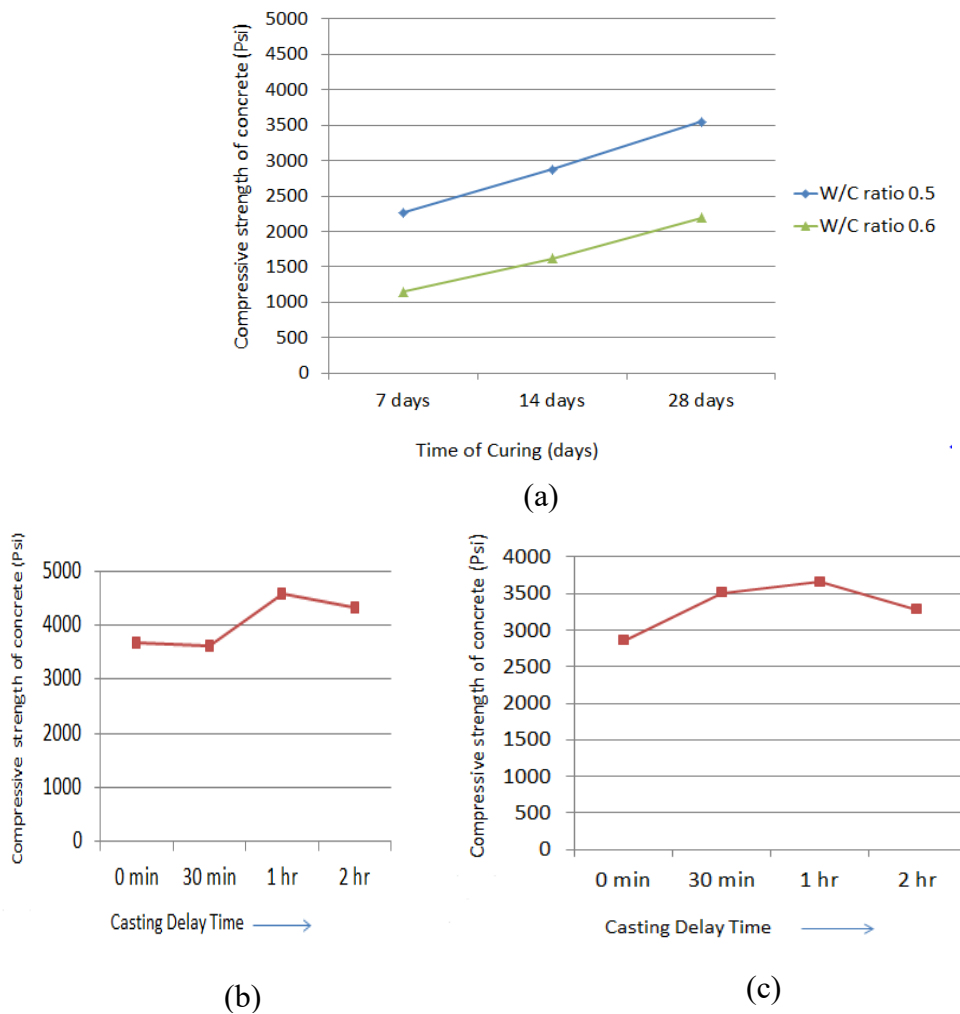


Fig. 1: (a) compressive strength vs. Time of curing (days); (b) compressive strength vs. Casting delay time(for w/c ratio 0.5); (c) compressive strength vs. Casting delay time(for w/c ratio 0.6).

By analysing those graph we observe the following behaviour:

- 1) Graph (a) indicates that with the increase of water cement ratio compressive strength increases. But we know up to a certain value of water cement ratio compressive strength increases after that compressive strength decreases with the increase of water cement ratio.
- 2) Graph (b) and (c) indicates that with an increase in casting delay time the strength of concrete increases (after an initial setting time until it cast). But after an optimum time, the strength of concrete begins to decrease.

## CONCLUSIONS

From the experimental investigation based on general and comparative study of cylinder compressive strength at different time and different age of two fixed w/c ratios, following conclusion can be drawn

- In the general compressive strength of concrete made with Ordinary Portland cement (OPC) increases due to casting delay (0 min, 30 min, 60 min, 120 min) up to an optimum time. (Initial setting time)
- In general, the casting attains maximum strength at 60 min. Casting delay time after which the strength starts decreasing.
- With the increase in W/C ratio compressive strength of concrete decreases

## **ACKNOWLEDGEMENTS**

First & foremost, thanks to almighty God for his graciousness, unlimited kindness &with the blessings of whom the good deeds are fulfilled.

I offer my sincerest gratitude to my supervisor Dr. SK. Sekender Ali, Professor, Department of Civil Engineering, BUET, Dhaka. Without his prudential advice and inspiring support, the project would not have been successful.

I wish to convey my special thanks to the staff of Civil Engineering Concrete lab, BUET who helped me to overcome the daily difficulties.

I would also like to thank all of my friends& well-wishers for their assistance.

## **REFERENCES**

Bako ca, A., Ozkul, M.H. and Artirma, S. “Effect of chemical admixtures on workability and strength properties of prolonged agitated concrete”, *Cem.& Conc. Res.*, 28(5), pp. 737–747 (1998).

Cheong, H.K. and Lee, S.C. “Strength of retempered concrete”, *ACI Mat. J.*,90(3), pp. 203–206 (1993).

Erdogdu, S., Arslantürk, C. and Kurultai, S. “Influence of fly ash and silica fume on the consistency retention and compressive strength of concrete subjected to prolonged agitating”, *Const. Build. Mat.*, 25, pp.1277–1281(2011).

Hawkins, M.J. “Concrete retemperingstudies”,*ACI J. Proc.*, 59(1), pp. 63–72 (1962).

Ravina, D. “Slump retention of fly ash concrete with and without chemical admixtures”, *ACI Conc. Int.*, 17, pp. 25–29 (1975).

## **EXPERIMENTAL STUDY TO INVESTIGATE THE USABILITY OF FLY ASH AS ADMIXTURE OF CEMENT**

Sampa\* & A T. M. Masum

*Department of Civil Engineering, Military Institute of Science and Technology, Dhaka, Bangladesh  
\*Corresponding Author: sampakhanam@yahoo.com*

### **ABSTRACT**

Concrete strength is considered as a function of water to cementitious materials (w/c) ratio, aggregates quality, admixtures and proper quality control. But the properties of cement such as cement ingredients and fineness also affect the strength and workability of concrete. In this research, total of four concrete trial mixes with different amount of fly ash were prepared and investigated for 45 days in which fly ash was used as the replacement of Ordinary Portland Cement (OPC) and other parameters were kept constant. The experimental results showed that the strength gaining rate (SGR) for concrete containing 100% OPC is higher at early ages and almost negligible at later ages. On the other hand, SGR of concrete containing 25% fly ash and 75% OPC is higher at later ages rather than at early ages. It is interesting to note that fly ash content more than 25% significantly decreases the concrete strength and workability. In industrial application where early strength is not a primary requirement, 25% fly ash as an admixture of OPC is recommended as materials cost, workability and compressive strength consideration.

Keywords: Fly ash; OPC; strength gaining rate; mineral admixture

### **INTRODUCTION**

In the year of 1950s, ready-mixed concrete with design strength of 35 MPa was considered as HSC. The increased use of chemical and mineral admixtures in the decade of 1960s quickly led to significant increases in attainable compressive strength and in the 1960s, 41 MPa and 52 MPa concrete were produced commercially. In the early 1970s, 62 MPa concrete was produced. Today, compressive strengths approaching 138 MPa have been used in cast-in-place buildings. Laboratory researchers using special materials and processes have achieved compressive strength of concrete in excess of 800 MPa [Schmidt and Fehling, 2004].

The major difference of HSC from conventional concrete is essentially the use of Supplementary Cementitious Materials (SCM) or mineral admixtures. The Supplementary Cementitious Materials physically act as a filler to decrease the average size of the pores in the matrix of HSC [Safiuddin and Zain, 2006] which is known as micro filling. Most of the SCMs contribute to increase the strength of HPC due to enhanced cementing efficiency resulting from secondary hydration or pozzolanic reaction [Safiuddin, 1998; Safiuddin and Zain, 2006]. Some of the SCMs are Fly Ash (type-F, type-C), Silica Fume, Ground Granulated Blast-furnace Slag (GGBS), carbon black powder, and anhydrous gypsum based mineral additives. Most widely used SCM for HSC are obtained as industrial by-products.

Fly ash reduces the water demand and thus improves the workability of concrete. In contrast, Silica Fume and rice husk ash increase the water demand due to lower particle size and excessive surface fineness and thus decrease the concrete workability for given water content but increase density of concrete mix [Safiuddin and Zain, 2006]. The content of Silica Fume differs from 3% to 30% by weight of cement depending on the strength and durability requirements. However, the practical and economical optimum content of Silica Fume is chosen toward 10% to 15% due to high cost and workability problem encountered in fresh concrete [De Larrard and Malier, 1994]. Class C Fly Ash has been used with a content varying from 20 to 40% [Ellis, 1992] whereas the content of Class F Fly Ash is usually limited to 15% to 25% and the GGBS is in the range of 30% to 50% in HSC [Safiuddin, 1998; Safiuddin and Zain, 2006].



The chemical admixtures used for HSC are mainly Water Reducer (WR), High Range Water Reducer (HRWR) or super plasticizers. Sometimes to increase the setting time, retarder is also used. HRWR can reduce the quantity of mixing water in the range of 12 to 45% [Safiuddin, 2008; ASTM C 494/C 494M-99a, 2002]. Very high dosage of HRWR might cause segregation and bleeding, delayed setting, plastic shrinkage, and air entrainment in fresh HSC and may delay cement hydration. The dosage limit of liquid HRWR for HSC generally varies from 5 to 20 l/m<sup>3</sup>, but dosage limit should be higher for hot weather than cold weather [Aitcin et al., 1994].

The plasticizing effect and water reduction will be higher if HRWR or WR are mixed with damp concrete [ACI 211.4R-93, 1998]. According to Canadian Association's Preliminary Standard A 266.5-M 1981, tests have shown that HRWR is most effective and produce the most consistent results when added at the end of the mixing cycle after all the ingredients have been introduced and thoroughly mixed.

Following are the objective of this study:

1. To investigate the parameters that affects the strength of concrete and finding the optimum Fly Ash content as ingredients of cement that produce High Performance concrete.
2. To develop a mix design with the above combination by trial and error procedures to achieve desired compressive strength and workability of concrete using locally available materials of Bangladesh.
3. To optimize the cost of concrete

## **METHODOLOGY**

In this study, ingredients used were ½” L/C Stone (Table 1), Sylhet sand of FM 2.5 (Table 2), Ordinary Portland Cement (OPC), Class F fly ash (Table 3) and admixture named as Glenium ACR 30 (JP) (Table 4) which are locally available in Bangladesh. The properties of materials such as specific gravity and absorption capacity of coarse and fine aggregates and crushing values of coarse aggregates are determined according to the procedure specified in ASTM C127, ASTM C128, ASTM C29 and BS 812. The graded aggregates, both fine and coarse aggregates, were washed and soaked in water for 24 hours and then air-dried to Saturated Surface Dry (SSD) condition before mixing with other ingredients. The proportioning of the materials was done according to British method of mix design. The mixer machine (rotating drum) was used for mixing the various constituents of concrete. The ingredients were fed into the machine into three layers. In the first layer one-third of estimated sand, cement, and coarse aggregate fed into the mixer machine and 30 sec time was allowed to mix the ingredients thoroughly. Simultaneously other two layers of ingredients fed into the machine and 30sec time was allowed for each layer to mix thoroughly. After the ingredients were mixed thoroughly about 70% of the water was poured in the machine then 60 sec time was allowed for the mixing of all three layers. Remaining 30% of the water was mixed with admixtures and then it was fed in the mixer machine with damp concrete and allowed to mix about 40 sec. If the admixture is fed with dry mix, it will not mix thoroughly with other ingredients. When mixing was completed, the mixtures were poured on a large tray. The workability of the fresh concrete was measured with a standard slump cone immediately after mixing. The test specimens were cast in steel mold of 100 x 200 mm cylinders. The concrete was poured into the mold in three layers each layer being compacted approximately 20 sec with a vibrator nozzle. After compaction of the third layer the upper surface of the concrete was levelled. Precautions were taken to avoid over compaction which leads to segregation of concrete. The test specimens were demolded 24 hours after casting and cured under water for 3, 7, 14, 28 and 45 days. Three cylinder of each strength level were tested after 3, 7, 14, 28 and 45 days. Concrete Compressive strength was performed on the cylinder at least after three hours of removal from the curing tank. Crushing strength was performed on the cylinder at least after three hours of removal from the curing tank. Load was applied continuously till the cracks in the specimen were developed with a rate of 2.4KN/sec according to ASTM C31. Casting procedures used in this study are shown in Figure-2.

Table 1: Properties of Coarse Aggregate

Properties	½ " LC stone
Bulk specific gravity (oven dry basis)	2.638
Bulk specific gravity (S.S.D basis)	2.652
Crushing value (%)	25
Crushed/uncrushed	crushed
Absorption capacity (%)	0.57

Table 2: Properties of Fine Aggregate

Properties	Sylhet sand
Bulk specific gravity (oven dry)	2.530
Bulk specific gravity (S.S.D)	2.579
Apparent specific gravity	2.659
Absorption capacity (%)	1.91
Fineness modulus (FM)	2.5

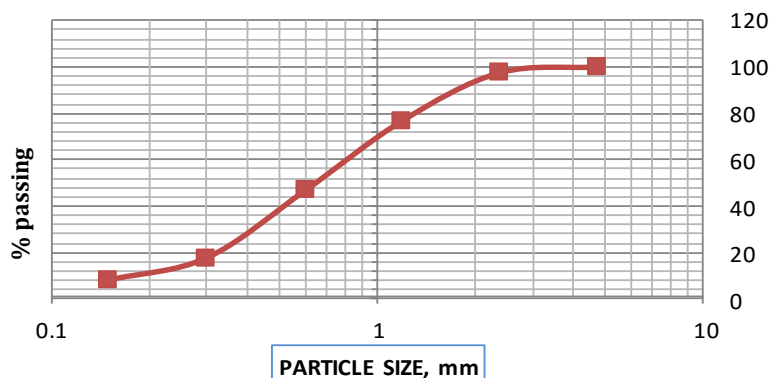


Fig. 1: Particles size distribution of fine aggregate

Table 3: Properties of Fly Ash

Properties	Fly Ash Class F
Pericles retained on 45µm sieve(%)	30%
Specific Surface Area (m <sup>2</sup> /kg)	200-250
Specific gravity	2.70

Table 4: Properties of Admixtures

Product information	Glenium ACR 30 (JP)
Specification Type	ASTM C 494 Type F
Polymer	2 <sup>nd</sup> generation poly-carboxylic ether based
Strength developments	Very early strength gain
Specific gravity	1.09±0.02 at 250C
Addition rates (per 100 cement)	400ml to 1200ml at 25 <sup>o</sup> C and dosage rate increase with temperature
Compatibility	Most of the POZZOLITH series products including POZZOLITH 55R

Table 5: Proportioning of Ingredients used to produce 1m<sup>3</sup> of concrete (Density=2400 Kg/m<sup>3</sup>)

Batch-ID	Fly Ash (%)	Design Strength (28 days) (MPa)	Ingredients used to produce 1m <sup>3</sup> concrete					
			Cement (Kg)	Coarse Aggregate (CA) (Kg)	Fine Aggregate (FA) (Kg)	Free water (Kg)	Admixture (Kg)	w/c ratio
A	0	80	636.4	990.90	633.00	140	8.30	0.22
B	15	80	540.6	990.90	633.00	140	8.30	0.22
C	25	80	467.15	990.90	633.00	140	8.30	0.22
D	30	80	445.48	990.90	633.00	140	8.30	0.22

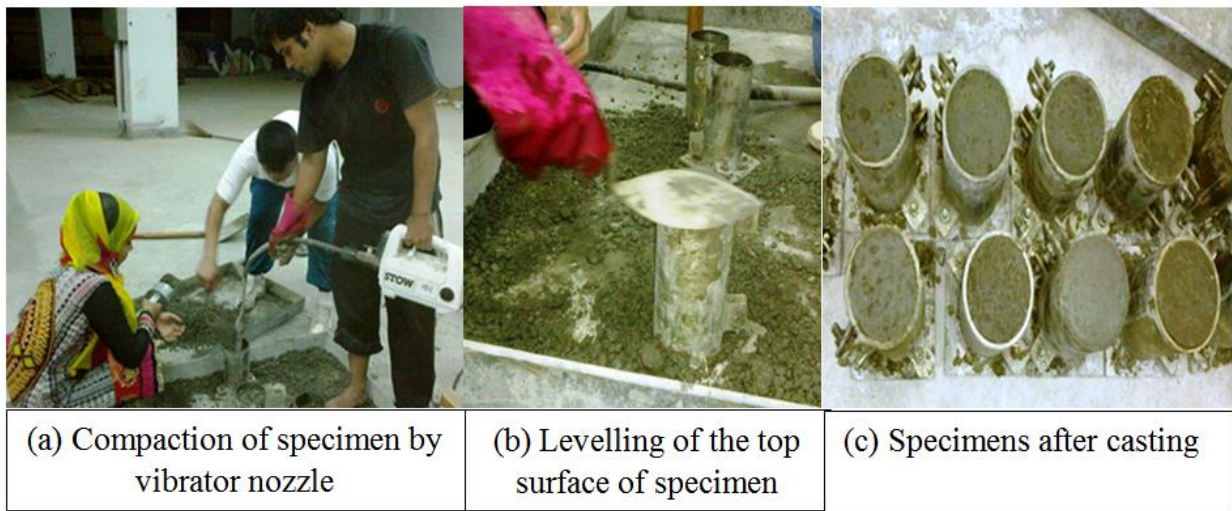


Fig. 2: Casting of Cylinder Specimens

## ANALYSIS OF RESULTS

In this section the experimental results of slump values and compressive strength of concrete for each trial mixes are represented.

Table 6: Slump values and compressive strength test results of concrete

Batch-ID	Fly Ash (%)	Design Strength(28 days) (MPa)	Experimental results of cylindrical concrete specimen					Slump values (mm)
			Compressive strength (MPa)					
			3 days	7 days	14 days	28 days	45 days	
A	0	80.00	70.97	75.38	77.84	83.41	84.10	75
B	15	80.00	38.87	47.82	55.87	63.85	69.24	100
C	25	80.00	38.00	47.33	58.33	62.28	82.23	125
D	30	80.00	33.00	40.35	45.67	50.66	60.00	150

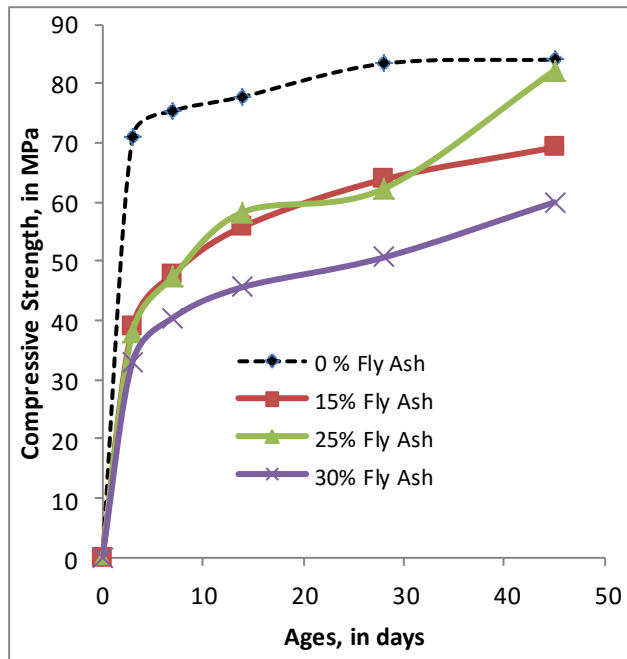


Fig. 3: Compressive Strength VS Ages of concrete

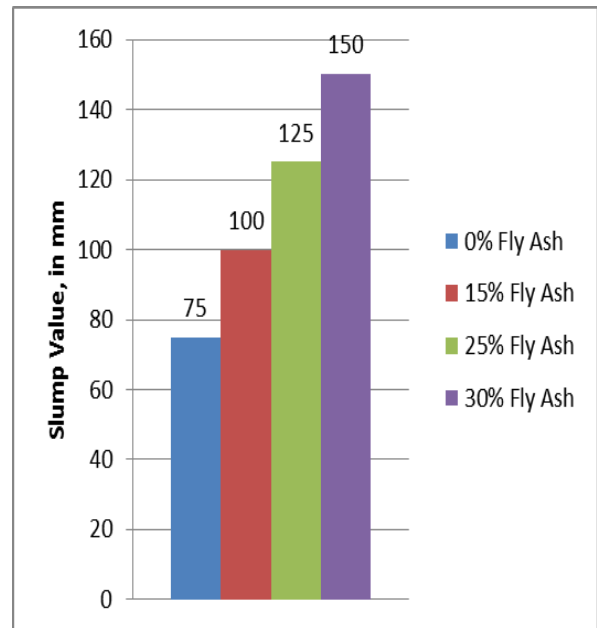


Fig. 4: Slump Value of concrete mixes with Fly Ash Content

Experimental result revealed that with the increment of fly ash content in concrete there was a significant increase in the workability. On the other hand, this increased amount of fly ash exhibited almost same compressive strength of concrete as that of prepared using only OPC at the latter stage (45 days) up to the optimum content (25%) of fly ash. It is mentionable that this phenomenon is due to the pozzolanic reaction of fly ash with cement.

### Compressive Strength:

From Figure-3, it is observed that all four trial mixes (Batch-A, B, C and D) of concrete were mixed with same materials as shown in Table-1, 2,3, and 4 except but the amount of Fly Ash varies. Moreover, these Batches were designed with 28 days compressive strength of 80 MPa but after experimental investigation it was not achieved. Followings are the sources of deviations:

1. Aggregate Size was not used as specified in the mix design. ½ inch downgrade aggregates was used.
2. According to design, the specified cement type was Type-1 Ordinary Portland Cement (OPC) but in the all three fly ash was also used which provides lower strength at early age due to the pozzolanic reaction of fly ash with cement.
3. Designed aggregate properties and used aggregate properties were different.
4. Gradation of Fine aggregate was not fully matched with the Specified (ASTM 136).

### Workability:

The workability of concrete as slump (in mm) is shown in Figure-4, slump values of concrete increase as the % of Fly Ash were increased, and thus workability of concrete also increases.

## **CONCLUSION**

I) Due to the POZALONIC reaction of Fly Ash with cement, it has lower strength at early age and higher at later age than Ordinary Portland Cement concrete. On the other hand, incorporation of Fly Ash as partial replacement of Ordinary Portland Cement increases the workability and decrease the materials cost of concrete.

II) Proper gradation of aggregate having smaller inter-particle voids, smaller size aggregate and appropriate compaction increase the strength of concrete

III) With the increase of cement contents the strength of concrete also increases.

IV) Lower water-binder ratio along with High Range Water Reducer and retarder are essential to produce High Strength

## **REFERENCES**

Aïtcin, PC., 1994. The use of superplasticizer in high performance concrete, *High Performance Concrete: From Material to Structure*, E & FN Spon, London, UK, pp.14-33.

De Larrard, F., and Malier, Y., 1994. Engineering properties of very high performance concretes, *High Performance Concrete: From Material to Structure*, 1st English Language Edition, E & FN Spon, London, UK, pp. 85-114.

Safiuddin M., 1998. Influence of Different Curing Methods on the Mechanical Properties and Durability of High Performance Concrete Exposed to Medium Temperature, M.Sc. Thesis, The National University of Malaysia, Bangi, Malaysia.

Safiuddin M., and Zain M.F.M., 2006, "Supplementary cementing materials for high performance concrete", *BRAC University Journal*, Vol. 3, No. 2, pp. 47-57.

Schmidt, M., Fehling, E., and Geisenhanslüke, C., 2004," *Proceedings of the International Symposium on Ultra High Performance Concrete*, ed., Kassel University Press, Kassel, Germany, pp. 11–23.

## **EFFECT OF WASTE GLASS ON THE PROPERTIES OF CONVENTIONAL CONCRETE**

S. Y. Morshed\*

*Department of Civil Engineering, Khulna University of Engineering & Technology, Khulna,  
Bangladesh*

*\*Corresponding Author: yadmorshed@gmail.com*

### **ABSTRACT**

World is producing a huge amount of waste glass, that is an environmental concern. These waste glass provide an available resource for potential use in concrete by partially replacing coarse and fine natural aggregates. The objective of this study was to test the fundamental properties of concrete that utilized 15%, 30%, 40% and 50% waste glass as a partial replacement for coarse and fine natural aggregates in conventional concrete. This study also compared the results with conventional concrete. The outcome of this research demonstrate that waste glass has negative impact on the compressive strength of concrete. On the other hand, waste glass improve resistance against chloride ion penetration and lesser the water sorptivity compared to the conventional concrete.

Keywords: waste glass; concrete; strength; chloride ion penetration and water sorptivity.

### **INTRODUCTION**

The generation of waste is vastly increased due to rapid growth of population and industry. So, worldwide recycling of waste materials has become a serious issue (Taha and Nounu, 2009). Numerous efforts have been made within the concrete industry to use waste glass (WG) as a partial replacement for natural aggregates or ordinary portland cement (OPC), with work using crushed WG as a concrete aggregate first being published in 1974 (Johnston, 1974). Numerous research works were performed to examine the opportunity of reusing waste recycled glass in concrete and construction industry as alternative solution to reduce the generated bulk of mixed-color waste recycled glass, and establish solid ground for clear understanding and further investigation (Dhir et al., 2004; Jin et al., 2000; Shayan and Xu, 2003). Most of the past research on the use of glass aggregates in concrete engrossed on the mitigation of the deleterious alkali-silica reaction (ASR).

Due to the strong reaction between the alkali in the cement and the reactive silica in the glass, the use of glass in concrete has been previously found to not be satisfactory due to excessive expansion and strength loss (Almesfer and Ingham, 2014). This effect of alkali-silica reaction (ASR) can be mitigated by using 20% fly ash of weight of ordinary Portland cement (Wright et al., 2014).

This paper investigated the effect of partially replacement of coarse and fine aggregate by glass aggregate in conventional concrete, where Portland Composite Cement was the key binding material. The objective of this study was to test the fundamental properties of concrete that utilized 15%, 30%, 40% and 50% waste glass as a partial replacement for coarse and fine natural aggregates in conventional concrete. This study also compared the results with conventional concrete.

### **METHODOLOGY**

One of the most important tasks of this study was collection of waste glass and preparation of glass aggregate. The main ingredient of study waste glass was collected from locally available glass stores, domestic wastes and wastes of construction work [Fig. 1]. The glass was crushed to sand size using a standard Los Angeles (LA) abrasion machine to obtain a fineness modulus similar to the natural sand

used in this study [Fig.2]. Although the FM is a rough estimation of consistency across mixtures, its simplicity evaluation provides a basis for quality control of workability (Mindess et al., 2003). The coarse glass aggregate [Fig. 3] was collected by separating from the crushed aggregate using a No. 4 ASTM standard sieve. Crushed glass retained on NO. 4 sieve was used as coarse aggregate and passing material was used as fine aggregate.



Fig. 1: Collected Waste Glass



Fig. 2: Fine Glass Aggregate



Fig.3: Coarse Glass Aggregate

The natural sand used in this thesis was locally available river sand, locally known as Sylhet sand, adhering to ASTM C33 (ASTM, 2011a), with a saturated surface dry (SSD) specific gravity of 2.4, water absorption 4.1% and fineness modulus (FM) of 2.9. The dry rodded unit weight of the natural sand was determined 1600 kg/m<sup>3</sup>. The glass sand adhered to the ASTM C33 (ASTM, 2011a) gradation and had a specific gravity of 2.6 and water absorption 0.00%. The FM was maintained at 2.9 ± 0.1. The glass sand also had dry rodded unit weight of 1795 kg/m<sup>3</sup>. The natural coarse aggregate used in this research was crushed stone chips adhered to the ASTM C33 (ASTM, 2011a) gradation as a #57 coarse aggregate with a dry rodded unit weight of 1495 kg/m<sup>3</sup>, SSD specific gravity of 2.73, and water absorption 0.70%. As mentioned earlier, coarse glass aggregate was separated from the crushed waste glass by using ASTM standard No. 4 sieve and then they were prepared to adhere the ASTM C33 (ASTM, 2011a) gradation as a #57 coarse aggregate with a dry rodded unit weight of 1522 kg/m<sup>3</sup>, SSD specific gravity of 2.6, and water absorption 0%.

Table 1: Proportion of concrete mixtures (kg/m<sup>3</sup>)

Mix Identifier	Cement	Coarse Aggregate		Fine Aggregate		Water
		Glass	Stone chips	Natural Sand	Glass Sand	
R0	364	-	930	777	-	200
R15	364	140	790	661	117	200
R30	364	279	651	544	233	200
R40	364	372	558	466	311	200
R50	364	465	465	389	389	200

In this study, total five batches of concrete were cast and all the mixture were designed for 4000 psi compressive strength at 28 days after casting. The proportion of different ingredients of concrete is given in Table 1. In the table R represent replacement and the lateral digits represents the percent of natural coarse and fine aggregate was replaced by glass aggregates. Proportioning of concrete was performed according to ACI 211.1 and 100×200 mm concrete cylinder was cast and compacted according to ASTM C31 (ASTM, 2000) in two layers with 25-rod blows per layer.

The uniaxial compressive strength of concrete was determined at 1, 3, 7 and 28 days after casting. Test for static elastic modulus was performed at 28 days and Rapid Chloride penetration test (RCPT) and water sorptivity test were at 90 days after casting.

### ***RCPT and Water Sorptivity Test***

The ability of concrete to resist penetration from aggressive elements (i.e., chloride ions) is key to the durability of reinforcing steel in concrete.

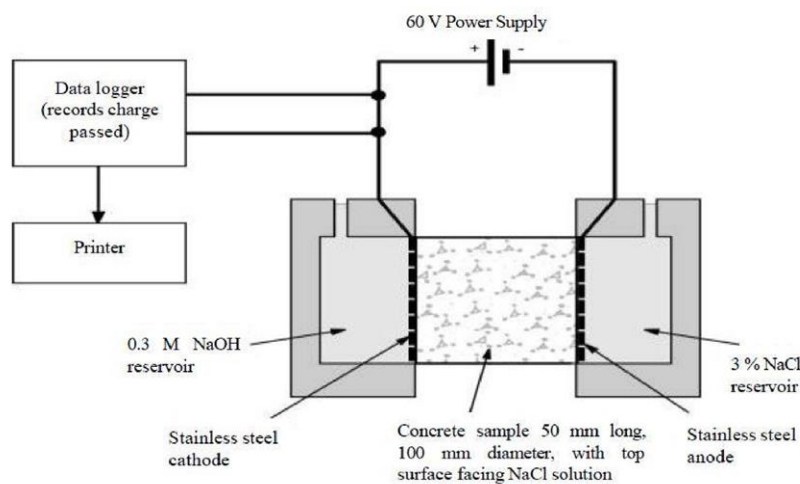


Fig. 4: Schematic diagram of RCPT test

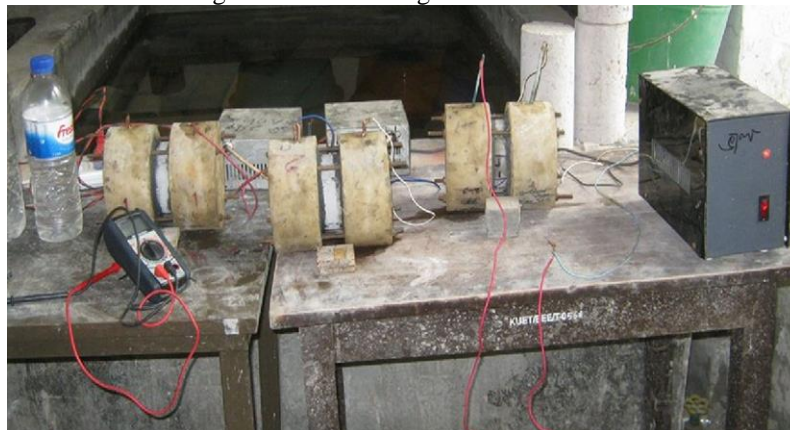


Fig.5: Experimental Setup of RCPT test

To evaluate the resistance of concrete against chloride penetration (RCPT), this test was performed on one specimen per mixture at the age of 90 days. Concrete cylinders 100×200mm in size were prepared and cut into 50mm thick disks from the center of the specimen. The test was performed according to ASTM C1202 (ASTM, 2010). A schematic diagram of RCTP test and experimental setup of this test are shown in Fig.4 and Fig.5 respectively.

Water sorptivity test of concrete was performed according to ASTM C1585 (ASTM, 2011b). For this test 50 mm thick disk from a 100×200mm concrete cylinder and they were kept at 60° C for three days. Then they were kept in atmospheric condition for 15 days.



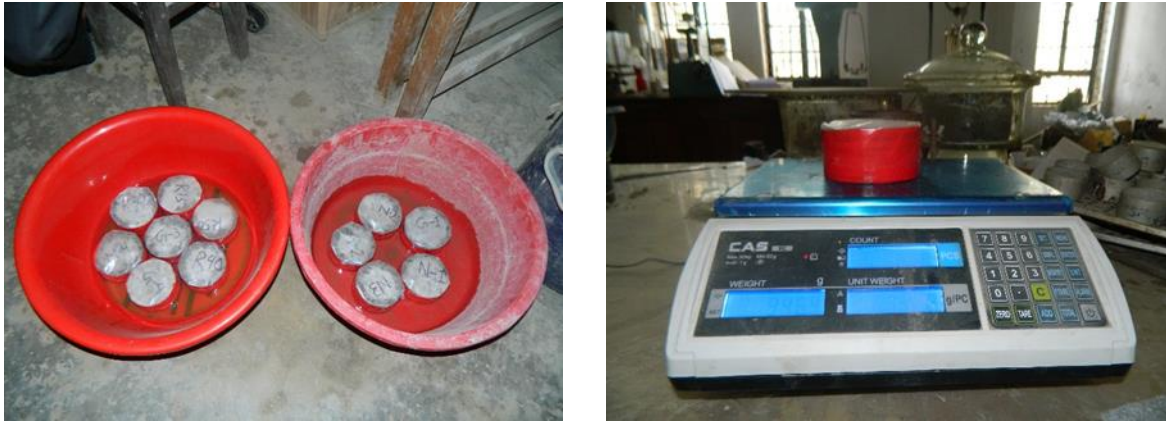


Fig. 6: Experimental setup of water sorptivity test

### RESULTS AND DISCUSSION

The compressive strength gain curve for all five mixtures are presented in Fig. 7 and comparison of compressive strength is made [Fig. 8] at 1, 3, 7 and 28 days after casting. All of the mixtures were designed for 4000 psi. None of the mixtures attained the designed strength 4000 psi except R 0, where no waste glass was used. The maximum strength gained 3755 psi for 30% replacement of natural aggregates by glass aggregates, which is 93.88% of the design strength. Minimum strength was found 74.98% of designed strength for 50% replacement of natural aggregates

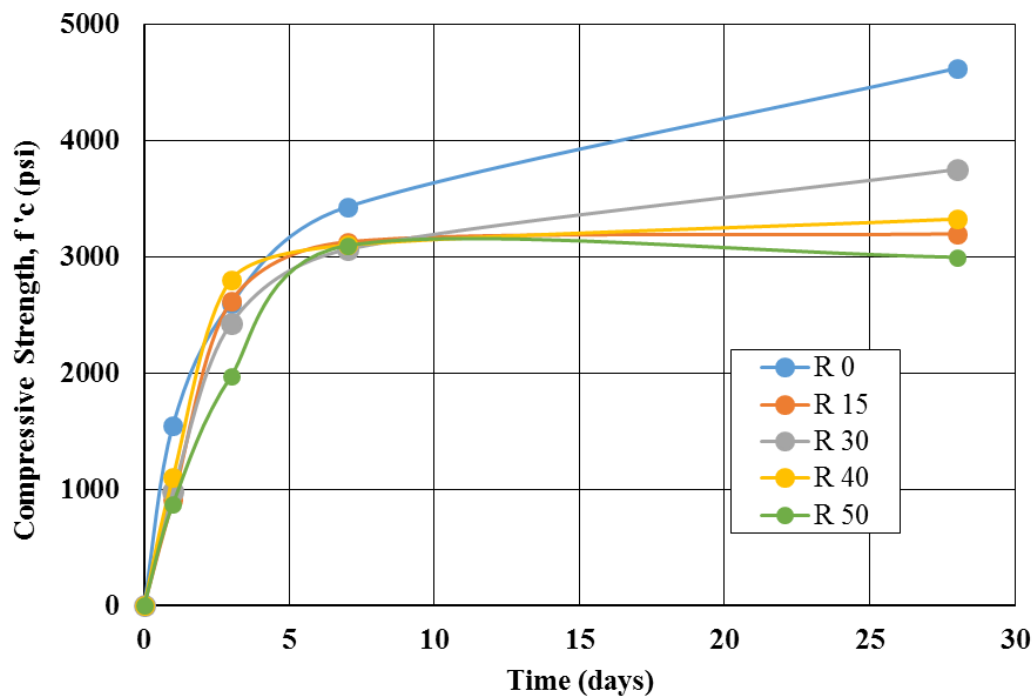


Fig. 7: Compressive Strength Gain Curves

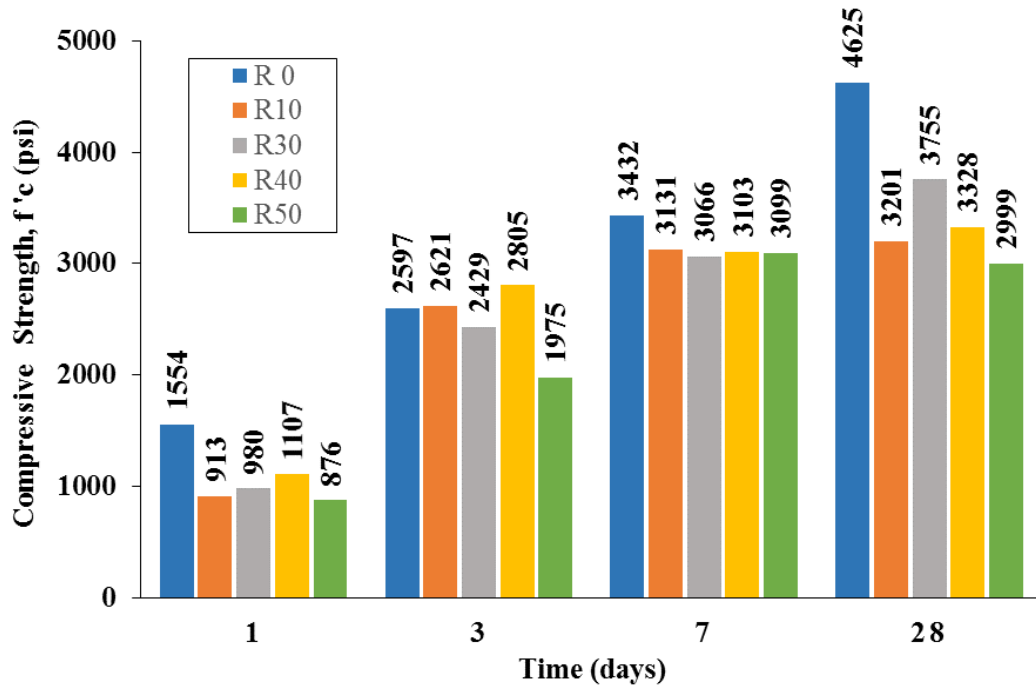


Fig. 8: Comparison of Compressive Strength

Elastic modulus of concrete was determined at 28 days after casting. Maximum elastic modulus was found 552 ksi for R50 mixture [Fig. 9], where 50% replacement of natural aggregate was made. On the other hand, conventional concrete (R0) attained 456 ksi which is less than that for R50.

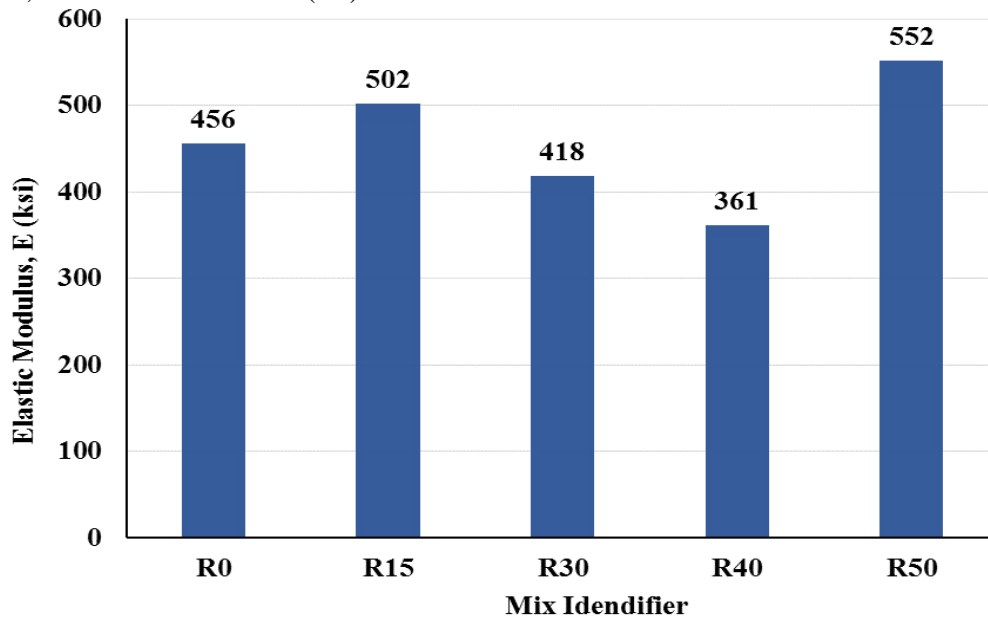


Fig. 9: Comparison of Static Elastic Modulus

The result showed with the percentile increased of glass aggregate in concrete, the charge passed through concrete decreased [Fig.10]. The strength may reduce for a lower fracture toughness of glass particles and weaker bond between glass aggregates and cement paste. On the other hand with the increase in glass aggregates, increased resistance in charge passing. Waste glass also improved the water sorptivity of concrete than conventional concrete.

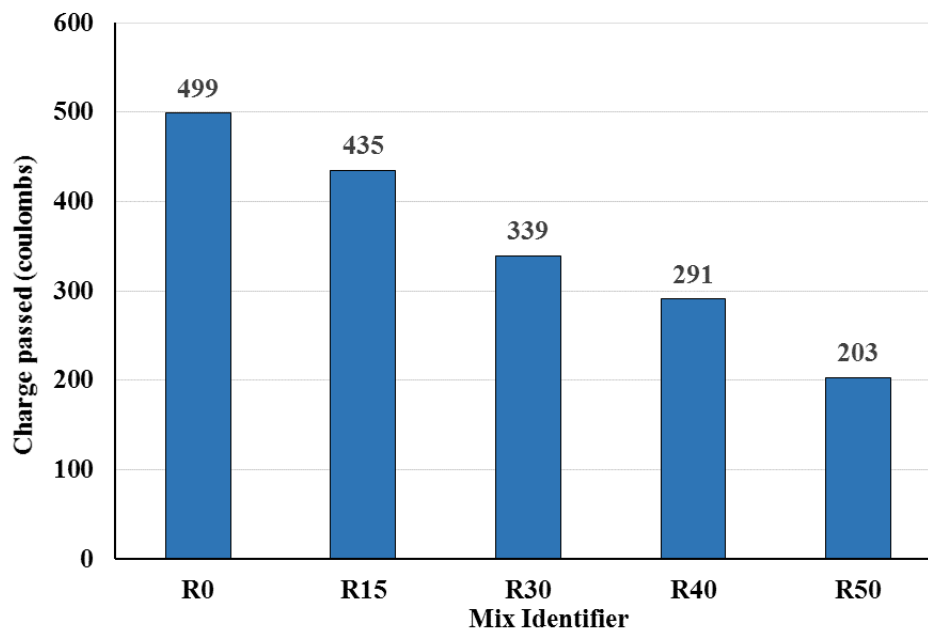


Fig. 10: Comparison of RCPT results

Table 2: Results of sorptivity test

Mix Identifier	R0	R15	R30	R40	R50
Initial sorptivity ( $10^{-4}$ mm/s <sup>0.5</sup> )	140	165	140	136	142
Final sorptivity ( $10^{-4}$ mm/s <sup>0.5</sup> )	14	14	17	15	11

The results of sorptivity test are presented in Table 2. The results showed that percentile increasing glass aggregates in conventional, both initial and final sorptivity (rate of water absorption) decrease. So introducing waste glass aggregate in conventional concrete reduce water absorption thus increase durability.

## CONCLUSION

This paper studied the effect of partially replacement of both natural fine and coarse aggregates by glass aggregate. Glass aggregate notably reduced the compressive strength of concrete. As concrete matures, the weaker bonding of glass aggregate to hydrated cement paste may become the weak link, which controls the compressive failure of glasscrete mixtures. Natural sand may allow for a better bond with cement paste given its greater surface roughness and moisture absorption capacity. On the other hand, considering durability performance glass aggregates have positive effect on conventional concrete. With percentile increasing glass aggregate in conventional concrete, RCPT and water sorptivity decreased.

## REFERENCES

- Almesfer, N., Ingham, J. 2014. Effect of waste glass on the properties of Concrete. *Journal of material Engineering*, ASCE, 06014022.
- ASTM. 2000. *Standard Practice for Making and Curing Concrete Test Specimens in the Field*. C31, West Conshohocken, PA.
- ASTM. 2007. *Standard practice for making and curing concrete test specimens in the laboratory*. C192-07, West Conshohocken, PA.
- ASTM. 2010. *Standard test method for electrical indication of concrete's ability to resist chloride ion penetration*. C1202-10, West Conshohocken, PA.
- ASTM. 2011a. *Standard specification for concrete aggregates*. C33-11, West Conshohocken, PA

- ASTM. 2011b. *Standard test method for measurement of rate of absorption of water by hydraulic-cement concretes*. C1585-11, West Conshohocken, PA.
- Dhir, RK., Dyer, RK., Tand, MC., 2009. Alkali-silica reaction in concrete containing glass. *Mater. Struct.*, 42(10), 1451–1462.
- Jin, W., Meyer, C., Baxter, S., 2000. Glasscrete—concrete with glass aggregate. *ACI Mater. J.*, 97(2), 208–213.
- Johnston, C D. 1974. “Waste glass of coarse aggregate for concrete.” *J. Test. Eval.*, 2(5), 344–350.
- Mindess, S., Young, J., Darwin, D., 2003. *Concrete*, 2nd Ed., Pearson Education, Upper Saddle River, NJ
- Shayan, A., Xu, A., 2004. Value-added utilization of waste glass in concrete. *Cem. Concr. Res.*, 34(1), 81–89.
- Taha, B., Nounu, G., 2009. Utilizing waste recycled glass as sand/ cement replacement in concrete. *J. Mater. Civ. Eng.*, 10.1061/ (ASCE) 0899-1561(2009)21:12(709), 709–721.
- Wright, J., Cartwright, C., Fura, D., Rajabipour, F., 2014. Fresh and Hardened Properties of Concrete Incorporating Recycled Glass as 100% Sand Replacement. *J. Mater. Civ. Eng.*, 10.1061/ (ASCE) MT.1943-5533.0000979, 04014073.

## **SEISMIC RISK ASSESSMENT OF EXISTING BUILDINGS OF CUET CAMPUS IN CHITTAGONG**

M. S. Uddin<sup>1\*</sup>, M. R. Alam<sup>2</sup>, M. A. R. Bhuiyan<sup>2</sup> & R. K. Mazumder<sup>3</sup>

<sup>1</sup>*Department of Civil Engineering, Southern University Bangladesh, Chittagong, Bangladesh*

<sup>2</sup>*Department of Civil Engineering, Chittagong University of Engineering and Technology,  
Chittagong, Bangladesh*

<sup>3</sup>*Institute of Earthquake Engineering Research, Chittagong University of Engineering and  
Technology, Chittagong, Bangladesh*

*\*Corresponding Author: saif08cuuet@gmail.com*

### **ABSTRACT**

Bangladesh is situated in the seismic prone area on the world seismic guide. Existing fault lines are capable of producing moderate to high magnitude earthquake in Bangladesh. The Chittagong city is quite substantial to earthquake according to proposed seismic map of Bangladesh National Building Code (BNBC). Chittagong University of Engineering and Technology (CUET) is located about 27 km away from the center of the city. This study was carried out to identify the condition of existing structures of CUET in terms of seismic risk. Rapid Visual Screening procedure especially FEMA 154 and Turkish two levels risk assessment procedures are applied to assess the seismically vulnerable buildings. A total number of 80 buildings are assessed in the first level investigation. Moreover, seven buildings (administrative and academic) were selected based on importance and considered in the second level investigation. Most of the buildings are found to be performed well during both first and second level assessments.

**Keywords:** Assessment; CUET; rapid visual screening; risk; seismic vulnerability

### **INTRODUCTION**

Bangladesh is located in the moderate seismic region in the world seismic map prepared by Global Seismic Hazard Assessment Program (GSHAP, 1992). The country is situated close to the boundary of two active plates: the Indian plate in the West and the Eurasian plate in the East and North. An earthquake of even medium magnitude on Richter scale can produce a mass graveyard in major cities of the country. For the existing buildings, it is important to identify the seismically vulnerable building before taking any strengthening measure. To survey all buildings in detail level is neither feasible nor possible. Rapid Screening Procedure is widely accepted before considering any structural detail level of investigation. Chittagong University of Engineering & Technology (CUET) region falls into zone 2 in Bangladesh National Building Code (BNBC 1993) with a seismic coefficient of 0.15 g and zone 3 with a coefficient of 0.28 g in the new seismic map. It has been felt necessary to prepare a structural database of existing buildings in CUET campus. The results of the current study will be a guideline in any future development plan. This study is carried out to assess the seismic safety of existing structures by considering rapid screening and preliminary approach. The first tire includes a simple walk-down assessment by visualizing the structural vulnerability parameters. In the second tire, buildings were assessed by checking structural integrity checks.

This study aims at evaluating the structural vulnerability of existing buildings by means of multiple assessment techniques. The main objectives of this study are to assess the seismic safety of existing buildings and to provide a direction how to judge in a practical way whether the minimum safety requirements are fulfilled.

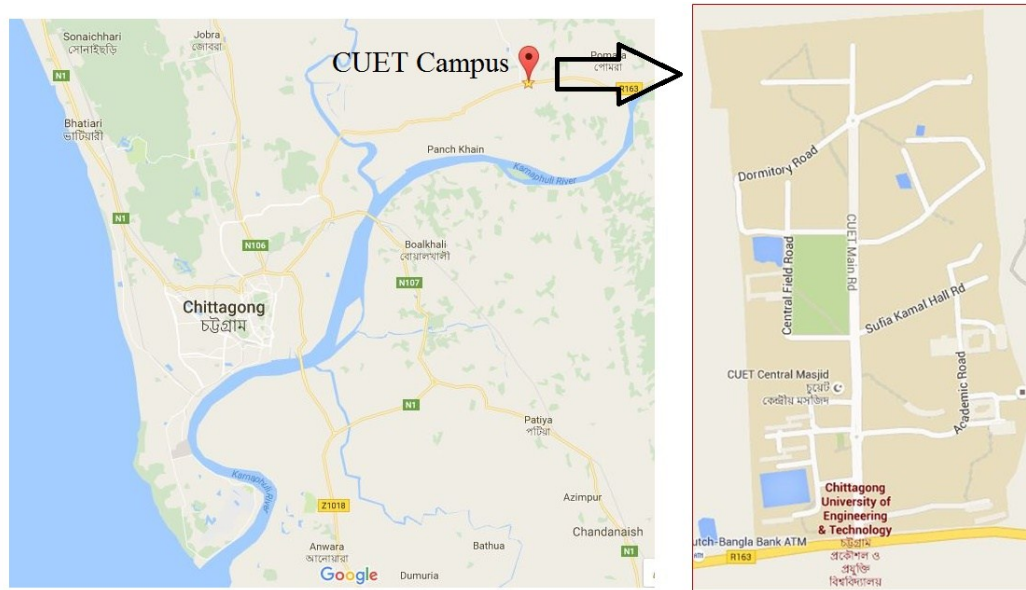


Fig. 1: Google map of CUET Campus

## METHODOLOGY

Mainly two major types of structures are present at CUET. Reinforced Concrete (RC) Frame Structures with masonry infill wall and Unreinforced Masonry Buildings with the flexible diaphragm and Unreinforced Masonry Buildings with fixed diaphragm. To evaluate the seismic condition of the existing buildings, two methodologies were mainly used named R.V.S (Rapid Visual Screening) suggested by FEMA (Federal Emergency Management Agency) and Turkish simple screening procedure developed by Ozcebe et al. in 2006.

The FEMA 154 methods assign a basic structural score based on lateral force resisting system of the building. Score modifiers are specified to take into account the effect of number of stories, plan, vertical irregularities, pre-code or post-benchmark code detailing and soil type. This approach enabled users to classify surveyed buildings into two categories: those acceptable as to “risk to life safety” or those that may be seismically hazardous and should be evaluated in more detail by a design professional, experienced in seismic design. Ozcebe et al (2006) developed seismic vulnerability evaluation methods that can be classified into three main groups. The first, the simplest level is known as “Walkdown Evaluation”. In this survey, major vulnerability factors are considered as soft story, heavy overhang, apparent quality, short column, pounding possibility and topographic effects. Evaluation of this first level does not require any analysis and its goal is to determine the priority levels of buildings that require immediate intervention. Preliminary assessment methodologies (PAM) are applied when more in-depth evaluation of building stocks is required. The procedures in the third tier employ linear or nonlinear analyses of the building under consideration and require the as-built dimensions and the reinforcement details of all structural elements.

## RESULTS AND DISCUSSIONS

There are mainly two types of structures exist in CUET campus. Most of the buildings are Unreinforced Masonry (URM) structure with the flexible and rigid diaphragm. Rest of the buildings are RC frame (C3) structures with masonry infill. A total number of 86 buildings exist in the campus area of which 80 buildings are surveyed and analyzed. However, remaining 6 buildings which are found to be under construction are not taken into consideration. All of the buildings are less than 6 storied. Figure 2 represents the number of buildings exists according to their story numbers. The figure illustrates that 92 percent buildings are less than 4 stories. Among the surveyed buildings, 68 percent buildings are RC structures, 32 percent buildings are Unreinforced Masonry structure (figure 3).

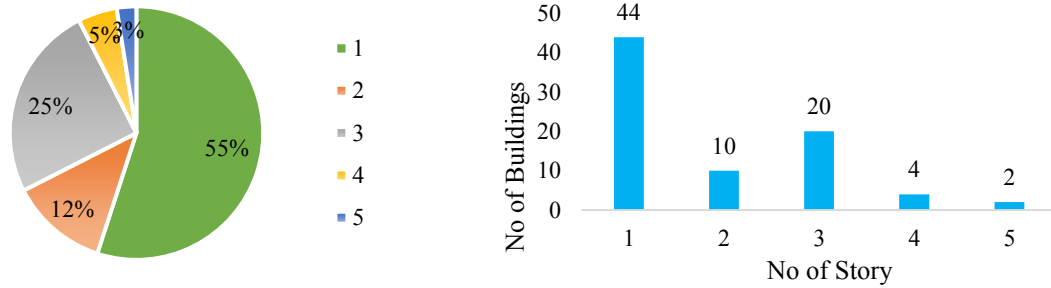


Fig. 2: Proportion of buildings according to no. of stories

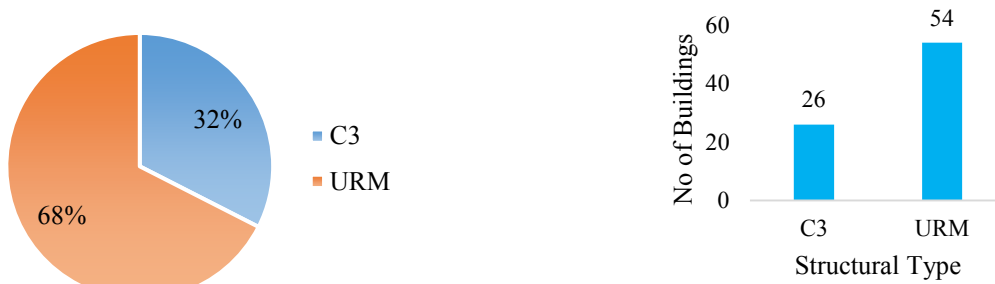


Fig. 3: Building structural types and no. of stories

Total buildings are classified into eight categories based on their purpose of uses. Figure 4 reflects existing building use categories in percentage. Majority numbers of the buildings were using for the residential purposes. Only 8 percent buildings are used for the academic purposes, 4 percent buildings are administrative and 1 percent buildings are emergency center.

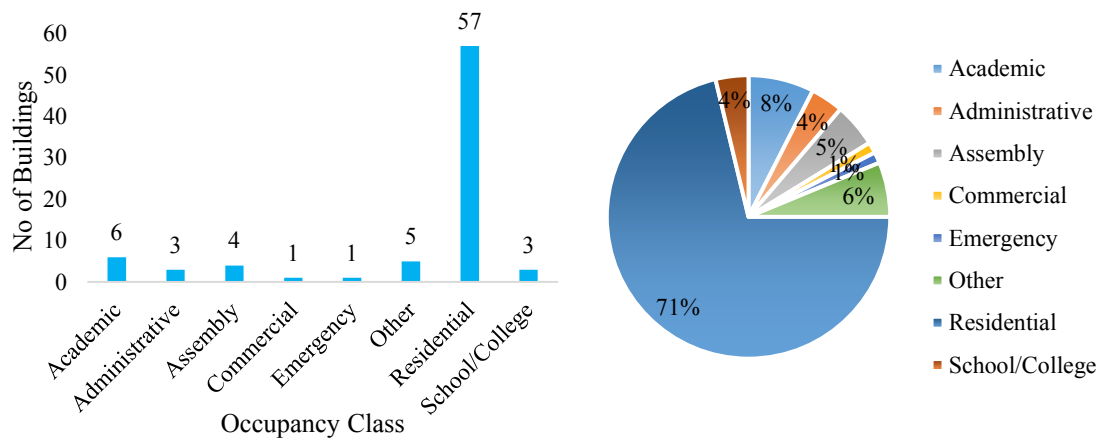


Fig. 4: Proportion of occupancy class of the buildings

### Level 1 Assessment

First stage assessment is basically rapid screening procedure including Turkish tier 1 Walkdown Survey and FEMA 154 Rapid Visual Screening. The prior one is followed for the RC structures and later method is used to evaluate unreinforced masonry types of buildings. Turkish level 1 survey method is used for 26 RC structures.

### Turkish Walkdown Procedure

In the Turkish level 1 survey, major vulnerability factors are surveyed and shown in tables and figures. Figure 5 represents the existing structural physical visible condition of the buildings in percentile form. Table 1 displays the relationship of the buildings apparent quality varies with

building number of stories. Figure 6 represents number of buildings present having short column effect. Table 2 shows short column presence with respect to different number of stories.

Table 1: Apparent Building Quality

No of Story	Average	Good	Poor	Total
1	3	3	2	8
2	5	2	0	7
3	5	0	1	6
4	3	0	0	3
5	0	2	0	2
<b>Total</b>	<b>16</b>	<b>7</b>	<b>3</b>	<b>26</b>

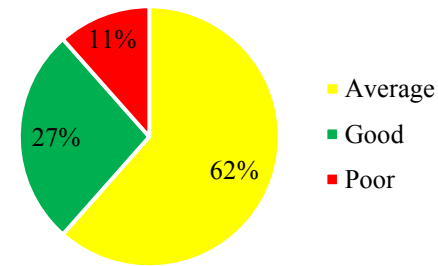


Fig. 5: Proportion of Apparent Quality

Table 2: Short Column Effect

No of Story	Identified	Not Identified	Total
1	2	6	8
2	6	1	7
3	5	1	6
4	3	0	3
5	1	1	2
	<b>17</b>	<b>9</b>	<b>26</b>

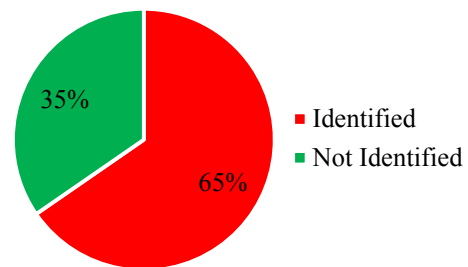


Fig. 6: Proportion of Short Column

There are only two buildings which are identified as pounding possibility with each other. However, three parameters such as soft story, heavy overhang and topographic effects are not found in any of the surveyed buildings. From the level 1 survey, performance scores are calculated for each building. Table 3 shows the performance scores are obtained for RC buildings. The buildings having a score above 80 are classified as low risk building. The building having a score below 60 is considered as high risk buildings. The score ranges from 61 to 80 marked as moderate risk class. Table 3 represents level 1 performance score variations with different number of stories.

Table 3: Summary of Performance Score (PS)

Number of Stories	PS < 60	60 ≤ PS ≤ 80	PS > 80	Total
1	0	0	8	8
2	0	0	7	7
3	0	6	0	6
4	3	0	0	3
5	1	1	0	2
<b>Total</b>	<b>4</b>	<b>7</b>	<b>15</b>	<b>26</b>

### Rapid Visual Screening

FEMA 154 RVS can be applied for both structures. Turkish method can't be applied for masonry structures, as a result, RVS is conducted for remaining 54 nos. masonry structures. Table 4 and Table 5 shows the no. of buildings having RVS score modifiers plan irregularity and pre-code/post-benchmark. The proportion of these modifiers are shown in figure 7 and figure 8. The modifier vertical irregularity is not considered as all the buildings are vertically regular. As the soil condition was unknown the soil type D is taken as a modifier as per FEMA 154 guideline. From the RVS procedure, final scores are calculated for each building. Table 6 shows the nos. of buildings require detailed evaluation based on cut-off score 2 suggested by the guideline.



Table 4: Plan Irregularity

No of Story	Irregular	Narrow Rectangular	Rectangular
1	19	6	11
2	0	0	3
3	0	2	12
4	1	0	0
<b>Total</b>	<b>20</b>	<b>8</b>	<b>26</b>

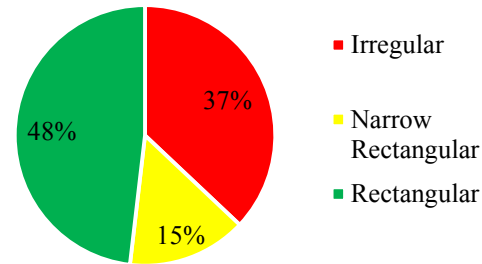


Fig. 7: Proportion of Plan Irregularity

Table 5: Pre-Code and Post-Benchmark

No of Story	Post-Benchmark	Pre-Code
1	17	19
2	0	3
3	1	13
4	1	0
<b>Total</b>	<b>19</b>	<b>35</b>

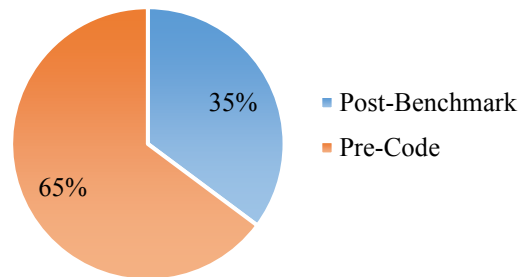


Fig. 8: Proportion of Pre-Code and Post-Benchmark

Table 6: RVS Final Score Summary

No of Story	Detailed Evaluation Required	
	Yes (Final Score $\leq$ 2)	No (Final Score $>$ 2)
1	18	18
2	0	3
3	2	12
4	0	1
<b>Total</b>	<b>20</b>	<b>34</b>

### Level 2 Assessment

Second level assessment is conducted for the RC buildings following Turkish Tier 2 guideline prepared by Ozcebe et al. in 2006. Seven buildings are analyzed based on building importance level in terms of building use. Academic and administrative buildings are preferred in this stage. Table 7 represents the risk class for each building that is obtained from the Turkish level 2 analysis. The building integrity values are checked after taking detail structural floor sketch and preliminary assessment calculation. Finally Table 7 shows the risk class for each buildings that is obtained from the Turkish level 2 analysis.

Table 7: Summary of assessment results and Risk Class in level 2

ID No.	Building Name	Risk Group
15	Dormitory	Low
57	EME Building	Low
61	Engg. Office Building	Low
63	CE Building	Low
65	Central Library	Low
66	Pre-Engineering Building	Low
68	Admin Building	Low

## CONCLUSIONS

It is seen that most of the single story residential building configuration are somewhat similar. Therefore the obtained performance for single story residential URM represents similar results in first level assessment. It is observed that building performance score decreases with increase in number of story. All the buildings in second level assessment procedure lie in the low risk group. The overall findings are summarized in table 1.

Table 8: Summary of findings based on first and second level assessments

Level of Assessment	First		Second
Assessment Approach	Walk-down Procedure	Rapid Visual Screening	Preliminary Assessment Method
Structural Type	RC frame with Masonry Infill	Unreinforced Masonry	RC frame with Masonry Infill
No. of Building Assessed	26	54	7
High	04	20	0
Moderate	07	-	0
Low	15	34	7

Among the applied methods, FEMA 154 covers all the structural types whereas Turkish method are limited to apply for RC frame buildings only in the first level of assessment. In FEMA 154, six parameters are dominated (mid-rise, high-rise, plan irregularity, vertical irregularity, pre-code, post-benchmark and soil condition). Masonry buildings need to be assessed in details for more consistent results. This study contains basic structural vulnerability information which can be employed for any decision making in any future development work. As under construction buildings are not considered in this study, these buildings should be assessed in future.

## REFERENCES

- BNBC. 1993. Bangladesh National Building Code (BNBC 1993).  
 Federal Emergency Management Agency. 2002. FEMA 154: Rapid Visual Screening of Buildings for Potential Seismic Hazards—A Handbook. Washington DC  
 GSHAP. 1992. World Seismic Map. Global Seismic Hazard Assessment Programme. [seismo.ethz.ch/GSHAP](http://seismo.ethz.ch/GSHAP)  
 Ozcebe, GH; Sucuoglu, SM; Yüccemen, A; Yakut and Kubin. J. 2006. Seismic Risk Assessment of Existing Building Stock In Istanbul—a Pilot Application in Zeytinburnu District. *8NCEE*, Paper No. 1737, San Francisco.

## **TORSIONAL CAPACITY ASSESSMENT OF COMPOSITE CROSS SECTIONS USING MATHEMATICA**

A. F. Mazumder, M. Nishat & M. A. A. Sarfin\*

*Department of Civil Engineering, Presidency University, Dhaka, Bangladesh*

*\*Corresponding Author: ony.sarfin@gmail.com*

### **ABSTRACT**

Torsional capacity is the ability of the cross section to resist a torque that attempts to twist the cross section. Mechanical properties, like shear stress and torsional stress, can be improved by using composite section rather than using single material. The main purpose of this paper is to improve the torsional capacity of Aluminium by combining with brass. Torsional capacity and shearing stress were calculated for five cross sections (Cases I, II, III, IV, and V), two of them were composed of one material (CS-I and II, Aluminium and Brass) and other three were composite sections with different arrangement of Aluminium and Brass (Case III and IV). Finite difference method was adopted to calculate the stress function, shearing stress and torsional capacity. The analysis of cross sections was performed in Wolfram Mathematica 8.0 software. The analysis result revealed that brass, individually, can provide higher torsional capacity among the studied materials and composite section having aluminium inside and brass outside, can bear highest shearing stress among the studied composite sections.

Keywords: Torsional stress; shear stress; composite section

### **INTRODUCTION**

A composite material is a combination of two or more different materials. Composite section produces a new material with new properties, which are not found in the individual materials and it is the key advantage of using combination of two or more different materials. It has high performance due to the high specific strength, high specific stiffness, high flexibility, low density, low thermal expansion, and easy to fabricate. There are two phases of composite materials. The first one is reinforcing phase. In this phase, material exhibits high strength with low specific densities. The second phase is the matrix. In this phase, the material shows ductility and toughness, these properties are improved by other reinforcing materials. Composite materials can be generally involved into three categories, which are dispersion strengthened, particle reinforced, and fiber reinforced. In Dispersion strengthened, the matrix of the material is reinforced by fine distribution of secondary particles. The secondary particles affect the performance of the material causing deformation in it. Particle reinforced materials have many particles impeded in the matrix. In case of Fiber reinforced materials, materials are reinforced by fibers and most of the load carried by the fibers.

Torsional capacity is defined as the ability of the cross section to resist a torque that attempts to twist a cross section of its axis. In order to improve the torsional capacity for two or more materials, a combination of materials should be performed. Some researchers studied various cross section to assess the torsional and shear stress capacity (Massa and Barbero, 1998; Rao, 2007; Roberts and Al-Ubaidi, 2012; Salim and Davalos, 2005; Tarn and Wang, 2001).

The main purpose of this study is to improve the torsional capacity of Aluminium material combining with brass material and to find suitable arrangement of materials so that cross section can bear higher torsion and shearing stress.

### **METHODOLOGY**

To investigate torsional capacity and shearing stress, square cross sections were chosen. Torsional capacity and shearing stress were found out for modulus of rigidity of two different materials by taking other parameters like dimensions and angle of twist as constant. To find out torsional capacity and shearing stress, the Saint Venant's theory of torsion and Prandtl stress function were used. Finite

difference method was used as analysis technique. All sections were analyzed to find out torsional capacity and shear stress by using Wolfram Mathematica 8.0 software.

**The Prandtl Stress Function**

The Poisson’s equation can be written like Eq. (1). Where  $\Phi$  is the Prandtl stress function and  $\theta$  is angle of twist.

$$\nabla^2\Phi = -2G\theta' \quad (1)$$

This equation can be rewritten as,

$$\nabla^2\Phi = -2 \text{ in the cross section, and}$$

$$\Phi = 0 \text{ on the boundary}$$

By using these governing equation and condition, Torque and shear stress can be determined as follows,

$$T = 2 \int_A \Phi dA$$

$$\frac{\partial \Phi}{\partial n} = -\tau$$

**Finite Difference Method**

Finite difference method is a techniques of replacing ordinary differential equation, partial differential equation and their boundary conditions by a set of algebraic equations. Let’s assume a 1-D structure with length L and let’s divide into ‘n’ nodes

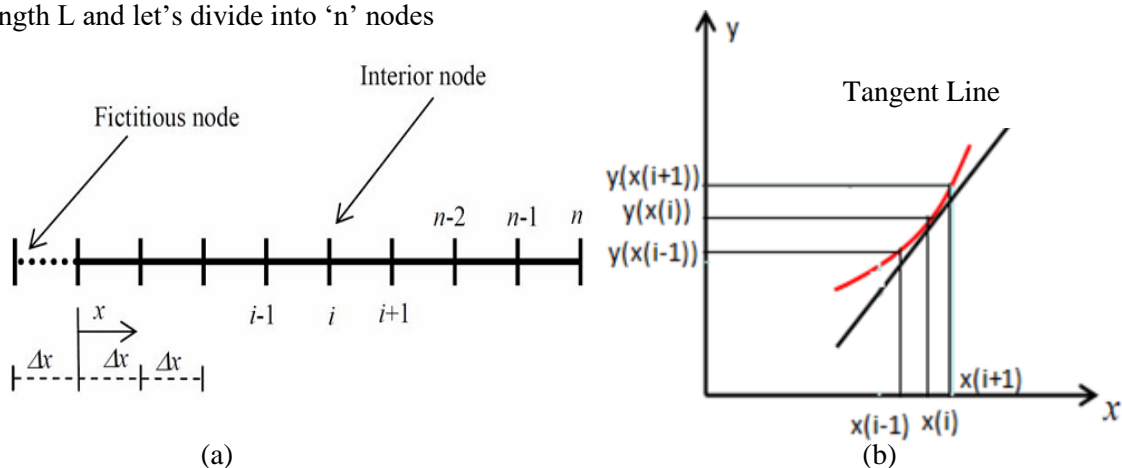


Fig. 1: (a) Nodes taking for 1 D, (b) Graphical representation of nodes

So, the differential equation for all nodes can be written as

$$\frac{d^ny}{dx^n} + \frac{d^{n-1}y}{dx^{n-1}} + \dots = f(x)$$

Now approximating each differential operator by a finite difference. From Taylor series, for first and second order central finite difference can be written as

$$y'_i = \frac{y_{i+1} - y_{i-1}}{2h}$$

$$y''_i = \frac{y_{i-1} - 2y_i + y_{i+1}}{h^2}$$

For 2-D, second order central finite different can be written as, (in y and z direction)

$$y''_i = \frac{y_{i-1,j} - 2y_{i,j} + y_{i+1,j}}{h_y^2}$$

$$y''_j = \frac{y_{i,j-1} - 2y_{i,j} + y_{i,j+1}}{h_z^2}$$

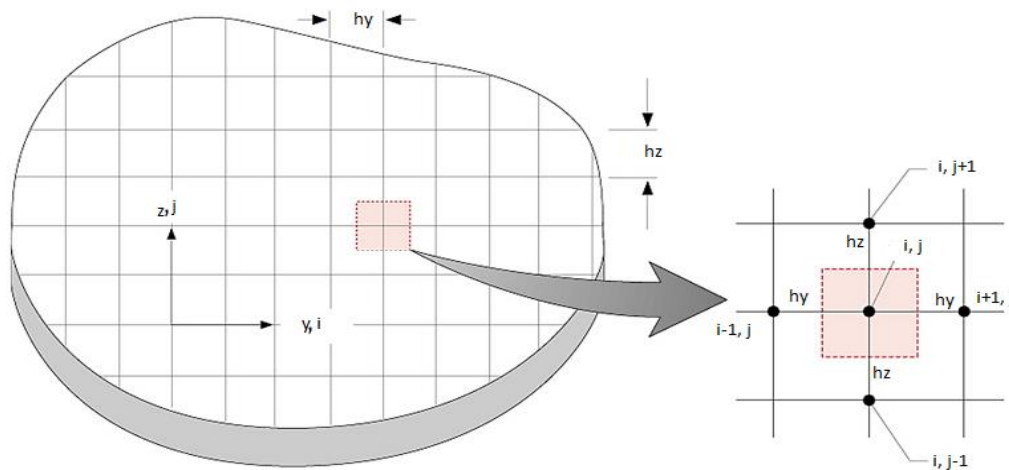


Fig. 2: Nodes taking for 2-D

From the derivation of stress function,

$$\nabla^2 \Phi = \frac{\partial^2 \Phi}{\partial y^2} + \frac{\partial^2 \Phi}{\partial z^2} = -2G\phi'$$

Here,

$$\frac{\partial^2 \Phi}{\partial y^2} = \frac{\phi_{i-1,j} - 2\phi_{i,j} + \phi_{i+1,j}}{h_y^2}$$

$$\frac{\partial^2 \Phi}{\partial z^2} = \frac{\phi_{i,j-1} - 2\phi_{i,j} + \phi_{i,j+1}}{h_z^2}$$

So,

$$\nabla^2 \Phi = \frac{\phi_{i-1,j} - 2\phi_{i,j} + \phi_{i+1,j}}{h_y^2} + \frac{\phi_{i,j-1} - 2\phi_{i,j} + \phi_{i,j+1}}{h_z^2}$$

For  $h_x = h_y = h$

$$\nabla^2 \Phi = \frac{\phi_{i-1,j} + \phi_{i+1,j} - 4\phi_{i,j} + \phi_{i,j-1} + \phi_{i,j+1}}{h^2}$$

### Experimental Cross Sections

To investigate torsional capacity and shearing stress square cross sections were chosen. Torsional capacity and shearing stress was found out for different modulus of rigidity by taking other parameters like dimensions and angle of twist as constant. Modulus of rigidity was taken as variable for different cross sections [Fig. 3].

The parameters are as follows,

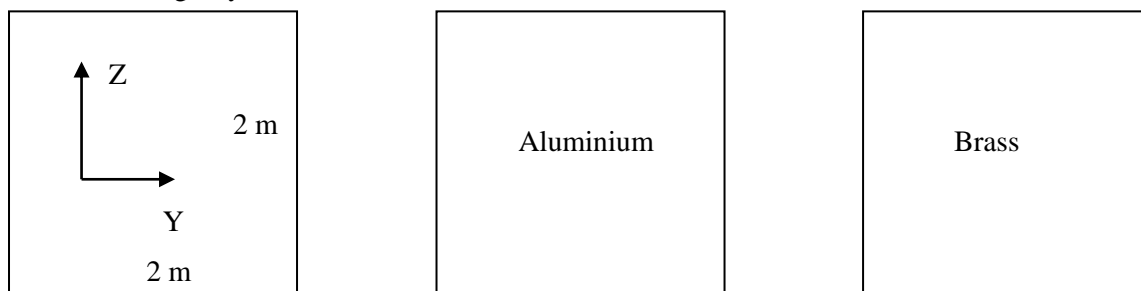
Length in Y direction = 2 meter

Length in Z direction = 2 meter

Angle of twist,  $\theta = 1$  radians

Modulus of rigidity of Aluminium = 24000 MPa.

Modulus of rigidity of Brass = 40000 MPa.



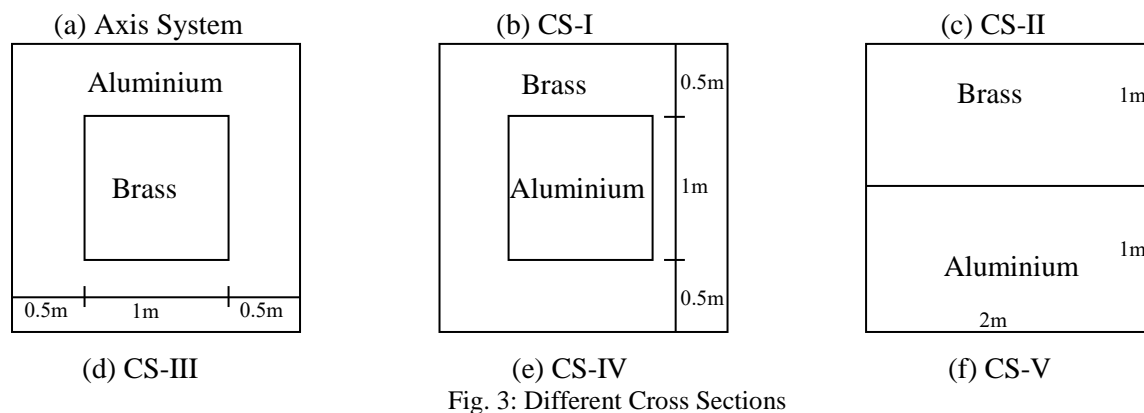


Fig. 3: Different Cross Sections

### RESULTS AND DISCUSSIONS

Result was recorded for four points [Fig. 4]. Torsional capacity and shearing stress were recorded and tabulated for these points.

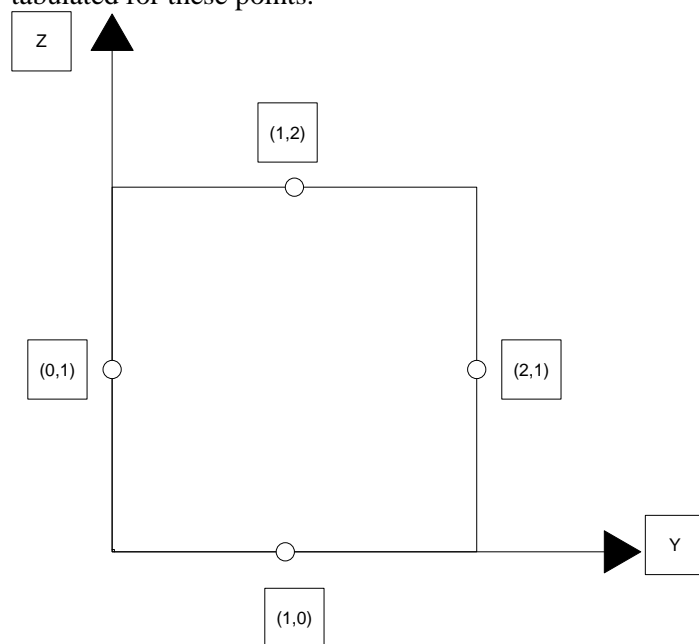


Fig. 4: Position of Recorded Shear Stress

By using Mathematica, torsional capacity and shearing stress was calculated. Table 1 shows the comparison among the cross sections.

### CONCLUSIONS

In this study, torsional capacity and shear stress were found out by analysing square composite sections, which were in different arrangement of two materials (Aluminium and Brass). Two cross sections of one material (CS-I and CS-II) were analysed, which has aluminium and brass, individually. Other three cross sections (CS-III, CS-IV, and CS-V) were analysed with different combination of aluminium and brass. It was found that for single materials, brass gives higher torsional capacity and can bear higher shearing stress among the cross sections having single material (CS-I and II), because brass has higher modulus of rigidity. Composite section having brass inside and aluminium outside (CS-III), gives higher torsional capacity. Because, the core material has higher modulus of rigidity. Composite section

Table 1: Torsional Capacity, Shearing Stress

Sl. No.	Cross Section	Shearing Stress, $\tau$ (MPa)				Torsional Capacity, T (N-mm)
		(1,0)	(2,1)	(1,2)	(0,1)	
01	CS-I	32357.68	32357.68	32357.68	32357.68	53864.31
02	CS-II	53929.46	53929.46	53929.46	53929.46	89773.86
03	CS-III	40165.51	40165.51	40165.51	40165.51	72925.5
04	CS-IV	46121.63	46121.63	46121.63	46121.63	70712.67
05	CS-V	43632.4	33776.33	32932.39	33776.33	58766.93

having brass outside and Aluminium inside (CS-IV) can bear higher shearing stress. It is known that shearing stress varies with the length and increases with the increase of distance from the centre and material having higher modulus of rigidity was placed outside. Due to this fact, CS-IV can bear higher shearing stress comparing with other composite cross section. So, it can be concluded that

- Materials having high modulus of rigidity should be used for high torque, where high torsional resistance is required.
- Materials having higher modulus of rigidity should be placed outside in a cross section for the resistance of higher shearing stress optimum material area.

#### REFERENCES

- Massa, JC and Barbero, EJ. 1998. A Strength of Material Formulation for Thin Walled Composite Beams with Torsion. *Journal of Composite Materials*, Vol. 32, No 17:1560-1594.
- Rao, CS. 2007. *Analysis of Tapered Laminated Composite Tubes under Tension and Torsion*. MSc Thesis, University of Texas at Arlington, USA.
- Roberts, TM and Al-Ubaidi, H. 2012. Influence of Shear Deformation on Restrained Torsional Warping of Pultruded FRP Bars of Open Cross-section. *Journal of Thin-walled Structures*, 39:395-414.
- Salim, HA and Davalos, JF. 2005. Torsion of Open and Closed Thin-Walled Laminated Composite Sections. *Journal of Composite Materials*, 39:497-524.
- Tarn, JQ and Wang, YM. 2001. Laminated Composite Tubes under Extension, Torsion, Bending, Shearing and Pressuring: a State Space Approach. *International Journal of Solid and Structures*, 38:9053-9075.

## USE OF SLAG AS COARSE AGGREGATE AND ITS EFFECT ON MECHANICAL PROPERTIES OF CONCRETE

M. A. Qurishee\*, I. T. Iqbal, M. S. Islam & M. M. Islam

*Department of Civil Engineering, Chittagong University of Engineering and Technology, Chittagong,  
Bangladesh*

*\*Corresponding Author: muradalqurishee@gmail.com*

### ABSTRACT

Traditional coarse aggregates are very costly and its reserve will be gradually finished, possessing a great threat. Slag is considered as third class hazardous waste that requires a large place for dumping. To transform the slag into an environment-friendly resource and to save the environment from the pollution, the possibility of the use of slag as coarse aggregate cannot be overlooked. The main objective of the study is to investigate the strength properties of slag incorporated as coarse aggregate in concrete. The proportion of slag and stone chips used as coarse aggregate was varied from 0 to 100%. A total of 500 specimens of 4 inches cube were cast using plain water in normal temperature for the curing periods of 7, 14, 28, 90 and 180 days. W/C ratios were varied as 0.60, 0.50 and 0.42 for making 20, 30 and 40 MPa concrete respectively and compressive as well as tensile strengths were evaluated. Concrete made by replacing coarse aggregate with BFS is observed to increase upto a replacement level of 40%.

Keywords: Coarse aggregate; compressive strength; concrete, slag tensile strength

### INTRODUCTION

Slag is a byproduct of steel production left over after a desired metal has been separated (i.e., smelted) from its raw ore and it is usually a mixture of metal oxides and silicon dioxide. Low iron slag is considered as third class hazardous waste which may require a large place for dumping. Traditional coarse aggregates like stone chips, brick chips are very costly and huge amount of stones are withdrawn from Sylhet every day and as a result one day the reserve of stones will be finished which will possess a great threat to us. As per the survey conducted by En Safe, Inc. (2002) a single ferroalloys industry produces 220,000 tons of low carbon slag per year. Also survey report of European Slag Association EUROSLAG conducted among its member (European steelworks and processing companies) since 2000, it is known that in 2008, 45.6 million tons of ferrous slag was produced and more than 400 million tons of iron and steel slag is produced each year in the world. Scarcity of coarse aggregate in future and problem of dumping place for slag can be minimized if slag can be used as the partial replacement of coarse aggregate, fine aggregate or cement. The objective of the study is to minimize the cost of construction by using slag as a replacement of coarse aggregate in making environmental friendly concrete and solving the dumping problem of slag. The compressive as well as tensile strength of concrete due to the use of slag as a replacement of coarse aggregates in various proportions and at different curing period are evaluated so as to observe the effectiveness of slag as coarse aggregate in concrete.

### *Reviews of literature survey are presented as below-*

Chen Meizhu, Zhou Mingkai, Wu Shaopeng (2007) worked on mortar made up of ground granulated blast furnace, gypsum, clinker and steel slag sand. The experimental results show the application of steel slag sand may reduce the dosage of cement clinker and increase the content of industrial waste product using steel slag sand.

Isa Yuksel, Omer Ozkan, Turhan Bilir (2006) experimented use of non ground granulated blast furnace slag as fine aggregate in concrete. The study concluded that the ratio of GGBs/sand is governing criteria



for the effects on the strength and durability characteristics.

Li Yun-feng, Yao Yan, Wang Liang (2009) investigated effects of steel slag powder on the workability and mechanical properties of concrete. Experimental results show that mechanical properties can be improved further due to the synergistic effect and mutual activation when compound mineral admixtures with steel slag powder and blast furnace slag powder mixed in concrete.

Saud Al-Otaibi (2008) studied use of recycling steel mill as fine aggregate in cement mortars. The replacement of 40% steel mill scale with that of fine aggregate increased compressive strength by 40%, drying shrinkage was lower when using steel mill scale.

Tarun R Naik, Shiw S Singh, Mathew P Tharaniyil, Robert B Wendfort (1996) investigated application of foundry by-product materials in manufacture of concrete and masonry products. Compressive strength of concrete decreased slightly due to the replacement of regular coarse aggregate with foundry slag however strengths were appropriate for structural concrete.

## **METHODOLOGY**

In this study, concrete strength of 20, 30 and 40MPa are considered with a W/C ratio of 0.60, 0.50 and 0.42 respectively for the replacement level of 0%, 10%, 20%, 30%, 40%, 50%, 60%, 70%, 80%, 90% and 100%.of natural coarse aggregate by slag and studied for compressive as well as tensile strengths for the curing periods of 7days, 14days, 28days, 90days, 180days. For each percent replacement and curing period 6 samples are prepared, 3 samples for compressive strength and 3 samples for tensile strength test.

### ***Mix Proportions***

The concrete mix proportions (design) were obtained for a control mix of slump  $4 \pm 1$  in. ( $100 \pm 25$  mm) for 20, 30 and 40 MPa of concrete with a W/C ratio of 0.60, 0.50 & 0.42 respectively.

### ***Materials***

ASTM Type I Ordinary Portland Cement (OPC) conforming to ASTM C-150 was used as binding material. Locally available natural sand passing through 4.75 mm sieve and retained on 0.075 mm sieve and stone chips passing through 20 mm sieve was used. Slag from the steel plant was consumed throughout the experimental investigations. Table 1 shows the properties of ingredient materials used in this experimental investigation. Table 2 shows the physical properties of OPC.

## **TEST CONDUCTED**

### ***(a) Compressive Strength tests***

Compressive strength of concrete specimens was tested at the ages of 7, 14, 28, 90 and 180 days in accordance with the BS EN 12390-3:2009. Reported strength is taken as the average of three tests results.

### ***(b) Tensile Strength tests***

Tensile strength of concrete specimens was tested at the ages of 7, 14, 28, 90 and 180 days in accordance with the BS EN 12390-3:2006. Reported strength is taken as the average of three tests results.

## **RESULTS AND DISCUSSIONS**

The test results of the study are shown below through the graphical presentation (Ref. Fig.1 to Fig.6).

### **Compressive strength and tensile strength:**

For making compressive & tensile tests specimens, compaction is done by a temping rod in place of vibrator machine. The specimens are cured in open air water tank in tap water in room temperature. The specimens were dried up before the tests. However, in the rainy season it is very difficult to dry which might cause the variation of test results. In normal consistency test, initial & final setting time test is affected by the temperature & the humidity of the surrounding medium. In this investigation, tests are

Table 1: Physical Properties of Ingredient Materials

Properties	Fine Aggregate	Coarse Aggregate	Slag
Fineness Modulus	2.40	6.55	--
Specific Gravity	2.58	2.67	2.57
Unit Weight (kg/m <sup>3</sup> )	1600	1700	1350
Absorption capacity (%)	2.05	1.63	1.55
Moisture content (%)	0.908	0.30	--
Bulk Specific Gravity	--	--	2.62

Table 1: Physical Properties of Cement

Properties	OPC
Fineness (cm <sup>2</sup> /gm)	98.5
Normal consistency	27%
Soundness	2.7 mm
Initial Setting	180 min
Final Setting	270 min

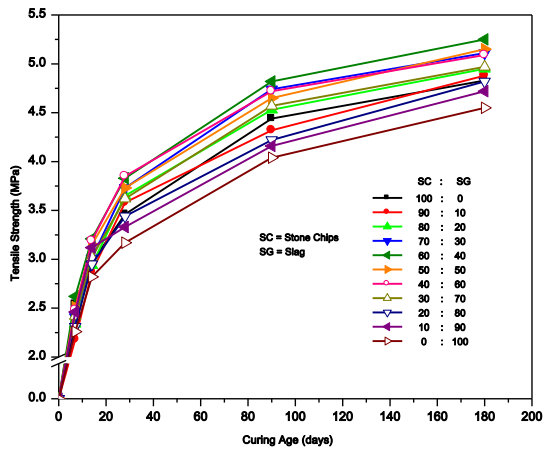


Fig.2: Tensile Strength - Curing Age for 20 MPa Concrete

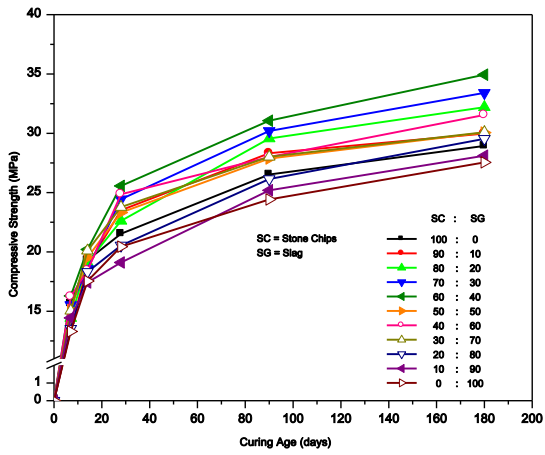


Fig.1: Compressive Strength - Curing Age for 20 MPa Concrete

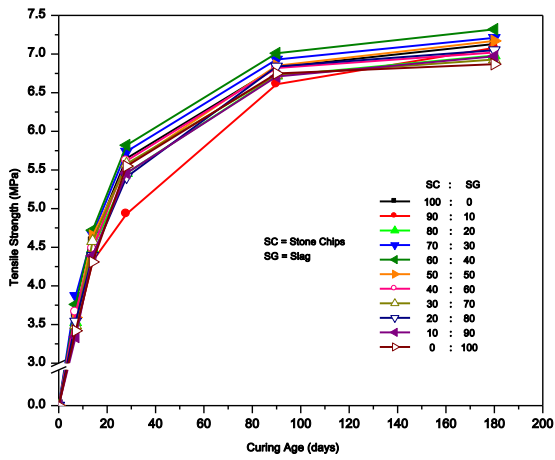


Fig.4: Tensile Strength - Curing Age for 30 MPa Concrete

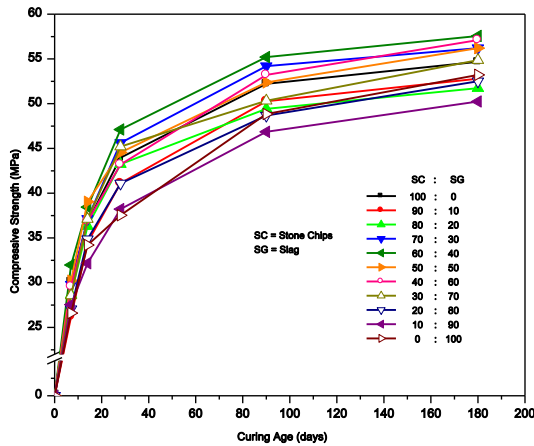


Fig.5: Compressive Strength - Curing Age for 40 MPa Concrete

carried out in room temperature and humidity condition.

The test result shows that 40% slag replacement shows good result. Also replacement levels of 50% and 60% shows reasonable improvement of concrete strengths at different ages. Table 3 shows the summary of the test results.

## CONCLUSION

The following conclusions can be drawn from the study:

- (1) Compressive strength of concrete made by replacing coarse aggregate by slag is higher than normal conventional concrete (concrete with stones chips).
- (2) Compressive strength as well as tensile strength for concrete made by replacing coarse aggregate by slag is observed to increase upto replacement level of 40%.
- (3) Concrete made by using 40% partial replacement of Slag shows the strength improvements that vary from around 6 to 20%.

Finally, it can be concluded that, Slag from Bangladesh Steel Re-Rolling Mills (BSRM) can be used as coarse aggregate at a proportion of 40% of total coarse aggregate which may offer more compressive and tensile strength and also considering the environmental issue.

## **PARAMETRIC STUDY ON REINFORCED CONCRETE JACKETED COLUMNS: COMPARISON OF CHANGES IN BEHAVIOR DUE TO CHANGES IN REINFORCEMENT PATTERN**

A. A. Saeem\*, M. S. Ahmed, M. M. Rahman, I. Chowdhury & M. R. Alam

*Department of Civil Engineering, Chittagong University of Engineering and Technology, Chittagong, Bangladesh*

*\*Corresponding Author: a.al.saeem@gmail.com*

### **ABSTRACT**

This paper contains a parametric study on re-strengthening of rectangular RC columns using different widely practiced RC jacketing techniques. Finite element program ANSYS Multi Physics is utilized for non-linear finite element analysis owing to its capabilities to predict and pictorially represent the response of RC columns in post-elastic range to the ultimate strength. Comparisons are done among four different popular techniques of RC jacketing to find out the link between reinforcement pattern and columns' structural behaviour, i.e., lateral and axial deformation response and crack formation. A rectangular RC column without retrofitting is analysed and then it is retrofitted to a target ultimate strength theoretically in four distinct ways: retrofitted with (i) one reinforcing bar at each corner; (ii) two reinforcing bars at each corner; (iii) three reinforcing bars at each corner with diagonal confinement bar at corners; and (iv) four reinforcing bars at each corner having two layers of additional tie bars and analysed. The study finds the jacketing technique (iii) to be the most efficient for jacket of RC column.

Keywords: ANSYS; finite element analysis; interface; RC column jacketing; re-strengthening

### **INTRODUCTION**

Reinforced concrete members are often damaged due to natural disasters, notably earthquakes, overloading, change in building usage and so on. Damage may take place in almost all parts of a structure, namely slabs, beams, columns, walls etc. Rehabilitation is needed after the damage has taken place to bring the damaged member to the strength previously existed. Re-strengthening is also carried out when the purpose of an existing structure changes, predicted load increases or environmental load increases than that was taken into account when designed. Re-strengthening of reinforced concrete members has become very common in the modern world. There are different retrofitting techniques for different members of a structure. Jacketing is the most popularly used method for strengthening of building columns. The most common types of jackets are steel jacket, reinforced concrete jacket, fiber reinforced polymer composite jacket, jacket with high tension materials like carbon fiber, glass fiber etc. Enlargement of the existing structural members such as column and beam sections by placing reinforcing steel rebars around its periphery and then concreting it is widely adopted option; which is referred as concrete jacketing. This method significantly increases the member sizes and thereby its stiffness. Concrete Jacketing primarily enhances the confinement along with the shear and axial behaviour in case of columns.

There is a wide spectrum of published work on column jacketing. The published work emphasizes finding out the minimum requirements, interface treatment and the failure type. Several experimental and numerical analyses show the minimum requirements for reinforced concrete column jacketing (Vedprakash et. al., 2014, Pravin et. al., 2011). Strength of the new materials will be equal or greater than those of the existing column. Minimum jacket thickness will be 4". All published work on RC jacketing recognize the importance of interface preparation to achieve a good bond between the original column and the added jacket so that the resulting element behaves monolithically (Ju'lio et. al., 2003). The current practice of surface treatment in several countries consists increasing surface roughness, application of bonding agent and application of steel connectors. Hand chipping, sand-blasting, jack-hammering, electric hammering, water demolition and iron brushing are the most common surface

roughening methods. Several authors state that increasing the roughness of the interface surface is necessary, but its influence has not been quantified (Rodriguez et. al., 1994, Bett et. al., 1988, Alcocer et. al., 1990). Several publications conclude that adding steel connectors crossing the interface does not meaningfully increase the debonding force, but increases almost directly the longitudinal shear strength considering slipping (Ju'lio et. al., 2001). In this work, a comparison among various techniques (Teran et. al., 1992) of RC jacketing is done using ANSYS Multi Physics computer program. This study aims to investigate and compute the lateral and axial deformation responses at different stages of axial incremental loading and find the effect of reinforcement pattern on lateral and axial deformation responses and crack formation.

## NUMERICAL MODELING IN ANSYS

The concrete material model predicts the failure of brittle materials. An eight-node solid element SOLID65 is used to model the concrete. The solid is capable of cracking in tension and crushing in compression. The element is defined by eight nodes having three degrees of freedom at each node: translations in the nodal x, y and z directions. Link8 element is used to model the steel reinforcement. LINK8 is a 3-D spar element which is a uniaxial tension-compression element with three degrees of freedom at each node: translations in the nodal x, y, and z directions. Interface surface is created using TARGE170 and CONTA174 geometries. For 3D modeling, the surface of old concrete is taken as contact surface and the surface of new concrete is taken as target surface by default. Then a contact pair is created using standard contact behavior. Default values of normal penalty stiffness and penetration tolerance are allowed for the surface to surface contact creation. Maximum friction stress is taken to be  $1 \times 10^{20}$  psi.

The criterion for failure of concrete due to a multi-axial stress is controlled by the expression given by Willam and Warnke (1975).

$$F/f_c - S \geq 0$$

where, F = a function of the principal stress state ( $\sigma_{xp}$ ,  $\sigma_{yp}$ ,  $\sigma_{zp}$ ); S = failure surface expressed in terms of principal stresses and five input parameters  $f_t$ ,  $f_c$ ,  $f_{cb}$ ,  $f_1$  and  $f_2$ ;  $f_c$  = uniaxial crushing strength;  $\sigma_{xp}$ ,  $\sigma_{yp}$ ,  $\sigma_{zp}$  = principal stresses in principal directions. However, the failure surface can be specified with a minimum of two constants,  $f_t$  and  $f_c$ . The other three constants default to Willam and Warnke:

$$f_1 = 1.45f_c; f_2 = 1.725f_c; f_{cb} = 1.2f_c$$

These default values are valid only for stress states where the condition

$$|\sigma_h| \leq \sqrt{3} f_c; \sigma_h = \text{Hydrostatic stress rate} = (1/3)(\sigma_{xp} + \sigma_{yp} + \sigma_{zp})$$

is satisfied. This condition equation applies to stress situations with a low hydrostatic stress component. All five failure parameters should be specified when a large hydrostatic stress component is expected. If condition equation is not satisfied, the strength of the concrete material may be incorrectly evaluated. When the crushing capability is suppressed with  $f_c = -1.0$ , the material cracks whenever a principal stress component exceeds  $f_t$ .

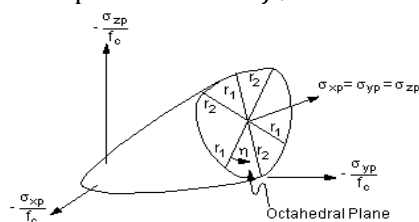


Fig. 1: 3-D failure surface in principal stress space (ANSYS, 2011)

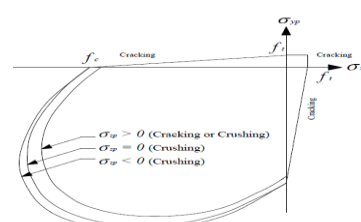


Fig. 2: Failure surface in principal stress space with nearly biaxial stress (ANSYS, 2011)

Both the function F and the failure surface S are expressed in terms of principal stresses denoted as,  $\sigma_1$ ,  $\sigma_2$ , and  $\sigma_3$  where:

$$\sigma_1 = \max(\sigma_{xp}, \sigma_{yp}, \sigma_{zp}); \sigma_3 = \min(\sigma_{xp}, \sigma_{yp}, \sigma_{zp}) \text{ and } \sigma_1 \geq \sigma_2 \geq \sigma_3.$$

The failure of concrete is categorized into four domains:

$$0 \geq \sigma_1 \geq \sigma_2 \geq \sigma_3 \text{ (compression - compression - compression)}$$

$$\sigma_1 \geq 0 \geq \sigma_2 \geq \sigma_3 \text{ (tensile - compression - compression)}$$

$$\sigma_1 \geq \sigma_2 \geq 0 \geq \sigma_3 \text{ (tensile - tensile - compression)}$$

$$\sigma_1 \geq \sigma_2 \geq \sigma_3 \geq 0 \text{ (tensile - tensile - tensile)}$$

In each domain, independent functions describe F and the failure surface S. The four functions describing the general function F are denoted as  $F_1, F_2, F_3$ , and  $F_4$  while the functions describing S are denoted as  $S_1, S_2, S_3$ , and  $S_4$ . The functions ( $i = 1-4$ ) have the properties that the surface they describe is continuous while the surface gradients are not continuous when any one of the principal stresses changes sign. In this work, a 12"x12" column is taken to be re-strengthened. The dimensions of jacket (4" at each side) for all four techniques are kept unaltered. Length of each model is 10 ft. The design is done in such a way that the compressive strength of the four models after re-strengthening are theoretically equal. The design compressive strength for non-jacketed (A) and jacketed (B, C, D, E) columns are 433.8 kips and 1115.2 kips whereas the nominal compressive strength are 667.4 kips and 1715.6 kips respectively. The modelling of interface surface is done in the same way for four models. These conditions ensure that the change in structural responses with incremental loading obtained in numerical analysis will be controlled only by reinforcement pattern.

Table 1: Details of numerical modelling in ANSYS

	A	B	C	D	E
Plan view					
Isometric view					
Size	12"x12"	20"x20"	20"x20"	20"x20"	20"x20"
Longitudinal Steel	4#8φ	8#8φ	Equivalent to 8#8φ	Equivalent to 8#8φ	Equivalent to 8#8φ
Transverse Steel	#3φ @12" c/c	#3φ @6" c/c	Equivalent to #3φ @6" c/c	Equivalent to #3φ @6" c/c	Equivalent to #3φ @6" c/c

### Material Properties

The properties of concrete and reinforcing steel are as the table below.

Table 2: Material Properties

Concrete		Reinforcing Steel	
Property	Value	Property	Value
Compressive Strength	4000 psi	Modulus of Elasticity	$2.9 \times 10^7$ psi
Modulus of Elasticity	$3.605 \times 10^6$ psi	Poisson's Ratio	0.3
Poisson's Ratio	0.18	Yield Strength	60000 psi
Uniaxial Cracking Stress	474.34 psi	Tangent Modulus	2900 psi
Open shear transfer coefficient	0.3		
Closed shear transfer coefficient	1		

### Element Meshing

After modeling and inputting all the data the models are meshed. The original column (A) is subdivided into  $6 \times 6 \times 20 = 720$  elements whereas the retrofitted columns (B, C, D and E) are subdivided into  $10 \times 10 \times 20 = 2000$  elements. Each element sizes 2"x2"x6". The mesh size is kept the same in contact surface i.e. 2"x6". Number of elements in contact surface is  $6 \times 20 \times 4 = 480$ .

### Loads and boundary condition

Displacement boundary conditions are needed to be constrained in the model to get a unique solution. To ensure that the model acts the same way as the experimental columns specimens, boundary conditions need to be applied where the supports and loadings exist. For concentric columns model the displacement of all nodes at bottom base of column in x, y and z. directions is held zero ( $U_x=0$ ,  $U_z=0$  and  $U_y=0$ ). To apply the axial load on the top of the concentric column specimens, loads were applied on each nodes at the top of the columns.

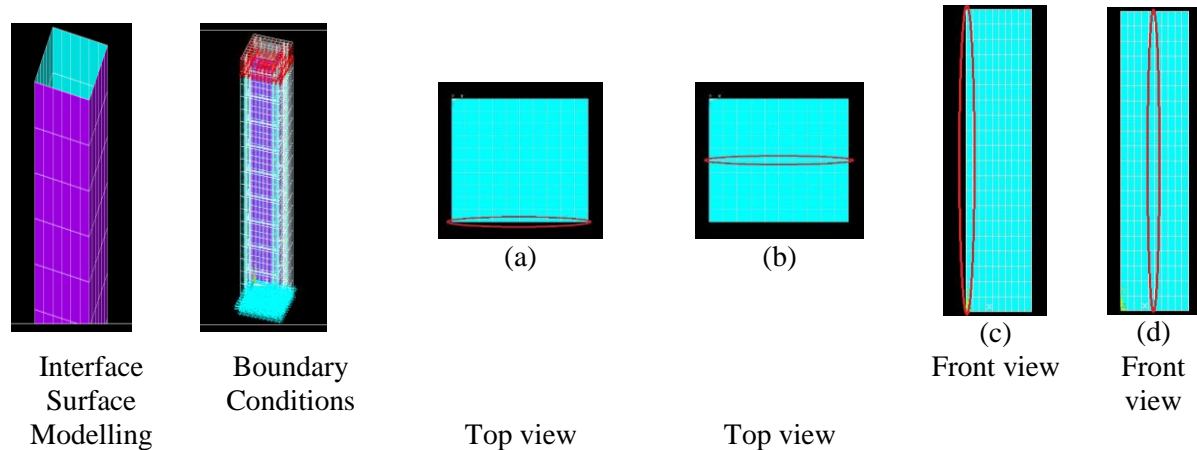


Fig. 3: Interface and Boundary Conditions Fig. 4: Selected directions for structural response comparison

## RESULTS AND DISCUSSIONS

In the following section, the four models of RC jacketing will be compared on the basis of load-deflection plots at selected locations on the columns, first cracking loads and loads at failure.

### First Cracking Load

The analysis of the five column models shows the following first cracking loads. The increment of the first cracking load with compared to model A is also shown in the Table 3.

Table 3: Comparison of first cracking load

Model	A	B	C	D	E
First Cracking Load (Kips)	230.6	648.6	619.9	652.1	648.3
Increment (compared to A), %	0.00	181.27	168.82	182.78	181.1

### Displacements and Stresses

Four directions are selected for the comparison of displacements and stresses as shown in Fig. 4. Total 72 different comparison are made on displacements (i.e. x-component of displacement, y- component of displacement, z- component of displacement and displacement vector sum) and stresses (i.e. 1st principal stress, 2nd principal stress, 3rd principal stress, stress intensity and equivalent Von Mises stress). Some of the comparisons are shown in Fig. 5 to Fig. 12.

Fig. 5 shows that at top edge nodes of plan displacement is maximum at two opposite sides and decreases from side to middle. Displacement plot shows that displacement both at middle and side are minimum for model D at the same concentric loading condition.



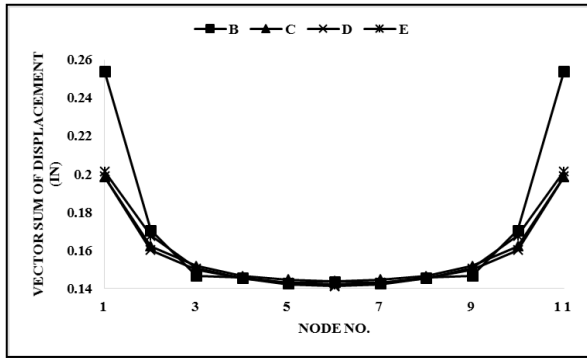


Fig. 5: Variation of Vector Sum of Displacement (direction shown in Fig. 4a)

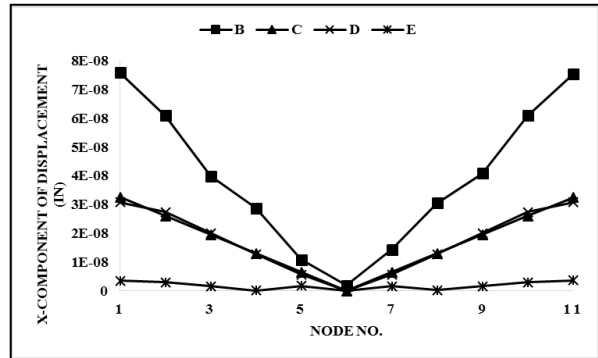


Fig. 6: Variation of x-component of Displacement (direction shown in Fig. 4b)

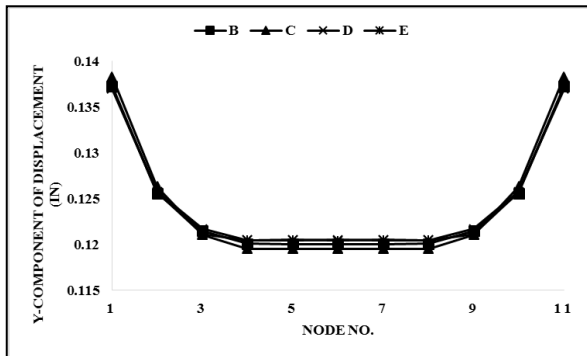


Fig. 7: Variation of y-component of Displacement (direction shown in Fig. 4b)

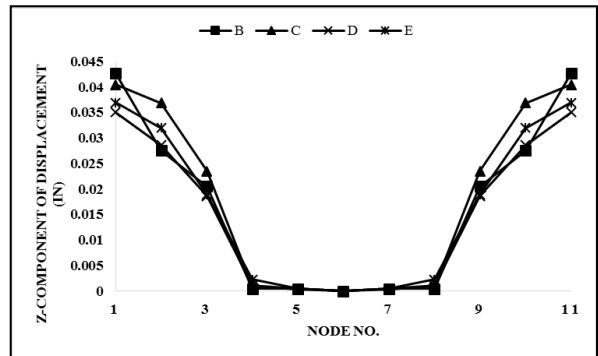


Fig. 8: Variation of z-component of Displacement (direction shown in Fig. 4b)

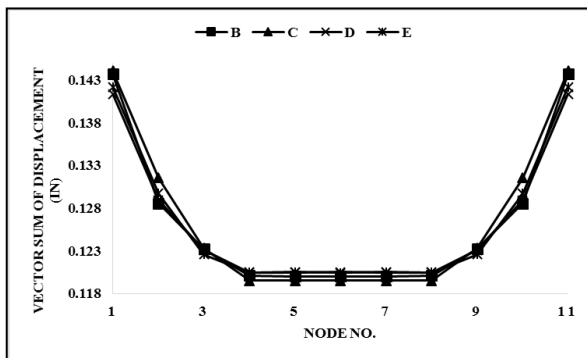


Fig. 9: Variation of Vector Sum of Displacement (direction shown in Fig. 4b)

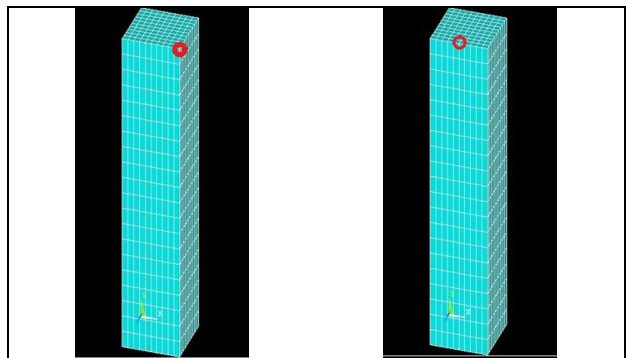


Fig. 10(a): Top corner Fig. 10(b): Top edge node location

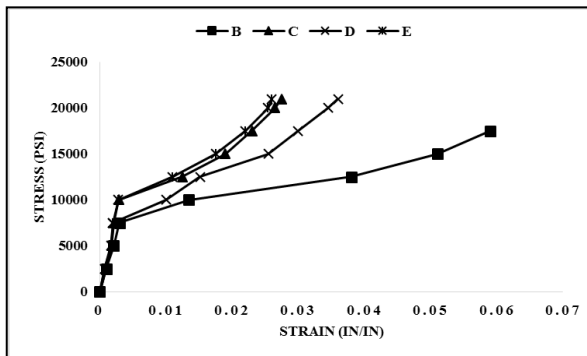


Fig. 11: Stress-strain diagram for top corner node.

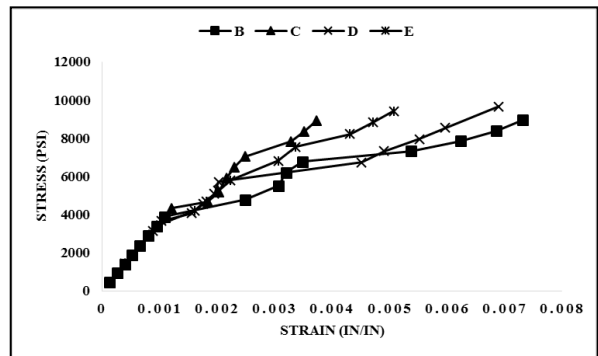


Fig. 12: Stress-strain diagram for top edge middle node

In Fig. 6, it is found that the x-component of displacement is always minimum for model E, then model C, and maximum value for model B. Fig. 7 describes the variation of y-component of displacement at

top middle nodes of plan and shows maximum displacement is for model C at edge whereas minimum displacement is for D at the edge node. The minimum displacement at the center node is for model C. In Fig. 8, the z-component of displacement is minimum for model D and maximum for model B. Displacement value decreases from edge to middle nodes. Fig. 9 describes the variation of vector sum of displacement at top middle nodes of plan and shows minimum displacement is for model D at the edge node whereas maximum displacement is for C. The minimum displacement at the center node is for model C.

## CONCLUSIONS

Based on the analysis and comparison of the four different models, conclusion may be stated as: In very low range of loading, the axial and lateral deformation responses of model B, C, D and E are almost similar. From the stress-strain diagram shown in Fig. 11 it can be concluded that all the four models act almost the same upto the proportional limit. After exceeding the proportional limit, the model E shows most brittle behavior. The model C also shows brittle nature whereas the model D shows a relatively flat stress-strain diagram which indicates its ductile nature. The model B also shows maximum strain at the same stress level but the curve ends before reaching the maximum stress level reached by the model D. From the stress-strain diagram shown in Fig. 12, it is established that all the four models act almost the same upto the proportional limit and after exceeding the proportional limit, the model C shows a steeper stress-strain diagram. The model E shows almost same behavior as model C but gives a flatter stress-strain diagram than that of the model C which indicates E to be more brittle than C. The stress-strain diagram for model B is flatter than that of the model D. The model B shows maximum strain at the same stress level as the model D but the curve ends before reaching the maximum stress level reached by the model D. Cracking starts at 652.1 kips load for model D, which is greater than the other three (B=648.6 kips; C=619.9 kips; E=648.3 kips). From the stress-strain diagrams (Fig. 11 and Fig. 12), it is observed that the model D shows more ductile behavior than model C and E. Model D is the best RC jacketing technique based on its axial and lateral deformation responses, such as strain at different stages of incremental loading; stresses at different points; and cracking load.

## REFERENCES

- A.Teran & J.Ruiz, Reinforced concrete jacketing of existing structures, *Earthquake Engineering, Tenth World Conference*, 1992 Balkema, Rotterdam. ISBN 9054100605.
- Alcocer S & Jirsa J. Assessment of the response of reinforced concrete frame connections redesigned by Jacketing. *Proceedings of the 4th US National Conference on Earthquake Engineering 1990*: 3: 295–304.
- ANSYS 11.0 user manual, ANSYS Corporation.
- Bett BJ, Klingner RE & Jirsa JO. Lateral load response of strengthened and repaired reinforced concrete columns, *ACI Structural Journal* 1988: 85(5): 499–508.
- Ju'lio E S, F Branco and V D Silva, *Structural rehabilitation of columns with reinforced concrete jacketing*, Prog. Struct. Engng Mater. 2003; 5:29–37 (DOI: 10.1002/pse.140).
- Ju'lio ES, Branco F & Dias da Silva V. *A influe'ncia da interface no comportamento de pilares refor,ados por encamisamento de beta'õ armado*. *Proceedings of the Congresso Construc,a'õ 2001*, IST, Lisbon, 17–19 December 2001: 1: 439–446.
- Julio ES., *A influe'ncia da interface no comportamento de pilares refor,ados por encamisamento de beta'õ armado*, PhD Thesis, Universidade de Coimbra. 2001.
- Rodriguez M & Park R., Seismic load tests on reinforced concrete columns strengthened by jacketing, *ACI Structural Journal*, March–April 1994: 91(2): 150–159.
- Shri. Pravin B. Waghmare, Materials And Jacketing Technique For Retrofitting Of Structures, *International Journal of Advanced Engineering Research and Studies* E-ISSN2249 – 8974(2011)
- Vedprakash C. Marlapalle, P. J. Salunke, N. G. Gore, Analysis & Design of R.C.C. Jacketing for Buildings, *International Journal of Recent Technology and Engineering (IJRTE)*, ISSN: 2277-3878, Volume-3 Issue-3, July 2014.

## **EFFECT OF VARIATION IN THE STRENGTH OF CONCRETE AND REINFORCING BARS ON THE BEHAVIOR OF RC BEAMS**

A. Amin<sup>1</sup> & N. H. M. K. Serker<sup>2\*</sup>

<sup>1</sup>*Department of Civil Engineering, European University of Bangladesh, Dhaka, Bangladesh*

<sup>2</sup>*Department of Civil Engineering, Rajshahi University of Engineering & Technology, Rajshahi, Bangladesh*

*\*Corresponding Author: kamrujjaman.serker@ruet.ac.bd*

### **ABSTRACT**

Reinforced concrete members are designed with specified code specifications. In general, the compressive strength of concrete and the yield strength of steel are assumed in the design process. Compressive strength of concrete depends on a number of factors and generally shows some degree of variation from the desired strength. On the other hand, reinforcing bars with higher yield strength than that recommended in the Bangladesh National Building Code is available in the market and being used in construction. Therefore, increase in yield strength of steel and decrease in compressive strength of concrete may have adverse effects on the flexural behavior of beams. This study includes the behavior of reinforced concrete beam due to this variation in strengths. This study shows that some certain beam turns into over-reinforced from under-reinforced state as well as compression controlled from tension-controlled state due to change in strengths. Besides, reduction in ductility is also observed due to strength variation in the properties of the major constituent materials. A complete theoretical analysis along with some experimental investigation is presented in this paper.

Keywords: Ductility; high-strength steel; BNBC; beam behavior

### **INTRODUCTION**

The building construction industry is one of the emerging sectors of Bangladesh and reinforced concrete (RC) building frames are the most popular choice in this regard. Recent earthquakes as well as some tragic incidents have raised the issue of performance of these buildings during an earthquake or under ultimate load. Concrete and reinforcing bars are the chief constituent materials in RC buildings. Since reinforcing bars are made in the factory its quality can be easily controlled and high strength steel bars are also available in the local market. The use of high-strength steel bars offers several advantages, such as the reduction of the reinforcement ratio, less cost for reinforcement placement, reduced reinforcement congestion, better concrete placement etc. On the other hand the quality of concrete is difficult to control and this job has become an impossible one in Bangladesh because of the crude construction technology and no-trained workers. Another important issue is the use of higher strength steel than that specified in the Bangladesh National Building Code (BNBC). BNBC (1993) adopted some of the ASTM Standards for structural steel and allowable yield strength of steel reinforcing bars was limited to 410 MPa (60 ksi). The important concern is that RC members are designed with Code specified maximum yield strength of 410 MPa and constructed with locally available higher grade steels such as thermo mechanically treated (TMT) high strength structural steel bars having yield strength up to 500 MPa or 72.5 ksi (Islam, 2010). Therefore such increase in yield strength of steel and decrease in compressive strength of concrete may have adverse effects on the behavior of RC flexural members and the beam would not achieve adequate ductility under ultimate load. This study aims to focus on

1. the behavior of beams using TMT high strength structural steel bars and concrete having specified design strength.
2. the behavior of beams using TMT high strength structural steel bars and concrete having strength less than the specified design strength.

## METHODOLOGY

The study is divided into two steps (i) analytical study with some typical beam sections (ii) experimental investigations. In each case ultimate load carrying capacity of the beam and ductility was measured.

Ductility is an important issue in the design of structure and structural member and is defined as the ability of the material/member to sustain deformation beyond the elastic limit while maintaining a reasonable load carrying capacity until total failure (Pam et. al., 2001). Ductility is a valuable structural property as it allows stress redistribution and provides warning of impending failure. The ductility of a reinforced concrete beam depends on the amount of tension reinforcement, the amount of compression reinforcement and the strength and ductility of the materials used (Sarkar et. al., 1997).

Generally, reinforced concrete beams are under-reinforced by design, so that failure is initiated by yielding of the steel reinforcement, followed, after considerable deformation at no substantial loss of load carrying capacity, by concrete crushing and ultimate failure. That is a ductile mode of failure is desired and is ensured by designing the tensile reinforcement ratio to be substantially below the balanced ratio, which is the ratio at which steel yielding and concrete crushing occur simultaneously. The mathematical expression of balanced reinforcement ratio (Nilson et. al., 2004) is

$$\rho_b = 0.85 \beta_1 \frac{f'_c}{f_y} \frac{\epsilon_u}{\epsilon_u + \epsilon_y} \quad (1)$$

where,

$f'_c$  = compressive strength of concrete,

$f_y$  = yield strength of steel,

$\epsilon_u$  = ultimate strain in concrete (usually taken as 0.003),

$\epsilon_y$  = yield strain of steel and

$\beta_1$  = constant depends on compressive strength of concrete. It is clear from Eq. (1) that for a particular beam section the balanced reinforcement ratio depends on the material properties. Besides upper limit of the reinforcement ratio has been introduced in the design Codes (e.g. ACI 318-05) to guarantee ductility

$$\rho_{max} = 0.85 \beta_1 \frac{f'_c}{f_y} \frac{\epsilon_u}{\epsilon_u + 0.004} \quad (2)$$

The reinforcement ratio thus provides a measurement for ductility and the ductility corresponding to the maximum allowable reinforcement ratio provides a measure of the minimum acceptable ductility. The mode of failure is another important issue which is defined as a function of net tensile strain. The net tensile strain is the tensile strain in the extreme tension steel at nominal strength. According to ACI Code (2005), a beam section is said to be tension-controlled if the net tensile strain is equal to or larger than 0.005 and compression-controlled if the net tensile strain is equal to or less than 0.002. A section is in a transition region between compression- and tension-controlled sections.

In this article the curvature ductility was considered. The ductility factor was taken as the ratio of the curvature at yield and ultimate condition. The ductility can be estimated as shown below:

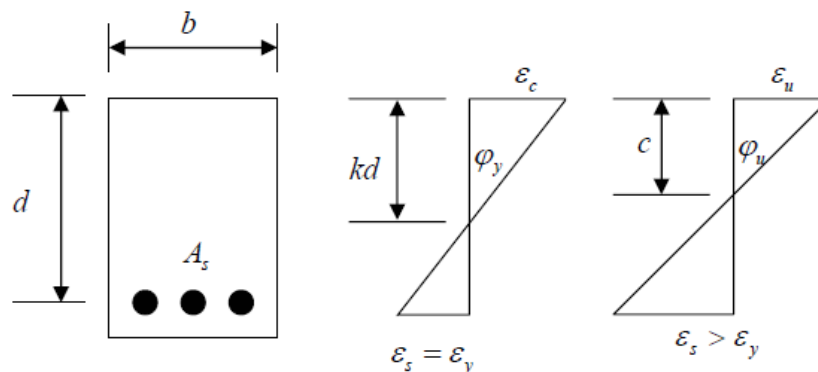


Fig. 1: Calculation of ductility

$$\text{The curvature at yield condition, } \phi_y = \frac{f_y}{E_s} \frac{1}{d(1-k)} \quad (3)$$

where,  $\phi_y$  = curvature at yield condition,  $k$  = constant,  $E_s$  = modulus of elasticity of steel,  $d$  = effective depth of the beam.

$$\text{The curvature at ultimate condition, } \phi_u = \frac{\epsilon_u}{c} = \frac{\epsilon_u \beta_1}{a} \quad (4)$$

where,  $\phi_u$  = curvature at ultimate condition,  $a$  = depth of rectangular compression stress block.

$$\text{Ductility } \mu = \frac{\phi_u}{\phi_y} = \frac{\epsilon_u}{f_y} \frac{d(1-k)}{a/\beta_1} \quad (5)$$

Another important factor, the strength reduction factor, is also incorporated in the design of the reinforced concrete members which is essentially based on the deformation capability of the member. The strength reduction factor depends on the net tensile strain of the beam. The purposes of the strength reduction factor are (1) to allow for the probability of under-strength members due to variations in material strengths and dimensions (2) to reflect the degree of ductility and required reliability of the member under the load effects being considered and (3) to reflect the importance of the member in the structure (ACI 318-05, 2005). Design strength or usable strength of a member or cross section is the nominal strength multiplied by the strength reduction factor.

### **NUMERICAL STUDY**

To understand the effect of the variation in chief constituent materials a numerical analysis was conducted on a beam section. A typical beam section (width = 12 inch, overall depth = 26 inch, effective depth = 22.5 inch) reinforced with three No.7 and two No. 9 bars was considered and analyzed. The analyses results are presented in Table 1. The beam section was analyzed considering two different grades of concrete to understand how the material strength affects the behavior of reinforced concrete beams. Balanced steel ratio, maximum steel ratio and ductility were calculated for each beam using the equations shown in the previous section and are presented in Table 1.

It is clear from Table 1 that the nominal strength of the beam increases as the yield strength of steel increases (Beams A2 and B2). However, the ultimate strength or the design strength of the beam may not increase in each case because the net tensile strain reduces appreciably. On the other hand, ductility of the member reduces with the inclusion of higher strength steel than that was primarily specified in the design. The minimum ductility may be obtained if the compressive strength of concrete decreases and the yield strength of the steel increase (Beams A3 and B3). The reduction in ductility is obvious and irrespective of concrete grade. Similarly, the net tensile strain reduces as the yield strength of the steel increases or the compressive strength of concrete reduces. Balanced steel ratio or the maximum steel ratio also decreases the yield strength of the steel increases or the compressive strength of concrete reduces.

### **EXPERIMENTAL INVESTIGATION**

To make the analysis more reliable, an experimental program was taken. Three rectangular singly reinforced concrete beams having dimensions 4in. x 10in. x 48in. (breadth x depth x length) were fabricated for testing. The beams were cast from normal strength concrete with cylinder compressive strength ranging from 2500 to 3000 psi. In order to study the effects of different materials strength yield strength of steel was also varied. The main bars (two No. 4 bars) were placed near the bottom of the beams. Near the top of the beams, two No. 3 bars (8 mm) bars were added as hanger bars for fixing the stirrups. All of the beams were simply supported at a span of 42 in. and were tested by subjecting them to monotonically applied point load at mid-span, as illustrated in Figure 2. Detailed properties of the beams are given in Table 2. During loading, the vertical deflections at mid-span of the beams were measured by a displacement dial gauge. Visual inspection of the cracks was carried

Table 1: Numerical analysis results

Sl. No.	$f'_c$ (ksi)	$f_y$ (ksi)	Steel ratio	Balance d steel ratio	Max. steel ratio	Net tensile strain	Strength reduction factor	Mode of failure	Ductility	Nominal Moment Capacity (k-ft)	Ultimate Moment Capacity (k-ft)
A1	3.0	60.0	0.014	0.0214	0.0155	0.0050	0.90	Tension	2.24	356.7	321.0
A2	3.0	72.5	0.014	0.0163	0.0128	0.0033	0.76	Transition	1.53	413.2	315.0
A3	2.5	72.5	0.014	0.0136	0.0107	0.0024	0.68	Transition	1.24	392.5	265.0
B1	4.0	60.0	0.014	0.0285	0.0206	0.0077	0.90	Tension	3.07	374.4	337.0
B2	4.0	72.5	0.014	0.0217	0.0171	0.0059	0.90	Tension	2.10	439.0	395.1
B3	3.5	72.5	0.014	0.0190	0.0150	0.0048	0.69	Transition	1.79	428.0	295.0

out throughout the tests. The test was terminated when the specimen failed completely, i.e. when the resistance of the specimen dropped. The load-deflection plot and failure patterns are shown in Fig. 3 and 4 respectively.

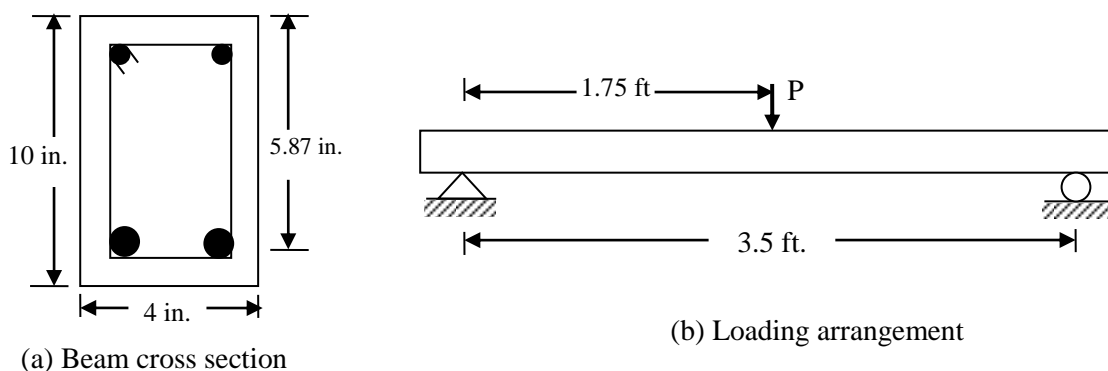


Fig. 2: Beam cross section and loading arrangement

Table 2: Properties of the beam specimen

Sl. No.	$f'_c$ (ksi)	$f_y$ (ksi)	Balance d steel ratio	Max. steel ratio	Net tensile strain	Strength reduction factor	Mode of failure	Ductility	Deflection (in)	Ultimate Load (k)
C1	2.93	60.0	0.021	0.015 <sub>1</sub>	0.005 <sub>3</sub>	0.90	Tension	2.51	0.26	10.5
C2	2.97	72.5	0.016	0.012 <sub>7</sub>	0.004 <sub>0</sub>	0.66	Transition	1.74	0.18	12.1
C3	2.52	72.5	0.014	0.010 <sub>8</sub>	0.002 <sub>9</sub>	0.61	Transition	1.44	0.14	12.5

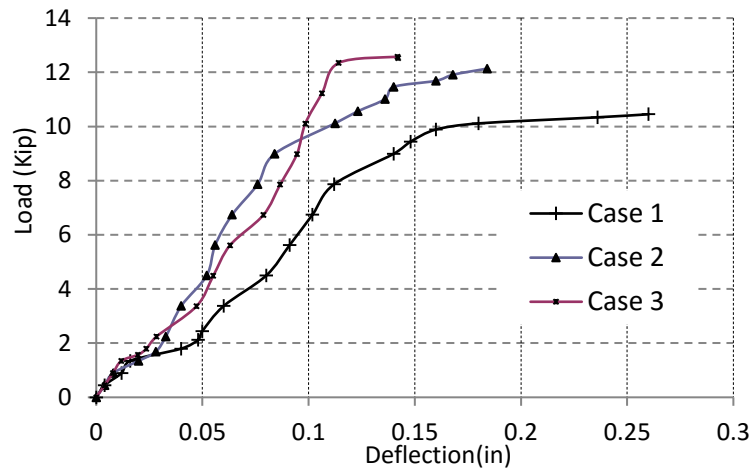


Fig. 3: Typical load- deflection curves

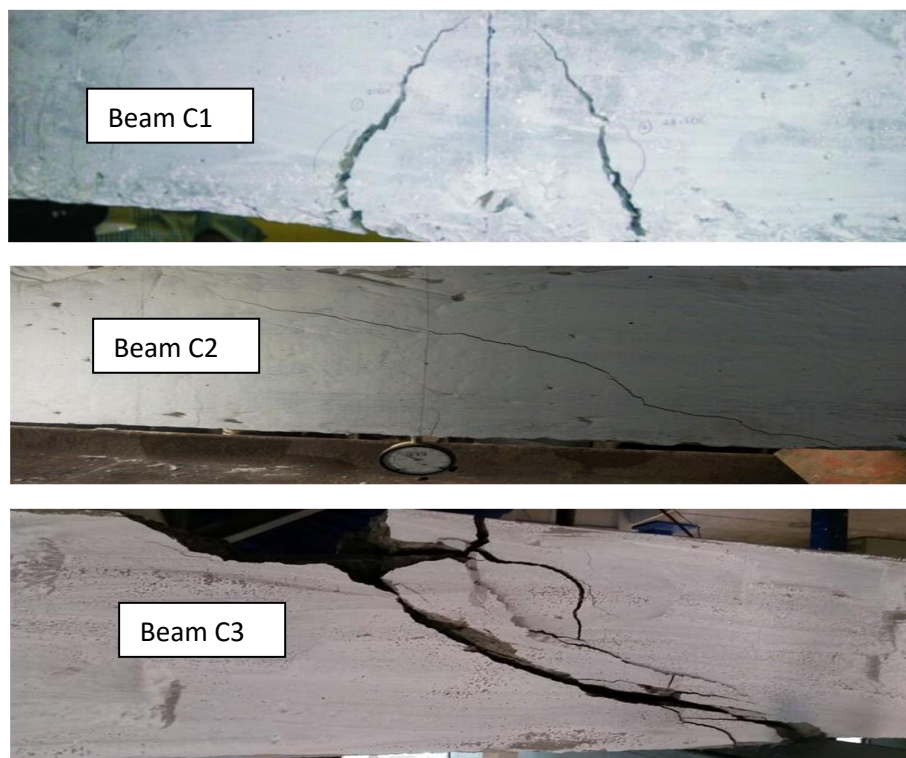


Fig. 4: Failure pattern of experimental beams

### Experimental Results

The experimental program was designed in such a way that the variation of the material strengths on the behavior of beam can be studied. From the numerical study results it is clear that a section may turn into over-reinforced if the strength of concrete decreases or strength of steel increases. Therefore, the tension reinforcement may or may not yield before the concrete in the compression zone is crushed. If the strength of the materials remains the same as it was considered in the design the reinforcement ratio may lie below the allowable maximum amount as a result the tension reinforcement will yield before the concrete is crushed and the beam will fail in a ductile manner. If the reinforcement ratio becomes larger than the allowable maximum, the concrete will be crushed without prior yielding of the tension reinforcement and the beam will fail in a brittle manner.

Beam C1 was designed considering compressive strength of 3000 psi and yield strength of steel as 60,000 psi. Due to some limitations, measurement of strain of steel or concrete was not possible. It was expected from the previous numerical study that the use of higher strength steel or lower strength concrete will affect the behaviour of the beam significantly. From the experiment the ultimate load

capacity of the beam was measured as 10.5, 12.1 and 12.5 kips for beam C1, C2 and C3 respectively. It is evident that the load carrying capacity of the beam has been increased after increasing the yield strength of steel. However, the ultimate load of beam C3 was larger than the expected. It is noteworthy that the deflection of the beam specimens reduces as the yield strength of steel increases or compressive strength of concrete decreases. The measured deflections are well correlated with the theoretical ductility. It is evident from the analytical study that there is a remarkable effect on the mode of failure of the beam and the beam which was initially designed as an under-reinforced section may turn into an over-reinforced section i.e. the beam may also fail by crushing of concrete instead of yielding of steel. The experimental beam also reflects the same as it can be seen from Figure 4.

## **CONCLUSIONS**

In the design of a reinforced concrete beam, both the flexural strength and ductility need to be considered. However, more importance is usually given to the flexural strength and only a simple check is carried out to ensure that a certain minimum level of ductility is provided by keeping the beam under-reinforced. From the structural safety point of view, ductility is as important as strength. A good ductility would provide the beam with a much better chance of survival when it is overloaded, attacked by a severe earthquake or subjected to an accidental impact.

From the above, it is evident that the major factors affecting the flexural strength and ductility of a reinforced concrete beam section are the concrete grade, yield strength of steel and tension steel ratio. In the case of a singly reinforced section, at a fixed concrete grade, the use of a higher tension steel ratio leads to a higher flexural strength but a lower ductility. Hence, the increase in flexural strength is achieved by compromising ductility.

When specified design strength and actual strength remain the same, then the steel ratio is below the allowable maximum steel ratio thus beam shows tension failure and produce higher deflection and ductility. When compressive strength remain the same but steel strength is increased, then beam shows larger nominal strength and produces relatively lower deformation and ductility. In case compressive strength is decreased but steel strength is increased which may be a common case in Bangladesh, the steel ratio increases and mode of failure of the beam is also changed and results lower deformation and ductility.

## **REFERENCES**

- ACI Committee 318. 2005. Building Code Requirements for Structural Concrete (ACI 318-05) and Commentary, American Concrete Institute, Farmington Hills, MI.
- ASTM A615/A615M-09. 2009. Standard Specifications for Deformed and Plain Carbon-Steel Bars for Concrete Reinforcement, ASTM International, West Conshohocken, PA.
- Bangladesh National Building Code. 1993. Housing and Building Research Institute, Dhaka, Bangladesh.
- Islam, MA. 2010. Thermo Mechanically Treated Advanced Steels for Structural applications, *Proceedings of MARTEC 2010, the International Conference on Marine Technology*, 11-12 December, 2010, Dhaka, Bangladesh.
- Nilson, AH; Darwin, D and Dolan, CW. 2004. *Design of Concrete Structures*, Thirteenth edition. McGraw Hill
- Pam, HJ; Kwan, AKH and Islam, MS. 2001. Flexural strength and ductility of reinforced normal- and high-strength concrete beams. *Proceedings of the Institution of Civil Engineers, Structures and Buildings*, 146(4): 381–389.
- Sarkar, S; Adwan, O. and Munday JGL. 1997. High strength concrete: an investigation of the flexural behaviour of high strength RC beams. *Structural Engineer*, 75(7):115–121.



## **A CASE STUDY OF STRENGTHENING OF AN EXISTING RESIDENTIAL BUILDING FOR USING IT AS A GARMENTS FACTORY**

M. R. Alam<sup>1\*</sup>, S. B. Ali<sup>2</sup>, A. Rafi<sup>1</sup> & M. O. B. Zahid<sup>1</sup>

<sup>1</sup>*Department of Civil Engineering, Chittagong University of Engineering and Technology,  
Chittagong, Bangladesh*

<sup>2</sup>*Institute of Earthquake Engineering Research, Chittagong University of Engineering and  
Technology, Chittagong, Bangladesh*

*\*Corresponding Author: rabiul@cuet.ac.bd*

### **ABSTRACT**

Recently, the rise of the commercial uses of building is enormously large, especially in urban areas of developing country like Bangladesh. Many of the investors are using a residential building as garments factory without any improvement of structure, which leads it to collapse such as, the tragedy of RANA PLAZA. The aim of this study is to provide a better solution of using a residential building safely and efficiently as a garments factory while it had not been predesigned for commercial use. The whole study includes analysis of structure elements with increasing loads, detect the failed members and provide them proper treatment of strengthening so that the building can sustain with moderated loading condition. There are number retrofitting methods are available in modern civil engineering works. In this study jacketing procedure is used for strengthening the existing building. The major analysis and design works, both in initial and retrofitted structural conditions are done by ETABS software. It is observed that, the correlative strengthening work can be carried out if any of structure members is damaged or cracked due to unsuspected loading or environmental disruptions.

Keywords: Strengthening method; retrofitting technique; jacketing; garments factory

### **INTRODUCTION**

The RC buildings are designed and constructed according to which purpose it is to be used such as residential purpose, industrial or commercial purpose. The elements of the building are though so that they are carried out according to their functions. If the purpose of use of a building is changed, the whole loading patterns is replaced by moderated loading system. So the behaviours of the structural elements may be changed. In some cases, some of the members need to be improved. The whole process requires strengthening the existing elements (Handbook, 2007).

The Garments sector has emerged as one of the biggest earner of foreign currency and day by day it is extending. The investors are opting to generate the factories in urban areas where the labours are available. The problem that arises includes limited resources with lack of place. It is much efficient, in this case, to convert a residential building into an industrial building.

The present study provides a better solution of using a residential building safely and efficiently as a garments factory while it had not been predesigned for commercial use. In the study analysis work is done of structure elements with increasing loads, detect the failed members and provide them proper treatment of strengthening so that the building can sustain with moderated loading condition.

### **RETTROFITTING TECHNIQUE USED FOR EXISTING BUILDING**

#### ***Jacketing of Columns***

Jacketing of columns consists of added concrete with longitudinal and transverse reinforcement around the existing columns. This type of strengthening improves the axial and shear strength of

columns while the flexural strength of column and strength of the beam-column joints remain the same.



Fig. 1: Construction Techniques for Column Jacketing.

### ***Jacketing of Beams***

Jacketing of beams is recommended for several purposes as it gives continuity to the columns and increases the strength and stiffness of the structure (Md. Akhter et al., 2013). While jacketing a beam, its flexural resistance must be carefully computed to avoid the creation of a strong beam-weak column system.

### ***Enlarging the Area of Footing***

The loads from a building get transmitted to the soil through the foundation. A seismic retrofit of a building includes strengthening of inadequate foundations or supplementing with new foundation. This covers the important aspects of deficiencies of foundation, analysis and assessment of foundation, the types of intervention to strengthen the foundation and the methods of execution.

## **STRUCTURAL PLANS**

A five-story residential building was designed and constructed according to the BNBC, 1993 code. The plan of typical floor is shown in Fig 2.

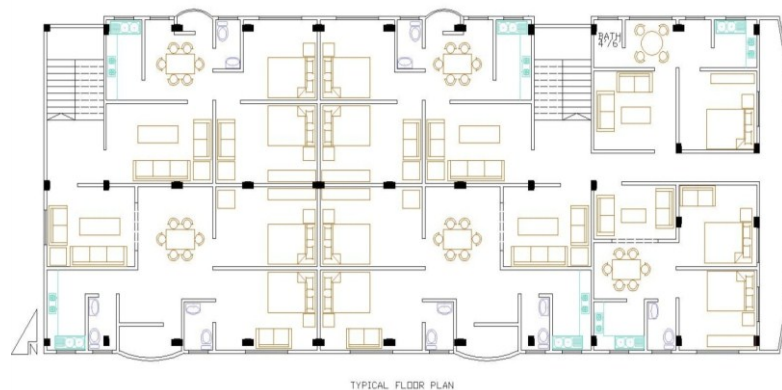


Fig. 2: Typical floor plan.

Initially the building was constructed for residential use. After some times, it was decided that the building is to be used as garments factory. Then remodeling of plans was necessary. The revised floor plans are given below:

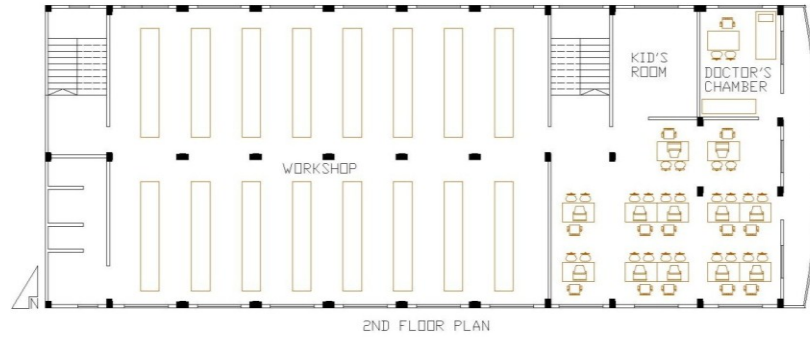


Fig. 3: Typical floor plan of Garments.

Table 1: Data of building element

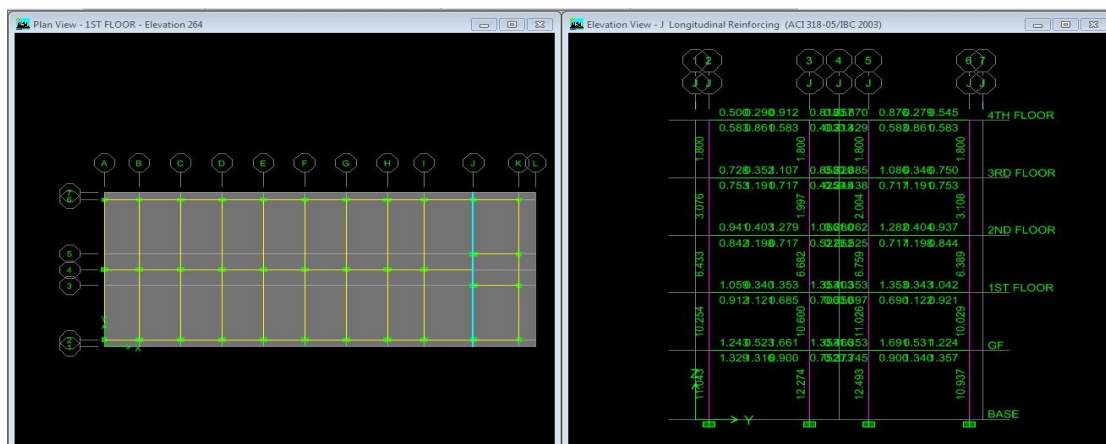
Ground floor space (sq. ft.)	Typical floor space (sq. ft.)	Columns			Beams		
		Types	Cross-Section	Number	Types	Cross-Section	Number
3925.76	4427.04	C1	10 × 20	8	B1	10 × 22	18
		C2	10 × 15	6	B2	10 × 20	1
		C3	10 × 15	18	B3	10 × 15	5
		C4	10 × 12	3	B4	10 × 15	31

### DESCRIPTION OF ANALYSED MODELS

In the present study the analysis is conducted with the aid of ETABS software. Three types of analysis was done according to ACI-318-05.

- i. Analysis as residential building
- ii. Analysis as garments factory of same structure
- iii. Analysis as garments factory of retrofitted structure

It is observed from Fig. 4 for section J, when the loading pattern was changed from residential to garments factory, some of the members are failed. It is occurred when a beam is subjected to loading, at the end of the beam, there is huge shear but the moment is comparatively small. Then due to the combination of shear stress and flexural stress, the principle stress is generated. Here, the failed beam sections are increased by beam retrofitting.



(a)

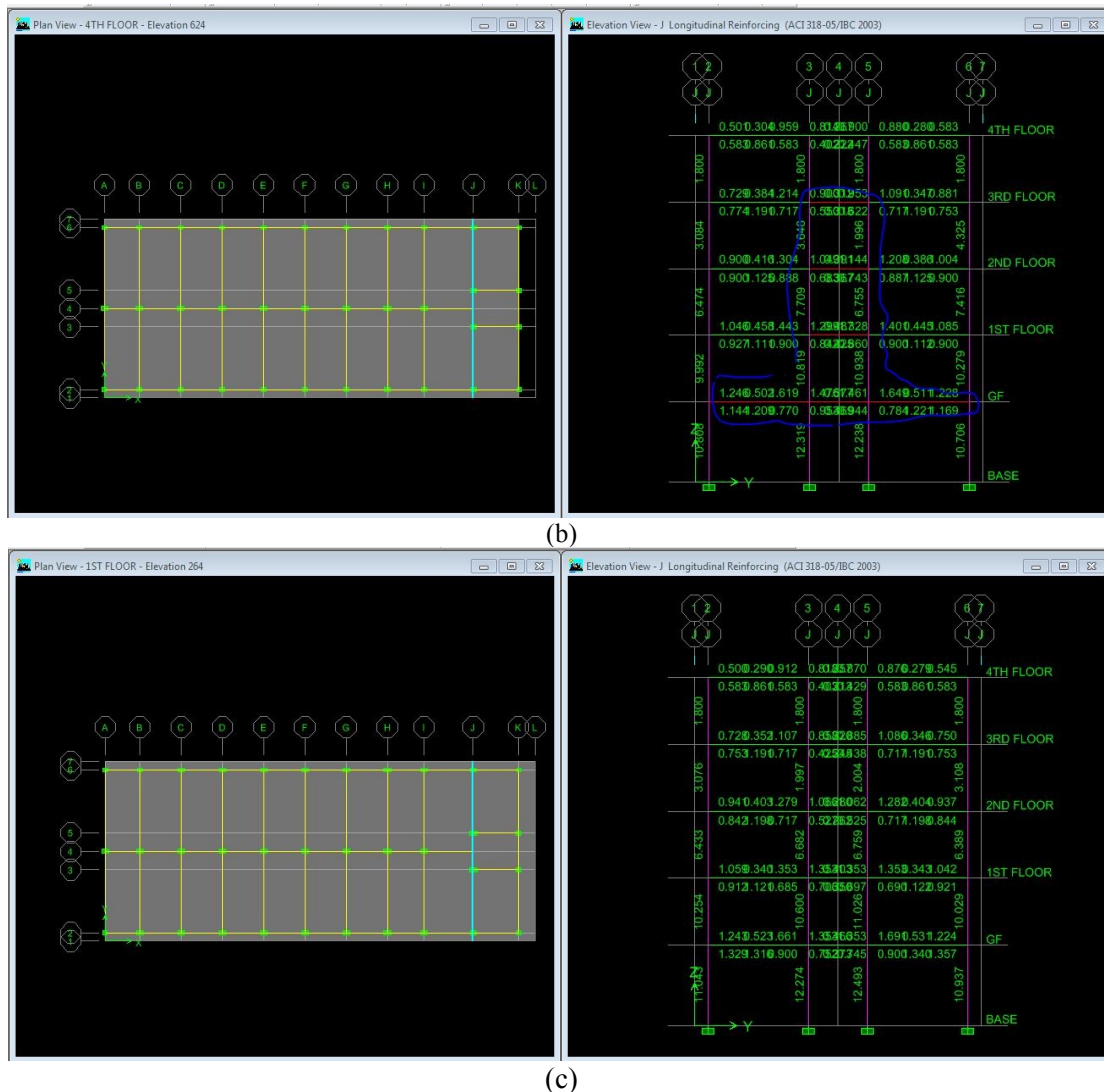


Fig. 4: Analysis data of section J for (a) Residential building, (b) Garments factory before retrofitting, (c) Garments factory after retrofitting

Similar observation can be made for section 4 and I. It is indicated that the ground floor columns requires extra reinforcement. So the short columns and ground floor columns are to be retrofitted.

## RETTROFITTING DESIGN

It is seen from the previous section that when the loading cases were changed for garments factory, some members of previously designed structure were failed. Therefore the failed members needed to be retrofitted. The structure is redesigned with retrofitted members.

### *Retrofitting of Beams*

When the manufactured load case is assigned in the structure, the result shows that B1 at grade beam (4I-6I section), the shear stress due to shear force and torsion together exceeds maximum allowed. Therefore the member is failed. Moreover, B2 beam at section 3J-5J, from ground floor to 2nd floor, is also failed due to the shear stress due to shear force and torsion together exceeds maximum allowed.

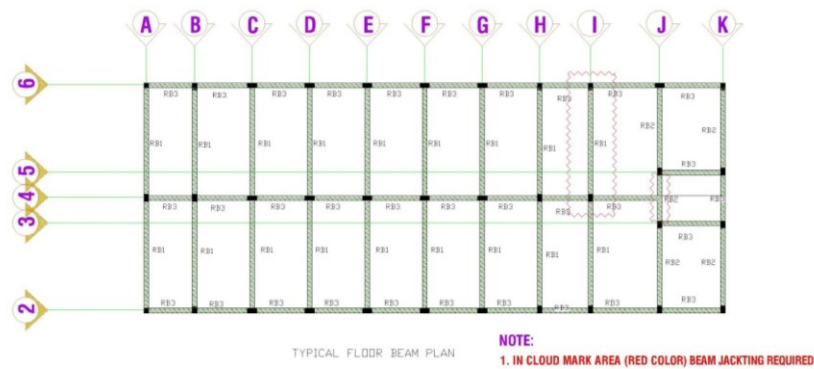


Fig. 5: Location of Beam Jacketing.

Those sections are needed to be increased by retrofitting. After retrofitting by concrete jacking method, those sections are adequate. According to the code, the minimum thickness of jacking i.e. 4 inch at each face is provided. Minimum reinforcement is also provided. The detailed analysis data of retrofitted beam is given at Table 2.

Table 2: Analysis data of retrofitted beams.

Beam NO	Size (in x in)	MAX +Mu(kip-in)	MAX -Mu(kip-in)	Req. Rebar Area (in <sup>2</sup> )		Provided Rebar (in <sup>2</sup> )		Shear Vu	Shear Rebar Req. (in <sup>2</sup> )
				Top	Bottom	Top	Bottom		
B1-R	18×32	1380	3137.9	Top	3.0	Top	5.72	63.31	.041
				Bottom	2.98	Bottom	4.84		
B2-R	18×30	868.66	1737.34	Top	2.5	Top	4.84	39.41	.005
				Bottom	2.5	Bottom	4.4		

### Retrofitting of Columns

After assigning the manufactured load case in the structure, the result shows that C1 (4B-4I section) at ground floor, reinforcing required exceeds maximum allowed. Therefore the member is failed. Those sections are needed to be increased by retrofitting. After retrofitting by concrete jacking method, those sections are adequate. According to the code, the minimum thickness of jacking i.e. 4 inch at each face is provided. Minimum reinforcement is also provided. Shear connector are used @ 12inch c/c in each face of column.

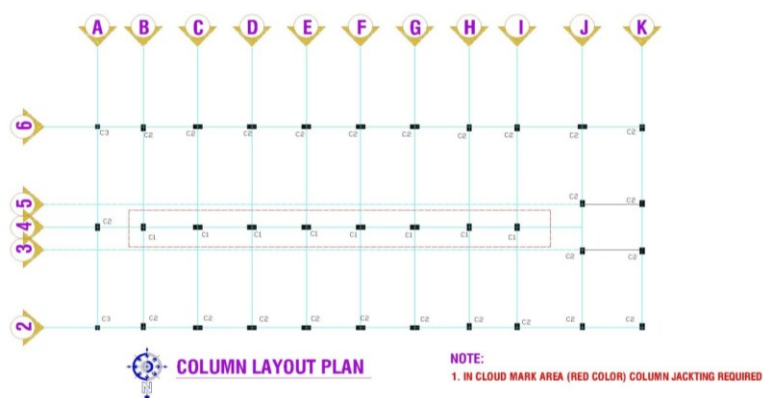


Fig. 6: Location of Column Jacketing

Table 2: Analysis data of retrofitted beams.

Column No.	Size (in x in)	MAX Mu(kip-in)	Req. Rebar Area (in <sup>2</sup> )	Provided Rebar (in <sup>2</sup> )
C1-R	18×28	-964.33	4.82	7.04

### **Retrofitting of Foundation**

When the load cases are changed for garments factory, the retrofitted columns required improved foundations. From manual calculation, the improved foundation area is 8'-6" × 8'-6" whereas the previous footing was 7'-6" × 7'-6". So the foundation has to be increased. As one layer of steel is provided in square footing, the outer faces of existing footing has to be roughly disrupted so that the internal rebar is freed at least 3inch. For new foundation, rebars are welded with the existing bars up to 1 ft. The retrofitted column rebars have to be inserted 10inch with epoxy. Then the concrete is casted at sufficient depth. The details of retrofitted foundation is shown in Fig. 7.

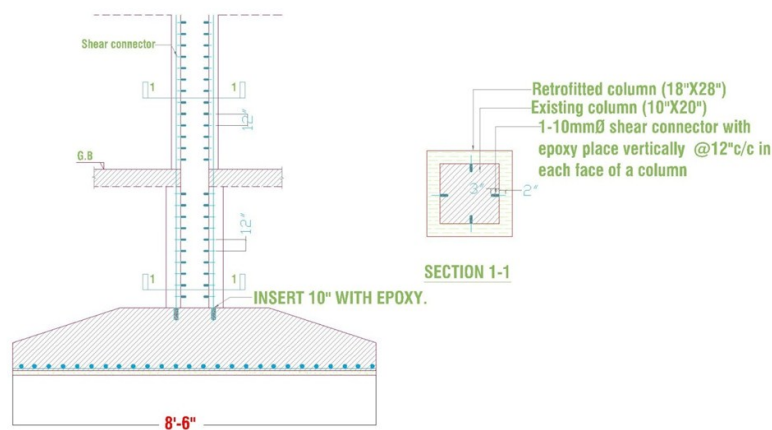


Fig. 7: Retrofitted foundation details.

### **CONCLUSIONS**

The structural failure occurs due to change in live load from residential building to garments factory. It includes failure of columns, beams and foundation. In this paper, a retrofit of beam, column and foundation is introduced. After considering several causes, it is concluded that,

- With respect to our country, concrete jacketing is the most economic and efficient process of retrofitting of beam, column and foundation.
- As a member section has to be increased at least 4inch in each face, the rebar requirement is decreased in some cases. In such a situation, minimum reinforcement must be provided.
- In jacketing, a new layer of concrete is applied on the surface. The bond between new and old concrete does not act monolithically. But they are considered monolithic in the analysis.
- As the building structure is symmetrical by loading pattern, torsion effect is ignored.

### **REFERENCES**

- ACI-318-05, 2005. *Building Code Requirements for Structural Concrete and Commentary*, American Concrete Institute.
- BNBC, 1993. *Bangladesh National Building Code*, Housing and Building Research Institute (HBRI) & Bangladesh Standards and Testing Institution (BSTI), Dhaka, Bangladesh.
- ETABS Nonlinear v9.6, 1995. *Extended Three-dimensional Analysis of Building Systems*, Computers and Structures Inc., Berkeley, California, USA.
- Indian Institute of Technology, 2011. *Handbook on Seismic Retrofit of Buildings*, Central Public Work Department & Indian Building Congress.
- Jamil, MA; Zisan, MB; Alam, MR and Alim, H. 2013. Restrengthening of RCC Beam by Beam Jacketing, *Malaysian Journal of Civil Engineering* 25(2):119-127.

## **FRACTURE TOUGHNESS DETERMINATION OF PLAIN CEMENT CONCRETE USING BRICK AGGRIGATE IN MARINE WATER**

M. R. Alam<sup>1</sup>, M. R. Mukhlis<sup>2\*</sup>, M. F. Rahman<sup>1</sup> & M. Shaheduzzaman<sup>1</sup>

<sup>1</sup>Department of Civil Engineering, Chittagong University of Engineering and Technology, Chittagong, Bangladesh

<sup>2</sup>Institute of Earthquake Engineering Research, Chittagong University of Engineering and Technology, Chittagong, Bangladesh

\*Corresponding Author: raihan.ce@live.com

### **ABSTRACT**

Fracture toughness of plain cement concrete using brick aggregate cured in marine water has been determined in this study. To determine the fracture toughness value for different depths having initial crack, thirty beams using brick chips were made according to ASTM specifications. During the casting of test specimen initial crack was introduced. Range of initial crack depths was taken 30%, 35% and 45% of the beam depth. Test specimens were then cured in marine water for 28 days. Experimental failure load for each beam, with the specified initial crack depth, was determined using the 4-point bending test of the beam. Fracture toughness values were then determined for failure loads and crack depths using the equation given by ASTM specifications for 4-point loading. Fracture toughness of concrete using brick aggregate cured in marine water in the study was found in the range of 0.376 to 0.608. The experimental investigation refers that the fracture toughness value increases with the decreasing of crack depth and increasing of beam width.

Keywords: Fracture toughness, plain cement concrete, brick aggregate, marine water

### **INTRODUCTION**

The resistance of a material to failure from fracture starting from a pre-existing crack is known as fracture toughness (Cardarelli, 2000). Most structural parts have flaws or defects present in them. These defects may be produced during manufacturing for fabrication process. The defects may be sharp corners, tool marks or damage due to shaping or construction.

When a fracture in the form of crack develops in the structure, its load bearing capacity reduces significantly. If it develops in the major structural components such as beams/girders, columns/piers, shear wall, retaining walls, dams, etc., to a significant amount, the entire structure could collapse within a minutes. Since inherent flaws (micro level) exist in concrete material and it could be activated for any accidental combination of loads, it is important to pay attention in minimizing flaws in any concrete structural elements and inhibiting their growth under normal and accidental loads. It is also important to study the behavior of concrete with inherent flaws under static or dynamic loading. For this reason fracture toughness test of concrete is important. The high strength materials have a low crack resistance (Fracture toughness) the residual strength under the presence of cracks is low. When only small cracks exist, structures designed in high strength materials may fail at stresses below the highest service stress they were designed for. The structure is made fail-safe by selecting materials with low growth rate and high residual strength and by adopting a design with inherent crack stopping capabilities (Broek, 1989). Due to the application of repeated loads or due to a combination of loads and environmental attack the existing crack will grow with time. The longer the crack, the higher the stress concentration induced by it. This implies that the rate of crack propagation will increase with time. For the presence of crack, the strength of the structure decrease. After a certain time the residual strength has become so low that the structure cannot withstand accidental high loads that may occur in service. From this moment on the structure is liable to fail. If such accidental high loads do not occur, the crack will continue to grow until the residual strength has become so low that fracture occurs under normal service loading. Some of the structures are designed to carry service loads that are high enough to initiate cracks, particularly when pre-existing flaws or stress concentrations are present. The designer has to anticipate this possibility of

cracking and consequently he has to accept a certain risk that the structure will fail. In order to ensure the safety of a structure, the designer must estimate the load carrying capacity of a structure after the propagation of cracks (Broek, 1984).

Brick chips are widely used for construction in rigid pavement, bridge, culvert, buildings, water tank, and drainage purposes in the countries like Bangladesh, India, Pakistan and many other countries. Cracks are formed in the concrete using brick aggregate due to the presence of void, improper curing, temperature changes, moisture content, w/c ratio, presence of joints in the structure. For the presence of cracks, the strength of the structure decrease.

Recent publications have shown that fracture mechanics has now been established as a fundamental approach that can explain certain nonlinear aspects of concrete behavior, help to prevent brittle failures of the structure and be an important aid in materials engineering (Kishen, 2005). Applications of fracture mechanics to failure of concrete structures have been demonstrated that experimental phenomena associated with the failure of concrete such as size effect on tensile strength and brittleness of concrete can be interpreted properly through fracture mechanics (Shah et. al., 1992). Fracture toughness of large concrete specimens have been investigated and found that fracture toughness increases initially as crack propagates but that a length-independent value is reached asymptotically and concluded that failure of large size concrete elements can be predicted realistically using linear elastic fracture mechanics (Wittmann et. al., 1985). Naturally cracked beams (pre-cracked) yield higher failure loads and stress-intensity values than notched beams with the same crack length (Swartz et al., 1982). Fracture toughness for the concrete using brick chips cured in normal water are determined by researchers but for the concrete using brick aggregate cured in marine water are rarely determined. Since brick chips are the very important material for construction and also the marine water is a huge resource of water that can be used for curing, it is aimed to determine the fracture toughness for concrete using brick chips cured in marine water in order to determine the service load under presence of cracks in the structure and to raise awareness of the engineer during the design of the structure.

### FRACTURE TOUGHNESS BY STANDARD ASTM TEST PROCEDURE

The Fracture toughness  $K_{IC}$  is the material toughness at the onset of fracture. The ASTM E1290-08 Standard suggests the formula for fracture toughness calculated based on the empirical equation (Eq. 1) given by (Srawley et. al., 1976) for single edge straight through cracked rectangular beam under four-point loading as given below:

$$K_{IC} = \frac{P(l_1 - l_2)\sqrt{a}}{BW^2} * \frac{3}{2(1-\frac{a}{W})^{\frac{3}{2}}} * \{ 1.989 - 1.33 \frac{a}{W} - \frac{[3.49 - 0.68 \frac{a}{W} + 1.35(\frac{a}{W})^2] * \frac{a}{W} * (1 - \frac{a}{W})}{(1 + \frac{a}{W})^2} \} \quad (1)$$

Where,

$K_{IC}$  = Fracture toughness in  $\text{MPa}\sqrt{\text{m}}$

$P$  = Load

$l_1$  = Center to center support length

$l_2$  = Loading span

$B$  = Width of the beam

$W$  = Depth of the beam

$a$  = Crack depth

### Materials and Test Specifications:

All beams were tested by following ASTM specification. Materials and test specifications are given in the following Table 1-

Table 1: Materials and Test specifications

Mixing ratio:	1: 1.5: 3
Type of cement:	Portland cement
Type of sand:	Local sand
Size of fine aggregate:	#16 passing & #30 retaining, #30 passing & #50 Retaining, #50 passing & #100 retaining = (1:2:3)
Size of coarse aggregate:	25 mm passing 19 mm retaining
Size of cylinder:	Diameter = 152 mm; Height = 305 mm
w/c ratio:	0.365



Different test results of cement, sand, aggregate and plain concrete are given in the following Table 2-

Table 2: Different Test results of Cement, Sand, Aggregate and Plain Concrete

Name of test	Test results
F.M. (Fineness Modulus) of sand	2.49
Slump value (average of 05 tests)	79 mm
7 days compressive strength of cement mortar (average of 10 tests)	25.9 MPa
28 days compressive strength of cement mortar (average of 10 tests)	33.5 MPa
7 days tensile strength of cement mortar (average of 10 tests)	2.25 MPa
28 days tensile strength of cement mortar (average of 10 tests)	3.30 MPa
28 days cylinder compressive strength of cement concrete with brick aggregates (average of 15 tests)	19.0 MPa
Aggregate crushing value of brick aggregate (average of 03 tests)	38.33%

### Preparation of Test Specimens

Six uncrack beams, six beams with 30% depth of crack and standard width (152 mm), six beams with 35% depth of crack and standard width (152 mm), four beams with 45% depth of crack (76 mm width), four beams with 45% depth of crack (102 mm width) and four beams with 45% depth of crack (127 mm width) were cast by using brick chips. Steel plates of 1 mm thickness were provided during casting for producing pre-cracked beam having 1 mm crack width as shown in [Fig. 1].



Fig. 1: Casting of pre-cracked beams inserting steel plates

The details of different test specimens are given in the following Table 3-

Table 3: Details of different test specimens

Test Specimen ID	Total no. of Test Specimen	Beam dimensions (mm)	Crack depth (% of beam depth)
1-1 to 1-6	6	813×152×203	uncrack
2-1 to 2-6	6	813×152×203	35
3-1 to 3-6	6	813×152×203	30
4-1 to 4-4	4	813×127×203	45
5-1 to 5-4	4	813×102×203	45
6-1 to 6-4	4	813×76×203	45

### Standard ASTM Test Procedure:

In specified formwork the specimens were casted. The formwork was removed after 24 hours and specimens were kept under marine water for curing for 28 days. Marine water was collected directly from Patenga sea beach of Chittagong. Specimens were removed after 28 days from the water and kept in dry place for 24 hours to evaporate the moisture from their external surface. Loading positions and supporting positions were clearly marked and uneven surfaces were made smooth surface by using sand paper and Weir brush. Swivelling supports (in one vertical plane, perpendicular to the length) were provided at a distance 12.5 mm from both ends of the beam. Four-point loading positions were fixed at one-fourth of span length from both supports. This loading was chosen for obtaining pure bending at the middle-half portion of the beam where crack was present. Load was applied on the beam monotonically without any jerk and it was increased continuously at a rate of 10kN/min until the test specimen failed. Failure load was recorded from a digital load meter. A dial gauge with a sensitivity of 0.01 mm was used for measuring the load point deflection. Displacement controlled load was applied on the specimen. Load was recorded at each 5 division increments of the dial gauge up to failure load. All specimens were tested under simply supported conditions. Experimental setups for standard ASTM Test procedure are shown in the following figures:



Fig. 2: Experimental setup for standard ASTM Test



Fig. 3: Experimental setup of crack beam by using brick chips



Fig. 4: Failure of crack beam by using brick chips



Fig. 5: Experimental setup of uncrack beam by using brick chips



Fig. 6: Failure of uncrack beam by using brick chips

## RESULTS AND DISCUSSIONS

The crack depth and peak load for each test beam and the corresponding computed fracture toughness are shown in Table 4. From this table it is seen that the magnitude of the maximum load varies with the depth of crack as well as width of the test beam. The peak load capacity decreases with the increasing depth of crack which can be easily described by the  $a/W$  ratios, where  $a/W$  is the ratio between depth of crack ( $a$ ) and height of beam ( $W$ ). Three types of  $a/W$  ratios used in the standard ASTM test procedure which are 0.3, 0.35, 0.45 among which test beams with  $a/W$  ratio 0.3 have shown larger peak load capacity whether test beams with  $a/W$  ratio 0.45 have shown smaller peak load capacity. In the other hand, peak load capacity decreases with the decreasing width of beam. Test beam with 152 mm width has shown larger peak load capacity whether test beam with 76 mm width has shown smaller peak load capacity.

Figure 7, 8, 9, 10 and 11 show the load-deflection plot for cracked beam with different depth of crack and width of test beam made with brick aggregates cured in marine water. Figure 12 shows the load-deflection curves for combined average load. From all the load-deflection curves it is seen that material behaves almost linearly at the beginning of the applied load and becomes nonlinear near the peak load. A part of this non-linearity could be attributed to the coalescence of tensile micro-cracks (development of fracture process zone) before the subsequent crack extension. The remaining part is due to the nonlinear compression behavior near maximum loads. It was found that when the load reached its maximum value, the test specimen began to lose its resistance very fast, which could not be plotted properly. For this reason, only the load deflection plots up to peak load have been showed in this study. The peak load was then used to determine the fracture toughness according to Eq. (1).

Table 4: Fracture Toughness of cracked Test Specimens

Sl no.	Test Specimen ID	Beam Dimension (mm)	Crack Depth (% of beam depth)	Load (KN)	Fracture toughness $K_{IC}$ (MPa $\sqrt{m}$ )
1	2-01	813×152×203	35	8.1	0.394
2	2-02			9.7	0.472
3	2-03			8.3	0.404
4	2-04			9.1	0.443
5	2-05			9.8	0.477
6	2-06			9.0	0.438
7	3-01	813×152×203	30	12.5	0.547
8	3-02			11.2	0.490
9	3-03			13.9	0.608
10	3-04			11.5	0.503
11	3-05			12.6	0.551
12	3-06			13.0	0.567
13	4-01	813×127×203	45	8.0	0.479
14	4-02			8.5	0.509
15	4-03			8.2	0.491
16	4-04			9.1	0.545
17	5-01	813×102×203	45	6.9	0.409
18	5-02			7.3	0.433
19	5-03			6.7	0.397
20	5-04			7.1	0.421
21	6-01	813×76×203	45	5.5	0.405
22	6-02			5.3	0.390
23	6-03			5.2	0.383
24	6-04			5.1	0.376

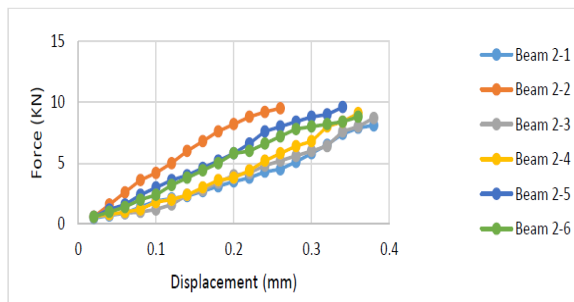


Fig. 7: Load deformation curves for crack of 35% depth of beam (152 mm beam width)

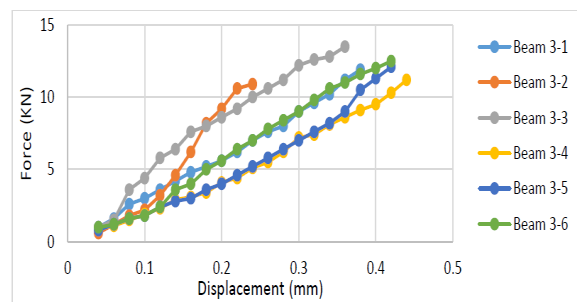


Fig. 8: Load deformation curves for crack of 30% depth of beam (152 mm beam width)

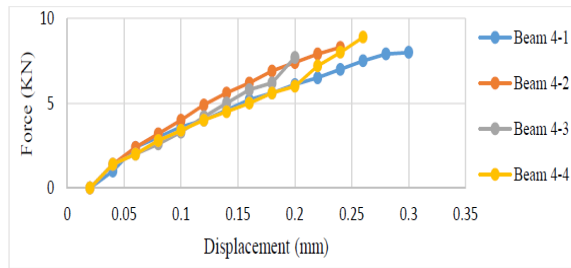


Fig. 9: Load deformation curves for crack of 45% depth of beam (127 mm beam width)

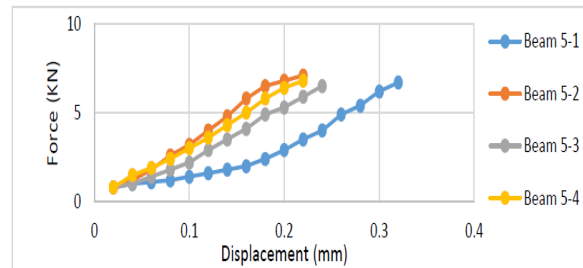


Fig. 10: Load deformation curves for crack of 45% depth of beam (102 mm beam width)

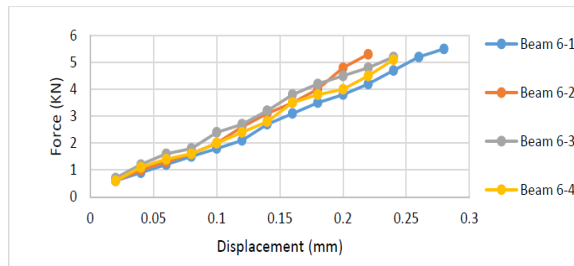


Fig. 11: Load deformation curves for crack of 45% depth of beam (76 mm beam width)

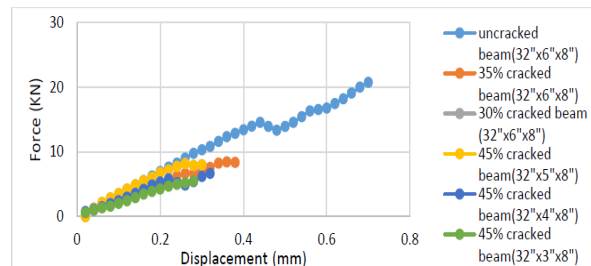


Fig. 12: Load deformation curves for combined average load

## CONCLUSIONS

- The fracture toughness values obtained from the experimental study with marine water curing increases with the decreasing of crack depth and increasing of beam width.
- It was found in case of beam with different crack depths, the failure loads of beam decrease when the crack depth increases.
- When the width of beams decreases, the failure load also decreases having constant crack depth.

## REFERENCES

- Broek, D., 1989, *The practical use of fracture mechanics*, 1<sup>st</sup> edition, Kluwer Academic Publishers, Dordrecht/ Boston/ London, pp. 5-14
- Broek, D., 1984, *Elementary Engineering Fracture Mechanics*, 3<sup>rd</sup> printing, Martinus Nijhoff Publishers, Hague, Netherlands, pp. 4-10
- Cardarelli, F., 2000, *Materials Handbook: A Concise Desktop Reference*, 2<sup>nd</sup> edition, Springer-Verlag London Limited, pp.16
- Kishen, J.M.C., 2005, Recent developments in safety assessment of concrete gravity dams, *Current Science*; 89(4), 650-656
- Shah, S.P. and Ouyang, C., 1992, Measurement and modeling of fracture processes in concrete in Materials Science of Concrete, *American Ceramic Society*, Westerville, OH, Vol.III, edited by Scalny, J., 243-270
- Srawley, J. E. and Gross, B., 1976, Side-cracked plates subjected to combined direct and bending Forces, *Cracks and Fractures, ASTM STP*; 601, 559-579
- Swartz, S.E., Hu, K. K. and Huang, C.M.J., 1982, Stress intensity factor for plain concrete in bending-prenotched versus precracked beams, *Experimental Mechanics*, 412-417
- Wittmann, F.H. and Metzener-Gheorghita, I., 1985, Fracture toughness of concrete determined on large specimens, *Materials and Structures*; 18, 93-95

## EFFECT OF CURING METHODS ON THE STRENGTH OF BRICK AGGREGATE CONCRETE

M. A. Rashid<sup>1\*</sup>, M. N. Islam<sup>2</sup> & M. A. K. Hasan<sup>2</sup>

<sup>1</sup>Department of Civil Engineering, Uttara University, Dhaka, Bangladesh

<sup>2</sup>Department of Civil Engineering, Dhaka University of Engineering & Technology, Gazipur, Bangladesh

\*Corresponding Author: marashid78@yahoo.com

### ABSTRACT

This paper describes the influence of mainly the curing method on the strength of brick aggregate concrete. Six types of curing method (CM-1: water submersion curing; CM-2: wet earth curing; CM-3: polythene sheet curing; CM-4: gunny sack curing; CM-5: water spraying curing; and CM-6: air curing) which are followed in various practical cases in Bangladesh have been considered. Other parameters considered are the concrete mix ratio (1:2:4 and 1:1.5:3 by volume) and the age of concrete (7, 14, 28 and 90 days). The Ordinary Portland Cement was used in making concrete and the water-cement ratio considered was 0.50 by weight. A total of 144 nos. of standard concrete cylinders were cast and tested for crushing strength of concrete. It has been found that curing method CM-1 gives the highest concrete strength and the curing method CM-6 gives the lowest strength to concretes irrespective of the concrete mix ratio. The rich concrete mix (1:1.5:3) gives higher strength than that of lean concrete mix (1:2:4) except the curing method of CM-4. For lean concretes, at the age of 28 days, the curing methods CM-3, CM-4 and CM-5 yielded 13%, 33% and 8% higher strengths than that of the CM-6 method. The increase of concrete strength at the age of 90 days over that at 28 days has been found to vary from 1% to 48% with a mean of 18%.

**Keywords:** Age of concrete, brick aggregate, compressive strength, curing method, mix proportion

### INTRODUCTION

Concrete is the most widely used man-made construction material. It is a stone like material obtained by permitting a carefully proportioned mixture of cement, sand, gravel or other suitable coarse aggregate, and water to harden in forms of the shape and dimensions of the desired structure. The compressive strength of concrete is commonly considered its most valuable property, although, in many practical cases, other characteristics such as durability and permeability may in fact be more important. Nevertheless, compressive strength usually gives an overall picture of the quality of the concrete. Moreover, the strength of concrete is almost invariably a vital element of structural design and is specified for compliance purpose (Nilson et al., 2010).

Curing of concrete is the process of controlling the rate and extent of moisture loss from concrete during cement hydration. It may be needed after concrete has been placed in position thereby providing time for the hydration of the cement to occur. Since the hydration of cement does take time – days, and even weeks rather than hours – curing must be undertaken for a reasonable period of time if the concrete is to achieve its potential strength and durability. Curing may also encompass the control of temperature since this affects the rate at which cement hydrates. The curing period may depend on the properties required of the concrete, the purpose for which it is to be used, and the ambient conditions, i.e. the temperature and relative humidity of the surrounding atmosphere. Curing is designed primarily to keep the concrete moist, by preventing the loss of moisture from the concrete during the period in which it is gaining strength. Curing may be applied in a number of ways and the most appropriate means of curing may be dictated by the site or the construction method (James et al., 2011).

The physical properties of concrete depend to a large extent on the extent of hydration of cement and the resultant microstructure of the hydrated cement. Upon coming in contact with water, the hydration

of cement proceeds both inward in the sense that the hydration products get deposited on the outer periphery of the cement grain, and the nucleus of un-hydrated cement inside gets gradually diminished in volume. At any stage of hydration the cement paste consist of the product of hydration, the remnant of un-reacted cement, calcium hydro-oxide and water. The product of hydration forms a random three dimensional network gradually filling the space originally occupied by the water. Accordingly, the hardened cement paste has a porous structure, the pore size varying from very small ( $4 \times 10^{-10}$  m) to very large and are called gel pores. As the hydration proceeds, the deposit of hydration products on the original cement grain makes the diffusion of water to the un-hydrated nucleus more and more difficult and so the rate of hydration decreases with time. Therefore, the development of the strength of concrete, where starts immediately after setting is completed, continue for an indefinite period, though at a rate gradually diminishing with time. Eighty to eighty five percent of the eventual strength is attained in the first 28 days and this strength is considered to be the criterion for the structural design and is called the characteristic strength (Sing, 2001).

In Bangladesh, depending upon the suitability and availability, different methods are followed for curing of concrete in different structures. Pounding method (blocking water on the surface of cast concrete) is normally used for curing the top surface of flat or near-flat surfaces such as floor slab, pavements, roof slab etc. Structural elements such as footings, pile cap, column below grade etc. are usually covered by soil after few hours/days of their casting. This is done with the view that the curing of these concrete will continue by the damp environment created by the surrounding soil. Sometimes concrete structures such as column, floor slab etc. are wrapped or covered with polythene sheets in order to keep the concrete moist by preventing evaporation of water from it. In some cases, after removing the formwork, concrete structures are wrapped or covered with gunny-sacks and then water is sprayed several times in a day for curing the concrete. This method of concrete curing is usually followed for column, pier, retaining wall and some other vertical structures. On the other hand, exposed side surfaces of floor beams are generally cured by spraying water on the concrete surfaces several times in a day. In some exceptional cases concrete elements are just left exposed in the open air which may be due to the non-availability of curing facilities or some other reasons. However, in all of the above mentioned cases, the representative concrete specimens (cylinder and/or cube) of various concrete elements are normally cured by full submersion of specimens into water. This difference between the curing conditions of real structural element and the representative concrete specimens may yield concretes of different qualities. As a result the strength of the representative specimens may differ from that of the concretes of actual structures.

In Bangladesh, both crushed stone and broken bricks are widely used as coarse aggregates in making concrete. However, due to non-availability and price considerations of stones, the use of broken bricks as coarse aggregate is getting popularity especially in the private sectors. Effect of the moist curing on the strength of brick aggregate concrete was investigated experimentally by Rahman et al. (2009). It was reported that moist-cured brick aggregate concrete show significant higher compressive strength in comparison with that of the air-cured concrete. An average value of the ratios of the compressive strengths of air-cured concrete to those of moist-cured concrete was found to be 0.74. Also the initial moist curing of 3, 7, 14 and 21 days yielded 67%, 68%, 81% and 89% respectively of the 28 days moist-cured compressive strength (all were tested at 28 days).

Experimental investigation on the effect of curing on the strength of brick aggregate concretes was also done by Ahmad and Amin (1998). They reported that the curing of concrete at any stage is beneficial to overcome the losses due to discontinuity in curing. The delayed curing was found to be helpful even in attaining the desired strength provided that the early age (1st one week) curing is not hampered. However, in such cases curing for a longer duration was reported to be required.

So far, no study on the influences of different curing methods on the real structural concrete elements (those are practically followed in Bangladesh) has been reported. This paper has, therefore, been aimed at to study the above mentioned issue considering the brick aggregate concretes.

## EXPERIMENTAL PROGRAM

In the experimental program a total of 144 standard cylindrical concrete specimens (150×300 mm) have been cast and then tested to get the concrete crushing strengths. Three parameters considered were curing method, age of concrete and concrete mix ratio. Six type of curing methods of concrete which are commonly followed in Bangladesh have been considered as the main parameter. The curing methods considered are:

- (i) Full submersion of concrete specimens into water (CM-1).
- (ii) Covering the concrete specimens with wet earth (CM-2).
- (iii) Wrapping the concrete specimens with polythene sheets (CM-3).
- (iv) Covering the concrete specimens with gunny sacks and then spraying water on this several times in a day (CM-4).
- (v) Spraying water on the exposed specimens at several times in a day (CM-5).
- (vi) Concrete specimens left in the open air outside the lab (i.e. air cured) (CM-6).

Two types of concrete mix ratio (1:2:4 and 1:1.5:3 by volume) along with the age of concrete (7, 14, 28 and 90 days) have also been considered in this study. Therefore, a total of 6×2×4 or, 48 nos. of mixes of concrete and hence a total of 48×3 or 144 nos. of cylindrical specimens were cast and then tested for compressive strength at the age of specified days. Ordinary Portland Cement (Type-I) was used in this experiment. Properties of the cement used are shown in Table 1.

Table 1: Properties of the cement (OPC) used in the experiment

Property of cement	Test value
Normal consistency	28.6%
Initial setting time	3 hr. 0 min.
Final setting time	6 hr. 0 min.
Compressive strength (3 days)	25.5 MPa
Compressive strength (7days)	34.3 MPa

The coarse aggregates used were 25 mm down well graded brick aggregates. The properties of fine and coarse aggregates used in the experiment are presented in Table 2. Potable water was used in making concretes with a water-cement ratio of 0.5 by weight.

Table 2: Properties of fine and coarse aggregates used

Property of materials used	Test values of	
	Fine aggregate (sand)	Coarse aggregate (brick aggregate)
Fineness modulus	2.4	7.4
Water absorption (%)	2.0	6.0
Unit weight ( kg /m <sup>3</sup> )	1492	1102

Required numbers of steel moulds each of 150×300 mm size were cleaned using wire brush and then their joints were tightened by nut-bolts. These cleaned moulds were placed on firm and level floor on concrete laboratory. Lubricating oil (Mobil) was used to smear the bottom and inside of the mould for its easy removal after hardening of concrete. Fresh concrete was prepared as per designed mix in a mixture machine. Immediately after unloading from mixture machine, the fresh concrete was placed in the mould in three layers and was compacted each layer of concrete by using nozzle type vibrator machine. The fresh concrete in the specimen molds were kept in the laboratory without any disturbance for about 24 hours. Then the concrete specimens were demoulded and were placed under the specified curing method. The maximum curing period considered was 28 days except for the curing method of CM-2 in which the maximum curing period was 90 days.

The test cylinders were collected from their specified curing conditions before 24 hours of their testing and kept in air dry condition in the laboratory. Both the ends of cylinders were ground by grinding machine in order to make the end surfaces smooth and level. Then the measurements for diameter of each specimen were taken using slide callipers. Average of three measurements those at top, middle

and bottom were considered in determining the diameter and then the cross sectional area of each specimen. Concrete cylinders were tested in the lab using the 2000 KN capacity Universal Testing Machine following the ASTM C39 specifications. At first the test cylinder was placed on the machine's base platen keeping it vertical and centered on the plate. Then load was applied on the top surface of the specimen. This load was increased gradually until the specimen failed. The crushing load was then recorded. The crushing load of each of the test specimens was divided by the average cross sectional area of respective cylindrical specimen and was recorded as the compressive strength of that concrete. The compressive strengths of all concretes along with different parameters are presented in Table 3.

Table 3: Compressive strength of test concretes

Age of concrete (day)	Compressive strength (MPa) of concrete under the curing condition of -					
	CM-1	CM-2	CM-3	CM-4	CM-5	CM-6
Mix ratio = 1:2:4 (by volume)						
7	23.7	24.4	25.8	27.6	25.4	17.6
14	27.5	25.4	32.9	32.3	27.5	22.4
28	32.2	28.7	32.6	38.5	31.3	28.9
90	39.4	42.4	43.3	41.9	38.4	34.8
Mix ratio = 1:1.5:3 (by volume)						
7	24.7	24.7	27.3	35.5	31.6	26.7
14	35.2	32.9	31.3	36.1	35.1	27.1
28	42.9	37.9	36.8	36.6	37.1	38.1
90	46.5	41.2	44.1	39.9	40.8	38.5

## ANALYSIS AND DISCUSSION OF TEST RESULTS

Test data have been analyzed with a view to study the influence of curing methods along with other variables considered in this study and are discussed in the followings.

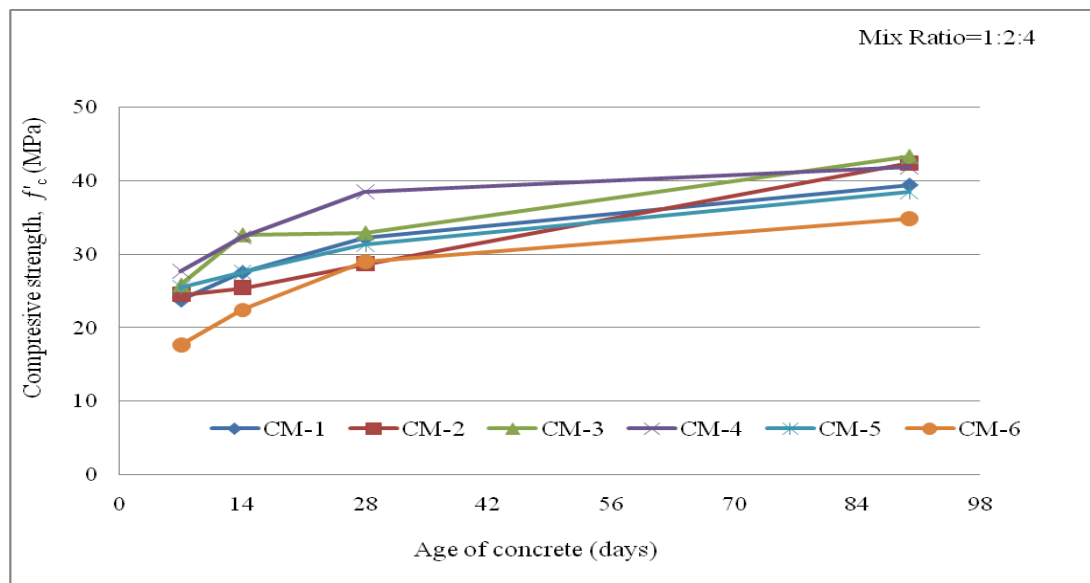
### *Influence of the Curing Methods on the Concrete Strength*

Fig. 1 shows the relative influences of curing methods considered in this study on the concrete crushing strength for a wide range of the age of concretes made with brick aggregate. It is seen that the curing method CM-1 (full submersion of concrete specimens into water) gives higher concrete strength than any other curing method irrespective of the concrete mix ratios except that of mix ratio of 1:2:4. The exceptional case may be due to a comparatively lean concrete mix along with the much higher absorption capacity of brick aggregates. On the other hand, the air curing method CM-6 (concrete specimens left in open air in the lab) gives the minimum strengths to concretes considered.

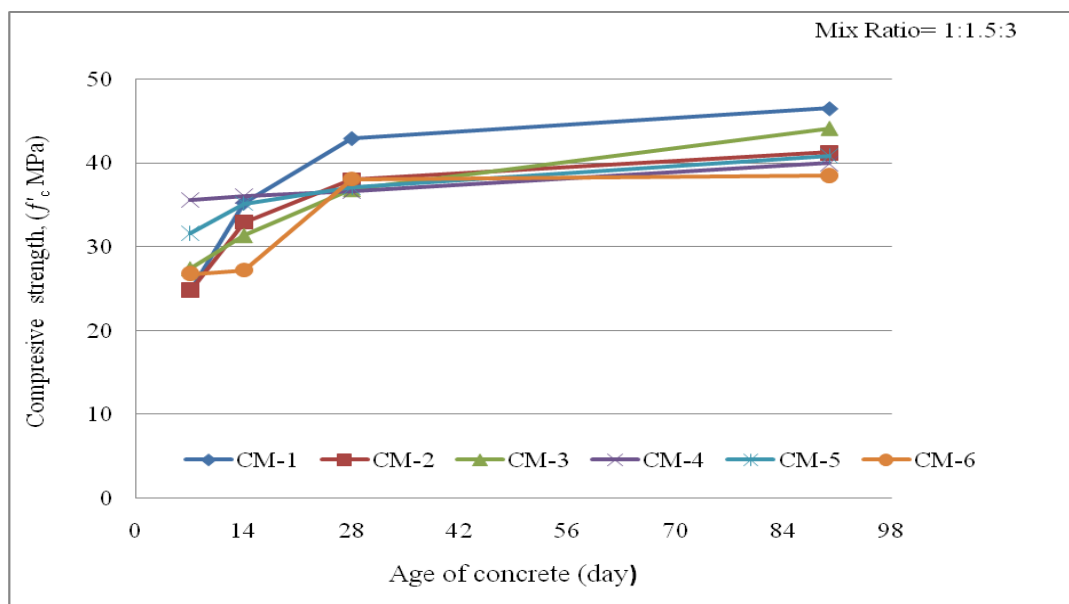
The curing methods CM-3 (wrapping the concrete specimens with polythene sheet) and CM-4 (covering the concrete specimen with gunny sack and then spraying water on this several times in a day) are seen to be the much influential in giving strengths to concrete. These may be due to the available moisture around the concrete specimens provided by the almost air-tight polythene sheet system and long time existence of sprayed water on concrete surface because of the coarse gunny sack. The curing method CM-5 (spraying water on the exposed specimens several times in a day) also gives higher strengths, but to a lesser amount, than those of the air-cured concretes.

A comparative study of the 28-days crushing strengths of concrete cured following the different methods is given in Table 4. Ratios of strength of concrete cured following either of CM-1, CM-2, CM-3, CM-4, and CM-5 to that of the concrete cured by CM-6 (air curing method) are presented in this table. From Table 4 it is seen that for rich concretes (mix ratio=1:1.5:3) curing methods CM-2, CM-3, CM-4 and CM-5 do not have any influence in increasing the concrete strength over that by CM-6 curing





(a)



(b)

Fig. 1: Influence of different curing methods on the strength of concrete

method. Whereas the CM-1 method gives a significant increase (an average of 12%) in concrete strengths for both the rich and the lean (mix ratio=1:2:4) concretes. On the other hand, the CM-2 method of curing has no influence in increasing concrete strength over those of CM-6 method for either rich or lean concretes. However, for lean concrete, CM-3, CM-4 and CM-5 show 13%, 33% and 8% increase, respectively, in concrete strength.

Table 4: Ratios of compressive strengths (28-days) obtained following different curing methods.

Coarse aggregate	Mix Ratio (by volume)	Ratio of concrete strengths at 28 days for curing methods				
		CM-1/CM-6	CM-2/CM-6	CM-3/CM-6	CM-4/CM-6	CM-5/CM-6
Broken bricks	1:2:4	1.11	0.99	1.13	1.33	1.08
	1:1.5:3	1.13	0.99	0.97	0.96	0.97
Mean		1.12	0.99	1.05	1.15	1.03
Standard Deviation (SD)		0.008	0.001	0.115	0.263	0.077

### Influence of the Concrete Mix Ratio on the Concrete Strength

The relative influences of the concrete mix ratios on the crushing strength of concretes made with brick aggregates are presented in Fig. 2. It is seen from this figure that the rich concrete mix (1:1.5:3) gives higher strengths than those of lean concrete mix (1:2:4) except the concrete cured with CM-4 method.

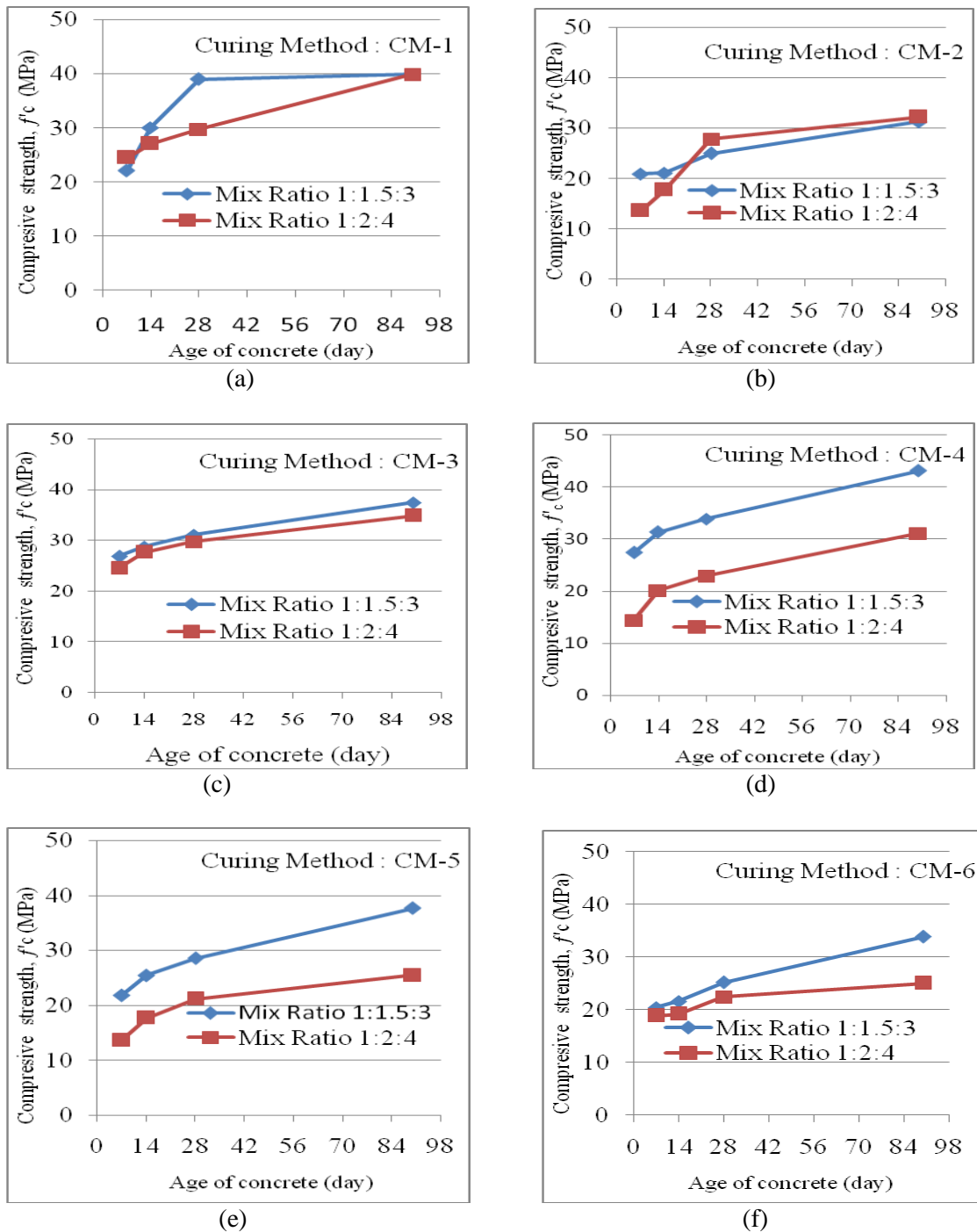


Fig. 2: Effects of mix ratio on the strength of concrete

### Concrete Strengths at 7 and 14 Days

The ratios of concrete strengths at 7 days to those of 28 days and the strengths at 14 days to those of 28 days are presented in Table 5. From the table, it is seen that the concrete continue to increase its strength with its age. The mean strength of concretes at the age of 7 days is 75% of that at 28 days. While the concrete reaches 87% of its 28-days strength at the age of 14 days.

Table 5: Comparison among compressive strengths (28-days) of concrete

Concrete mix ratio (by vol.)	Curing method	$f'_{c,7}$ (MPa)	$f'_{c,14}$ (MPa)	$f'_{c,28}$ (MPa)	$\frac{f'_{c,7}}{f'_{c,28}}$	$\frac{f'_{c,14}}{f'_{c,28}}$
1:2:4	CM-1	23.7	27.5	32.2	0.74	0.85
	CM-2	24.4	25.4	28.7	0.85	0.89
	CM-3	25.8	32.9	32.6	0.79	1.01
	CM-4	27.6	32.3	38.5	0.72	0.84
	CM-5	25.4	27.5	31.3	0.81	0.88
	CM-6	17.6	22.4	28.9	0.61	0.78
1:1.5:3	CM-1	24.7	35.2	42.9	0.58	0.82
	CM-2	24.7	32.9	37.9	0.65	0.87
	CM-3	27.3	31.3	36.8	0.74	0.85
	CM-4	35.5	36.1	36.6	0.97	0.99
	CM-5	31.6	35.1	37.1	0.85	0.95
	CM-6	26.7	27.1	38.1	0.70	0.71
Mean					0.75	0.87
SD					0.1120	0.083

### Increase in Concrete Strength after 28 Days

The ratios of concrete strengths at 90 days to those of 28 days are presented in Table 6. It is to be mentioned here that after 28 days no curing was applied to any concrete specimen except those for the curing method of CM-2 in which the maximum curing period was 90 days. From Table 6 it is seen that the gain in concrete strength at the age of 90 days over that at 28 days ranges from an insignificant value (1%) to a quite high value (48%) and the mean increase is 18%.

Table 6: Ratio of concrete strength at 90 days to that of 28 days

Concrete mix ratio (by vol.)	Curing method	$f'_{c,28}$ (MPa)	$f'_{c,90}$ (MPa)	$\frac{f'_{c,90}}{f'_{c,28}}$
1:2:4	CM-1	32.2	39.4	1.22
	CM-2	28.7	42.4	1.48
	CM-3	32.6	43.3	1.33
	CM-4	38.5	41.9	1.09
	CM-5	31.3	38.4	1.23
	CM-6	28.9	34.8	1.20
1:1.5:3	CM-1	42.9	46.5	1.08
	CM-2	37.9	41.2	1.09
	CM-3	36.8	44.1	1.20
	CM-4	36.6	39.9	1.09
	CM-5	37.1	40.8	1.10
	CM-6	38.1	38.5	1.01
Mean				1.18
SD				0.129

### CONCLUSIONS

Following conclusions can be drawn based on the findings of this study-

- (i) Curing method CM-1 (full submersion of concrete specimens into water) gives higher concrete strength than any other curing method irrespective of the concrete mix ratios. On the other hand, curing method CM-6 (air curing) gives minimum strengths to concretes considered.
- (ii) The rich concrete mix (1:1.5:3) gives higher strength than that of lean concrete mix (1:2:4) except the curing method of CM-4.
- (iii) For lean concretes, the curing methods CM-3, CM-4 and CM-5 yielded 13%, 33% and 8% higher strengths (28 days) than that of the CM-6 method (air curing).

- (iv) The increase in concrete strength at the age of 90 days over that at 28 days (maximum curing period except the CM-2 method of curing) varies from an insignificant value (1%) to a quite high value (48%) and the mean increase is 18%.

#### **ACKNOWLEDGMENT**

The experimental work described was supported by and executed at the Department of Civil Engineering, Dhaka university of Engineering & Technology, Gazipur-1700, Bangladesh. This support is greatly appreciated by the authors.

#### **REFERENCES**

- Ahmad, S and Amin, AFMS. 1998. Effect of curing conditions on compressive strength of brick aggregate concrete. *Journal of Civil Engineering, The Institution of Engineers, Bangladesh*, CE 26(1): 37-49.
- James, T; Malachi A; Gadzama EW and Anametemfiok, V. 2011. Effect of curing methods on the compressive strength of concrete. *Nigerian Journal of Technology*, 30(3): 14-20.
- Nilson, AH; Drawin, D and Dolan, CW. 2005. *Design of concrete structures*. New Delhi: McGraw-Hill Publishing Company Limited. pp.779.
- Rahman, MA; Chakma, S and Rahman, MM. 2009. *Effect of the moist curing on the strength of brick aggregate concrete*. B. Sc. Engineering Thesis, Department of Civil Engineering, DUET, Gazipur.
- Sing, MGH. 2001. *Handbook on concrete mixes*. New Delhi: Bureau of Indian Standards. pp.11.

## **A TENTATIVE METHODOLOGY TOWARDS SEISMIC FRAGILITY ASSESSMENT OF HIGHWAY BRIDGES IN BANGLADESH**

A. K. M. T. A. Khan\* & M. A. R. Bhuiyan

*Department of Civil Engineering, Chittagong University of Engineering and Technology, Chittagong,  
Bangladesh*

*\*Corresponding Author: thohidul.ce@gmail.com*

### **ABSTRACT**

Bridges are the economic benchmark for the countrywide transportation development which facilitates emergency rescue operation, first aid, fire fighting, medical services and relief operation for disaster prone areas. As a transportation lifeline, it seems very important to minimize the seismic induced losses of bridge function as much as possible. At past, the performance of highway bridges against moderate to high seismic thrust was quite unsatisfactory at different part of the world which proves that bridges are highly susceptible to damages during earthquake. A significant amount of global bridges collapsed in the recent years have exposed inadequacy of the design of existing bridge structures which pushes engineers to rethink about the optimization of seismic provision. A fragility curve (FC) illustrates the conditional probability that a structure surpasses some defined limit states at different levels of load or seismic shock. This study clarifies the research importance of developing the seismic fragility functions (FF) and FC for the major bridge classification in Bangladesh. This literature based study reconfirm the necessity of FF and FC of existing bridges in a particular territory so that, the prediction of damage probability for a certain ground motion may possible. Both the FF and FC could be fruitful in damage state assessment for a defined seismic event as well as financial seismic losses prediction following density and speed of traffic, environmental exposure, soil condition, degree of uses and structural importance of the major bridge classification in Bangladesh. To do so, at the very infant stage of this study, a tentative methodology flowchart have been tried to establish which cordially urges further refinement.

Keywords: Fragility function; fragility curve; seismic induced losses; damage state analysis; seismic performance; highway Bridge

### **INTRODUCTION**

Bridges are a crucial part of the overall transportation system as they play very important roles in evacuation and emergency routes for rescues, first-aid, fire fighting, medical services and transporting disaster commodities to expatriates. In this regard, bridges serve as a transportation lifeline of modern society. In view of the importance of the bridge structure, it is a contemporary key issue to minimize as much as possible the loss of the bridge functions against earthquakes to enhance continued functioning of the community life. A large number of bridge structures collapsed in recently occurred destructive earthquakes in different places in the world have exposed inadequacy of the design of existing bridge structures, which have led engineers rethink widely on how to design bridge structures against earthquakes. These occurrences have indicated that the necessity to construct/rehabilitate bridge structures to withstand seismic forces in earthquake prone regions is more than a mere philosophy (Khan, 2014; Khan and Bhuiyan, 2015). The performance of highway bridge systems observed in past earthquakes — including the 1971 San Fernando earthquake, the 1994 Northridge earthquake, the 1995 Great Hanshin earthquake in Japan, the 1999 Chi-Chi earthquake in Taiwan, the 2010 Chile earthquake, and the 2010 Haiti earthquake — have demonstrated that bridges are highly susceptible to damages during earthquakes (Alim et al., 2015). Bridges give the impression of being rather simple structural systems. Indeed, they have always occupied a special place in the affections of structural designers because their structural form tends to be a simple expression of their functional

requirement. Bridges, possibly because of their structural simplicity, have not performed well as might be expected under seismic thrust. In recent earthquakes in California in 1989, Japan in 1995, etc. modern bridges designed specifically for seismic resistance have collapsed or have been severely damaged when subjected to ground shaking of an intensity that has frequently been less than corresponding to current code intensities (Alim, 2014; Alim et al., 2015). FC displays the conditional probability that a structure surpasses some defined limit state at different levels of load or other actions. For seismic fragility, the curves represent the probability of seismic damage at various levels of ground shaking, which is described for the purposes of this research in terms of peak ground acceleration (PGA).

## **LITERATURE REVIEW**

Since last decade, several authors have tried to explain this term with different parameters from different seismic eyesight's (Alim, 2014; Alim et al., 2015). Most of these assumptions and explanations were mainly focused on different civil engineering structures - particularly on buildings and bridge structures. Yamazaki et al. (2000) developed a set of empirical FC based on the actual damage data acquired from the 1995 Hyogo-ken Nanbu (Kobe) earthquake. Shinozuka et al. (2000) presented both empirical and analytical approaches for FC. Kim and Shinozuka (2004) then developed FC for concrete bridges retrofitted by column steel jacketing. The FC were expressed in the form of a two parameter lognormal distribution function with the estimation of the two parameters performed an optimization algorithm, and it could be achieved through ground motion records and seismic structural response analyses (Alim, 2014; Alim et al., 2015).

In the seismic fragility analysis, different forms of engineering demand parameters (EDP) are used to monitor the structural responses under earthquake ground motion and measure the damage states (DS) of the bridge components. DS for bridges should be defined in such a way that each DS indicates a particular level of bridge functionality. A capacity model is needed to measure the damage of bridge component based on prescriptive and descriptive DS in terms of EDP (Choi et al., 2004; Neilson, 2005). Four DS as defined by Federal Emergency Management Authority (FEMA, 2000) through HAZUS are commonly adopted in the seismic vulnerability assessment of engineering structures, namely slight, moderate, with extensive and collapse damages. Bridge piers are one of the most critical components, which are often forced to enter into nonlinear range of deformations under strong earthquakes. Alim et al. (2015) affirmed that, the displacement ductility of the bridge pier is adopted as damage index (DI). Hwang et al. (2001) recommended four different DS for bridge pier based on ductility limit. But retrofit affects the seismic response and demand of the bridge pier and the capacity as well. For the retrofitted bridge pier new limit states (LS) need to be defined (Alim, 2014). LS capacities for the retrofitted bridge bent might be obtained by transforming the ductility LS proposed by Hwang et al. (2001). The use of ductility limit for retrofitted reinforced concrete (RC) columns is well documented in literature of Ramanathan et al. (2012), Billah and Alam (2012), Alim (2014) and Alim et al. (2015).

In Incremental Dynamic Analysis (Vamvatsikos and Cornell, 2002; Alim, 2014; Alim et al., 2015), the structure is subjected to a series of non-linear time-history analysis of the increasing intensity (e.g. Peak ground motion acceleration is incrementally scaled from a low elastic response value up to the attainment of a pre-defined post-yield target limit state). Incremental Dynamic Analysis (IDA) is a new methodology which may postulate a clear indication of the relationship between the seismic capacity and the demand. An analysis scheme was carried out for the as-built and retrofitted concrete bridge bent (Alim, 2014). The peak values of base shear are plotted against their top displacement counterparts, for each of the dynamic runs, giving rise to the so-called dynamic pushover or IDA envelop curves (Alim et al., 2015). FC allows the evaluation of potential seismic risk assessment of any structure. Fragility function describes the conditional probability i.e., the likelihood of a structure being damaged beyond a specific damage level for a given ground motion intensity measure (Alim, 2014; Alim et al., 2015). In order to develop FC, different methods and approaches have been developed. Depending on the available data and resources, fragility functions can be generated empirically based on post-earthquake surveys and observed damage data from past earthquakes

(Basoz and Kiremidjian, 1999; Yamazaki et al., 2000; Alim, 2014). However, limited damage data and subjectivity in defining DS limits the application of empirical FC (Padgett and DesRoches, 2008).

In absence of adequate damage data, fragility functions can be developed using a variety of analytical methods such as elastic spectral analyses (Hwang et al., 2001), nonlinear static analyses (Shinozuka et al., 2000) and nonlinear time-history analyses (Hwang et al., 2001; Choi et al., 2004). In order to generate analytical FC, structural demand and capacity needs to be modelled. Alim (2014) and Alim et al. (2015) studied the Probabilistic Seismic Demand Model (PSDM) that was used to derive the analytical FC using nonlinear time-history analyses of the retrofitted bridge bents. Though this is the most rigorous method, yet this is a dominating reliable analytical method (Shinozuka et al., 2000). The PSDM establishes a correlation between the EDP and the ground intensity measures (IM). Displacement ductility demand of retrofitted bridge bent was considered as the EDP, and the PGA was utilized as IM of each ground motion records (Alim, 2014; Alim et al., 2015). Two approaches are used to develop the PSDM. These are (i) the Scaling Approach and (ii) the Cloud Approach (Alim, 2014; Alim et al., 2015). Following Scaling Approach, all the ground motions are scaled to selective intensity levels and an IDA is conducted at each level of intensity; however, in the Cloud Approach, un-scaled earthquake ground motions are used in the nonlinear time-history analysis and then a PSDM is developed based on the nonlinear time history analyses results. Alim (2014) and Alim et al. (2015) studied the Cloud method that was utilized in evaluating the seismic fragility functions of the retrofitted bridge bents. In this approach, a regression analysis is carried out to obtain the mean and standard deviation for each limit state by assuming the power law function (Cornell et al., 2002), which gives a logarithmic correlation between the median EDP and selected IM. In order to create sufficient data for the Cloud Approach, IDA is carried out instead of nonlinear time history analysis where the median and dispersion value of the DS are described by Ramanathan et al. (2012).

Effect of isolation on FC of thirty highway bridges based on simplified method was assessed by Karim and Yamazaki (2007) where strong ground motion records were utilized for dynamic analysis towards FC development. Another fragility assessment of a multi-span highway bridge (i.e., isolated by shape memory alloy restrainers and lead rubber bearing) was postulated by Bhuiyan and Alam (2012). The authors offered fragility functions of the bridge components that are generated and then combined to approximate the overall system fragility functions at different damage states. A comprehensive Bayesian methodology for developing probabilistic capacity and demand model for structural component of highway bridge system was formulated by Gardoni et al. (2002) where both aleatory and epistemic uncertainties were considered. The PSDM are used in conjunction with the component capacity models to objectively assess the seismic fragilities of RC bridge bent for a set of ground excitations. Analytical probabilistic fragility studies require extensive computer simulations to account for the randomness in both input motions and response characteristics. Jeong and Elnashai (2007) initiated an approach where a set of fragility relationships with known reliability was derived based on the fundamental response quantities of stiffness, strength and ductility of bridge frames.

A set of seismic FC for the bridges commonly found in the Central and Southern United States (CSUS) was developed to predict economic losses due to earthquake and prioritization of retrofit action (Choi and Jeon, 2003). The authors assessed the seismic resistance of several retrofitted bridges and also evaluated using fragility analysis and compared with that of the as built bridges to verify the effect of each retrofit measures aggressively. A method was presented for the evaluation of seismic fragility function of RC bridge structures subjected to both rigid and spatially varying excitation in association with nonlinear dynamic analysis and plain Monte-Carlo simulation (Lupoi et al., 2004). An expanded methodology for the generation of analytical FC for highway bridges in CSUS was presented by Nielson and DesRoches (2007a). The methodology considered the contribution of the major bridge components (i.e., pier, abutment and bearing) to its overall bridge system fragility. The fragility of individual bridge component was then compared with the overall bridge system and it was observed that, the overall bridge as a system is more fragile than any one of the individual components. Seismic FC for nine major classes of highway bridges at CSUS was developed by Nielson and DesRoches (2007b). The methodology adopted three dimensional analytical models and nonlinear time history analysis to develop FC and further compared with the HAZUS-MH procedure.

Analytical FC for typical Algerian RC bridge piers was developed by Kibboua et al. (2011) in association with forty one worldwide accelerometer records and nonlinear dynamic analysis to assess the damage indices express in terms of the bridge displacement ductility, the ultimate ductility, the cyclic loading factor and the cumulative energy ductility. Combining the damage indices defined for five damage rank with the ground motion indices, the FC for the bridge piers were derived assuming a lognormal distribution. Mackie and Stojadinovic (2004) addressed the analytical and numerical formulation of FC for single bent RC highway bridges. FC was derived at the demand, damage and decision variable levels that are useful for traffic network modelling. El-Arab (2012) proposed an analytical methodology of seismic FC for RC pier bridges in Egypt. The study strongly argued that, the peak ground acceleration for 50% probability of exceeding slight, moderate and severe damage ranges from approximately 0.15g to 0.4g for the typical Egyptian RC pier bridges.

FC for two span simply supported concrete bridge pier in near fault region was developed by Shirazian et al. (2011) incorporating several earthquake time histories. To assess the loss estimation due to bridge damage, FC (both empirical and analytical) have been developed for various bridge types across America (Nielson, 2003). FC alone cannot predict the indirect losses associated with a given level of damage. Therefore, damage-functionality relationships are required in addition to FC that might be able to assess the indirect losses associated with a particular seismic event. Dukes et al. (2012) studied the sensitivity of design parameters used to develop bridge specific FC. A bridge specific fragility methodology can be developed that takes into account certain design aspects of a bridge design in order to provide FC particular to a bridge design. The authors conducts a sensitivity study to test which design parameters have a significant impact on bridge response and should therefore be consider as predictive variables in bridge specific fragility analysis used in the design procedures.

Tanaka et al. (2000) presented a methodology for developing the seismic fragility function that takes both physical and functional aspects into account. The authors deals with the fragility functions that can be used for post earthquake transportation management system where both space and time factors are relevant and follows three step procedure. (i) Construct the GIS based damage database, (ii) estimates spatial distribution of ground motion and assign to facility and (iii) develops the seismic FC for the highway bridges to estimate possible seismic losses. Fragility analysis of wall pier supported highway bridges of Southern Illinois in USA was initiated by Bignell and LaFave (2010). A series of hammerhead and regular wall pier supported bridges were randomly selected to analytical procedure and hundred three dimensional finite element model that are excited by synthetic earthquake records. Second stage liquefaction potentiality was also considered in the fragility analysis and it was observed that, the Southern Illinois wall pier supported bridges are moderately vulnerable to structural damage in a 2% probability of exceeding in a 50 years earthquake, and in some cases they could be highly vulnerable to on-site liquefaction arousal.

Evaluation of effectiveness and optimum design of isolation devices for highway bridges might be possible by using fragility function methodology (Zhang and Huo, 2009). The author adopts the performance based evaluation approach to investigate the effectiveness of isolation devices incorporating probabilistic seismic hazard analysis and IDA to produce fragility functions. The study shows that, the mechanical properties of isolation devices have significant effect on the damage probability of isolated bridges and these issues should be effectively considered under the fragility function framework. PSDM and fragility estimates for highway bridges with single column bent was assessed by Huang et al. (2010). The PSDM was proposed considering ground motion characteristics, prevailing uncertainties, statistical uncertainties and model errors in association with Bayesian updating approach. The uni-variate deformation shear fragility and the bi-variate deformation shear fragility were crucially assessed for the target bridge.

Fragility analysis of a highway overcrossing bridge with soil structure interaction was comprehensively discussed by Kwon and Elnashai (2010) for Central and Eastern USA. Four different modelling methods were adopted to represent abutment and foundations of the bridges and



FC of the components and bridge system are derived. Four different SSI approaches results different seismic FC. The authors argued that, careful consideration is necessary when selecting an analytical representation of a soil and foundation system to obtain reliable seismic impact assessment. It was also observed that, abutment bearings are the most critical components of the bridge systems.

Mechanistic quantification of RC bridges DS under earthquake through fragility analysis was performed by Banerjee and Shinozuka (2008). Bridge damageability information in a succinct form as FC is needed to pursue the seismic risk assessment of a highway network consisting of as large as thousand of bridges that could be affected by a high magnitude earthquake with in and near the service area of the network. FC for seismically retrofitted RC bridge was evaluated by Kim (2003). The CALTRANS specified bridges were seismically strengthened and then Monte-Carlo simulation was performed to study nonlinear dynamic responses of the bridges before and after retrofit. The effect of retrofit is expressed in terms of the increase of the median value of the FC for retrofitted bridge from that of the before retrofit. The comparison clarifies that, the retrofitting effort shows excellent performance for the ascertained damage states. Preliminary study on the FC for highway bridges in Taiwan was initiated by Liao and Loh (2004). The FC was used to represent the probabilities that structural damage, under various levels of seismic excitation, exceeds specific DS. Since, it is neither necessary nor practical to evaluate individual bridges, bridge classification and mapping scheme plays an important role. Calculation of site-specific seismic demand and demand function (i.e., capacity curves and fragility curves) are the key factors in bridge damage assessment and seismic losses prediction.

In the light of above discussion, it becomes appealing to critically assess the fragility functions of highway bridges in Bangladesh based on which a meaningful and representative fragility curves should be developed. Both these fragility function and fragility curves will be synergistically supportive in damage state assessment for a particular seismic event as well as financial seismic loss prediction incorporating the socio-economic context, density and speed of traffic, environmental exposure, soil condition, degree of use and structural importance of the major bridge classifications in this seismic region.

## **OBJECTIVES OF THE PROPOSED RESEARCH WORK**

Motivated by the study done so far, the current work is aimed to conduct the following works stated hereunder:

- i) To propose a major classification of bridges in terms of structural importance and serviceability based on existing bridge inventory in Bangladesh.
- ii) To develop physical and analytical modelling scheme of the proposed bridge classification for probabilistic seismic hazard analysis.
- iii) To select a set of ground motion records for incremental dynamic analysis incorporating the finite element procedure of the major bridge classification towards seismic performance assessment.
- iv) To derive the analytical seismic fragility function for the major bridge classification considering engineering demand parameters, different damage states, ground motion intensity measures and probabilistic seismic demand model based on available literature.
- v) To develop seismic fragility curves following steps (iii) and (iv) for major bridge classification of Bangladesh that will best suited for seismic losses determination and retrofit prioritization.

## **POSSIBLE OUTCOMES**

A meaningfully sophisticated and more objectively tuned fragility function and fragility curves for major bridge classification of Bangladesh will be developed. It is expected that, this more comprehensive fragility function with fragility curves will be better capable of evaluating the probabilistic seismic hazard analysis by accurately assess damage states that are important to estimate possible loss estimation and taking retrofitting decision for overall bridge systems in Bangladesh.

## TENTATIVE FLOWCHART OF METHODOLOGY

A tentative flowchart of the research methodology have been tried to discussed by following steps given hereunder which might helpful to reach the research goal positively [Fig. 1]. This research work still in very primary stage which needs further modification and cordially promote comments and valuable suggestions from research community.

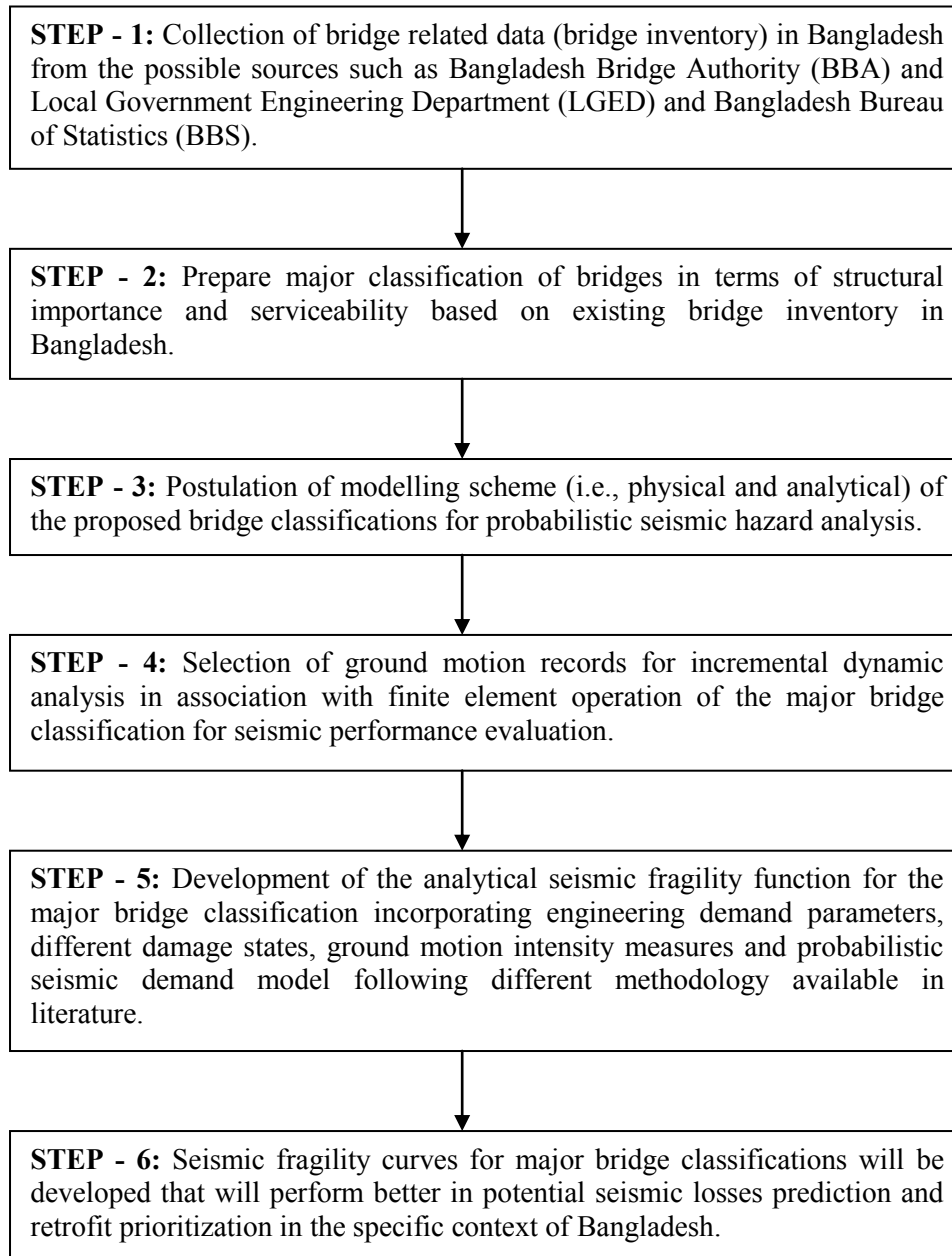


Fig. 1: Proposed methodology flowchart for fragility assessment of highway bridges in Bangladesh

## REFERENCES

- Alim, H. 2014. *Reliability Based Seismic Performance Analysis of Retrofitted Concrete Bridge Bent*, M. Engineering Thesis, Department of Civil Engineering, Chittagong University of Engineering and Technology (CUET), Chittagong, Bangladesh.
- Alim, H; Khan, AKM. TA and Bhuiyan, MAR. 2015. *Reliability Bases Seismic Performance Analysis of Retrofitted Bridge Bent*, IABSE-JSCE Joint Conference on Advances in Bridge Engineering III, 21-22 August, Bangladesh.

- Banerjee, S and Shinozuka, M. 2008. Mechanistic Quantification of RC Bridge Damage States under Earthquake through Fragility Analysis, *Probabilistic Engineering Mechanics*, 23: 12–22.
- Basoz, N and Kiremidjian, AS. 1999. *Development of Empirical Fragility Curves for Bridges*, Proceedings of the 1999 5<sup>th</sup> U.S. Conference on Lifeline Earthquake Engineering: Optimizing Post-Earthquake Lifeline System Reliability, August 12-14, 16: 693–702.
- Bhuiyan, AR and Alam, MS. 2012. *Seismic Fragility Assessment of Multi-span Continuous Highway Bridge Isolated by Shape Memory Alloy Restrainer and Lead Rubber Bearing*, Proceedings of the 15<sup>th</sup> World Conference on Earthquake Engineering, Lisbon, Portugal.
- Bignell, J and LaFave, J. 2010. Analytical Fragility Analysis of Southern Illinois Wall Pier Supported Highway Bridges, *Earthquake Engineering & Structural Dynamics*, 39: 709–729.
- Billah, AHMM and Alam, MS. 2012. *Development of Fragility Curves for Retrofitted Multi-Column Bridge bent Subjected to Near Fault Ground Motion*, Proceedings of the 15th World Conference on Earthquake Engineering, Lisbon, Portugal.
- Choi, E DesRoches, R and Nielson, B. 2004. Seismic Fragility of Typical Bridges in Moderate Seismic Zones, *Engineering Structures*, 26(2): 187–199.
- Choi, E and Jeon, JC. 2003. Seismic Fragility of Typical Bridges in Moderate Seismic Zone, *KSCE Journal of Civil Engineering*, 7(1): 41-51.
- Cornell, CA; Jalayer, F; Hamburger, RO and Foutch, DA. 2002. Probabilistic Basis for 2000 SAC Federal Emergency Management Agency Steel Moment Frame Guidelines, *Journal of Structural Engineering*, 128(4): 526–532.
- Dukes, J; DesRoaches, R and Padgett, E. 2012. *Sensitivity Study of Design Parameters used to Develop Bridge Specific Fragility Curves*, Proceedings of the 15<sup>th</sup> World Conference on Earthquake Engineering, Lisbon, Portugal.
- El-Arab, IME. 2012. Analytical methodology of Seismic Fragility Curve for Reinforcement Concrete Pier Bridges in Egypt, *International Journal of Engineering and Advanced Technology (IJEAT)*, ISSN: 2249 – 8958, 2(2): 392-299.
- FEMA 366/September 2000. *HAZUS<sup>®</sup>99 Estimated Annualized Earthquake Losses for the United States*, Reported by Federal Emergency Management Agency, Washington D.C., US.
- Gardoni, P; Kiureghian, AD and Mosalam, KM. 2002. Probabilistic Models and Fragility Estimates for Bridge Components and Systems, *Pacific Earthquake Engineering Research Center, PEER Report 2002/13*, University of California, Berkeley.
- Huang, Q; Gardoni, P and Hurlbauss, S. 2010. Probabilistic Seismic Demand Models and Fragility Estimates for Reinforced Concrete Highway Bridges with One Single-Column Bent, *Jour. of Engg. Mech. @ ASCE*, ISSN 0733-9399/2010/11, 136(11): 1340–1353.
- Hwang, H; Liu, JB and Chiu, YH. 2001. *Seismic Fragility Analysis of Highway Bridges*. Reported under Project MAEC RR-4, Mid-America Earthquake Center, USA.
- Jeong, SH and Elnashai, AS. 2007. Probabilistic Fragility Analysis Parameterized by Fundamental Response Quantities, *Engineering Structures*, 29: 1238–1251.
- Karim, KR and Yamazaki, F. 2007. Effect of isolation on fragility curves of highway bridges based on simplified approach, *Soil Dynamics and Earthquake Engineering*, 27: 414–426.
- Khan, A.K.M. TA. 2014. *An Improved Rheology Model of Laminated Rubber Bearings for Seismic Analysis of Multi-Span Highway Bridge*, M.Sc. Engg. Thesis, Dept. of Disaster and Environmental Engineering, Chittagong University of Engineering & Technology (CUET), Chittagong, Bangladesh.
- Khan, AKMTA and Bhuiyan, MAR. 2015. *Damage State Analysis of Seismically Isolated Multi-Span Continuous Bridge*, IABSE-JSCE Joint Conference on Advances in Bridge Engineering III, 21-22 August, Bangladesh.
- Kibboua, A; Naili, M; Benouar, D and Kehila, F. 2011. Analytical Fragility Curves for Typical Algerian Reinforced Concrete Bridge Piers, *Structural Engineering and Mechanics*, 39(3): 411-425.
- Kim, SH. 2003. *Fragility Curves for Seismically Retrofitted Concrete Bridges*, Proceedings of the Pacific Conference on Earthquake Engineering, New Zealand, Paper ID – 168, pp. 1-8.
- Kim, SH and Shinozuka, M. 2004. Development of Fragility Curves of Bridges Retrofitted by Column Jacketing, *Probabilistic Engineering Mechanics*, 19: 105–112.
- Kwon, OS and Elnashai, AS. 2010. Fragility Analysis of a Highway Over-Crossing Bridge with Consideration of Soil–Structure Interactions, *Structure and Infrastructure Engg.*, 6(1–2): 159–178.

- Liao, WI and Loh, CH. 2004. Preliminary Study on the Fragility Curves for Highway Bridges in Taiwan, *Journal of the Chinese Institute of Engineers*, 27(3): 367-375.
- Lupoi, G; Franchin, P; Lupoi, A and Pinto, PE. 2004. Seismic Fragility Analysis of Structural Systems, Proceedings of the 13<sup>th</sup> World Conference on Earthquake Engineering, Paper ID - 4008, August 1-6, Vancouver, B.C., Canada.
- Mackie, K and Stojadinovic, B. 2004. *Fragility Curves for Reinforced Concrete Highway Overpass Bridges*, Proceedings of the 13<sup>th</sup> World Conference on Earthquake Engineering, Paper ID - 1553, August 1-6, Vancouver, B.C., Canada.
- Nielson, BG. 2003. Bridge Seismic Fragility-Functionality Relationships: A Requirement for Loss Estimation in Mid-America, Reported by *CBE Institute, Texas A&M University*, US.
- Neilson, BG. 2005. *Analytical Fragility Curves for Highway Bridges in Moderate Seismic Zones*, Ph. D. Thesis, School of Civil and Env. Engineering, Georgia Institute of Technology.
- Nielson, BG and DesRoches, R. 2007a. Seismic Fragility Methodology for Highway Bridges Using a Component Level Approach, *Earthquake Engineering and Structural Dynamics*, 36: 823–839.
- Nielson, BG and DesRoches, R. 2007b. Analytical Seismic Fragility Curves for Typical Bridges in the Central and Southeastern United States, *Earthquake Spectra*, 23(3): 615–633.
- Padgett, JE and DesRoches, R. 2008. Methodology for the Development of Analytical Fragility Curves for Retrofitted Bridges, *Earthquake Engineering & Structural Dynamics*, 37: 1157–1174.
- Ramanathan, K; DesRoches, R and Padgett, JE. 2012. A Comparison of Pre and Post-seismic Design Considerations in Moderate Seismic Zones through the Fragility Assessment of Multi-span Bridge Classes, *Engineering Structures*, 45: 559–573.
- Shirazian, S; Ghayamghamian, MR and Nouri, GR. 2011. Developing of Fragility Curve for Two-Span Simply Supported Concrete Bridge in Near-Fault Area, Reported by *World Academy of Science, Engineering and Technology*, 51: 571-575.
- Shinozuka, M; Feng, MQ; Lee, J and Naganuma, T. 2000. Statistical Analysis of Fragility Curves, *Jour. of Engineering Mechanics @ ASCE*, 126(12): 1224-1231.
- Tanaka, S; Kameda, H; Nojima, N and Ohnishi, S. 2000. *Evaluation of Seismic Fragility for Highway Transportation Systems*, Proceedings of the 12<sup>th</sup> World Conference on Earthquake Engineering, Paper ID - 0546, New Zealand.
- Vamvatsikos, D and Cornell, CA. 2002. Incremental Dynamic Analysis, *Earthquake Engineering and Structural Dynamics*, 31(3): 491-514.
- Yamazaki, F; Motomura, H and Hamada, T. 2000. *Damage Assessment of Expressway Networks in Japan Based on Seismic Monitoring*, Proceedings of the 12<sup>th</sup> World Conference on Earthquake Engineering, Paper ID – 0551, Auckland, New Zealand.
- Zhang, J and Huo, Y. 2009. Evaluating Effectiveness and Optimum Design of Isolation Devices for Highway Bridges Using the Fragility Function Method, *Engineering Structures*, 31: 1648-1660.

## **ADOPTION OF REGULAR COLUMN INSTEAD OF SHEAR WALL AT LIFT-CORE OF MODERATELY TALL RC FRAME STRUCTURE**

A. K. M. T. A. Khan\* & M. R. Alam

*Department of Civil Engineering, Chittagong University of Engineering and Technology, Chittagong, Bangladesh,*

*\*Corresponding Author: thohidul.ce@gmail.com*

### **ABSTRACT**

Shear wall are prominently used in lift-core of reinforced concrete (RC) frame structure for their optimum lateral stiffness and dynamic vibration resistivity. The ambient lateral load resistance, high stiffness and vibration resilience are the prime motivation to use such kind of solid element in the building structure. Providing shear wall, the deflection might be significantly reduced and therefore structural engineers are frequently choose this option. This study investigates the optimization of shear wall and evaluating the potentiality of regular column (instead of shear wall) in lift-core of a typical RC building frame. Two different modelling approaches of the lift-core (shear wall oriented and column oriented) have been employed to assess the seismic performances of a RC frame by nonlinear dynamic analysis. The RC building frame was considered as a intermediate moment resisting frame (IMRF) and a fixed restraint condition at foundation level of the building frame was considered. Five optimization schemes were adopted for both models by changing the relative position of shear wall and column arrangement. The seismic performance considered in this studies are storey deflections for both models, which further compared with the maximum permissible storey deflections following BNBC-2006, ACI Code 9.5.2 and Nilson et al. (2003). The numerical result shows that, the shear wall oriented lift-core posses less storey deflection than the column oriented lift-core whereas, for moderately tall structure (i.e., up to 9 storey), column oriented lift-core may use instead of shear wall as the permissible limit allows this initiation. But, for more than 9 storey, column oriented lift-core may not be adequate and then mandatorily shear wall have to adopted at lift-shaft because of the exceeding of permissible storey deflection at top storey.

Keywords: Shear wall, rc frame structure, nonlinear dynamic analysis, maximum permissible deflection, seismic performance, building code

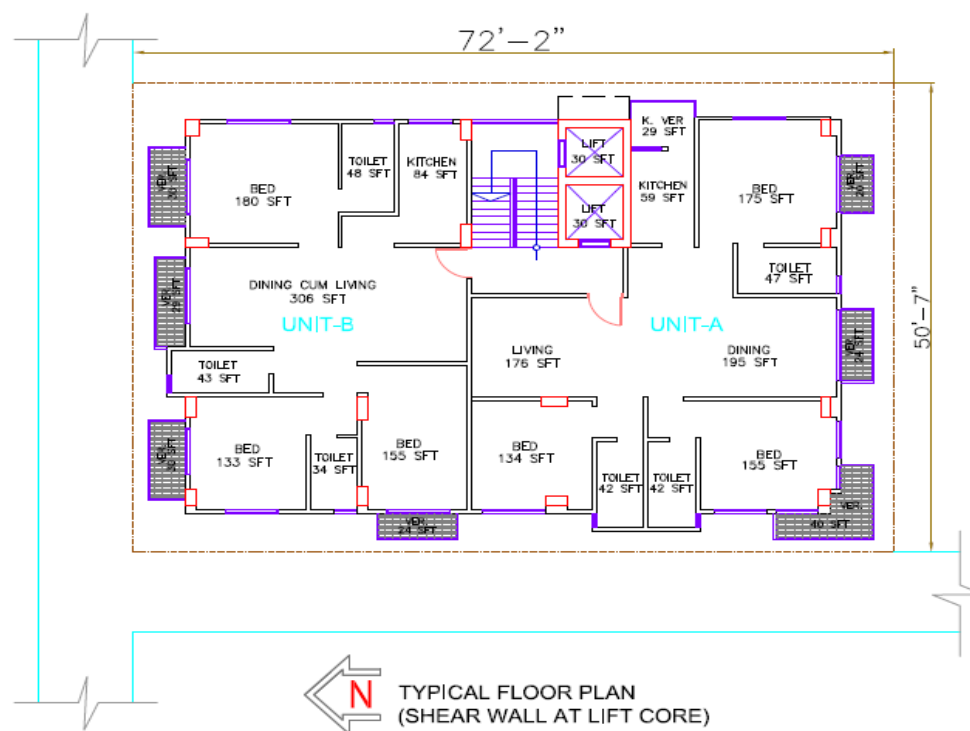
### **INTRODUCTION**

Shear wall is a common practice in lift-core for the multi-storied reinforced concrete (RC) building construction. At the RC building frame, lift-core is the most vibratory portion as the lift-cabin moves up and down continuously for transporting human being and goods at different floors of structure. The vibration produced by the lift in a RC frame may cause dilemmatic situation. In the very early stage of its invention, the weight of the lift's machine unit and cabin was quite heavy. But trend of modern science makes this issue a simple one. Recently, most of the lift is made from light fiber materials and they are comparatively lighter than earlier one. Earlier heavy lifting unit produced huge vibratory effect and they are dominantly manually operated (i.e., Pulley-Crane subsystem), so that structural engineers tried to emphasis on thicker lift-core (10 to 12 inch) with adequate reinforcement to reduce the vibration phenomena. Today's nominal-weighted lift is fully automated by the modern electromagnetic interaction and is appealing to rethink about the lift-core mechanism i.e., simple column instead of shear wall (Khan, 2015). Different authors focused on the shear wall and column analogy in the lift-core and the vibration effect of the continuous movement of lift-core. The optimization of shear wall has been assessed by Katkhoda and Knaa (2012) in the selection of structural systems for the design of RC high rise building for seismic resilience. The authors studied RC high rise building (10, 15, 20 storied), where the genetic algorithm was applied to access optimum solution, which ensures the economic dimensions that achieve the saving in concrete and steel amount thus gain lower cost also. The authors consider shear wall system, moment resisting frame and the

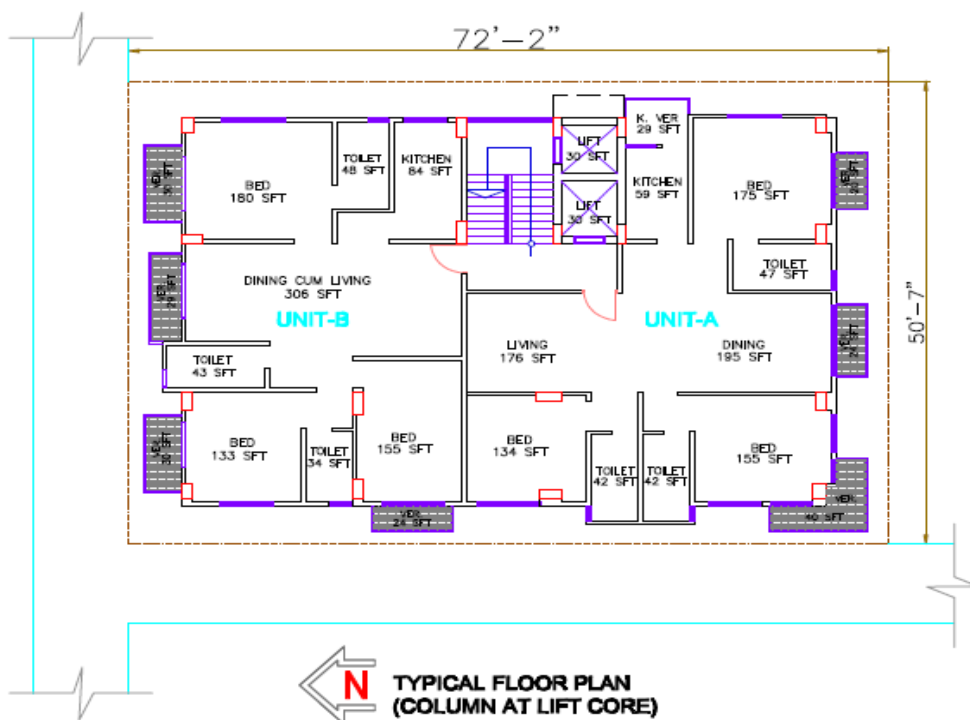
optimum combination of frame and shear wall system. Effect of change in shear wall location on storey drift of multi-story building was critically observed by Agrawal and Charkha (2012) when structure subjected to lateral loads. The authors argued that, shear wall is very prominent for high plain stiffness and strength which can be used to resist large gravity loads. It is very important to determine effective, efficient and ideal location of shear wall. The analysis proceeds by changing various position of shear wall with different shapes for determining parameters like storey drift, displacement and axial load etc. incorporating ETABS software. Shear wall are oblong in cross section, i.e., one dimension of the cross section is much higher than the other. While rectangular cross section is common, box shaped, L-shaped, U-shaped and other required sections are also used. Husain (2013) argued that, the hollow RC shaft around the lift-core of RC building act as shear walls and could be utilize to significantly resist seismic forces. Properly designed and detailed shear walls have shown very good performance in past earthquake as lateral loads caused by wind. Shear wall buildings are a popular choice in many earthquake prone countries, like Chile, New Zealand, USA, India and even in Bangladesh. Optimum structural modelling for tall buildings was performed by Jameel et al. (2012) where more emphasis was adopted on shear wall at lift-core. The authors argued that, dual system modelling combining frame and shear wall is appropriate for multi-storied buildings at lift-core and stair case portion. The investigation promotes the effects of multi-storied framed and shear wall structure in terms of storey displacement, natural frequency and natural time periods. Lateral displacement and storey drift were measured and it was observed that shear wall is a fruitful solution with cost effectiveness. Effect of different configuration of shear walls on seismic behaviour of high rise building was evaluated by Kharade and Chore (2014) where shear wall mainly used at lift-core. In multi-storied building, presence of lift-core wall causes localized increase of lateral stiffness of the overall system. Effect of placement and opening in shear wall on the displacement at various levels in a building subjected to seismic thrust was evaluated by Gupta and Pande (2014). Considering column at lift-core might reduce significant amount of costing in compare to shear wall construction. Moreover, the structural self weight could be noticeably reduced at the lift-core portion which finally helps to reduce foundation volume. In the BNBC-2006, ACI Code 9.5.2 and Nilson et al. (2003), a guideline provided for maximum permissible computed deflections for the residential building structure. It could be earnestly possible to analyse the effectiveness of simple column in compare with shear wall made lift-core and check the deflection limits accordingly. Column based lift-core allows the deflection limit for certain height (i.e., up to 9 storey) might be a cost effective alternative. The objective of this work is to carry out the optimization of shear wall in lift-core of RC building structure and evaluating the effectiveness of regular column instead of shear wall at lift-core.

## MODELLING OF THE RC FRAME BUILDING

A RC building frame [Fig. 1 & Fig. 2] suitable for FE software analysis was selected after taking the necessary permission from the project owner. Geometric and material data of RC building frame have been assigned after critically analyse the collected information. Some initial hand approximation has been initiated to primarily consider the tentative section of beam, column, slab and shear wall members. A Professional finite element (FE) based software namely Extended Three Dimensional Analysis of Building System (i.e., ETABS Nonlinear Version 9.7.0) was incorporated for dynamic analysis of the RC building frame. A new model was initiated from the software opening interface and assign total number of stories (B+G+7). The grid spacing have to be defined according to the column to column distance following the spacing in X and Y direction. The grid ID in X direction are delimited to A - J with corresponding spacing with 50", 182", 118", 109", 74", 83", 84", 47" and 42", respectively. Again, the grid ID in Y direction are delimited to 1 - 10 with corresponding spacing were 34", 63", 74", 32", 96", 92", 32", 35", 41", 45" and 30", respectively. The storey ID has been assigned according to features including level, height and comparative elevations. In this study, the height of typical floor was 10 ft and the basement floor was at 5 ft top of foundation level. "Define" menu helps to confirm the materials properties and frame sections. Four structural elements of the RC frame were Beam ( $f_c'=3500$  lb/in<sup>2</sup>), Column ( $f_c'=4000$  lb/in<sup>2</sup>), Slab ( $f_c'=3500$  lb/in<sup>2</sup>) and Shear wall ( $f_c'=4000$  lb/in<sup>2</sup>). 72 Grade ( $F_y=72000$  lb/in<sup>2</sup>) steel was blended in each structural elements.



(a)



(b)

Fig. 1: Physical model (typical plan) of the RC building frame (a) shear wall at lift-core (Model A), (b) only column at lift-core (Model B)

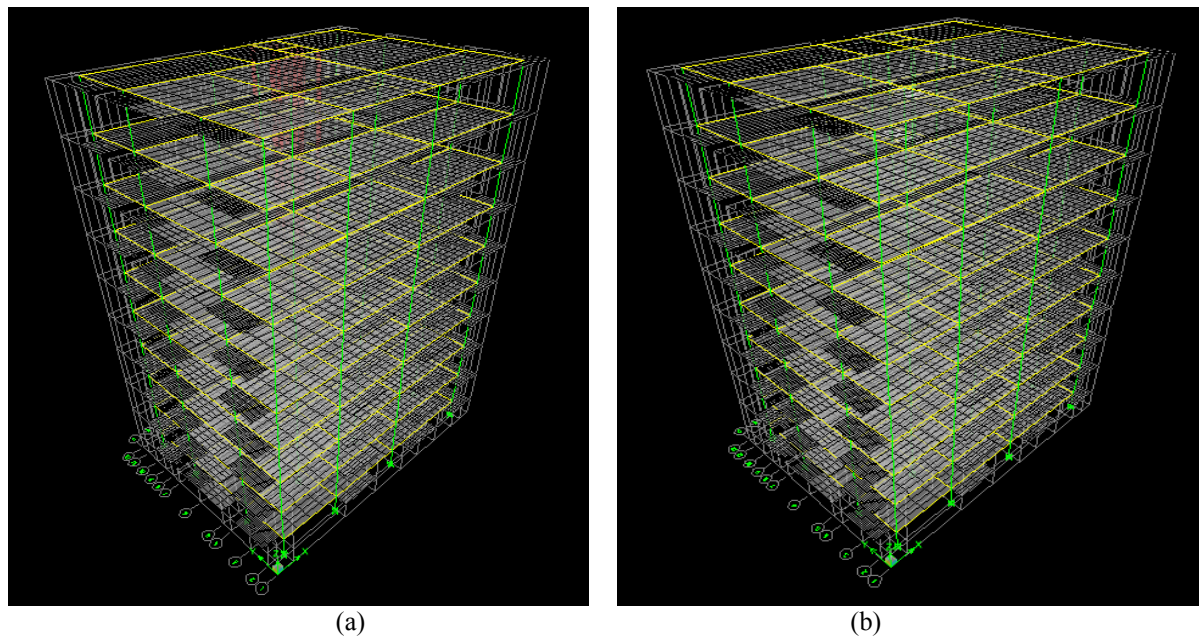


Fig. 2: 3D Model at FE scheme (a) shear wall at lift-core (Model A), (b) only column at lift-core (Model B)

The modulus of elasticity was assigned following the formula  $[E = 57000\sqrt{f'_c}]$ , where  $f'_c$  is in  $\text{lb/in}^2$ . Frame sections of the structural elements were ensured with the relevant cross section of Beam (10" x 24"), Column (10" x 25") and Column (10" x 30") at lift-core, Column (12" x 20") at corner, Column (12" x 25") at side span and Column (12" x 30") at mid span. All sections are rectangular in shape. Slab is 5.5" thick and shear wall is 10" thick with pier level P1. All the structural members have been digitally drawn based on the grid and following the sequence of columns  $\rightarrow$  beams  $\rightarrow$  shear walls  $\rightarrow$  slab chronologically. The base support condition was assigned as fixed. The dead load and live load at each floor slab was assigned as uniformly distributed in nature. The entire slab member and shear wall elements was meshed to 4 by 4 for accurate analysis. The inner portion of lift-core was assigned as opening. The centre of diaphragm was checked which should be nearly at centre of RC building frame. The model was critically checked for the FE software ETABS analyse. After successful analysis, the design combination following the "select design combo" was initiated for both USD (Ultimate Strength Design) and WSD (Working Strength Design) loading pattern. Both the concrete frame and shear wall member was designed individually to find the deformed shape and storey deflection. The storey deflection was then compared with the code provided allowable deflection values for shear wall based lift-core and simple column based lift-core. Other optimization models was analysed and designed following aforementioned steps chronologically to find out the storey deflections at every grid of each model.

## LOADS AND LOAD COMBINATIONS

Following expert based opinion, assume that, the dead load is  $100 \text{ lb/ft}^2$  and live load is  $40 \text{ lb/ft}^2$ . These loads were uniformly distributed on the top of each slab from basement floor to 7<sup>th</sup> floor. At the top roof, the entire distributed loads assigned as its half of the regular floor by the practical observation. Earthquake and wind load was assigned according to UBC (Uniform Building Code) 1994. For earthquake loads, seismic zone factor (Z) is 0.15, site coefficient (S) is 1.2 and structural importance factor (I) is 1.0 with time period 0.030 and numerical response modification factor ( $R_w$ ) is 8.0. The active zone for seismicity is base to top roof. For wind load, basic wind speed is 150 mph (mile/hour), exposure type is B, and structural importance factor is 1.0 with windward coefficient is 0.8 and leeward coefficient is 0.5. The active zone for wind induced vibration is ground floor to top roof. Two load combinations are considered in this study, namely WSD and USD combination. For WSD combination, both the dead load and live load coefficient is 1. Whereas, for USD combination, dead load coefficient is 1.2 and live load coefficient is 1.6. Some other default combinations were automatically initiated by the professional finite element environment of ETABS 9.7.0.



## ALLOWABLE DEFLECTION BY BNBC-2006 AND OTHER CODES

According to BNBC–2006 (Table 6.6.4), ACI Code 9.5.2 and Table 6.2 of Nilson et al. (2003), the maximum permissible computed deflection for RC frame structure is  $[(L/480)++]$  with complying some other conditions. Current study incorporates  $(L/500)$  to compute the maximum permissible deflection, where  $L$  means total height of building structure in "inch". The allowable deflection at top roof becomes 2.28". Following same approximation, the allowable deflections at basement floor to 7<sup>th</sup> floor were 0.12", 0.36", 0.60", 0.84", 1.08", 1.32", 1.56", 1.80" and 2.04", respectively. The allowable deflection at foundation level was considered as zero for fixed support condition.

## NUMERICAL OUTCOMES

Table 1: Comparison of maximum and allowable storey deflection for different modelling approaches

Model	Storey ID	Grid ID	Maximum Storey Deflection, $\delta_U$ (inch)	Allowable Storey Deflection by BNBC – 2006, $\delta_A$ (inch)	Comparison of Maximum and Allowable Storey Deflection	% Change in between $\delta_U$ & $\delta_A$
Model A (Shear wall at Lift)	Top Roof	Grid 2	1.194	2.280	$\delta_U < \delta_A$ (Safe)	90.888
1 <sup>st</sup> Optimization of Model A	Top Roof	Grid B	1.464	2.280	$\delta_U < \delta_A$ (Safe)	55.749
2 <sup>nd</sup> Optimization of Model A	Top Roof	Grid B	1.470	2.280	$\delta_U < \delta_A$ (Safe)	55.052
3 <sup>rd</sup> Optimization of Model A	Top Roof	Grid B	1.646	2.280	$\delta_U < \delta_A$ (Safe)	38.534
4 <sup>th</sup> Optimization of Model A	Top Roof	Grid 2	1.573	2.280	$\delta_U < \delta_A$ (Safe)	44.915
5 <sup>th</sup> Optimization of Model A	Top Roof	Grid B	1.689	2.280	$\delta_U < \delta_A$ (Safe)	35.013
Model B (Column at Lift)	Top Roof	Grid B	1.665	2.280	$\delta_U < \delta_A$ (Safe)	36.956
1 <sup>st</sup> Optimization of Model B	Top Roof	Grid B	1.862	2.280	$\delta_U < \delta_A$ (Safe)	22.436
2 <sup>nd</sup> Optimization of Model B	Top Roof	Grid B	1.931	2.280	$\delta_U < \delta_A$ (Safe)	18.056
3 <sup>rd</sup> Optimization of Model B	Top Roof	Grid B	1.826	2.280	$\delta_U < \delta_A$ (Safe)	24.856
4 <sup>th</sup> Optimization of Model B	Top Roof	Grid B	1.891	2.280	$\delta_U < \delta_A$ (Safe)	20.601
5 <sup>th</sup> Optimization of Model B	Top Roof	Grid B	1.786	2.280	$\delta_U < \delta_A$ (Safe)	27.680

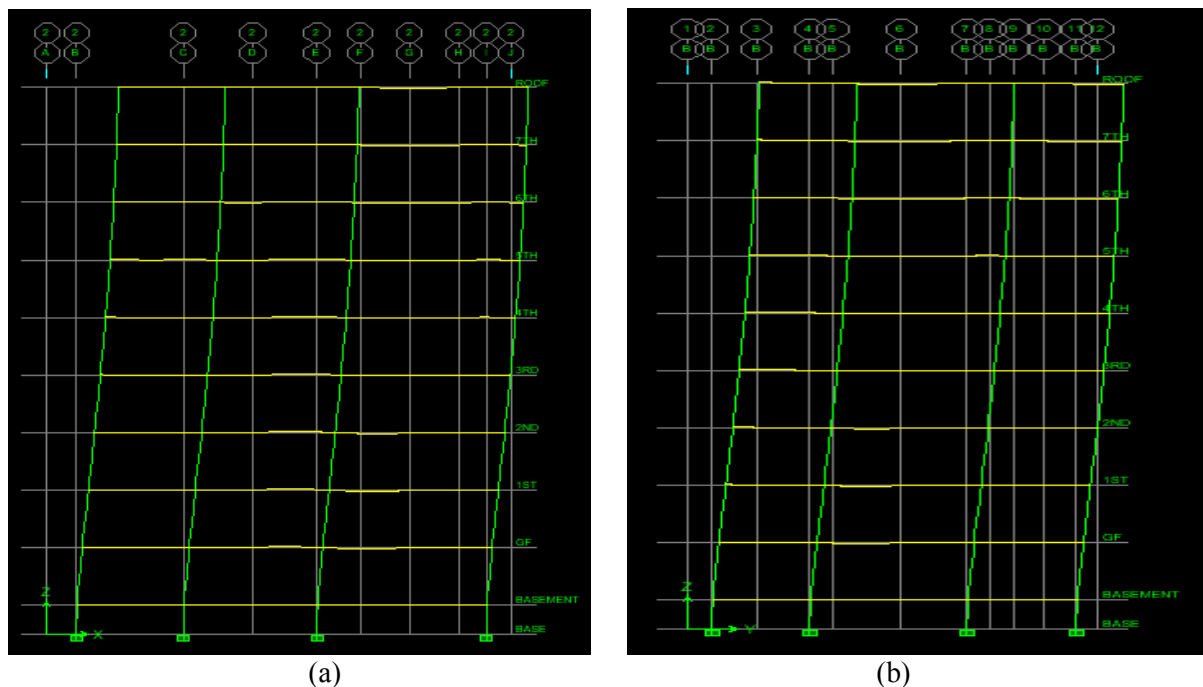


Fig. 3: Deformed shape with maximum deflection (a) Model A (at grid 2), (b) Model B (at grid B)

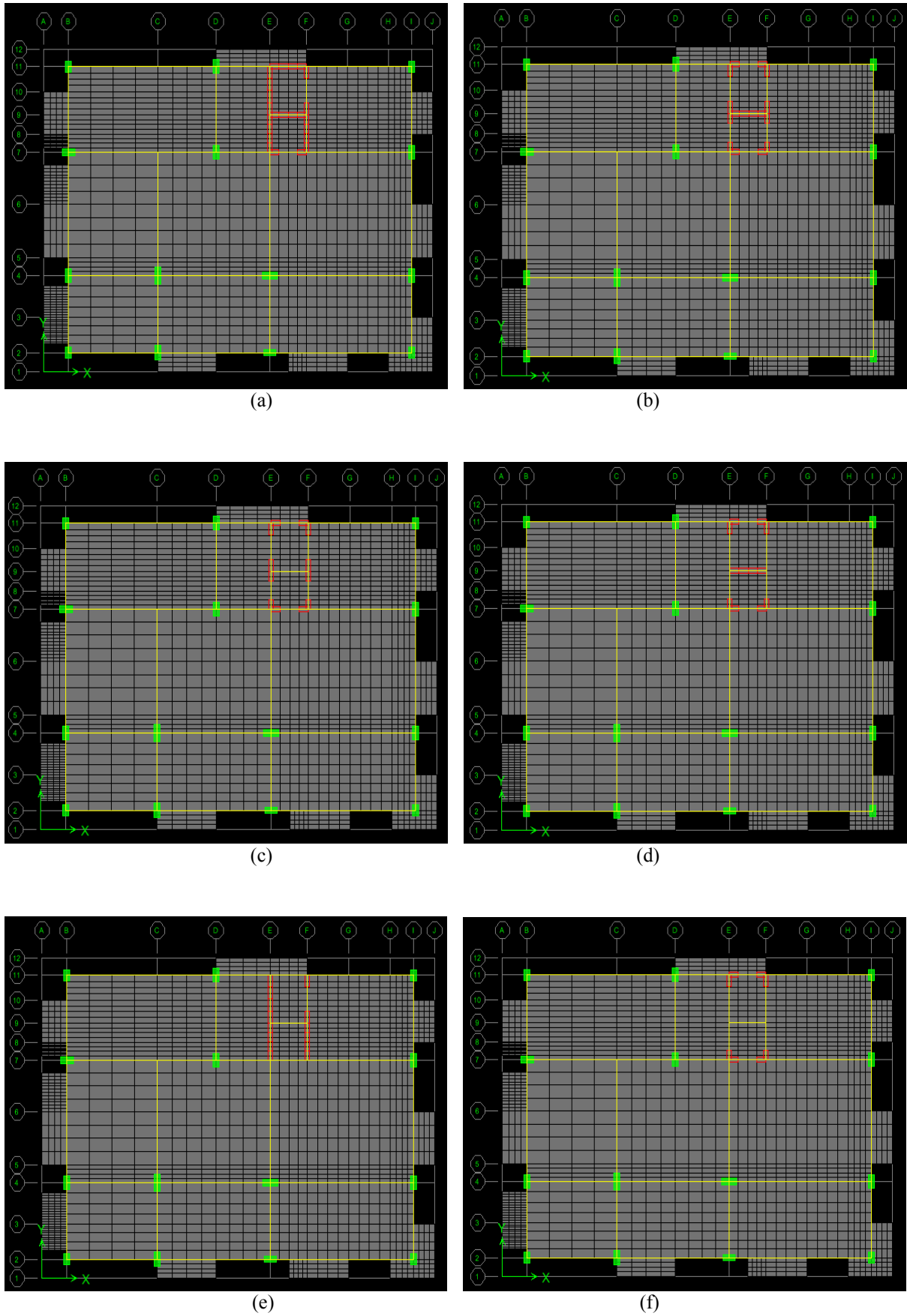


Fig. 4: Plan of the RC frame (shear wall provided at lift-core) (a) Model A, (b) 1st Optimization, (c) 2nd Optimization, (d) 3rd Optimization, (e) 4th Optimization, and (f) 5th Optimization

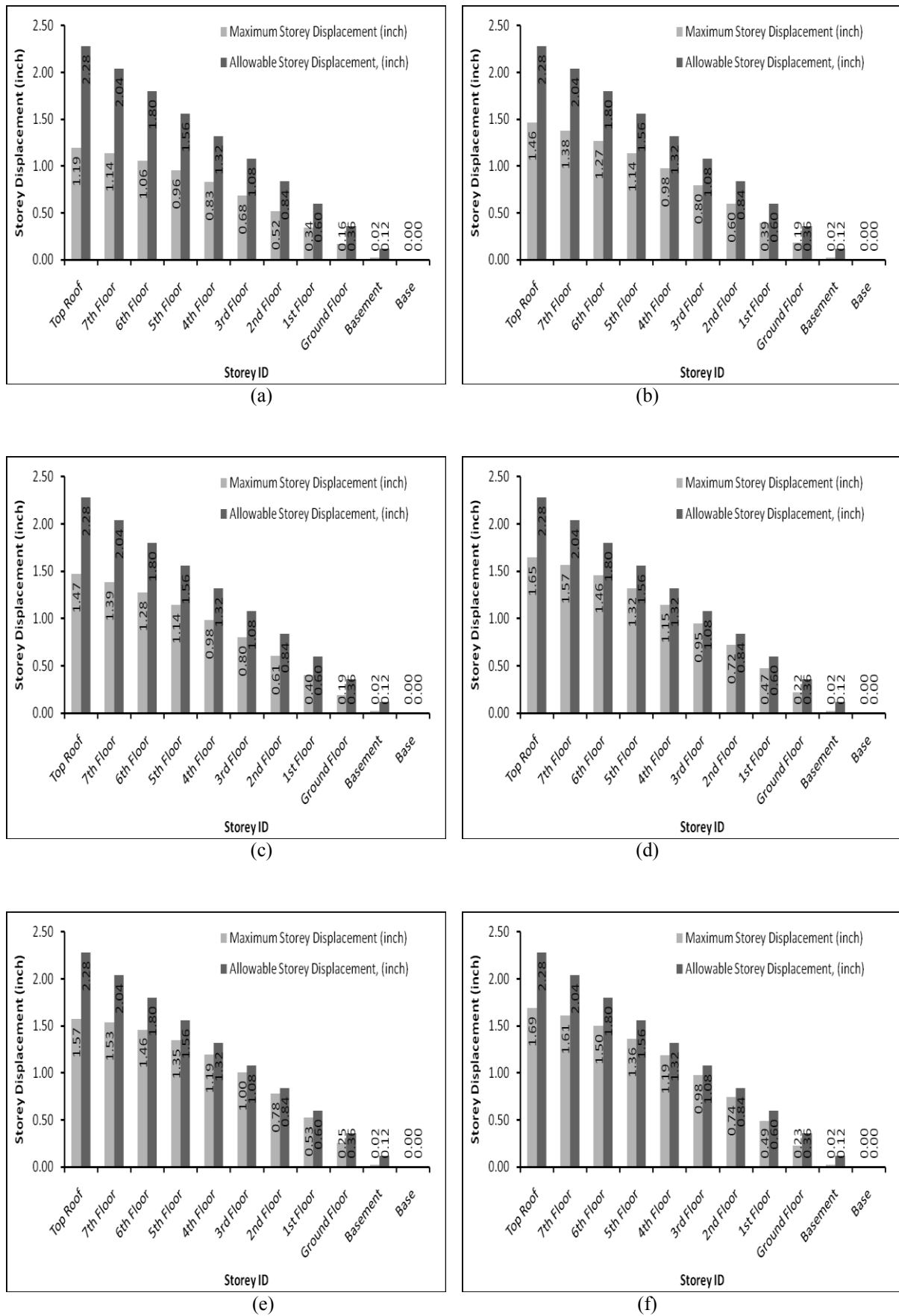


Fig. 5: Comparison of maximum & allowable storey deflection for (a) Model A (shear wall at lift-core), (b) 1st Optimization, (c) 2nd Optimization, (d) 3rd Optimization, (e) 4th Optimization and (f) 5th Optimization

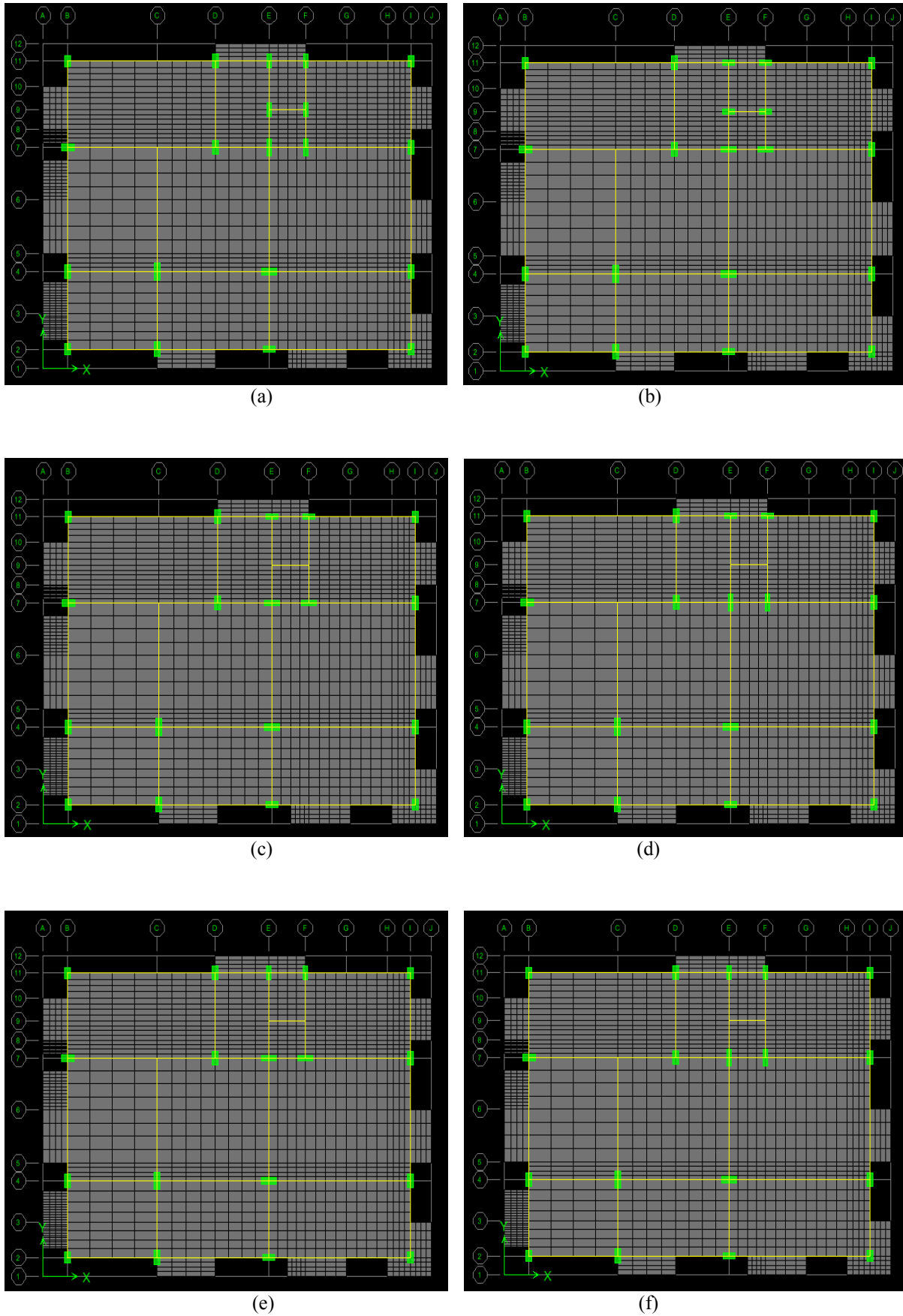
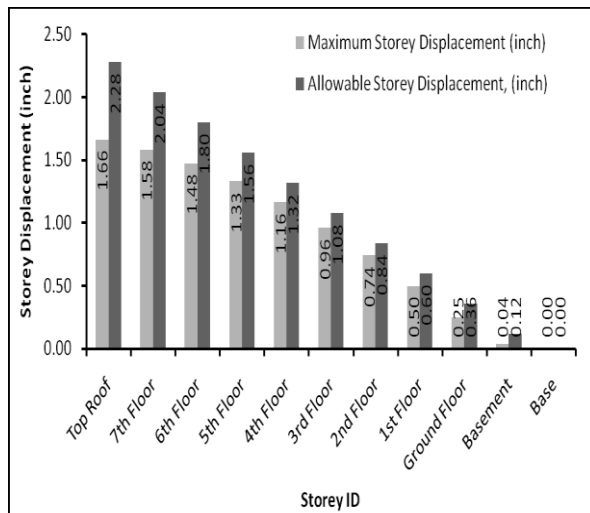
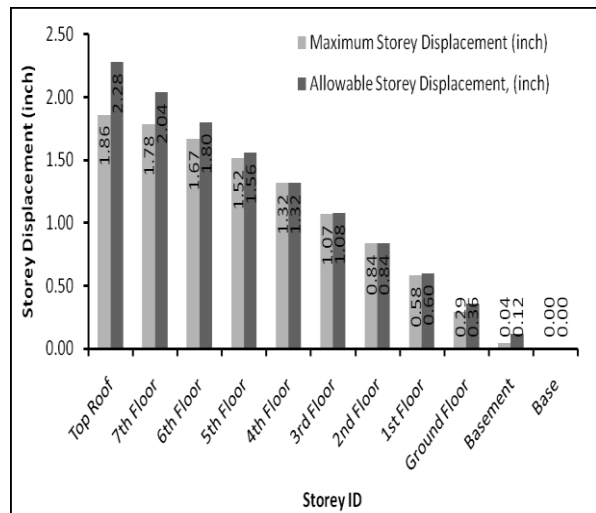


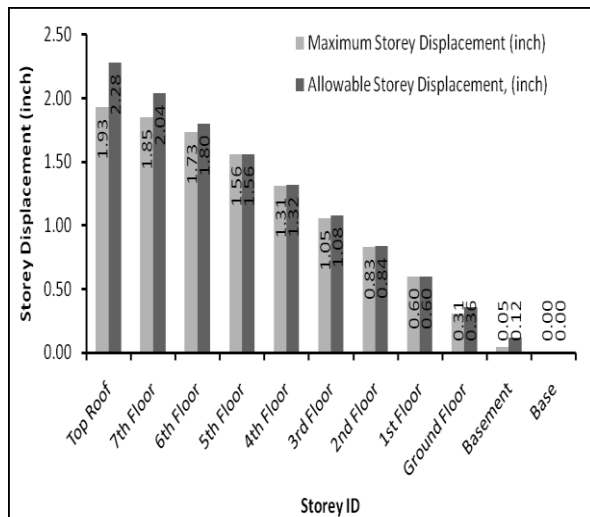
Fig. 6: Plan of the RC frame (only column provided at lift-core) (a) Model B, (b) 1st Optimization, (c) 2nd Optimization, (d) 3rd Optimization, (e) 4th Optimization and (f) 5th Optimization



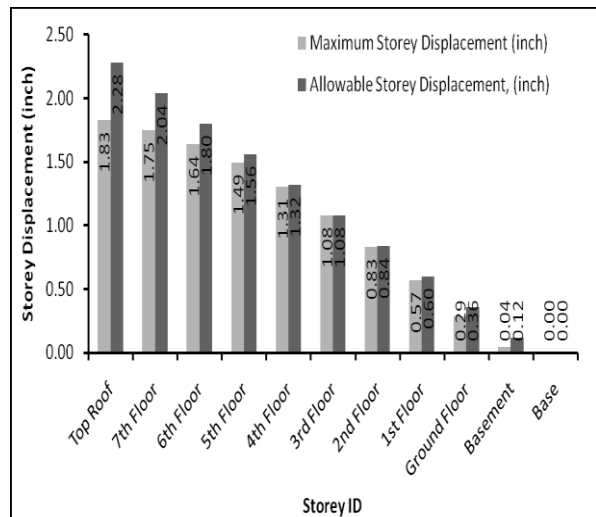
(a)



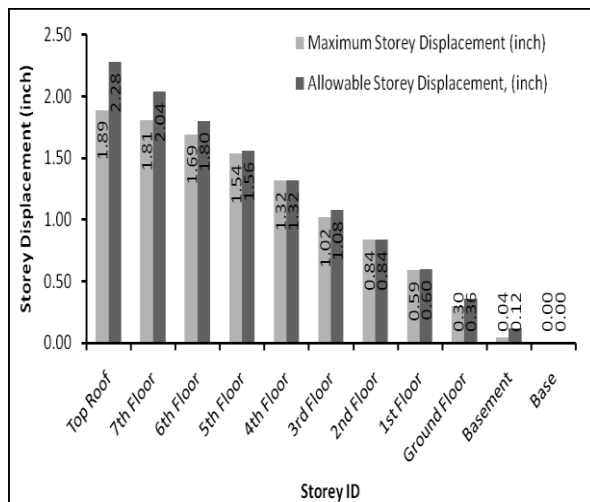
(b)



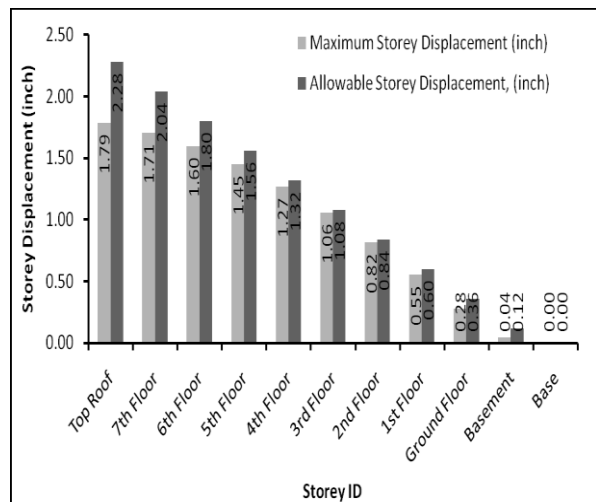
(c)



(d)



(e)



(f)

Fig. 7: Comparison of maximum & allowable storey deflection for (a) Model B (only column at lift-core), (b) 1st Optimization, (c) 2nd Optimization, (d) 3rd Optimization, (e) 4th Optimization & (f) 5th Optimization

## CONCLUDING REMARKS

This study presents the optimization of shear wall and evaluating the effectiveness of traditional column instead of shear wall in lift-core of a typical residential RC building frame. Two individual situation of the lift-core have been considered to assess the seismic performances of the target RC frame by nonlinear dynamic analysis. These are lift-core made by shear wall (Model A) and lift-core made by regular column instead of shear wall (Model B). The RC building frame was considered as an intermediate moment resisting frame (IMRF) following the provision of building codes. A fixed restraint condition at foundation level of the building frame was considered which causes zero deflection after dynamic analysis. Five optimization schemes were adopted for both Model A and Model B by changing the relative position of shear wall and column arrangement. Storey deflection has been considered as the seismic performance for both Model A and Model B, which further compared with the maximum permissible storey deflection following BNBC-2006, ACI code 9.5.2 and Nilson et al. (2003). The numerical results revealed that, the shear wall based lift-core possess less storey deflections than the column based lift-core. For moderately tall (i.e., up to 9 storey) building frame, column based lift-core may practice instead of shear wall because, the permissible limit allows this operation. For high-rise/tall RC frame (i.e., more than 9 storey) column based lift-core may not be adequate and then obviously shear wall have to exercised at lift-core because of the exceeding of permissible storey deflection at top storey. For both the model A and B, 5<sup>th</sup> optimization possess the most cost effective and convenient alternatives. More rigorous analysis is required using further sophisticated finite element software to gain refined knowledge about this column-shear wall analogy at lift-core of RC building frame which might be dealt as a future work.

## REFERENCES

- Agrawal, AS and Charkha, SD. 2012. Effect of Change in Shear Wall Location on Storey Drift of Multistorey Building Subjected to Lateral Loads, *International Journal of Engineering Research and Applications (IJERA)*, 2(3): 1786-1793.
- American Concrete Institute (ACI) Code Clause 9.5.2.
- Bangladesh National Building Code (BNBC) - 2006.
- Gupta, PR and Pande, AM. 2014. Effect of Placement and Openings in Shear Wall on the Displacement at Various Levels in a Building Subjected to Earthquake Loads, *International Journal of Research in Engineering and Applied Sciences (IJREAS)*, 02(02): 5-9.
- Husain, FAB. 2013. *Shear Walls in Reinforced Concrete Building*, Article published by Civil Engineering Division, Baghdad University, Iraq, Paper ID: 7913, pp. 1- 7.
- Jameel, M; Islam, ABMS; Hussain, RR and Khaleel, M. 2012. Optimum structural modelling for tall buildings, *Struc. Design of Tall & Special Building*, wileyonlinelibrary.com/journal/tal, pp. 1-13.
- Katkhoda, A and Knaa, R. 2012. Optimization in the Selection of Structural Systems for the Design of RC High-rise Buildings in Resisting Seismic Forces, *Energy Procedia*, 19: 269–275.
- Khan, AKMTA. 2015. *Optimization of Shear Wall and Evaluate the Effectiveness of Regular Column instead of Shear Wall in Lift-Core of Reinforced Concrete Building Structure*, Term Paper Submitted to the Department of Civil Engineering, CUET, Chittagong, Bangladesh.
- Kharade, VV and Chore, HS. 2014. Effect of Configuration of Shear Walls on Behavior of High-Rise Buildings, *Integrated Journal of Engg. Research and Technology*, 1(6): 336–342.
- Nilson, AH; Darwin, D and Dolan, CW. 2003. *Design of Concrete Structures* (E-Book), 13<sup>th</sup> Edition, Published by McGraw Hill Publishers Inc., United States of America, ISBN No. 007-123260-5.

## **BOROPUKURIA FLY ASH - A PROSPECTIVE GREEN MATERIAL FOR COASTAL CONCRETE**

M. M. Islam\*, M. T. Alam & M. S. Islam

*Department of Civil Engineering, Chittagong University of Engineering and Technology, Chittagong,  
Bangladesh*

*\*Corresponding Author: moinul91@yahoo.com*

### **ABSTRACT**

Coastal concrete i.e. structural concrete exposed to sea environment needs special care regarding its durability. Fly ash, coal burnt waste products, is reported to be well effective as blending material with cement for its contribution in making impermeable concrete and also in reduction the CO<sub>2</sub> emission associated with the production of cement. Bangladesh government has made a mega plan to reach a capacity 40,000 MW of electricity by 2030, half of which will be generated from coal. Now in Bangladesh 250 MW coal based power plant is in running condition at Boropukuria. Additional 5250 MW coal based power plant is going to be installed. This paper investigates the performance of fly ash concrete exposed to artificially made sea water (SW). Fly ash concrete specimen of 100 mm cubical size made by cement fly ash mix ratio 100:0, 80:20, 70:30, 60:40 and 40:60 have been studied in PW, normal and accelerated SW environment (1T & 6T) and also in submerged (SUB) and alternate wetting drying (AWD) condition up to 12 months. After 12 months of curing, the loss in compressive strength as compared to PW cured specimens of similar age are reported to lie in the range of 12% to 28% for OPC and 4% to 17% for 70:30 fly ash concrete. Fly ash concrete of cement replacement level 30 to 40% showed relatively less negative half cell potential (HCP) value as compared to other concretes. The study reveals that fly ash concrete of cement fly ash mix 70:30 may be effective for concrete exposed to coastal environment form strength and durability point of view.

**Keywords:** Cement; compressive strength; fly ash; marine environment; half cell potential

### **INTRODUCTION**

Reinforced concrete is one of the most widely used building materials all over the world due to abundance of materials, speed and versatility in construction, strength, durability, economy and relatively long life spans. However, corrosion of the reinforcement in concrete structures is of utmost important to the life cycle of these structures especially to those areas exposed to marine environment. The expanded uses of concrete have increased the interest of scientists / researchers for its use in aggressive environments although a well designed concrete structure is reported to survive up to its design life without any major repair/maintenance work in adverse environment. SW is a complex solution of many salts containing living matter, suspended silt, dissolved gases and decaying organic material. The average salt concentration of SW is about 3.5%. Compound of chloride present in SW is around 89%; whereas the presence of sulphate compounds is around 10%. Reinforced Concrete structures in SW environments are often found to be deteriorated. So prior to the construction of any concrete structure in such location, proper steps should be taken to overcome the risk of deterioration of concrete due to chloride and sulfate attack. Depending on the tidal range, nature, extent and mechanism of deterioration process, a reinforced concrete structure exposed to SW environment can be divide into different zones like Atmospheric zone, Splash zone, Tidal zone and Submerged zone. The tidal zone experiences alternate wetting drying action in SW and is considered as corrosive area (Gowda, 1981). In coastal environment, chloride ion penetrating into the concrete from SW reacts with Ca(OH)<sub>2</sub> liberated from cement hydration and form calcium chloroaluminate (Friedels Salt). On the other hand, sulfate ions that penetrates inside concrete forms gypsum and a complex compound namely calcium sulphoaluminate (Ettringite). Both the products occupy a greater volume after crystallization in the pores of concrete than the compounds they replace. The formation of gypsum hydrate may cause an increase in volume of 17.7% in concrete (Islam et al., 2010).

The use of blended cement containing supplementary cementitious materials as a replacement of certain percentage of Portland cement is more effective than ordinary Portland cement in reducing the rate of chloride diffusion when properly cured (Juenger, 2015). The four primary types of SCMs are slag, fly ash, silica fume, and metakaolin. Fly ash has been shown to drastically improve chloride ingress resistance (Basheer, et al. 2002, Thomas, 2004). Fly ash, a byproduct of burning pulverized coal at electric power generating plants, is a fine-grained material consisting of spherical, glassy particles comprised of silicate glass containing silica, alumina, iron and calcium. Due to its chemical composition, fly ash exhibits both pozzolanic and hydraulic activities (Plank et al., 2015). These properties allow it to be added to Portland cement as a mineral additive at the time of batching, or it can be interground with the cement clinker during the production of the cement. In the hardened state, the addition of fly ash greatly reduces the permeability of concrete which provides great resistance to chloride ion ingress (Scrivener et al., 2015). This is primarily due to higher fineness of fly ash compared to cement which leads to more compact concrete mix that reduces pore sizes in the cement paste and reduces the space available for chlorides to penetrate into the concrete (Erdogan et al., 2014). Some of the benefits of including fly ash admixtures in concrete include improved workability, reduced segregation, bleeding, heat evolution and permeability, inhibiting alkali-aggregate reaction and enhanced sulfate resistance (Federal Highway Administration 2011). Bangladesh has a long coastline along its southern border. Structural concrete in such location are always under the adverse effect of marine environment. Hence prior to construction of concrete structures at such locations care should be taken to mitigate the risk of chloride and sulfate attack. Relevant literature reveals that addition of fly ash as a partial replacement of cement in making structural concrete reduces the permeability of concrete, which in turns may resist the penetration of harmful salt ions within the concrete structure. Studies on the use of fly ash concrete in aggressive environments show that the percentage of cement replacement with fly ash and their relative proportion for making concrete in such environment is very important and still debatable as well. Bangladesh government has launched a mega plan to reach 40,000 MW capacity of electricity generation by 2030, half of which will be generated from coal. There already exist a 250 MW coal-based power plant at Barapukuria in Dinajpur utilizing coal from Barapukuria Coal Mining Company Limited. Adjacent to the Barapukuria Power Plant, another 250 MW plant is supposed to be set up. The 1200 MW coal based power plant will be built at Matabari, Cox's Bazar using ultra super critical technology with the funding from both GOB and JICA. In addition 1320 MW coal fired power plant, "Maitree Super Thermal Power Project" at Rampal, Khulna is going to be established as a joint venture between India and Bangladesh. Also a MOU between GOB and Huadian Hong Kong Co. Ltd has been signed for setting up a coal-fired power plant of Further Bangladesh government has planned to install one of the similar plants at Mawa of Munshiganj with a capacity of 522 MW, while two others with the total capacity of 566 MW in Khulna region, all of which are coal based. According to the EIA report, 28.1 million tons of coal will be burnt to produce the estimated 5500 MW of electricity at the proposed power plant. Considering 10% ash generation, it will produce around 2.8 million tons of fly ash. These ashes comprising of fly ash, bottom ash and liquid ash which are extremely hazardous contain hazardous and radioactive metals like arsenic, lead, mercury, nickel, vanadium, beryllium, barium, cadmium, chromium, selenium and radium. About managing the waste, the EIA report states that the fly ash "could" be used in cement factories and brickfields. Taking Barapukuria as an example, it produces more than 300 metric tons of fly ash in one day, none of which has ever been used in cement factories and brickfields. Rather, they are found dumped in surrounding locations including at the ponds, lagoons or landfills which is spirally affecting the environment. The unused fly ash and bottom ash disposed from coal combustion power plants, makes major negative environment effects such as air pollution and groundwater quality problem due to leaching of metals from the ashes, specially unused fly ash which has very small particle size. The aim of this research is to evaluate and explore the suitability of the use of Bangladeshi fly ash in structural concrete and its efficiency in enhancing concrete durability performance as well as strength characteristics through improvement of the concrete microstructure.

## **EXPERIMENTAL PROGRAMS**

The experimental program was planned to study the effect of fly ash replacement with cement in concrete as per following steps:



### Properties of materials used

(a) **Cement:** ASTM Type-I Portland Cement was used as binding material. Chemical compositions of ASTM Type-I (OPC) are given in **Table 1**.

(b) **Fly ash:** A low calcium ASTM Class F fly ash collected from Barapukuria Power Plant, Bangladesh was used. Chemical analysis of fly ash as conducted using XRF study is shown in **Table 1**.

(c) **Aggregate:** Locally available natural sand with fineness modulus 2.58, specific gravity 2.61, passing through 4.75 mm sieve and retained on 0.075 mm sieve was used as fine aggregate. The coarse aggregate was crushed stone with a maximum nominal size of 12.5 mm with fineness modulus 6.58 and specific gravity 2.70.

Table 1: Chemical composition of ordinary Portland cement and fly ash

Types	ASTM Type-I Cement	ASTM Class F Fly Ash
<b>Chemical analysis (%)</b>		
Calcium oxide, CaO	65.18	8.6
Silicon dioxide, SiO <sub>2</sub>	20.80	59.3
Aluminum oxide, Al <sub>2</sub> O <sub>3</sub>	5.22	23.4
Ferric oxide, Fe <sub>2</sub> O <sub>3</sub>	3.15	4.8
Magnesium oxide, MgO	1.16	0.6
Sulfur trioxide, SO <sub>3</sub>	2.19	0.1
Sodium Oxide, Na <sub>2</sub> O	--	3.2
Loss on ignition	1.70	--
Insoluble residue	0.6	--

Table 2: Composition of Artificial Sea Water (Mayers, 1969)

Salt	Amount (gm/ liter)	% of total salt
Sodium chloride (NaCl)	27.21	77.74
Magnesium chloride (MgCl <sub>2</sub> )	3.81	10.89
Magnesium sulfate (MgSO <sub>4</sub> )	1.66	4.74
Calcium sulfate (CaSO <sub>4</sub> )	1.26	3.60
Potassium sulfate (K <sub>2</sub> SO <sub>4</sub> )	0.86	2.46
Calcium carbonate (CaCO <sub>3</sub> )	0.12	0.34
Magnesium bromide (MgBr <sub>2</sub> )	0.08	0.23
<b>Total</b>	<b>35.00</b>	<b>100.00</b>

### Variable Details

Different variables used in this experimental program are listed below:

(a) Five different mix proportions of cement fly ash (100:0, 80:20, 70:30, 60:40, 40:60) were used as cementitious material.

(b) Artificial SW of two different concentrations (1T and 6T) was used as curing water. PW was also used for comparison. SW (1T) is simulated in laboratory by mixing tap water with exact amount and proportion of different chemical compounds found in natural SW (**Table 2**). 6T simulated SW is obtained by mixing 6 times chemical compounds respectively as that of 1T solution.

(c) Two different exposure states namely submerged (SUB) and alternate wetting drying (AWD) were used to simulate immersed and tidal zone condition.

### Mix design

#### Sample description

A total of 400 no's of cubical specimen of size 100 mm were also cast from M38 concrete for different test as per program. The specimens were demoulded after 24 hours of casting and cured in PW at ambient temperature for 28 days. After that specimens were placed in SW of different concentration (1T, 6T) as well as PW for different exposure periods. Some of the specimens were subjected to AWD cycles (12 hours wetting followed by 12 hours drying) to simulate the tidal marine zone condition. Concrete specimens were designated as per grade of concrete and amount of fly ash as a percentage of total cementitious material. Thus M38FA40 concrete means grade of concrete is M38 and cement fly ash mix ratio is 60:40.

### TEST CONDUCTED

#### (a) Strength tests

Compressive strength of concrete specimens was tested at the ages of 1, 3, 6 and 12 months in accordance with the BS EN 12390-3:2009. Reported strength is taken as the average of three tests results.

**(b) Half Cell Potential measurement**

Half-cell potential of the steel reinforcement placed at two depth level 15 and 25 mm in fly ash concrete specimens that were exposed to SW of different concentration under SUB and AWD state of exposure was measured at every month upto 12 months of curing in accordance with ASTM C 876.

**RESULTS AND DISCUSSION**

Fly ash concrete specimens that are exposed to PW and SW of different concentration for various exposure periods were tested after specific exposure periods. The test results are graphically presented and discussed in the following sections:

**(a) Compressive strength**

The compressive strengths of OPC and fly ash concretes exposed to different marine environment, have been graphically represented in Fig.1 and Fig.2. Also for the ease of comparison, the relative compressive strengths are plotted in Fig.3 and Fig.4.

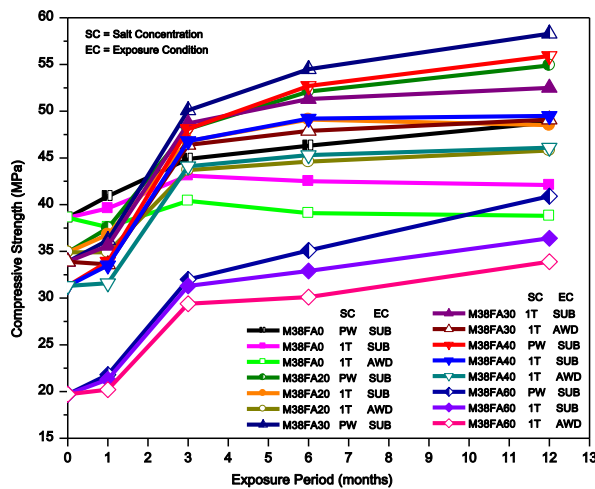


Fig.1: Compressive Strength - Exposure Period Relation for Concrete Exposed to 1T SW

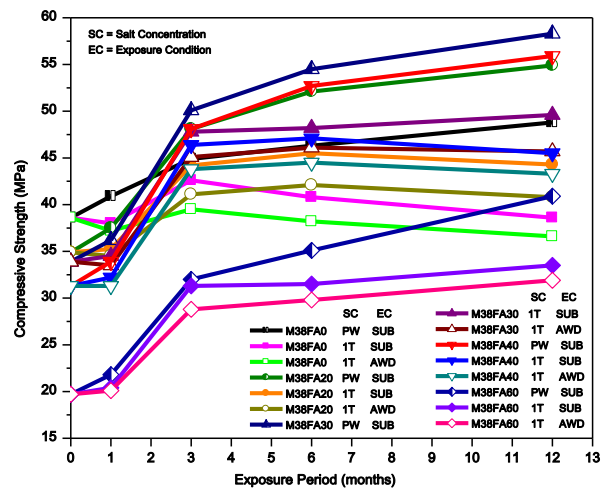


Fig.2: Compressive Strength - Exposure Period Relation for Concrete Exposed to 6T SW

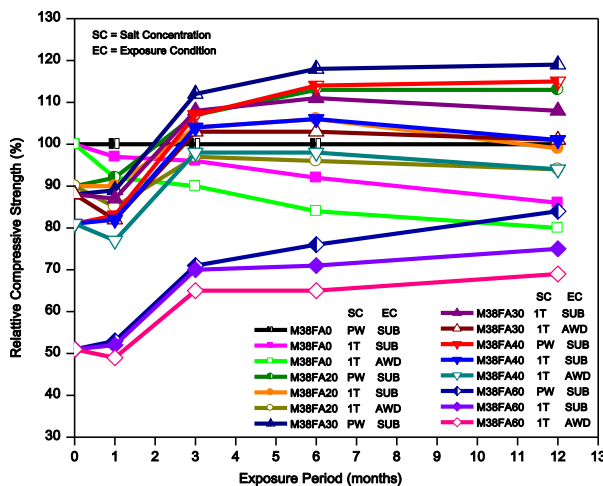


Fig.3: Relative Compressive Strength - Exposure Period Relation for Concrete (1T SW)

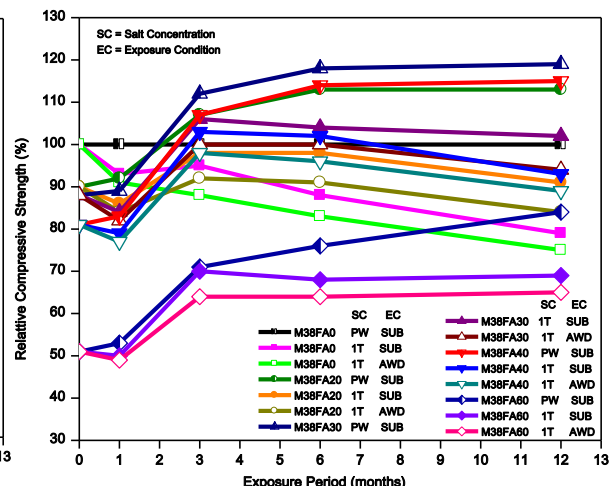


Fig.4: Relative Compressive Strength - Exposure Period Relation for Concrete (6T SW)

Compressive strengths corresponding to “0” month curing age represent the 28 days PW cured strength. In case of PW curing, the specimens for compressive strength were kept in SUB condition only and for SW curing, both SUB and AWD state of exposure conditions are used. In case of PW curing, OPC concrete shows higher strength at initial ages than that for fly ash concrete. But for relatively longer curing periods, the differences between the results are seen to be decreased. In case of PW curing, compressive strengths for 1 month exposure period is 38.6 MPa for OPC concrete, and 34.9, 33.9, 31.3, 19.7 MPa for fly ash concrete of cement fly ash mix ratio 80:20, 70:30, 60:40, 40:60 respectively; whereas the same values after 12 months curing, are 48.8 MPa for OPC concrete and 54.9, 58.3, 55.9, 40.9 MPa for fly ash concrete of similar replacement level. This is due to slow hydration rate

of fly ash at early age of curing. Test results show that compressive strength of concrete cured in SW and under SUB condition show relatively higher values than those for AWD condition. In case of fly ash concrete with cement fly ash mix ratio 100:0, 80:20, 70:30, 60:40 and cured in SW of 6T concentration, compressive strength for SUB condition are 40.8, 45.5, 48.2, 47.1 and 38.6, 44.3, 49.6, 45.5 MPa for 6 and 12 months of curing; whereas the corresponding values are 38.2, 42.1, 46.1, 44.5 and 36.6, 40.8, 45.7, 43.3 MPa respectively for AWD condition of similar curing period. During wetting cycle, SW enters into the pore spaces of the concrete and during drying cycles the penetrated salt ions become dried up and react with the cement hydrates that result in the formation of expansive compound and leads to the strength deterioration. Also during drying cycle, moisture inside the concrete may come out from the specimens for which normal hydration process is disturbed. Rate of strength deterioration for different types of concrete is observed to vary with SW concentration as well as exposure condition.

The compressive strength data also provide important information regarding the gain in strength of concrete under SW curing. In case of AWD condition and for 12 months of curing under 1T SW shows a gain in strength of 17%, 27%, 19% for fly ash concrete of cement fly ash mix ratio of 80:20, 70:30, 60:40 respectively; whereas the same value for 6T SW curing under similar exposure condition are 6%, 18%, 12% respectively. Thus in aggressive environment, gain in strength for fly ash concrete of cement fly ash mix ratio 70:30 is observed to be higher than that for any other concrete studied. The loss in compressive strengths as compared to 12 months compressive strength of PW cured OPC concrete, are observed to lie in the range of 12% to 28% for OPC concrete, 8% to 22% for 80:20, 4% to 17% for 70:30, 7% to 20% for 60:40 and 18% to 40% for 40:60 fly ash concrete when exposed to SW of different concentration. Cause for strength reduction may be the formation of expansive compounds includes ettringite or frields salt when concrete specimens are cured in SW. Due to formation of these expansive materials, micro cracks are developed inside the concrete and their subsequent propagation with the progress of hydration weakens the bond between hydrated product and aggregate particles. Ultimate result is the deterioration of concrete and the loss in compressive strength. Fly ash concrete specially cement fly ash mix ratio 70:30 shows higher resistance to SW penetration as compared to OPC concrete at longer exposure periods. Gain in compressive strength after 12 months exposure period for fly ash concrete of cement fly ash mix ratio of 80:20, 70:30, 60:40 are in the range of 106% to 126%, 118% to 136%, 112% to 128% with respect to 28 days compressive strength of PW cured concrete, whereas this value is 95% to 105% for OPC concrete. For longer exposure periods with the progress of hydration, fly ash concrete offers better resistance against the penetration of SW due to its impermeable nature that results in higher gain in strength at later ages.

Overall observation reveals that fly ash concrete shows relatively lower rate of strength reduction as compared to OPC concrete. Fly ash concrete specially cement fly ash mix ratio 70:30 shows higher resistance to SW penetration as compared to OPC concrete over longer exposure periods as well as least reduction in compressive strength. Overall reduction of compressive strength was 22% for OPC concrete, 16% for 80:20 fly ash concrete, 12% for 70:30 fly ash concrete, 15% for 60:40 fly ash concrete and 27% for 40:60 fly ash concrete. From all the above discussion it is clear that fly ash concrete shows comparatively higher gain in compressive strength in SW and fly ash concrete of cement fly ash mix ratio 70:30 shows lowest strength deterioration at larger curing periods in any curing condition among all the concretes studied.

### **(b) Half Cell Potential**

Half-cell potential (HCP) of the steel reinforcement placed at two depth level 15 and 25 mm in fly ash concrete specimens made from five different replacement level of fly ash which were exposed to SW of different concentration under SUB and AWD state of exposure are shown in **Fig.5** to **Fig.8**. Half cell potential was measured at an interval of one month for all the specimens. The reinforced concrete specimens were air dried for one hour before the half cell potential measurement. All potential values of concrete specimens become more negative with the increase of curing period. HCP value of M38FA0, M38FA20, M38FA30, M38FA40, M38FA60 concrete at a depth level of 15 mm were -122, -126, -119, -120, -125 mV respectively when exposed to SW of concentration 6T after 9 months of curing; whereas the same values for the same concretes after 12 months of curing in 6T SW were -274, -266, -255,

-262, -268 mV respectively. From the Figures, it is observed that there is a sudden drop of HCP values of all the concretes within the period of 10 to 11 months of exposure and this value drops from -100 to -200. This sudden drop can be attributed to the change in the condition of the potential of steel-concrete interface, possibly due to the ingress of sufficient amount of chloride at the rebar level. Therefore the chloride concentration at rebar level at the time of sudden drop can be considered as the critical chloride concentration responsible for depassivation of the steel reinforcement. Correspondingly the time at which this sudden drop had occurred was the corrosion initiation period under specific circumstances of the present investigation.

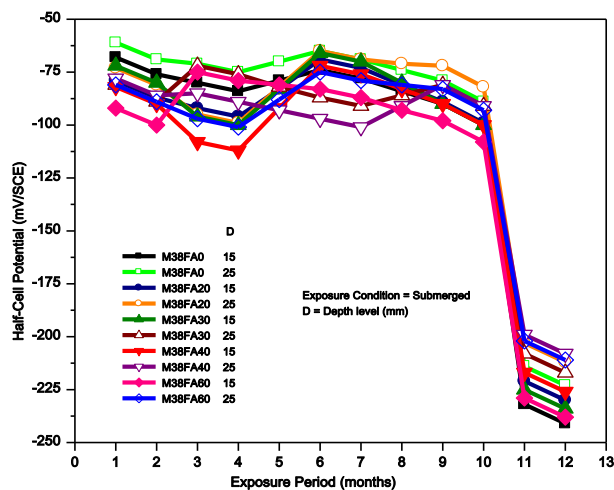


Fig.5: Half Cell Potential - Exposure Period Relation for Concrete Exposed to 1T SW (SUB)

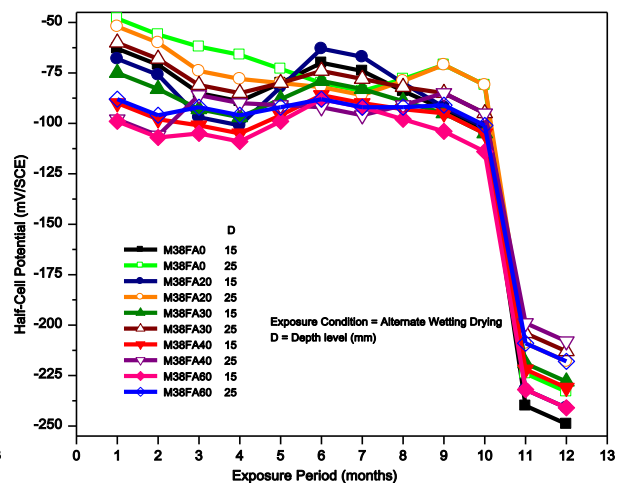


Fig.6: Half Cell Potential - Exposure Period Relation for Concrete Exposed to 1T SW (AWD)

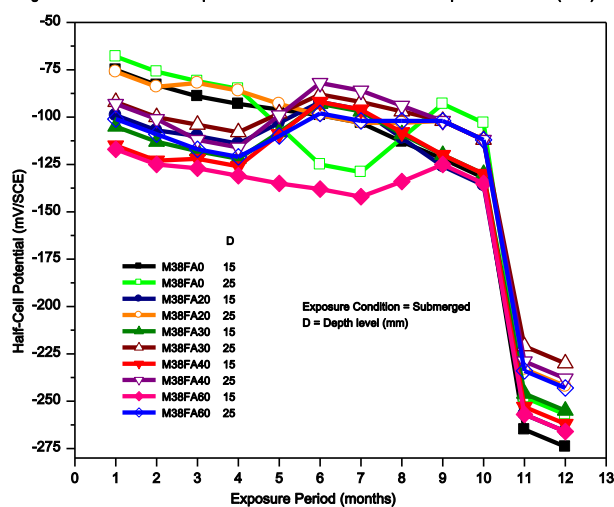


Fig.7: Half Cell Potential - Exposure Period Relation for Concrete Exposed to 6T SW (SUB)

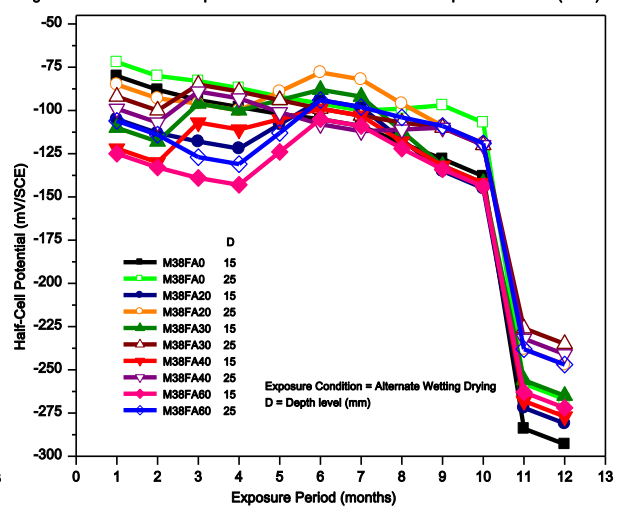


Fig.8: Half Cell Potential - Exposure Period Relation for Concrete Exposed to 6T SW (AWD)

It is also revealed from the HCP readings that fly ash concrete has better resistance against corrosion of steel as compared to OPC concrete for long exposure periods. In case of M38FA20, M38FA30, M38FA40, M38FA60 concretes, HCP values are -241, -228, -231, -240 mV for the steel at a depth level of 15 mm after 12 months of curing in SW of 1T concentration and in AWD condition; whereas the HCP values for same concretes are -281, -265, -277, -272 mV for 6T SW of similar condition. On the other side HCP values for OPC concrete are -249 and -293 mV respectively. From these HCP values, it is clear that fly ash blending can increase the resistance of concrete against rebar corrosion. Corrosion of reinforcement takes place due to ingress of chloride inside concrete. The passive oxide film surrounding the steel bar was destroyed due to presence of chloride ions. But in case of Fly ash concrete, ingress of chloride ion is observed to be reduced as compared to OPC concrete. Overall observation reveals that fly ash concrete of cement replacement level 30 to 40% shows relatively less negative HCP as compared to other concretes used in this study.

## CONCLUDING REMARKS

Based on the test results of plain and reinforced concrete of five different replacement levels of cement by fly ash exposed to simulated SW of 1T and 6T concentrations under SUB and AWD state, the following conclusions may be drawn:

- (1) Fly ash concrete shows relatively slower rate of strength gaining as compared to OPC concrete at early age of curing. But after 56 days of curing, compressive strength gaining rate increases for fly ash concretes as compared to OPC concrete.
- (2) Compressive strength of concrete specimens cured in SW of different salt concentration and in different exposure show a decreasing trend with the increase of exposure periods. Also for concrete specimens exposed to AWD state exhibited higher loss in strength than that of SUB state of exposure.
- (3) Effect of SW on strength reduction is lower for fly ash concrete as compared to OPC concrete. Upto 12 months of exposure in SW, overall losses in compressive strength lie in the range of 12 to 28% for OPC concrete, 8 to 22%, 4 to 17% and 7 to 20% for 20, 30 and 40% cement replaced fly ash concrete respectively. Concrete of cement: fly ash ratio 70:30 shows the least strength deterioration in all SW environments.
- (4) At the initial stage of curing, HCP values were almost constant before the initiation of rebar corrosion. After the dipassivation of steel, HCP rapidly decreased to more negative values. Fly ash concrete showed relatively lower negative value of HCP values as compared to OPC concrete.
- (5) The use of fly ash as partial replacement of cement clinker in cement production will reduce CO<sub>2</sub> emission to the environment and the problem of its disposal, saving the valuable fertile lands. Also it will save the national revenue by reducing the import of fly ash from foreign country.

## REFERENCES

- Basheer, L; Kropp, J and Cleland, D. 2002. Assessment of the durability of concrete from its permeation properties: A Review. *Construction and Building Materials*, 15: 93-103.
- Erdogan, ST. Over, D and Tokyay, M. 2014. Effect of pozzolan content and fineness on early hydration of interground blended cements. *Journal of Advanced Concrete Technology*, 12: 101–110.
- Federal Highway Administration. (2011). U.S. Department of Transportation Federal Highway Administration. Retrieved from <http://www.fhwa.dot.gov/infrastructure/materialsgrp/flyash.htm>
- Gowda, S. S. 1981. Corrosion fatigue of tubular joints in offshore structures. *First Indian Conference on Ocean Engineering*, V52-V61.
- Islam, MS; Islam, MM and Mondal, BC. 2010. Effect of freeze - thaw action on physical and mechanical behavior of marine concrete. *The institution of Engineers, Malaysia*, 71(1): 53-64.
- Juenger, MCG and Siddique, R. 2015. Recent advances in understanding the role of supplementary cementitious materials in concrete. *Cement Concrete Research*, 78: 71-80.
- Mayers, JJ; Holm, GH and Mc Allister, R. F. 1969. *The Hand Book of Ocean and Underwater Engineering*, McGraw-Hill London, , pp. 1094.
- Plank, J; Sakaib, E; Miao, CW; Yu, C. Hong, J. X. 2015. Chemical admixtures - Chemistry, applications and their impact on concrete microstructure and durability. *Cement Concrete Research*, 78: 81-89.
- Scrivener, K; Lothenbach, B; De Belie, N; Gruyaert, E; Skibsted, J; Snellings, R and Vollpracht, A. 2015. Hydration and microstructure of concrete with SCMs. *Material Structure*, 48: 835–862.
- Thomas, MDA and Matthews, JD. 2004. Performance of PFA Concrete in a Marine Environment – 10 Year Results. *Cement and Concrete Composites*. 26: 5-20

## CONSTRUCTION WASTE MANAGEMENT PRACTICE: BANGLADESH PERCEPTION

F. H. Chowdhury<sup>1,2</sup>, M. T. Raihan<sup>1,3\*</sup>, G. M. S. Islam<sup>1</sup> & F. Ramiz<sup>4</sup>

<sup>1</sup>Department of Civil Engineering, Chittagong University of Engineering & Technology, Chittagong, Bangladesh

<sup>2</sup>MAX Infrastructure Limited, Dhaka, Bangladesh

<sup>3</sup>Development Design Consultants Limited, Dhaka, Bangladesh

<sup>4</sup>Design Planning & Management Consultants, Dhaka, Bangladesh

\*Corresponding Author: tanveerraihan.m2n@gmail.com

### ABSTRACT

Construction sector involves several regulation policies including environmental protection, energy efficiency, work safety, taxation, and public procurement. Environment friendly and sustainable construction practice with competitiveness is essential for the balanced development of a country. Being and part of that, proper management of construction wastes is an important issue now a days. Being a developing country, Bangladeshis in the face of massive construction development work considering its current socio-economic condition. However, construction waste management practice is very poor in most cases. It is high time to think about some timely steps in order to implement different strategies for overall management. For successful waste management strategies, reliable and examined case studies are necessary. This study considered reviews on construction wastes, their generation and available management strategies. Finally, recommendation is provided on Bangladesh perspective.

Keywords: Waste management; construction waste; project management; sustainable development

### INTRODUCTION

In recent years, landfill loading and operation is heavily burdened with construction and demolition (C&D) waste. Eurostat reports illustrates that around 2 billion waste is being produced every year in European Union, which includes 31% of construction waste (DEFRA, 2007). About 29% of world's municipal solid waste is generated at China; among which 40% comprised of construction waste (Wang *et al.*, 2010). Study reported that 3158 tons material waste were disposed every day at landfills which is 23% of the total solid waste generated at Hong Kong (EPD, 2008). Land filling process is inefficient due waste of resources as well as inducing substantial adverse impacts on environment. Old landfills are almost reaching their capacity to its fullest, uncontrolled landfill sites chose for C&D waste are enlarging, because, strong pressure still exists to merely landfill construction debris (Kartam *et al.*, 2004).

Construction waste generation has become a major concern owing to its direct impacts on environment while affecting the efficiency of this industry (Formoso *et al.*, 2002). Building activity has huge environmental impacts from air pollution, noise pollution and water pollution (EPD, 1999). The most important and unpleasant environmental effect is from incineration which discharge pollutants to air (Kartam *et al.*, 2004). Contractors have to bear profit loss because of additional overhead costs and delays and loss of efficiency due to further time spend for cleaning (Skoyles and Skoyles, 1987). Since subcontractors have to estimate the amount of cost and involvement of time for waste generation during bidding, subcontractors are often blamed for construction waste generation (Johnston and Mincks, 1995). Construction organizations are willing to imply environmental friendly ways towards waste management only if they are profitable since profit maximization is their main objective (Hao *et al.*, 2008).

Any practices that might induce waste reduction must be prompted while deciding optimum waste handling methods by considering cost implications. A successful waste management can be promoted by developing a CWM plan and thus incorporation of the plan in construction specification. Reduction of construction waste on a project site can meet its sustainability objectives.

Depending on the economic and cultural characteristics the amount of waste generation, data used for categorization of waste and recording methods differs country wise (Kourmpanis *et al.*, 2008). Similarly, the effective execution of WM strategy is swayed by the affinity of WM plans with the actual situation (Manowong, 2012). Being a densely populated country Bangladesh cannot afford waste management by land filling, therefore, research is required to identify useful methods to mitigate construction waste generation and its management. This research aims to explore effective approaches to sort out and/or reduce waste generation in construction projects in Bangladesh.

### CONSTRUCTION WASTE & ITS GENERATION

Construction waste is principally a mixture of surplus materials generated during new construction or a demolition waste. It can be a mixture of lot many materials or in some cases can be individual ones depending on the type of work. C&D waste could be formed due to excavation work, clearance of any project site, road works and renovation or demolition of structures etc. Masonry wastes can be easily mixed up with other wastes such as wood and drywall.

Some of the more common C&D wastes can be lumber, drywall, metals, masonry (brick, concrete), carpet, plastic, pipe, rocks, dirt, paper, cardboard, or green waste related to land development (AIA,2008). Inert materials such as brick, concrete, rock etc. generally considered as masonry construction waste. Dirt removed from a demolition site is also included in that part. Waste materials from new wood for construction works like plywood, chipwood, dimensional lumber, shavings and sawdust and different demolition wood waste is considered as wood waste in construction site. Cut pieces of metallic materials such as new metal studs, metal beams, pipes are considered as metallic waste. Besides these, plastic and other different types of waste materials can be found in any construction site. Table 1 shows sequential list of construction wastes considering hazardousness nature adopted from the government of UK website.

Table 1: Construction and demolition waste classified according to hazardous characteristics. (Adapted from Govt.UK (2016))

Hazardous	Non-hazardous
Insulation and asbestos materials	Insulation and asbestos materials
Concrete, bricks, tiles and ceramics in mixtures	Concrete
Treated wood, glass, plastic (alone or in mixtures) containing hazardous substances	Bricks
Mixed metals containing hazardous substances	Tiles & ceramics
Cables containing oil, coal tar and other hazardous substances	Concrete, bricks, tiles and ceramics in mixtures
Soil and stones	Wood - untreated
Dredging spoil	Glass - uncontaminated
Gypsum materials	Plastic - excludes packaging waste
Un-used or un-set cement	Metallic waste, including cable Copper, bronze and brass, Aluminum Lead, Iron and steel, Tin
Paints and varnishes	Soil and stones
Paint cans	Dredging spoil
Adhesive or sealant containers	Gypsum materials
	Paints and varnishes

Cheung (1993) defined construction waste as the “by-product generated and removed from construction, renovation and demolition work places or sites of building and civil engineering structures”. Similar to definition of waste, waste measured is considered in different ways. While Treloar *et al.*, (2003) in terms of embodied energy of materials, Bossink and Brouwers (1996) described three case studies where waste of each type of material considered in different ways such as (i)

percentage of total construction waste; (ii) percentage of purchased materials and (iii) percentage of total cost of waste. However, categorization of waste streams along with volume/weight waste generated is essential to calculate these percentages. Some factors always influence the production of wastes during the life cycle of any construction projects, viz. design, procurement, materials handling, construction/renovation, demolition (Graham and Smithers, 1996). Patel *et al.* (2016) stated a conceptual framework at their study, where the sources of construction waste was organized into five categories as presented in figure 1. Ekanayake and Ofori (2000) limited the causes of waste into four major categories such as Design, Procurement Operation and Material handling.

Design	<ul style="list-style-type: none"> <li>• Blueprint Error</li> <li>• Detail Error</li> <li>• Design Changes</li> </ul>
Procurement	<ul style="list-style-type: none"> <li>• Shipping Error</li> <li>• Ordering Error</li> </ul>
Handling of Materials	<ul style="list-style-type: none"> <li>• Improper Storage or deterioration</li> <li>• Improper handling (off site and on site)</li> </ul>
Operation	<ul style="list-style-type: none"> <li>• Human Error</li> <li>• Equipment malfunction</li> <li>• Catastrophes, accidents, Weather</li> </ul>
Residuals	<ul style="list-style-type: none"> <li>• Leftover Scrap</li> <li>• Irreclaimable non consumables</li> </ul>

Fig. 1: Waste generation sources; adapted from Patel *et al.* (2016)

## ENVIRONMENTAL ISSUES

Impact of construction waste on the environment is always a major issue and proper management is required to avoid environmental liabilities. Natural resources of a region are affected during construction activities required for the development work. From the study of Kumar & Kaushik (2005), it can be inferred that construction related energy consumption, including both direct and indirect activities, amounts to around 50% of national energy use. The activities also associated with transport of materials. The negative effect of construction wastes inaugurates by dumping activities viz. dumping into forests, streams, ravines, empty land etc. which leads to cause erosion, contaminates wells and affects water tables and surface water (Arslan *et al.*, 2012). With proper synergy between build environment and natural environment can influence the hydrological system (Dixon, 2010). Using thoughtful planning system, design of buildings and landscapes can play role in operating construction development activities without causing any desolation of environment.

## IMPLEMENTATION OF CONSTRUCTION WASTE MANAGEMENT

Construction waste management (CWM) can be termed as reduction and diversion of construction waste, demolition debris and land cleaning rubbishes from disposal and rerouting recyclable resources back into the construction process (AIA, 2008). It is seen that construction solid waste management is given low priority when there is financial limitations and considerable amount of waste minimization can be attained when waste management is implemented as part of project management functions (Coffey, 1999).

Construction waste management plans require cooperation between all personals involved in a construction project. The client, designer, contractor, site engineers, technicians, sub-contractors, workers, material providers all need to work from the pre planning stage till end of any projects for ensuring an effective and efficient waste management plan. A framework called Leadership in Energy



and Environmental Design (LEED) in which Green Building System is widely applied. A bunch of standards are set to practice environmentally sustainable construction including practices for sound waste management into construction activities (LEED, 2004). Several research studies promoted the importance of incorporating waste management process in design and procurement phases. (Lingard *et al.*, 2000; McDonald and Smithers, 1998). Some research outcomes support the attitudinal approaches than the technological improvements (Kulatunga *et al.*, 2006; Wong and Yip, 2004). Disparity among construction waste management performance can be caused by client contractor relationship even standing within same jurisdiction has been noticed by Tam *et al.* (2007). According to Kulatunga *et al.*, (2006) attitudinal variances between different working groups and inadequate training to support the importance of waste minimization practices have obstructed proper waste management practices in the construction industry. Further, lack of communication of strategies from the top level to the bottom level of the organization, and insufficient data flow from construction sites to estimators, negatively disturbs waste management applications. Moreover, research on CWM performance has commonly suffered from insufficient quality data to support an informed debate on CWM performance. One can link different construction techniques, work procedures and common practices during construction work with construction waste management performance and provide quantitative data for benchmarking construction waste management practices across different projects by investigating Waste generator rate (WGR) (Lu *et al.*, 2011). WGR is widely used as an indicator to measure construction waste management performance which can be calculated by dividing the waste volume ( $m^3$ ) or quantity by the amount of virgin materials purchased or the amount required by the design or per  $m^2$  of gross floor area (GFA) (Formoso *et al.*, 2002).

In an Australian federal government study (DOE, 2013), four key points were pointed out for improving the resource recovery from construction and demolition wastes viz. (i) design buildings or structures considering their deconstruction ability enabling resource recovery and reduction of integral energy; (ii) reduction of on-site contamination of wastes and segregation of materials; (iii) encouragement for using recovered waste materials with improved specifications and knowledge of implementation; and (iv) Promoting research and development activities for overcoming the business and technical barriers with innovation approaches. Yuan (2013) conducted an SWOT (strength, weakness, opportunity and threat) analysis aiming to understand the status of construction waste management of a particular city in south China and suggested some government efforts for enhancing the awareness through some methods viz. launching of series of promotional activities via public advertisement, newspaper, radio and outdoor advertising, enhancing contractors, engineers and architects awareness through vocational training and establishment of awards for general public and industry stakeholders who actively participated in CWM activities.

### **CONSTRUCTION WASTE MANAGEMENT IN BANGLADESH:**

Being a developing country, Bangladesh continuing huge development works. Mega projects such as Padma River Bridge are ongoing around the country are copious and many to start in upcoming days. According to previous reviews, before starting construction work at any region waste generation and management becomes an important issue. But research and technical resource related to construction waste management scenario in Bangladesh is very poorly disregarded. Some statistics are available relating to solid waste generation and management. But when it comes to construction and demolition wastes, sufficient information is not available to predict a future condition and thus take preventive measures. Zahur (2007) published a research work considering the solid waste generation in Bangladesh, added brick, wood, metal, glass and industrial wastes as a part of solid waste. The prediction of solid waste generation gives us some idea about overall waste generation. The urban areas in Bangladesh generate approximately 16015 tons of waste per day and it is projected to grow up around 47000 tons/day in the year 2025 (Bahauddin & Uddin, 2012). So, serious thoughts should be given to construction waste generation and its management incorporating detailed research and study. Field survey can be an effective approach at the for the kick start. Collaboration and communication at different level of construction starting from client to field workers are essential. In Bangladesh concerns about construction waste management are hardly seen among consumers as well as clients. When profit maximization and completion of project within due time is the main goal, CWM could be regarded as extra burden. In addition to that skilled manpower is an important issue for the overall management.

However, minimizing the waste generation rates by effectively using raw materials represents an effective construction manager.

## CONCLUSION

For sustainable development, practice of sustainable construction process has received great importance throughout the world. The consumption of materials for construction purposes being huge, this sector has great responsibility to contribute to the term 'Sustainability'. With the continuing research activities and practical experiences of the personals related to this industry, proper management of construction waste is necessary. The government should introduce incentives and benefits to the projects implementing an effective construction waste management plan. Planning, assessment, selection of consultants and contractors, design, operation, each step has contribution to a successful waste management output. We would consider one step ahead towards the green building technology after being able to implement proper waste management practices in all major construction projects in Bangladesh.

## REFERENCES

- Arslan, H, Salgin, B, & Coşgun, N .2012. Construction and demolition waste management in Turkey. *INTECH Open Access Publisher*.
- Bahauddin, KM, & Uddin, MH. 2012. Prospect of solid waste situation and an approach of Environmental Management Measure (EMM) model for sustainable solid waste management: Case study of Dhaka city. *Journal of Environmental Science and Natural Resources*, 5(1), 99-111.
- Bossink, BAG, & Brouwers, HJH. 1996. Construction waste: quantification and source evaluation. *Journal of construction engineering and management*, 122(1), 55-60.
- Cheung, CM; Wong, KW; Fan, CN & Poon, CS. 1993. Reduction of construction waste: final report. *The Hong Kong Polytechnic University and Hong Kong Construction Association, Hong Kong*.
- Coffey, M. 1999. "Cost-effective systems for solid waste management." *Waterlines*, 17(3), 23-24.
- DEFRA. 2007. UK purchases and expenditure on food and drink and derived energy and nutrient intakes in 2005-06, 18 January 2007. London: Defra
- Dixon, W. 2010. The Impacts of Construction and the Built Environment. *WILLMOTT DIXON, Perry Bar*.
- DOE. 2013. National Waste Reporting 2013 - Construction and Demolition (C&D) Waste Profile. Canberra ACT: Australian Government.
- Ekanayake, LL and Ofori, G. 2000. Construction material waste source evaluation. In: *Proceedings of the Second Southern African Conference on Sustainable Development in the Built Environment: Strategies for a Sustainable Built Environment*, Pretoria, 23–25 August.
- EPD. 1999. Environmental Protection Department, *Environment Hong Kong annual report, Hong Kong Government*.
- Formoso, CT; Soibelman, L, De Cesare, C, & Isatto, EL. 2002. Material waste in building industry: main causes and prevention. *Journal of construction engineering and management*, 128(4), 316-325.
- Govt.UK 2016. *Waste and environmental impact*. [Online] Available at <https://www.gov.uk/how-to-classify-different-types-of-waste/construction-and-demolition-waste> [Accessed 27 July, 2016].
- Graham, P. and Smithers, G. 1996. Construction waste minimization for Australian residential development, *Asia Pacific Building and Construction Management Journal* 2(1), 14-19.
- Li Hao, J; Hill, MJ & Yin Shen, L. 2008. Managing construction waste on-site through system dynamics modelling: the case of Hong Kong. *Engineering, Construction and Architectural Management*, 15(2), 103-113.
- Johnston, H & Mincks, WR. 1995. Cost-effective waste minimization for construction managers. *Cost Engineering*, 37(1).
- Kartam, N; Al-Mutairi, N; Al-Ghusain, I, & Al-Humoud, J. 2004. Environmental management of construction and demolition waste in Kuwait. *Waste management*, 24(10), 1049-1059.
- Kourmpanis, B; Papadopoulos, A; Moustakas, K; Stylianou, M; Haralambous, K. J., & Loizidou, M. 2008. Preliminary study for the management of construction and demolition waste. *Waste Management & Research*, 26(3), 267-275.

- Kulatunga, U; Amaratunga, D; Haigh, R & Rameezdeen, R. 2006. Attitudes and perceptions of construction workforce on construction waste in Sri Lanka. *Management of Environmental Quality: An International Journal*, 17(1), 57-72.
- Kumar, R., & Kaushik, S. C. 2005. Performance evaluation of green roof and shading for thermal protection of buildings. *Building and Environment*, 40(11), 1505-1511.
- Leadership in Energy and Environmental Design (LEED). 2004. Construction Waste Management for LEED 2.1 in Seattle. [Online] Available at <http://www.resourceventure.org> [Accessed 24th July 2016].
- Lu, W & Yuan, H. 2011. A framework for understanding waste management studies in construction. *Waste Management*, 31(6), 1252-1260.
- Manowong, E. 2012. Investigating factors influencing construction waste management efforts in developing countries: an experience from Thailand. *Waste Management & Research*, 30(1), 56-71.
- Patel, S and Patel CG. 2016. "Cost Optimization of The Project by Construction Waste Management." *International Research Journal of Engineering and Technology (IRJET)*, 05 (03), 734-740.
- Skoyles, ER & Skoyles, JR. 1987. *Waste prevention on site*. BT Batsford Limited.
- Tam, VW; Tam, CM; Zeng, SX & Ng, WC. 2007. Towards adoption of prefabrication in construction. *Building and environment*, 42(10), 3642-3654.
- The American Institute of Architects (AIA). 2008. Construction Waste Management Strategies: Best Practices", AIAP072739- BP 10.05.36. [Online] Available at <http://www.aia.org/aiaucmp/groups/secure/documents/pdf/aiap072739.pdf>. [Accessed 24 July, 2016].
- Treloar, GJ; Gupta, H; Love, PE & Nguyen, B. 2003. An analysis of factors influencing waste minimisation and use of recycled materials for the construction of residential buildings. *Management of Environmental Quality: An International Journal*, 14(1), 134-145.
- Wang, J; Yuan, H; Kang, X & Lu, W. 2010. Critical success factors for on-site sorting of construction waste: a China study. *Resources, Conservation and Recycling*, 54(11), 931-936.
- Yuan, H. 2013. A SWOT analysis of successful construction waste management. *Journal of Cleaner Production*, 39, 1-8.
- Zahur, M. 2007. Solid waste Management of Dhaka City: Public Private Community Partnership, *BRAC University Journal*, IV (2), pp. 93-97.

# **THIN WALL REINFORCED CONCRETE AS LOW COST SUSTAINABLE ALTERNATIVE FOR SINGLE FAMILY HOUSES IN PAKISTAN**

M. A. Saleem\* & U. Ahmed

*Department of Civil Engineering, University of Engineering and Technology, Lahore, Pakistan  
\*Corresponding Author: msale005@fiiu.edu*

## **ABSTRACT**

As per the statistics of the Pakistan Government, approximately 1/4<sup>th</sup> of the country's population is living in single room house. Natural calamities like floods and earthquakes also leave thousands homeless. There is an urgent need of research to devise low cost construction techniques and develop cheap materials in order to make available inexpensive housing to common people. The main purpose of this study was to explore potential of ferrocement panels for quick construction in order to achieve economical housing in the country. To fulfil the said objective, eighteen ferrocement panels reinforced with galvanized iron mesh were tested in compression and flexure. Cost comparison of ferrocement panels with traditional brick construction was also carried out for a small unit of 65 m<sup>2</sup> (three marla) area. The results of testing demonstrate that ferrocement panels are capable to take care the expected loading in a single story house. Their high ductility and energy absorption make them favourable for the areas which are prone to seismic activity. The material cost of ferrocement panel construction is close to the conventional brick and mortar construction, however, a ferrocement panel house can be ready for living in almost 1/4<sup>th</sup> of the time as compared to its brick counterpart.

Keywords: Low cost housing; thin wall concrete; ferrocement

## **INTRODUCTION**

Cost of constructing new houses is increasing rapidly throughout the world, therefore, building new houses has become very challenging for low income families. In the wake of rapidly growing population, need of affordable housing has become a much discussed and researched topic. Owning a dwelling is not an affordable proposition for a major section of the society (Sumadi and Ramli 2008). According to the data of Pakistan Government (2011) almost 1/4<sup>th</sup> of the total population in Pakistan is living in a single room housing unit. Natural disasters make the situation even worse and leave hundreds of thousands of people homeless and for these displaced people the principal need is to have a safe place to live.

Economical housing is a comparative term, which does not mean achieving low cost through reduction in quality (Tam 2011) or compromise on function. Instead, low cost is achieved through alternative construction techniques, light-weight materials, better resource management of resources etc. According to Miles (2003), housing is considered low cost if it can be acquired for up to 30% of the house hold income.

Cost of housing can be achieved either by using locally available low cost materials or by reducing time of construction through accelerated/innovative construction techniques. Pre-engineered steel structure is one such option, however this is more common for industrial buildings. Using steel prefabrication for housing may not be appropriate due to high initial cost and low serviceability attributes. On similar lines, some kind of cementitious material may be a better choice to carry out prefabricated house construction. Ferrocement is a material which has great potential to be used in cheap housing. Thin wall ferrocement panels can be easily manufactured in plants using common materials in a very short time and be assembled quickly in to a housing unit. Ferrocement is a thin wall concrete reinforced with layers of wire mesh, which are embedded in cement sand mortar (ACI 549R-97). In comparison to conventional concrete, the tensile strength to self-weight ratio of ferrocement is greater and it also has

improved cracking behaviour. These are the reasons which make ferrocement a favourable material for water-tight and light-weight structures. Ferrocement is a very suitable alternative material for the construction of prefabricated houses. Non structural application of ferrocement like plant pots, chairs, tables and boats are being constructed since 1884 (Aboul-Anen et al. 2009).

The ductile behaviour of ferrocement is attributed to close distribution of reinforcement in the form of mesh. Ferrocement has great potential to become an economical choice for the construction of temporary as well as permanent structures (Saleem and Ashraf 2008). Use of ferrocement as a roofing material in less privileged communities has been previously reported by Ibrahim in 2011. Ferrocement has potential to be used to construct almost all kinds of structures which can be constructed using traditional materials and this is one of its major advantages. Although there are some limitation of ferrocement, however, within the limitation it be considered as one of the most suitable composite construction materials.

One of the primary reasons of selecting ferrocement for this project is that all its ingredients are coming available in Pakistan at a very reasonable price. The ferrocement panels are easy to manufacture, light weight, easy to transport and assemble which make them a very suitable choice for low cost prefabricated houses. The concept of assembling ferrocement housing unit has been previously proposed as a do-it-yourself concept by Saleem and Ashraf (2008).

The main purpose of the current research was to explore the viability of ferrocement panels as a substitute material for the construction of cheap housing units. An effort was made to reach an economical and structurally suitable design of section of the panel in terms of dimension and number of layers of wire mesh. A minor objective was to carry out comparison of cost between the traditional brick and mortar construction and the ferrocement construction.

## EXPERIMENTAL WORK

Table 1 provides the test matrix which was developed to achieve the desired objectives of the research. A total of nineteen ferrocement panels were tested including one trial specimen. Size of each panel was 450mm x 1500mm. Number of galvanized iron (GI) mesh layers in each panel and the thickness of panels were varied, as presented in Table 1. Every panel had its own ID number which had information about the No. of mesh layers, thickness of panel and mode testing; flexure or compression. For instance, 30-2-F1 means that the panel is 30 mm thick with 2 mesh layers, it will be tested in flexure and it specimen 1 of such nature. For the specimen tested in axial, 'F' was replaced with 'A'. Two specimens with each unique specification were tested.

Mortar for the ferrocement panels was prepared using ordinary portland cement which was acquired afresh for every batch of casting. Also, for consistency, cement from same source was used for the entire stock of specimens.

Fine aggregates were used as per the recommendation of ACI 549 which recommends using sand which passes through sieve #8 (2.36 mm). Use of only small size aggregate is necessary because of thin section of panels and small opening size of mesh reinforcement. Sand from lawrancepur was used, which is considered one the best in Pakistan. Cement/sand ratio was kept as 1:2. This rich mix results in a dense matrix which in turns provides good compressive strength. The water to cement ratio varied between 0.4 and 0.43. Ferrocement can be prepared by using several types of reinforcement including chicken wire mesh, one dimensional fiber mats and discrete fibers etc. For this project, galvanized iron chicken mesh having square openings was selected, since it is locally available in abundance at a very cheap price. The opening size of the square mesh was 12.5 mm with a 1.4 mm diameter of wire. The

Table 1 Test Matrix

No.	Panel ID	Reinforcement	
		Mesh Layers	Volume Fraction
1	30-2-F1	2	1.67
2	30-2-F2	2	1.67
3	30-3-F1	3	2.51
4	30-3-F2	3	2.51
5	40-3-F1	3	1.88
6	40-3-F2	3	1.88
7	40-4-F1	4	2.51
8	40-4-F2	4	2.51
9	50-4-F1	4	2.01
10	50-4-F2	4	2.01
11	50-5-F1	5	2.51
12	50-5-F2	5	2.51
13	30-2-A1	2	1.67
14	30-2-A2	2	1.67
15	40-3-A1	3	1.88
16	40-3-A2	3	1.88
17	50-4-A1	4	2.01
18	50-4-A2	4	2.01

volume fraction of reinforcement was varied by using different number of mesh layers from two to five. The ACI 549 allows using skeletal steel which keeps the wire mesh at correct spacing and position during the casting. Therefore, 6 mm diameter steel rebars were used as skeletal steel, which is the highest size allowed by ACI 549.

In order to achieve smooth finish, plywood was used in the formwork to cast the specimens. Three separate formworks were prepared for casting 30, 40, and 50 mm thick panels. Fresh mortar was prepared for casting each specimen. A pan type mixer was used to prepare the mortar. First of all dry mixing of the materials was carried out for 2 to 3 minutes and then water was added while the mixer was running. Wet mixing took another three minutes which ensured a uniform mix. The formwork was put on the flat table vibrator and the first, layer of mortar was placed, which would serve as clear cover for the wire mesh. It was then vibrated. On this first mortar layer, the wire mesh was positioned along with the skeletal steel on top of it. Then next mortar layer was then poured, which was followed by the next layer of wire mesh. In this manner, the specimens with the desired number of mesh layers were prepared. The final layer of mortar was placed on the top and was levelled with the help of a float to achieve a smooth finish. The panels were then transported to the curing room. After 48 hours of casting, the formwork was disassembled and the curing was carried out for four weeks with the soaked jute cloth.

Specimens tested in flexure were applied with two-point loading as presented in Figure 1. The spacing between the loads, and between loads and supports was kept as  $1/3^{\text{rd}}$  of the center-to-center span of the panel, which turns out to be 450 mm. A 75 mm clear distance was provided from the edge of the panel to the center of the support. A high speed data acquisition system was used to record the load and mid-span deflection at a sampling rate of 1 *hz*. Test was carried out by applying displacement at the rate of 0.5 mm per min. A pair of all the unique specimens was also tested in compression (see Fig. 2). For the axial case, a displacement transducer was positioned at the middle height to acquire the horizontal deflection. Compression test was run displacement control having the displacement rate of 0.5mm per min.



Fig. 1 Test Setup for Flexural Test



Fig. 2 Test Setup for Compression Test

As a criterion for acceptance, the expected bending moment and compressive load was calculated for a 5 m x 5m single story unit. The bending moment was based on the wind forces produced due to a wind velocity of 160 km per hr. The factored moment comes out to be 0.1 kN-m. The compressive load due to roof and snow comes out to be 121 kN for the most heavily loaded wall.

## DISCUSSION ON RESULTS

### *Strength of Mortar in Compression*

To determine the strength in compression, 100 mm dia. and 200 mm high cylinders were prepared from every batch. These cylinders were tested on 7<sup>th</sup>, 14<sup>th</sup>, and 28<sup>th</sup> day. Table 2 provides the summary of 28

days compressive strength of these cylinders. The maximum and minimum cylinder strength attained was 49.7 and 33.1 MPa, respectively. The average compressive strength of all eighteen batched was 41.6 MPa having a standard deviation of 5.0.

### **Flexural Tests**

The Fig. 3 present the load-deflection response for the all the specimens. The specimens 50-5-F1 and 50-5-F2 achieved the ultimate loads of 8.17 and 5.9 kN, and max. deflection of 30.7 and 30.8 mm, respectively. The specimens 50-4-F1 and 50-4-F2 exhibited very similar responses in terms of ultimate loads, maximum deflection and stiffness. The ultimate load for both the specimens was nearly 16.5 kN. The failure mode of 50-5 F1,2 specimens was however more ductile than the specimens 50-4-F1,2.

The 40 mm thick specimens exhibited consistent trend of increase in ultimate loads with the increase of GI wire mesh. The specimens 40-4-F1 and 40-4-F2 attained the ultimate loads of 7.85 and 12.84 kN, and max. displacement of 38.6 & 42.2 mm, respectively. The specimens 40-3-F1 and 40-3-F2 reached max. displacement of 36.9 mm & 16.6 mm, respectively.

The wall panel with 30 mm thickness gained higher deflections in comparison with 40mm & 50mm thick specimens. However, their failure loads were smaller. The maximum deflection achieved by specimen 30-3-F1 was around 81 mm. For a constant volume fraction the ultimate load increases as the thickness of panel increases. The max. deflection, however, goes up with the reduction in the panel thickness.

Table 2 Compressive Strength at 28 Days

S. No.	Panel ID	28 Days Compressive Strength (Mpa)
1	50-5-F1	42.6
2	50-5-F2	44.7
3	50-4-F1	40.9
4	50-4-F2	37.1
5	40-4-F1	47.1
6	40-4-F2	39.1
7	40-3-F1	35.1
8	40-3-F2	47.2
9	30-3-F1	44.1
10	30-3-F2	43.1
11	30-2-F1	33.1
12	30-2-F2	48.1
13	50-4-A1	38.3
14	50-4-A2	42.1
15	40-3-A1	38.1
16	40-3-A2	49.7
17	30-2-A1	33.1
18	30-2-A2	43.1

The flexural cracks in all the specimens initially appeared in the mid-span region and then propagated towards the top with the increase in the crack width. As the applied load increased, more cracks started appearing in the region of constant bending moment. The appearance of cracks continued till the specimen failed. A typical pattern of the flexural cracks is shown in Figure 4.

### **Compression Tests**

Figure 5 presents the load displacement responses for the compression tests. The slenderness ratio of the panels with 30, 40 and 50 mm thickness was 173, 130 and 104, respectively. The ultimate capacity and the vertical displacement at collapse increased as the panel thickness increased. The ultimate loads for specimens 30-2-A2, 40-3-A2, and 50-4-A1 were 284, 494 and 666 kN, respectively. The specimens with 30 mm thickness finally buckled at failure, while the panels with 40 and 50 mm thickness exhibited compression failure close to the support area.

### **First Crack and Ultimate Load**

An increasing trend was observed in the magnitude of first crack load with the increase in the number of mesh layers and thickness of the panel. A comparison of first crack loads of twelve flexural specimens is presented in Figure 6. The ultimate load also followed a trend similar to the first crack load except the 50-5-F1,2 specimens. In the compression tests, ultimate loads increased with the increase in the panel thickness and number of mesh layers.

### Energy absorption

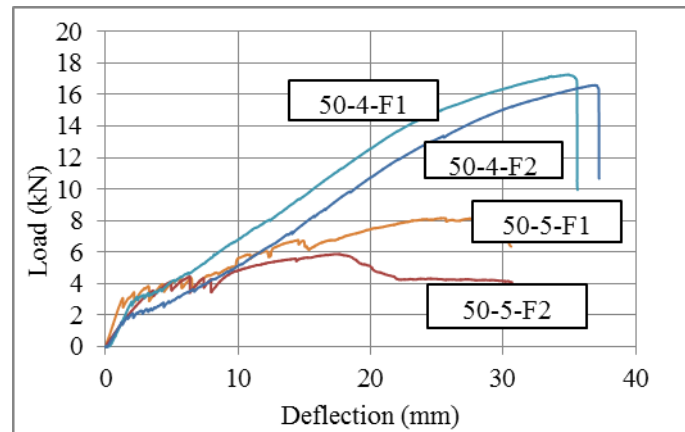
The area under the load deflection responses was calculated and reported as energy absorbed by the specimens. The specimens with 30 and 40 mm thickness exhibited increasing trend of energy absorption with the increase in numbers of mesh layers, however the 50 mm specimens showed in consistent behaviour (see Figure 7)

### COST ANALYSIS

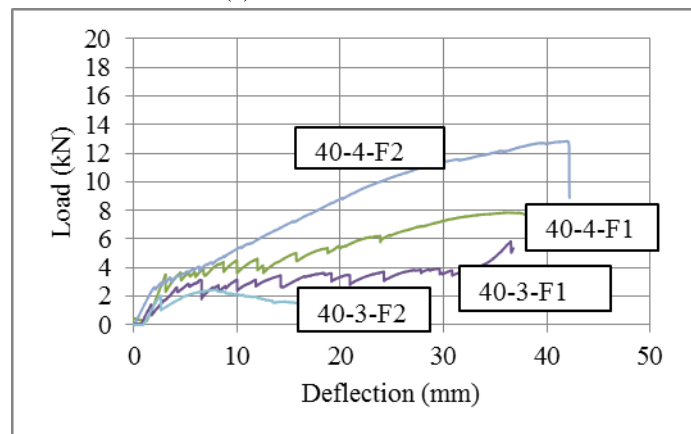
Material cost and labour cost are two main contributors towards the final cost of the housing unit. If a 50 mm thick wall panels with 5 layers of GI wire mesh are used to construct a house, its material cost is almost same as the conventional brick and mortar house. This comparison was carried out for a single family, single storey house having an area of 65 m<sup>2</sup> (3 Marlas). Table 3 provides a comparison of man hours break-up for the two types of construction. It is evident from this comparison that a prefabricated ferrocement house can be constructed in almost 1/4<sup>th</sup> of the time as compared to the traditional brick and mortar house. The reduction in the man hours requirement is the major contributor towards cost saving.

### SUMMARY AND CONCLUSION

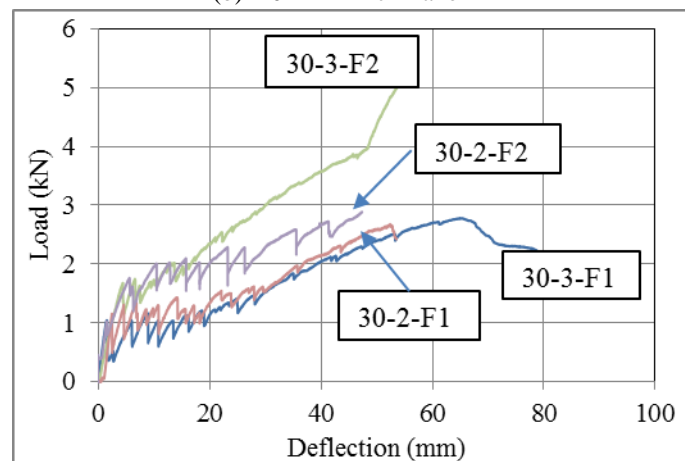
The ferrocement wall panels proved to have sufficient strength to take care of the loading expected in a single family house. For a single story house the most heavily loaded wall of a 5m x 5m room has to bear an ultimate compressive load of 121 kN, which is just 42% of the minimum compressive collapse load of 284 kN, achieved by 30 mm thick panel. The highest compressive load among all panels was 666 kN, achieved by the 50 mm thick panel. For the wind velocity of 160 km/hr. the flexural demand for the panel comes out to be 0.1 kN-m which is much lower than the lowest achieved moment capacity of 0.6 kN-m for the 30 mm thick panel. The absolute maximum moment capacity was attained by 50 mm thick panel which amounts 3.88 kN-m. The entire stock of panels fulfils the moment requirement, however it is suggested to use at least 40 mm thick panel because the 30 mm thick panels fail in buckling unlike the 40 and 50 mm thick panels which fail in compression.



(a) 50 mm Thick Panel



(b) 40 mm Thick Panel



(c) 30 mm Thick Panel

Fig. 3 Load Deflection Responses for Flexural Tests



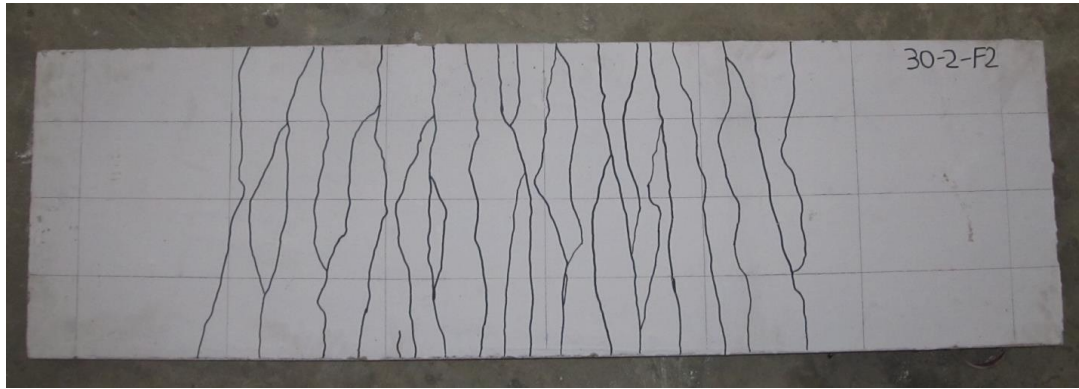


Fig. 4 Flexural Cracks in Specimen 30-2-F2

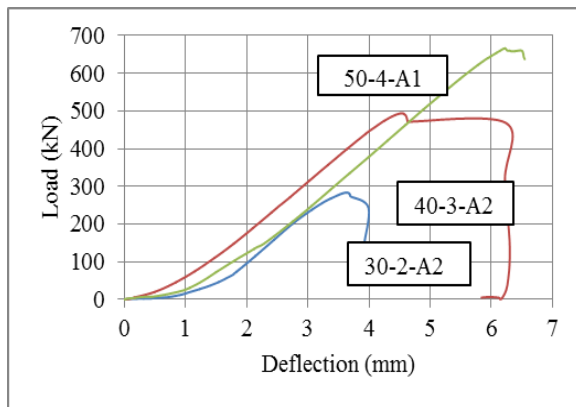


Fig. 5: Load Deflection Responses for Axial Load Tests

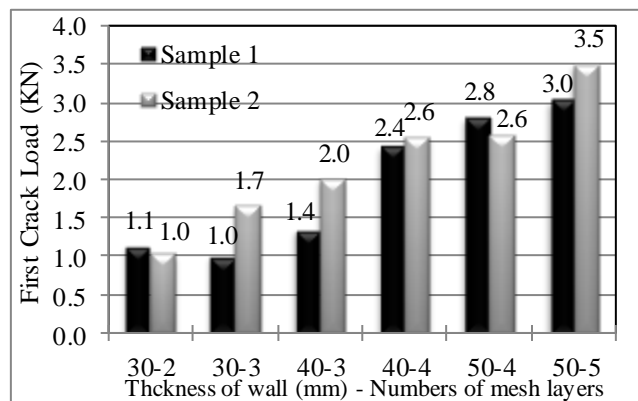


Fig. 6: First Crack Comparison for Flexural Test

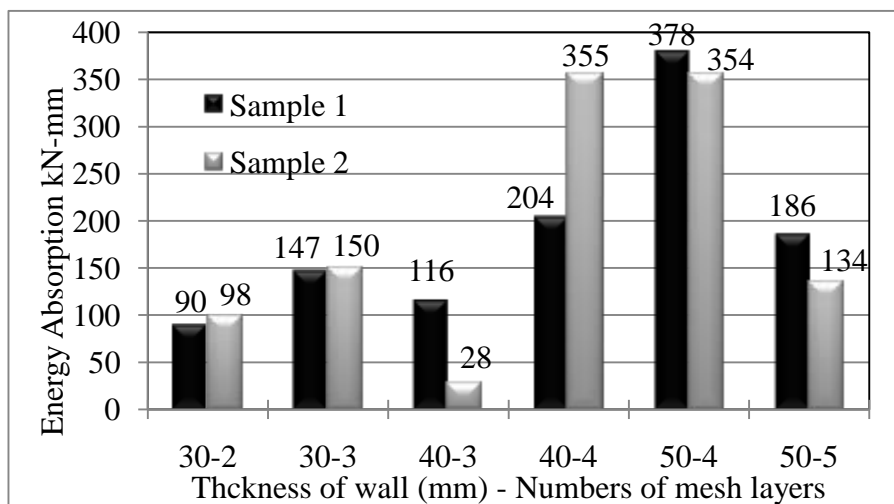


Fig. 7: Energy Absorption for the Flexural Tests

The material cost of 50 mm thick wall panel is similar to 230 mm thick wall made of traditional burnt clay bricks. The real saving in cost comes from the man hours. Only 1/4<sup>th</sup> time is required to assemble a ferrocement cement house as compared to the brick and mortar house.

Ferrocement panels have shown great promise to be used in house construction, however, work is still needed to evaluate their performance under impact loading and punching shear. Reinforcement meshes

made of other non-corrosive materials like polypropylene may be used to develop corrosion free panels, which will be suitable for areas with high humidity. A scaled room made of ferrocement panels may be tested on shake table to prove their effectiveness in the earthquake prone areas.

Table 3 Breakup of Man Hours

No.	Activity	Brick Construction		Ferrocement Construction	
		Days	Man Hours	Days	Man Hours
1	Excavation/Back Filling	3	96	3	96
2	Strip Foundation	5	120	-	-
3	Block Foundation	-	-	1	24
4	Damp Proffing	1	24	-	-
5	Joint Sealing	-	-	1	16
6	Brick Wall	10	400	-	-
7	Ferrocement Panels Erection	-	-	2	48
8	Roof Shuttering	3	120	-	-
9	Concreting	1	80	-	-
10	Curing of Roof slab	14	-	-	-
11	Formwork removal	2	48	-	-
12	Wooden Truss Installation	-	-	1	24
13	Roof Sheeting Installation	-	-	1	24
	<b>Total</b>	<b>39</b>	<b>888</b>	<b>9</b>	<b>232</b>

## REFERENCES

- Aboul-Anen, B; El-shafey, A. & El-Shami, M. 2009. Experimental and analytical model of ferrocement slabs. *International Journal of Recent Trends in Engineering* 1(6): 25-29.
- ACI 549R-97. 1997. State-of-the-Art report on ferrocement. American Concrete Institute. Farmington Hills, MI.
- Government of Pakistan, 2011. *Pakistan social and living standards measurement survey*. Government of Pakistan Statistics Division Federal Bureau of Statistics. Islamabad.
- Ibrahim, H. M. 2011. Shear Capacity of Ferrocement plates in Flexure. *Engineering Structures*. 33(5): 1680-1686.
- Miles, ME. 2013. Real estate development, principles and processes. 4th ed. Urban Land Institute. Washington D.C.
- Saleem, MA & Ashraf, M. 2008. Low Cost Earthquake Resistant Ferrocement Small House. *Pakistan Journal of Engineering and Applied Sciences*. 2(1): 59-64.
- Sumadi, SR & Ramli, M. 2008. Development of lightweight ferrocement sandwich panels for modular housing and industrialized building system. Universiti Teknologi Malasia.
- Tam, VW. 2011. Cost Effectiveness of using low cost housing technologies in construction. *Procedia Engineering*. 14(2011): 156-160.

## **PARAMETRIC STUDY ON LIVE-LOAD DISTRIBUTION IN LATERAL DIRECTION OF A SKEW COMPOSITE BRIDGE**

M. Hossain\* & M. B. Zisan

*Department of Civil Engineering, Chittagong University of Engineering and Technology, Chittagong, Bangladesh*

*\*Corresponding Author: mhossain.cuet@gmail.com*

### **ABSTRACT**

Determination of Live-load distribution factors is an important step in the analysis of bridge structure. This paper describes a numerical study on live load distribution factor of a three dimensional (3-D) finite element model of a skew composite bridge which was developed by using commercial software ANSYS. The finite element model was developed from an existing work and then accuracy of the model was verified by comparing the numerical results to the existing experimental results. The bridge models investigated the effects of skew angle and different vehicle position on the live-load distribution factors for shear and moment. To evaluate the skew effect, the skew angle of the bridges was varied from 0° to 60°. Load distribution factors (LDFs) from finite element were compared with those calculated according to the American Association of State Highway and Transportation Officials (AASHTO) specifications. It is found that AASHTO's standard specification "S-over" equation is simple to use but this equation may underestimate the distribution factor for some bridges and overestimate for others. Though AASHTO LRFD formula considered more parameters such as skew correction continuity but it is complex to use.

Keywords: Load distribution factor; vehicle position; skew bridge; numerical study; ANSYS

### **INTRODUCTION**

Nowadays skew bridges are very commonly used all over the world. The skew bridges are built to cross railways, waterways, roadways that are not perpendicular to the bridge at the intersection. The skew bridges can be defined as the bridge where the center line of the bridge is not perpendicular to the center line of the abutment and pier. Proper live-load distribution factor is important for bridge design. The American Association of State Highway and Transportation Officials (AASHTO) Standard Specifications for Highway Bridges did not account for the effect of skew. The distribution of load in a skew bridge is different than a normal straight bridge because of skewness. Usually the load transfer in short direction more than the long direction. The load distribution factors in lateral direction for live load moment and shear is determined using the AASHTO *Load and Resistance Design Specifications* (AASHTO LRFD). The specification additionally require the application of skew correction factors (SCFs) to beams when the line of bridge support is skewed.

#### ***Live-Load Distribution Factors***

Live load distribution is the proportion of the vehicular load carried by each girder. The AASHTO Standard Specifications for Highway Bridges have given live load distribution factors since 1931. The earlier approaches were based on the work done by Westergaard (1930) and Newmark (1938), but the factors were modified as new research results became available. To calculate the distribution factor, American Association of State Highway and Transportation Officials (AASHTO 2002) standard gave a simple "S-Over" equation. This "S-Over" equation is developed for straight bridges and the effect of skew angle and continuity are not considered in this code. Several investigation have been carried out to find the effect of skew angle on the live load distribution factor. Some researchers suggest new equations of live load distribution factor for moment and shear. In addition, AASHTO load and resistance factor design (AASHTO 2008) takes into account more bridge parameters such as girder spacing, girder stiffness, span length, continuity and the skew effect than the AASHTO standard

(AASHTO 2002). AASHTO LRFD presented skew correction factor for shear and moment distribution factor for skew bridge, however, the accuracy of those is still questionable (Huo et al., 2003; Zhang, 2008). According to Zokaie et al. (2000) study the LRFD code distribution factors lie within 5% of the distribution factors calculated with detailed finite-element models. The main objectives of this study are: (1) Development and verification of Finite Element Model of the skew bridge; (2) Disparity between the live-load distribution factor obtained from the finite element analysis to the present practiced code; (3) To figure out the effect of skew angle and vehicle position on live-load distribution factor; (4) Behavior of typical skew bridges; (5) To develop better design guidelines for bridge designers.

## FINITE ELEMENT MODELING

### *Model Description*

The finite element model developed for this study is taken from an existing work done by J. Meng et al. (2004) at the Federal Highway Administration Turner-Fairbank Highway Research Center. Here, approximately 1/6 reduced scale model was used for the finite element analysis. A two-span continuous bridge with a span length and deck width of 12 ft. and 7 ft., respectively was designed. The actual bridge would have a span of 72 ft. and width of 42 ft. The skew angle was selected based on practical skew angles used for real skew bridges. For most skew highway bridges, the skew angles fall in the range of 30°~60°. The existing model has a skew angle 36.87°.

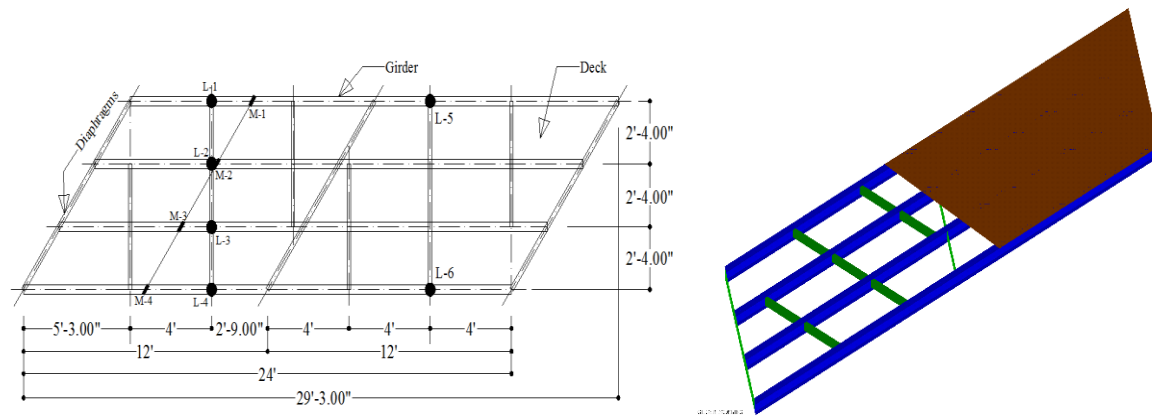
The girders and diaphragms were model using SHELL63 element. The girders were connected using diaphragms. Diaphragms are generally used to (1) transfer lateral wind loads to the deck and then to the bearings, (2) provide stability to the stringer or girder flanges during erection and placement of the deck, and (3) distribute laterally the vertical dead and live load from one stringer to other adjacent.

Bridge decks are used to carry the traffic load and to transfer the loading to the supporting girders and piers. Although most bridge decks are made of reinforced concrete, a 3/8 in. steel plate was used as the deck. Based on the theory of transformed section, this steel deck roughly simulated a 9 in. thick reinforced concrete Deck. Here the deck was modeled by using the SHELL63 element.

To simulate actual bridge bearings, pinned supports were provided at one end of the two span bridge and roller supports were provided to middle and other end of the bridge. The pin supports are designed to allow only the rotational movement about the pin and roller supports were designed to allow rotational movement plus translations along the length of the bridge.

Table 1 Basic geometric property of the bridge model

Span length	12 ft.
Width	7 ft.
Girder spacing	2 ft. 4 in.
Girder depth	6 in.
Web thickness	0.23 in.
Flange width	4 in.
Flange thickness	0.28 in.
Diaphragm cross-section	6 in. x 0.234 in.
Deck thickness	3/8 in.



(a) Plan View (J. Meng *et al.*, 2004)

(b) Finite element model (ANSYS)

Fig. 1: Bridge model

**Model Verification by Incremental loading test**

As a precursor to Live Load distribution factor calculation, two numerical incremental loading test was performed to verify the finite element model. For each numerical test, the load was applied in four increments of 200 lbs. each to a maximum of 800 lbs. The loading procedure is depicted in Table 2.

In the table 2, M1, M2, M3 and M4 refer to the load applied point in Fig. 1(a). Thus, for numerical test 1, load was applied to the model at only one location. However, for numerical test 2, loads were applied to two location. For each numerical test, displacement measurements were recorded at six location named L1, L2, L3, L4, L5 and L6 in Fig. 1 (a).

The value of the six displacement records from numerical analysis, experimental results (J. Meng *et al.*, 2004) are shown in Fig. 2. The results obtained from finite element analysis are very similar to the experimental results which verified the model accuracy. Due to errors in measurements, instrumentation, uncertainty in support conditions, material properties and load placement, as well as approximations and assumptions used in any experimental test, it is difficult for the experimental and numerical values to compare to a high degree of accuracy.

Table 2 Loading procedure (units: lbs., 1 lb. = 4.45 N)

		M1	M2	M3	M4
Numerical test 1	Step 1	-200	-	-	-
	Step 2	-400	-	-	-
	Step 3	-600	-	-	-
	Step 4	-800	-	-	-
Numerical test 2	Step 1	-	-200	-200	-
	Step 2	-	-400	-400	-
	Step 3	-	-600	-600	-
	Step 4	-	-800	-800	-

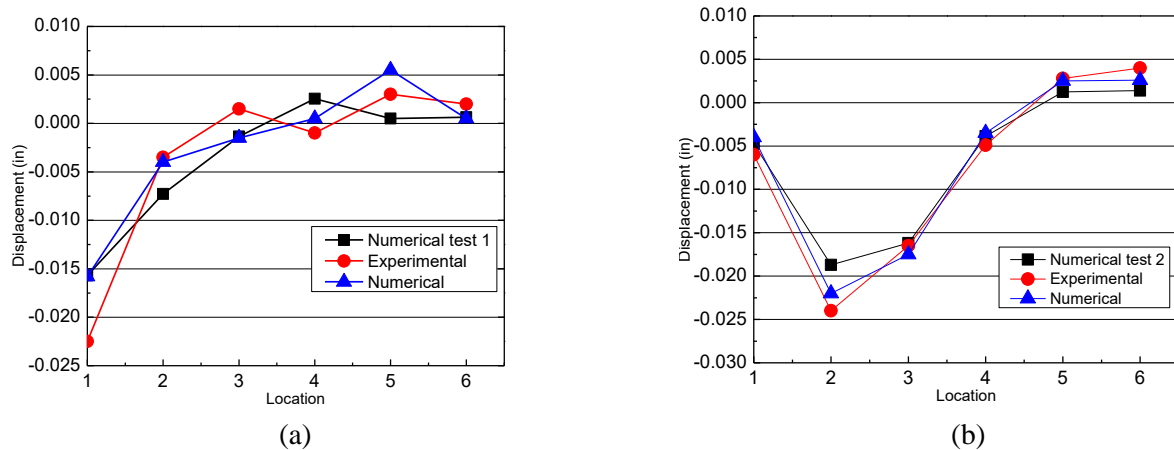


Fig. 2. Displacement comparison. (a) Numerical test 1; (b) Numerical test 2;

## LIVE-LOAD DISTRIBUTION FACTOR

### Shear Distribution Factor

Skew angle has significant effect on live load distribution factor. The ratio of distribution factor at any skew angle to the distribution factor at zero skew shows the effect of skew (Barr et al., 2001). For a bridge with skew, the shear at the obtuse corner has been found to be higher than that at the acute corner. As a result, the presence of skew can significantly increase the exterior girder shear and reduce the interior girder shear.

In Fig. 3, there are four location was selected to apply vehicle load on the bridge named as P1, P2, P3 and P4. The girders are designated by G1, G2, G3 and G4. Here, when load applied at location P1 and measured distribution factor in girder G1 (Exterior) than it is denoted by G1 P1 and similarly others. Since this research is carried using a scaled bridge model, to similitude with bridge model a scaled vehicle (HS20-44 truck) load were used.

The effect of skew was investigated by performing a finite element analysis with skew angle varies from  $0^\circ$  to  $60^\circ$  and at different position of the vehicle load. The FE results for different skew angle under the single-lane loading on exterior and interior girder shown in Fig. 4. The live-load distribution factor by AASHTO standard specification (S-over equation) is very much conservative for both exterior and interior girder shown in Fig. 4(a). In finite element analysis, curve G1P1 and G1P3 shows that the distribution factor of the loaded girder is decreased with the increase of skew angle up to  $45^\circ$  and then for  $60^\circ$ , the distribution factor increased slightly when the load was applied at acute corner. In contrast, curve G4P2 and G4P4 shows that the distribution factor increased with the increase

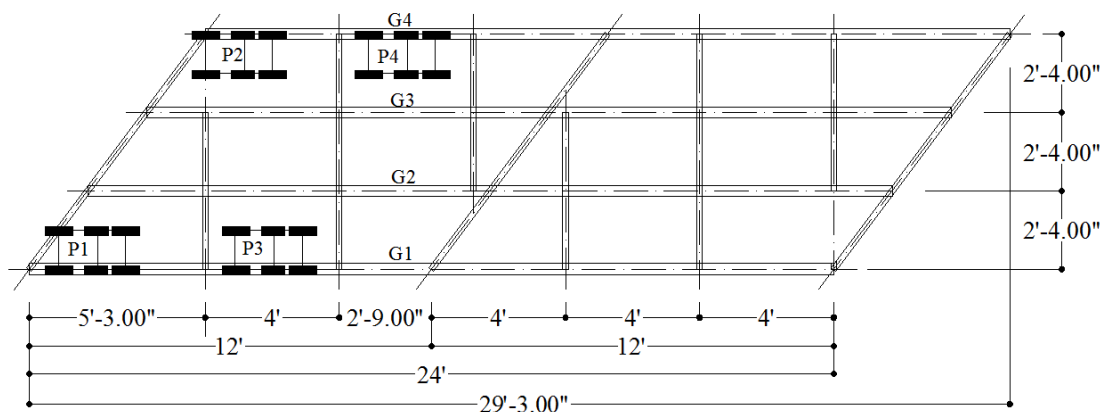


Fig. 3: Vehicle location and girder numbering

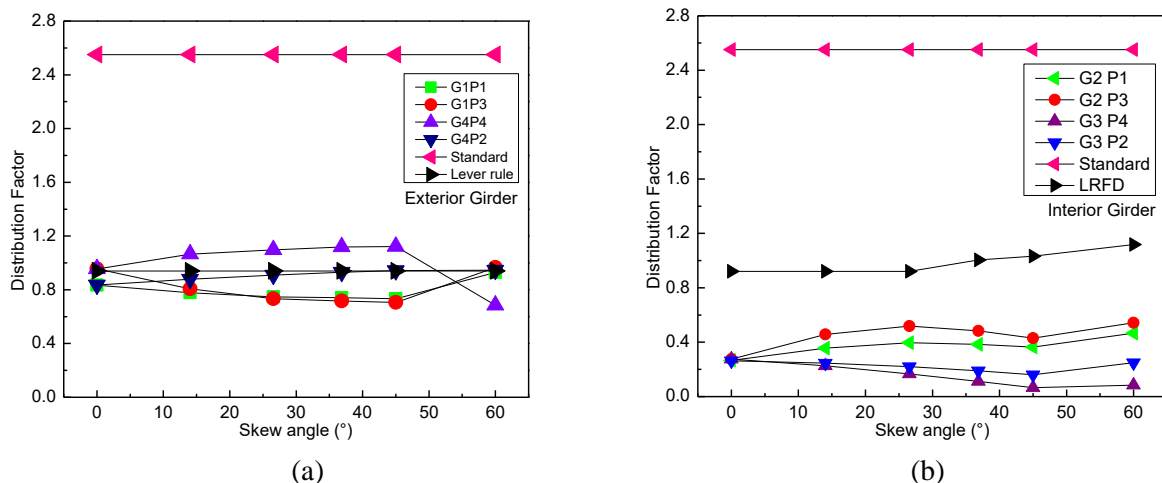


Fig.4: Comparison of LLDFs for shear with code

of skew angle up to  $45^{\circ}$  and then for  $60^{\circ}$ , the distribution factor decreased slightly when the load was applied at obtuse corner. Here the distribution factor by lever rule method for exterior (loaded) girder is slightly unconservative for load applied at obtuse corner and conservative for acute corner.

For interior girder both AASHTO standard and LRFD gave conservative distribution factor. In Fig. 4 (b) curve G3P4 and G3P2 shows that for the interior girder there was nearly a linear decrease in the distribution factor for skew angles up to  $45^{\circ}$  and then above  $45^{\circ}$ , the distribution factor increased slightly when load applied at obtuse corner. Curve G2P1 and G2P3 shows a slight up and down in distribution factor when load applied at acute corner.

### Moment Distribution Factor

Fig. 5(a) shows a variation of moment distribution factor in exterior girder with increasing skew angle. Also it shows the difference in between the codes to finite element distribution factor. AASHTO specification gave highly conservative moment distribution factor for both exterior and interior girder. Curve G1P3 and G4P4 shows a gradual increase in distribution factor for exterior girder. Due to the skew angle, the moment at the acute corner has been found to be higher than that at the obtuse corner. Here, curve G2P3 and G3P4 shows a slight decrease with increase in distribution factor.

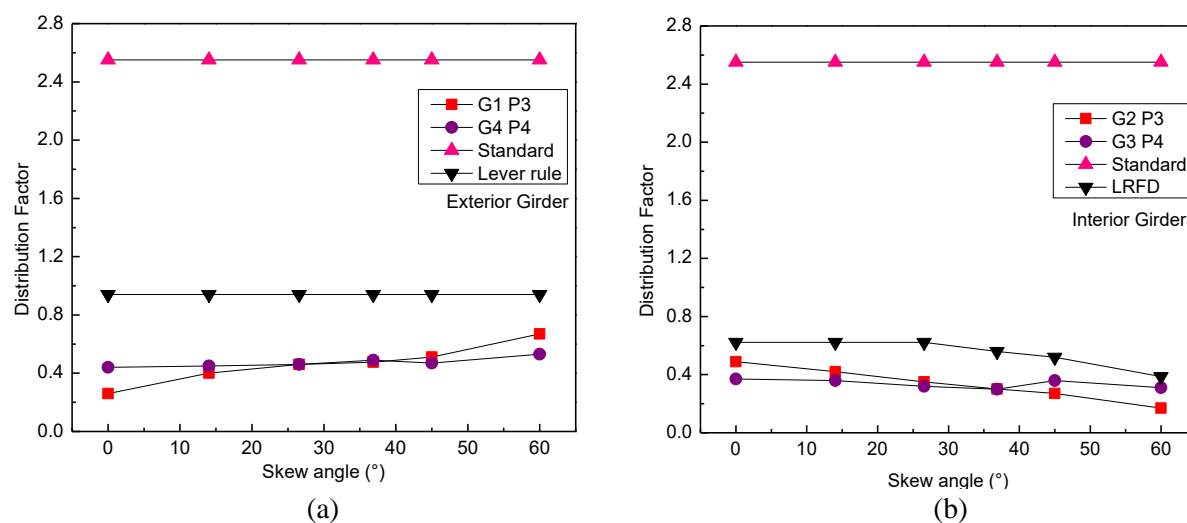


Fig. 5: Comparison of LLDFs for moment with code

## CONCLUSIONS

Based on this FE study and result, the following conclusion are made: (1) the shear distribution factor for exterior girder increasing and decreasing depending upon the position of vehicle with increasing skew angle. (2) For interior girder both AASHTO LRFD and standard equation overestimate the shear distribution factor and (3) Also for interior and exterior girder AASHTO gives higher value for moment distribution factor. Here the study shows that the lever rule method can very well predict the shear distribution factor for exterior girder. In the authors' opinion, the lever rule method with skew correction factor can be used to obtain fairly well live-load distribution factor for skew bridge. It is also recommended that more research should be performed to quantify a good distribution factor for skew bridge design.

## REFERENCES

- American Association of State Highway and Transportation Officials (AASHTO). 2002. Bridge design specifications, 14<sup>th</sup> edition, Washington, D.C.
- American Association of State Highway and Transportation Officials (AASHTO). 2008. *LRFD bridge design specifications*, Customary US Units. 5th Edition., Washington, D.C.
- Barker, R.M. and Puchett, J.A. 1997. *Design of highway bridges*. New York, NY: John Wiley & Sons.
- Barr, P. J.; Eberhard, M. O. and Stanton, J. F. 2001. Live-Load Distribution Factors in Prestressed Concrete girder Bridges. *J. Bridge Eng.* 6(5), 298-306
- Eom, J. and Nowak, A. S. 2001. Live load distribution for steel girder bridges. *J. Bridge Eng.*, 6(6): 489–497.
- Fu, G.k. and Chun, P.J. 2013. Skewed Highway Bridges. Final Report to “Michigan Department of Transportation”.
- Hughs, E., and Idriss, R., 2006. Live-Load Distribution Factors for Prestressed Concrete, Spread Box-Girder Bridge
- Huo, X., Conner, S. and Iqbal, R., 2003. Re-examination of the Simplified Method (Henry's Method) of Distribution Factors for Live Load Moment and Shear. Final Report, *Tennessee DOT Project No. TNSPR-RES*, 1218.
- Meng, J.Y.; Ghasemi, H. and Lui, E.M. 2004. Analytical and experimental study of a skew bridge model. *Engineering Structures* 26: 1127–1142
- Schuring, D.J. 1977. *Scale models in engineering*. Elmsford, New York, NY: Pergamon Press.
- Skoglund, V.J. 1967. *Similitude theory and applications*. PA: International Textbook Company.
- Szucs, E. 1980. *Similitude and modeling*. New York: Elsevier Scientific Publishing Company.
- Zhang, Q. 2008. Development of skew correction factors for live load shear and reaction distribution in highway bridge design.
- Zokaie, T.; Osterkamp, T. A. and Imbsen, R. A. 1991. Distribution of wheel loads on highway bridges: Final report. *National Cooperative Highway Research Program*.
- Zokaie, T. 2000. AASHTO-LRFD live load distribution specifications. *J. Bridge Eng.*, 5(2): 131–138.



# NUMERICAL STUDIES OF SHAPE EFFECT OF SQUARE AND CIRCULAR FOOTING PLACED ON COHESIVE-FRICTIONAL WEIGHTLESS MEDIUM

M. Rokonzaman\*, M. S. Islam & G. Sarkar

Department of Civil Engineering, Khulna University of Engineering & Technology, Khulna-920300,  
Bangladesh

\*Corresponding Author: rokoncekuet@yahoo.com

## ABSTRACT

In this study, three-dimensional finite element models, incorporating Mohr-Coulomb elasto-plastic material model, are validated for the evaluation of the shape effect of the square and circular surface footing under vertical loading in  $c-\phi$  soil. The numerical models have closely predicted experimental load-settlement relationships. The shape effects on the results are also discussed in relation to the progressive failure around the foundations and the shape of the failure mechanism inside the soil. Having detailed parametric studies, the shape factors of square footing are fitted by a simple exponential function of the soil friction angle and shape factors of circular footing are expressed as a function of shape factor of square footing.

Keywords: Bearing capacity; square footing; circular footing; numerical analysis

## INTRODUCTION

Bearing capacity of soil is one of the most interesting research subjects in geotechnical engineering as this problem has multi-dimensions with respect to the geometry of footing, loading and supporting foundation soil. Extensive studies were conducted for bearing capacity in two dimensions for infinitely long strip footing rest on a horizontal and inclined slope surface. In this regard, different methods of analysis and theories were developed over last few decades to determine the bearing capacity of soil. But the basic structure of formulae used for calculations of bearing capacity today, was first proposed by Terzaghi in 1943. The first important contributions are due to Prandtl (1920) and Reissner (1924), who considered a rigid perfectly plastic half space loaded by a strip punch and Sokolovski (1965), in regard to ponderable soil, all under plain strain conditions. Keverling Buisman (1940) and Terzaghi (1943) proposed the following formula to calculate the ultimate bearing pressure of soil beneath the footing, where the influence of soil cohesion ( $c$ ), surcharge ( $q$ ) and the weight of soil ( $\gamma$ ) are considered independently.

$$\frac{Q_{ult}}{B} = q_{ult} = cN_c + \gamma D_f N_q + 0.5\gamma B N_\gamma \quad (1)$$

Where  $Q_{ult}$ ,  $q_{ult}$  = Ultimate load and pressure respectively;  $B$ = footing width;  $D$ = depth of embedment;  $\gamma$ =unit weight of the soil; and  $c$ =soil cohesion and  $N_c$ ,  $N_q$  and  $N_\gamma$ =bearing capacity factors dependent only on the angle of the internal friction of soil. Terzaghi calculated all three components in Eq. (1) based on limit equilibrium. Prandtl (1920) and Reissner (1924) calculated the bearing capacity factor  $N_c$  and  $N_q$  for weightless soil using the method of characteristics assuming that the soil satisfied associate flow rule. The stress field for two independent solutions by Prandtl (1920) and Reissner (1924) has identical trajectories of principal stress and, even though the stress equation is nonlinear, the superposition of first two terms yields the correct solution. However, once the soil weight is considered, the Eq. (1) is not strictly valid, but it is used in design as a reasonable estimate. These two factors in Eq. (1) take the form

$$N_q = \tan^2 \left( \frac{\pi}{4} + \frac{\phi}{2} \right) \quad (2)$$

$$N_c = (N_q - 1) \cot \phi \quad (3)$$

Where  $\phi$  = internal friction angle. Michalowski (2001) obtained  $N_c$  directly for frictional soil by applying "rules of equivalent states" (Caquot 1934). There are several solutions in the literature for the

third factor  $N_\gamma$ . Meyerhof (1951, 1963); Hansen (1970); Vesic (1973); Hjjaj et.al (2005); Kumar and Khatri (2008) and Chakraborty and Kumar (2013) subsequently proposed different equation to calculate this bearing capacity factor. In contrast, there are large differences among the published numerical solutions for  $N_\gamma$ .

In recent years, both theoretical and experimental investigation on the ultimate bearing capacity of square and circular footings received the attention of many researchers (Cerato and Lutenegeger 2006; Merifield and Nguyen 2006; Cerato and Lutenegeger 2007; Yu et al. 2010; Lavasan and Ghazavi 2012; Ma et al. 2014). However, according to the author knowledge, very few experimental studies (Pathak et al. 2008) were performed that estimate the bearing capacity of square and circular footing placed on c- $\phi$  soil. Therefore, an extensive experimental investigation is required to determine the ultimate capacity of footing on c- $\phi$  soil, which would be a helpful tool for the design engineers.

This paper deals with the experimental and numerical investigation of ultimate bearing capacity of c- $\phi$  soil beneath square and circular footing subjected to vertical load, exploring the differences of failure mechanism of soil under the both footings. A detailed parametric study is carried out to determine the shape effect of square and circular footing as a function of soil property. Finally a new set of equations of shape factor for square and circular footing is proposed comparing its performance with past studies.

### **MODEL FOOTING TESTS**

Plate load test provide a direct measure of compressibility and occasionally the bearing capacity of soils. The technique adopted in this investigation for carrying out the plate loading test is described in D1194-94. (1998). The size of the square and circular model footings used were 400 mm and 420 mm, respectively, having a steel base with thickness of 30 mm. All tests were performed with the footing resting on the soil surface on the saturated clayey soils. The load was applied to the plate incrementally via a factory calibrated hydraulic load cell and a hydraulic jack, and the settlement was measured using computerized data acquisition system. In order to measure any tilt that may occur, two gauges on the perimeter of the plate were used. These gauges supported on rigid uprights fixed firmly into the ground at a distance of more than twice the plate width from the plate center. From the load-settlement data, a load settlement curve for square and circular footing was produced. The ultimate bearing capacity and the settlement of the footings were determined from load settlement curve for the test plates (Figure 2). Collecting the undisturbed samples from the soils of the test locations, following soil properties were obtained in the laboratory.

### **FINITE ELEMENT MODEL AND VALIDATION**

Finite element engine ABAQUS was used to determine the failure load (ultimate bearing capacity) of square and circular footing. The program is most suitable for analyzing nonlinear behavior of material, failure phenomena and related instability. The three-dimensional finite-element mesh used for analysis of a circular footing and square footing of as shown in Figure 1. It represents a half-footing cut through one of the orthogonal planes of symmetry. In numerical simulations, the elastic-perfectly plastic, associative Mohr-Coulomb material model was used. The material parameters used in the analysis is given in Table 1. Eight node linear brick elements with reduced integration were used for discretization of the foundation soil. The distance between the boundaries parallel to the footing length is 15 times the width of footing and the depth of the model is half of that distance (Zhu and Michalowaski 2005). The base of soil layer is fixed in all directions. All vertical boundaries are fixed in horizontal direction but free in vertical direction. The rigid surface footing is modeled by applying uniform vertical downward displacements at all nodal points below the footing at the top surface of domain.

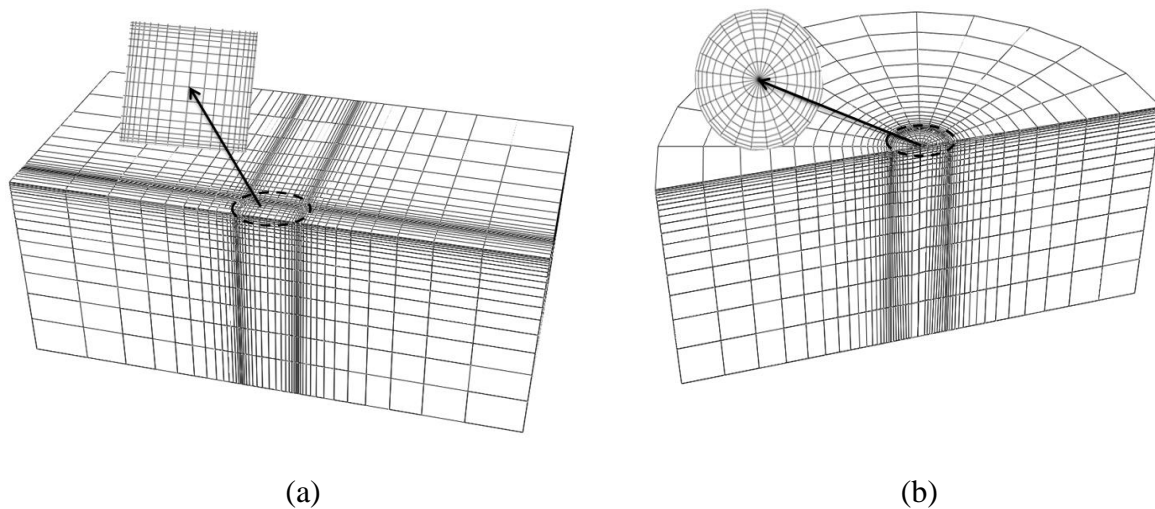


Fig. 1. Finite element meshes: (a) Half square footing and (b) Half circular footing.

Horizontal displacements at the footing-soil interface were restrained to against movement to model the perfect rough base of the footing. To determine the collapse load of the footing, displacement based analyses were performed. The total displacement was applied over a number of sub-steps and the bearing pressure was then calculated by summing the vertical components of the forces at the nodal points immediately beneath the footing divided by the footing area. The mesh is refined in the vicinity of foundation edge since it is in the zone of stress concentration. In this study, mesh convergence studies were performed to optimize the mesh size especially at the neighborhood of footing.

Table 1. Material Parameters

Parameter	Value
Bulk density, $\gamma$ (kN/m <sup>3</sup> )	15.83
Elastic modulus, $E_s$ (kPa)	4,800
Cohesion, $c$ (kPa)	10.75
Internal frictional angle, $\phi$ (Degrees)	20

## RESULTS AND DISCUSSIONS

The load-displacement curves obtained from the analysis for square and circular surface footings are shown in Figure 2. It is observed that the FE model can satisfactorily predict the experimental data points. It is noticed that the settlement curves of the circular and square footing is almost same up to the settlement of 13 mm and then, they deviates. The bearing capacity of square footing is 1.21 times higher than the circular footing. This is consistent with the experimental results obtained by Terzaghi (1943) and Cerato and Lutenegeger (2006), where the bearing capacity of square footing is approximately 1.33 and 1.25 times higher than a circular footing according to Terzaghi and Cerato et al, respectively. Terzaghi (1943) proposed the shape factors  $s_c=1.3$ ,  $s_q=1$ ,  $s_\gamma=0.8$ , and  $s_c=1.3$ ,  $s_q=1$ ,  $s_\gamma=0.6$  for square and circular footing, respectively. The factors  $s_c=1.3$ ,  $s_\gamma=0.8$  for square footing in Terzaghi's suggestion was derived from Golder (1941)'s experiments on clay soil with 3 in. square, 18 by 3 in. rectangular and sand with 6 in. square footing. These test data were highly scattered and Terzaghi disregarded the scatter for establishing a provisional equation. Terzaghi also ignored the influence of internal friction angle on shape factors.

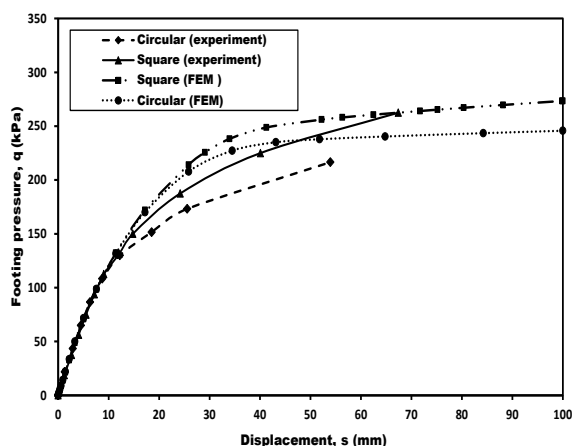


Fig. 2. Load displacement curves of square and circular footing

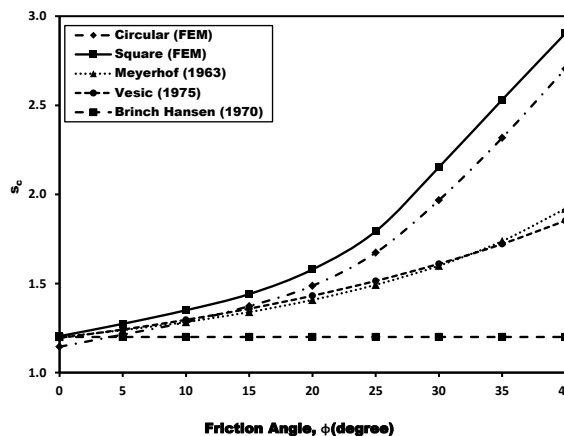


Fig. 3. Cohesion shape factor ( $s_c$ ) as a function of internal friction angle

Terzaghi's proposal for shape factors ( $s_c$  and  $s_q$ ) of square and circular footing was same, but there was small difference in  $s_\gamma$ . Variation of  $s_c$  for both square and circular footing with earlier approaches (Meyerhof, 1963; Hanssen, 1970; Vesic, 1973) are shown in Figure 3. Earlier approaches that are presented here for square footing only, which are based on small size experiments or semiempirical considerations. Hence, the bearing capacity of circular footing is being considered same as that of the square footing in many design codes. Factor  $s_c$  calculated using

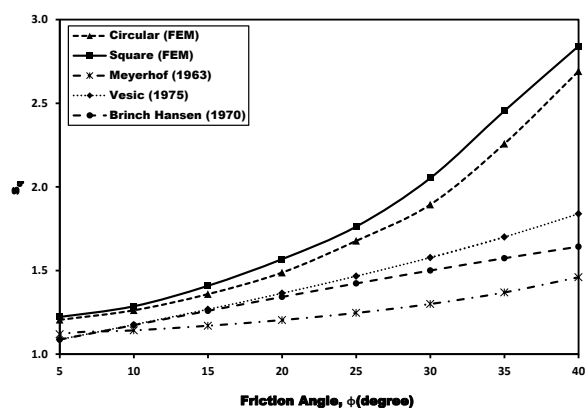


Fig. 4. Variation of surcharge shape factor ( $s_q$ ) as a function of friction

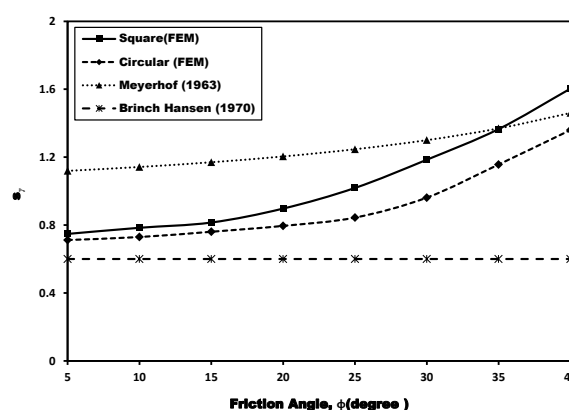


Fig. 5. Surcharge shape factor  $s_\gamma$  as a function of friction angle

Meyerhof (1963) and Vesic (1973) methods fall very close to one another especially lower friction angles. The newly proposed  $s_c$  for square footing or circular footing is greater than Meyerhof and Vesic's solution and the differences are below 1% at  $\phi=0^\circ$  and increased to 30% at  $\phi=40^\circ$ . Zhu and Michalowski (2005) also proved with their finite element analysis that the shape factors of Meyerhof are far too low. On the other hand, Hansen's proposal for cohesion shape factor of square footing is constant ( $s_c = 1.2$ ) and it is independent of friction. From experimental and numerical results, it can be concluded that Terzaghi and Brinch & Hanssen proposals for  $s_c$  are invalid.

Figure 4 presents the effect of friction angle on the shape modifier ( $s_q$ ) for both square and circular footing. It indicates that the difference of  $s_q$  is found small at lower values of friction angle and it increases with the increase of friction angle. The trends that are shown are similar to the trends of  $s_c$  (Figure 3). The maximum difference between the shape factor  $s_c$  and  $s_q$  for square footing is below 5% and this difference decreases to 4% for circular footing. For this reason,  $s_q$  can be expressed as a function of  $s_c$ . But in this paper,  $s_c$  and  $s_q$  of circular footing is expressed as a function of  $s_c$  and  $s_q$  of square footing, respectively. Earlier proposals (Meyerhof 1963; Brinch Hansen 1970; Vesic 1973) show conservative estimation of  $s_q$  as compared to the finite element results for both footings.

Figure 5 shows that the Meyerhof's proposal and Brinch and Hanssen's proposal for  $s_\gamma$  is contradictory to one another. According to the Brinch Hanssen's proposal,  $s_\gamma$  is constant and independent of  $\phi$ . On the other hand, Meyerhof's proposal shows that  $s_\gamma$  increases with the increase of  $\phi$ . According to this proposal  $s_\gamma=1$  when  $\phi=0^\circ$ ,  $s_\gamma=s_c$  when  $\phi \geq 10^\circ$  and  $s_\gamma$  will never less than 1. But, Terzaghi's suggestion for shape modifiers  $s_\gamma$  for square ( $s_\gamma=0.8$ ) and round ( $s_\gamma=0.6$ ) load is less than 1. Meyerhof's proposal is quite contrary with Terzaghi's suggestion as well as numerical results of this study. The work done by the soil weight during deformation is called the effect of soil weight on bearing capacity. When soil is incompressible ( $\phi=0^\circ$ ), the net work will be zero, because the negative work of soil volume that moves upward is equal to the positive work of the soil volume that moves downward. In this way, the influence of soil weight on bearing capacity is negligible,  $N_\gamma=0$  when  $\phi=0^\circ$  and  $N_\gamma>0$  when  $\phi>0^\circ$ . Erickson and Drescher (2002) and Zhu and Michalowski (2005) also proved that for small dilatancy angles the volume of displaced soil for a circular and square footing is less than the volume of displaced soil in plane-strain mechanism. But at larger dilatancy angle this relationship is opposite. For this reason,  $s_\gamma$  can be less than 1 as similar to the result shown in Figure 5. It shows that,  $s_\gamma$  for circular footing is always lower than the  $s_\gamma$  of square footing.  $s_\gamma$  for circular footing changes from 0.71 to 1.36 at a friction angle ranging from 5 to 40°. Consequently,  $s_\gamma$  for square footing changes from 0.75 to 1.60 at a friction angle ranges from 5 to 40°.

## CONCLUSIONS

This paper presents that numerical models have predicted closely the experimental data points of the load-settlement relationships of square and circular footings under vertical loading on homogeneous clay soil. It is observed that there is a difference between their load-settlement behaviors and ultimate bearing capacities. Based on this study, it is fair to conclude that square footing exhibits higher bearing capacity as well as shape factors than the circular footing on homogeneous clay soil. Detailed parametric studies are conducted to compare the shape effect of circular and square footing as a function of frictional angle. This study has proposed new set of shape modifiers,  $s_c$ ,  $s_q$  and  $s_\gamma$  for circular and square footings.

## REFERENCES

- Caquot, A. I. (1934). *Équilibre des massifs à frottement interne: stabilité des terres, pulvérulentes ou cohérentes. pulvérulentes ou cohérentes*, Gauthier-Villars, Paris.
- Cerato, A. B., & Lutenegeger, A. J. (2006). "Bearing capacity of square and circular footings on a finite layer of granular soil underlain by a rigid base." *Journal of Geotechnical and Geoenvironmental Engineering*, 132(11), 1496–1501.
- Cerato, A. B., and Lutenegeger, A. J. (2007). "Scale effects of shallow foundation bearing capacity on granular material." *Geotechnical and Geoenvironmental Engineering*, 133(10), 1192–1202.
- Chakraborty, D., & Kumar, J. (2013). "Dependency of  $N_\gamma$  on footing diameter for circular footings." *Soils and Foundations*, 53(1), 173–180.
- D1194-94., A. (1998). *Standard Test Method for Bearing Capacity of Soil for Static Load. Spread Footings*. Philadelphia, PA: American Society for Testing and Materials.
- Erickson, H. L., & Drescher, A. (2002). "Bearing capacity of circular footings." *Journal of geotechnical and geoenvironmental engineering*, 128(1), 38–43.
- Hansen, J. B. (1970). "A revised and extended formula for bearing capacity." *Geoteknisk Inst., Bulletin* 28, 5–11.
- Hjiaj, M., Lyamin, A. V., & Sloan, S. W. (2005). "Numerical limit analysis solutions for the bearing capacity factor  $N_\gamma$ ." *International Journal of Solids and Structures*, 42(5), 1681–1704.
- Keeverling Buisman, A. S. (1940). *Grondmechanica*. Uitgeverij Waltman, Delft.
- Kumar, J., & Khatri, V. N. (2008). "Effect of footing width on bearing capacity factor  $N_\gamma$  for smooth strip footings." *Journal of Geotechnical and Geoenvironmental Engineering*, 134(9), 1299–1310.
- Lavasan, A. A., & Ghazavi, M. (2012). "Behavior of closely spaced square and circular footings on reinforced sand." *Soils and Foundations*, 52(1), 160–167.
- Ma, Z. Y., Liao, H. J., & Dang, F. N. (2014). "Influence of Intermediate Principal Stress on the Bearing Capacity of Strip and Circular Footings." *Journal of Engineering Mechanics*, 140(7), 04014041.

- Merifield, R. S., & Nguyen, V. Q. (2006). "Two-and three-dimensional bearing-capacity solutions for footings on two-layered clays." *Geomechanics and Geoengineering: An International Journal*, 1(2), 151–162.
- Meyerhof, G. G. (1951). "The ultimate bearing capacity of foundations." *Geotechnique*, 2(4), 301–332.
- Meyerhof, G. G. (1963). "Some recent research on the bearing capacity of foundations." *Canadian Geotechnical Journal*, 1(1), 16–26.
- Meyerhof, G. T. (1953). "The bearing capacity of foundations under eccentric and inclined loads." *In Proceedings, 34th International Conference on Soil Mechanics and Foundation Engineering*, Zürich, Switzerland, 440–445.
- Michalowski, R. L. (2001). "The rule of equivalent states in limit-state analysis of soils." *Journal of geotechnical and geoenvironmental engineering*, 127(1), 76–83.
- Pathak, S. R., Kamat, S. N., & Phatak, D. R. (2008). "Study of Behaviour of Square and Rectangular Footings Resting on Cohesive Soils Based on Model Tests." *Sixth International Conference on Case Histories in Geotechnical Engineering*.
- Prandtl, L. (1920). "Über die härte plastischer körper." *Nachrichten von der Gesellschaft der Wissenschaften zu Göttingen, Mathematisch-Physikalische Klasse*, 74–85.
- Reissner, H. (1924). "Zum erddruckproblem." *Proc. 1st Int. Congress for Applied Mechanics*, Delft, The Netherlands, 295–311.
- Sokolovski, V. V. (1965). *Statics of Granular Media*. Pergamon Press, New York.
- Terzaghi, K. (1943). *Theoretical soil mechanics*. Wiley, New York.
- Vesic, A. S. (1973). "Analysis of ultimate loads of shallow foundations." *J. Soil Mech. Found. Div.*, 99(1), 45–76.
- Yu, L., Liu, J., Kong, X. J., & Hu, Y. (2010). "Three-dimensional large deformation FE analysis of square footings in two-layered clays." *Journal of geotechnical and geoenvironmental engineering*, 137(1), 52–58.
- Zhu, M., and Michalowski, R. L. (2005). "Shape factors for limit loads on square and rectangular footings." *Journal of geotechnical and Geoenvironmental Engineering*, 131(2), 223–231.

## NUMERICAL ANALYSIS OF VERTICAL UPLIFT RESISTANCE OF HORIZONTAL STRIP ANCHOR EMBEDDED IN COHESIVE-FRICTIONAL WEIGHTLESS SOIL

M. S. Islam, M. Rokonuzzaman \* & G. Sarkar

*Department of Civil Engineering, Khulna University of Engineering & Technology, Khulna,  
Bangladesh*

*\*Corresponding Author: rokoncekuet@yahoo.com*

### ABSTRACT

With an application of the finite element analysis, the vertical pullout capacity of a horizontal strip plate anchor placed in a cohesive-frictional ( $c-\phi$ ) soil has been computed. The variation of the uplift factors  $N_c$ ,  $N_q$  and  $N_\gamma$ , due to the contributions of soil cohesion, surcharge pressure and unit weight, respectively, has been evaluated for different friction angles ( $\phi$ ) and embedment ratios ( $H/B$ ). These break-out factors increase continuously with the increase of embedment ratios. The variation of  $N_q$  and  $N_\gamma$  has found almost linear and  $N_c$  varies nonlinearly with the friction angle.

Keywords: Anchor; numerical analysis; uplift capacity; finite element analysis

### INTRODUCTION

Plate anchors are light structural members employed to withstand uplift forces for conditions, where immediate breakaway occurs. Plate anchors are commonly used in transmission tower, sheet piles, retaining wall, deep water offshore developments, and airport hangars. (Hanna et al. 2014; Merifield and Smith 2010; Sahoo and Kumar 2012a; Sutherland et al. 1983). During the last 50 years, numerous experimental and numerical investigations have been conducted by several researchers to evaluate the pullout capacity of plate anchor. Experimental studies include (i) conventional 1-g laboratory model tests (Das and Seeley 1975; Neely et al. 1973; Ranjan and Kaushal 1977; Rokonuzzaman and Sakai 2012) and (ii) centrifuge model tests (Dickin and Laman 2007). While, numerical study consists of (i) lower bound limit analysis (Merifield et al. 2006; Meyerhof 1973), (ii) upper bound limit analysis (Kouzer and Kumar 2009; Merifield and Sloan 2006; Sahoo and Kumar 2012a), (iii) method of characteristic (Kumar and Rao 2004; Neely et al. 1973) and (iv) Finite element method (Kumar and Kouzer 2008; Merifield et al. 2006; Murray and Geddes 1987; Rowe and Davis 1982; Sahoo and Kumar 2012b). The pullout capacity of soil anchors are mainly influenced by anchor geometry, embedded ratio, soil-anchor interfaces and local soil conditions. Several researchers have investigated the effect of anchor geometry on the pullout capacity of plate anchor and recommended shape factors for the design engineers (Hanna and Ranjan 1992; Hanna et al. 2011). Kumar and Kouzer (2008) studied the effect of embedment ratio and frictional angle on the pullout capacity of plate anchor in sand and found that the uplift capacity increases with the increases with the increase in the embedment ratio and the frictional angle. Furthermore, plate anchor could be installed vertically and horizontally as per the requirements. Horizontal anchors are generally used to resist vertical uplift forces for the foundations of structures such as transmission towers, pipelines buried under water, and dry docks (Deshmukh et al. 2011; Kumar and Kouzer 2008; Merifield and Sloan 2006; Merifield et al. 2001). Moreover, it is noted from the literature that most of the study are conducted to evaluate the pullout capacity factor in either dry sand ( $c=0$ ) or saturated clay ( $\phi=0$ ). According to the author's knowledge, limited information is available in the literatures that estimate the pullout capacity of plate anchor in  $c-\phi$  soil. Although, Kumar and Naskar 2012 studied on the vertical uplift capacity of a group of two axial anchors in a  $c-\phi$  soil using the lower bound finite element limit analysis and showed the variation of the uplift capacity factors,  $N_c$  and  $N_\gamma$ , with the change in embedment ratio and vertical spacing.

In this study, an extensive elasto-plastic finite element analysis has been performed to investigate the pullout behavior of horizontal plate anchor in frictional cohesive soil ( $c-\phi$  soil). In order to investigate the effect of embedment ratio on the pullout capacity, anchor plates were buried at different embedment

ratio. Furthermore, the effect of frictional angle of soil on the pullout capacity factors  $N_c$ ,  $N_q$  and  $N_\gamma$ , due to the components of cohesion, surcharge pressure and soil weight, respectively are also investigated. The results have been compared with the existing results reported in the literature and design charts have been proposed for predicting the pullout capacity of anchor plates

### PROBLEM DEFINITION

A typical layout of a strip plate anchor having width  $B$  and thickness  $t$  is shown in Figure 1. The anchor plate is considered perfectly rigid and embedded in a cohesive-frictional ( $c-\phi$ ) medium. The ground surface is horizontal and a uniform surcharge of  $q= 18 \text{ kN/m}^2$  is applied on the top surface. The anchor plate is embedded at a depth of  $H$  from the ground surface, which is varied through a wide range of embedment ratio ( $H/B=1$  to  $10$ ). The collapse load ( $q_u$ ) per unit length of the plate anchor is computed for the immediate breakaway (vented) of the anchor plate i.e. anchor interface separates immediately upon pullout action. The uplift capacity factors  $N_c$ ,  $N_q$  and  $N_\gamma$  are calculated by assuming the principle of superposition using equation (1).

$$q_u = cN_c + qN_q + BH\gamma N_\gamma \dots \dots \dots (1)$$

The bearing capacity factor  $N_c$ ,  $N_q$  and  $N_\gamma$  have been computed separately by taking, (i)  $c \neq 0$ , but  $q=0$  and  $\gamma=0$ , (ii)  $c=0$ , but  $q \neq 0$  and  $\gamma=0$  and (iii)  $c=0$ , but  $q=0$  and  $\gamma \neq 0$ , which signifies the validation of the principle of superposition.

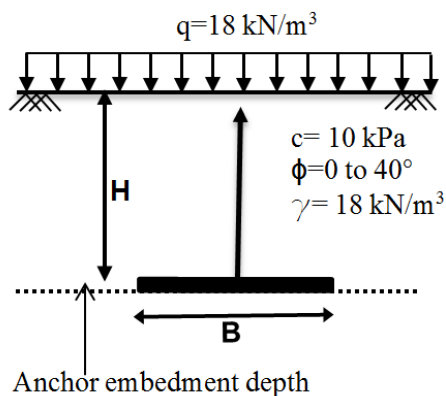


Fig. 1. Definition of the problem

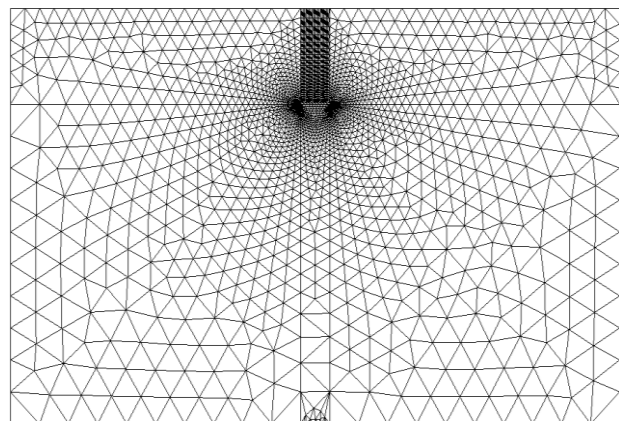


Fig. 2. FE mesh ( $H/B=3$ ,  $B=1\text{m}$ )

### FINITE-ELEMENT MODEL

An extensive elasto-plastic finite element (FE) analysis was conducted using ABAQUS to determine the ultimate pullout load of strip anchor in  $c-\phi$  soil. The present numerical analysis are carried out on isotropic and homogeneous soil with associative Mohr-Coulomb yield criterion and is defined by the cohesion value  $c$ , angle of internal friction  $\phi$ , and dilatancy angle  $\psi$ . In this study, a strip rigid plate is made contact with the soil domain, which is displaced progressively along the pullout direction. The interfaces between the anchor plate and soil domains are defined as (i) tangential behavior and (ii) normal behavior. In tangential behavior, a penalty friction formulation is used with a friction coefficient of 0.4, while in normal behavior hard contact is defined for pressure overclosure. Separation after contact is also allowed. The FE analyses are based on six-noded modified triangular elements. Figure 2 presents a typical two-dimensional finite-element mesh for a strip plate anchor embedded at  $H/B=3$  and  $B=1\text{m}$ . The analyses assume a perfectly rigid plate anchor, with incremental displacement being prescribed on the anchor nodes in contact with the soil. The dimensions of soil domain are selected in such a way that the stress and displacement gradients at boundaries would decrease and become zero. The soil domain is extended to  $10B$  in horizontal directions from the edge of the anchor for the embedment ratio ( $H/B$ ) 1 to 9. However, it is not sufficient for the  $H/B=10$  and therefore, the soil domain is extended to  $20B$ . This extension of soil boundaries is sufficient for the computation of  $N_c$ , but it is proved insufficient for determination of  $N_q$  and  $N_\gamma$ , especially when the rotation of anchor is greater than  $67.5$  degree. Thus, the soil domain is extended to  $20B$  in horizontal directions for embedment ratio 6 and 8, and  $30B$  for 10. However, the vertical boundaries are remaining  $10B$  from the bottom of the anchor



for all cases. Zero-displacement boundary conditions are applied to prevent out-of-plane displacements of the vertical boundaries and the base of the mesh is fixed in all three coordinate directions. To obtain more accurate results, elements are kept very small near the plate, increasing gradually in size and moving away from the plate. To determine the collapse load of the footing, displacement based analyses are performed. The total displacement is applied over a number of sub-steps and the uplift pressure is then calculated by summing the nodal forces along the pullout direction divided by the footing area.

## RESULTS AND DISCUSSIONS

The validity of the numerical results for the horizontal anchor is established through verification against published results before conducting the detailed parametric study. The designed FE model is validated for the pullout capacity factor  $N_c$  of a strip anchor in weightless soil ( $\gamma=0$ ). It can be seen in Figure 3 that  $N_c$  for horizontal anchor agrees well with the numerical solution obtained by Yu et al. (2011) and Merifield et al. (2001).  $N_c$  values for horizontal are closer with the upper bound solution up to a embedment ratio of 3 then deviates and maximum differences are found 6.6% for horizontal anchor. Note that, the current FE results, Yu et al. (2011), Merifield et al. (2001) and Rowe & Davis (1982a) stay close together for shallow embedment ratio ( $H/B=2$ ). FE result of Rowe & Davis (1982a) shows lower values and almost constant at large embedment ratio ( $H/B>3$ ). These differences may be due to truncation criterion, where the pullout capacity was taken at a displacement as 15-20 % of anchor width rather than the ultimate capacity for large embedment ratio.

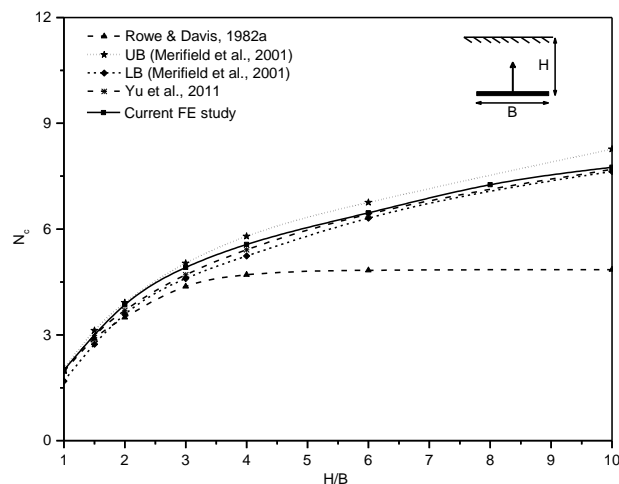


Fig. 3. Comparison of the bearing capacity factor  $N_c$  for plate anchors in weightless uniform soil

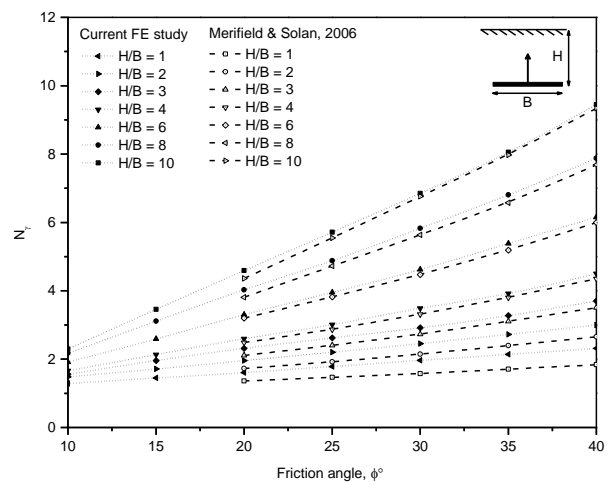


Fig. 4. Effect of friction angles,  $\phi$  on  $N_\gamma$  at different embedment depth ( $H/B$ )

The pullout capacity factor  $N_\gamma$  due to the contribution of soil weight for different embedment ratio and friction angle is shown in figure 4. The effect of friction angle on anchor breakout factor due to the contribution of soil weight is obtained for different combination of embedment depth and anchor rotation is shown in figure 4. For the purpose of validation, the current finite element results are compared with the lower bound solution obtained by Merifield and Solan (2006) which is shown in figure 4. The anchor break-out factor  $N_\gamma$  varies almost linearly with the friction angle as found by Merifield and Solan (2006). This trend is found similar as the variation of  $N_q$  (see Fig. 7) but in contrast with the variation of  $N_c$  (see Fig. 5). The current finite element results are found higher than the lower bound solution of Merifield and Solan (2006) at all embedment depths and the difference between the two decreases at higher embedment depth.

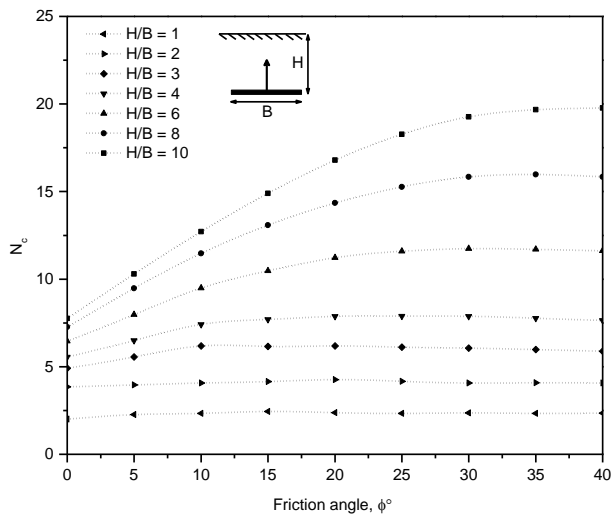


Fig. 5. Effect of friction angles,  $\phi$  on  $N_c$  at different embedment depth ( $H/B$ )

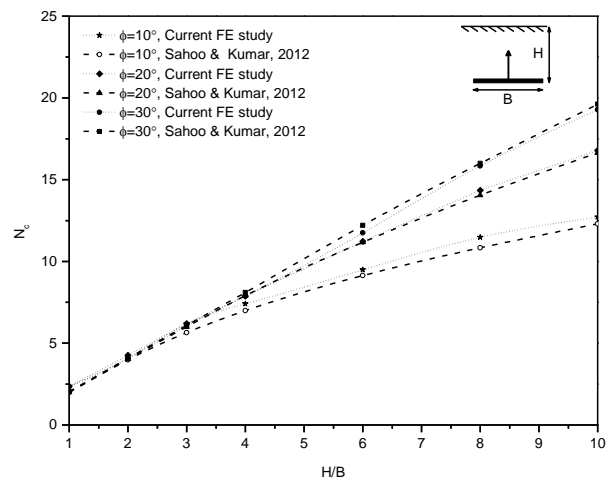


Fig. 6. Comparison of factor  $N_c$  for horizontal anchor at different friction angles,  $\phi$

The variation of break-out factor  $N_c$  with friction angle ( $\phi$ ) ranging from  $0^\circ$  to  $40^\circ$  at an interval of  $5^\circ$  corresponding to different embedment depth ( $H/B$ ) is presented in Figure 5. It can be seen that  $N_c$  increases gradually with friction angle upto the peak point and after that friction angle does not show any significant effect. This trend is found similar as found by Rowe and Davis (1982a) and Kumar and Naskar (2012). It is also noted that,  $N_c$  increases with the friction angle upto 20 degree for embedment ratio 1 to 3. After that, the peak value of  $N_c$  is shifted to 5 degree apart (i.e.  $25^\circ$  for  $H/B=4$ ) from embedment ratio 4 to 10. This peak value is different for different embedment ratio.

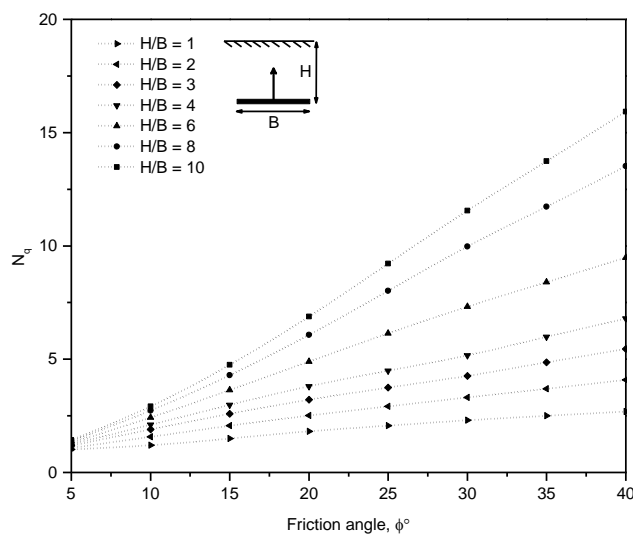


Fig. 7. Effect of friction angles,  $\phi$  on  $N_q$  at different embedment depth ( $H/B$ )

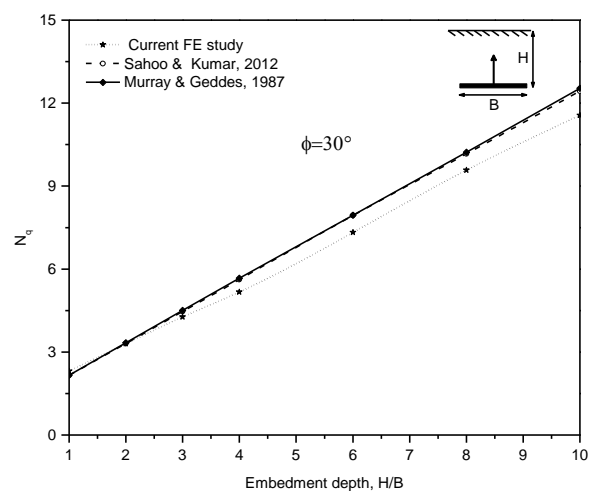


Fig. 8. Comparison of factor  $N_q$  for horizontal anchor at  $\phi=30^\circ$

For example, maximum value of  $N_c$  is found 6.18 and 11.74 at a friction angle  $20^\circ$  and  $30^\circ$ , for embedment ratio of 3 and 6, respectively. For the purpose of validation, the values of  $N_c$  obtained from current finite element studies are compared with the Sahoo and Kumar (2012) based on upper bound finite element analysis. Three friction angles (i.e.  $20^\circ$ ,  $30^\circ$ ,  $40^\circ$ ) are considered in the following comparisons, which are shown in the Figure 6. Present finite element results are found almost same as Sahoo and Kumar (2012) particularly at friction angle  $30^\circ$  and  $40^\circ$ , respectively. But, a small difference upto 5.6% are found at friction angle of  $10^\circ$  and embedment ratio of 8.

The variation of uplift factor ( $N_q$ ) due to the contribution of surcharge pressure with friction angle is obtained for different embedment ratio is shown in Fig. 7. Friction angle,  $\phi$  varies from  $5^\circ$  to  $40^\circ$  at an

interval of  $5^\circ$ . It is found that for a given embedment ratio, the breakout factors increase almost linearly with an increase the soil friction angle, which is in contrast with the variation of  $N_c$ . It also represents the comparison of break-out factor with previous available data. As per author knowledge, little studies were performed to determine the effect of surcharge pressure on anchor break-out factor  $N_q$ . For this reason, the values of  $N_q$  (see Fig. 8) obtained in current finite element analysis are compared only with those obtained in simple upper bound analysis by Murray and Geddes (1987) and Sahoo and Kumar (2012), respectively. It shows that, at a low embedment depth upto 2, the break-out factor  $N_q$  is found same as Murray and Geddes (1987) and Sahoo and Kumar (2012). The difference increases with the increase of embedment depth and the variation is almost linear as found by Murray and Geddes (1987) and Sahoo and Kumar (2012).

## CONCLUSION

A rigorous finite element investigation has been performed to determine the pullout capacity of strip anchor in  $c-\phi$  soil. Consideration has been given to the effect of soil friction angle and anchor embedment ratio on anchor pullout capacity factor  $N_c$ ,  $N_q$  and  $N_\gamma$ . At a given embedment ratios, anchor break-out factors  $N_\gamma$  and  $N_q$  increase continuously with the friction angle. But, their does not exist any peak point on  $N_\gamma$  and  $N_q$  which is in contrast with the trend of  $N_c$ . The variation of  $N_q$  and  $N_\gamma$  has found almost linear and  $N_c$  varies nonlinearly with the friction angle.

## REFERENCES

- Dickin, E. A., & Laman, M. (2007). Uplift response of strip anchors in cohesionless soil. *Advances in Engineering Software*, 38(8), 618-625.
- Das, B. M., and Seeley, G. R. (1975). "Load-displacement relationships for vertical anchor plates." *Journal of Geotechnical Engineering Division*, 101(7), 711-715.
- Deshmukh, V. B., Dewaikar, D. M., and Choudhary, D. (2011). "Uplift Capacity of Horizontal Strip Anchors in Cohesionless Soil." *Geotechnical and Geological Engineering*, 29(6), 977-988.
- Hanna, A., Foriero, A., and Ayadat, T. (2014). "Pullout Capacity of Inclined Shallow Single Anchor Plate in Sand." *Indian Geotechnical Journal*, 45(1), 110-120.
- Hanna, A., Rahman, F., and Ayadat, T. (2011). "Passive earth pressure on embedded vertical plate anchors in sand." *Acta Geotechnica*, 6(1), 21-29.
- Hanna, A., and Ranjan, G. (1992). "Pullout-displacement of shallow vertical anchor plates." *Indian Geotech J*, 22(1), 46.
- Kouzer, K. M., and Kumar, J. (2009). "Vertical Uplift Capacity of Equally Spaced Horizontal Strip Anchors in Sand." *International Journal of Geomechanics*, 9(5), 230-236.
- Kumar, J., and Kouzer, K. M. (2008). "Vertical uplift capacity of horizontal anchors using upper bound limit analysis and finite elements." *Canadian Geotechnical Journal*, 45(5), 698-704.
- Kumar, J., and Naskar, T. (2012). "Vertical uplift capacity of a group of two coaxial anchors in a general  $c-\phi$  soil." *Canadian Geotechnical Journal*, 49(3), 367-373.
- Kumar, J., and Rao, V. B. K. M. (2004). "Seismic horizontal pullout capacity of shallow vertical anchors in sand." *Geotechnical and Geological Engineering*, 22(3), 331-349.
- Merifield, R. S., and Sloan, S. W. (2006). "The ultimate pullout capacity of anchors in frictional soils." *Canadian Geotechnical Journal*, 43(8), 852-868.
- Merifield, R. S., Sloan, S. W., and Lyamin, A. V. (2006). "Three-dimensional lower-bound solutions for the stability of plate anchors in sand Three-dimensional lower-bound solutions for the stability of plate anchors in sand." *Geotechnique*, 56(2), 123-132.
- Merifield, R. S., Sloan, S. W., and Yu, H. S. (2001). "Stability of plate anchors in undrained clay." *Geotechnique*, 51(2), 141-153.
- Merifield, R. S., and Smith, C. C. (2010). "Computers and Geotechnics The ultimate uplift capacity of multi-plate strip anchors in undrained clay." *Computers and Geotechnics*, Elsevier Ltd, 37(4), 504-514.
- Meyerhof, G. G. (1973). "The Uplift Capacity of Foundations Under Oblique Loads." *Canadian Geotechnical Journal*, 10(1), 64-70.
- Murray, E. J., and Geddes, J. D. (1987). "Uplift of anchor plates in sand." *Journal of Geotechnical Engineering*, 113(3), 202-215.
- Neely, W. J., Stuart, J. G., and Graham, J. (1973). "Failure Loads of Vertical Anchor Plates in Sand." *Journal of Soil Mechanics and Foundations Division, ASCE*, 99(9), 669-685.

- Ranjan, G., & Kaushal, Y. P. (1977). Load-deformation characteristics of model anchors under horizontal pull in sand. *Goetech Eng Bangkok, Thailand*, 8, 65-78.
- Rokonuzzaman, M., & Sakai, T. (2012). Evaluation of Shape Effects for Rectangular Anchors in Dense Sand: Model Tests and 3D Finite-Element Analysis. *International Journal of Geomechanics*, 12(2), 176-181.
- Rowe, R. K., and Davis, E. H. (1982). "The behavior of anchor plates in sand." *Geotechnique*, 32(1), 25-41.
- Sahoo, J. P., and Kumar, J. (2012a). "Horizontal Pullout Resistance for a Group of Two Vertical Plate Anchors in Clays." *Geotech Geol Eng Geotechnical and Geological Engineering*, 30(5), 1279-1287.
- Sahoo, J. P., and Kumar, J. (2012b). "Vertical uplift resistance of two horizontal strip anchors with common vertical axis." *International Journal of Geotechnical Engineering*, 6(4), 485-496.
- Sutherland, H. B., Finlay, T. W., and Fadl, M. O. (1983). "Uplift capacity of embedded anchors in sand." *Int Conf Behav Offshore Struct*, 451-463.
- YU, L., LIU, J., KONG, X.-J., and HU, Y. (2011). "Numerical study on plate anchor stability in clay." *Geotechnique*, 61(3), 235-246.

## **INFLUENCE OF HANDRAIL TYPES ON AERODYNAMICS OF LONG-SPAN BRIDGE DECK**

M. N. Haque\*

*Department of Civil Engineering, Chittagong University of Engineering and Technology, Chittagong,  
Bangladesh*

*\*Corresponding Author: naimulce@gmail.com*

### **ABSTRACT**

Aerodynamic response is one of the main design consideration for long-span bridge deck and this is quite sensitive to the shape of the bridge deck. This paper numerically investigates the influence of handrail types such as solid handrail, perforated handrail with curb and without curb on aerodynamic responses of bridge deck with fairing. Edge fairing is attached at the side of the bridge deck to make it more practical and improve the aerodynamic responses. The steady state force coefficients and the flow field were taken as a parameter of interest. It was found that the types of handrail alter the aerodynamic behaviour of the bridge deck noticeably.

**Keywords:** Deck equipment; handrails; curb; aerodynamic response; bridge deck; CFD

### **INTRODUCTION**

Long span bridges are susceptible to various aeroelastic phenomena under the wind action and in the design stage of the bridge deck, aerodynamic responses are considered as one of main design aspect. Accurate prediction of aerodynamic responses is required to ensure safety and stability of the bridge deck against wind. To obtain the exact responses under wind action, bridge deck should be modelled along with its deck equipments. There are a number of common deck equipments such as handrail, safety barrier, median divider, inspection rails and light post etc attached to the deck. Even though, the size of these deck equipments are small as compared to the deck, their presence will influence the aerodynamic responses as it is already shown that aerodynamic response is a quite sensitive to the shape of the bridge deck (Shiraishi and Matsumoto, 1983 and Larsen and Wall, 2012).

Among these deck equipments, handrail is one the most common and often attached to the deck. Nagao et al. (1997) investigated the effects of perforated handrail on vortex-shedding vibration. They found that the size of the horizontal bars affects the vortex-shedding vibrations significantly. Later, Bruno and Mancini (2002) showed that addition of perforated handrails increases the overall bluffness of the deck by employing Large Eddy Simulation (LES). In previous studies only the perforated handrails were taken into consideration, however, for practical bridges, along with the perforated handrail, solid handrail is also attached. Further, perforated handrails are provided along with the curb or without curb. Therefore, it is required to know how the variation of the handrail types affects the aerodynamic responses due to its practical demand.

In the present study a numerical investigation was carried out by employing Unsteady Reynolds Averaged Navier-Stokes simulation (URANS) to show the influence of handrail types on aerodynamics of bridge deck with edge fairing. Fig.1 shows the cross section of the considered bridge deck. The top and bottom plate slopes of the fairing are set to  $40^\circ$  and  $20^\circ$ , respectively. The side ratio ( $R$ ) of the bridge deck is maintained at 5 and Reynolds number ( $Re$ ) is set to  $6.0 \times 10^4$ . Three different types of handrail namely, solid handrail, perforated handrail with curb and without curb is taken into consideration as shown in Fig.2. The steady state force coefficients and the flow fields are taken into consideration as parameter of interest.

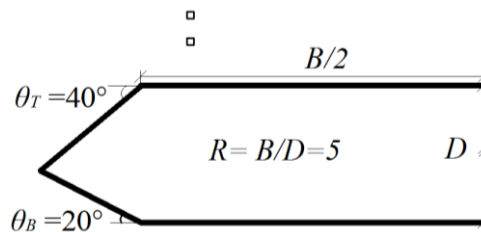


Fig. 1: Cross section of the bridge deck (with perforated handrails without curb) considered in the present study

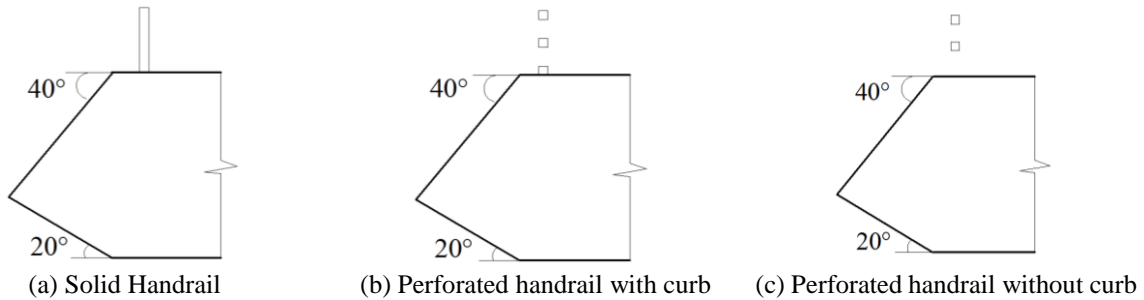


Fig. 2: Types of handrail considered in the present study

## NUMERICAL FORMULATIONS

The ensemble averaged Navier-Stokes equations called unsteady Reynolds-Averaged Navier-Stokes (URANS) equation was used to model the flow around the bridge deck. The flow was assumed to be two-dimensional and incompressible in nature. The governing equations were as follows;

$$\frac{\partial \bar{U}_i}{\partial x_i} = 0 \quad (1)$$

$$\frac{\partial \bar{U}_i}{\partial t} + \bar{U}_j \frac{\partial \bar{U}_i}{\partial x_j} = -\frac{1}{\rho} \frac{\partial \bar{P}}{\partial x_i} + \frac{\partial}{\partial x_j} \left[ \nu \left( \frac{\partial \bar{U}_i}{\partial x_j} + \frac{\partial \bar{U}_j}{\partial x_i} \right) - \overline{u_i' u_j'} \right] \quad (2)$$

where,  $\bar{U}_i$  and  $x_i$  were the averaged velocity and position vectors respectively,  $t$  was the time,  $\bar{P}$  was the averaged pressure,  $\rho$  was the air density,  $\nu$  was the fluid viscosity. The turbulence modeling was attained by utilizing the  $k-\omega$  SST turbulence model (Menter, 1994; Menter et al., 2003). Convective and diffusive terms in the governing equations were discretized with second order accurate central differencing schemes. For time integration second order accurate backward differentiation formulae method was utilized. PISO (Pressure implicit with splitting of operator) algorithm was utilized to solve these discretized equations. An open source code OpenFOAM was used as a solver.

Simulations were performed in a two dimensional domain with 48D in length and 25D in height, where  $D$  was the height of the bridge deck section. The object was placed at 18D downstream of the inlet. The outlet boundary was placed at 25D downstream of the object and height of the domain was 25D. The domain was sufficiently large to avoid unnecessary disturbance of the boundary conditions. At the outlet, pressure boundary condition, at the top and bottom of the domain, slip boundary condition and at the body, non-slip boundary condition was implemented. The domain was discretized spatially by a non-uniform structured grid and the cell size was varied gradually with a geometric progression of 1.05 in all directions. Further details of the model, grid system and validation can be found in (Haque et al., 2015a and 2015b).

## RESULTS AND DISCUSSIONS

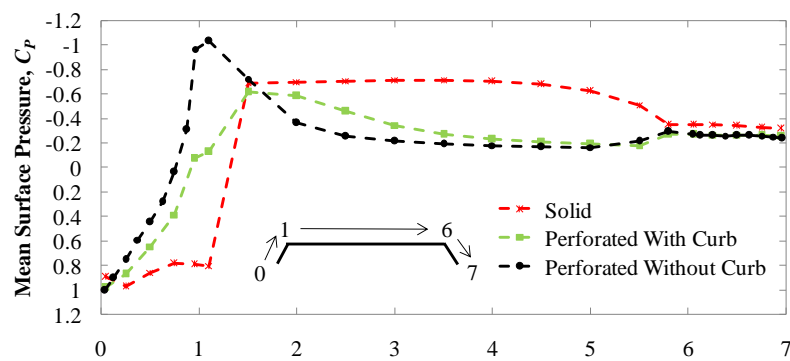
The mean and rms values of the steady state force coefficients of the considered bridge decks are compared in Table 1. All the force coefficients are normalized with the width of the deck ( $B$ ). As can be seen the reduction of the solidity ratio of the handrails improves the static aerodynamic responses of the

bridge decks. A trend can be noticed that both the mean and rms value of the force coefficients decreases from solid to perforated with curb and perforated with curb to without curb case. However, the perforated handrail with curb has the highest negative lift force value among the three, which means the deck with this type of handrail has increased stability against wind. Most interestingly, only the absence of the curb has noticeable influence on the force coefficients as reflected in the last column where a comparison was made between the perforated handrail with and without curb cases.

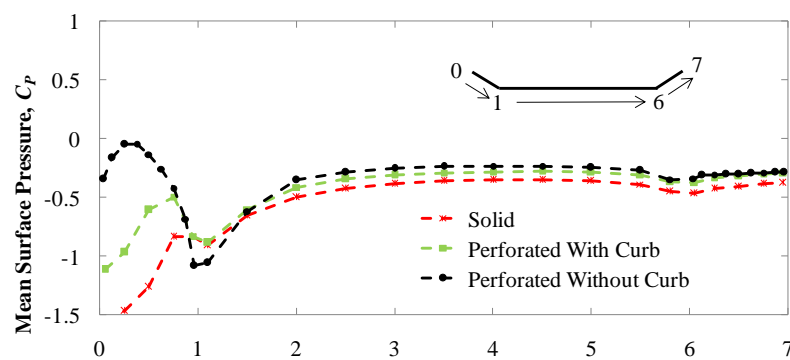
To better understand the responses, the time averaged pressure distributions are plotted in Fig. 3. Various important flow features can be noticed in the pressure field. For the case of perforated handrails without curb, very large suction appears at the leading edge side just before the handrail, after that,

Table 1: Steady state force coefficient comparison of the considered bridge decks

Force coefficients	Solid	Perforated	Perforated	Percentage variation (%)	
	(1)	With Curb (2)	Without Curb (3)	(1) & (2)	(2) & (3)
Mean value of drag force coefficient ( $C_D$ )	0.732	0.649	0.553	11.33	13.12
Mean value of lift force coefficient ( $C_L$ )	-0.156	-0.246	-0.176	57.69	44.87
Mean value of moment coefficient ( $C_M$ )	0.202	0.099	0.051	51.00	23.75
rms value of lift force coefficient ( $C_L'$ )	0.007	0.002	0.001	71.42	14.29
rms value of moment coefficient ( $C_M'$ )	0.001	0.0004	0.0002	60.00	20.00



(a) Top surface of the bridge deck



(b) Bottom surface of the bridge deck

Fig. 3: Time averaged pressure distribution around the bridge deck (Contd.)

suddenly pressure recovery occurs at the top surface of the deck. However, reverse phenomenon can be observed for the case of solid handrail case. Similar to the deck top surface, pressure field are mainly affected at the leading edge side of the deck bottom surface. Large suction appears at the leading edge bottom surface of the deck for the cases of solid and perforated handrail with curb. In the case of

perforated handrail without curb the deck has the highest negative lift value, which implies that the pressure distribution at the deck top surface is the influential one as it has the least magnitude of suction.

The time averaged velocity distribution around the bridge deck for the considered types of handrail are compared in Fig. 4. The observation made earlier is also reflected in the velocity distribution. Large shear layer separation can be noticed both at the deck top surface and leading edge bottom surface. Basically, this separated shear layer creates the suction at the top and bottom surface of the deck. In the all the three cases clear after-body vortex shedding can be seen at the trailing edge side. However, the size of the vortex decreases for the case of perforated handrail with and without cases as compared to the solid handrail case.

## CONCLUSIONS

A relative comparison of steady-state aerodynamic characteristics of bridge deck for various handrail types was made. At the current Reynolds number ( $R_e$  of  $6.0 \times 10^4$ ) and considered geometry ( $R=5$ ), we found that the types of handrail has noticeable influence on the force-coefficients and flow field. As the solidity ratio of the handrail decreases, the steady-state aerodynamic responses of the bridge deck improve. Even though, the variation in handrail types is made at the top surface of the deck, it affected the bottom surface of the deck pressure and velocity fields as well. Due to the presence of the handrail, the follow separation occurs both the leading and trailing edge side of the deck and depending on the solidity ratio of the handrail, the intensity of separation varies. Therefore, handrail should be properly modelled during the time of numerical and experimental investigation for actual estimation of the aerodynamic responses of the bridge deck.

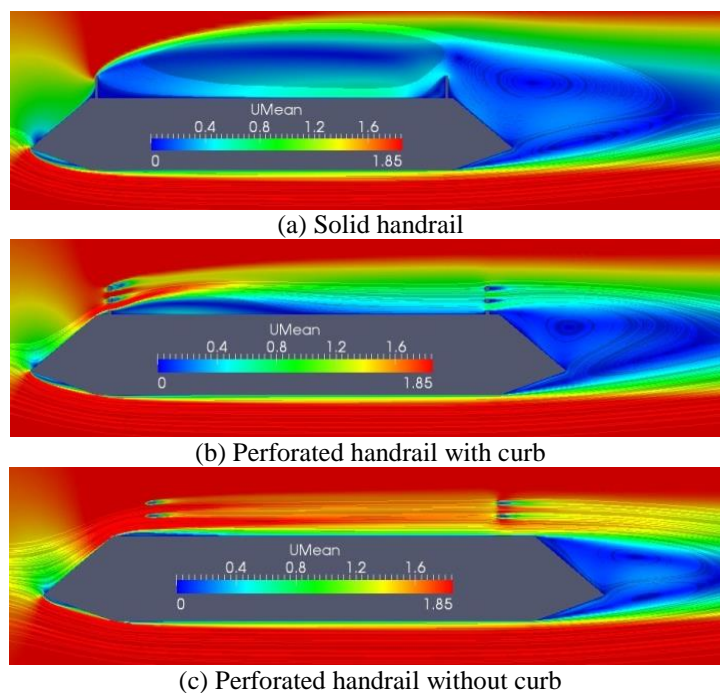


Fig.4: Time average velocity distribution around the bridge deck

## REFERENCES

- Bruno, L and Mancini, G. 2002. Importance of deck details in bridge aerodynamics. *Structural Engineering International*, 12(4):289-294.
- Haque, MN, Katsuchi, H, Yamada, H and Nishio, M. 2015a. Strategy to develop efficient grid system for flow analysis around two-dimensional bluff bodies. *KSCE Journal of Civil Engineering*, 20(05): 1-12.
- Haque, MN, Katsuchi, H, Yamada, H and Nishio, M. 2015b. Flow field analysis of a pentagonal-shaped bridge deck by unsteady RANS. *Engineering Application of Computational Fluid Mechanics*, 10(1): 1-16.



- Larsen, A, and Wall, A. 2012. Shaping of bridge girders to avoid vortex shedding response. *Journal of Wind Engineering and Industrial Aerodynamics*, 104-106: 159-165.F.R.
- Menter, F. 1994. Two-equation Eddy-viscosity Turbulence Model for Engineering Applications. *AIAA Journal*, 32:1598–1605.
- Menter, FR, Kuntz, M and Langtry, R. 2003. Ten years of industrial experience with the SST turbulence model. *Proceedings of Turbulence, Heat and Mass Transfer 4*, 12-17, October, Antalya, Turkey, 625–632.
- Shiraishi, N, and Matsumoto, M. 1983. On classification of Vortex-Induced oscillation and its application for bridge structures. *Journal of Wind Engineering and Industrial Aerodynamics*, 14: 419–430.
- Nagao, F, Utsunomiya, H, Yoshioka, E, Ikeuchi, A and Kobayashi, H. 1997. Effects of handrails on separated shear flow and vortex-induced oscillation. *Journal of Wind Engineering and Industrial Aerodynamics*, 69-71: 819-827.

## **SEISMIC PERFORMANCE OF REINFORCED CONCRETE FRAME BUILDING WITH AND WITHOUT URM INFILL WALLS**

R. Dey<sup>1</sup>, M. A. R. Bhuiyan<sup>2</sup>, R. K. Mazumder<sup>3</sup> & A. K. M. T. A. Khan<sup>1</sup>

<sup>1</sup>*Structural Engineer, Building Design and Development, Chittagong, Bangladesh*

<sup>2</sup>*Department of Civil Engineering, Chittagong University of Engineering and Technology, Chittagong, Bangladesh*

<sup>3</sup>*Institute of Earthquake Engineering Research (IEER), Chittagong University of Engineering and Technology, Chittagong, Bangladesh*

*\*Corresponding Author: rajen.ce08@gmail.com*

### **ABSTRACT**

In the conventional practice masonry walls are considered as non-structural element and its load is considered on the corresponding elements. Effect of infill is mostly ignored during analysis of the structure. To obtain the perfect model of a building the behaviour of all the primary components is needed and their load carrying capacities are required. This study attempts to simulate the nonlinear behaviour of URM infill frames using SeismoStruct v7.0 where diagonal strut model is used to idealize the effect of infill wall. A six storied ordinary moment resisting frame is considered with and without infill walls and capacity of the structure is evaluated and compared using capacity spectrum method. Prior to that pushover analysis was carried out for both configuration of the structure. It is observed from pushover analysis that the bare frame comprises lesser stiffness when compared to the frame with infill within a range of displacement. Ductility of bare of frame also reduces with inclusion of infill masonry walls as is observed from capacity demand curve of the structure. However inclusion infill walls increases the capacity of the structure to withstand stronger ground motion compared to bare frame structure.

Keywords: Diagonal strut model; stiffness; ductility; un-reinforced masonry; capacity spectrum method

### **INTRODUCTION**

The Reinforced Concrete frame building with URM infill walls are very common in Bangladesh and many other countries. Easy and low-cost constructing is known as a main reason for uses of the brick masonry in the developing countries. The purpose of masonry is mostly to protect inside of the structure from the environment and to separate internal spaces. In most of the cases of seismic resistant design, particularly in Bangladesh, the brick masonry infill walls in RC frame building is typically considered as non-structural elements. Therefore, this consideration may result inaccurate prediction of the lateral stiffness, strength, and ductility of the structure. Reluctance of numerous engineers to take into account the contribution of brick masonry infill is due to the inadequate knowledge in structural modelling and uncertainty involved in interaction between infill and RC frame.

In recent times several researchers (Decanni et al., 2004; Baran and Sevil, 2010 etc.) have compared experimental and analytical results of interaction between RC frame and URM infill walls. Such experimental results revealed that performance of URM infill walls inside RC frame varied with lateral loads applied on the structure (Decanni et al., 2004; Baran and Sevil, 2010). URM infill remains in contact with RC frame under very low lateral loads and hence there is composite action between RC frame and URM infill walls. Initial lateral stiffness increased for the URM infill model in compare to bare frame model. A number of research works have been done in past decades to generate acceptable model for structural analysis in order to account interaction between URM infill and RC frames. Among several models, equivalent diagonal strut model for infill panels is preferred

due to its simplification in URM behaviours. In this study, the structural model was developed in a software package Seismostruct v7.0 to perform structural analyses for the index building. The objective of this work is to compare the seismic performance of RC frame building with and without inclusion of unreinforced masonry walls.

## METHODOLOGY

### Modelling of Infill Wall

The most critical part of modelling of a RC frame with URM infill wall is to model the URM infill properly. There have been several research conducted in past studies to develop micro model for the numerical simulation of infill panels using two dimensional finite element (Ellul and D' Ayala, 2012), however, the diagonal strut model (see Fig.1) is still the most widely used and accepted by the researchers as its simplified approach for bulk analysis, and has been advocated in many documents and guidelines (CSA, 2004 and NZSEE, 2006).

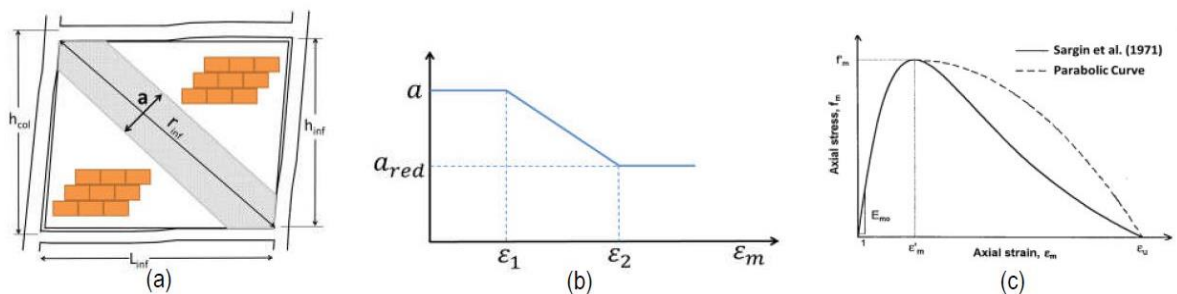


Fig.1: Diagonal strut for masonry infill panel modelling; (a) Equivalent diagonal strut representation of an infill panel, (b) Variation of the equivalent strut width as function of the axial strain, (c) Envelope curve in compression

Diagonal strut model utilizes a four-node masonry panel element for the modeling of infill panel. Six strut members are used to illustrate each panel. Every diagonal direction characterizes two parallel struts to carry axial loads across two opposite diagonal corners and a third one to carry the shear from the top to the bottom of the panel. The operation of fifth and sixth strut members activate on deformation of the panel as they only act across the diagonal that is on compression. Stiffness and strength of an infill panel is calculated from width of equivalent strut using formula proposed by Mainstone and Weeks (1970) and Mainstone (1971).

$$a = 0.175(\lambda_I h_{col})^{-0.4} r_{inf} \quad (1)$$

Where,

$$\lambda_I = \left[ \frac{E_m t_{inf} \sin 2\theta}{4E_c I_{col} h_{inf}} \right]^{\frac{1}{4}} \quad (2)$$

Where  $\lambda$  is the coefficient used to determine equivalent width of infill strut;  $h_{col}$  is column height between centerlines of beam;  $h_{inf}$  is height of infill panel;  $E_c$  is expected modulus of elasticity of frame material;  $E_m$  is expected modulus of elasticity of frame material;  $I_{col}$  is moment of inertia of column;  $r_{inf}$  is diagonal length of infill panel;  $t_{inf}$  is thickness of infill panel and equivalent strut; and  $\theta$  is angle whose tangent is the infill height-to-length aspect ratio.

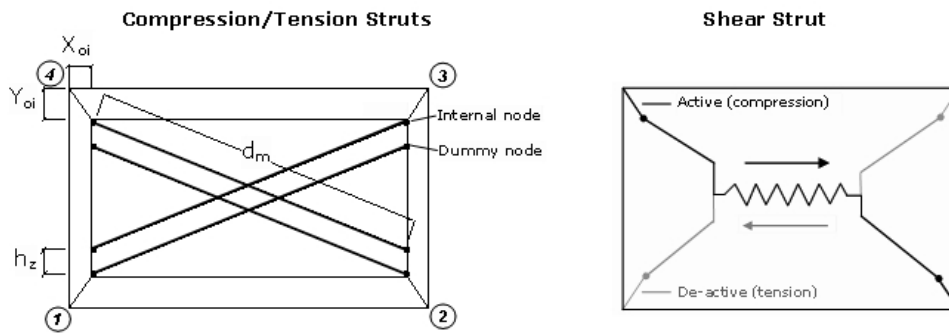


Fig.2: Equivalent strut model for infill panel (Crisafulli, 1997)

The selected building is modelled using finite element package software named SeismoStruct. SeismoStruct is able to predict large displacement behavior of space frames under static or dynamic loading, taking in to account both geometric nonlinearities and material inelasticity. Bare frame and infill frame model of the building is shown in Fig.3(a) and Fig.3(b) respectively.

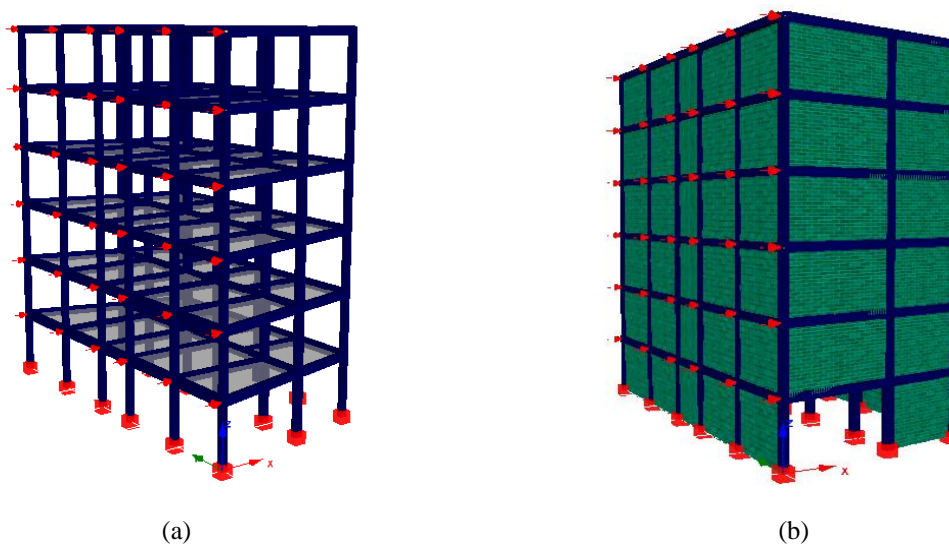


Fig.3: (a) Bare frame model; (b) URM Infill frame model

### Design Spectrum and Seismic Design

The design spectra in proposed BNBC is developed based on following relationship,

$$C_s(T) = \left[ 1 + (\eta \cdot 2.5 - 1) \frac{T}{T_B} \right], 0 \leq T \leq T_B \quad (3)$$

$$C_s(T) = S \cdot \eta \cdot 2.5, T_B \leq T \leq T_C \quad (4)$$

$$C_s(S) = S \cdot \eta \cdot 2.5 \left( \frac{T_C}{T} \right), T_C \leq T \leq T_D \quad (5)$$

$$C_s(T) = S \cdot \eta \cdot 2.5 \left( \frac{T_C T_D}{T} \right), T_D \leq T \leq 4S \quad (6)$$

$C_s$  depends on  $S$  and values of  $T_B$ ,  $T_C$  and,  $T_D$  which are all functions of the site class (in Fig.4) is the damping correction factors.  $Z$  represents seismic zoning coefficient,  $I$  is the structural importance factor and  $R$  is the response reduction factor.

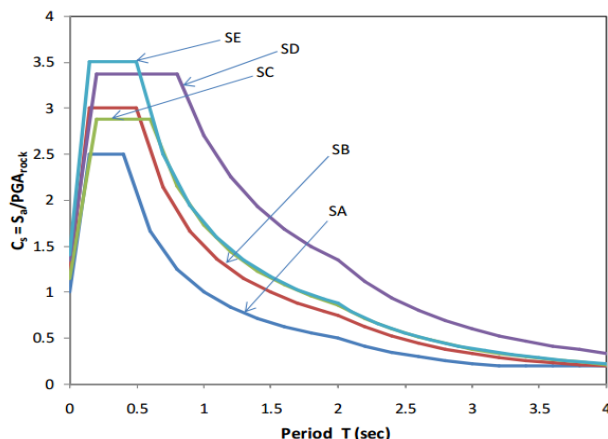


Fig.4: Normalized acceleration response spectrum for different site classes for proposed BNBC 2010.

## RESULTS AND DISCUSSION

Pushover analysis is performed by applying a controlled displacement (Response control) at the top of a particular frame. Capacity curve is determined for both configuration of the building. Pushover analysis provides non-linear force-displacement relationship of the Multi Degree of Freedom (MDOF) system. Relation between Normalized lateral forces and normalized displacements are assumed as Eq. (7) where,  $m_i$  is the mass of the  $i$ -th story. Displacements are normalized in such a way that  $n = 1$ , where  $n$  is the control node whereas  $n$  denotes roof level. Fig.5 to Fig.11 describes the step by step procedure for the determination of performance point for bare frame and URM masonry infill frame structure.

$$F_i = m_i \Phi_i \tag{7}$$

### Step-1: Pushover Curve for Bare and URM Frame Model

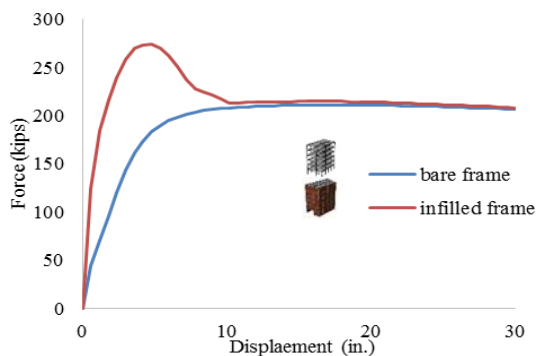


Fig.5: Pushover curve for bare frame and infill frame model

### Step-2: Demand Spectra in AD Format

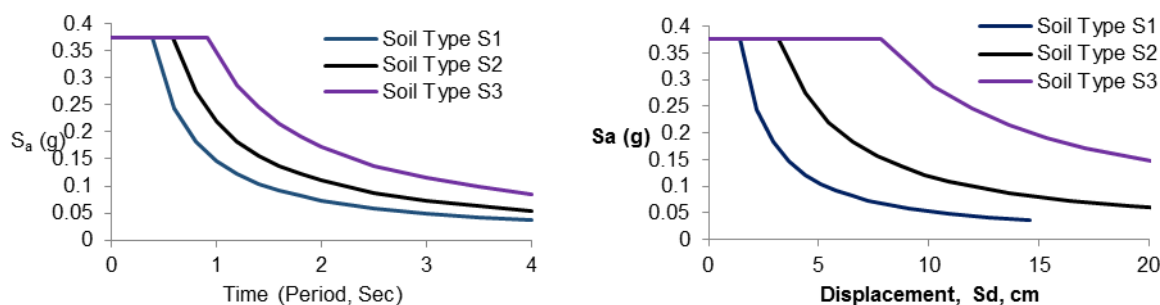


Fig.6: conversion of elastic acceleration spectra to demand spectra

### Step-3: Equivalent SDOF Model

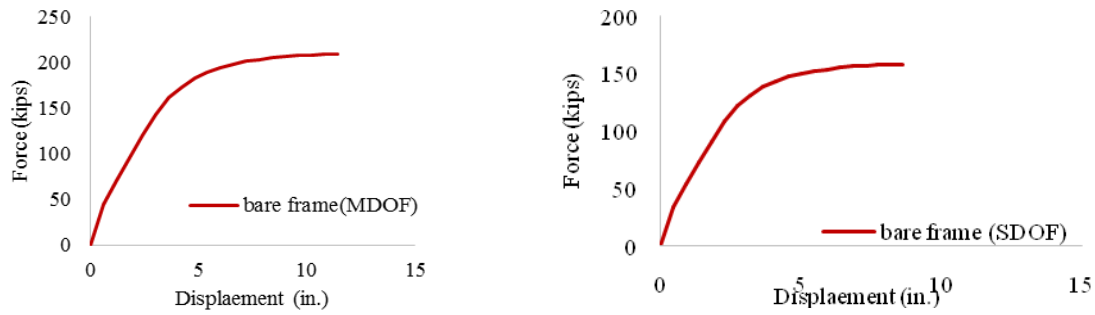


Fig.7: Pushover curve for MDOF bare frame model (left) and for equivalent SDOF model (right)

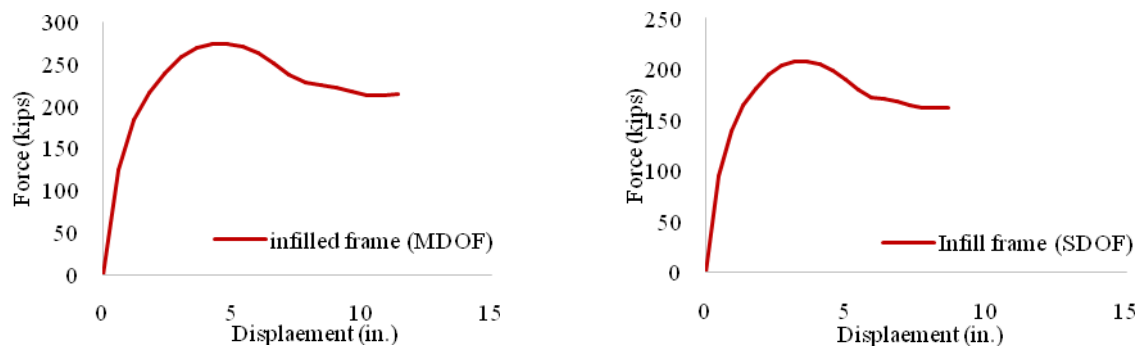


Fig.8: Pushover curve for MDOF infill frame model (left) and for equivalent SDOF model (right)

### Step-4: Equivalent Conversion of Pushover Curve to Capacity Curve

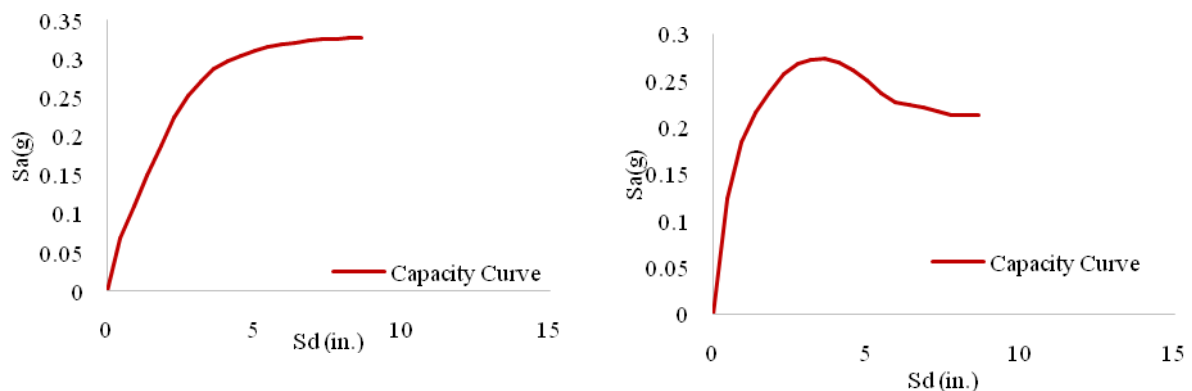


Fig.9: Capacity curve for bare frame model (left) and for infill frame model (right)

### Step-5: Superposition of Capacity Curve and Demand Curve

Intersection point of the capacity curve and the demand curve gives the displacement demand. Performance point of the selected building is obtained for both infill and bare frame model by superposition of capacity curve and demand spectra for soil type 1.

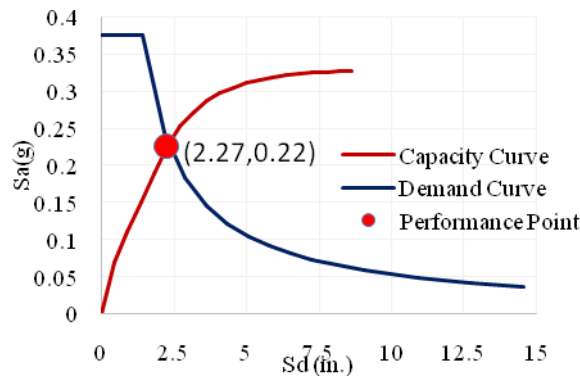


Fig.10: Capacity curve versus demand curve for bare frame model

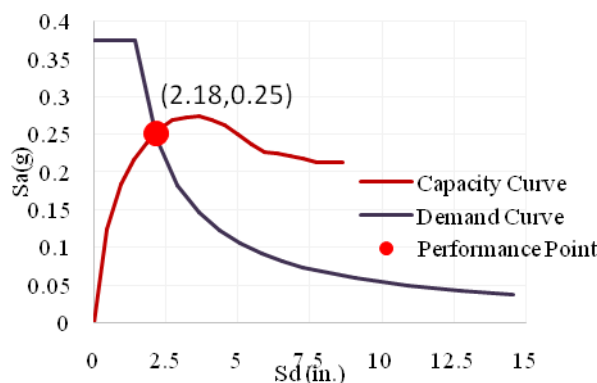


Fig.11: Capacity curve versus demand curve for infill frame model

## CONCLUSIONS

By closely observing, Fig.5 reveals that the pushover curve for infill frame structure has larger gradient than of structure without infill walls up to a certain displacement which indicates higher stiffness of the structure. However, this stiffness drops sharply at a particular value of displacement and the same trend is observed for further displacement value. Such behaviour figures out the fact that Inclusion of masonry wall in bare frame structures increases the lateral stiffness and resistance of RC frame building significantly. Although, Seismic performance of bare frame is found to be inferior to infill frame, ductility of the structure decreases with the inclusion of URM infill. Comparative response of bare frame and infill frame is summarized in Table 1.

Table 1: Comparative response of bare frame and infill frame model

Analysis types	Parameters	Bare Frame Structure	Infill Frame Structure
Nonlinear Static (Pushover)	Approximate Peak Loading Capacity (Kips)	200	280
	Yield Displacement (inch)	4.8	4.2
	Ultimate Displacement (inch)	11.4	11.4
Capacity Spectrum	$S_a$ (g)	0.22	0.25
	$S_d$ (inch)	2.27	2.18

## ACKNOWLEDGEMENT

The authors would like to acknowledge SeismoSoft for providing SeismoStruct v7.0 academic license which was used in this study.

## REFERENCES

- Baran, M and Sevil, T. 2010. Analytical and experimental studies on infilled RC frames. *International Journal of the Physical Sciences*, 5(13):1981-1998.
- Canadian Standards Association (CSA), Design of masonry structures (S304.1), Ontario, Canada, 2004.
- Crisafulli, FJ. 1997. *Seismic Behaviour of Reinforced Concrete Structures with Masonry Infills*, PhD Thesis, University of Canterbury, New Zealand.
- Decanini, L; Mollaloli, F; Mura, A and Saragoni, R. 2004. *Seismic performance of masonry Infilled R/C Frames*, Proceeding of the 13th World conference on Earthquake Engineering. Vancouver, B.C., Canada.
- Ellul, FL and D'Ayala, D. 2012. Realistic FE models to enable push-over nonlinear analysis of masonry infilled frames, *The Open Construction and building Technology Journal*, 6: 213-235.
- Mainstone, RJ and Weeks, GA. 1970. *The influence of bounding frame on the racking stiffness and strength of brick walls*, 2nd International Brick Masonry Conference, Stoke-on-Trent, UK.
- Mainstone, RJ. 1971. *On the stiffness and strengths of infilled frame*. Proceedings, Institution of Civil Engineers, Supplement IV, 57-90.
- Assessment and Improvement of the Structural Performance of Buildings in Earthquakes, 2006. Reported by New Zealand Society for Earthquake Engineering (NZSEE).



## **APPLICATION OF RECYCLED AGGREGATE IN CONCRETE: A REVIEW**

M. Nuruzzaman\* & M. Salauddin

*Department of Civil Engineering, Chittagong University of Engineering and Technology, Chittagong,  
Bangladesh*

*\*Corresponding Author: mnzshuvo@gmail.com*

### **ABSTRACT**

This study presents an overview of the development and application of recycled aggregate in the production of concrete. Nowadays, in a large part of the world, demolition of old and deteriorated buildings and traffic infrastructure, and their replacement with new ones is a usual phenomenon. As a consequence, the volume of demolished concrete is increasing day by day, which generates a lot of waste and ultimately pollutes the environment. However, because of rapid industrialization, production and utilization of concrete is rapidly increasing, which results in increased consumption of natural aggregate as the largest concrete component. Hence, the preservation of natural aggregates sources is being threatened day by day. On the other hand, the protection of the environment has become one of the major issues of our present world. The reduction of raw material consumption and energy consumption is critical elements in this regard. Therefore, recycling of demolished concrete for new construction is essential to preserve the natural resources as well as to solve the disposal problems of demolished concrete.

**Keywords:** Demolished concrete; recycling; recycled coarse aggregate

### **INTRODUCTION**

Nowadays, in a large part of the world, demolition of old and deteriorated buildings and traffic infrastructure, and their substitution with new ones is a usual phenomenon (Malešev et al., 2010). It is worth mentioning that the prime reasons behind these are a rearrangement of a city, expansion of traffic directions, changes of purpose, structural deterioration, & increasing traffic load, natural disasters, etc (Malešev et al., 2010; Kumar & Babu, 2015). As a consequence, the volume of demolished concrete is increasing day by day, which generates a lot of waste and ultimately pollutes the environment. Uddin (2007) stated that the global production of demolished concrete is estimated at 2–3 billion tons per year. Furthermore, Fisher & Werge (2009) reported that about 850 million tons of construction and demolition of waste are generated in the EU per year, which represent 31% of the total waste generation. Also, in the USA, the construction waste produced from building demolition alone is estimated to be 123 million tons per year (FHWA, 2004). Similar to many other countries also in Bangladesh, the volume of demolished concrete is increasing alarmingly due to the deterioration of concrete structures as well as the replacement of many low-rise buildings by relatively high-rise buildings due to the booming of real estate business (Uddin, 2007). The typical way of managing this material has been through its disposal in landfills. Consequently, the human environment is getting polluted incessantly because of such disposal of huge amount of construction waste.

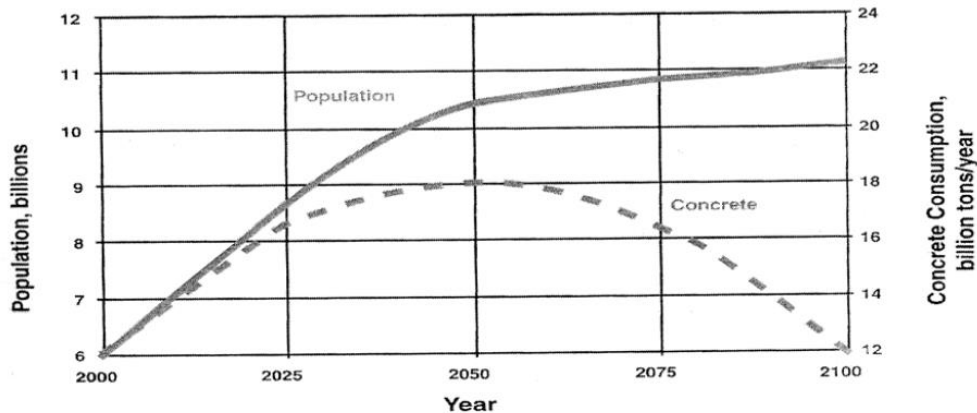


Fig. 1: Consumption of concrete and population in the world (Uddin et al., 2006)

However, because of rapid industrialization, production and utilization of concrete is rapidly increasing, which results in increased consumption of natural aggregate as the largest concrete component. For instance, two billion tons of aggregate are produced each year in the United States, is expected to raise to more than 2.5 billion tons per year by the year 2020 (FHWA, 2004). Crushing of concrete to produce coarse aggregate for the production of new concrete is one common means for achieving a more environmentally-friendly concrete. Hence, the preservation of natural aggregates sources is being threatened day by day. One of the ways to preserve natural aggregate is to utilize the recycled aggregate in the production of concrete (Uddin et al., 2006; Khalaf et al., 2004). Therefore, recycling of demolished concrete for new construction is essential to preserve the natural resources as well as to solve the disposal problems of demolished concrete. Recycling of demolished concrete will also provide other benefits, such as the creation of additional business opportunities, saving the cost of disposal, saving money for local government and other purchaser, helping local government to meet the goal of reducing disposal, etc. Based on this perspective, it is realized that concrete industry can be made sustainable through recycling of the demolished concrete.

### RECYCLED AGGREGATE

Recycling is the act of processing the used material for use in creating a new product. The usage of natural aggregate is getting more and more intense with the advanced development in infrastructure area. Recycled aggregate is comprised of crushed, graded inorganic particles processed from the materials that have been used in the constructions and demolition debris. Recycled aggregates are produced from the re-processing of mineral waste materials, with the largest source being construction and demolition waste. These wastes are normally composed of concrete rubble usually, constitutes the largest proportion of C&D waste. It has been shown that crushed concrete rubble, after separation from other C&D waste and sieved, can be used as a substitute for natural coarse aggregates in concrete or a sub-base or a base layer in pavements.

Recycling concrete wastes will lead to reduction in valuable landfill space and savings in natural resources. In addition to the environmental benefits in reducing the demand on land for disposing the waste, the recycling of construction and demolition wastes can also help to conserve natural materials and to reduce the cost of waste treatment prior to the disposal. If the technology and public acceptance of using recycled aggregate are developed, there will be no requirement for normal aggregate if 100% of demolished concrete is recycled for new construction (Malešev et al., 2010; Uddin et al., 2006). Therefore, the topic of recycling of the demolished concrete is getting considerable attention under sustainable development nowadays.

### RECYCLED CONCRETE AGGREGATE

Generally, recycled concrete aggregate (RCA) is made by following two-stages, crushing of demolished concrete and screening for the removal of contaminants such as reinforcement, paper, wood, plastics and gypsum (Malešev et al., 2010). A lot of research has been done with respect to the applicability of

recycled concrete in the production of concrete. The researchers applied different techniques in order to examine the suitability of RCA to produce sustainable concrete. Based on the literature study, it has been found that of recycled aggregates are suitable mainly for non-structural concrete applications (Yong & Teo, 2009).

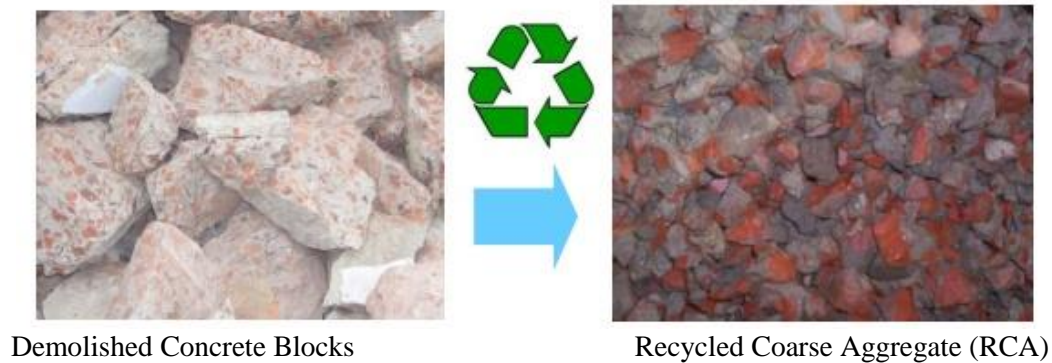


Fig. 2: Demolished Concrete Block and Recycled Coarse Aggregate (Uddin et al., 2006)

Concrete made with such recycled concrete aggregate is called recycled aggregate concrete (RAC). The activities of renovation and demolition in the maintenance and modernization of buildings generate large amounts of solid waste and rubble, adding to the already vast and continuously increasing solid waste stream. Currently, there is a widespread move to adopt new operational strategies aimed at prevention and minimization of the waste generation as close as possible to the sources aiming for a responsible pursuit of environmentally sustainable developments. This development is primarily induced by aspects of economics such as rising tip charges, transport distances and fuel costs, which are forcing demolition contractors to find other less costly options to dispose of building and demolition waste than at waste management centers and landfill sites.

The use of recycled concrete aggregate (RCA) as an alternate for dense-graded aggregate base course (DGABC) applications over the recent years have been approximately 10% to 15%. Presently 60 to 70 percent of demolished concrete is using as sub-base course aggregate for road construction. Researchers are continuing investigations to utilize recycled aggregate in new construction effectively. Most of the contractors are left with the decision as to which material to be used where their usage of RCA is seemingly based on cost. The aggregate particles of recycled concrete compare well to conventional mineral aggregates in that they possess good particle shape, high absorption, and low specific gravity. Recycled concrete aggregate has also been shown to have no significant effect on the volume response of specimens to temperature and moisture effects.

### PROPERTIES OF RECYCLED AGGREGATE

Based on the literature study, when demolished concrete is crushed, a certain amount of mortar and cement paste from the original concrete remains attached to stone particles in recycled aggregate. Certainly, this attached mortar is the main reason for the lower quality of RCA compared to natural aggregate (NA). Recycled aggregates typically are of poor quality compared with natural aggregates due to lower stiffness caused by crushing of waste concrete and higher water absorption capacity given by old cement paste attached to the surface of recycled aggregate. The properties of RCA in comparison to the Natural aggregate are listed below (Malešev et al., 2010):

- ✓ increased water absorption
- ✓ decreased bulk density
- ✓ decreased specific gravity
- ✓ increased abrasion loss
- ✓ increased crushability
- ✓ increased quantity of dust particles
- ✓ increased quantity of organic impurities if concrete is mixed with earth during building demolition

## **APPLICATION OF RECYCLED AGGREGATE**

Application of recycled concrete is important as it helps to promote sustainable development in the protection of natural and reduces the disposal of demolition waste from old concrete. After World War II, the applications of recycled aggregate in construction have started by demolished concrete pavement as recycled aggregate in stabilizing the base course for road construction (Olorusongo, 1999). Yong (Khalaf et al., 2004) reported that recycled concrete can be applied as many types of general bulk fills, bank protection, sub-basement, road construction, noise barriers and embankments. Furthermore, it can be applied to soil-cement pavement bases, lean-concrete bases, structural grade concrete and bituminous concrete (FHWA, 2004; Yong & Teo, 2009). Recycled concrete can be also used in the production of concrete for pavements, shoulders, median barriers, sidewalks, curbs and gutters, building and bridge foundation. Growth in the use of recycled concrete for retaining wall backfill, portland cement concrete mix, landscaping rock, drainage aggregates, and erosion control is also happening (Uddin et al., 2006).

## **BENEFITS OF RECYCLED AGGREGATE**

The advantages associated with the recycling of demolished concrete can be pointed as below (Kumar & Babu, 2015; Poon et al., 2002, Xiao & Falkner, 2007; Olorusongo, 1999):

- ✓ Saving of natural resources
- ✓ Creation of additional business opportunities
- ✓ Saving cost of disposal of demolished concrete
- ✓ Saving money for local governments and other purchasers
- ✓ Saving energy when recycling is done at site
- ✓ Helping local government to meet their goal of reducing disposal and
- ✓ Minimizing hazards to collect coarse aggregate from different natural resources

## **CONCLUSIONS**

In this day and age, the world is concern as well as passionate about reducing, recycling and reusing. Earlier, the waste from non-biodegradable material like demolished concrete or this type of project would end up in a landfill, costing a huge amount of space. Auspiciously, the scenario is not the same any longer. In recent years, the researchers have found that it is possible to recycle the old concrete. Even though the word “recycled concrete” could be a little bit perplexing, this recycled concrete is extremely robust and reliable. Review of several studies suggested that the use of recycled materials has a positive impact on different aspects. This includes the benefits in enhancing the sustainability of the construction industry while reducing cost, providing solutions to environmental pollution and reducing the need for natural resources.

## **REFERENCES**

- and Technology, Vol. 4, pp. 18584-18591, ISSN 2319 - 8753.
- Assessments for Construction Applications—A Materials Flow Analysis.*” U.S. GEOLOGICAL SURVEY, Bolden, J., Lebdeh, T. A. and Fini, E. (2013), “*Utilization of recycled and waste materials in various Central Region, Denver, Colorado.*”
- Concrete Aggregate—State of the Practice*”, National Review 2004; U.S. Department of Transportation *Concrete as Coarse and Fine Aggregates.*” Paper presented at the International Conference on the *Concrete Production*”, Journal of Sustainability, Vol. 2, pp. 1204-1225, ISSN 2071-1050.
- Concrete*”, UNIMAS E-Journal of Civil Engineering, Vol.1, Issue 1, pp. 1-6.
- Conference on Sustainable Construction Materials and Technologies, June 28 - June 30, 2010, *construction applications.*” American Journal of Environmental Science, Vol.9, Issue 1, pp. 14-24.
- Federal Highway Administration: Washington (FHWA) (2004), “*Transportation Applications of Recycled*” Federal Highway Administration: Washington, DC, USA, 2004; pp. 1-47.
- Fisher, C.; Werge, M. (2009), “*EU as a Recycling Society*”, ETC/SCP Working Paper 2/2009; Available

- Infrastructure, Lahore, Pakistan, Vol. 2, pp. 1077-1090.
- International Conference on Advances in Cement Based Materials and Applications to Civil  
International Seminar on Exploiting Wastes in Concrete held at the University of Dundee, Scotland, UK
- Khalaf, F.M. et al. (2004), "Recycling of demolished masonry rubble as coarse aggregate in Concrete:  
Kumar K. S., Babu S. D. (2015), "Experimental Study of Recycled Aggregate Concrete with Partial  
Malešev M.; Radonjanin V. and Marinković S. (2010), "Recycled Concrete as Aggregate for Structural  
Olorusongo, F.T. (1999). "Early Age Properties of Recycled Aggregate Concrete". Proceeding of the  
on 7 September 1999, pp. 163-170.  
online: <http://scp.eionet.europa.eu.int> (accessed on 10 January 2013).
- Poon, C.S., Shui, Z.H. and Lam, L. (2002), Advances in Building Technology, Pages 1407 – 1414.  
Regeneration and Conservation of Concrete Structures (RCCS), Nagasaki, Japan.  
Replacement of Cement by Fly Ash", International Journal of Innovative Research in Science, Engineering  
review. " ASCE J Mater Civil Eng (2004); pp. 331–340.
- Uddin, M.T. (2007), "Sustainable Development of Concrete Technology", CBM-CI International  
Uddin, M.T., Khan, A. Z. and Mahmood, A.H. (2015), "Recycling of Demolished Brick Aggregate  
Uddin, M.T. et al. (2006), "Recycling of Demolished Concrete as Coarse Aggregate", ACBM/ACI  
Uddin, M. et al. (2006), "Recycling of Concrete Made with Brick Aggregate." Second International  
Università Politecnica delle Marche, Ancona, Italy.
- Wilburn, D. R. and Goonan, T. G. (1999), "Aggregates from Natural and Recycled Sources-Economic  
Workshop, Karachi, Pakistan, December 10-11, 2007.
- Xiao, J. and Falkner, H. (2007), Construction and Building Materials, Vol. 21, Issue 2, pp. 395 – 401.
- Yong, P.C. and Teo, D.C.L. (2009), "Utilisation of Recycled Aggregate as Coarse Aggregate in

## **UTILIZATION OF PLASTIC WASTE IN CONCRETE AS A PARTIAL REPLACEMENT OF FINE AGGREGATE**

S. Das<sup>1\*</sup>, M. T. Alam<sup>2</sup> & I. Chowdhury<sup>2</sup>

<sup>1</sup> *Institute of Earthquake Engineering Research, Chittagong University of Engineering and Technology, Chittagong, Bangladesh*

<sup>2</sup> *Department of Civil Engineering, Chittagong University of Engineering and Technology, Chittagong, Bangladesh*

*\*Corresponding Author: shagata.joy@gmail.com*

### **ABSTRACT**

The onset of industrialization and the sustained urban growth of large population causes the build-up of large amount plastic wastes. Because of the non-biodegradable property of plastics, decomposition is not possible. So, they remain in the environment for a long time, pollute soil and water that creates ecological problems. If these harmful non-biodegradable materials can be substituted as a construction material by using in concrete, that will be a significant source of plastic wastes management. This paper deals with the investigation of using grinded plastic wastes as a partial replacement of fine aggregate in concrete and to find the optimum percentage of plastic that can be used in concrete without reduction of concrete strength or with a slight amount of strength reduction which are considered as negligible. Plastic wastes consist of discarded old computers, TVs, refrigerators, radios, old electrical and electronic equipment were collected at first and then grinded through using a pulverizing machine. Through ACI method, a mix design was made for concrete of grade M-28. The proportion of mixing of the grinded plastic wastes are 2 %, 4 %, 6 %, 8 % & 10 %. The specimens have been cured for 7 & 28 days. Compressive strength and Tensile strength test of concrete were conducted. As the melting temperature of the plastic is low thus it is susceptible to temperature. So, it is important to focus on the impact of heat in concrete strength when using grinded plastic. Post-heat compressive strength test was also conducted. After obtaining the data, they were analyzed by comparing with a controlled specimen. Result had showed that there was slight reduction in strength with the mix proportion of 2%, 4% and 6% of grinded plastic wastes.

Keywords: Non-biodegradable materials; plastic waste; compressive strength; tensile strength; temperature

### **INTRODUCTION**

Plastic waste is a pertinent part of the complete amount of waste worldwide. Due to rapid industrialization and civilization the quantity of plastic waste generated each year, especially computers, televisions and all other kinds of electronic wastes has assumed alarming proportions. According to a projection of the International Association of Electronics Recyclers (IAER) in 2006 that 3 billion electronic and electrical appliances would become WEEE (Waste Electrical and Electronic Equipment) by 2010. Now it is 2015 and so obviously the projected amount have already acceded. Each year more than 22.88 million tons of electronic waste generated in Bangladesh (ESD, 2010). A report shows that, About 50% assembler companies are sold out the generated waste, 30% are dumped, 20% are stored for long time. 30% repairers stored the old TV sets for repairer and farther uses, 15% dumps it, 5% didn't give any importance to inform. Among the customers 40% sold rejected sets to the repairers, 10% through away and 20% reuses it after repairing. Also, Some eight million metric tons of plastic waste makes its way into the world's oceans each year and the amount of the debris is likely to increase greatly over the next decade unless nations take strong measures to dispose of their trash responsibly, new research suggests. The report, which appeared in the journal Science on Thursday, is the most ambitious effort yet to estimate how much plastic debris ends up in the sea. The amount of plastic that entered the oceans in the year measured, 2010, might be as little as 4.8 million metric tons or as much as 12.7 million. So it is a great concern to dump it. But Traditional landfill is not

environmentally friendly way to get rid of. In the disposal process is also very difficult to accomplish the EPA regulations. How to reuse the non-biodegradable Electronic Waste and Plastic Waste become an important research topic. And so we have made an effort to use this non-biodegradable components in concrete industry as partial replacement of fine aggregate. This study alleviates the crisis in decomposition of non-biodegradable thermoplastic. It will also provide a significant substitutional way to control the huge amount of wastes plastic and a substitute construction materials at a very low cost. The main purpose of this project is to study the strength of concrete due to replacement of fine aggregate by plastic wastes in concrete. The variation of compressive strength, tensile strength of concrete using plastic, the optimum replacement level of sand by plastic for maximum strength, minimization of the cost of construction and making environmentally friendly concrete by using plastic as a replacement of sand, which otherwise been dumped and make environmental hazard, all are the main objectives of this project.

## METHODOLOGY

### *Experimental Investigation*

The aim of the experimental programme is to compare the properties of concrete made with and without plastic, used as fine aggregate.

### *Experimental Programme*

For preparing the testing specimen, an ACI mix design has been conducted for concrete with strength of M28. Fine aggregate has been replaced by plastic as proportion of weight by 0%, 2%, 4%, 6%, 8% and 10%. The specimen have been tested for 7 days & 28 days curing period.

### *Mix Design*

An ACI Mix Design has been conducted for M28 strength of concrete. Specification of Materials according to ACI Mix Design- Fine Aggregate (796 kg/m<sup>3</sup>), Coarse Aggregate (992 kg/m<sup>3</sup>) & Cement (422.22 kg/m<sup>3</sup>).

### *Material Properties*

Cement:		Ordinary Portland Cement(OPC)	
SL No.	Characteristics	Value Obtained	Value ASTM
1.	Fineness (cm <sup>2</sup> /gm.)	253	>=280
2.	Normal Consistency		
3.	Soundness		
4.	Setting Time: Initial Setting: Final Setting:	56 min 108 min	>=45 min <=6 hr. 15 min

Properties of Aggregate		
Properties	Fine Aggregate	Coarse Aggregate
Fineness Modulus	2.6	4.54
Specific Gravity	2.4	2.8
Unit Weight	1580 kg/m <sup>3</sup>	1600 kg/m <sup>3</sup>
Absorption Capacity	.36 %	.25 %
Moisture Content	5.26 %	2.04 %

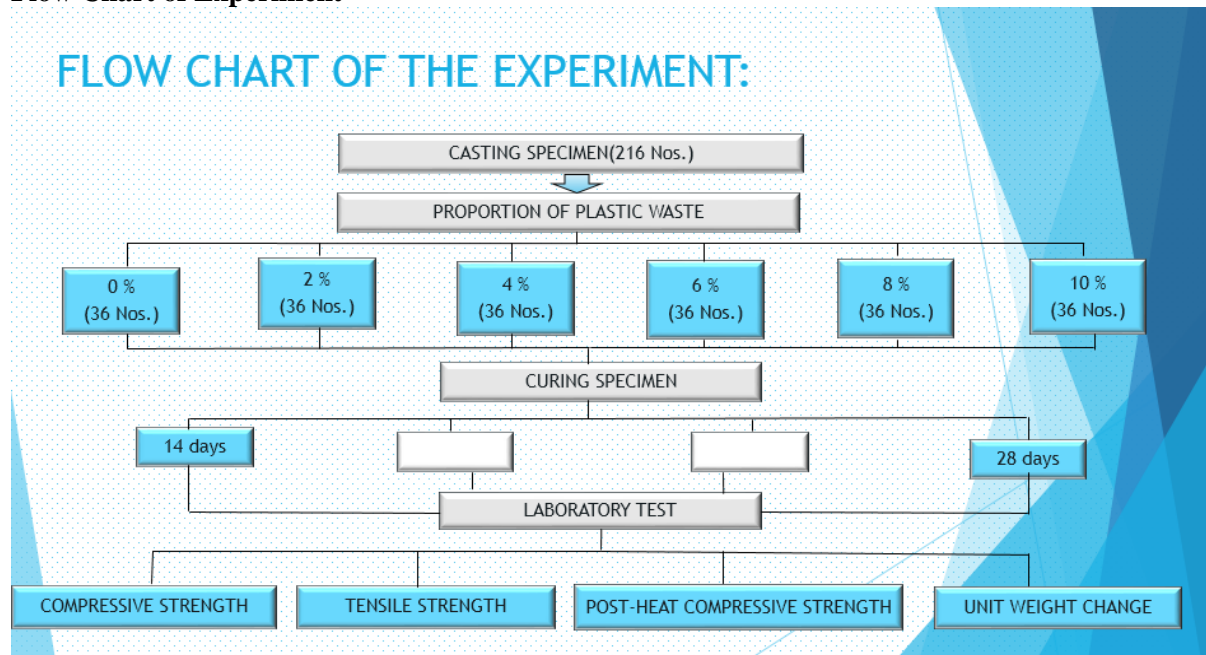
### *Plastic Wastes*

At first, various types of plastic are collected from different sources like old TV, electronic board, old computer monitor etc. Then all of them are grinded through grinded machine into small pieces. As there residues some big particle of plastic after grinding process, they are sieved through No.4 sieve. Then they have been collected for further use in concrete as a partial replacement of fine aggregate.

### Properties of Plastic Wastes

PROPERTIES NAME	VALUE
Specific Gravity	1.01
Absorption (%)	<0.2
Color	White
Fineness Modulus	6.58
Shape	Angular
Melting Temperature	80-85° C

### Flow Chart of Experiment



### Design Strength Test:

For the testing specimen, mix design of 28 MPa concrete have been conducted. For the design strength test, 3 cylindrical specimens of 6 inch dia and 12 inch length, have been casted with different water cement ratio. They have been cured for 28 days in fresh water. After 28 days curing period, they have been taken for the compressive strength test. Three different water ratio i.e .40, .45 and .50 have been used for casting the test specimens. After conducting the test, it has been found that .40 water cement ratio have given the required strength for the design test specimen. So we have used .40 w/c ratio for casting the concrete cube specimen.

### Compressive Strength with regard to Different Water Cement Ratio

Water Cement Ratio	Specimen No	Applied Load(KN)	Average Applied Load(KN)	Average Compressive Strength(MPa)
0.4	1	50	51.67	28.41
	2	52		
	3	53		
0.45	1	49	49.00	26.80
	2	48		
	3	50		
0.5	1	48	47.33	25.79
	2	48		
	3	46		





Fig. 1 : Cylinder Compressive Strength Test



Fig. 2 : Specimen Under Applied Compression Force



Fig. 3 : Specimen Under Applied Tensile Force



Fig. 4 :Crushed Concrete Cube

## RESULTS AND DISCUSSIONS

### GRAPHICAL REPRESENTATION OF COMPRESSIVE STRENGTH(MPa):

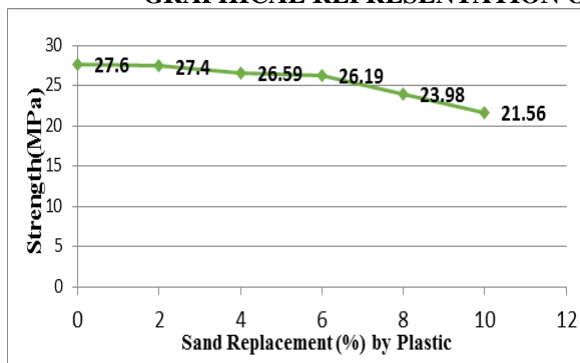


Fig. 5: Compressive Strength of Concrete(7 Days)

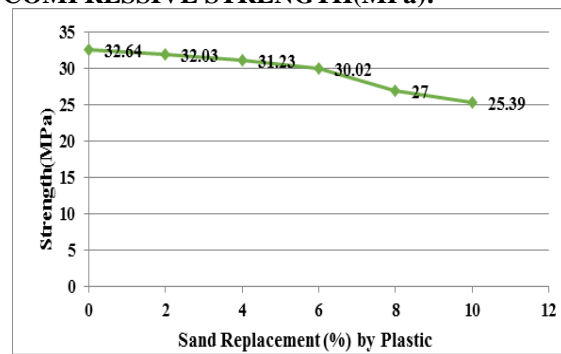


Fig. 6: Compressive Strength of Concrete (28 Days)

### GRAPHICAL REPRESENTATION OF POST HEAT COMPRESSIVE STRENGTH(MPa):

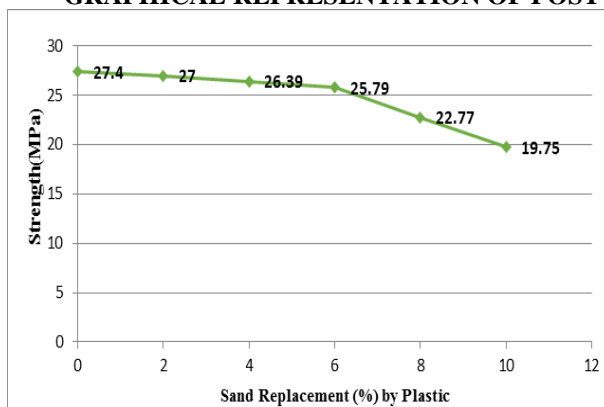


Fig. 7: Post Heat Compressive Strength of Concrete (7 Days)

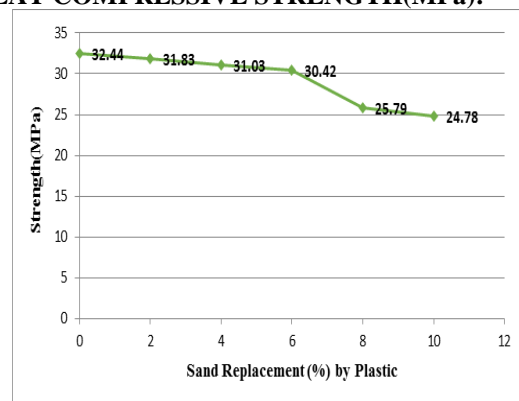


Fig. 8: Post Heat Compressive Strength of Concrete (28 Days)

**GRAPHICAL REPRESENTATION TENSILE STRENGTH(MPa):**

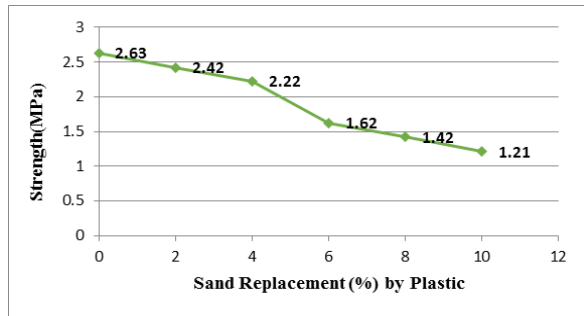


Fig. 9: Tensile Strength of Concrete(7 Days)

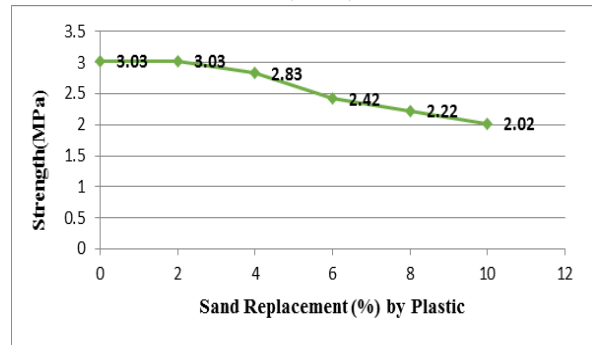


Fig. 10: Tensile Strength of Concrete (28 Days)

**GRAPHICAL REPRESENTATION OF VARIATION BETWEEN COMPRESSIVE STRENGTH AND POST HEAT COMPRESSIVE STRENGTH:**

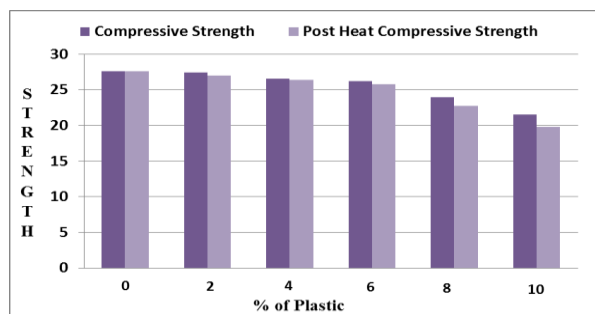


Fig. 11: Compressive Strength vs Post Heat Compressive Strength(7 Days)

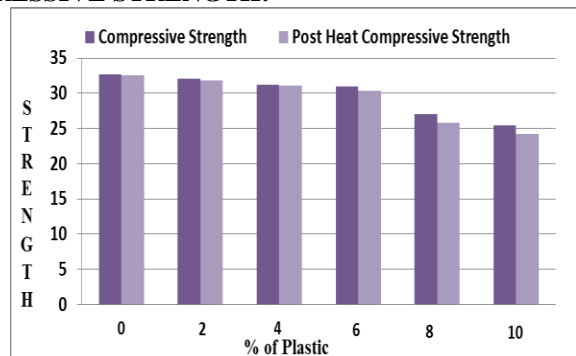


Fig. 12: Compressive Strength vs Post Heat Compressive Strength(28 Days)

**DISCUSSION:**

In this test all laboratory test are done carefully. In spite of these experimental result may vary from actual result due to following reason:

In the compressive, tensile and post heat compressive strength test mixing is done manually whereas mechanical mixing give actual strength.

The specimen are cured in open air water tank, which may contain impurities. As a result the strength may affected.

Although the specimen must be dried up before the test, in the rainy season it is very difficult to dry, so actual result may vary.

In post heat compression test the thermal exposure of mechanical oven could not be controlled properly due to mechanical error, so the actual result may vary.

**CONCLUSIONS**

Following conclusions can be made based upon the studies we have conducted:

1. Compressive strength of concrete has been found decreasing gradually with increasing of adding plastic. From our investigation, it has been found that 28 days compressive strength for 2 % is 32.03 MPa, 4% is 31.23 MPa, 6% is 30.02 MPa, 8% is 27 MPa and 10% is 25.39 MPa. There is also a sharp decrease in compressive strength with percentage of 8 % and 10 % of plastic. That clearly represents that plastic can be used as a substitute material by 2%, 4 % and 6 % of sand by weight because it provides sufficient compressive strength. But for further increase in percentage of plastic the compressive strength goes down rapidly.

2. With the increase in percentage of plastics that is used as a partial replacement of sand the post-heat compressive strength also decreases. From the results, the 28 days Post-heat compressive strength for 0% is 32.44 MPa, 2% is 31.83 MPa, 4% is 31.03 MPa, 6% is 30.42 MPa, 8% is 25.79 MPa & 10% is 24.78 MPa. It clearly shows that if we increase the percentage of plastics beyond 6% the post-heat compressive strength reduces rapidly.

Introduction of plastics in concrete tends to make concrete ductile, hence increasing the ability of concrete to significantly deform before failure. This characteristic makes the concrete useful in situations where it will be subjected to harsh weather such as expansion and contraction, or freeze and thaw.

3. For 1 m<sup>3</sup> concrete, It has been found that replacing sand by 2 % of plastic wastes, sand is substituted by 15.92 Kg of plastic .Replacing sand by 4 % of plastic wastes, sand is substituted by 31.84 Kg of plastic. Replacing sand by 6 % of plastic wastes, sand is substituted by 47.76 Kg of plastic .So, when it would be used in large scale in construction site, there would be a significant way to control this huge amount of plastic wastes that have to be dumped.

#### **SCOPE FOR FURTHER RESEARCH:**

The use of recycled plastics in concrete is relatively a new development in the world of concrete technology and lot of research must go in before this material is actively used in concrete construction. The use of plastics in concrete lowered the strength of resultant concrete, therefore, the research must be oriented towards ternary systems that helps in overcoming this drawback of use of plastics in concrete. Emphasis has been given to grind the waste into fine powder and mix into such proportion so as to achieve maximum packing density which may result to increase in compressive strength.

#### **NEED FOR FURTHER WORK:**

It is necessary to work out a project proposal to carry out further studies on various aspects such as collection, processing and effective utilization of this waste material. To start with, such a study could be initiated with the following components:

1. Estimation of the types, quantity and useful components present in the waste plastic materials in the city and surrounding areas.
2. Methodology for collection and sorting out the useful components of the plastic waste.
3. Methodology for processing the plastic bags as required for use in the preparation of modified bitumen, including cleaning, shredding and further processing of the plastic waste materials.
4. Identification of two or three construction companies / entrepreneurs who could incorporate appropriate mixing units in their hot mix plant to add and mix the required proportion of the processed plastic additive.
5. Carrying out further laboratory investigations, construction of some test tracks and field studies on the performance of concrete using the modified concrete.
6. Preparation of specifications and standards for the construction industry. It is hoped that on completion of the above project, the plastic waste materials will be put to effective use in construction industry, resulting in improved environmentally friendly concrete structures and also relief from the waste plastic materials being littered all around urban areas.

#### **REFERENCES**

- Ghernouti Y; Rabehi B; Safi B and Chaid R. 2012. Use of recycled plastic bag waste in the concrete, Volume 8, ISSN 1314-7269.
- Kumar M and Goyal, S. 2008. Laboratory investigation of the properties of concrete containing recycled plastic waste.
- Tomas, UG. 2014. Effect of Thermoplastic as Fine Aggregate to Concrete Mixture, IJAST, 62:31-42.
- Zoorob SE and Suparma BL. 2000. Laboratory design and investigation of continuously graded asphaltic concrete containing recycled plastic aggregate replacement, Cement and Concrete Composite 22-233-242.
- Pantsios A. 2015. 8 Million Metric Tons of Plastic Dumped Into World's Oceans Each Year, <http://ecowatch.com/2015/02/16/8-million-tons-plastic-dumped-into-oceans/> [Accessed 16 February 2015].
- Schwartzfeb J. 2015. Study Finds Rising Levels of Plastics in Oceans, [http://www.nytimes.com/2015/02/13/science/earth/plastic-ocean-waste-levels-going-up-study-says.html?\\_r=0](http://www.nytimes.com/2015/02/13/science/earth/plastic-ocean-waste-levels-going-up-study-says.html?_r=0) [Accessed 13 February 2015].
- Wikipedia, Compressive Strength, [https://en.wikipedia.org/wiki/Compressive\\_strength](https://en.wikipedia.org/wiki/Compressive_strength) .

# **A DETAILED INVESTIGATION OF REINFORCED CONCRETE COLUMN JACKETING: EXPERIMENT, THEORY AND NUMERICAL ANALYSIS**

K. S. Ahmed & M. Riaz\*

*Department of Civil Engineering, Military Institute of Science & Technology, Dhaka, Bangladesh  
\*Corresponding Author: riazcity7239@gmail.com*

## **ABSTRACT**

In recent days, Reinforced Concrete (RC) column jacketing is been increasingly used in structural strengthening in Bangladesh. This research work investigates the structural capacity enhancement of column by RC jacketing. Twelve jacketed short column samples composed of 25 mm and 31.5 mm jacket thickness were experimented for axial capacity. Samples vary in terms of use of surface preparation, welded ties, and change of clear cover in jacketed part. Analytical equations in terms of Interaction Diagram are formulated. As an outcome, a software is developed to analyse and compare the capacity under combined compression with uniaxial bending. Tested sections are modelled in ETABS 2015 and SAP 2000 for Finite Element analysis. Experimental result shows that new concrete collapses earlier at the interface than that of the old concrete. Welding jacket ties contribute to axial capacity by resisting rebar buckling. Proposed analysis accounts the effect of interface bonding thus differs with Japanese code, ETABS, and SAP. However, test results validated the analytic axial capacity at an accuracy of 89 to 96%. Hence a bondage coefficient of 0.85-0.95 is proposed in determining axial capacity.

Keywords: Column; retrofitting; jacketing; interaction diagram; Finite element

## **INTRODUCTION**

In order to avoid potential earthquake hazard, latest Bangladesh National Building Code (BNBC)-2015 guideline demands more structural resistance that suggests to strengthen many existing building structures of Bangladesh. Recent earthquakes, Rana Plaza incident and some other structural hazards raised the attentions towards the structural strengthening. Previously, many buildings were designed neither following the guideline nor considering lateral load. In addition, changes in live loads and user facilities, deterioration of the load carrying elements, design errors, poor construction quality during erection, and aging of structure, addition and alteration of existing structure force the users to strengthen the structural elements. Column being the most important structural element requires the utmost priority to be retrofitted. In recent years, column jacketing is commonly used to enhance the strength and stiffness of existing RC structure. Applications of RC column jacketing has already been executed in some garments buildings of Bangladesh. Still there is a large number of building structures that requires strengthening work immediately.

Effect of surface preparation, failure criteria and capacity of concrete jacketing has been experimentally and analytically investigated in the past by Bett et al. (1988), Saatcioglu and Ozcebe (1989), Alcocer and Jirsa,(1993), Erosy et al.(1993), Park and Rodriguez(1994), Stoppenhagen et al. (1995), Abu-Tair et al.(1996), Austin et al.(1999), Climaco and Regan (2001), Julio et al.(2003), Eduardo et al. (2005), Beushausen and Alexander (2008), Yuce et al. (2007), Roberto et al. (2008), H. Sezen and Eric A. Miller (2009), Stephanos E. Dritsos et al. (2010), D. W. Zhang et al.(2013), Veena M and Mini Soman (2014) and M. G. Marques et al. (2015). Indian code [3] and Japanese code [4] has separate methodology and equations for designing jacketed section. In Bangladesh, analysis and constructional methodology are recently published as guideline [6] that is modified and based on Japanese guidelines. Due to increasing use of RC jacketing, engineers need a simplified, time saving design and analysis approach. However, no significant research work has been reported yet and also the analysis and design guideline for RC column jacketing is yet to be established authentically.

This paper investigates the structural capacity enhancement of column by RC Jacketing. Hence, experimental investigation on jacketed column were carried out to determine load carrying capacity under pure compression. Simplified analytical equations are proposed to estimate jacketed column capacity in terms of Interaction Diagram which was compared with that of derived from Japanese retrofitting codes. Tested samples are modelled in ETABS 2015 & SAP 2000 v17 for Finite Element (FE) analysis. Finally, a computer program is developed which is able to analyse and compare the capacity of jacketed sections under combined compression with uniaxial bending.

## EXPERIMENTAL INVESTIGATION

Twelve short column samples of 610 mm height with a cross section of 102 mm x 102 mm were used as Reference Sample (RS). Four 8 mm bar were used as longitudinal reinforcement. Tie (2.5 mm) with 6.5 mm clear cover (CC) were used at 150 mm spacing. To depict old column section comparatively weaker concrete was used in RS. Eleven samples were retrofitted using RC jacketing with 25 mm and 31.5 mm jacket thickness. Eight longitudinal bars were used with the same diameter as RS. Ties were spaced at 100 mm. Other than two samples as mentioned in Table 1, typical CC was kept as 12.7 mm. Brick and stone chips of 19 mm and 12.7 mm downgraded respectively were used. Local and Sylhet sand of Fineness Modulus (FM) 1.1 and 2.2 respectively were used in test. Mix ratio was 1:2:4 and 1:1.5:3 by percent of volume for RS and jacketed samples respectively. Before jacketing surface were roughened using hand chisel. Afterwards, sand blasting was carried out using coarse sand of FM 2.2. Samples are named according to their thickness. Suffix letter used to describe the jacketing process; 'N'-no bonding agent, 'B'-surface prepared and bonding agent, 'M'- monolithic casting, 'W'-welded ties, and 'C' change of clear cover. CC was changed from 12.7 to 8.5 mm and 15 mm for 25 mm and 31.5 mm jacket thickness respectively.

Compressive capacity was tested in Universal Testing Machine (UTM) as in Fig. 1. Steel base plate of 205 mm x 205 mm cross section and 15 mm thick was used for uniform distribution of axial load. Load was applied at a rate of 1 mm/ min rate. Machine was programmed to stop at 40 % strain after reaching to the maximum axial load. Peak axial capacity was displayed in both the dial meter and in computer monitor system generating required graph of load, stress and strain.

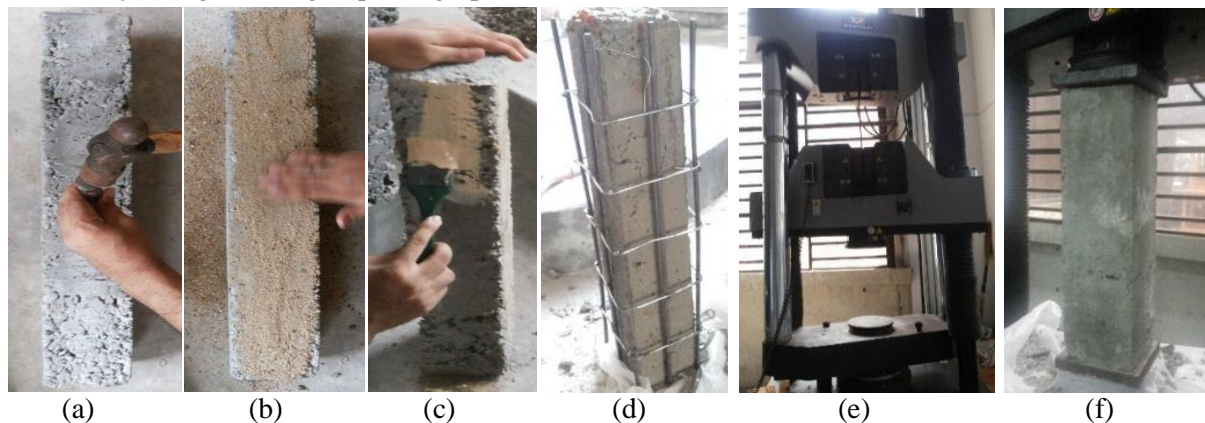


Fig. 1: (a) Surface roughening (b) Sand blasting (c) application of epoxy bonding agent (d) Jacketing of sample (e) UTM machine (f) Test Setup

## ANALYTIC ASSESSMENT

Both weighted average concrete strength ( $f'_{c' avg}$ ) and old concrete strength ( $f'_{c' old}$ ) are used for analysis of jacketed section as in [6] and [7]. However, lower elastic modulus need to be considered in design as mentioned in [2]. Compressive strength is increased for the active confinement determined by various equations by Scott et al. (1982), Uzumeri (1982), Mander et al. (1988) and Yong et al. (1988). In this regard, a concrete model is proposed to account confining stress generated by the jacket thickness. Effect of longitudinal reinforcement is negligible in pure compression according to P. Christou et al. (2013). Thus, thickness of jacket concrete in between longitudinal bar and old column face  $t_{jacket inner}$  is only used to determine confining stress. Volumetric ratio of the concrete to old column sections  $\rho_{concrete} = (4 \times t_{jacket inner}) / b_0$  [Modified to concrete according to FRP formula of R. Benzaid and H.A.

Mesbah, (2013)]. Confinement coefficient  $k_e = 1 / (1 - \rho_{concrete})$ . Tensile strength of concrete  $f_{rc}$  and volume of confine concrete to the volume of column section ratio  $\rho_{cc}$  is determined to find out confining stress  $fl' = 0.5 \times k_e \times \rho_{cc} \times f_{rc}$ . Finally jacketed compressive stress  $f_{c' Jacket}$  is determined using Mander concrete model [5].

### Proposed Interaction Diagram Equations

Simplified five-point interaction diagram is formulated by deriving equations which are based on column interaction diagram with ACI code 318-08. It is considered that, old rebar is corroded hence cross sectional area is considered negligible in analysis to contribute in compression which is agreed with V. C. Marlapalle et al. (2014). Thus, pure compression for jacket sections can be written as:

$$P = CB \times [0.85 f_{c' jacket} \times (A - A_{s old} - A_{s jacket})] + (A_{st jacket} + A_{sc jacket}) \times f_{y jacket} \quad (1)$$

$CB$  = Coefficient of bondage; to account the reduction factor due to bonding effect at interface of different concrete.  $A$  = cross section after jacketing,  $A_{s old}$  and  $A_{s jacket}$  = area of longitudinal steel in existing column and jacket respectively,  $A_{st jacket}$  and  $A_{sc jacket}$  = area of tension and compression steel respectively in jacket,  $f_{y jacket}$  = yield strength of jacket longitudinal steel.

Bending capacity of old rebar is considered to contribute along with jacketed bar. To account for the remaining contribution of old longitudinal bar, a partial value of their original bending capacity is assumed. It is denoted as Coefficient of moment ( $CM$ ). It is considered that, these bar had reached to yield strength and their remaining ductility is added in the bending capacity of jacketed section. Thus  $CM = 1 - (f_{y old} / f_{u old})$  in which  $(f_{y old} / f_{u old})$  is ratio of yield and ultimate strength of old column rebar. Generally  $CM$  gives a value ranging from 0.20-0.35. Thus pure bending point is denoted as:

$$M = [A_{st jacket} \times f_{y jacket} + CM \times A_{st old} \times f_{y old}] \times (dn - \frac{a_n}{2}) \quad (2)$$

$A_{st old}$  = area of tensile steel in old column,  $dn$  = distance of centroid of tensile jacketed steel from top fibre,  $a_n$  = dimension of equivalent stress block in jacketed section.

Jacketed concrete strain  $\epsilon_{ujacket}$  is taken as 0.003 in analysis. However, old concrete strain  $\epsilon_{uold}$  is considered up to 0.005. Basing on strain compatibility a single concrete strain is considered for simplification. Basing on strain and force, weighted average concrete strain  $\epsilon_{uavg}$  is calculated. Finally following equations are proposed for balanced, compression and bending control points:

$$P = 0.85 f_{c' jacket} \times a_n \times b_{new} + A_{sc jacket} \times f_{s' jacket} + A_{st jacket} \times f_{y jacket} \quad (3)$$

$$M = 0.85 f_{c' jacket} \times a_n \times b_{new} \times (\frac{h_{new}}{2} - \frac{a_n}{2}) + A_{sc jacket} \times f_{s' jacket} \times (\frac{h_{new}}{2} - d'_{new}) +$$

$$A_{st jacket} \times f_{y jacket} \times (d_{new} - \frac{h_{new}}{2}) + CM \times A_{st old} \times f_{y old} \times (d_{old} - \frac{h_{old}}{2}) \quad (4)$$

### Interaction Diagram using Japanese equations

Following [4] and [6] maximum theoretical axial capacity  $P_{max}$  and bending equations are formulated.

$$P_{max} = A_{st jacket} \times f_{y jacket} + A_{st old} \times f_{y old} + b_{new} \times h_{new} \times f_{c' avg} \quad (5)$$

[According to 3.3.4-2 a of Japanese guidelines]

$$M = (A_{st jacket} \times f_{y jacket} \times g_{jacket} + A_{st old} \times f_{y old} \times g_{old} + 0.12 \times b_{new} \times h_{new}^2 \times f_{c' avg})$$

$$\times (\frac{P_{max} - P}{P_{max} - 0.4 \times b_{new} \times h_{new} \times f_{c' avg}}) \quad (6)$$

$g_{old}$  and  $g_{jacket}$  are distance between tensile and compressive longitudinal steel in jacket portion and existing column respectively

### FINITE ELEMENT MODELLING USING ETABS 2015 AND SAP 2000

Section designer is used to model jacketed column section in ETABS 2015 and SAP 2000 v17. Material properties were defined according to the test samples. Rectangle and box section was used to model

samples. Longitudinal and tie bar were placed in the model following the actual dimensions of samples. After modelling, interaction diagram and moment vs. curvature diagram can be extracted as output. SAP 2000 produces advance features for analysis stress and strain in different conditions as well as moment vs. concrete and steel strain and compression data. Interaction diagram are formulated using these data. Fig. 2 displays the model and stress distributions.

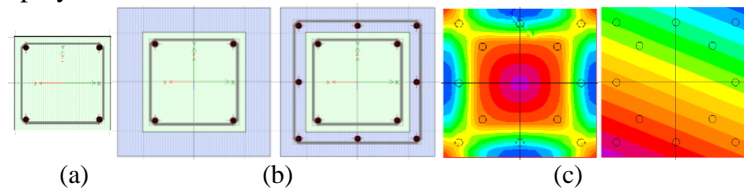


Fig. 2 (a) Old column section (b) Jacketed column (c) Stress distributions

## RESULTS AND DISCUSSIONS

Results of the test and analytical assessment are shown in Table 1. Bonding does not follow a linear behaviour and vary greatly according to construction, material property and types of surface preparation, moisture content of substrate [8]. Effect of creep and any direct tension stress caused by shrinkage are ignored in analysis. All these factors contribute in the deviations of test with analytic results. Monolithic samples 25-M and 31.5-M had the less deviation due to absence of different concrete interface. Whereas 25-N and 31.5-N had the larger deviation. Since there is no provision of reduction factors due to bonding interface in FE analysis and Japanese code therefore proposed pure compression point differs as much as 26% as in Fig. 3. Other points agree with the Japanese code by a variation of 8-12% while pure bending resulted deviation by only 1-2.5%. On the other hand, for maximum bending capacity, proposed analysis agrees well with an accuracy of 93.5-98 % with the Japanese code. However, both differ with ETABS and SAP with a deviation of 16.5-25% due to liner addition and composite action account which is shown in Fig. 7.

Table 1. Experiment vs. Analytical Results

Sample Name	$f'_{c,old}$ (MPa)	$f'_{c,jacket}$ (MPa)	Analytic capacity (KN)	Test capacity (KN)	% variation	Area Ratio $A/A_{old}$	Capacity ratio $P_n/P_{old}$	
							Analytic	Test
25-N	11.12	19.35	243.29	226.21	7.02	2.220	1.522	1.521
25-B	11.13	21.63	289.64	258.51	10.74		1.948	1.739
25-B-W		21.98	289.75	264.38	8.78		1.813	1.778
25-M		21.80	289.69	302.5	4.36		1.812	2.030
25-B-C		21.89	329.83	298.83	9.46		2.064	2.010
31.5-N	11.12	24.98	336.9	305.67	9.26	2.617	2.108	2.056
31.5-B	12.20	29.42	441.00	416.78	5.51		2.759	2.803
31.5-M		29.87	441.72	452.86	2.69		2.764	3.046
31.5-B 2		20.85	403.70	379.45	6.01		2.526	2.552
31.5-B-W		20.21	402.43	382.78	4.88		2.518	2.575
31.5-B-C	11.12	21.32	372.08	342.68	7.74	2.328	2.305	
RS	-	-	159.80	148.65	6.97	-	-	-

### Failure Pattern

Samples failed with generation of full and partial depth longitudinal crack as in Fig. 5. Few lateral cracks were generated also. Local failure occurred due to stripping out of concrete at the new and old concrete interface which agrees with [7]. This happens as the jacketed column is unable to maintain strain compatibility at the interface of new and old concrete. Crushing of jacket concrete along with failure of ties were seen. Concrete failed at the corner due to the high concentration of stress which agrees with [9]. Significant increase of axial capacity was found up to 178% depending on compressive strength of jacket. From Table 1 it is seen that, for same area ratio bonding and surface prepared sample had increased capacity ratio from 18-22% than the nonbonding sample.

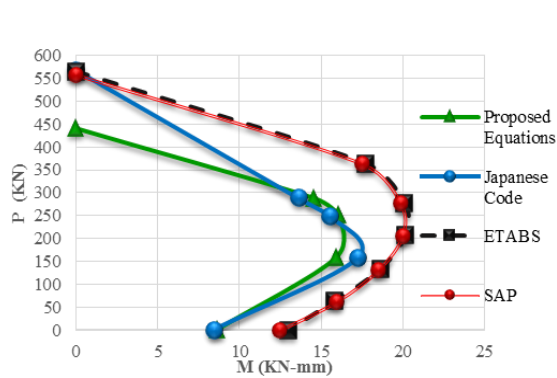


Fig. 3: Comparison of Interaction Diagram.

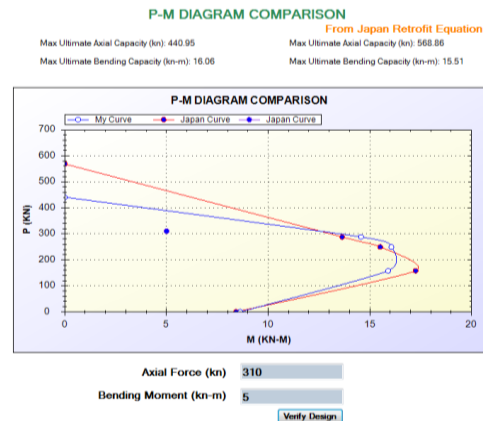


Fig. 4: Developed software output interface

### Development of Analysis Software

A software is developed to analyse jacketed column using Eq. (1)-(6) in the programming language of 'Microsoft C#'. Interface takes the input of material properties and dimensions to generate interaction curve both with and without phi. A comparison is also generated with Japanese code in the output interface as shown in Fig. 4. User facility like print, save as image, and zoom options are incorporated. Jacket design verification can be performed using the dynamically generated point.

### Stress-strain Behaviour

Maximum loading occurred in an average strain of 0.012-0.013 mm/mm for all the sample as in Fig. 6. However, 25-M, 31.5-M and RS samples had lesser rate of 0.011 and 0.01 respectively. Thus ultimate strain of confined concrete increases due to jacketing as tensile reinforcement undergoes strain hardening well agreed with S. Chun and H.C. Park (2012). 0.3% ductility is achieved in axial loading corresponding to 1.61% increase of size. This approves the seismic effectiveness of jacketing.



Fig. 5: Typical failure pattern of samples

### Effect of Surface Preparation, Confinement Stress and Welded Ties

Increase capacity can be achieved without using any bonding agent and surface preparation. However, use of this increased the capacity to 24-30%. A detailed trial method was carried out with different value of CB ranging from 0.85-1 for bonded and 0.60-0.70 for non-bonded. Hence CB in the range 0.85-0.95 is proposed. For perfect bonding the value is 1. Tabulated capacity is calculated with the minimum value of CB as 0.85 and 0.65 for surface prepared and non-prepared sample respectively. Test result verified the analysis with an accuracy of 89 to 96%. For same jacket thickness, clear cover of bars in jacket determines the effective thickness of confinement concrete. Thus the reduction of clear cover will increase the capacity with a ratio varying from 0.45-0.50 and vice versa. For constant clear cover, confinement stress increased due to increase in the thickness and compressive strength of jacket concrete. Welding of ties prevent buckling of main and tie bar in failure with an increase of axial



capacity at a range of 1-2.5% only. Thus for construction convenient welded ties may not be applicable except joint.

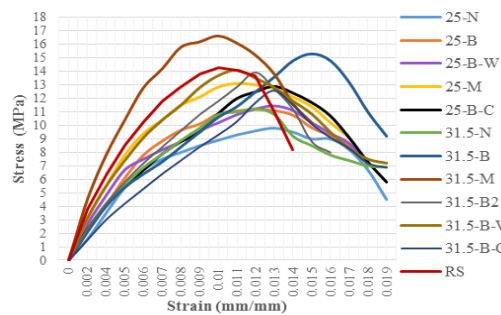


Fig. 6 Stress vs. Strain

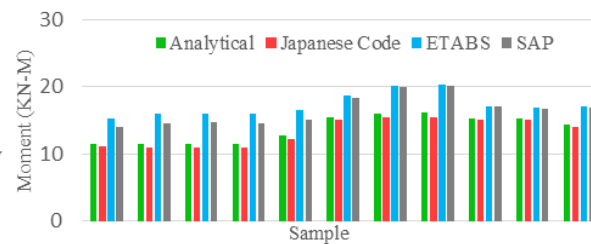


Fig. 7 Maximum bending capacity comparison

## CONCLUSIONS

Based on the results and findings presented in the paper, following conclusions can be drawn:

- Capacity enhanced significantly (up to 178% in this research) by RC jacketing depending on compressive strength, clear cover, use of surface treatment and bonding agent. Outer concrete and interface bonding governs the failure pattern.
- Developed compressive stress of RC jacketing can be used instead of weighted average or existing value. Proposed equations can be used for simplified analysis of RC column jacketing.
- Idea of using commercial software (such as ETABS, SAP) in analysing and designing jacketed column is controversial. Engineers should be careful in case of retrofitting column design.
- The developed program can be a useful tool in jacketed column capacity prediction. It can be effectively used by the engineers to analyse and design for simplicity and enhanced time efficiency.
- Proposed CB and bending capacity analysis can further be evaluated for precision by axial and bending test of actual size column.
- This research work may contribute to develop a design guideline for column strengthening using RC jacketing.

## REFERENCES

- Aysha H, Ramsundar, K. R. Arun M and Velraj Kumar. G, "An Overview of Interface Behavior between Concrete to Concrete", International Journal of Advanced Structures and Geotechnical Engineering, Vol. 03, No. 02, April 2014.
- CEB bulletin no. 162, "Assessment of Concrete Structures and Design Procedures for Upgrading (Redesign)". Bulletin Information, Euro international concrete committee, Paris, 1983.
- Indian Standard, "Seismic Evaluation and Strengthening of Existing Reinforced Concrete Buildings-Guidelines", Bureau of Indian Standards, February 2013, chapter 8.
- Japanese Standard, "Guidelines for Seismic Retrofit of Existing Reinforced Concrete Buildings", Japan Building Disaster Prevention Association, 2001, chapter 3, pp. 2-23.
- Mander, J.B., Priestley, M.J.N, and Park, R. "Theoretical Stress-Strain Model for Confined Concrete" Journal of Structural Engineering, American Society of Civil Engineers, vol.114, No. 8, 1988, pp. 1804-1825.
- "Manual for Seismic Retrofit Design of Existing Reinforced Concrete Buildings", Public Works department, Bangladesh, 2015, chapter 3.
- Stephanos E. Dritsos, "Seismic Strengthening of Columns by Adding New Concrete", bulletin of the New Zealand Society for Earthquake Engineering, Vol. 40, No. 2, June 2007, pp. 65-66
- S. Mohsen S. Asaei, Tze Liang Lau and Norazura Muhammad Bunnori, "Modelling FRP-confined RC Columns using SAP2000", World Applied Sciences Journal 27 (12): pp.1717-1720, 2013.

## **STRENGTH BEHAVIOR OF SLAG (GGBS) BASED GEOPOLYMER CONCRETE IN CHLORIDE ENVIRONMENT**

S. Sarker\*, M. A. Hossain, O. C. Debnath, N. Tabassum & M. S. Islam

*Department of Civil Engineering, Chittagong University of Engineering and Technology, Chittagong,  
Bangladesh*

*\*Corresponding Author: sarkercuet11@gmail.com*

### **ABSTRACT**

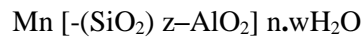
Concrete is the most abundantly used manmade material in the world. The main component of concrete is the Ordinary Portland Cement (OPC) which is the second most utilized material after water. After automobile, OPC production is the second major generator of carbon-dioxide which pollutes the atmosphere. Geopolymer has been widely used as a cement replacement material which leads to reduce the carbon dioxide emission by using the industrial by-product as a base material. Ground Granulated Blast Furnace Slag (GGBS) is a latent hydraulic material that can directly react with water in presence of an alkali activator. After activation, GGBS in alkali activator solution is termed as alkali activated slag (AAS) and act as the main constituent of geopolymer. This paper focuses on experimental results of a study conducted to assess the strength of AAS concrete over 7, 14, 28 & 60 days exposure in normal & sodium chloride environment. This programme covers the immersion of cubical specimen in NaCl solution of different concentration. The performance of the specimen was evaluated in terms of visual appearance, change in weight & compressive strength over the stated exposure periods. From this study, it is observed that the strength of geopolymer concrete specimens increase with the increase of dosages & ages in normal environment while in chloride environment, the corresponding gain in strength is observed to be lower as compared to normal environment.

Keywords: Geopolymer; GGBS; alkali activators; strength; chloride environment

### **INTRODUCTION**

Concrete is the most widely used construction material due to its versatility and energy efficient next to steel and aluminium (Hardjito et al., 2004). The main component of concrete is the ordinary Portland cement (OPC) which is conveniently used as the binder in concrete still now. But the production of OPC is a concerning issue for the environment now a days. In the production of OPC, carbon dioxide gas is produced which is the main source of greenhouse gas and global warming. Statistics shows that the amount of carbon dioxide production is almost one ton for every ton of OPC produced. Alarming issue is that, this carbon dioxide contributes to greenhouse gas emission approx. 7% of the total greenhouse gas (GHG) emission to the earth's atmosphere. Among the GHGs CO<sub>2</sub> contributes 65% of the total global warming. It can be seen that even a small reduction of greenhouse gas emissions per ton of manufactured concrete can make a significant impact on environment (Flower and Sanjayan, 2007). Each year the concrete industry produced almost 12 billion tons of concrete (Attwir and Kabir, 2010) globally and utilized 1.65 billion tons of cement for that purpose. Production of 1 ton of cement requires around 2.8 tons of raw materials including fuel as reported on four different studies (Björk, 1999; Reddy et al., 2010; Anuar et al., 2011; Guo et al., 2010). The increase of cement production is reported to be almost 3% per year. Geopolymers are inorganic polymeric binding materials, firstly developed by Joseph Davidovits in 1970s. Geopolymerisation involves a chemical reaction between an aluminosilicate (Al-Si) material and a strong alkaline solution yielding amorphous to semi crystalline three-dimensional polymeric structures, which consist of Si-O-Al bonds. In 1978, Davidovits proposed that an Al-Si compound could polymerise with an alkaline solution. Davidovits (1988) discovered that the concrete used in ancient structures is alkali-activated aluminosilicate binders and named it as geopolymer concrete because of polymerization reaction. This led to the idea of cement replacement and the

subsequent creation of “Geopolymer Concrete”. Geopolymer is a type of amorphous aluminohydroxide product that exhibits the ideal properties of rock-forming elements, i.e., hardness, chemical stability and longevity. Geopolymer binders are used together with aggregates to produce geopolymer concretes which are ideal for building and repairing infrastructures and for precasting units because they have very high early strength. The polymerization process involves a substantially fast chemical reaction under alkaline condition on Si-Al minerals, that results in a three dimensional polymeric chain and ring structure consisting of Si-O-Al-O bonds, as follows (Davidovits 1999):



Where: M = the alkaline element or cation such as potassium, sodium or calcium; the symbol – indicates the presence of a bond, n is the degree of polycondensation or polymerisation; z is 1, 2, 3, or higher, up to 32.

The chemical reaction may comprise the following steps (Davidovits 1999; Xu and van Deventer 2000):

1. Dissolution of Si and Al atoms from the source material through the action of hydroxide ions.
2. Transportation or orientation or condensation of precursor ions into monomers.
3. Setting or polycondensation/polymerisation of monomers into polymeric structures.

However, these three steps can overlap with each other and occur almost simultaneously, thus making it difficult to isolate and examine each of them separately (Palomo et al. 1999).

The main objective of this study is to evaluate the strength, durability and suitability of Slag (GGBS) based geopolymer concrete as an alternative of conventional concrete. However, the specific objectives are listed as follows:

- ▶ To optimize the mix design for AAS (alkali activated slag) concrete.
- ▶ To evaluate the compressive strength of AAS concrete at different age.
- ▶ To evaluate the performance of AAS concrete in Chloride environment compared to normal environment.

## METHODOLOGY

The following articles discuss the materials and methodologies used for the study.

### Materials and Sample Preparation

Slag sample used for this study was collected from Royal Cement Company, Chittagong (Bangladesh). Table-1 shows the chemical properties of slag used for the experiment.

Table 1: Chemical Composition of GGBS (% mass)

Composition	SiO <sub>2</sub>	Al <sub>2</sub> O <sub>3</sub>	Fe <sub>2</sub> O <sub>3</sub>	MnO	CaO	MgO	Na <sub>2</sub> O	K <sub>2</sub> O	LOI
GGBS	29.27	17.07	1.76	0.49	40.07	8.35	0.61	0.23	0.06

\*LOI- loss of ignition

### Combined Aggregate:

Combined aggregate means the mixture of fine aggregate (43%) & coarse aggregate (57%). Fine aggregate were collected from locally available source. Fine aggregate & coarse aggregate were prepared in accordance with ASTM C778-02 & ASTM C33-03 respectively. The grading & material properties of coarse & fine aggregate are shown in the Table-2 & Table-3.

Table 2: Grading of Combined Aggregate

Coarse Aggregate	Sieve size(mm)	Passing	Retain	%
		19	12.5	19.95
		12.5	9.5	17.1
	9.5	4.75	19.95	
Coarse aggregate=57%				
Fine Aggregate			43%	

Total combined aggregate=100%

Table 3: Properties of Aggregates

	Fine Aggregate	Coarse Aggregate
Specific Gravity	2.52	2.67
Absorption Capacity	1.45(%)	0.8(%)
Moisture Content	1.25(%)	0.57(%)
Fineness Modulus	2.57	NA
Unit Weight (kg/m <sup>3</sup> )	1580	1560

### **Alkaline Activators:**

The alkali activators used in this study is a sodium silicate based solution which is a mixture of sodium silicate ( $\text{Na}_2\text{SiO}_3$ ) & sodium hydroxide ( $\text{NaOH}$ ). The  $\text{NaOH}$  solution was prepared in laboratory by dissolving  $\text{NaOH}$  pellets in deionized water at least 1 day prior to mixing. 15 molar  $\text{NaOH}$  solution was used (prepared by dissolving 600g of  $\text{NaOH}$  per liter of water). The  $\text{Na}_2\text{SiO}_3$  was collected from local suppliers. Table-4 shows the chemical properties of activator solution.

Table 4: Chemical properties of activator solution

Components	$\text{Na}_2\text{O}$	$\text{SiO}_2$	$\text{H}_2\text{O}$	Molarity(M)
$\text{Na}_2\text{SiO}_3$	8%	26%	66%	NA
$\text{NaOH}$	29.05%	0%	70.95%	15

## **EXPERIMENTAL PROGRAMME**

### **Mix Design:**

The combined solution of sodium silicate ( $\text{Na}_2\text{SiO}_3$ ) and  $\text{NaOH}$  solution was used as alkaline activators. Two dosage of  $\text{Na}_2\text{O}$  (% $\text{Na}_2\text{O}$ ) was selected for experiment those were 5% & 7% respectively which was the ratio of  $\text{Na}_2\text{O}$  content of alkaline solution to GGBS. Two activator modulus having 1.0 and 1.5 respectively was selected for this experiment which is the mass ratio of  $\text{SiO}_2$  to  $\text{Na}_2\text{O}$ . The alkaline activator was prepared by mixing a sodium silicate and  $\text{NaOH}$  solution with a concentration of 15 M. Specimen notation used for alkali activated slag concrete is given in Fig.1

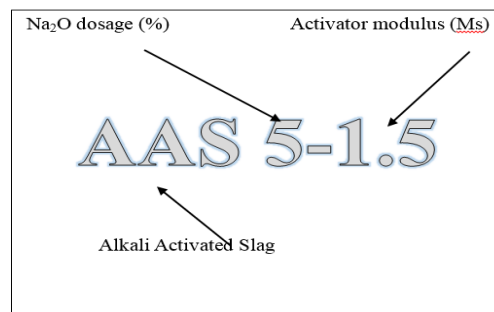


Fig. 1: Specification notation for AAS concrete specimen

### **Mix Details:**

The mass ratio of combined aggregate to slag was fixed at 3 for all batches. A water binder ratio of 0.45 was used & kept constant for all batches. A total 96 nos. of 100mmX100mmX100mm cubical specimens were prepared for compressive strength test using four mix combination. The variables of AAS concrete are shown in Table-5.

The proportioning of ingredients (binding materials, activator solution, fine sand, coarse aggregate and water) were conducted based on the absolute volume method (Neville, 1996) which assumed that the volume of compacted concrete is equal to the sum of the absolute volume of all the ingredients. The mix proportion for the concrete are given in Table-5

### **Mixing, moulding and curing:**

The sodium hydroxide and sodium silicate solutions are mixed in a plastic container 24 hours before casting. The other ingredients like fine aggregate, coarse aggregate, extra water, and binder (GGBS) were measured in required amount and mixed for 5 minutes. Then the alkaline activator was mixed gradually and the mixture were poured into 100mm cubic moulds and compacted by tamping rod. The curing regime for AAS concrete was 24 hours at room temperature prior to demoulding followed by heat curing continuously at 40°C for 72 hours in temperature controlled room. After completion of heat curing the specimens were kept at room temperature up to the completion of corresponding testing. Various stages of mixing, preparation and curing of AAS concrete specimens are shown in Fig.2 – Fig.6.

Table 5: AAS concrete mixes and variables

Mix	Variables		Mass of materials (kg/m <sup>3</sup> )				
	Na <sub>2</sub> O Dosage (%)	Activator Modulus (Ms)	GGBS	Combined aggregate	Added water	Na <sub>2</sub> SiO <sub>3</sub>	NaOH
AAS 5-1.0	5	1.0	537.42	1612	128.19	103.4	64.04
AAS 5-1.5	5	1.5	538.29	1615	104.35	155.3	49.83
AAS 7-1.0	7	1.0	536.32	1609	82.558	144.4	89.48
AAS 7-1.5	7	1.5	537.54	1613	49.128	217.1	69.75



Fig.2: Alkali activator solution



Fig.3: Mixing



Fig.4: Moulding



Fig.5: Demoulding



Fig.6: Heat Curing

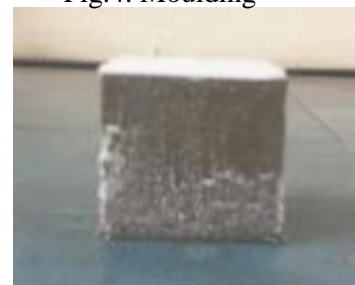


Fig.7: After curing at NaCl solution

#### **Durability Study:**

The cubical specimens were submerged in NaCl solution of different concentration i.e. 2<sup>T</sup> & 3<sup>T</sup> concentration. Sea water contains around 2.78% of NaCl and hence 2<sup>T</sup> & 3<sup>T</sup> concentration means 5.56% (two times) and 8.34% (three times) NaCl solution. The enhanced salt concentrations were used to get the accelerated effects in short time. For durability study, compressive strength and % weight loss data after 14, 28 & 60 days exposure periods (Fig.7), were studied to evaluate the performance of specimens.

#### **RESULTS AND DISCUSSIONS**

The compressive strength gain of AAS concrete having different combination is shown graphically in figure 8. It also shows the compressive strength gain of AAS concrete exposed to NaCl environment of two different concentration. The AAS concrete showed significantly higher strength for the 7% Na<sub>2</sub>O compared to the 5% Na<sub>2</sub>O. At the age of 60 days, maximum strength for 5% dosage of Na<sub>2</sub>O is recorded as 45 Mpa and for 7% dose is 65 MPa. Thus increase of Na<sub>2</sub>O that increases the alkalinity of the dosage, increases the strength of the specimens in normal as well as chloride environment. However strength of AAS specimens in chloride environment is observed to be lower than the normal environment for all mix combination. It is also seen that the strength gain in concrete higher dosage of Na<sub>2</sub>O is more rapid i.e. in case of AAS 7-1.5, almost 76% of strength is gained after 7 days.

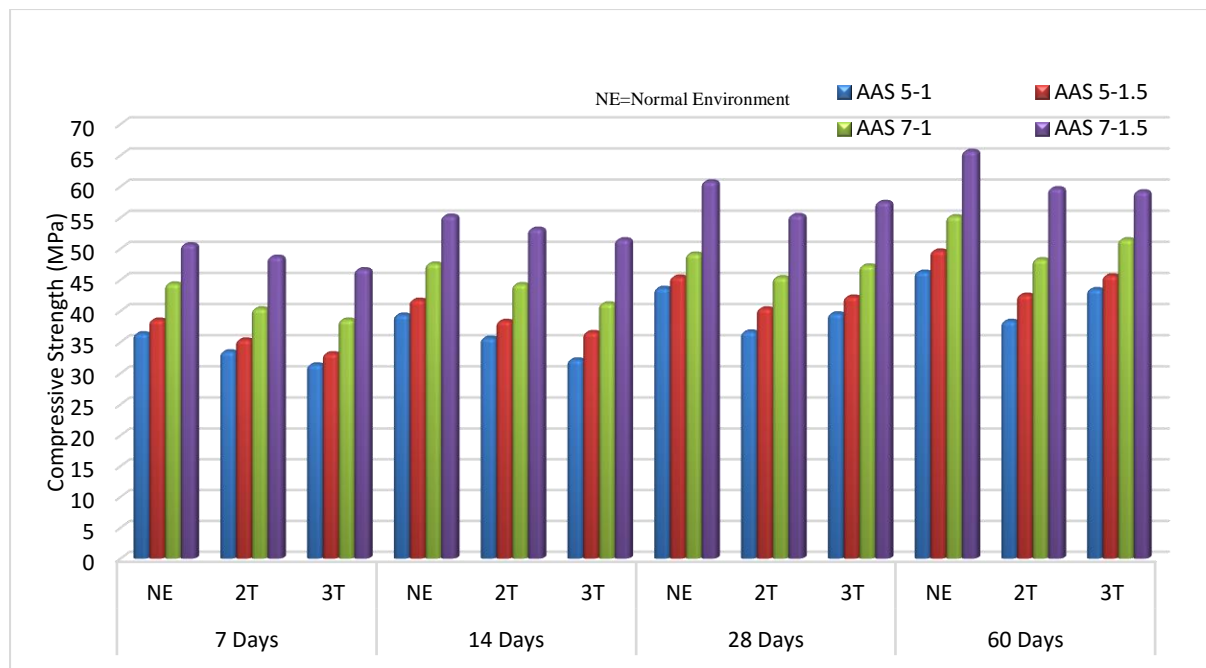


Fig 8: Compressive strength of AAS concrete in normal & chloride environment

The results of weight change for concrete specimens in chloride environment ( $2^T$  &  $3^T$ ) are presented graphically in Fig.9. The negative value of weight change data indicate the loss of weight due to immersion in NaCl environment which may be associated with surface erosion. After 60 days exposure, it has been seen that the AAS concrete made of higher dosage (7%Na<sub>2</sub>O) shows less deterioration & lower weight change. It also indicates the stability of specimen increase with the increase of dosage of Na<sub>2</sub>O & activator modulus of alkaline solution. From weight change study it has been seen that the mixed combination AAS 7-1.5 shows relatively better performance as compared to other mixes.

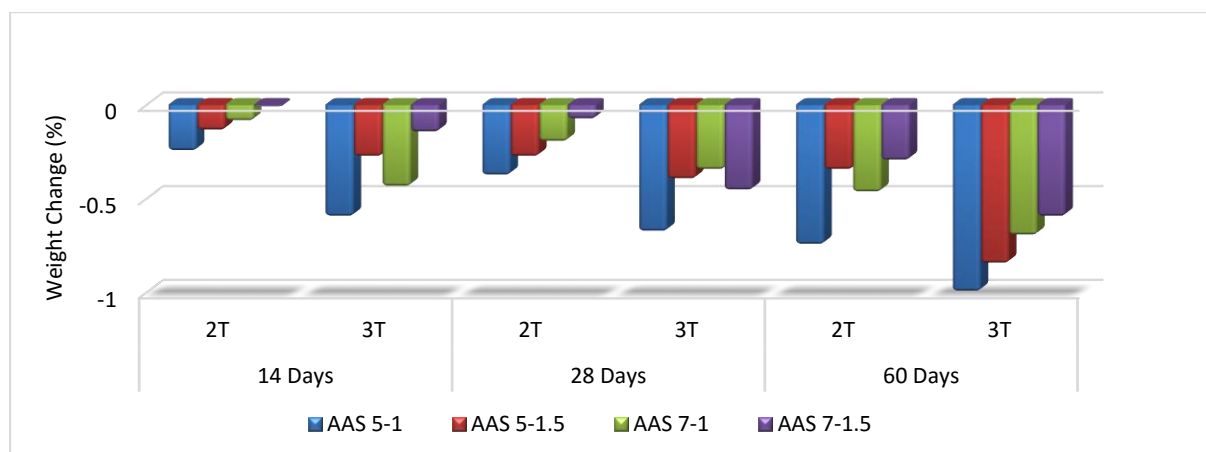


Fig 9: Weight Change (%) of AAS concrete in chloride environment

### CONCLUSION:

The followings are the conclusions drawn from the study:

1. AAS 7-1.5 mix attained 50 MPa compressive strength (almost 76% of 60 days) after 7 days which indicates that geopolymer mixes having higher dosage of Na<sub>2</sub>O can attain ultimate strength very rapidly.
2. The compressive strength of AAS concrete is observed to increase with the increase of Na<sub>2</sub>O dosage & activator modulus.

3. In NaCl environment, AAS concrete showed no noticeable signs of surface degradation, i.e. change of color, sign of cracks/spalls etc. although few signs of salt deposition is noticed at some location of specimen surfaces. It indicates that AAS concrete can offer ample resistance against chloride attack.

## REFERENCES

- Anuar, K. A., Ridzuan, A. R. M. and Ismail, S. (2011). Strength characteristic of geopolymer concrete containing recycled concrete aggregate. *International Journal of Civil and Environmental Engineering*. 11 (1), 81-85.
- ASTM International. C 778-02. *Standard Specification for Standard Sand*. ASTM International, West Conshohocken, USA.
- ASTM International. C 33-03. *Standard Specification for Concrete Aggregate*. ASTM International, West Conshohocken, USA.
- A.Palomo, M.W. Grutzeck, M.T. Blanco (1999) 'Alkali-Activated flyashes, a cement for future.' *Cement and concrete research* 29(8): 1323-1329
- Bjork, F.1999. *Concrete Technology and Sustainable Development*. Vancouver Symposium on Concrete Technology for Sustainable Development. Vancouver, Canada.
- Davidovits JSPE PA CTEC'79, Society of Plastic Engineers, Brookfield Center, USA,(1979)  
151
- Davidovits J (1988), "Structural Characterization of Geopolymeric Materials With X-Ray Diffractometry and MAS NMR Spectroscopy", *Geometry and MAS NMR Spectroscopy*", Geopolymer'8: First European Conference on Soft Mineralogy, Compiègne, France, Vol 2,1988,PP. 149-166.
- Davidovits J, (1999). 'Chemistry of Geopolymeric system, Terminology. Geopolymer.'99 International Conference, France.
- D. Hardjito, B. V. Rangan (2005). 'Development and Properties of Low-Calcium Fly Ash-Base Geopolymer Concrete.' Research report GC 1, Faculty of Engineering, Curtin University of technology, Perth, Australia.
- Flower, D. J. M. and Sanjayan, J. G. (2007). Green House Gas Emissions Due to Concrete Manufacture. *International Journal of Life Cycle assessment*. 12(5), 282-288
- Guo, X., Shi, H. and Dick, W. A. (2010). Compressive strength and microstructural characteristics of class C fly ash geopolymer. *Cement and Concrete Composites*. 32 (2), 142-147.
- N. M Attwir, and S. Kabir, 'Reducing Environmental Impacts through Green Concrete Technology.' The 3rd Technology and Innovation for Sustainable Development International Conference (TISD2010)
- Reddy, B. S. K., Varaprasad, J. and Reddy, K. N. K. (2010). Strength and workability of low lime fly-ash based geopolymer concrete. *Indian Journal of Science and Technology*. 3 (12), 1188-1189.
- Xu, H. and J. S. J. van Deventer (2000). *The polymerization of Alumino-Silicate Minerals*. *International Journal of Mineral Processing* 59(3):247-266